ANL-76-8

ANL-76-8

PROCEEDINGS

OF THE

SYMPOSIUM AND WORKSHOP

ON

ADVANCED BATTERY RESEARCH AND DESIGN

March 22-24, 1976

Sponsored by

Chicago Section, The Electrochemical Society

and

Argonne National Laboratory

Printed in the United States of America
Available from
National Technical Information Service
U. S. Department of Commerce
5285 Port Royal Road
Springfield, Virginia 22161
Price: Printed Copy $12.75; Microfiche $2.25

Distribution Category:
Energy Storage—
Electrochemical
(UC-94c)

ANL-76-8

ARGONNE NATIONAL LABORATORY
9700 South Cass Avenue
Argonne, Illinois 60439

PROCEEDINGS OF THE SYMPOSIUM AND WORKSHOP ON ADVANCED BATTERY RESEARCH AND DESIGN

March 22-24, 1976

Sponsored by

Chicago Section, The Electrochemical Society
Chemical Engineering Division, Argonne National Laboratory

Symposium Committee and Proceedings Editors

J. Robert Selman, Illinois Institute of Technology
Robert K. Steunenberg, Argonne National Laboratory
John J. Barghusen, Argonne National Laboratory
William C. Howard, Gould Incorporated

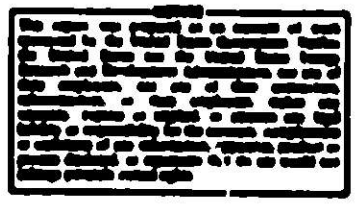

PREFACE

This volume contains the proceedings of the Symposium and Workshop on Advanced Battery Research and Design sponsored by Argonne National Laboratory and the Chicago Section of The Electrochemical Society. The idea for this meeting evolved from interest expressed by members of the Chicago Section in convening a symposium on the development of high-energy secondary batteries. The relevance of this subject is evidenced by the several research programs that have been initiated recently in the United States and Europe to develop advanced batteries for use as energy storage devices on electric utility networks and as power sources for electric automobiles.

The meeting was divided into two parts: a symposium on the state of the art in secondary batteries emphasizing new applications for secondary batteries; and a workshop on new developments in high-temperature batteries. This format has been retained in the publication of these proceedings, with each part having separate pagination.

The symposium committee extends their appreciation for the assistance of all who participated in this symposium. In particular, we express our gratitude to Mrs. Miriam Holden and her staff of the Conference Planning and Management Department for making the arrangements for this symposium, and to Mrs. Sherry Grisko for assistance in preparing the manuscripts for publication.

TABLE OF CONTENTS

Symposium on Secondary Batteries

TABLE OF CONTENTS (cont'd.)

High-Temperature Battery Workshop

TABLE OF CONTENTS (cont'd.)

TABLE OF CONTENTS (cont'd.)

PART A

SYMPOSIUM ON

SECONDARY BATTERIES

SECONDARY BATTERIES FOR LOAD LEVELING

James R. Birk
and
Fritz R. Kalhammer
Electric Power Research Institute
Palo Alto, California

ABSTRACT

More than fifty years ago, secondary batteries were used advantageously to store and deliver electric energy for electric rail and city emergency power systems. Today, batteries are being considered seriously for storage of off-peak energy because they promise a possibly unique combination of favorable operational characteristics, flexible siting and environmental compatibility. These prospects have given rise to broad and growing activities in research, development and engineering of advanced battery concepts and systems for utility energy storage. In this paper, we will briefly discuss the technical and cost criteria for utility energy storage. Candidate battery systems will then be reviewed in terms of their characteristics and basic prospects to meet utility criteria. The question of the technoeconomic feasibility of lead-acid batteries for utility energy storage will also be examined. Significant technical and economic obstacles on the way to practical utility batteries will be identified and related to the major ongoing development efforts.

INTRODUCTION

Batteries have become indispensable sources of electric power in a host of important applications that demand relatively small amounts of energy delivered with high reliability by small (in many cases, portable) packages. It is interesting to note that more than 50 years ago batteries were also used to deliver much larger blocks of energy in a number of DC power systems for electric streetcar and municipal emergency power service. In these now historical applications, the key to the usefulness of batteries was their ability to store energy and deliver power with high reliability, at the rate demanded, and at a competitive cost.

Since then the development of modern AC power systems for technical and economic reasons has gone almost entirely the route of primary power generation in response to the instantaneous electric load; the only exception has been a gradually increasing use of pumped hydroelectric storage. As is by now well known, the electric utilities use a mix of AC generating equipment with different technical and economic characteristics to meet the fluctuating demand for electricity in a cost-effective manner. Base load plants serve the part of the system load that continues 24 hours a day through most of the year. Such plants are designed to operate with the

highest practical efficiency and reliability on the least expensive fuels. Because of this, base load plants generate the lowest cost power despite their high capital costs.

The broad daily demand peaks of a typical utility are satisfied by intermediate cycling generating equipment, typically a system's older, less efficient fossil steam plants and, not necessarily by choice, with gas turbine driven generators. Finally, the upper increment of the daily load peak is served by a system's oldest, least efficient steam plants, and increasingly by gas turbines.

In the past, this approach has permitted the electric utilities to supply electric power on demand, with high reliability and at rather low energy cost; it has also permitted utility systems to grow in an orderly fashion through addition of modern power plants for base load and demotion of older equipment to cycling and peaking service. Presently, this mode of operation and system expansion is becoming increasingly problematical for several reasons that developed primarily during the past few years:

- sharply higher fossil fuel costs are resulting in greatly increased cost of power especially from intermediate cycling and peaking equipment
- future availability of distillate fuel for the combustion turbines used increasingly for peaking and intermediate service is becoming uncertain
- greatly escalated costs of nuclear and fossil steam baseload plants are penalizing such plants heavily for less-than-maximum capacity factors
- future availability of economical cycling plants is in doubt because modern fossil fuel base load plants will not be suitable for eventual cycling service

These problems could be solved or greatly mitigated if combinations of base load plants (operated at the highest possible capacity factors) and energy storage systems were used to also provide the electric energy now generated by peaking and cycling equipment. This prospect explains why many electric utilities now are looking to energy storage as a necessity, rather than merely a useful complement to conventional generating equipment. Further, because the potential of pumped hydro development appears too limited, interest is high in new ways of utility energy storage. Presently, a good part of this interest is being focussed on use of secondary batteries as the potentially most versatile method of storing energy on electric utility systems, and significant efforts are underway to develop advanced batteries that will meet utility requirements.

In this paper, we will briefly discuss the technical and economic requirements that have to be met by competitive methods of utility energy storage. The specific advantages and limitations of batteries for this new and potentially large application will be examined, and candidate battery systems will be reviewed in terms of their basic characteristics, their current development status and problems, and their prospects for application in utility energy storage.

TECHNICAL AND ECONOMIC CONSIDERATIONS

Pumped hydroelectric storage is firmly established as an operationally advantageous and economically attractive component of electric power systems. This storage method thus can serve as a baseline in assessing the competitiveness of more advanced concepts for utility energy storage. In Table 1, representative technical and cost characteristics of pumped hydro installations are compared with those considered achievable for batteries.

Table 1

CHARACTERISTICS OF PUMPED HYDROELECTRIC AND BATTERY ENERGY STORAGE

Characteristic	Pumped Hydro	Batteries	
		Lead-Acid	Advanced
Efficiency (round trip)	67-75	60-75	60-80
Energy Density (kWh/cu.ft.)	0.03	1-2	1-5
Duty Cycle (typical daily)			
charge time (hours)	6-8	possibility of	
discharge time (hours)	8-10	shorter duty cycles	
Response			
load change (min)	1-5	rapid response	
charge to discharge (min)	2-20	(<1 sec)	
Capital Cost			
power-related components (C_p, $/kW)	120-160	60-100	60-100
energy storage-related components (C_s, $/kWh)	3-12	40-70	20-40
total capital cost* (C_T, $/kW)	200-300	500-800	250-400
O & M Cost (mills/kWh)	~1	1-2 (?)	2-4 (?)
Availability (%)	85-90	90 (?)	?
Useful Plant Life (years)	50	7-10	?

---

* total capital cost is given by

$C_T = C_p + t_{max} \times C_s$ where

t_{max} = maximum time during which storage system can deliver energy at rated power; total storage system cost calculated for t_{max} = 10 hr.

As shown in the table, batteries are likely to have competitive efficiency when operating on a typical daily duty cycle; they are expected to be superior with respect to other technical characteristics such as energy density and response time. On the other hand, batteries are unlikely to match pumped hydro in most of the categories bearing directly on energy storage economics: life, capital cost of energy storage capacity, and the costs of operation and maintenance. Batteries appear to have a cost advantage only with respect to the power-related components of the energy

storage system. A detailed analysis of how the advantages and limitations of batteries might be traded off in their optimum use on electric utility systems is beyond the scope of this paper. However, it is possible to present some simple considerations that will illustrate major trends and point to economically advantageous ways of using battery energy storage.

In Table 2, we have summarized technical and operating advantages of energy storage in general and dispersed battery energy storage in particular, and we have listed possible capital cost credits relative to conventional methods and equipment for power generation. Some of these credits have not yet been quantified. The numerical values given in Table 2 are based on the few rather simplifying estimates available at present;[1-3] their magnitude is still being questioned by several utility planners. Actual values depend strongly on a power system's equipment and operating parameters which can be rather different for different utilities. Furthermore, not every credit will apply for a given installation, and applicable credits tend to be interdependent. Credits thus cannot simply be added to arrive at a total storage system credit. Clearly, this situation and the potential importance of capital cost credits for the competitiveness of battery energy storage call for more detailed analyses. For the purpose of this paper, we have assigned batteries a rather conservative capital cost credit of $50/kW.

Figure 1 presents an economic comparison, in terms of total annual power cost, of two energy storage systems and representative utility equipment for generation of base load, intermediate cycling and peaking power. The favorable economics of pumped hydro -- including projected underground installations -- are readily apparent. Advanced batteries with capital costs near the lower end of the range given in Table 1 are attractive for shorter periods of annual and daily operation, especially if the expected capital cost credit is applied. It is apparent that a combination of base load capacity with more than one method of energy storage -- a "storage mix" -- would tend to result in the lowest overall cost of power delivered by the system. It should be noted* that the lines for batteries and pumped hydro represent envelopes for all optimally used storage systems -- that is, for systems whose energy storage capacity is used fully and equally for 250 days every year. For example, battery systems with a maximum discharge time t_{max} = 4 hr. represent a single point on the battery line, determined by the condition $T = 250 \times t_{max} = 1000$ hr/yr. This somewhat unusual method of presentation permits a graphic distinction between energy storage systems with different sets of power- and storage capacity-related capital costs.

Figure 2 is intended to show that batteries, with their relatively high costs of specific storage capacity, are economically rather sensitive to less-than-optimum use. For example, operating a battery of given power rating and a 10 hr discharge capacity for 100 days per year results in a 60% higher power cost compared to a 4 hr-battery used 250 days (and, hence, for the same total of 1000 hours) per year at the same power level. The corresponding difference is much smaller for pumped hydro. Thus, while utilities do not have to be overly concerned with operating pumped hydro at

---

*For a derivation, see Reference 4.

Table 2

IMPACTS OF ENERGY STORAGE ON
ELECTRIC POWER SYSTEMS

	IMPACTS	ECONOMIC BENEFITS*
CENTRAL ENERGY STORAGE	Improved base load capacity factor	Low cost charging energy
	Conservation of oil, natural gas	Reduced fuel costs
	Contribution to spinning reserve	Capital cost credit ($20-50/kW)
	Higher reliability/reduced reserve margin	Capital cost credit (t.b.d.)
	More efficient load following	Capital cost credit (t.b.d.)
DISPERSED ENERGY STORAGE	Impacts above, plus:	
	1) Deferral of new T & D lines	Capital cost credit ($50-100/kW)
	2) Deferral of substation reinforcement	Capital cost credit ($30-60/kW)
	3) Misc. (T&D loss, VAR control, short circuit)	Capital cost credit ($10-20/kW)
	4) Increased security of supply/reduced reserve	Capital cost credit (t.b.d.)
	5) Rapid Installation (factory built)	Reduced interest during construction
	6) Modular/incremental capacity growth	High capacity factor of storage

*Probable ranges; actual benefits depend on specific conditions in individual power systems.

full capacity for as many days per year as possible, this is economically very desireable for batteries, and the question arises whether utilities are likely to operate batteries this way. A partial answer is provided by the results of the load curve analysis performed by the Public Service Electric & Gas Company as part of an energy storage assessment study funded by EPRI and ERDA. As presented by V. Sulzberger of PSE&G during the Workshop on Lead-Acid Batteries at EPRI on November 18-19, 1976, and shown in Table 3, these results suggest that energy storage systems capable of delivering their rated power for a few hours per day could be fully utilized during most weekdays throughout the year. Operation of battery energy storage in the economically most advantageous and competitive mode thus appears compatible with the on-peak energy requirements of representative electric power systems. However, whether the electric utilities would actually use batteries in this way is likely to depend on several other factors as well, including use of batteries for some of the functions listed in Table 2, variations in the cost of charging power within a given utility system, and the feasibility of dispatching power from storage systems in small and relatively short increments.

The PSE&G study data may also be used to generate a very rough estimate of the total battery capacity that might be supportable in the U.S. electric utilities. Referring to Table 3, it is noted that 6% of a typical system's peak load could be satisfied by batteries of 4 hour discharge capacity. Assuming a U.S. peak load of 800,000 MW in 1985, this translates into 800,000 MW x 6% x 4 h = 200 million kWh of storage capacity. At a cost of $25/kWh, this represents a total investment of $5 billion -- a large incentive for developing the battery technologies discussed in the following section.

CANDIDATE BATTERIES FOR UTILITY ENERGY STORAGE

Lead-Acid Batteries

Recent studies by ESB, C&D and Gould (the three largest U.S. manufacturers of industrial lead-acid batteries) indicate a high probability that lead-acid batteries can be designed to meet the technical requirements for utility energy storage (see Table 1). The battery cost projections developed in these studies are shown in Table 4. Significantly, battery costs are nearly identical when expressed in terms of a cost linearly amortized over the anticipated cycle life, despite rather different design philosophies: C&D's design involves a 20 kWh, closed cell with pasted plates, ESB uses the same cell size but prefers tubular plates, and Gould uses a 125 kWh, open cell with large pasted plates*. This result tends to support the view that designs having the required, long cycle life but substantially lower costs are unlikely to emerge.

---

*When viewed over the 20-year life span of interest for utility applications, Gould's concept of replacing the positive electrodes twice (at a cost of $22/kWh each time) may have some advantage, provided this approach is technically feasible and does not involve costly operations.

Table 3

PEAK LOAD DURATION FREQUENCY DISTRIBUTION FOR A REPRESENTATIVE UTILITY SYSTEM

Description	Characteristics						
Load Duration Interval (Hrs.)	1-2	3-4	5-6	7-8	9-10	11-12	13-14
Avg. Frequency of Occurrence	172	154	91	62	43	45	32
Avg. Annual Hours of Operation	269	554	464	473	403	500	450
Avg. Magnitude of Interval Load (% of Peak Load)	3	3	3	3	3	3	3
Load Duration Interval (hrs.)	0-2	0-4	0-6	0-8	0-10	0-12	0-14
Frequency of Occurrence (Single Device)	172	209	223	223	223	223	223
Expected Annual Operation (Hrs.)	269	639	892	1078	1260	1453	1570
Avg. Magnitude of Interval Load (% of Peak Load)	3	6	6.8	7.5	8	9	9

Table 4

CAPITAL COSTS AND SPECIFICATIONS FOR UTILITY LEAD-ACID BATTERIES

Cost/Specification[1]	BATTERY SYSTEM C & D	ESB	Gould
Lead Cost ($/kWh)	22.10	19.80	13.00
Other Materials Costs ($/kWh)	11.70	14.40	10.70
Price ($/kWh)[2]	62.90	65-70	43.30
Cycle Life (cycles)	2500	2500	1750[3]
(years)	10	10	7
Price/cycle (¢/kWh/cycle)	2.51	2.60	2.47
Efficiency[4]	83	82	80

(1) costs are based upon rated (end-of-life) capacity
(2) assumes 1 million kWh/year of sales
(3) positive plate only
(4) ten-hour discharge and 7-hour charge with additional 3-hr taper charge

The high capital costs raise serious doubts regarding the economic feasibility of using lead-acid batteries for utility energy storage. This point is illustrated in Figure 3 which compares total annual costs of power delivered by lead-acid batteries with power costs for pumped hydro storage and combustion turbines: unless very large capital cost credits are justified by special circumstances (e.g., a combination of strict environmental constraints and very high cost of needed transmission/subtransmission reinforcements), lead-acid batteries appear to be non-competitive.

Note that the battery lines in Figure 3 are drawn for a storage-related capital cost of $50/kWh. Actually, lead-acid battery energy storage installations are expected to cost closer to $75-100/kWh since substantial balance-of-plant costs -- in the order of $25 - 40/kWh -- are involved. Major contributions to these costs include (1) a building to house the battery, (2) a massive pad for the heavy (110-130 lbs/kWh) batteries, (3) hydrogen monitoring and ventilating equipment, and (4) environmentally acceptable drainage and handling of battery acid.

The discussions and questionnaire responses during EPRI's Lead-Acid Battery Workshop indicate substantial utility industry interest in a near-term application of lead-acid batteries if total capital costs (in $/kW) can be brought to lower levels. Since this can be achieved -- with some sacrifice in the universal usefulness of a battery -- by reducing the extent of energy storage capacity (maximum discharge time) for a given power level, the teams at ESB, C&D and Gould are being asked to provide technical and cost information on lead-acid batteries designed for discharge in 3 and 5 hours. The results of these efforts, together with closer studies of the benefits and credits that would result from battery

energy storage on electric power systems, should provide an answer to the currently open question whether a near-term demonstration of lead-acid battery energy storage on a utility system is justifiable.

To date, a closer look at utility-oriented lead-acid batteries has provided us not only with a firmer cost base but with several rather useful (although not necessarily unexpected) insights:

- balance-of-plant costs are a significant cost factor, and their minimization will require development of compact battery systems capable of being installed with a minimum of shelter
- achievement of utility-type battery life is likely to require both, high-quality materials and sophisticated engineering designs; this suggests caution in projecting costs of advanced batteries from materials and designs used in the R&D phase
- even if engineering approaches are available to compensate for life-limiting processes, the complexity and cost associated with such approaches may become prohibitive; this suggests concentration of future developments of systems with inherently long life
- use of special charging techniques to maintain capacity and (or) extend life of batteries is likely to be compatible with battery operation in a utility environment

Advanced Battery Systems

The high cost of the lead-acid battery suggests that its penetration into the utility market will be very small, at most. Hence, there remains an urgent need and a large business opportunity to develop other battery systems that will have substantially lower costs while retaining or improving on the life prospects of the lead-acid system. Because a battery's active and containment materials can contribute substantially to total cost, the first criterion for utility batteries must be low materials cost per unit of storage capacity. As is well known, this criterion demands that a battery system meet several or all of the following requirements:

- low specific cost ($/kWh) of active materials
- high utilization of active materials
- high energy density to minimize containment materials
- low cost ($/ft^2) of containment materials
- high current density to minimize electrode and separator area and cost

Fundamental considerations of electrochemical engineering and practical experience in developing advanced batteries make it clear that several of these requirements are conflicting. For example, a high current density is generally incompatible with high utilization of active materials; if the conflict is partially resolved by using a higher temperature to reduce electrode polarization and cell resistance, more expensive containment materials might be required. Other, similarly fundamental conflicts result from the low-cost criterion. Development and engineering of cost-

competitive, advanced batteries thus tend to involve complex trade-offs between conflicting requirements. Some of these depend on unconventional battery configurations or designs, as will be discussed below in conjunction with the sodium-sulfur and lithium-metal sulfide systems.

Approaches to achieve long battery life -- the other major requirement for utility energy storage -- are more difficult to quantify but generally involve one or more of the following:

- soluble or liquid reactants and (or) products to avoid the cumulative degradation of structure and (or) morphology typical of solid electrodes
- electrode materials and cell conditions conducive to a high degree of electrochemical and morphological reversibility
- a high level of control of conditions (temperature; reactant distribution; impurities) inside cells, usually via circulation of electrolytes

These general considerations to achieve battery systems of low cost and long life have led to the present, widespread interest in the following electrode (active) materials

negatives	positives
sodium (liquid)	sulfur (liquid)
lithium (liquid; alloy)	chlorides (soluble)
zinc (soluble product)	sulfides (reversible solids)
iron (soluble product)	chlorine (soluble gas)
redox couples (soluble)	bromine (soluble liquid)
	redox couples (soluble)

Of the various possible combinations, the following systems currently appear to be the most promising:

- sodium - sulfur
- sodium - antimony chloride
- lithium (alloy) - metal sulfide
- zinc - chlorine (bromine)
- all redox
- iron redox

Technological aspects of these battery systems have been reviewed recently[5] and will be discussed in some detail later during this workshop. Accordingly, the following remarks will be limited to a brief survey of a few key problems and uncertainties that need to be resolved on the way to practical batteries.

A somewhat ironic aspect of advanced battery development is that one of the major technical problems encountered in achieving long life is the same as one of the key problems of lead-acid batteries--namely, positive current collector and container (grid) corrosion. While it is possible to

solve this corrosion by use of exotic materials, this approach is expensive and possibly prohibitive for utility applications. For example, the use of molybdenum for the lithium-iron pyrite system and of catalyzed titanium for the zinc-chlorine system might turn out to be too expensive. The reactivity of positive active materials, the strongly oxidizing conditions, and, in many cases, the high temperature are severe conditions for long-term use of any practical, electrically conducting material. The degree of success in circumventing or solving this problem will have a large impact on the ultimate success of almost every advanced battery system.

A second important problem area for most batteries (certainly all high-temperature batteries) is the identification of technically acceptable and economically practical separators. Unfortunately, the implications of technical acceptability are not always fully understood. For example, in the case of the beta alumina electrolyte/separator for high-temperature sodium systems, good (i.e. dense, strong, and conductive) ceramics have been fabricated, yet long life of cells using separators made by reasonably practical methods has not yet been achieved. Apparently, we still lack a complete understanding as to what is a good electrolyte and (or) what makes it fail. A somewhat similar situation exists for the lithium-metal sulfide system: corrosion resistant ceramic separators such as aluminum nitride, silicon nitride, yttria, yttria stabilized magnesia, and possibly boron nitride, have been found. Also, electrode reversibility and potential for long cycle life has been established in laboratory test cells that did not use conventional separator shapes. However, compact cells, which require and utilize separators such as those described above, have yet to show long cycle life. Thus, it appears that separator corrosion resistance, strength, and porosity are necessary but not sufficient criteria to achieve long life -- wetting, chemical interaction and other properties also appear to be important.

A common problem to most battery development is the difficulty of achieving uniform current densities in laboratory-scale cells. Non-uniform current density can result in localized stresses due to overcharge/overdischarge, temperature variations, etc. Examples of detrimental effects can be found in almost all advanced battery systems. One example is a suspected failure mode of β-alumina in which high local charging current density results in excessive pressure of sodium deposited in capillaries. Another good example is provided by the Dow sodium-sulfur battery. The electrolyte used in this system is a borate glass which, like all conducting glasses, has a rather high temperature coefficient of resistivity. Hence, small temperature deviations within the cell can cause major changes in current density among the individual electrolyte capillaries. This effect, in turn, tends to amplify the temperature deviations within the cell and can result in an overdischarged situation at certain points within the cell. This may cause formation of solid sodium polysulfides which, in turn, can cause the capillary electrolyte tubes to break. While this cause of failure has not been confirmed, it is suggested by the fact that failures occur most frequently near the end of discharge of cells operated at greater depth of discharge. Again, this is not a unique potential problem to Dow's sodium-sulfur system but rather a major concern for all high-temperature battery systems.

The status of the advanced battery programs has not yet justified the testing of cell groups (i.e. batteries). This may be a major hurdle for many of the battery systems in that current sharing of parallel cells and under/over utilization caused by capacity deviations of cells in cell strings might be serious problems which could limit life and performance. Until this hurdle is passed, extrapolations of performance from the level of individual cells to the multicell battery level must be regarded with caution.

A final problem that tends to be common to most advanced battery systems is that of impurities and their effect of life and performance. Most notable is the effect of certain electrode-derived impurities (e.g. silicon and corrosion products) on the life of beta alumina in the sodium-sulfur system. Also important is the effect of metallic impurities on the quality of the zinc deposit and the extent of hydrogen gassing o. the zinc-halogen systems. There are even some recent indications that impurities may have a significant effect on the degradation of active material in lead-acid batteries. Once identified, impurity problems are relatively easy to solve although the obvious approach -- using high-purity materials -- may prove to be economically impractical.

Solving the various technical problems while remaining within the cost constraints for utility application is a major goal in developing battery systems for utility applications. At this time, it is difficult to determine how well this is being accomplished because our ability to accurately assess manufacturing and materials costs for the advanced batteries is still very limited. In most cases, an economic judgement has to be made on eventual materials costs, assuming successful development of high volume production methods. The question becomes as to how realistic these judgements can be considering, for example, that laboratory-scale lithium-metal sulfide cells have a materials cost of over $2000/kWh, cells produced for pilot-plant scale are estimated to have a materials cost of $130/kWh, and cells produced at a manufacturing plant are projected to have a materials cost of $16.30/kWh. Another question relates to the required quality or purity of materials. If highly purified materials are required for any of the advanced battery systems, the cost for materials, fabrication, and quality control is likely to severely impact the economic feasibility of these systems.

One area of activity, still largely unexplored, is how costs can be reduced and/or life extended through optimization of operating conditions. Results obtained with both the sodium-sulfur and lithium metal sulfide system show that utilization of active materials, current density, and efficiency can be substantially and simultaneously improved by operating the cells at higher temperatures. In principle it seems possible to substantially reduce the requirements and costs for separator and current collector materials. The question yet to be answered is: how does this temperature increase impact materials stability? Another relatively unexplored area is the utilization and optimization of charge control procedures, as discussed previously. For the sodium-antimony chloride system, occasional (e.g. weekend) constant potential charges might well be instrumental in achieving long life; on the other hand, for the zinc-chlorine system constant time (e.g. 4 hrs) charge and discharge appear to result in lowest cost and optimum performance. Further work to pursue this aspect of cell and battery operation appears amply justified.

The degree to which the aforementioned technical problems have been solved for the various advanced battery systems can be assessed by the cell test results shown in Table 5. All of the life data shown in the table are for cells built and tested in 1975, and many of the cells are still on test. It is apparent, therefore, that the past year has yielded some rather encouraging cell-testing results in that life and/or capacity have dramatically increased for all systems; subsequent papers will no doubt amplify on the major accomplishments. Equally important, a better understanding of major failure mechanisms should result in continued progress toward achieving long-life capability in the near future.

REFERENCES

1. Lewis, P. A. and J. Zemkoski, "Prospects for Applying Electrochemical Energy Storage in Future Electric Power Systems, Presented at the 1973 IEEE International Convention, New York, N.Y., March 26-30, 1973.

2. Fernandes, R. A., "Optimium Peak Shaving Mix for Electric Utilities," Presented at the IEEE Power Engineering Society Winter Meeting, New York, N.Y., January 26-31, 1975.

3. Fernandes, R. A., "Hydrogen Cycle Peak Shaving," Final Report on Work under Contract with Empire State Electric Energy Research Corp., Niagara Mohawk Power Corporation, Syracuse, N.Y., April 1975.

4. Kalhammer, F. R., "Energy Storage: Applications, Benefits and Candidate Technologies," Presented at the Symposium on Energy Storage, Fall Meeting of the Electrochemical Society, Dallas, October 5-10, 1975.

5. Yao, N. P. and J. R. Birk, "Battery Energy Storage for Utility Load Leveling and Electric Vehicles: A Review of Advanced Storage Batteries," p. 1107 in Record of the 10th Intersociety Energy Conversion Engineering Conference, University of Delaware, Newark, Delaware, August 18-22, 1975.

Table 5

OBJECTIVES AND STATUS OF LOAD-LEVELING BATTERY DEVELOPMENT

System	Current Status: Cell Capacity (kWh)	Current Status: Life (cycles)	Next Level of Development	MWh-Size Battery For BEST Facility
Development Objectives	≥ 2	≥ 2000	Prototypes for BEST Facility	ASAP after 1978
Lead-Acid	20 - 125	1750-2500[1]	(Prototypes of full size cells could be available in 1977)	(1978)
Zinc-Chlorine	1	> 100[2]	20 kWh battery by early 1977	1979
Lithium-Metal Sulfide	0.15 0.15	- 400[4] 100-200[5]	1 kWh cell by late 1976	1981
Sodium-Sulfur	0.005 0.02-0.05	2000[2,3] 100-200	2.5 kWh full size cell in 1978	1982
Sodium-Antimony Chloride	0.002 0.01	- 500[2,3] - 100	15 kWh full size cell in 1978	1981
Zinc-Bromine	small experimental cells	?	laboratory prototypes (0.02 - 0.1 kWh)	?
Redox		?		?

1. Projections for state-of-the-art designs
2. Cells still on test
3. Primarily tests of β-alumina electrolyte life
4. Data for laboratory cells
5. Data for compact (engineering) cells

Figure 1

ANNUAL OPERATING COSTS FOR BASE LOAD, INTERMEDIATE CYCLING AND PEAKING POWER GENERATING EQUIPMENT

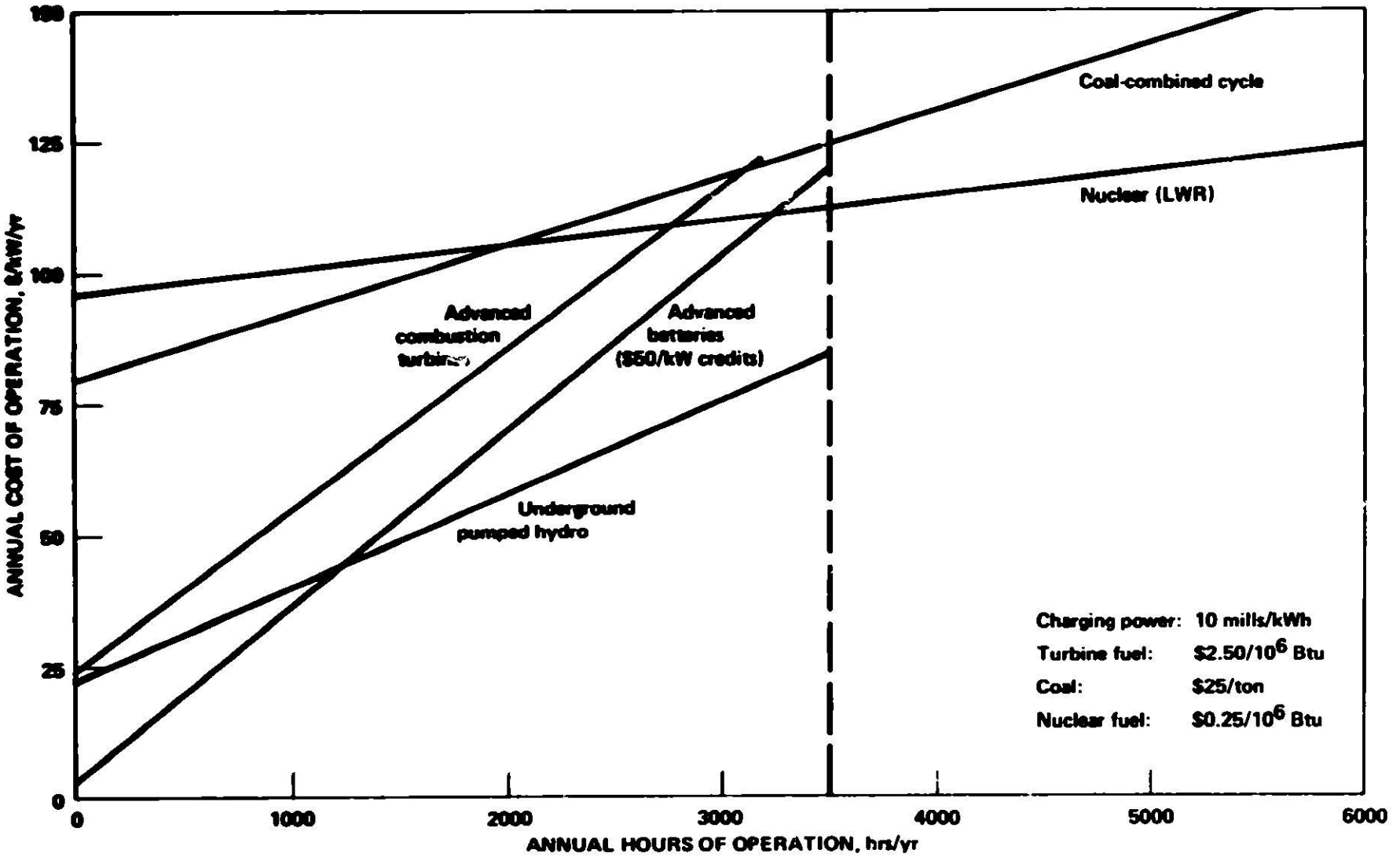

Figure 2

ANNUAL OPERATING COSTS FOR PUMPED HYDRO AND BATTERY ENERGY STORAGE

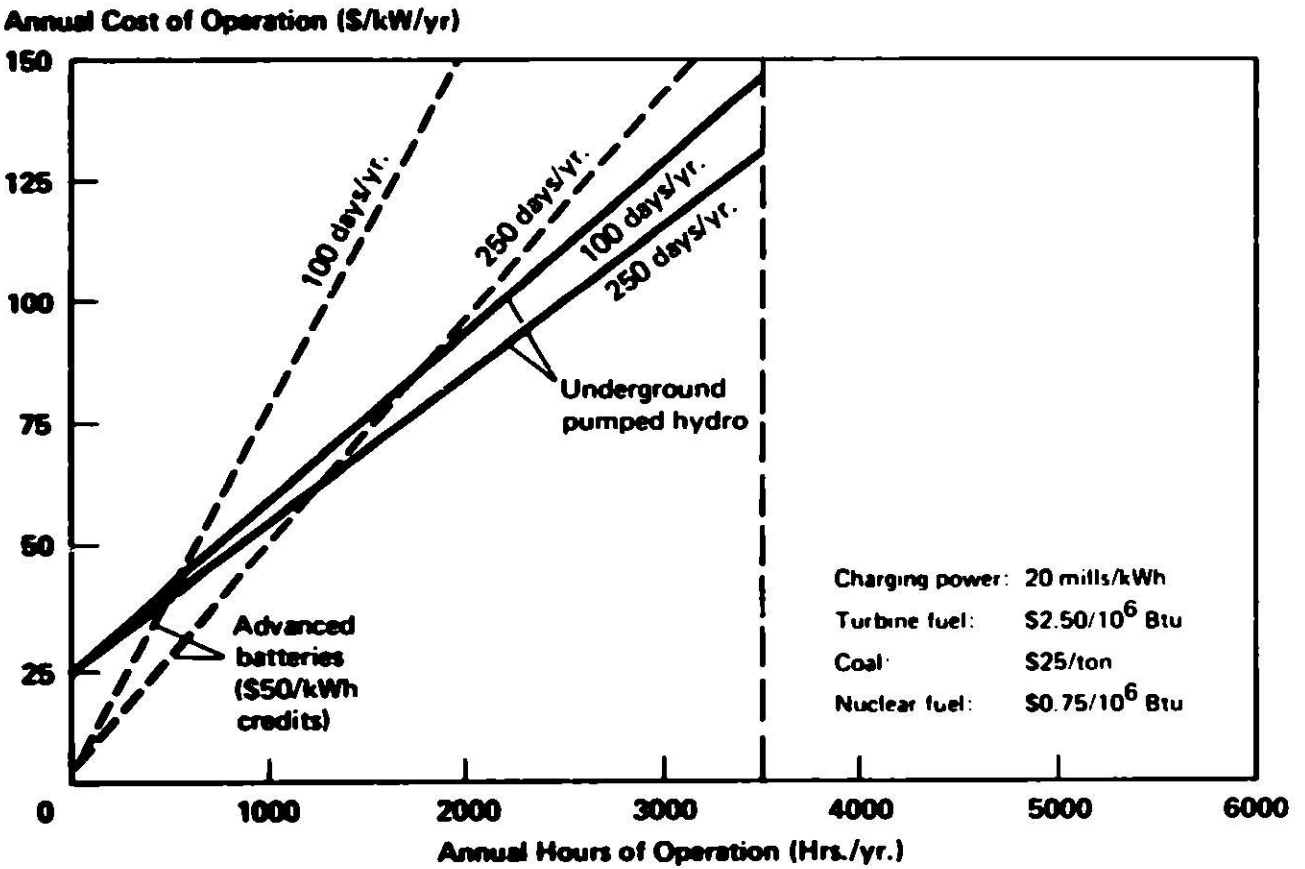

Figure 3

ANNUAL OPERATING COSTS FOR NEAR-TERM
PEAKING POWER GENERATORS

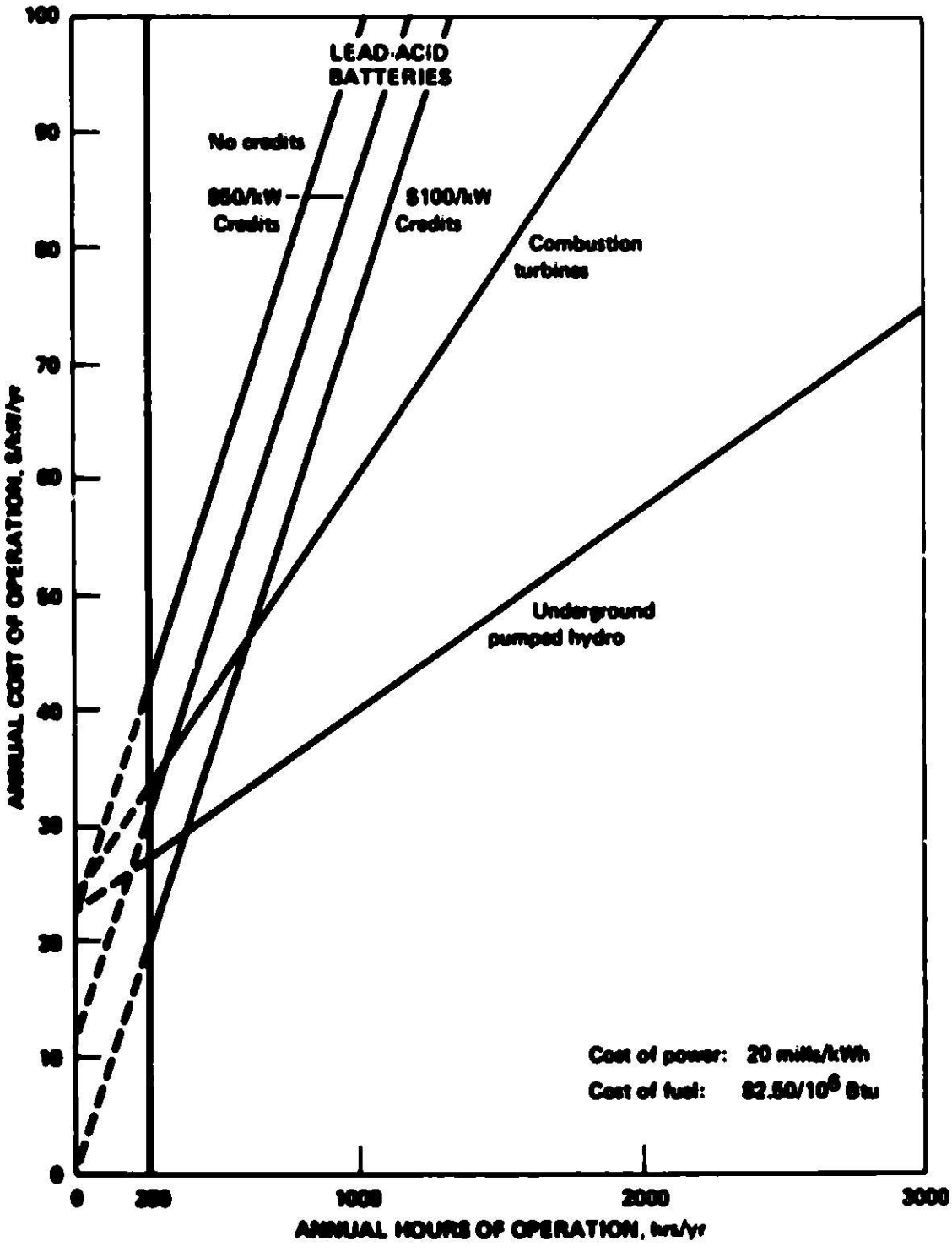

SECONDARY BATTERIES FOR ELECTRIC VEHICLES

Albert R. Landgrebe
U.S. Energy Research and Development Administration
Washington, D.C. 20545

An important part of the Energy Storage Program of the U.S. Energy Research and Development Administration is the development of secondary storage batteries for automotive propulsion applications. The successful development of batteries for this purpose will provide significant savings of oil resource and will also have beneficial environmental effects.

Of the battery systems being developed, major efforts are presently or will be concentrated on the following seven systems: advanced lead-acid, nickel-iron, nickel-zinc, zinc-air; iron-air, lithium-metal sulfide and sodium-sulfur batteries. The probability of one or more of these systems meeting the technical requirements for the intended application within the next several years appears good. The ultimate technical/economic feasibility of these systems cannot be assessed at this time because many engineering problems must still be resolved. However, the high temperature systems, Li-MS and Na-S systems appear to be good candidates for electric vehicles in the long term.

Introduction

Major electrochemical storage systems in the form of batteries are used in most facets of everyday life: the starter batteries which provide cranking power for automobiles, flashlight and transistor radio batteries, telephone and emergency standby power batteries, and the small batteries which power consumer products such as toothbrushes and electronic calculators. Also, battery-powered vehicles are used extensively as golf carts and as transportation conveyances in such facilities as airports, large warehouses, and manufacturing facilities. Battery development is being pressed today to power electric and hybrid vehicles through the ERDA's programs.

The common forms of present day electrochemical storage systems such as lead-acid and nickel-iron (Edison) cells were developed during the 19th century. At the turn of the century, electric vehicles were in wider use than heat engine powered vehicles with as many as 10,000 in operation. Batteries also found application in numerous lighting, especially emergency lighting, and signaling applications. With the widespread introduction of low cost, available petroleum products, internal combustion engines overcame the early advantage of electric cars and the major portion of battery use was and still is relegated to engine starting and automobile/truck/bus electric system regulation.

Justification for Electric Vehicles

The need for reducing the consumption of scarce, expensive petroleum-derived fuels has focused attention on systems which, through their implementation, will reduce the demand for these petroleum products and, at the same time, allow an orderly shift in energy dependence to other energy sources as coal, nuclear, solar, etc. This demand reduction and shift must be carried out over a reasonable time span to allow appropriate market adjustments and with acceptable environmental affects.

Electrochemical systems and technology have been identified as major candidates to achieve significant energy savings through storage techniques in a number of application sectors -- transportation, electric utilities, and industry. Electric vehicle development is currently in the limelight-for good reasons-and is receiving support and direction from both the executive and legislative branches of government. (e.g., House Bill HR 8800 and Senate Bill S 1632).

The major obstacle to the acceptance of electrically-propelled vehicles has been the energy storage system--the well-known, contemporary lead-acid battery does not offer the combination of high cycle life, high specific energy and power, and low cost that would result in a long-lived acceptably performing automobile. This statement needs some qualification because the electric van and bus could use advanced lead-acid batteries in the near term and a limited performance passenger vehicle could be introduced with a range of 40-60 miles for urban driving. However, benefit analyses have shown that if an acceptable electrochemical propulsion source were to be developed, the penetration of vehicles using this source into the national automotive fleet could be significant and could save approximately 10% of the annual projected automotive-related petroleum demand by the year 2000.

Electrochemical propulsion units would involve all electric vehicles (full battery power) or in a companion propulsion role for the hybrid vehicles using either a small heat engine (Stirling engine) or flywheel unit to complete the propulsion package.

The electric vehicle market has developed on a low profile basis over the years; until now there are something like 280 electric vehicles and component manufacturers in the United States and at least one major technical journal, Electric Vehicle News, devoted to this industry. Over 1800 battery powered passenger cars of less than 2000 pounds curb weight are currently in operation in the U.S., with similar numbers reported in Great Britain, Sweden, and Italy; and larger numbers in Japan. A single charge, 160 km range, battery-powered taxi was just recently introduced in Great Britain on an experimental basis. The incentive for battery development in the electric vehicle and related market place is therefore strong, and, indeed, urgent.

Goals

In general, today's batteries have been custom-tailored for specific applications that are frequently designed for either low cost or high performance but not both simultaneously. Table I reviews the performance characteristics and the cost of present secondary batteries.

TABLE I. Comparison of Today's Secondary Batteries (1)

Battery Type	Cost[a] ($/kWh)	Energy Density By[b] Weight (Wh/kg)	Volume (kWh/ft^3)	Life[c] (Cycles)
Silver-Zinc	900	120	8.8	100/300
Nickel-Cadmium	600	40	3.6	300/2000
Nickel-Iron	400	33	1.4	3000
Lead-Acid				
Motive Power	50	22	2.6	1500/2000
Submarine	80	28	2.0	400
Golf Car	35	35	2.2	300
Elec Vehicle	100	35	2.8	500/800

[a]Cost to the user.

[b]Battery capacity is inversely related to rate of discharge. The values shown are for the 6-hour rate.

[c]Cycle life depends on a number of factors, including depth of discharge, rate of charge and discharge, temperature, and amount of overcharge. Range shown is from most severe to modest duty.

Battery requirements for vehicular applications are represented by a new set of stringent technical and cost goals that will be difficult to meet with the existing commercial batteries. Table 2 shows the interim battery development goals that have been tentatively identified as the battery requirements for viable electric vehicle applications. Of the existing batteries in Table I, the lead-acid battery is the only candidate that comes close to meeting the combined performance and cost goals. Although the lead-acid battery is not expected to meet the interim specific energy goal, its existing technology with one hundred years of effort behind it, argues for a worthwhile pursuit for the near-term vehicle applications. The above discussion points out the need for a concerted development of advanced batteries that have potential of meeting the application goals. Such a concerted effort is expected to be expensive (>100 million dollars) and long

(>5 years) in order to explore and evaluate potential battery systems, but these factors may very well be inconsequential to the impact of the successful implementation and benefits of electric vehicles.

TABLE II. Interim Battery Requirements for Electric Vehicle Applications

	Tentative Goals
Duty Cycle	2-4 hour Discharge 1-6 hour Charge
Energy Efficiency	>50%
Specific Energy	>70 Whr/kg
Specific Power	
Sustaining	> 20 W/kg
Peak	> 100 W/kg
Cycle Life	>1000 Cycles (3-10 years)
Cost	$25-35/KWhr
Environmental Impact	Minimal

The performance requirements for automotive vehicles, Table III, and the effects of battery characteristics on electric car design, Table IV, present some characteristics that may be acceptable for electric vehicles. It is evident that various types of batteries may be acceptable for different types of vehicles depending on the characteristics which are shown as goals. The complex question of trade-off between cost and performance characteristics requires more careful analysis. However, it is evident that there is a need for development of high-energy batteries for electric automobiles.

TABLE III. Performance Requirements For Automotive Categories (2)

Automotive Categories and Types	STORED ENERGY PROPULSION ONLY			HYBRID PROPULSION* (Heat Engine/ Stored Energy)	
Characteristics and Performance Parameters	General Purpose Family Car	Commuter Car	Utility Car	General Purpose Family Car	Commuter Car
Gross Vehicle Weight (lbs)	4000	2500	1700	4000	2500
Passenger	6	4	2	6+	4
Range Between Recharge (Miles)	150-200	100	50	200+	100+ (Limited By Heat Engine Fuel Capacity)
Top Speed (MPH)	60	60	30	60	60
Maximum Acceleration (MPH/SEC)	4	3	2	4	3
Allowable Storage System Weight (Lbs)	900-1400	600-1000	400-650	300-500	100-200
Storage System Target Performance					
Power (Watts/Lb)	70-100	45-70	30-50	190-300	170-300
Energy (Watt-Hrs/Lb)	85-150	25-45	15-30	<10	<10
Cycle Life	>1000 Deep Discharge Cycles	>1000 Deep Discharge Cycles	>1000 Deep Discharge Cycles	$>10^5$ Shallow Cycles	$>10^5$ Shallow Cycles

*Thermal storage/heat engine (Stirling) is not considered a hybrid

Batteries for Electric Vehicles

Seven advanced secondary battery concepts have been identified for their potential for use in electric vehicles and about another six battery concepts have been identified. These are: advanced lead-acid, nickel-iron, nickel-zinc, zinc-air, iron-air, lithium-metal sulfide and sodium-sulphur batteries. Other battery concepts having merit but not covered herein include zinc-chlorine, zinc-bromine, nickel-hydrogen, lead-manganese dioxide, zinc-manganese dioxide and a whole class of batteries containing organic electrolytes. In addition to secondary batteries, at least one primary battery concept is being investigated for its application to electric vehicles, that is Lockheed's Li/water/air battery.

TABLE IV. Effect of Battery Characteristics on Electric Car Design (3)

	Battery				Assumed Vehicle Characteristics					
Type	Specific Energy W-hr/lb	Specific Power, W/lb	Cost, $/kW-hr	Veh., lb	Weight Batt., lb	Batt., %	Energy Stored, kW-hr	Power, kW	Battery Cost, $	Range for J-227, mi
Lead-Acid	12.5	12.5	30	3000	1200	40	15	15	750	90
Ni-Alka-line	30	30	100	2250	750	30	22.5	22.5	2250	80
Near-Term Mid-Size	35	35	-	2500	800	32	28	28	-	110
High Power	70	100	30	2400	625	25	43.8	42.5	1300	190
Low Power	80	40	25	4000	1200	35	112	56	2950	300

Lead-Acid Battery

Improvements are possible with the lead-acid battery and development of this technology could result in an improved battery in a short period of time. By decreasing the weight of the battery case, increasing the specific gravity of the electrolyte in order to have better utilization of the active materials and decreasing the weight of the plates it should be possible to obtain a battery having a life of 500-700 cycles and a specific energy of 50 W-hr/kg. There is a need to reduce the grid corrosion to increase the cycle life. Major improvements have been made in the past decade and more developmental type improvements will be made in this old technology.

Nickel Systems

Nickel systems such as Zn//β-NiOOH, Fe//β-NiOOH and H_2//β-NiOOH have been developed for other applications and the Fe//β-NiOOH and H_2//β-NiOOH have demonstrated very long cycle life, i.e., several thousand cycles. However, the development of such systems into a suitable vehicle battery is contingent upon the successful development of an economical nickel electrode. This must be accomplished without sacrificing the lifetime and performance of the conventional sintered-nickel electrode. A summary of the nickel systems is given in table V.

Because the basic technology for these systems already exist, and substantial effort is still being expended, the likelihood of the successful development of an acceptable battery system (of intermediate specific energy) for the interim electric vehicle market is high and the time frame for development and demonstration would be relatively short.

TABLE V. Present or Estimated Characteristics of Nickel Battery Systems

Battery Type	Energy Density ($KWHR/ft^3$)	In-Out WHR Efficiency	Cycle Life (Deep Cycles)	Cost To User ($/KWHR) (Est.*)	State Of Development	Critical Technical Problems
H_2/NiOOH	50	75-80	2000	100	Moderate to High	1. Production of an inexpensive high performance NiOOH cathode. 2. Reduce degradation of anode. 3. Improve H_2 storage
Zn/NiOOH	60	65-70%	300	50	Moderate to High	1. Dendrite growth and shape change. 2. Utilization on Ni. 3. Recycle Ni
Fe/NiOOH	30-50	No Data	1000	120	High	1. Reduce self-discharge 2. Improve utilization of Ni

Metal-Air Systems

From an energy density point of view, an air cathode is attractive as a battery component because the electrochemical reactant is supplied continuously from the surrounding battery. Two alternatives that present possibilities for power sources are iron-air and zinc-air battery systems.

The use of air cathodes is not a recent development. A zinc-air battery with air electrodes of wet-proofed carbon has been commercially available for fifty years for use in channel marker buoys, highway flashing systems, railway signals, radio receivers and transmitters, and similar applications. Although reliable, a battery of this type could be discharged only at low rates because of air electrode limitations. Consequently, the power density would be unacceptably low for vehicular applications.

The considerable research efforts on fuel cells and metal air cells in the last 10 years that led to the development of high-rate air electrodes has created a renewed interest in metal-air batteries.[4]

The development and technical problems related to zinc electrode are well known (Table VI).

Edison's work on iron electrodes for nickel-iron cells date back to the early 1900's.[5] At that time, extensive work by Thomas Edison on the iron electrode resulted in his pocket plate electrode that was used in Edison Ni-Fe cells manufactured up to 1974. This electrode uses a synthesized Fe/Fe_3O_4 mixture of active materials that is contained within nickel plated steel perforated compartments. This arrangement represented a durable long-lived (to 50 years) stable electrode that was very suitable for specialty applications such as railroad lighting, industrial trucks, and mining lighting. However, the ruggedness of the iron plate design, coupled with an equally rugged nickel electrode and case design, led to low stored energy and power density electrodes (33 Wh/kg and 22 W/kg, respectively, in the finished cell). Consequently, although iron electrode technology existed and was available, it was never suitable or considered for use in the construction of a high-energy-density iron-air cell.

Recently, work has been conducted on an iron electrode at Seimens in Germany[6], Matshushita in Japan[7], SU in Sweden[8], McGraw-Edison[9], GT&E[10], and Westinghouse in the United States. The development and technical problems related to the zinc electrodes are well known and will not be discussed herein. Both the iron-air and zinc-air system have the potential for use in hybrid vehicles and perhaps in electric vehicles. Table VI lists the characteristics of these systems.

Table VI. Present or Estimated Characteristics of Metal-Air Battery Systems

Battery Type	Energy Density ($KWHR/M^3$)	In-Out WHR Efficiency	Cycle Life (Deep Cycles)	Cost To User ($KWHR) (Est.*)	State of Development	Critical Technical Problems
Zn/Air Slurry	No Data	40%	3000 Hours	25-40*	Moderate	1. Recycling of slurry 2. Catalyst deactivation 3. Contamination from CO_2
Zn/Air Mechanically Rechargeable	No Data	N.A.	No Data	No Data	Low	1. H_2O loss 2. Leakage of electrolyte 3. Rapid replacement 4. Contamination from CO_2
Zn/O_2	No Data	No Data	200	No Data	Low	1. Zinc dendrite and shape change 2. Control of O_2 pressure
Fe/Air	110	30-40	300	25-40	Moderate	1. Low cost Fe electrode 2. Rechargeable air electrode 3. Low efficiency

High Temperature Battery Systems

Both the Li/LiCl-KCl/metal sulfide and Na/β-Al_2O_3/S systems were reviewed in recent papers by N.P. Yao and J.R. Kirk[11] and by D.L. Douglas[1].

Substantial development efforts on versions of the lithium-metal sulfide cell are underway at Argonne National Laboratory and General Motors Company. Working with Argonne are Atomics International Division of Rockwell International Corporation, Eagle-Picher Industries, Inc. and Gould, Inc.

The electrolyte most commonly used is the LiCl-KCl eutectic (m p 325°C) and operating temperature range is 350°C-400°C. Cell voltages for Li/LiCl-KCl/FeS_2 and Li/LiCl-KCl/FeS are high with open circuit voltages of 2.03 and 1.62, respectively. Large current densities are possible, promising compact batteries with high energy and power density. Yet, various material problems remain to be solved in the area of separators, current collectors for the positive electrode, and insulators for electrical feed-through. A greater understanding of the complex chemistry is required for confident

predictions of calendar life at high temperatures, e.g., cycle life. Cells of about 60 A-hr capacity have operated for over 6000 hours. Demonstration of minimum performance and life in a 40 Kw-hr battery is two to three years away. Good progress has been made in developing this system.

The major developers of sodium-sulfur batteries are the Ford Motor Company, British Railways Board, Electric Council Research Center in the United Kingdom, Compagnie General I' Electricite in France, Yuasa Battery Company in Japan, General Electric Company, TRW, and the Dow Chemical Company. The essential feature of the sodium-sulfur cell is the use of a ceramic or a glass as an electrolyte. With the single exception of the cell being developed by Dow Chemical, the electrolyte consists of some version of the ceramic, beta alumina ($Na_2O.11Al_2O_3$). The material is ionically conductive at elevated temperature, the charge carrier being sodium ions. Volume specific resistance of beta alumina ranging from 5 to 30 ohm-cm at 300°C is used in test cells. The resistivity is a function of "dopants," pressing and sintering conditions and composition. The active materials, sodium and sulfur, are both liquid at the temperature of operation and the solid electrolyte also serves the function of the separator.

Laboratory cells of capacities of a few watt-hours have operated for over 7000 hours. Power and energy densities have been obtained that extrapolate to useful values for electric vehicle applications. Failures are normally due to seals or electrolyte shortcomings. Cracks and/or pinholes appear which cause internal short circuits. Accordingly, the principal thrust of development work is toward improving the beta alumina electrolyte. While the sodium electrode (anode) shows relatively little polarization, under most conditions, the sulfur electrode is the source of some material problems. Perhaps the most severe of these is that of corrosion of the container by the polysulfide melt. No metal or coating has yet been found to be completely satisfactory.

In the case of the Dow-Chemical sodium-sulfide cell, the electrolyte is a sodium ion conducting glass. This is drawn into hollow fibers. The fibers are sealed onto a header which is connected to a sodium reservior. Thus, the fibers are filled with molten sodium. The fibers are immersed in molten sulfur containing a grid current collector. In this design, a very large surface area of electrolyte/separator is accomplished. Accordingly, a cell with a large output can be designed based on fiber current densities of a few milliamperes per cm^2.

Recently the removal of calcium and "oxides" from the sodium anolyte has led to improved cell lifetimes as defined by numbers of deep charge-discharge cycles and total coulombs passed through the glass fibers. Cells containing 1000 fibers (0.55 A-hr capacity) are still operating with no increase in cell resistance after over 550 deep cycles and 6624 mA hours per cm^2 of fibers. These are being operated at 12 mA per cm^2 of fiber--six times the design current density. At normal current densities, this corresponds to over 3300 hours of operation. Larger 40 ampere-hour cells have been assembled and will be tested.

Conclusion

Secondary batteries for electric vehicles offer several potential advantages including conservation of resources and favorable environmental features such as no thermal and air pollution.

Several advanced batteries under development show promise of meeting the requirements for electric vehicles within the next decade. Potential vehicle batteries include lead-acid, nickel-iron, and nickel-zinc for the near term (one to three years); advanced lead-acid and nickel-zinc for the intermediate term (three-to-five years); and metal-air, lithium-metal sulfide, sodium-sulfur and other advanced systems for the longer term (greater than five years).

Table VII presents a summary of Research and Development effort on potential vehicle batteries; the batteries are divided accordingly for near-term, intermediate-term, and long-term development on the basis of the state of the technology for each of the battery systems. The development time that is required for the technology demonstration varies from one to two years for the near-term batteries, three to five years for the intermediate-term batteries, and five years or more for the long-term batteries. The current development status and the projected performance for each of the battery systems are shown in the table in terms of specific energy, specific power, cycle life, and the installed energy cost. Generally, the projected values for the near-term systems can be made with a higher level of confidence than those for the long-term systems, because the technology of the latter systems is still in its infancy. Accordingly, the risk associated with the technology development increases from the near-term to the long-term systems.

The incentive for developing the higher-risk, long-term battery systems is the potentially higher payoff, as examplified by the "Relative Figure of Merit" in the table. The Relative Figure of Merit (RFM) is a combined measure, relative to the state-of-the-art (SOA) lead-acid battery, of the projected performance capability, battery and cycle life costs, and the number of years to commercial deployment. The numbers shown here are the relative measure on an arbitrary scale (SOA=1.0), and are not to be interpreted as the projected improvement factor of the battery systems relative to the SOA lead-acid battery.

The RFM was calculated on the basis of the following functional relationship:

$$\text{"RMF"} = K(EPL/CY^{1/2})^{1/2}$$

where K = a proportionality constant
E = relative specific energy
P = relative specific peak power
L = relative cycle life
C = relative battery cost
Y = relative number of years to commercial deployment

TABLE VII. Potential Electric Vehicle Batteries

Batteries			Current (January 1976)				Projected				Relative Figure* of Merit
Systems	Electro-lytes	Temp. °C	W-hr/kg	W/kg (peak)	Cycle Life	Cost. $/KWH	W-hr/kg	W/kg (peak)	Cycle Life	Cost. $/KWH	
[illegible]											
[illegible]	Aq. H_2SO_4	Room Ambient	30	90	700	100	50	150	>1000	60	1.0
[illegible]	Aq. [illegible]	Room Ambient	65	140	<600	1000	60	150	>1000	120	2.1
[illegible]											
[illegible]	Aq. H_2SO_4	Room Ambient	—	—		—	50	150	>1000	60	3.9
[illegible]	Aq. [illegible]	Room Ambient	77	150	200	800	110	150	>1000	50	4.6
[illegible]											
[illegible]	Aq. [illegible]	Room Ambient	80-120	60	<150	2000	90	80	>1000	60	2.3
[illegible]	Aq. $ZnCl_2$	Room Ambient	<65	<60	<100	>2000	130	130	>1000	50	4.3
[illegible]	LiCl-KCl eutectic	400-430[a]	100	120	<250	>2000	150	200	>1000	60	7.2
[illegible]	β-alumina	300-350[a]	90	100	<200	>2000	170	200	>1000	60	6.3

*"Relative Figure of Merit" is a function of driving range capability, power capability, battery and cycle life costs, and the number of year to commercial deployment, based on the projected performance of the battery systems. The higher the figure, the better the system is.

The development risk for each system, while important, was not assigned in the formulation because it is a more subjective factor. Energy efficiency was also not considered. The equation is not rigorous nor complete, but it does give the same importance factor to the performance capability factors, E and P, and to the battery and cycle life costs, L and C. The relative number of years to commercial deployment, Y, was considered of secondary importance.

The RPV value for the metal/air system is not impressive for an advanced battery system because of the modest specific power and specific energy that are projected. Furthermore, metal/air systems have generally a low energy efficiency, 35 to 50%, because of the high polarization at the air electrode and the corrosion at the metal electrodes. The efficiency is, however, expected to improve with development. The arguments for the development of metal/air systems are that technology already exists for the systems and that they have the potential to serve as a backup for the interium batteries. Metal/air systems may be applicable to hybrid vehicles coupled with a high power storage source, as concluded by the Japanese developers.

As progress is made from the near-term batteries to the long-term batteries, the vehicle range capability is expected to increase correspondingly from 20-40 miles (with near-term batteries) to 60-100 miles (with intermediate-term batteries), and to 120-180 miles (with long-term batteries) for compact vehicles in typical urban driving. Such performance progression will greatly improve the public acceptance and the viability of electric vehicles.

Acknowledgment: I wish to acknowledge Dr. N. P. Yao, who developed the figure of merit and who supplied valuable input to this paper.

References

1. D. L. Douglas, "Batteries For Energy Storage"
Preprinted papers presented at 168th National Meeting A.C.S.
September, 1974

2. George Pezdirtz, ERDA, private communication

3. Paul Nelson, Argonne National Laboratory, private communication

4. E. S. Buzzelli "Low Cost Bifunctional Air Electrodes," paper 46,
ECS Dallas Meeting, October, 1975

5. V. Falk and F. J. Salkind, Alkaline Storage Batteries, John Whiley
and Sons, Inc., New York (1969) pp. 16, 21

6. H. Cnoblock, et al, "Performance of Iron-Air Secondary Cells Under
Practical Operation Conditions" preprint 17, International Power
Sources Symposium, Brighton, England (1972)

7. M. Mori, et al, Japanese Patent Application 50-72-137, June 14, 1975
(Matshushita).

8. O. Lindstrom, "Rechargeable Metal-Air Battery Systes," 23rd Meeting, International Society of Electrochemistry, Stockholm, Sweden (1972)

9. J. D. Moulton, et. al., U.S. Patent 2, 871, 281 Alkaline Storage Battery with Negative Iron Electrodes," January 27, 1959

10. E. R. Bowerman, Proceeding, Power Sources Symposium, Atlantic City (1968)

11. N. P. Yao and J. R. Birk, "Battery Energy Storage For Utility Load-Leveling and Electric Vehicles: A Review of Advanced Secondary Batteries," IECEC Newark, Delaware, (August 1975).

THE LEAD-ACID BATTERY

A. C. Simon
Naval Research Laboratory, Washington, D.C.

S. M. Caulder
International Lead Zinc Research Organization
Research Associate at NRL

ABSTRACT

The lead-acid battery has shown a slow but steady development over the years of its history. Most of its improvements have been obtained through engineering development and there has been relatively little basic research. At a period when there is the possibility of two major markets for batteries, those of energy storage and electric vehicles, one should not too soon dismiss this battery from consideration. Although at present marginal for both of these applications, there is the distinct possibility that with the proper research the life and energy density of this battery can be increased to the point where it may look a lot more attractive than at present. Some of the problem areas and possible solutions are discussed.

INTRODUCTION

At the present time the lead-acid battery appears to be in a very auspicious position. Despite temporary set-backs caused by the present state of the economy, the starting, lighting and ignition battery market has shown a steady increase that promises to continue with population growth. There is also a growing market for specialty batteries for self-powered tools, recreational vehicles, toys and various other self-powered equipment. With serious consideration now being given to batteries as a means of energy storage for the electric power generating industry and also as the main power source for electric service vehicles, we are faced with the realization that, at least for the near future, the lead-acid battery is the only feasible contender for these services.

On the other hand there are a number of factors that could seriously alter the present favorable position of this battery. There are alternate battery systems now being developed that promise to have much higher energy densities than does the lead-acid battery. There are constantly changing conditions in the materials supply situation that may drastically change the availability or cost of various battery components. Environmental protective regulations are causing increasingly difficult problems in product waste disposal. Energy shortages not only could greatly curtail automobile usage, with attendant disaster to the SLI market, but could also increase the cost of production of such items as containers, separators and other battery components. Even now, changes in grid alloy composition, required to meet the demand for maintenance-free batteries, are making it increasingly difficult to use recycled lead in production.

In order to meet these problems a great deal more reliance must be placed upon research efforts than has been the case in the past. Some of this research and development effort is currently underway, some is in the planning stage, and there are some areas where research will be needed that as yet have not even been explored.

CURRENT STATE OF THE ART

A. General

The most significant recent developments in lead-acid battery engineering have been the introduction of light weight, high temperature and impact resistant plastic containers; the manufacturing of sealed and maintenance-free batteries and the development of lighter weight electrodes and connectors.

Attempts at discrediting the lead-acid battery usually concentrate on the low energy density of this system. Until recently the container was a large factor in the overall weight of the battery. The development of plastic containers has made possible a package that not only looks better but is also smaller and of less weight than its predecessors.

The use of thermo-plastics such as polyethylene, polypropylene, polyvinylchloride and polycarbonate is rapidly becoming standard in automotive and stationary batteries. These plastics may be transparent or translucent (for easy monitoring of electrolyte level) or highly colored to increase their sales appeal. The decrease in weight not only permits a greater energy density but, since a decreased wall thickness is required, a greater internal volume, thus allowing for a greater number of plates and giving an increase in capacity.

In addition, the self extinguishing flammable plastics such as polyvinyl chloride reduce the fire hazard and the semi-flexible nature of some of the plastics greatly reduces the possibility of breakage. Along with these advantages have come better methods of sealing the tops and terminals so that leakage problems have been greatly reduced, if not eliminated.

A relatively new and fast growing field is that of specialty batteries such as those used to provide power for emergency lighting, burglar and fire alarms, portable medical instruments, toys, handyman tools, etc. The first maintenance-free, non-spill batteries were developed for such applications. These batteries either contain a gel electrolyte or an electrolyte-containing separator, and the grids are usually of a lead calcium alloy or pure lead to reduce gassing and its accompanying problems.

In all such batteries care must be taken to limit the end of charge voltage. They are not truly sealed since they provide a Bunsen type valve for venting in an emergency, such as overcharging. Most such batteries are designed for low to medium discharge rates. They have a linear charge loss of about 3 to 4% a month, so that their shelf life is long as compared with other lead-acid batteries.

A different approach to obtaining maintenance-free batteries is to use recombination catalysts such as platinum or palladium alloys. These proprietory alloys are incorporated into the electrodes or placed in specially designed caps so that the hydrogen and oxygen that are formed during electrolyte decomposition are recombined and no loss of water occurs.

Recently there has been a demand for maintenance-free SLI batteries. The manufacturers of SLI batteries in this country have on the market or under development long life maintenance-free SLI batteries, the success of which is dependent principally upon the use of lead-calcium alloys in the grid, high purity active material and a somewhat larger than usual electrolyte reservoir. By the use of lead-calcium, rather than lead-antimony, grid alloys the deposition of antimony on the negative is avoided, so that very little water undergoes decomposition. Most modern car batteries, during car use, tend to be maintained at almost constant potential by the alternator and voltage regulation systems. This makes possible the use of lead-calcium grids, which normally do not stand up well to charge-discharge cycling. Thus maintenance-free service can be obtained with these grids without loss of battery life. Although maintenance-free batteries for car use appear to be sealed, investigation shows that venting is provided.

Maintenance-free batteries are also being tested in Europe. The approach used there, however, has been to develop low antimony-lead alloys (less than 3% Sb) which are apparently satisfactory. The much lower rate of antimony transfer to the negative, using these low antimony grids, reduces self-discharge to acceptable levels.

A great deal of unusable battery weight resides in connectors and grids, and the industry in the past few years have been highly successful in reducing this toward a minimum. By the use of cell connectors that pass through the cell wall rather than out of the top of the cell a considerable weight reduction has been achieved as well as lower electrical resistance. Studies of grid design have recently shown relationships between grid resistance and grid design that have made possible the design of grids that achieve the maximum support with the least electrical resistance and minimum weight consistent with the type of service for which they are intended.

Three considerations limit the possible weight reduction of the grid. One is the need for sufficient grid conductors to be present and properly distributed to supply the necessary electrical conductivity at specified rates of charge and discharge. A second consideration is the necessity for sufficient grid material to support the active material throughout the steps of manufacture and in subsequent use. Finally, it is necessary that the grid be of sufficient thickness to provide for the two above considerations throughout the required service life, since during this period there is a continuous reduction of grid thickness by a corrosion process.

No corrosion-free grid, that is economically feasible, has as yet been produced and grids continue to be made of lead or lead alloys. At present lead-antimony and lead-calcium appear to be the most feasible alloys although research is continuing in this area to develop other alloys with equal or greater corrosion resistance.

There has been considerable interest in the use of lead plated aluminum as a grid material since it would improve conductivity and provide a lighter grid. Most attempts to use this or other plated metals have been unsuccessful although Sweden's Axel Johnson Institute for Industrial Research claims to have developed lead coated aluminum grids that have been successful in tests and they are now offering this process to battery manufacturers. In this country, claims have been made for an undercoat process that makes the lead coated aluminum impervious to attack even if the lead plating is not perfect. This latter process is now being tested by the Electric Power Research Institute. One hopes that these claims will be proved valid, since such a lead plated aluminum grid would not only increase the energy density and reduce internal resistance but could possibly also reduce costs of manufacture.

A battery development claimed to give extremely long life is the computer designed battery of Bell Telephone Laboratories. This battery uses pure lead grids of a conical construction. This is supposed to be the best compromise between grid growth and active material expansion, and thus best suited to retain the active material pellets throughout life. The active material paste is made from chemically prepared tetrabasic lead sulfate, and does not require the curing steps of conventional paste formulations. A very long life is claimed for this battery under the emergency stand-by, float potential operation required by the telephone industry.

B. Environmental Pollution Considerations

As the populace gradually becomes aware that the environment is becoming poisoned by society's own waste products, there is a growing hue and cry to control all manufacturing processes to the point where there are no harmful environmental pollutants. Since, in many cases, there are no reliable figures as to what constitutes harmful pollution for a given product there has no doubt been a tendency to impose unrealistic limits.

In this respect lead is no exception. The battery manufacturers are finding it increasingly difficult and expensive to comply with restrictions on pollution being enforced by Federal and local agencies. This applies equally to the lead content in the waste water from battery plants, to the lead content in the air surrounding such plants and to the lead content in the workers within the plant. Similar and perhaps worse problems of lead control will be faced by the primary and secondary lead smelters. It is also probable that arsenic and antimony will face similar regulation as their properties become better known to the public.

Manufacturing dry charged batteries contributes greatly to lead bearing waste water. It has been necessary in the past to wash the plates after formation to remove excess acid. Considerable effort is now being directed toward eliminating this washing. Gould and Globe have produced, by slightly different procedures, batteries that eliminate the washing procedure. These batteries can be shipped and stored "dry" and activated when desired by the addition of electrolyte, although the plates in such batteries are not really dry but contain 20 to 40% of the acid that would normally be present in a wet battery. The elimination of the washing step saves up to 40 gallons of wash water per battery and gas savings also occur

from not having to dry the battery plates. The cost of such processes are substantially lower than for the drying ovens, washing equipment, water clarification, etc. required for dry charging.

Although the public has now become accustomed to dry charged batteries an alternate route is to return entirely to the shipment of wet charged batteries. Some manufacturers are considering this option and are experimenting with methods to reduce loss of charge and to minimize corrosion during storage.

A final point is the increasing hazards faced by the manufacturer in the marketing of his product. The formation of the Consumers Products Safety Commission and applicable regulations such as the Hazardous Substances Act are examples of the trend in government today to protect the rights and safety of consumers while increasing the responsibilities of the manufacturers.

According to the Kierney Management Consultants the product liability claims in 1972 totaled 12.5 billion dollars, which represented a 100-fold increase from 1965. It is foreseen that, at this rate, the 1975 claims may reach 50 billion dollars. Because of possible mishaps with the acid electrolyte as well as the possibility of explosion, electrical burns, etc., the lead-acid battery can well be considered hazardous. This applies particularly when the many new uses to which this battery is being applied are considered. Therefore research and development into providing a hazardproof battery must also be considered by manufacturers. It has truly become an age in which environmental impacts and environmental protection costs must be considered in every step of manufacture and distribution.

We mention these burdens on the manufacturer, not as an indictment of the lead-acid battery, but only to show the increasing headaches that all manufacturers must face. It is also well to consider what such legislation and restrictions will mean to manufacturers of sodium-sulfur, lithium-chlorine, lithium sulfide, or similar high energy density batteries that contain highly reactive, extremely dangerous materials. When one is tempted to paint too optimistic a future for such batteries these points should be kept in mind.

C. Separators

Separators are an essential part of battery construction, and properly built separators contribute greatly to both battery life and power. Needless to say, the separators serve the multiple purposes of preventing electrical contact of plates of opposite polarity, restraining the movement and bridging of sediment particles, providing needed electrolyte space at the surface of the plate and assisting in the retention of the active material. There is also evidence that they reduce self-discharge by restraining the migration of antimony to the negative plate. At the same time they have the detrimental effect of increasing the internal resistance of the battery by interfering with current flow through the solution.

There are several essential requirements that must be met by successful separators. The first is mechanical strength sufficient both for the handling during assembly and in subsequent life service. Next is an ability

to withstand both the corrosive effects of the acid electrolyte and the redox conditions generated during battery operation. Third, the separator is required to have low electrical resistance and uniform and controlled pore size. Fourth, the separator must not contain soluble impurities, such as chloride or metals, that would interfere with cell performance or produce side reactions. Finally, a demonstrated ability to inhibit the transfer of antimony is desirable when lead-antimony grid alloys are used.

At the present time many different separator materials are available, of different porosity and thickness, and separators can be tailored to specific uses of the battery. The original wood separators were first replaced by microporous rubber separators which are produced by compounding sheet rubber formulations with a silica hydrogel and subsequently driving off the water to develop the necessary porosity. This separator material has pore dimensions in the order of one micron and is relatively pure. Unfortunately it is fairly brittle so that it normally is not produced with a rib thickness of less than .020". It has now been largely replaced by other types, but is used in some applications.

Cellulose separators have been in use for a long time and are currently still in use. Cellulose mats of suitable pore size and corrosion resistance are made up and impregnated with phenolic resin and cured. These phenolic impregnated cellulose separators can be produced in corrugated form or with extruded ribs on a flat sheet. While the porosity of these separators may be as high as 60%, they are brittle and the mechanical strength and corrosion resistance are only fair. Pore size is not particularly uniform and averages about 15-25 microns.

A major improvement in separators is provided by the microporous polyethylene separator, which is compounded of a mixture of silica, ultra high molecular weight polyethylene and a plasticizing oil. These components are extruded as a continuous sheet which is then treated to extract most of the oil, thus developing the required porosity. The material produced in this way has extreme toughness combined with flexibility and has excellent corrosion resistance and mechanical strength. The pores are much finer than in other separator material, averaging about .05 micron. This material can also be made into very thin separators because of its excellent mechanical strength and flexibility.

Polyethylene separators are also made from 1-5 micron fibers produced by blowing from the melt. The filaments are thinned and aligned by a high velocity hot air blast. The resultant mat is then sintered by pressure and heat into a continuous structure. Although this material has the same mechanical strength as the microporous polyethylene described above it has a larger pore size, averaging about 15 microns. Since it is made without the use of fillers or binders its purity is exceptional.

Sintered polyvinyl chloride was a pioneer polymeric material for separator use. Its manufacture involves forming the required shapes from finely divided PVC powder and then sintering the particles. Over the years this product has been improved somewhat, principally by the development of finer grades of PVC powder and by reducing the separator thickness. This separator also appears to be undergoing replacement by materials of greater

flexibility, mechanical strength and porosity, although recent developments have brought the pore size down to about .05 microns and considerably increased the flexibility.

Fiberglass separators are also made. These are made from glass fibers that are subsequently bonded by heat and pressure. They may contain an intermediate layer of silica powder and latex coating to reduce pore size and inhibit antimony transfer. These separators are tough and flexible enough for most applications. Fiberglass is usually found as an active material retaining layer in partnership with one of the above mentioned separators.

For high power applications low electrical resistance can be obtained by reducing rib thickness and using material of high porosity. Such advantages are usually accomplished at the expense of corrosion resistance and mechanical strength. A primary consideration, in addition to those mentioned above, is cost. This may in many cases determine which of the above types of separator is chosen, irrespective of other advantages. In this area, also, energy shortages have had an effect on cost, and safety and health have become a source of concern.

As to the future, consideration is being given to thinner separators, with lower electrical resistance. Sealed separators or wrapped separators would prevent edge shorting and probably greatly extend life, as well as retaining sediment. For this purpose flexibility and sealability would be paramount among desirable properties. The increasing use of maintenance-free batteries will require separators of exceptional purity. When lead-calcium grids are used their tendency to cause active material softening will best be controlled by enveloping the plates with separator material of great flexibility and very small pore size.

D. Batteries for Vehicle Propulsion

There is no battery now available or in prospect that can drive a vehicle with the performance and range that can be achieved with an internal combustion engine. There is no compact, packaged, electrochemical energy system that can compete in weight, portability or economy with gasoline.

However, the time may be fast approaching when the fossil fuels are either not available or become so much more expensive that the public will gladly accept vehicles of the limited range and speed offered by battery power. Increasing atmospheric pollution from internal combustion engines is also a factor that will act to promote the use of all-electric vehicles or hybrids.

Electric vehicles using lead-acid batteries, such as fork lifts, trucks and similar commercial applications have been able to successfully compete with the internal combustion engine for a number of years because of economical service and the non-polluting characteristics that electric vehicles offer. This type of battery use will undoubtedly become more popular in the future. In fact, a number of recent studies here and abroad have shown that, for various types of stop and go vehicles, such as milk vans, mail trucks and buses, the battery propelled vehicles show much lower

operating and maintenance costs over their service life than do their internal combustion engine counterparts.

Thus, for industrial vehicle applications, there is no doubt that the lead-acid battery has proven practical. Recent improvements in charger design, which permit fast charging yet prevent overcharging and allow a minimum of supervision have done much not only to extend the life but improve the popularity of such vehicles. At the same time there have been continuing improvements in cases, grids and separators that have increased the dependability and life of the batteries used in such applications. In this type of application, performance and range are secondary to economic or special environmental consideration and the lead-acid battery has proven itself acceptable.

The case is quite different with automobiles used in normal family pursuits. Here economic considerations have been consistently sacrificed to the goal of ever increasing performance and it will take extensive consumer education to gain acceptance for electric automobiles, unless energy shortages make their use mandatory.

Even in this case, however, the low energy density lead-acid battery is the only feasible electric storage system currently available and one might say that, for automobile operation, this battery is not inspiring. The electric car designer is faced with a vicious cycle. Increasing the battery size to obtain increased performance adds sufficient additional weight to largely defeat the effort, not to mention the mounting cost. According to Dr. Paul D. Agarwal of the G. M. Research Laboratory, to equal the heat energy stored in a 20-gallon tank of gasoline would require 15,000 lbs of batteries. In comparison, a sub compact internal engine car with a full 20-gallon tank need not weigh more than 2200 pounds.

However, the Electric Vehicle Council has compiled figures that indicate that most existing automobiles usually run short trips and stay under 35 miles per hour. Considering our large urban population this is probably correct. It would seem especially true in the case of second cars in a family and there are about 25 million such multicar households in the U.S.

While it would appear that an electric car must be designed with all elements keyed to the propulsion system there have been numerous conversions of existing cars to battery propulsion. While these demonstrate the feasibility they must be considered as short term intermediates to the true electric automobile.

The Fiat X1/23, for example, has a curb weight of about 1800 pounds, uses nine 12-volt batteries and has a 65 mile range and a 40 mph top speed. The CGE-Gregoire is powered by eight 12-volt batteries, has a curb weight of about 2000 pounds and claims a 60 mile range with a 55 mph top speed.

An example of a car specifically designed for electric operation is the British Enfield 8000. This two passenger vehicle has a maximum speed of 40 mph, with a 62 mile range under peak traffic conditions through the heart of London. The vehicle uses four 12-volt 110 Ah batteries, providing power through a series/parallel control system. The curb weight is 1800 lbs.

Although not generally realized, there has been a steady gain in energy density by the lead-acid battery over the past years. According to figures presented to the 5th International Lead Conference in Paris, November, 1974 by the Chloride Group, Inc., England, the typical energy density at the 5 hr rate has increased from 20.9 Wh/kg (9.5 Wh/lb) in 1920 to 29.2 Wh/kg (13.2 Wh/lb) in 1970. Current U. S. traction batteries have energy densities of 31.5 Wh/kg (14.2 Wh/lb) while batteries in certain Japanese vehicles have energy densities of 36 Wh/kg (16.32 Wh/lb). The Japanese have set a goal of 60 Wh/kg (27.2 Wh/lb) but so far have achieved only 48 Wh/kg (21.7 Wh/lb) with a life of only 150 charge-discharge cycles. While waiting for high energy density batteries it is well to ponder the following.

The higher energy density batteries that are promised for the future can no doubt greatly improve these performance figures. But in order for electric vehicles to be successful the vehicle itself must be specifically designed for batteries and there must be improvement in motor design, control mechanisms, power transmission and vehicle design. These concepts can be tested with the lead-acid battery.

Serious development on electric vehicles should therefore start now, using the lead-acid battery as a basis. There is a waiting second car market for electrics that will increase as gasoline becomes more scarce and expensive. As we approach the convenience and economy of mass production of electric vehicles, with attractive financing programs for the consumer and nationwide sales and service this market should continue to grow, even without super batteries.

The sodium-sulfur, the lithium chlorine, the lithium-sulfide systems all have a very attractive theoretical energy density. But practical compromises to obtain a working cell have in each case greatly reduced the actual energy density below the theoretical value, just as is the case in the lead-acid battery. In each case the high temperatures required for operation would make intermittent operation difficult. Various operational problems have also made it difficult in each case to produce batteries of extended service life, even under laboratory conditions. In the case of the sodium-sulfur, a limited power density would almost certainly require operation in parallel with another power source (hybrid application).

The zinc-air battery gives performance superior to the lead-acid but rechargeability remains one of the major problems. Other systems that might be considered require circulating pumps, heat exchangers and other supplemental equipment that reduce their actual energy density and add considerably to the complexity of operation.

The high temperature systems make claims of being very inexpensive, because of the abundance and low cost of their components. This may be more than offset in actual production by the high costs associated with the rigid quality control that such batteries will require throughout all steps in fabrication and assembly.

On the basis of these considerations we believe that if electric automobiles are produced in quantity, a large number of them will be lead-acid battery powered for a long time.

E. Batteries for Energy Storage and Peak Shaving

The steadily increasing demands for electrical power and the fact that there are peak periods of electrical demand much larger than the average load are a matter of concern to the suppliers of electrical power. These peak demands can be met by a large capital outlay for new equipment but this is uneconomical because of the long periods during which such equipment would remain idle. Electric utilities therefore use their most efficient and economically obtained power for base loading, while using less efficiently generated power for intermediate and peak energy demand periods. For example, plants using nuclear fuel or water power might meet peak demand with less efficient and more costly fossil fuel sources of power.

It is obvious that methods of storing excess power generated during off-peak periods to be used at periods of peak demand offers an economical means of fully utilizing generating equipment and avoiding crisis in electrical supply. The practicality of this has been proven in the past by systems using pumped hydroelectric storage. However, there are relatively few areas where conditions are suitable for this type of storage. One practical alternative system is that using secondary batteries to store energy. This idea is attractive because batteries would allow a very efficient energy transfer and the modular construction, non-polluting character of the installation would have very little, if any, effect on local environments. Consequently, such load leveling systems could be distributed throughout the utility network at sites near load centers or wherever their use would result in savings in transmission line costs. Since the batteries are modular units they could be efficiently scaled to whatever size local conditions required, and easily modified for changing requirements. In addition, as has been well demonstrated, batteries have additional advantages such as surge suppression, voltage regulation, filtering, etc., that would not be obtainable from other methods of storage.

As a point of fact, such energy storage plans were originally based on the use of high energy density batteries that are not yet available. However, as plans progressed it became evident that lead-acid batteries are capable of meeting this need now and possibly even in the more distant future when such high energy batteries do appear.

At the present time there are two design studies that illustrate this point. The first is that sponsored by the Energy Research and Development Administration and the Electric Power Research Institute that proposes to build a test facility (BEST) for testing various batteries for applicability to energy storage. As presently conceived this test facility will have three bays, each capable of testing a 1MW, 10MWh battery, with a fourth bay containing the control equipment, computer facilities and test instruments. At the present time the lead-acid battery is the only system available for test and plans are being formulated to obtain suitable lead-acid batteries for this facility.

The second design study involves the construction of a 20 MW, 200 MWh lead-acid battery energy storage demonstration plant, sponsored by the Energy Research and Development Administration.

The feasibility studies have brought out the fact that the principal problem at present is that of producing these batteries at a cost that will be attractive to the electric utilities. However, with careful planning, it appears that this difficulty can be overcome. Past experience with scale-up of large industrial batteries and submarine cells have given the lead-acid battery companies sufficient experience with large cells so that state-of-the-art batteries are presently available that can probably meet the requirements of the BEST facility, with its 1 MW, 10 MWh capacity.

With the 20 MW, 200 MWh facility the situation is somewhat different. In this case larger modules are proposed than are currently available and the manufacturers are being asked for designs that they feel would most economically meet the requirements. One problem that is immediately evident is that present commercial facilities are inadequate to produce either the case required for such modules or the separators. Other problems concern the difficulty of transporting and handling such large modules, intercell connectors, switching and circuit breakers, but none of these problems appear to be insurmountable.

There appear to be no problems that cannot be solved in connection with the use of lead-acid batteries for this project, once the manufacturers are themselves sufficiently convinced of the commitment of Government and the electric utilities to the project. On the other hand, Government and the electric utilities are unwilling to become this committed without a practical demonstration. Under these circumstances the project could reach a stalemate, disasterous to all concerned.

This idea of energy storage in batteries, however, suggests a potential market for lead acid batteries that is enormous. Since in such a market, almost all parts of the battery would be salvageable, it would seem that batteries for this use can be made cheap enough to appear attractive as energy storage facilities. The initial amount of lead required would be very large, but lead is a metal that is plentifully distributed in the U.S. and friendly nations, so that it is not in critical supply. In addition, there is the added advantage that there are not so many competing uses for lead that supply would become a problem. There is, of course, the additional factor that after a few years and as batteries began to fail there would be practically 100% recovery of lead from facilities installed earlier. There is the final advantage that in this application the problem of energy density would not be as important as in some other applications, so that the weight of lead-acid batteries would not be as great a determent as in the usual case.

Because of already demonstrated reliability and low maintenance requirements, as well as long life (yet to be demonstrated for this type of application) it is possible that the lead acid battery could remain competitive for power storage even with the arrival of the higher energy density batteries that have been promised in the next decade.

LEAD-ACID BATTERY RESEARCH

The foregoing discussion should serve to illustrate that there has been an on-going improvement in the lead-acid battery during the past several

decades. This has been accomplished for the most part by engineering advances. Because of the highly cost competitive nature of the lead-acid battery business there has been very little funding available for research of a basic nature. Emphasis has been rather on engineering development, automation of processes, improved machinery and other achievements aimed toward improved efficiency and reduced cost.

Although each of the major battery companies has maintained a research laboratory, much of the effort of such laboratories has in the past been expended on the development of other battery systems or to other products that would help the economic position of the company. Relatively little effort has been directed toward understanding the basic mechanisms of the battery. This may be due in part to the fact that the lead-acid battery has proven sufficiently reliable and satisfactory for past needs without the necessity for research of this nature.

Eventually a point will be reached in engineering development where little or no additional improvement will be possible, and at this point further improvement will require more fundamental research than has been used up to this point.

That such research is needed is indicated by the low efficiency of active material utilization; the continuing problems of grid corrosion; the lack of knowledge as the causes of poor active material cohesion and its lack of adhesion to the grid in the positive plate; the continuing problems with both positive and negative degradation with continued cycling; and by the continuous loss of capacity that takes place throughout life. Very little is known about the effect of impurities; what impurities are harmful, and what impurities are of possible benefit; what constitutes acceptable limits of impurities, etc.

Fortunately, in the past few years a change has taken place and the principal battery manufacturers are now employing more people to study battery problems and are obtaining the necessary equipment to make more fundamental research possible.

A very good sign is a cooperative effort being made by a number of American and European manufacturers who have banded together to support a study of grid corrosion at the Battelle Research Institute in Switzerland.

An example of battery research by other than battery manufacturers is that furnished by the International Lead Zinc Research Organization, Inc. (ILZRO). For over a decade ILZRO has been supporting various projects that pertain directly or indirectly to battery problems. While this organization naturally cannot address itself to problems resulting from the use of proprietary products or procedures, it can and does undertake research on some of the lead acid battery problems that are of general importance to the entire industry, and more specifically to those problems likely to be encountered in the use of lead-acid batteries for electric vehicle propulsion.

Aside from an occasional project supported at the universities by one of the battery manufacturers, there seems to be no university interest in lead-acid batteries, at least in the United States. In England, Europe,

Japan and the eastern European countries there is a great deal more research into lead-acid battery problems than has been evident here, in universities, government supported institutions and the battery companies themselves.

One government laboratory in this country, the Naval Research Laboratory, has supported basic work in lead-acid battery research, but this effort has been small in the past, involving no more than two or three people at any time, except during the period of World War II. This effort, although small, has been given considerable cooperation from the battery companies and NRL has received contributions of battery components, test specimens and cooperation in various experiments from the various manufacturers, as well as valuable information, advice and criticism and all of this cooperation is hereby gratefully acknowledged.

Work at NRL has been primarily directed toward study of the properties of the positive and negative active material and in the determination of how these properties are affected by changes in such factors as paste composition, discharge or charge rate, acid specific gravity, temperature, etc. We have also directed a great deal of effort toward determining those factors responsible for capacity loss, battery failure and poor utilization of active material.

In making these studies we have confirmed that the physical condition of the active material plays a most important part in battery performance and life. For upon the physical nature of the active material depend such characteristics as surface area, porosity, chemical activity, solubility and other factors upon which the rate and extent of reaction occur.

Although the reactions of the lead-acid battery are theoretically completely reversible, they are less so in practice and each charge-discharge cycle yields slightly less capacity than the preceding. This loss of capacity may be traced in some cases to purely physical factors such as crystal size, cases in which the crystal becomes passivated by a reaction layer that stops reaction before the entire crystal remainder can be utilized; or by such more complex factors, such as changes in lattice spacing due to adsorbed impurities that may deactivate the crystal.

Two recently found properties of the positive active material appear to be of great significance in the search for better active material utilization and more prolonged capacity retention. The first of these was the discovery that part of the PbO_2 formed initially was electrochemically inactive in subsequent charge-discharge cycles and, moreover, that the inactive portion increased with increasing number of such cycles. This discovery was the result of earlier investigations based on thermal methods of analysis.

These thermal studies showed that the thermal degradation process was different for chemically and electrochemically prepared PbO_2. Differential thermal analysis studies also showed that after long periods of cycling, the PbO_2 in the plates yielded a decomposition curve very similar to that of the chemically prepared samples. Differential scanning calorimeter studies showed that an exothermic peak occurred at 180°C for the electrochemically prepared material but no similar curve appeared when

the chemically prepared samples were run. High temperature mass spectroscopy at 10^{-6} mm showed that this peak was associated with water evolution. To determine more about the structure that yielded this water on decomposition, pulsed NMR studies of the hydrogen nuclear relaxation times were made of the chemically and electrochemically prepared PbO_2 and of the product obtained after prolonged cycling. It was evident from the relative magnitudes of the hydrogen signals that the electrochemically prepared form contained more hydrogen than the other two. The nonexponential character of the relaxation time also indicated that the electrochemically prepared samples had hydrogen present in at least two different configurations. The chemically prepared and cycled samples showed uniform hydrogen behavior, as evidenced by a single exponential relaxation curve.

The course of the relaxation curve for the electrochemically prepared PbO_2 can be separated into short term gaussian behavior and long term exponential behavior. The long term exponential portion of the curve is similar to that found for the chemically prepared form. From the magnitude of the short term gaussian portion of the curve one can calculate a hydrogen-hydrogen separation of slightly more than 2Å. Since water molecules have a lower separation of 1.6Å, this means that the fast relaxation component is not due to water but corresponds to some other form of hydrogen bonding, the exact nature of which has not yet been determined.

Another recent discovery concerning the lead-acid positive plate that has been made at NRL was that the originally compact and dense PbO_2 found in the formed plate was transformed by cycling into a much more porous and open structure that appears to be continuous throughout the plate. This new structure has been named coralloid because of its resemblance to coral. The transformation to the coralloid form takes place as a gradual process, beginning at the surface and proceeding to the center of the plate. The length of time for the conversion to the new structure varies, decreasing with increasing depth of discharge and with increasing discharge current density.

The configuration of the PbO_2 is apparently an ideal structure since it has strength, rigidity, good electrical conductivity and a large surface area, while providing adequate porosity for electrolyte flow. Unfortunately, any benefits derived from the occurrance of this type of structure are masked by the simultaneous increase in the inactive form of PbO_2.

Eventually, as the battery approaches the end of its life, this coralloid structure disappears and is replaced by a very loosely connected, nondescript structure that resembles neither the original as-formed nor the coralloid structures. Numerous tests have shown that this metamorphous seems to take place in all plates, regardless of their source or method of manufacture. However, the study was originally made only on battery plates that had lead-antimony grid alloys. We are now repeating these investigations to determine whether the absence of antimony, as is the case with plates with lead-calcium grids, will give different results than those previously obtained.

Auger spectroscopy has also been used to study the distribution of impurities within the electrodes during charge and discharge and it has been found that the mobility of some of these impurities is greater than had previously supposed. Results so far have been too rudimentary to analyze but it would appear that some of these migrations of the elements may correlate with capacity loss and disruption of the coralloid structure. This is also an area where more thorough investigations are planned.

We consider these recent observations to be highly significant in the quest for longer life, higher energy density and higher capacity. In particular the discovery that there is an inactive form of PbO_2 present is important. If this inactive form can by some means be prevented from forming, or can be converted to the active form, significant improvement in the battery is possible, both in performance and life.

The Energy Research and Development Administration has recently sponsored this work at NRL, so that additional people can be assigned to the project. This additional support, plus the cooperation of the battery companies and ILZRO, should enable answers to be found to some of the principal problems that limit energy and power density as well as cycle life of the lead-acid battery.

CURRENT STATUS AND PROSPECTS OF THE Zn-AIR AND Na-S BATTERIES IN FRANCE

A. J. Appleby
Laboratoires de Marcoussis
91-Marcoussis, France

J.-P. Gabano
S.A.F.T.
92-Levallois Perret, France

The Compagnie Générale d'Electricité is currently conducting development work on both a circulating-slurry zinc-air battery with either built-in or external recharging facility and on the sodium-sulfur - β-alumina battery. The first system promises to be an effective vehicle power unit with sufficient energy density to give useful vehicle performance (110 wh/kg : about 150 km range for a practical city-car with normal payload). Power units have been extensively tested over the past three years in the form of laboratory modules, and sufficient data to predict practical lifetime, perforance and manufacturing cost have been obtained. An upper-limit system cost of $40 (1974)/kw is expected. Practical lifetime will be at least 2000 running hours. The sodium-sulfur battery, whose development time will be longer, may be applied to either vehicles or to industrial purposes for which the efficiency of the zinc-air system (40% overall) is not sufficiently high (e.g., offpeak storage). Over 6000 cycles (24000 hours total) have been obtained with laboratory cells using pure β-alumina electrolytes. Problems that must be solved to develop practical battery systems are summarized.

INTRODUCTION

The EEC countries and Japan have economies that are largely dependent on imported oil, which represented 67% of their total primary energy consumption in 1973.[1] The present objective of the EEC is to limit oil use to 40% of total primary energy by 1985,[2], mainly by the development of nuclear energy, which will save the equivalent of 260 million tonnes of crude oil (43% of 1973 consumption) at that time. About 31% of this installed nuclear capacity will be situated in France. In view of the commitment to an economy which will be eventually largely based on nuclear energy, it is likely that an important electric vehicle market will develop between now and the end of the century. The electric vehicle will serve both as a secondary means of oil conservation* and as a device for partial nuclear load-leveling. Other nuclear load-leveling will be provided by hydrogen production (on a seasonal basis), initially destined for the chemical industry, and by electrical storage (electrochemical and pumped storage).

It seems clear that if suitable vehicle power sources become available, the electric vehicle market will become of importance in the early '80s. The C.G.E. in France currently working on two candidate power source systems,

* Only 18% of oil use in the EEC was in road transport in 1973 (U.S. 43%)[1].

namely zinc-slurry - air and sodium-sulfur β-alumina. The former will be capable of approximately 110 wh/kg, the latter 180 wh/kg, both at the 3-hour rate. These figures are 2.4 to 4 times higher than the most optimistic current estimates for future long-life lead-acid traction batteries under the same conditions (45 wh/kg), and will result in vehicle payloads and ranges that will be acceptable for general use. Currently, the zinc-air system,[3-7] which uses zinc powder as active material in a circulating electrolyte, is closest to practical application. Prototypes up to a size of several kw have been constructed and successfully run under laboratory conditions, and have given lifetimes and performances within the desired specifications. In contrast, the sodium-sulfur system is being currently examined only at the single-cell level, at which excellent performance, particularly in respect to lifetime, has been achieved. In view of the new technology required, stepwise progress to the prototype battery level, and eventually to industrial application, will be inevitably slower than that for zinc-air. In consequence, we feel that the first successful electric vehicle will be a utility van or bus, which will be powered at first by the zinc-air system. Vehicles of this type will be eventually supplemented and replaced for many purposes by those based on sodium-sulfur or other advanced systems (perhaps fuel cells), which will have more attractive energy characteristics (in terms of battery weight and overall efficiency) and lifetimes.

The circulating slurry zinc-air system, while technologically relatively simple, suffers from the same fundamental disadvantage of all energy storage devices based on the charge and discharge of a low temperature oxygen electrode (e.g., hydrogen electrode - fuel cell combinations): a relatively low overall efficiency. This efficiency will be about 40% in practice. Despite its low cost, which will be much less than that of corresponding hydrogen fuel cell - electrolyzer combinations, it is not certain that it will find general use outside the transportation field, which is best adapted to its lifetime. In contrast, the sodium-sulfur battery will have a per-kilowatt* capital cost about twice as high, but in this case lifetimes of several years with no maintenance whatever may be expected. This factor, together with its potentially lower cost than that of the lead-acid battery, will make it a candidate for all current and anticipated industrial-scale secondary battery applications. However, its use for discontinuous applications (e.g., in private vehicles) may be difficult because of the problem of temperature maintenance. The problem of safety will also require attention. A distinct advantage of the sodium-sulfur battery, that sets it apart from conventional secondary cells, is the fact that its energy storage capability can be engineered indepenently of its power producing capability (as in the case of fuel cells or of the circulating zinc-air system). This factor will be especially important for heavy vehicle applications and for reserve storage or peak-shaving.

Some of the factors involving end-use of the above systems, and the problems that must be solved for their eventual large-scale application, are discussed below. In addition, they are briefly compared with alternative secondary batteries, with emphasis on the transportation field.

---

* The relevent cost parameter for both circulating zinc-air and sodium-sulfur systems is the per kw cost (on charge for Na-S, on discharge for Zn-air), as both systems will be limited by the available active area (of β-alumina and current collectors and air electrodes respectively), not storage volume.

ELECTRIC POWER SOURCES FOR USE IN VEHICLES

A summary of electric vehicle performance requirements, based on the 1968 Arthur D. Little evaluation[8], is given in Fig. 1. For all but the smallest vehicles, at least 100 wh/kg will be required to give a satisfactory practical range between recharges. In addition, if electric vehicles are to make a substantial penetration of the market, battery cycle lifetime should be such that overall kilometric costs are similar to those for (future) vehicles using untaxed gasoline. The latter factor will be of particular importance in Europe, where gasoline taxes provide a substantial amount of national administrative budgets. It is reasonable to suppose that in the future the corresponding sums will be recovered by special taxation on transportation kwhs. In addition, because present European gasoline prices without tax are similar to overall U.S. prices at the pump, such calculations are useful for indicating the economic requirements for preliminary penetration of the U.S. market.

In spite of recent developments in energy density, the lead-acid battery will never provide sufficient performance for more than a minor fraction of the overall vehicle market, e.g., for short-range utility cars or door-to-door delivery vans. In addition, its fixed costs per kilometer are too high

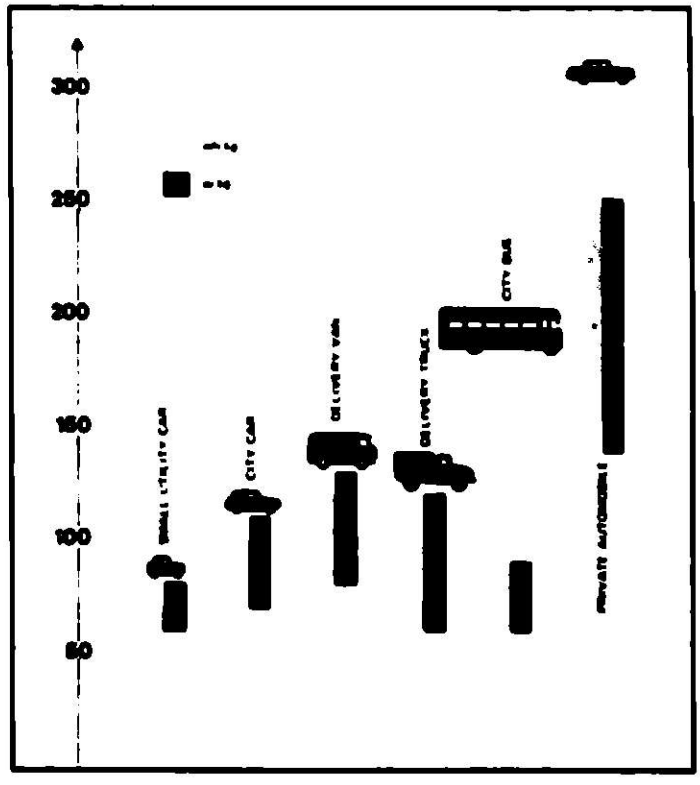

Fig. 1. Power source energy and power densities for electric vehicles.

to meet the economic goals given above.

Practical power sources that will attain the required performance and economic criteria do not at present exist. However, major candidates currently receiving study are low temperature batteries based on the Ni-Zn, Zn-air (also Zn-compressed oxygen[9]), Fe-air[10], $Zn-Cl_2$[11] and $Zn-Br_2$[12] couples, as well as low-temperature fuel cells[13]. The most widely studied high-temperature systems are based on the Na-S[14] and Li-Al[15a] and Li-Si[15b] -FeS_x couples. Other possible candidates (ambient-temperature $Ni-H_2$, high-temperature solid-state batteries) are discussed elsewhere in this symposium.

The limitations of the nickel-zinc system, resulting from the solubility of zincate ions in the electrolyte, are well known. Research to limit the shape-change phenomenon is currently in progress (c.f. Ref. 16), and it is reasonable to assume that lifetimes in excess of 1000 cycles under practical conditions will be eventually attained. System energy density will be from 1.5 to 2 times greater than that of future lead-acid batteries, and few problems of industrial production are anticipated. However, a major difficulty is system capital cost, which will be at least 50% higher per wh than that of lead-acid. This factor, together with a probably limited cycle life, will give an unacceptable overall cost per km for generalized use.

The zinc-compressed oxygen and zinc-air concepts have good energy densities (about 120 and 100+ wh/kg respectively), but they suffer at present from the electrode shape-change problem. In addition, the difficulties of making satisfactory long-life low-cost rechargeable oxygen electrodes have yet to be overcome. Cost of the basic module in these systems should ultimately be lower than for lead-acid, but the pressure container (for zinc-oxygen) will be expensive and will constitute a safety hazard. The circulating electrolyte system required in the case of zinc-air (to prevent carbonate build-up) will also increase cost and system complexity. In addition, limitations resulting from the use of an ambient temperature air electrode limit power density. Vehicle fuel cells, and aqueous $Zn-Cl_2$ or $Zn-Br_2$ batteries, should allow higher energy densities to be attained, but their stage of development is too limited to make any predictions possible. Industrial development of the molten salt systems requires the solution of many technological problems that are new to the battery industry. However, their potentially low costs will certainly make them attractive, and they may be regarded as second-generation power sources for vehicle applications.

The most promising system for achieving the necessary initial penetration of the potential market is therefore the zinc-air system, both from the viewpoint of cost and energy density, provided that its intrinsic problems can be overcome. Lower energy density and very poor charge-discharge efficiency remove the only other possible candidate secondary battery (Fe-air) from consideration. Systems requiring industrial processing for recharge (e.g., those based on alkali metals) seem unlikely to provide the impetus for early market penetration.

The C.G.E. slurry zinc-air battery was devised as an engineering solution to the problems posed by the classical zinc-air battery. By the use of a fluid electrode, it avoids the shape-change effect. In addition, current densities are considerably greater than those in classical systems, so that hardware weight is reduced and power density increased. This is achieved

by running at temperatures above ambient and by avoiding zinc passivation by maintaining the reaction product (zincate ion) in solution. In addition, the air electrode is optimized for high discharge rates, since recharge is carried out in a separate unit with an oxygen electrode optimized for the evolution process. This concept immediately removes the difficulties inherent in the use of bifunctional air electrodes[17], which have relatively low performance and short lifetimes.

THE CIRCULATING ZINC-AIR BATTERY

General

Work on the concept started at the Laboratoires de Marcoussis, Research Center of the C.G.E., in 1971. From the beginning, the system was conceived of as a rechargeable fuel cell, in which the negative electrode was simply a current collector brought into continuous contact with a fluidized fuel (zinc powder in KOH electrolyte). The C.G.E. system differs from other proposed zinc-powder - air batteries[3-5] in using a very high electrolyte flow rate (about 0.8 m/s), which prevents the appearance of any passivation effects and results in excellent zinc particle - current collector contact. A constant cross-section tubular system of relatively large diameter (ca. 2 cm) gives optimum hydrodynamic conditions (constant velocity turbulent flow of the zinc powder - electrolyte slurry*), and eliminates segregation. Auxiliary power requirements are therefore minimized, since pressure drops are small.

The addition of colloid stabilisers has allowed a threefold increase of the thermodynamic threshold concentration for zincate precipitation. At the same time, passivation of the zinc electrode is thereby prevented under all current density conditions. The useful attainable zincate concentration corresponds to 300 g Zn/liter of 12M KOH before precipitation and passivation limit performance. Self-discharge of the zinc powder has been shown to be very low, and no complex zinc metering (c.f. Ref. 3) is needed. No separation of zinc oxide or zincate from the electrolyte is attempted. As in all zinc-powder battery concepts, simple rapid mechanical recharge is possible. This proposal, with its advantages, has been discussed elsewhere.[6,7,18] Our studies have shown that onboard recharge is indispensable from the viewpoint of marketing an electric vehicle equipped with a circulating zinc-air battery, due to the cost of installing the logistic support required for external regeneration. Only the integrated secondary system is considered in the present paper.

The zinc powder regenerator is a small unit attached to the primary power system. Both use the same electrolyte circulation. The power source may therefore be regarded as a three-electrode secondary zinc-air cell in which the ionic circuit, not the electronic circuit, is broken, as in some classical flate-plate cells. The system is modular, so the power-producing section (tubular electrodes), the regenerator and the energy storage section (reservoir) are capable of a great variety of geometrical arrangements to suit vehicle space and power and energy requirements. An overall scheme of the whole system is given in Figure 2.

---

*The zinc - electrolyte slurry has been granted the trademark 'Elosine'.

Unit cells

As indicated above, the unit cells are tubular, and comprise (from inside to outside) :

(1) A copper-plated steel exmet, welded to form a tubular current collector.
(2) A copper-plated steel screen separator support.
(3) Asbestos separator ($\sim$0.3 mm).
(4) Air electrode.
(5) Steel screen current collector.
(6) Outer steel exmet tube, serving as primary positive current collector. This is mechanically compressed onto the air electrode and its backing screen and produces and extremely rugged and rigid structure.
(7) Porous Teflon outer coating.

The tubular structure has been optimized from the viewpoint of performance and manufacturing cost. Its performance and lifetime result from the air-electrode structure which consists entirely of an extended Teflon-bonded active carbon with no noble metal catalyst. Lifetimes of individual electrodes have been shown to be greater than 3,000 working hours, under practical conditions. The tubular cell system and its auxilliaries are designed so that emptying automatically takes place on stand-by. No air electrode degradation occurs during these periods. The tubes and system are shown schematically in Refs. 7 and 18.

Typical current-voltage curves for individual tubes at 50° C are given in Figure 3, which shows improvements made since 1973. The data used as the basis of performance evaluation indicates a maximum power of 75 watts/tube at 0.9 v. The gain in performance results from electrode and separator improvements: Zn electrode polarization is negligible ($\sim$20 mv at 300 ma/cm^2). Polarization is practically independent of state of discharge of the system, but starts to increase rather suddenly as the solubility limit for zincate is approached. As for all fuel cells, ah capacity is independent of rate.

Hydrodynamics

The tubular electrodes are connected in modules by plastic U-junctions. Modules consist of closely-spaced bundles of electrode tubes arranged with series electrolyte flow. Flow to the self-emptying modules is started by the use of a small self-priming pump at the inlet to the group of modules constituting the battery. The latter serves as a choke under normal conditions, and creates the correct negative internal pressure for functioning, flow being maintained by a suction pump at the module exit. The use of negative pressure prevents weeping of the air electrode. However, for correct functioning of the latter the total pressure drop across the system should be small. This factor governs the maximum number of tubes per module. A module is shown in Figure 4.

Recharging

Spent electrolyte typically contains 295 g/l zinc in the form of zincate, of which 280 g is regenerated on charge. 270 g ($\sim$270 wh) is usable, 10 g representing a typical self-discharge loss. Long-term self-discharge losses on stand in quiescent solutions are not very much greater, since passivation of zinc occurs rapidly under these conditions. Typical increase in carbonate concentration per cycle is 2×10^{-2} mole/l. Approximately 50 charge-discharge

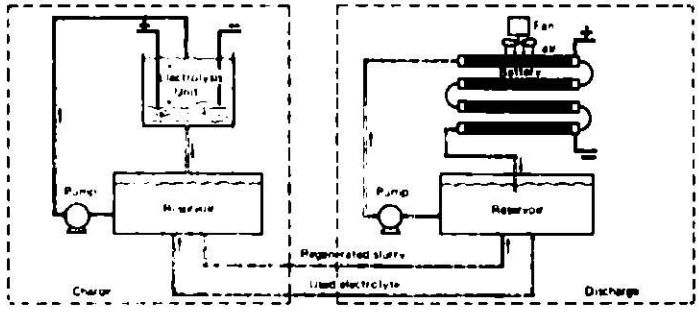

Fig. 2. Circulating zinc-air overall system concept.

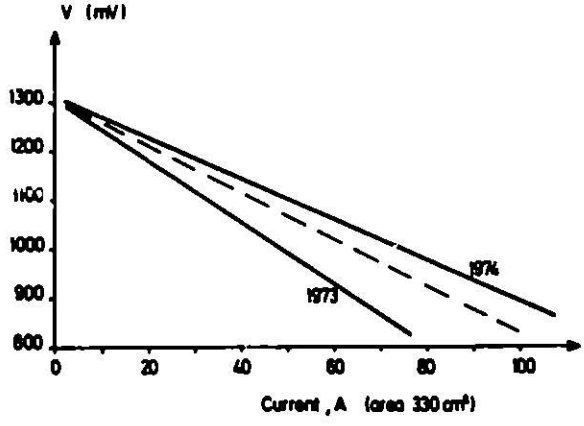

Fig. 3. V - I curves for individual tubes.

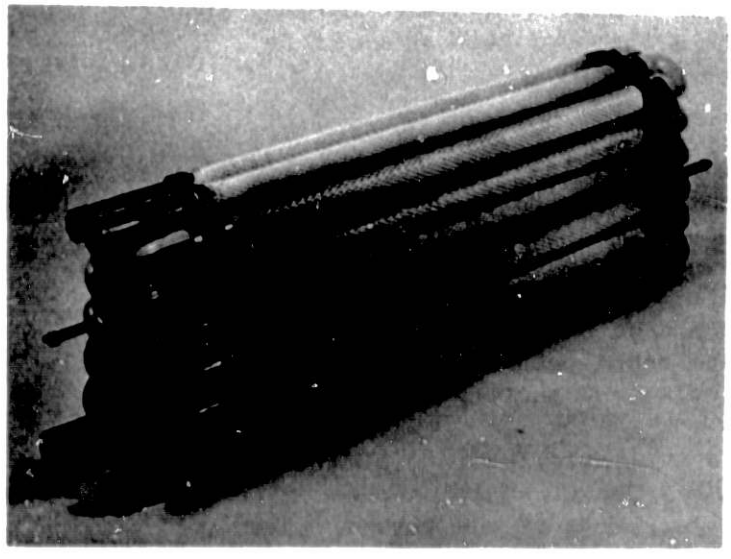

Fig. 4. 1.8 peak kw power module (24 tubes).

cycles can be obtained before removal of carbonate is necessary.

Studies undertaken since the beginning of 1975 have illustrated the feasibility of on-board electrical recharging. A prototype system consisting of a 1 kw generator and electrolyzer is at present under test. The electrolysis unit which will be installed in the vehicle uses a modular construction of tubular electrodes of similar size to those in the fuel cell. The oxygen electrode, of proprietary structure, is at the outside of the system, the zinc powder electrode being in the center. Laboratory experiments indicate a mean of 2.4 v on charge at high current densities. Since charging is over an 8 hr period, the total electrolyzer area required for a full charge in this time is small compared with the total fuel cell area, so that the electrolyzer weight is about 10 % of the total. Overall efficiency (with all losses) is 40%.

Operation and system performance

Excess heat from the system is rejected via the air flow. Normal air flow is 3-8 times stoichiometric, depending on power output. Air is given a cursory decarbonation by bubbling through the electrolyte, which is sufficient to prevent any problems due to carbonate build-up in the air electrodes. Normal working temperature is 50-55° C, automatically maintained by air-flow control via a blower. Using the performance datum given in Figure 5 maximum power for the optimized zero-capacity limiting case will about 280 w/kg, which includes auxiliaries, electrode tubes and the supporting framework, together with a typically dimensioned reservoir. System maximum energy density for the zero-power limiting case (zinc-powder plus electrolyte only) is about 145 wh/kg at nominal current densities. Typical systems for automobiles will have performance of 80 w/kg peak power and 110 wh/kg energy density at nominal rates (this represents a 3-hr discharge rate, approximately 80 ma/cm^2). Systems optimized for different rates and capacities will have different empty specific power characteristics (see Table 1). These figures include losses due to the circulating currents, which represent 1.0 % of nominal power. Auxiliary power requirements are predicted to be 1.4 % of full power output (5 % of nominal) in scaled-up systems. Overall specific gravity is close to unity. A proposed system has been shown in Ref. 7.

Economics

Comparative changes in zinc, gasoline and electrical kwh prices, together with the taxes that may be imposed on the use of vehicles with different power sources must be considered to be unknown quantities over the next ten or so years. In addition, the principle application of the circulating zinc-air battery will be to electric traction, for which the total market cannot at present be predicted. No first hand experience of the system is available, since no prototype vehicles have as yet been built and tested. Consequently, any economic calculations must be used with caution.

Based on the available laboratory data, and on estimates of the amortization costs of the types of equipment needed for the manufacture of electrode tubes and mechanical parts of the system, an overall manufacturing cost for the rechargeable system equal to $40/kw at 1974 prices has been estimated. This figure assumes a volume production of 100,000 20kw units* per year, and

*Figures are peak kilowatts, corresponding to the one-hour rate.

corresponds to $4.50-$5.00/lb of system hardware. This figure is rather insensitive to zinc cost, since the initial charge of zinc powder in typically-dimensioned systems represents only a small fraction of the above figure. In regard to zinc availability, an annual production of 150,000 zinc-air urban vehicles represents a zinc requirement equal to only 5% of current French production (currently about 270,000 tonnes/yr). Similarly, if a loss of 0.1% of zinc per cycle is considered (reasonable for internally-recharged batteries), then the quantity of zinc that must be replaced annually for a constant vehicle pool is equal to only 2% of the total inventory.

Since the most important part of the total cost involves the electrode tubes and auxiliaries, the per kwh cost of the zinc-air system falls as the stored energy/peak power ratio of the installed battery increases. This is particularly true for the case of heavy vehicles. A comparison of the initial battery cost and performance for lead-acid (32.5 wh/kg) and zinc-air (primary system corresponding to 100-125 wh/kg) for various classes of electric vehicles is given in Table 1. It can be seen that the initial cost of the circulating zinc-air system is of the same order as (in some cases less than) that of a lead-acid system giving much less range. Since the cycle life of the zinc-air system (at least 600 cycles at the C/3 rate, 80% d.o.d., based on laboratory module performance) will be at least equal to that of lead-acid batteries under the same cycling conditions, fixed costs per km will be correspondingly lower.

In terms of overall per km costs, this advantage is clearly shown in Fig. 4 (calculations for 1 tonne urban vehicle - economic assumptions are stated in Ref. 7). An electricity cost at the power point of 3.6 cents (1974) per kwh has been assumed. Since the latter represents a very small part of the total running costs, the lower overall efficiency of the zinc-air system is not significant. Overall, the true cost per km of a zinc-air powered vehicle, amortized over the same chassis lifetime as a conventional car, should be approximately the same as that for a gasoline-powered vehicle at current U.S. pump prices (or untaxed European prices). Since gasoline costs will almost certainly rise more rapidly in future than prices of coal- or nuclear-based electricity, the economic advantage of the zinc-air battery vehicle should become even more marked.

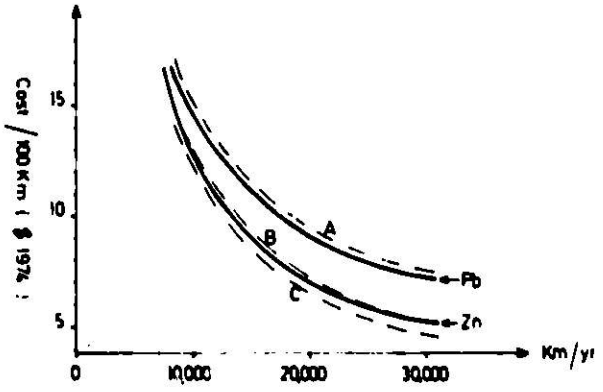

Fig. 5. Calculated total cost per 100km for lead-acid, zinc-air and gasoline vehicles. A: Present European gasoline costs (with taxes, 39c/l); B. U.S. costs (15.4c/l); C. U.S. untaxed costs (9c/l).

	City Car Chassis Weight : 500 kg Useful Load : 250 kg 30 hp		Delivery Van Chassis Weight : 1,000 kg Useful Load : 1,000 kg 75 hp		Truck or Minibus Chassis Weight : 4,500 kg Useful Load : 3,500 kg 180 hp	
	Lead-Acid Battery	C.G.E. Circulating Zn/Air Battery	Lead-Acid Battery	C.G.E. Circulating Zn/Air Battery	Lead-Acid Battery	C.G.E. Circulating Zn/Air Battery
Battery Volume (liters)	200	300	500	800	2,000	2,000
Elozine Volume (liters)	-	100	-	310	-	910
Total Battery Weight (kg)	400	250	1,000	700	4,000	2,000
Elozine Weight (kg)	-	180 (72 %)	-	548 (79 %)	-	1,638 (82 %)
kwh Installed	13	26	32.5	80	130	238
Range (km)*	50 to 80	100 to 170	50 to 80	120 to 200	50 to 80	100 to 170
Installed Battery Cost**	1	1,25	2.5	2.75	10	6
Installed cost/kwhr	1	0,63	1	0.45	1	0.33

* Depending on driving cycle.
** Based on unit cost of Lead-Acid Battery for City Car = 1.

TABLE 1. Investment cost/performance comparison for different electric vehicles.

Present status of development - problems requiring solution

To date, the majority of work on the project has consisted of improvements to the tubular reaction cells and of the optimization of electrode structures. Large numbers of tubes, either singly or in the form of 12-tube modules, connected hydraulically and electrically in series, have been life-tested and cycled to within technical specifications (>600 cycles, 80% d.o.d. at C/3). Even longer lifetimes can be expected at lower depths of discharge (lower final zincate concentrations). The primary power system can therefore at this point be regarded as being out of the laboratory stage - its major problems now involve optimization of tube dispositions, of module sizes and of the auxiliaries required for practical vehicle applications. The basic technical limits currently identified are as follows:
1) At low ambient temperatures, battery start-up power is much less than nominal (ca. 25% at -15°C). While warm-up is relatively rapid (the total amount of electrolyte in the system is the same as that in a lead-acid battery of the same capacity), work is currently in progress to reduce internal I.R. drop, which is the principal cause of this difficulty. This modification will further improve overall system performance.
2) System energy density is limited by that of the Elozine , which corresponds to a figure of 145 wh/kg. It does not seem possible to increase this energy density level, given the present technological system concept, without extensive further research.

Work on the internal recharge modules, having started at a later stage than that of the power system, requires further laboratory testing. In contrast to other reported research[19], no basic problems concerning zinc powder formation have been identified. Optimization of current density, temperature and hydrodynamic conditions is currently being conducted. Special non-noble-metal catalyzed oxygen electrode stuctures that allow efficient electrolysis in the presence of high zincate concentrations have been developed. The major engineering problem is the reduction of module I.R. drop.

Passage from the present state of research to the required engineering objectives is no longer dependent on the successful resolution of fundamental problems. The principles involved, and the feasibility of the solutions adopted are known and have been demonstrated. Technical success is dependent on the outcome of a program of development and assembly of optimized components.

THE SODIUM-SULFUR β-ALUMINA SYSTEM

General

Work on β-alumina started at Marcoussis in 1968, as a general extension of a high-temperature solid-electrolyte program for the development of doped zirconia fuel cells. From the beginning, the electrophoretic deposition method for tube formation was adopted. Using laboratory-prepared β-alumina powders as starting material, this technique permits fabrication of high-quality green tubes of reproducible properties and finely controlled wall-thickness and surface finish. The green tubes were completed by an isostatic pressing operation and were fired in β-alumina crucibles to avoid sodium losses. An account of the fabrication techniques has been given elsewhere[20]. In parallel with this work, fundamental studies to establish the sodium oxide - alu-

minum oxide phase diagram were conducted[21].

In preliminary work, a wide range of β and β" compositions was examined. Early cycling experiments used electrolytic filling of the tubes with sodium from molten sodium nitrate, which involves application of high initial cathodic current densities. It was noted that tubes containing more than 3% MgO as a sintering aid did not survive the filling operation. Other tubes showed cycle lifetimes under the conditions described below that depended on MgO content[22]. It was therefore decided that only pure stabilizer-free β-alumina of two-block composition was suitable for long cycle lifetimes. Details of its composition and method of fabrication are given in Ref. 20. The specific resistance of this material is 15Ω-cm at 300°C.

The type of failure seen in MgO-doped tubes was characteristic of all early β-alumina work. It has been discussed in terms of Griffith crack formation at the β-alumina-Na interface[23]. It was suggested that this results in stress concentration at the crack head, since the effect of I.R. drop and radial diffusion favor formation of sodium under high Bernouilli pressures at these points. Impedance measurements using β-alumina close to failure and an analog model[24] have also produced evidence in favor of such a mechanism. However, contemporary work at Marcoussis suggested that this failure mechanism does not necessarily apply to all types of β-alumina and to all battery environments, as discussed below.

All early work at Marcoussis was performed in all-glass (SOVIREL S 74701) hardware for ease of fabrication, using β-alumina tubes of 8 mm diam., 45 mm length with various wall thicknesses. The sulfur electrodes contained graphite felt and Mo wire spiral current collectors. Cycling was generally restricted to between Na_2S_3 and Na_2S_5 compositions in life-tests to optimize β-alumina properties, which also involved tests on Na-Na, and polysulfide-polysulfide cells. Current densities were 67 mA/cm^2 charge (3 hour rate), 200 mA/cm^2 discharge (1 hour rate) for Na-S cells (2.25 Ahr. total capacity) and 0.2 and 0.15 A/cm^2 for both charge and discharge for Na-Na and polysulfide-polysulfide respectively. Other life-tests were conducted under open-circuit conditions. Cell ageing was followed by progressive impurity analysis, electrical resistance measurements, crystallographic analysis, and SEM-electron microprobe examinations. Test variables were tube wall thickness, temperature, initial purity of β-alumina, and foreign ion concentration in the melt.

It was shown that ageing was associated with a progressive increase in resistance at higher temperatures (300°C and above). Failure occured immediately following a rapid drop in resistance. Lifetimes were strongly dependent on temperature (> 10,000 hours at 200°C ; 300 - 400 hrs at 330°C) and on tube wall thickness. At higher temperature (~330°C), lifetime was shown to be independent of whether or not charge was passed. Na-Na cells also were shown to fail more rapidly than Na-S cells. Ageing (increase in resistance) and failure were strongly dependent on reservoir material used: cells in all-glass hardware showed failure that occured much more rapidly than for ceramic or metal hardware. Details are given in Ref. 25.

The above results were accounted for by chemical analysis of failed tubes. In all cases, K^+ ion was detected in substantial quantities (approaching 1 %) at failure, whereas other trace elements (with the exception of Si) re-

mained substantially constant. The K^+ ion was shown by electron-probe microanalysis have a regular distribution through the material, which results from diffusion alone since results obtained under cycling and non-cycling conditions were not substantially different. The K^+ ion resulted from ion-exchange with the glass envelopes, as confirmed by the fact that degradation was proportional to glass area in contact with Na metal. Properties of K^+-exchanged 2-block β-alumina were examined by electrical and X-ray measurements. The $\vec{c}$ axis was substantially expanded in exchanged material, causing surface strain. The exchanged material also possessed a higher electrical resistance. Tests were conducted to determine the effect of likely corrosion products of metallic envelopes on the ageing of β-alumina. However, after cycling of polysulfide cells containing known amounts of transition metal salts, chemical analysis of β-alumina showed that ageing effects due to incorporation of transition metal ions were negligible even after several thousand of hours of operation[24]. Corrosion products of transition metal hardware may therefore be ignored in considering failure of β-alumina.

Results showed that the critical level for K^+ incorporation is about 1000 ppm. Provided this figure is not exceeded, seemingly infinite lifetime can be expected with the pure 2-block β-alumina material. This condition may be achieved by testing Na-S cells in all-glass hardware at slightly lower temperatures (285 - 290°C). Under such conditions the leaching rate of K^+ ion from the walls of the glass cell is low. This procedure was resorted to in 1972 for testing, after the degradation mechanism was established, but before definitive metal hardware was available. Since this time, no ceramic failures have occured. The longest-lived Na-S cell thus far has completed over 7,000 cycles (67 mA/cm^2 charge, 3 hour rate, 200 mV/cm^2 discharge, 1 hour rate) or over 3 years continuous operation. Results have shown that higher charge rates (150 mA/cm^2) have no effect on lifetime.

Present status of program

No ceramic failures have occurred in testing since the failure mechanism of pure β 2-block ceramic was determined. Consequently, we are confident that ceramic of this composition, made on an industrial scale, will be suitable for very long-life applications. Present emphasis is on tackling those other areas requiring technical solution before practical small prototype long life cells can be constructed. These problem areas are as follows :

(1) Fabrication of β-alumina with the required properties (electrical conductivity, lifetime) by methods that are capable of cheap mass production.
(2) Development and manufacture of optimized metal containers.
(3) Development of seals with suitable properties (thermal cycle and corrosion resistance), that are capable of mass production.
(4) Possible corrosion problems (anode and cathode compartments, seals, current collectors).
(5) Sulfur electrode optimization (charge capability, geometry, effects of overcharge, effect of inversion, development of economic current collectors).
(6) Problems associated with batteries (cell capacity imbalance, overcharge, inversion, thermal cycling, thermal properties, safety, economic optimization).

Currently, we are examining the possibility of eliminating the need for using β-alumina crucibles in the sintering operation by introducing other me-

thods of atmospheric sodium buffering. Present emphasis is on the use of lower sintering temperatures (<1700°C), which necessitates starting materials having higher reactivities. This will permit the use of existing industrial furnace technology and eliminate the need for extensive development expenditure. Flash sintering is also being examined, but this solution requires a new technology. While the ceramic purity required has been emphasized, the degree of purity is no higher than that for many other industrial applications. Starting materials have a current price of only 30 c/lb, so we have confidence that a low-cost ceramic with the required properties and lifetime will be available at the end of the development program.

Development of low-cost, long-lifetime seals and metal containers involves essentially corrosion problems . For light weight and low cost, aluminum and its alloys are primary choices, but for certain applications and system parts, various alloy steels may be appropriate. New types of cheap ceramic-metal seals have been developed, which show great promise and are currently under accelerated life-testing. The problem of material optimization of the cathode current-collector interface is receiving close attention. Optimization of system geometry depends on energy density-power density requirements, and will depend on the application. Cells are shown in Figs. 6,7.

Work on the sulfur electrode has been emphasized, both from the viewpoint of increasing capacity per cm^2 and depth of discharge, and with regard to finding substitutes for expensive laboratory compcnents (e.g. graphite felt). 100 % d.o.d. (i.e. $S \rightarrow Na_2S_3$) has been consistently demonstrated and capacities over 1 Ahr/cm^2 have been obtained. This figure can be increased to even higher values by the use of special current collector geometries, so that the battery will not be limited by the geometrical cell area required in particular applications for which low capital cost is important. As well as providing for almost unlimited storage capacity per unit area (a feature of liquid-electrode, but not solid-electrode, cells), the sodium-sulfur battery has the enormous additional advantage of a 100% Faradaic efficiency and a zero self-discharge rate. Problems involved in battery construction may therefore prove to be much easier to solve than for classical systems. The formation of insulating sulfur layers or solid sulfides may be used in special current collector designs to give automatic overcharge and inversion protection. Finally, present results indicate that thermal cycling is unlikely to present major problems in large batteries.

CONCLUSIONS

The circulating zinc-air battery system promises to be the first high-energy-density battery (>100 wh/kg) to be introduced as a practical electric vehicle power source. As such, it will offer the performance necessary to open up a large electric vehicle market. Its simple modular design will permit capital costs on the same order as those for lead-acid batteries giving less than half the range. In addition, its overall costs per km will correspond to those for vehicles using gasoline at present U.S. pump prices (or at untaxed European prices) based on the same rate of chassis depreciation. Despite its low cost and advanced stage of development, its relatively low overall efficiency (40 %) will restrict its wide use to the transportation field.

The sodium-sulfur β-alumina battery has already demonstrated potential

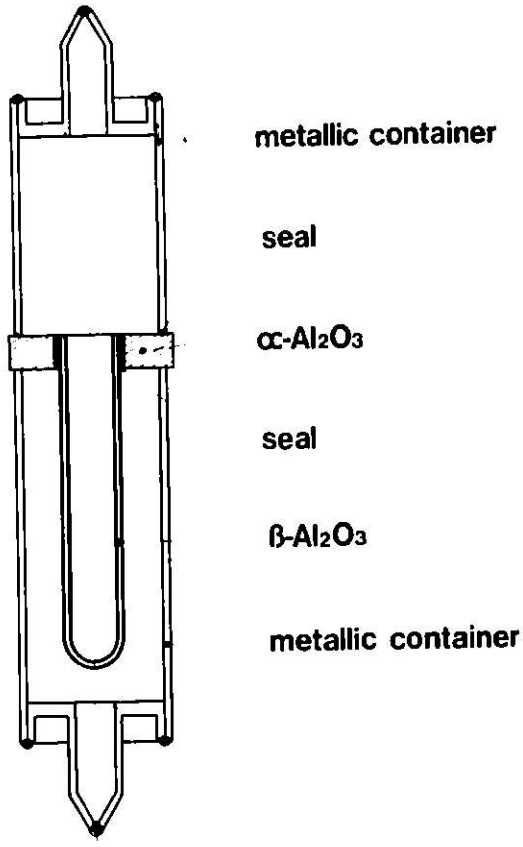

Fig. 6. Schematic view of Na-S cell design concept.

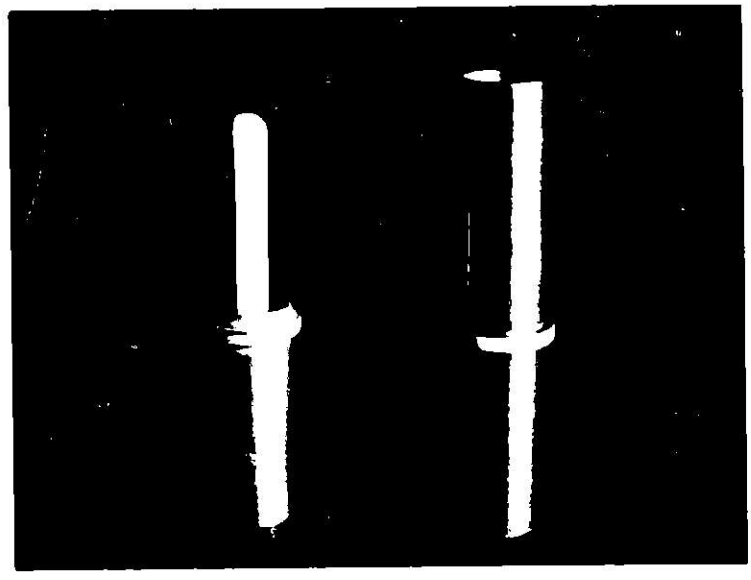

Fig. 7. Present laboratory test hardware, showing seals.

cycle lifetimes of several years for the ceramic electrolyte. Since its introduction will require extensive development of a new materials technology together with very long term testing of all components, its employment on an industrial scale will come some time after that of the circulating zinc-air battery. Due to its high energy efficiency (>75 %) and energy density (>180 wh/kg at C/3), it will replace the zinc-air battery in traction applications where intensive use (no temperature cycling) occurs, and where its amortization over very long lifetimes will be advantageous. Its greatest applications promise to be in the industrial field, where its zero maintenance, low potential cost, long lifetime and zero self-discharge rate will be distinct advantages. The energy necessary to maintain battery temperature will be lower than that for floating in conventional systems. The greatest problem area of the battery in early work, the β-alumina membrane, is now seen as its greatest asset. Unlike other high-temperature battery concepts, the liquid electrode materials used are not only time-stable, but can present a storage capacity that will be virtually independent of ceramic area in advanced designs. Very low cost systems of high storage capacity are therefore possible.

REFERENCES

(1) Statistics of Energy, 1959 - 74, O.E.C.D., Paris 1974.
(2) M. Banal, Rev. Française Electricité, No 249 - 50, 21, 1975.
(3) H. Baba, assigned to Sony Corp., U.S.P. 3555032, 3560262.
(4) Battelle Memorial Institute, Franch Patent 2096046.
(5) D. Doniat, K. Beccu and A. Porta, assigned to S.A. Automobiles Citroën, German Pat. 2125576.
(6) A. J. Appleby, J. P. Pompon and M. Jacquier, 3rd Intl. Electric Vehicle Symp. Washington DC, February 1974.
(7) A. J. Appleby, J. P. Pompon and M. Jacquier, Proc. I.E.C.E.C., 759121, 1975.
(8) J. H. B. George, L. J. Stratton and R. G. Acton, "Prospects For Electric Vehicles" Arthur D. Little, Inc. Report to U.S. Dept. H.E.W., N.A.P.A.C., Arlington, Va., May 1968.
(9) M. Klein, Proc. I.E.C.E.C., 729017, 1972.
(10) H. Cnobloch, D. Gröppel, D. Kühl, W. Nippe and G. Siemsen "Power Sources 5", D. H. Collins ed., Academic Press, New York, 1975, p. 261; O. Lindström, ibid., p. 283.
(11) P. C. Symons, Intl. Conf. Electrolytes for Power Sources, Brighton, England, Dec. 1973; A. F. Sammells, Ext. Abstracts Electrochem. Soc. Fall Meeting, p. 600, Dallas Tex, October 1975.
(12) G. Clerici, M. de Rossi and M. Marchetto "Power Sources 5", D. H. Collins ed., Academic Press, New York 1975, p. 167; M. Walsh, F. Walsh and D. Crouse, Proc. I.E.C.E.C. 758171, 1975.
(13) Y. Bréelle, A. Grenier and J. Cheron, Proc. 4th Intl. Symp. Fuel Cells, R.U.C.A., Antwerp, Belgium, 1972.
(14) N. Weber and J. T. Kummer, Proc. 21st Ann. Power Sources Conf., p. 37, 1967; S. Gratch, J. V. Petrocelli, R. P. Tischer, R. W. Minck and T. J. Walden, Proc. I.E.C.E.C., 729008, 1972.
(15a) E. C. Gay, F. J. Martino and Z. Tomczuk, Proc. I.E.C.E.C., 759097, 1975.
(15b) L. R. Mc Coy and L. A. Heredy, 759099, 1975.
(16) K. W. Choi, D. Hamby, D. N. Bennion and J. Newman, Ext Abstracts Fall Meeting Electrochem. Soc., Dallas Tex. 1975, P. 135, 137.
(17) H. Cnobloch, G. Siemsen and F. von Sturm, "Power Sources 4", D. H. Collins ed., Oriel Press, Newcastle-upon-Tyne, England, 1973, p. 311.

(18) A. J. Appleby and M. Jacquier, to be published in J. Power Sources.
(19) M. I. Gillibrand, J. Gray and J. F. Gudger "Power Sources 4", D. H. Collins ed., Oriel, Newcastle-upon-Tyne, England, p. 297, 1973.
(20) J. Fally, C. Lasne, Y. Lazennec, Y. Le Cars and P. Margotin, J. Electrochem. Soc. 120, 1296 (1973).
(21) E. Le Cars, J. Thery and R. Collongues, Compt. Rend. Acad. Sci. (Paris) 274, 4 (1972).
(22) J. Fally, C. Lasne, Y. Lazennec and P. Margotin, J. Electrochem. Soc. 120, 1292 (1973).
(23) G. H. Tennenhouse and T. J. Whalen, Ford Motor Co.; Annual Report, NSF - RANN Contract C. 805, July 1974.
(24) R. D. Armstrong, T. Dickinson and J. Turner, Electrochim. Acta 19, 187 (1974).
(25) Y. Lazennec, C. Lasne, P. Margotin, J. Fally, J. Electrochem. Soc 122, 734 (1975).

BATTERIES FOR ELECTRIC VEHICLES IN WESTERN EUROPE

by G. Lander and E. Voss

Forschungs- und Entwicklungszentrum der VARTA Batterie AG,
Kelkheim/Taunus, Germany

ABSTRACT

In Western Europe a number of electric vehicle projects are currently underway. At present all vehicles are powered by lead-acid batteries. Lead-acid cells operate at an energy density of 30 to 40 Wh/kg depending on cell design. Cycle life is in the range of 500 to 1600. Maintenance has been reduced to a minimum. The capability of lead-acid batteries to power vehicles for city transport has been demonstrated.

INTRODUCTION

A report on batteries for electric vehicles (e.v.) in Western Europe is enfaced with one major difficulty: there are very little informations officially published by the various companies working on or producing already special e.v. batteries. This lack of information, certainly an indication for development in progress, concerns items which are of utmost interest to battery engineers, such as construction details and production procedures. It is very significant for the situation prevailing to-day that even serious battery makers are presenting much more design details of the cars their batteries are used in than on these batteries themselves.

As a consequence of the information gap this report is restricted to a few countries in Western Europe only, because there is not known any publication from Eastern Europe, and it is further restricted to batteries existing at least in some prototype versions which are tested in a car. Keeping these limitations in mind the following countries remain to be discussed: France, Great Britain and the Federal Republic of Germany, and there remains one battery system only, namely the lead-acid system. There are, of course, a number of companies which are doing development work on systems other than lead-acid, such as Fe/O_2, Ni/Zn, Ni/Co and Na/S. However, at present no prototype battery thereof is on test in a car.

The lead-acid system as a power source for road vehicles has a long tradition in Europe. Just for curiosity some of the early

vehicles are shown in fig. 1 and fig. 2. For several decades European post administrations have used battery powered delivery cars especially in Austria, where still a number of them is in operation, and in Germany, where they have disappeared by the end of the 1950 decade due to the German tax legislation and to their low velocity. In Great Britain a fleet of about 60 000 grocery and milk delivery vans is on the roads. All these cars operating at a rather low speed have used and still are using normal commercial lead-acid batteries with flat or tubular plates. At the end of the 1960ies, when new techniques of low loss high power electronics were made available, the development of new lead-acid batteries started in different countries which resulted in batteries having higher energy and power density, lower maintenance and better control during operation.

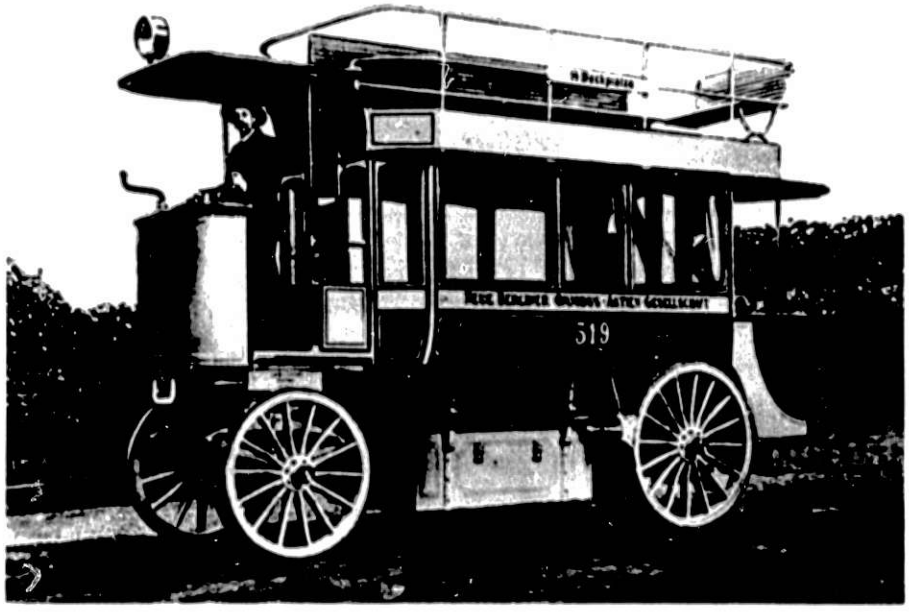

Fig. 1: Berlin bus 1905

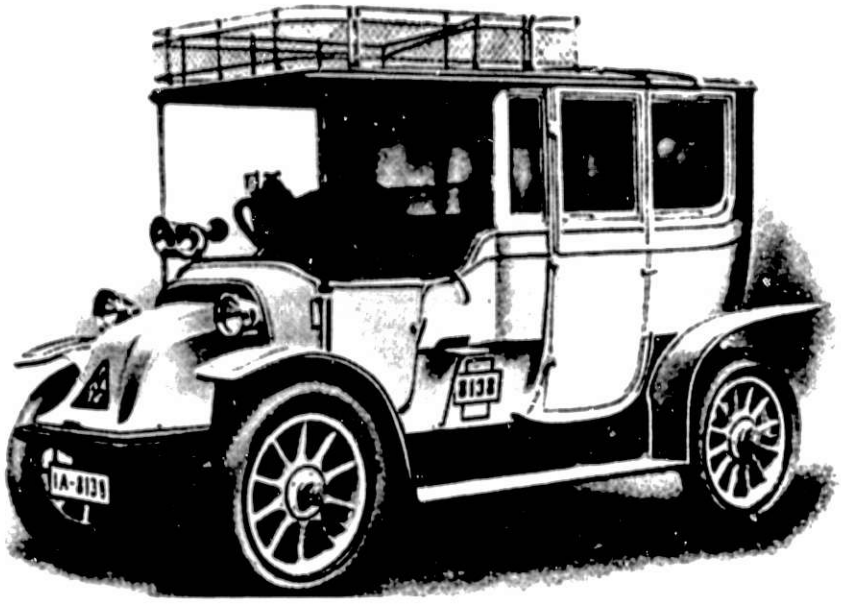

Fig. 2: Berlin taxi 1904

ELECTRIC VEHICLE PROJECTS IN WESTERN EUROPE

The different projects on e.v. currently underway in Western Europe are summarized in tables 1 - 3. In France there are two projects using batteries of FULMEN (table 1), one bus project for testing two prototypes and one transporter project running with 60 models in 1975. Great Britain, besides its 60 000 delivery vans, has a number of buses as well as passenger cars in operation. The lead-acid batteries used are made by CHLORIDE and LUCAS. As in France the battery mostly is installed in the car or on a trailer. The City Taxi of LUCAS only uses a battery exchange technique (table 2). This technique is predominand in Germany as can be seen from table 3. It is applied to buses and transporters as well. Batteries in this country are made by VARTA and also by W. HAGEN and HOPPECKE.

The philosophy of developing and applying battery powered vehicles has often been discussed at length (1) - (5). There is no need to repeat the arguments alleged. It should be pointed out, however, that from our present state of knowledge and experience the economics are of high priority. The engineer engaged in the development of e.v. lead-acid batteries is forced to raise the question whether a decrease of costs rather than an increase on energy density should have preference.

Table 1

Electric Vehicle Projects in France

vehicle	developed in co-operation of	status	number of vehicles 1975	additional planned	battery type	batteries by	system	mode of operation	sponsor
Sovel-Bus	EDF-Sovel	proto-type	2		lead-acid (improved)	FULMEN	battery installed	rush hour peak looping	EDF
Grégoire	EDF	field test	60	1978 = 200	lead-acid 40 Wh/kg flat plate	FULMEN	battery installed	service-vehicle city-traffic	EDF (GES)

Table 2

Electric Vehicle Projects in Great Britain

vehicle	developed in co-operation of	status	number of vehicles 1975	additional planned	battery type	batteries by	system	mode of operation
Silent-Rider City Bus	Chloride, Selnec Greater Manchester Transport	proto-type	2	20	lead-acid 36 Wh/kg tubular	Chloride	battery installed	rush hour 4/5 h peak looping
Lucas City Bus		proto-type	2		lead-acid 40 Wh/kg flat plate	Lucas	battery installed	rush hour 4/5 h peak looping
Leyland City Bus		proto-type	1		lead-acid (improved) flat plate	Chloride	battery on trailer	rush hour 4/5 h peak looping
Lucas Taxi		proto-type	1		lead-acid 40 Wh/kg flat plate	Lucas	battery exchange	city traffic
Enfield Passenger-car		field test	10		lead-acid 40 Wh/kg flat plate	Golf-Batt.	battery installed	city traffic

Table 3

Electric Vehicle Projects in Germany

vehicle	developed in co-operation of	status	number of vehicles 1975	additional planned	battery type	batteries by	system	mode of operation	sponsor
MAN-Bus	GES, MAN, VARTA, Bosch, Siemens	field test	20		lead-acid 33 Wh/kg tubular	VARTA	battery exchange	16 h/day	GES, North Rhine Westphalia
Daimler-Benz OE 305	GES, Daimler, VARTA, Bosch, Siemens	proto-type	2	1977 = 20	lead-acid 33 Wh/kg tubular	VARTA	Hybrid battery Diesel	16 h/day (full service)	GES
Daimler-Benz OE 302 Duo-Bus	Dornier, Daimler, Bosch, VARTA	proto-type	1	1977 = 6	lead-acid 33 Wh/kg tubular	VARTA	Hybrid battery overhead line	16 h/day (full service)	BMFT: 7,6 Mio VARTA: 0,75 : 50%
Daimler-Benz LE 306 1 t-Transporter	GES, Daimler, VARTA, Bosch, Siemens	field test	30	1977 = 80	lead-acid 40 Wh/kg	VARTA W. Hagen Hoppecke	battery exchange	service-vehicle 5 – 8 h/day	GES
VW-Transporter 0,75 t	GES, VW, VARTA Bosch, Siemens	field test	40	1977 = 50	lead-acid 40 Wh/kg	VARTA W. Hagen Hoppecke	battery exchange	service-vehicle 5 – 8 h/day	GES

BATTERIES DEVELOPED FOR E.V.'S

As already mentioned the aims of the development work on new lead-acid e.v. batteries during the last seven or ten years have been to improve the energy density and to reduce the maintenance by introducing more sophisticated control systems. The electrodes used are of the well-known flat plate or tubular plate design. New ideas did not appear on the scene.

The highest energy density of lead-acid e.v. batteries obtained by 1975 is around 40 Wh/kg at the 5 hrs rate. Although there is very little information on how this increase by more than 10 % was achieved, it can be concluded from general knowledge that this progress partially was possible by reducing drastically the weight of the inert materials, such as top lead, cell container etc. As is known from SLI batteries the application of the cast on strap (COS) technique and through the partition (TTP) connectors in combination with cell containers of polyethylene is very successful. As can be seen from fig. 3 FULMEN has used the TTP connectors for individual cells made from blow-molded polyethylene (6). A so-called monobloc 6 cells arrangement based on this principle is shown in fig. 4. Eight of these monoblocs (96 V, 180 Ah 5 hrs) are forming the battery for the CGE Grégoire electric car (7). VARTA made use of the COS technique in combination with flexible copper connectors and blow-molded polyethylene jars as shown in fig. 5. This 360 V, 455 Ah (5 hrs) battery is the power source for the MAN buses (8). Both methods are effecting favourable the internal resistance and the discharge voltage of batteries which again is a contribution to a higher energy density.

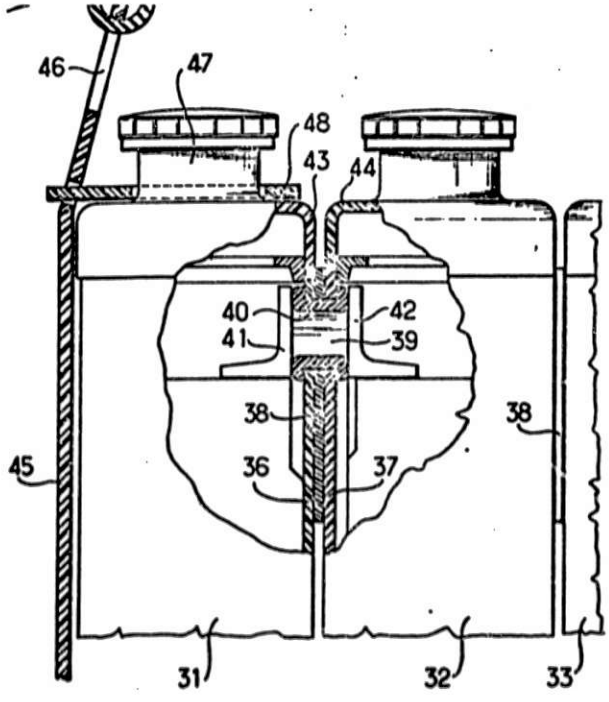

Fig. 3: FULMEN TTP connector

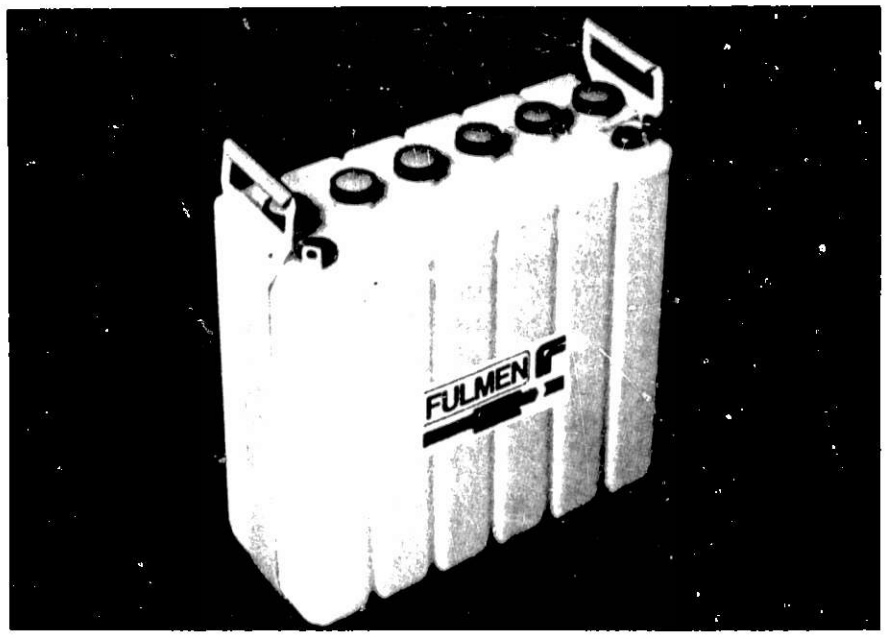

Fig. 4: FULMEN 12 V monobloc

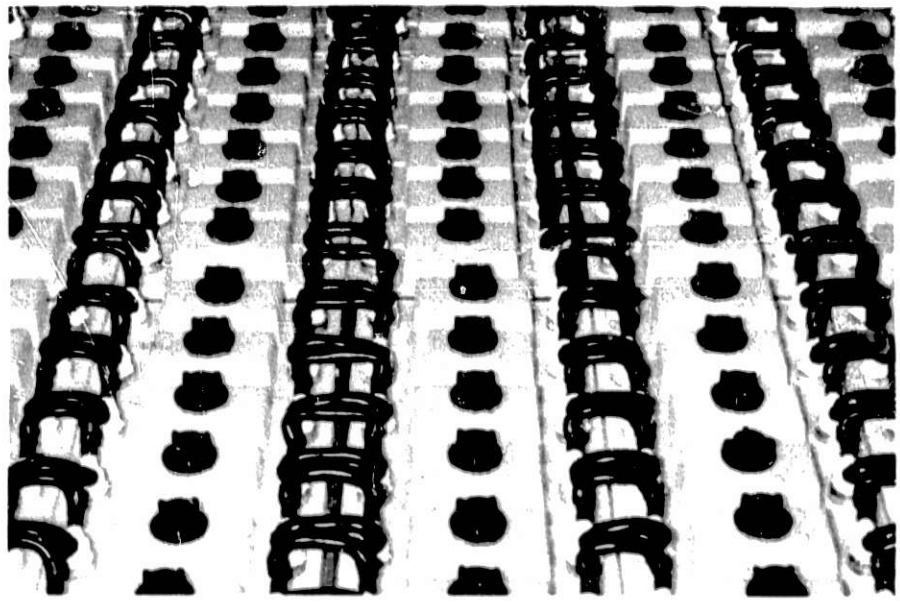

Fig. 5: VARTA flexible Cu connector "Polflex"

Apart from the reduction of inert material weight there must also have taken place an improvement of active material utilization, an optimal choice of the amount and density of the electrolyte as indicated by FULMEN (7) and a reduction of grid weight. It is self-evident that no company has made any detailed publication on these highly confidential items. However, the old rule of battery engineers: the less lead spent for a given amount of energy the shorter the cycle life and vice versa, seems to be still valid.

To clarify the situation, typical and estimated data for conventional and new cells are summarized in table 4 (cf. (9)). In this summary are also included estimated data which might give an indication of the potential capability of the lead-acid system. It is considered that an energy density of 45 to 50 Wh/kg at the 5 hrs rate will be a reasonable upper limit for a lead-acid cell still having a life of several hundred cycles.

Table 4

Detailed data on the lead-acid system (5 hrs rate)

	conventional traction cell	modern e.v. cell (estimates)	estimated limit of lead-acid system
pos. act. material g/Ah	14	10	8 - 7
neg. act. material g/Ah	13	10	8 - 7
acid g/Ah	13	12	11 - 10
pos. grid g/Ah	10	7	7 - 6
neg. grid g/Ah	8	6	6 - 5
top lead g/Ah	5	2	1 - 1
container separator g/Ah	7	5	3 - 3
total, g/Ah	70	52	44 - 39
medium discharge voltage, V	1.92	2.0	2.0
energy density Wh/kg	27	38	45 - 51

The maintenance of a lead-acid battery primarily consisting of controlling the electrolyte level and watering a number of cells is of importance for the capacity and for the life of the battery as well. A constant electrolyte level and as a consequence a constant electrolyte concentration is maintained, for instance, by an automatically working central watering system developed by VARTA (10). Each individual plug is equipped with a float-gauge consisting of a soft rubber tube which is closed or opened by more or less bending as soon as the electrolyte level deviates from normal. The choice of material for the soft rubber tube is critical because of the aggressive conditions in the cell. The plug configuration is shown in fig. 6.

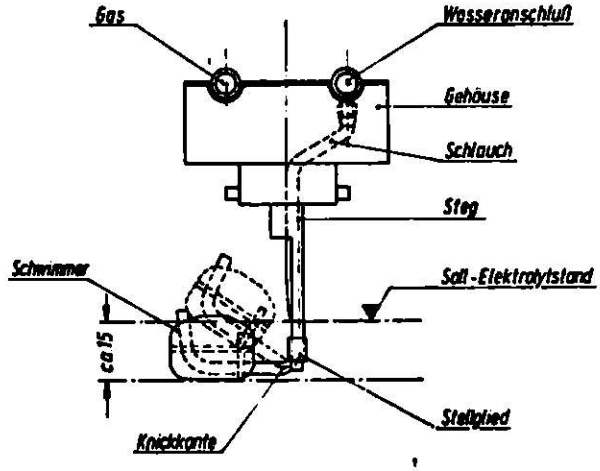

Fig. 6: VARTA watering system

Each plug is connected to a tube system which automatically is coupled up to a water resevoir as soon as the battery is moved into the charging station. The arrangement of the tube system can be seen from fig. 7. It may also be noticed that this battery carries an additional system of tubes which are provided for the degassing of the battery to the outer atmosphere thus avoiding the accumulation of highly explosive amounts of hydrogen/oxygen mixtures.

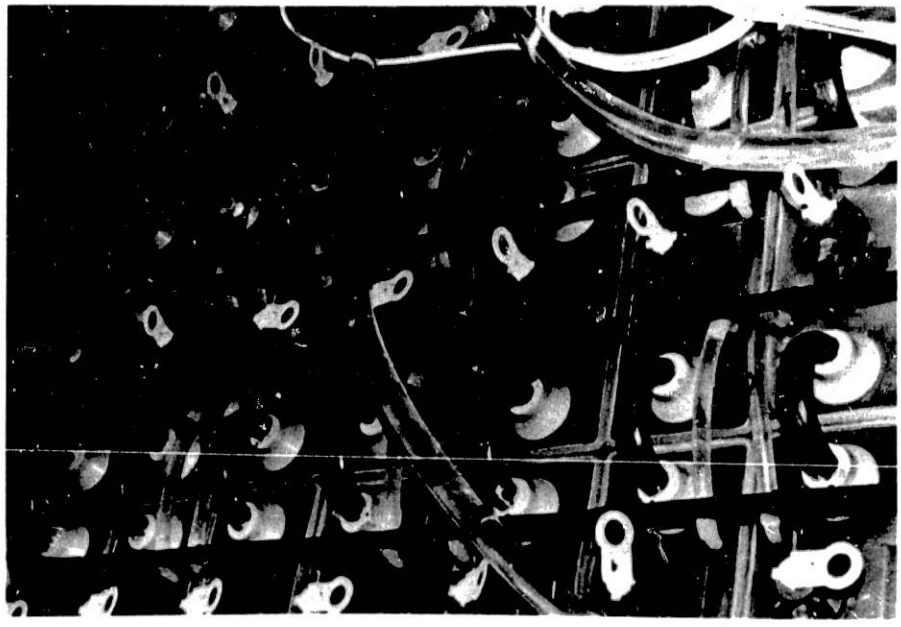

Fig. 7: VARTA watering and degassing system

An automatic watering system has also been developed by CHLORIDE (16) for the Silent-Rider bus battery. The supply of topping up water is controlled by the principle of increasing air pressure in the cell as the electrolyte level rises.

Another possibility to reduce water loss is the use of low antimonial alloys as grid material. LUCAS has applied this principle in her new e.v. battery (11). It seems that such batteries are in use in the bus as well as in the taxi cab project promoted by LUCAS (12), (13).

Heavy duty batteries as they are in use in buses may suffer from heat development. Temperatures of 80° C and more have been measured. High temperatures are disadvantageous for the battery life. Cooling, therefore, will be of beneficial effect. A cooling system has been developed by VARTA for the 360 V, 455 Ah MAN bus battery already mentioned. Each individual cell is equipped with a cooling circle consisting of a plastic tube the terminals of which are visible in fig. 8. In the multi-cell battery all these tubes are connected to a central heat exchanger which is able to remove 3 kW of heat (14). The system is shown in fig. 9. It is evident that the peripheric equipment described must be added to the debit of the energy density of the whole battery system. Therefore, and also because of the higher costs, the application of such heavy duty battery system is justified only in big electric vehicles.

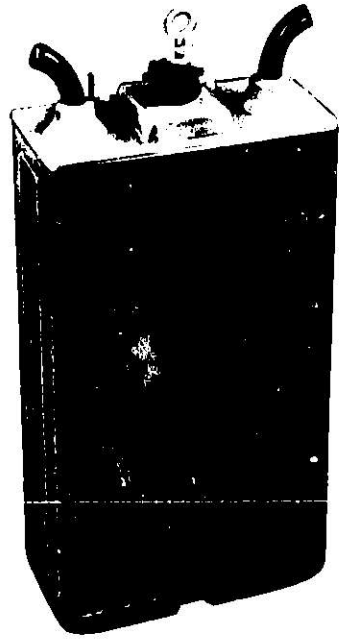

Fig. 8: VARTA heavy duty e.v. cell with cooling equipment

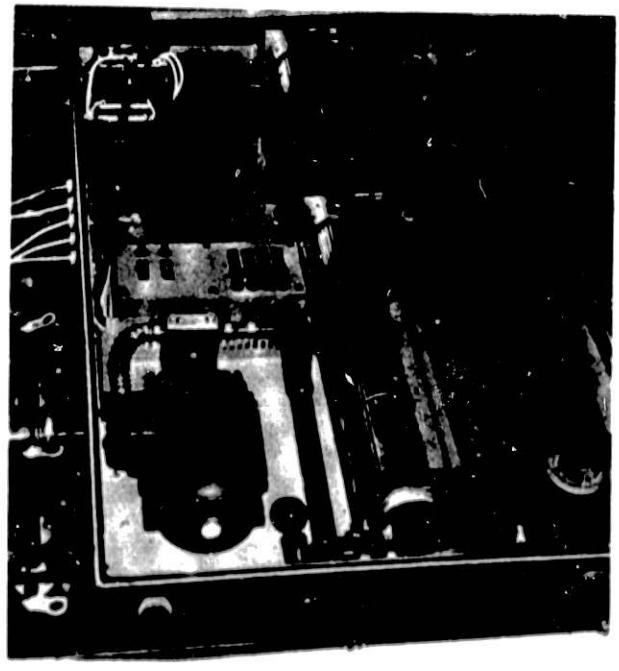

Fig. 9: Heat exchange of MAN bus battery

A simple watering and degassing device, however, may be of value already in medium duty batteries as shown in fig. 10. As is known from published data (15), (8) the energy density decreases from 31.4 Wh/kg of a single cell to 26.9 Wh/kg of the total battery system all accessories included.

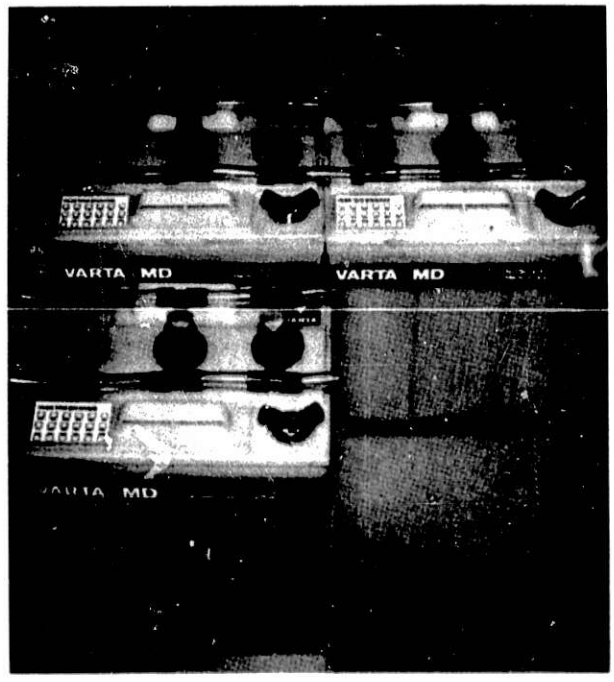

Fig. 10: VARTA medium duty batteries with central watering and degassing system

A proper charging method may also significantly contribute to battery life and reliability. On the other hand quick charge very much effects the economic efficiency. As an example how this problem can be solved the CHLORIDE "Programmed Rate of Rise of Voltage" (PRV) charger should be mentioned (16). This charger is capable to recharge the Silent-Rider battery (cells with tubular plates) of 330 Volts, 329 Ah within 3,5 hrs.

TESTING OF E.V. BATTERIES

The laboratory testing of lead-acid e.v. batteries mainly is restricted to capacity and cycle life testing. Standard specifications are not known so far. It seems, however, that capacity and cycle life testing as well at 2,5 x I_5 A are now preferred which roughly is equal to the 1,5 hrs rate. The average energy at this rate is about 67 to 75 % of the 5 hrs rate energy depending on the cell design. The product of energy per cycle and number of cycles is equal to the integrated energy the battery is able to deliver during its

lifetime. The value of the integrated capacity is of importance for economic considerations.

CONCLUSIONS

In a variety of e.v. projects in France, Great Britain and Germany the behaviour of new lead-acid batteries is evaluated. At present systems other than lead-acid are not on the road. It has been possible to increase the energy density of lead-acid cells from 25 - 28 Wh/kg to 30 - 40 Wh/kg, the life ranging from 500 to 1600 cycles. Maintenance of batteries may considerably be reduced by special peripheric installations such as automatic watering devices, cooling and proper charging methods. It is expected and partially it has already been demonstrated that these battery systems are capable to supply sufficient power to electric vehicles for city transport.

REFERENCES

(1) G. Wilke et.al., Denkschrift Elektrospeicherfahrzeuge, ed. Deutsche Forschungsgemeinschaft, Wiesbaden, 1970

(2) H. Niklas, Status Report on Electric Vehicles and their Batteries in West Germany, 85th BCI Convention San Francisco, May 1973 p. 109

(3) Diff. Authors, Elektrotechnische Zeitschrift, Ausgabe A, 94 (1973), p. 617 - 712

(4) H.G. Müller et.al., Elektrisch angetriebene Kraftfahrzeuge, Studie der Gesellschaft für elektrischen Strassenverkehr mbH (GES), Düsseldorf, 1973

(5) R.L. d'Arcy, Ein systematisches Batteriekonzept für Elektrofahrzeuge in "Elektrizitätsverwertung" 7/8 (1974)
Konzepte für Fahrzeug-Antriebsbatterien, in "Elektrotechnische Zeitschrift" b 27 (1975), p. 97 - 99

(6) B. Gicquel, A. Mensvier, French Patent 7317006 (FULMEN), 10.5.1973

(7) FULMEN leaflet "The Electric Vehicle", 1974

(8) VARTA leaflet "VARTA Blei-Batterien für Elektrofahrzeuge", No. 12301

(9) H. Bode, Energiequellen, in Denkschrift Elektrospeicherfahrzeuge, ed. Deutsche Forschungsgemeinschaft, Wiesbaden, 1970, p. 96

(10) VARTA leaflet "VARTA Peripherie-Systemspeicher für Elektro-Strassenfahrzeuge", No. 12306

(11) LUCAS traction cells, in Lead Power News, Nov. 1975, p. 6

(12) LUCAS, A description of electric vehicles (1975 ?)

(13) LUCAS News, October 1975 "Hail the electric taxi ...!"

(14) N.N., How Mönchengladbach organises its battery buses, in Lead Power News, April 1975, p. 2

(15) VARTA leaflet "VARTA Fahrzeug-Blei-Akkumulatoren", No. 12302

(16) CHLORIDE publication, Silent-Rider a project for city centre transport

HIGH-TEMPERATURE BATTERIES

by

Elton J. Cairns and John S. Dunning
Research Laboratories, General Motors Corporation
Warren, Michigan 48090

ABSTRACT

The state of the art for high-temperature batteries will be presented and discussed. Emphasis will be given to the lithium alloy/metal sulfide and sodium/sulfur cells. Other systems to be considered include lithium/chlorine and sodium/metal halide. Cell chemistry and performance and life-limiting factors will be reviewed for all of the systems, and the status of investigations in critical problem areas will be given. Recent advances in the demonstration of high specific energy and expectations for future improvement will be presented.

INTRODUCTION

The current awareness of the developing shortage of inexpensive sources of energy has given new impetus to the search for and development of means for making more effective and more efficient use of the energy sources and energy conversion systems that we possess. The most rapidly-growing sector of our energy economy is that of electrical energy generation. Fortunately, we possess the capability of generating electrical energy from a wide variety of primary fuels, including coal and nuclear fuel, which are in much larger supply in the United States than petroleum. In order to more effectively utilize our electrical energy system, it is important to have an efficient, flexible, economical means of storing off-peak electrical energy for later use during peak demand periods. In addition, the demand for petroleum could be reduced by the use of rechargeable batteries as a power source for automobiles.

The performance, lifetime, and cost goals for the battery applications mentioned above tend to exclude all of the presently-available batteries, and many proposed batteries. The class of batteries which is projected to have the best combination of performance, life, and cost for large-volume application in multikilowatt sizes is that of high-temperature batteries, which are being developed to meet the following general goals:

	Peak Specific Power (W/kg)	Specific Energy* (W·h/kg)	Minimum Cycle Life	Minimum Lifetime (yr)	Cost ($/kW·h)
Off-peak energy storage	15-50†	100-200†	1000-2000	5	20
Automobiles	200	200	500-1000	3	20

† not very important for this application

* at 50 W/kg

Of course, only those systems using abundant materials can be considered for widespread use.

In the field of high-temperature cells, there are two types of electrolytes in use: molten salts (almost exclusively alkali halides), and solids (almost exclusively sodium-ion conductors). Nearly all of the cells with molten-salt electrolytes use lithium as the reactant at the negative electrode (usually as an alloy) because other candidate reactants are relatively soluble in their molten salts. All of the cells with solid electrolytes use sodium as the negative electrode reactant because the only solid electrolytes of adequate conductance for a low electronegativity metal conduct only sodium ions. The positive electrode reactants are elements of high electronegativity and low equivalent weight, or compounds containing them. These conditions result in the focusing of effort on the following systems: lithium/alkali halide/metal sulfide (or sulfur), sodium/solid electrolyte/sulfur, sodium/solid electrolyte/metal halide, lithium-aluminum/alkali halide/carbon-$TeCl_4$, and lithium/alkali halide/chlorine.

In the sections that follow, the systems just listed will be discussed, with emphasis on current status (based on the latest publicly available information) and problems remaining to be solved.

LITHIUM/METAL SULFIDE CELLS

The current efforts on lithium/metal sulfide cells evolved from earlier work on lithium/sulfur cells,[1-3] which experienced gradual loss of sulfur from the positive electrode and a corresponding decline in capacity. The use of a sulfur compound such as FeS_2, FeS, or Cu_2S reduces the solubility of sulfur-bearing species in the electrolyte, and provides for greatly improved stability of operation without capacity loss,[4-6] at the expense of cell voltage (tenths of a volt) and lower specific energy. (Compare the values in Table I to 2600 W·h/kg for Li/S.)

Table I. PERFORMANCE SUMMARY - HIGH TEMPERATURE BATTERIES

System	Theoretical Specific Energy W·h/kg	Operating Temperature °C	Small Cell Tests (<20 A·h)					Large Cell or Battery Tests (>20 A·h)			
			Capacity Density & Current Density A·h/cm² @ A/cm²		Peak Power Density W/cm²	Cycle Life	Lifetime h	Specific Energy W·h/kg*	Specific Power W/kg*	Cycle Life	Lifetime h
Li/LiCl-KCl/FeS_2	1321	400-450	0.4	0.4	1.4	92	300	-	-	115	617
Li/LiCl-KCl/FeS	869	400-450	-	-	-	-	-	-	-	-	-
Li-Al/LiCl-KCl/FeS_2	650	400-450	0.65	0.64	(1.0)	300	6400	80-150	8-80	300	6400
Li-Al/LiCl-KCl/FeS	458	400-450	0.75	0.064	0.8	(300)	(5000)	70-85	8-150	121	3700
Li-Si/LiCl-KCl/FeS_2	944	400-450	-	-	-	-	-	-	-	-	-
Li-Si/LiCl-KCl/FeS	637	400-450	-	-	-	-	-	-	-	-	-
Na/β-Al_2O_3/S*	758	300-400	1.7	0.16	0.3	-	-	77	154	N.A.	N.A.
Na/β-Al_2O_3/S**	521	300-400	-	-	-	-	-	-	-	-	-
Na/β-Al_2O_3/Na_2S_{3-2}***	308	300-400	-	-	-	8500	10000 (1000 A·h/cm²)	-	-	-	-
Na/β-Al_2O_3/$NaAlCl_4$-M_xCl_y	792-1036	210	0.4	0.015	0.375	>200	5000 (>60 A·h/cm²)		-	-	-
Li-Al/LiCl-KCl/C-$TeCl_4$	N.A.	400	-	-	-	200	-	60-80	468	100	288
Li/LiCl-KCl-LiF/Cl_2	2167	450	0.33	1.05	~2.8	325	650	277**	230**	210	668

* Reaction to Na_2S_3

** Reaction to Na_2S_{3-7}

*** Reaction in the single phase region Na_2S_{3-7} + Na_2S_3

† Excluding weight of thermal insulation

†† Excluding weight of case, insulation, and Cl_2 storage

Introduction of a metal sulfide in place of sulfur modifies the chemistry of the cell reactions. For the Li/LiCl-KCl/FeS cell, the predominant discharge reactions and corresponding potentials (*vs.* Li) are:

$$4Li + 3FeS_2 \rightarrow Li_4Fe_2S_5 + FeS \quad 2.1\ V \qquad (1)$$

$$2Li + Li_4Fe_2S_5 + FeS \rightarrow 3Li_2FeS_2 \quad 1.9\ V \qquad (2)$$

$$6Li + 3Li_2FeS_2 \rightarrow 6Li_2S + 3Fe. \quad 1.6\ V \qquad (3)$$

The theoretical specific energy for these cell reactions is 1321 W·h/kg, about half that for the Li/S cell, largely because of the weight of the Fe.

Each of the above reactions is associated with a plateau in the voltage-capacity curve for the cell, as shown in Fig. 1. Reaction 1 is associated with the upper plateau, Reaction 2 with the small second plateau, and Reaction 3 with the longer plateau near 1.6 V. All of the compounds in Reactions 1-3 have been identified in the electrodes of cells that had been cycled and then examined at the appropriate state of charge.[7,8] It is difficult to return to the fully charged state in which only FeS_2 is present, but little loss of capacity is evident. Even though the reactions above appear to be rather complex, FeS_2 electrodes have demonstrated stable operation for extended time periods.[9]

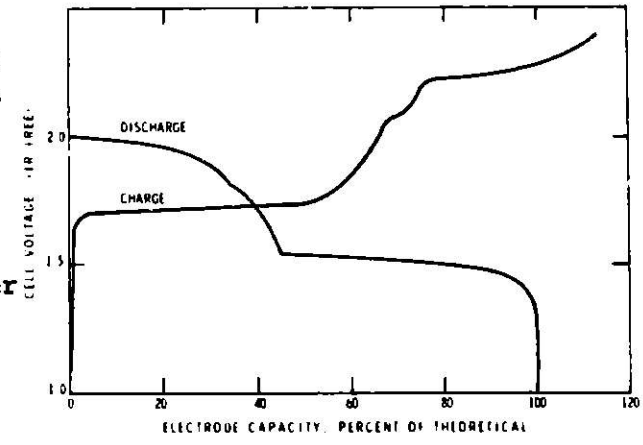

Fig. 1. Voltage-capacity curve for a Li/FeS_2 cell.

Another cell under investigation makes use of FeS in the positive electrode. The most commonly used electrolyte with FeS is the LiCl-KCl eutectic. For the Li/LiCl-KCl/FeS cell, the reactions appear to be:

1st Discharge

$$2Li + FeS \rightarrow Li_2S + Fe \qquad (4)$$

Recharge

$$8Li_2S + 8Fe + 2KCl \rightarrow K_2Fe_7S_8 + Fe(?) + 2LiCl + 14Li \qquad (5)$$

$$K_2Fe_7S_8 + Fe(?) + 2LiCl \rightarrow 8FeS + 2KCl + 2Li \qquad (6)$$

The leftover iron in Reaction 5 has not been found conclusively, but has been included in the reactions to preserve the 1:1 ratio of iron and sulfur. The compound $K_2Fe_7S_8$* has been identified in large amount in electrodes from cycled cells.[8,9] Reaction 6 only proceeds with some difficulty, and $K_2Fe_7S_8$ probably is the major reactant at the positive electrode of the Li/LiCl-KCl/FeS cell after the initial discharge. The voltage-capacity curve for this cell is characterized by a single, flat plateau at 1.5-1.6 V. It is interesting that $K_2Fe_7S_8$ is not an important phase in the FeS_2 electrode, and that Li_2FeS_2 is not important in the FeS electrode (with LiCl-KCl

* The exact formula for this compound is in doubt, but this is the best available.

electrolyte). The theoretical specific energy of the Li/FeS cell is 869 W·h/kg. Improvements in stability of operation can also be obtained with other metal sulfides, such as Cu_2S,[6] NiS,[8] CoS,[8] and $CuFeS_2$,[8] but the theoretical specific energies for these Li/MS cells are lower than for Li/FeS_2 cells, and these materials are more expensive than FeS_2 or FeS.

Liquid lithium electrodes have not been as stable as desired, because of capacity loss related to both physical and chemical losses of lithium from the electrode.[10] The physical losses are caused by a lack of sufficient wetting of the current collector during recharge, and inadequate wicking of the deposited lithium into the current collector. Various additives to the lithium have been evaluated in an attempt to improve the wetting and wicking properties of the lithium electrode. Chemical losses of lithium from open cells with LiCl-KCl electrolyte have been experienced because of the displacement reaction

$$Li + KCl \rightarrow K + LiCl \qquad (7)$$

and the evaporation of potassium. The rates of both of the above losses have been reduced significantly by the proper choices of current collector materials (nickel, stainless steel, low carbon steel), additives (e.g., copper, zinc), and the use of sealed cells or potassium-free electrolytes (to avoid the potassium-loss mechanism). Even so, further work is necessary before liquid lithium electrodes are acceptable for stable, long-lived cells.

As an alternative to the liquid lithium electrode, the solid lithium-aluminum alloy electrode has been investigated, and shows good stability, at the cost of a lower cell voltage (by about 0.3 V over a large composition range, ∿7 a/o to 45 a/o Li) and a greater weight (about 80 w/o of the fully charged electrode is aluminum).[11,12] Compare the theoretical specific energies of corresponding cells in Table I with lithium and lithium-aluminum electrodes, which show a loss of 50%. In addition, some of the lithium in the lithium-aluminum alloy is not available at reasonable current densities (20-30% unavailable at 0.1 A/cm^2) in contrast to the liquid lithium electrode which exhibits essentially 100% utilization. The best operation of these electrodes is found at an electrolyte volume fraction of 0.2 in the electrode.

Solid lithium-silicon is also under investigation as a negative electrode,[13] and at a composition of Li_4Si, shows a significant weight advantage over LiAl, as indicated by the theoretical specific energy values in Table I. Since silicon is not as good an electronic conductor as aluminum, a more elaborate current collector probably will be required for Li_4Si. Voltage plateaus were found at 48, 158, 280, and 336 mV *vs.* Li at 400°C, in locations consistent with the existence of compounds of the following stoichiometries: Li_5Si, $Li_{4.1}Si$, $Li_{2.8}Si$, and Li_2Si. No information was presented concerning the ability of the electrode to support current. Lithium-boron alloys have also been investigated,[9,14] and are able to support high discharge current densities (up to 8 A/cm^2) at 500°C in LiCl-KCl. Performance is much poorer at lower temperatures. Little information is available on recharge characteristics or cycle life,[9] but it appears that it is difficult to remove lithium from the composition LiB_2.

The scaleup and engineering efforts on lithium-aluminum/iron sulfide cells have progressed to the point of performance and cycle-life measurements on lightweight cells of about 100 A·h capacity,[8,9,11] of the design shown in

Fig. 2. These cells have typically been operated at current densities in the range 0.04 to 0.25 A/cm^2, corresponding to complete discharge in 4 to 24 h, which is in the range of interest for off-peak energy storage. The cell weights have been near 1 kg, corresponding to a specific energy of 100 to 150 W·h/kg (see Table I and Fig. 2). Repeated cycling of these cells has shown the capacity retention to be good. Lifetimes of more than 3000 h have been demonstrated for these lightweight Li-Al/LiCl-KCl/FeS_2 cells.[9] In tests involving heavier cells with larger amounts of electrolyte, lifetimes as long as 6400 h have been achieved.[12] Prismatic cells, of vertical orientation with similar capacities (∿100 A·h) are also being developed.

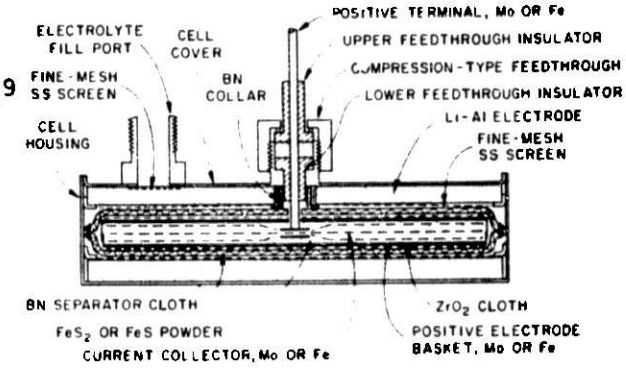

Fig. 2. Lightweight Li-Al/MS cell design. Cell diameter ∿13 cm, weight 1-1.7 kg.[9]

The factors which are serving to limit the performance of Li-Al/FeS and Li-Al/FeS_2 cells include swelling of the positive electrode (especially of the FeS cells) which accompanies discharge of the cell. The swelling of the FeS electrode has been associated with the formation of $K_2Fe_7S_8$. Prevention of the formation of this phase by elimination of potassium from the electrolyte should reduce the amount of swelling.

Incomplete utilization of the FeS or FeS_2 has been a problem, and is at least partially caused by inadequate current collection within the positive electrode. The use of CoS_2 (or CoS) improves the electronic conductivity of the active material,[15] reducing the current collector requirement so that 40-60% utilization can be obtained at 0.1 A/cm^2, and 415°C. It has also been found that CuS added to FeS (in amounts near 40 w/o) improves the utilization of the active material,[9] and probably reduces the extent of formation of $K_2Fe_7S_8$, (and perhaps the extent of swelling as well). Further improvement in utilization of the active material is necessary especially at the higher current densities required for automobile propulsion. Values near 70% utilization at 0.4 A/cm^2 and 450°C are desired for this application.

Inexpensive, corrosion-resistant current collectors for FeS and FeS_2 electrodes are needed. Various forms of carbon have been used with some success, but carbon has only a marginally-acceptable electronic conductivity, poor strength, and is not easy to join to other materials. Tungsten and molybdenum have also been used, but they are heavy and expensive. A large number of candidate materials have been evaluated for possible use in Li/S and Li/MS cells, with only a few showing reasonable corrosion resistance, as indicated in Table II.[8,16]

The development of a lightweight, corrosion-resistant feedthrough for sealed cell operation requires an electronic insulator which will remain stable at potentials near that of lithium. Many ceramics have been rejected because they are readily attacked by lithium. The most promising materials currently being investigated are high-purity boron nitride and high-purity aluminum nitride. High-purity BeO is also good but poses a health question. Yttria and some double metal oxides may prove to be acceptable (e.g., $CaZrO_3$,

Table II. COMPATIBILITY OF PROSPECTIVE POSITIVE ELECTRODE MATERIALS IN LITHIUM/IRON SULFIDE CELLS

Material	Positive Electrode	Results of Corrosion Tests or Cell Tests
Mo	FeS_2, FeS	Little or no attack of properly prepared material
W	FeS_2	
C, Graphite	FeS_2, FeS	
TiN, FeB Coating on Fe	FeS_2	
Fe	FeS	Moderate attack or dissolution
Ni	FeS	
Fe	FeS_2	Severe attack or dissolution
Ni	FeS_2	
Cu	FeS	
Nichrome	FeS_2	
Nb	FeS_2	

$MgAl_2O_4$), but more work remains in this area. Bonding techniques are required for the most compact feedthroughs. The conductor of the feedthrough which operates at positive electrode potential must resist oxidation at these high potentials, and must be joined with low resistance to the electrode. The most popular materials for this use are molybdenum and tungsten. Molybdenum is attacked slowly, and both metals are heavy. At present, mechanical feedthroughs are commonly used, tut they leave something to be desired in terms of size, weight, and leak rate.

Next in importance to the improvements in the positive electrodes indicated above are better separators. Boron nitride cloth, about 2 mm thick, together with zirconia cloth 1 mm thick has been used most successfully as a separator, preventing contact between the positive and negative electrodes, and helping to retain particles of active material. Thinner, less expensive, and highly corrosion resistant materials are needed for this purpose. Thinner, nonwoven, high purity boron nitride may serve well, if developed. The separator should have very small pores (a few micrometers or less) in order to prevent movement of fine particles of lithium-aluminum, iron, and other solids from the electrodes. It must be thinner (perhaps 1 mm thick) in order to reduce the internal resistance of the cell, and should not be sensitive to air or moisture (for ease in handling and cell assembly). Yttria may be another good candidate. It has shown good stability in preliminary tests, is thermodynamically stable, but is not yet available as a strong, flexible, high-purity cloth or mat.

As a convenience in cell assembly (and as a cost-saving measure), it would be advantageous to develop a simple means for assembling cells in the discharged state (using Fe and Li_2S in the positive electrode) avoiding the need for metallic lithium and the handling of it. Some experiments have been performed on the assembly and startup of discharged cells, with promising results.

The outlook for the continued development of cells with lithium alloy negative electrodes and iron sulfide positive electrodes is good. It is likely that within the next few years, cells can be developed having specific energies approaching 200 W·h/kg at a specific power of 100 W/kg with a life of over 5000 h and 1000 cycles using FeS_2 electrodes, and 140 W·h/kg at a specific power of 60 W/kg and a life of over 5000 h and 1000 cycles using FeS electrodes. The cost will probably continue to be high (compared to $20/kW h) until inexpensive feedthroughs, current collectors, and separators are available. Figure 3 shows a conceptual design for a 43 kW·h, 270 kg Li-Al/FeS_2 battery for electric vehicle propulsion.

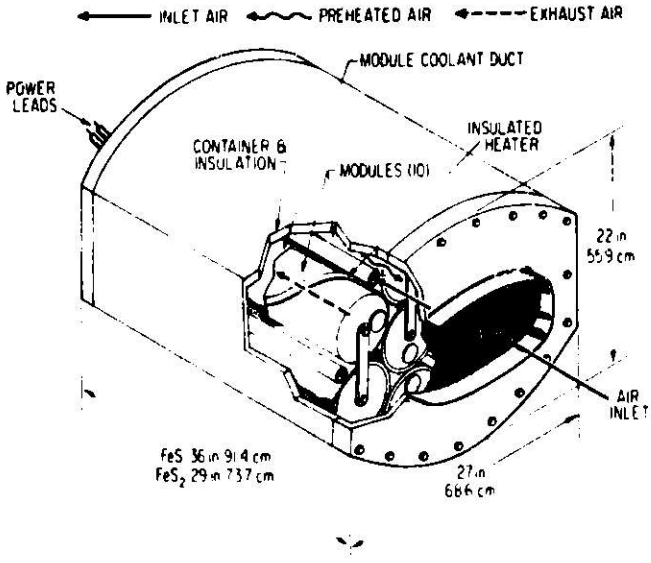

Fig. 3. Conceptual design of an electric vehicle battery using Li-Al/MS cells.[17]

SODIUM/SULFUR CELLS

In 1967, the Ford Motor Company[18] revealed their work on the development of a sodium/sulfur cell with a ceramic, sodium-ion-conducting electrolyte. This cell is appealing because it is very simple in concept: molten sodium separated from molten sulfur by a ceramic electrolyte, penetrable only by sodium ions, as shown in Fig. 4.[19] The cell operates at 300-400°C, sodium serves as its own current collector and a carbon felt serves as the current collector for the sulfur electrode.

The overall electrode and cell reactions are rather simple:

$$2Na \rightarrow 2Na^{+} + 2e^{-} \quad \textit{anode} \quad (8)$$

$$2Na^{+} + 3S + 2e^{-} \rightarrow Na_2S_3 \quad \textit{cathode} \quad (9)$$

$$2Na + 3S \rightarrow Na_2S_3 \quad \textit{overall} \quad (10)$$

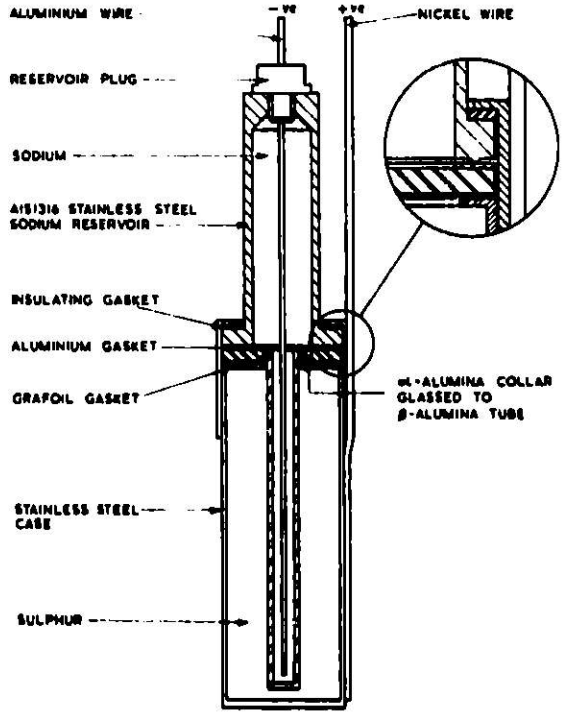

Fig. 4. Conceptual design of a tubular Na/S cell.[19]

The Na_2S_3 is not a compound, but merely the stoichiometry at which the compound Na_2S_2 begins to precipitate from the sodium polysulfide melt at operating temperature. The phase diagram of the Na-S system shows that at 350°C, as the sulfur electrode receives sodium during the discharge reaction, a separate liquid phase, $Na_2S_{5.2}$ forms, causing a voltage plateau at 2.07-2.08 V *vs.* Na, extending from essentially pure sulfur to $Na_2S_{5.2}$. As more Na is added to $Na_2S_{5.2}$, the voltage declines through a single-phase region, until the composition Na_2S_3 is reached, at which point Na_2S_2 begins to precipitate. This is the end of discharge.

The details of the sulfur electrode reactions are rather complex because two sulfur-containing phases and many sulfur-containing species are involved in both chemical and electrochemical reactions. The present state of knowledge of the reactions is as follows.[20] The major species in the polysulfide melt are believed to be $S_4^=$, $S_5^=$, and $S_2^=$ (and not $S_3^=$ or any singly-charged sulfur species), and of course Na^+. The electroactive species are primarily $S_4^=$, $S_5^=$, and $S_2^=$. The overall discharge of a Na/S cell starts with essentially pure sulfur, but very soon a separate polysulfide phase forms, which is believed to be the seat of the electrochemical reactions, and a number of chemical equilibria. The sulfur-rich phase is believed to be involved via reaction with the polysulfide phase. The discharge reactions in the two-phase region ($Na_2S_{5.2}$ and sulfur) are:

Electrochemical reduction of Na_2S_5,[20] via a two-step reaction

$$^-S_3 - S_2^= + e^- \rightarrow {}^-S_3 \cdots S_2^= \qquad (11)$$

$$^-S_3 \cdots S_7^{\prime\prime\prime} + e^- \rightarrow S_3^= + S_2^= \qquad (12)$$

Equilibria among the polysulfides and disproportionation of $S_3^=$ (nonelectrochemical)

$$S_2^= + 2S_5^= \rightleftarrows 3S_4^= \qquad (13)$$

$$2S_3^= \rightarrow S_4^= + S_2^= \qquad (14)$$

The sulfur phase reacts with the polysulfide phase, and is consumed in the process by such reactions as:

$$2S_2^= + S_4 \rightarrow 2S_4^= \qquad (15)$$

$$2S_2^= + S_6 \rightarrow 2S_5^= \qquad (16)$$

$$2S_4^= + S_2 \rightarrow 2S_5^= \qquad (17)$$

The potential of the sulfur electrode remains constant at about 2.075 V *vs.* sodium across this two-phase region of the phase diagram.

After all of the sulfur phase is consumed, the electrochemical reduction of polysulfides continues (with declining potential to about 1.75 V) through the single-phase region extending from $Na_2S_{5.2}$ to Na_2S_3 at about 350°C, according to Reactions 11 and 12 above, and the analogous two-step reduction of $S_4^=$:[20]

$$^-S_2 - S_2^= + e^- \rightarrow {}^-S_2 \cdots S_2^= \qquad (18)$$

$$^{-}S_2\cdots S_2^{=} + e^{-} \rightarrow 2S_2^{=} \quad (19)$$

Reactions 11, 12, 18, and 19 are very fast, with exchange current densities in the 1 A/cm^2 range. When the overall stoichiometry of the polysulfide melt reaches Na_2S_3, Na_2S_2 precipitates, blocking further access of melt to the electrolyte-current collector interface. Normally the discharge process is halted before this occurs.

The recharge process is believed to take place as follows, with the two-electron oxidation of $S_4^{=}$:

$$S_4^{=} \rightarrow S_4 + 2e^{-} \quad (20)$$

followed by the reaction of sulfur with the polysulfide melt:

$$S_4 + 2S_4^{=} \rightarrow 2S_6^{=} \quad (21)$$

$$\text{or} \quad S_4 + 4S_4^{=} \rightarrow 4S_5^{=} \quad (22)$$

When the solubility limit for sulfur in polysulfide is exceeded, a separate sulfur phase is formed. At high current densities, this sulfur phase, being a poor electronic and ionic conductor, blocks further reaction as it is formed on the electrolyte and current collector. One problem in the design and operation of sulfur electrodes is to prevent this blockage by sulfur until the cell is nearly fully recharged. The voltage-capacity curves of Fig. 5 exhibit the behavior just discussed for the end of charge and end of discharge.[21]

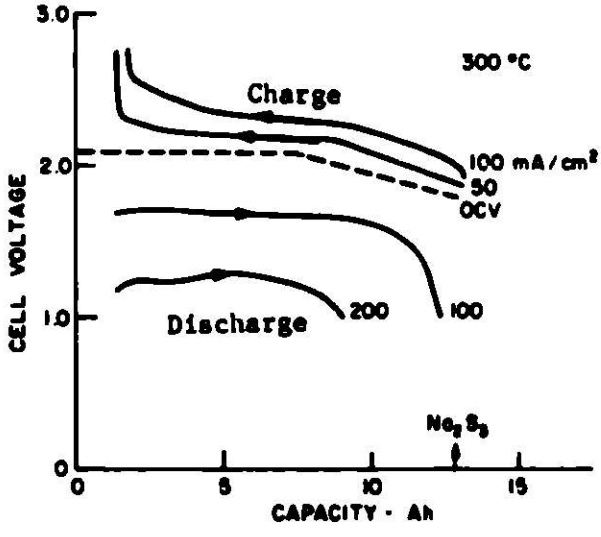

Fig. 5. Voltage-capacity curve for a Na/S cell at 300°C.[21]

The electrolytes which are used in sodium/sulfur cells are ceramics[18-22] or glasses[23,24] which conduct sodium ions. The glass electrolytes have rather low conductivity ($\sim 5\times10^{-4}\Omega^{-1}cm^{-1}$), and must therefore be very thin ($\sim$10 μm) in order to yield a cell with an acceptably low internal resistance. In order to have an electrolyte geometry compatible with a 10 μm thick electrolyte, hollow fibers ($\sim$50 μm, OD) are used (Fig. 6). Thousands of borate glass fibers are bundled together with one end bonded to a low-melting B_2O_3-Na_2O glass "tube sheet," and the other end sealed. Sodium is fed to the insides of the hollow fibers from one side of the tube sheet. Among the fibers on their outsides are sulfur and a metal foil current collector.[23] The glass fibers are operated at a current density of 2 mA/cm^2, and have experienced failure by cracking after a number of charge-discharge cycles, and failure by cracking near the joint with the tube sheet. Thicker fiber walls favor longer cell lives. Recently,[23] glass fiber cells of the 1000-fiber, 0.4-A h size have exhibited lifetimes of up to 3300 h, and cycle lives of 1600 cycles at 10-25% depth of discharge (Na_2S_3 is 100%). Shorter lives are experienced at greater

depths of discharge.

The ceramic electrolytes for sodium/sulfur are composed of Na_2O and Al_2O_3 in varying ratios in the range $Na_2O \cdot 5Al_2O_3$ to $Na_2O \cdot 11Al_2O_3$, usually with small amounts of other oxides such as Li_2O or MgO to stabilize the β" structure[19,21] which is more conductive (3-5 Ω·cm at 300°C) than the β structure[22,25] (20-30 Ω·cm).

The β- and β"-alumina electrolytes (tubular, 1-3 cm OD, 1-2 mm wall, 10-30 cm long) can be prepared by a number of combinations of processing steps, as indicated by Table III. The overall process can be divided into three main steps: powder preparation, green body formation, and sintering. There are a number of options for each of the three main steps, however

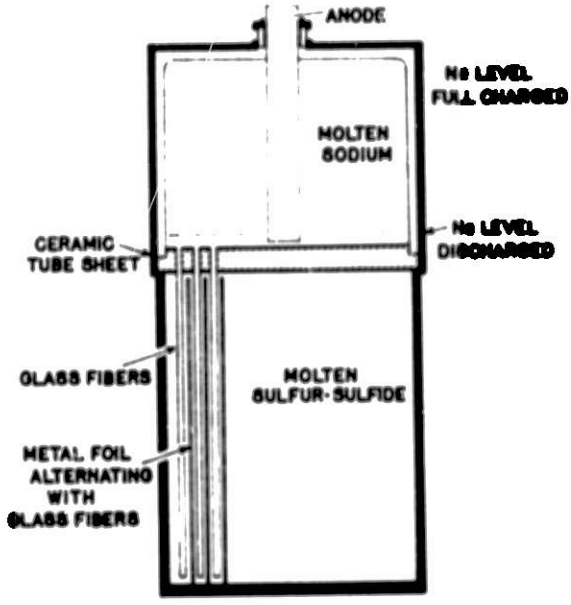

Fig. 6. Design of a hollow-glass-fiber Na/S cell.[23]

Table III. β- AND β"-Al_2O_3 FABRICATION METHODS

Powder Preparation	I	Direct mixing of compounds
	II	Decomposition of salt(s)
	III	Gel
	IV	Spray drying
	V	Complete reaction to β- or β"-Al_2O_3
Green Body Formation	A	Isostatic pressing
	B	Extrusion
	C	Electrophoretic deposition
Sintering Method	1	Encapsulated (in Pt or inert material)
	2	Enclosed with powder (high-temperature sintering)
	3	Zone pass-through

certain combinations of steps have been more popular than others:

IA1 has been used at Ford,[21] British Rail,[19] and others for preparation of β"-Al_2O_3

VC2 has been used by Compagnie Générale d'Electricite[25] and by General Electric[26] for β-Al_2O_3

IA3 has been used by Chloride Silent Power, and is being investigated in the Ford program[21] for β"-Al_2O_3.

Powder preparation by methods II and III is being evaluated in the Ford program, as well as green body formation by method B, extrusion. Each major step

in electrolyte preparation has associated with it a number of important variables that have an influence on the chemical, microstructural and mechanical properties of the final product.

It is beyond the scope of this paper to review the details of β-Al_2O_3 electrolyte preparation, but some information on the major points is appropriate.

Powder Preparation: It is important to have fine-structured, uniformly mixed reactants. This is the objective of methods I-IV of Table III. The compositions favored[21] are in the range 9% Na_2O, 0.8% Li_2O, balance Al_2O_3, from α-Al_2O_3, Na_2CO_3 and $LiNO_3$ starting materials.

Green Body Formation: The emphasis here is to prepare green bodies of optimum density with well-controlled tolerances and good uniformity for subsequent sintering to high density (>96% of theoretical).

Sintering: This may be the most difficult step in the process requiring minimum loss of Na_2O by volatilization at reaction-sintering temperatures in the range 1520-1600°C for a precise time (in the range 1 to 10 min), followed by annealing at a lower temperature (~1400°C for ~8 h) to complete the formation of the β''-Al_2O_3 phase with good conduction (~5 Ω·cm), but grain growth (beyond ~25 μm) is to be avoided for good strength (~1500 kg/cm^2).

Beta-alumina electrolytes have been operated in cells of various shapes and sizes, the most popular being tubular, with electrolytes about 1 cm diameter, and 1-2 mm thick. Various modes of failure of the electrolyte have been observed, the most common being sodium penetration from the sodium side toward the sulfur side, forming "fingers" of sodium which penetrate the electrolyte, eventually causing cracking. At the sulfur side, contamination of the beta alumina by potassium has been troublesome, causing cracking and flaking, as has been the formation of a thin coating of silica on the electrolyte, blocking the electrode reaction. Improvement of the purity and corrosion resistance of the sulfur electrode and housing extends the cell life considerably, as does improvement of the density and strength of the electrolyte.

Cells with two sodium electrodes have demonstrated lifetimes of more than 1000 A·h of charge passed per cm^2 of electrolyte.[21] Carefully prepared Na/S laboratory cells (1-2 A·h size) containing no metals (avoiding iron, manganese, chromium, and silicon contamination) have sustained 600-1000 A·h of charge passed per cm^2 corresponding to 4000-8000 cycles without any loss of capacity, as shown in Fig. 7.[21] However, these cells have been operating only in the single-phase (Na_2S_5 to Na_2S_3) region. This is impractical because it corresponds to a theoretical specific energy of only about 300 W·h/kg, which would probably result in a well-engineered cell of only 60-70 W·h/kg. Some cells with stainless steel containers have shown long lifetimes, but have suffered capacity loss because of silica coating of the electrolyte, and blockage of mass transport in the sulfur electrode because of the formation of solid lumps of iron, manganese, and chromium sulfides. Operation over the composition range S to Na_2S_3 (or nearly so) corresponding to a more attractive theoretical specific energy of 756 W·h/kg has been difficult, especially during recharge, because of problems with segregation of polysulfide and formation of sulfur films on the electrolyte, resulting in capacity loss. Even with these problems, hundreds of cycles have been obtained (Table I), but with declining

capacity. Recent work with specially-shaped graphite current collectors for the sulfur electrode[21] has resulted in higher capacity densities at reasonably high current densities because of the promotion of favorable mass-transport conditions, avoiding the buildup of the products of electrochemical reaction at the electrolyte surface, and providing for the transport of reactant to the surface. Other interesting results include the use of metallic current collectors which are well wetted by polysulfide and not well wetted by sulfur, to promote more complete recharge.[21]

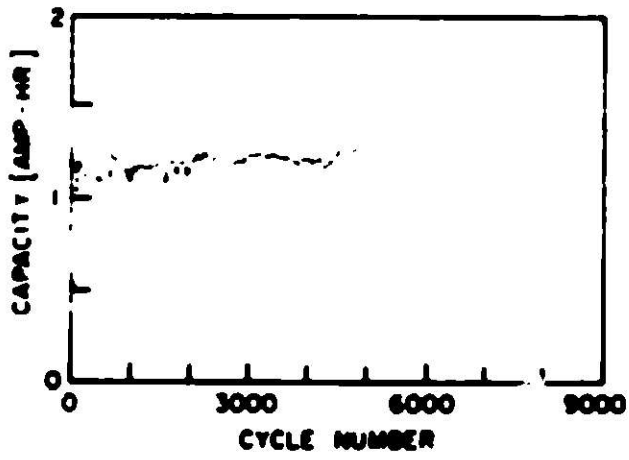

Fig. 7. Capacity-cycle number relationship for a long-lived, metal-free positive electrode $Na/Na_2S_{5.2}$ cell.[21] Discharge current density 250 mA/cm^2, charge current density 125 mA/cm^2.

A few batteries of Na/S cells have been built and operated for relatively short periods of time, demonstrating in small sizes (15 A·h, 11 V, 165 W·h) a specific energy of 77 W·h/kg and a specific power of 154 W/kg exclusive of insulation, etc. A larger battery of 1000 cells[27] yielded 50 kW·h and a power of 20 kW, but with a high total system weight, so that the specific energy and specific power were not very high.[28]

The problems receiving emphasis for the Na/S cell are rather similar to those for the Li/MS cell. Corrosion-resistant metallic materials for use in contact with the sulfur electrode are needed for use as containers and possibly current collectors. A large number of materials have been tested, as shown in Table IV, with only graphite surviving well so far. A number of

[illegible]

Other candidate materials have been identified in static corrosion tests, and await testing in cells. Chromium oxide is an interesting electronic conductor which might be useful as a coating on a stainless steel cell case. Other problems include the need for corrosion-resistant seals and feedthroughs, and improved joining techniques to seal beta alumina to alpha alumina. More work is needed on the operation of cells across the full composition range S to Na_2S_3 at reasonable rates (>0.1 A/cm^2) without capacity loss for at least 1000 cycles. Of course, inexpensive fabrication procedures for the electrolyte are a necessity. As more work is carried out on battery design and operation, cell charge balancing techniques must be worked out, and thermal control methods must be perfected. These latter two areas are important for all high temperature cells.

SODIUM/METAL CHLORIDE CELLS

Another cell which has recently been investigated[30,31] that makes use of a beta alumina electrolyte is the $Na/\beta\text{-}Al_2O_3/M_xCl_y$ in $NaCl\text{-}AlCl_3$ cell, which operates at temperatures near 200°C. During discharge, sodium is transferred to the M_xCl_y compartment which contains $SbCl_3$, $CuCl_2$, $FeCl_3$ or $NiCl_3$ as the reactant. Cells have been assembled using either disk- or tube-shaped electrolyte. Early tests have been confined to relatively small (<10 A·h) laboratory cells of low specific energy. Operating current densities of 20 mA/cm^2 are typical.

Fig. 8. Voltage-capacity curve for a $Na/\beta\text{-}Al_2O_3/M_xCl_y$ cell.[30]

Little information is available on cell performance, other than curves such as those of Fig. 8, which shows a voltage-capacity curve for operation at a constant current of 30 mA (the 18-h rate) for a 0.56 A·h cell.[30] Disk electrolyte cells have achieved 5000 h and 200 cycles of operation whereas tubular electrolyte cells, failing by electrolyte penetration by sodium or by cracking have not yet demonstrated long life.[31] Information on voltage vs. current density has not been publicly available. At this workshop, additional information is expected to be provided.

LITHIUM-ALUMINUM/C-$TeCl_4$ CELL

Investigation and development of the Li-Al/LiCl-KCl/C-$TeCl_4$ cell operating at 475°C have been performed over about the last decade by Standard Oil (Ohio)[32] and more recently by ESB.[33] The negative electrode is 45 a/o Li-Al alloy, as discussed in the Lithium/Metal Sulfide Cells section of this paper. The electrolyte is the LiCl-KCl eutectic in a boron nitride cloth separator, and the positive electrode is a special porous carbon of high specific area, containing $TeCl_4$. The high-area carbon provides for the adsorption of chloride and alkali metal ions:

$$-\overset{|}{\underset{|}{C}} - Cl + e^- \rightarrow -\overset{|}{\underset{|}{C}}\cdot + Cl^- \qquad (23)$$

$$-\overset{|}{\underset{|}{C}}\cdot + M^+ + e^- \rightarrow -\overset{|}{\underset{|}{C}} - M \qquad (24)$$

The $TeCl_4$ adds to the capacity of the positive electrode by means of the following reactions:

$$TeCl_x + xLi^+ + xe^- \rightarrow xLiCl + Te \qquad (25)$$

$$Te + 2Li^+ + 2e^- \rightarrow Li_2Te \qquad (26)$$

The $TeCl_4$ addition yields a flatter voltage plateau at about 2.7 V than is obtained from Reactions 23 and 24. Lightweight, sealed cells having two square, 58 cm negative electrodes between which is a two-sided positive electrode of equal area are now being constructed and tested. A typical voltage vs capacity curve is shown in Fig. 9.

Single cells have yielded specific energies as high as 79 W·h/kg. A 12-cell experimental battery weighing 5.4 kg delivered 264 W·h (49 W·h/kg) at the 2-h rate, and operated for 100 cycles over a period of about 300 h.[32] Currently, single cells are being constructed and tested after a pause in the program.

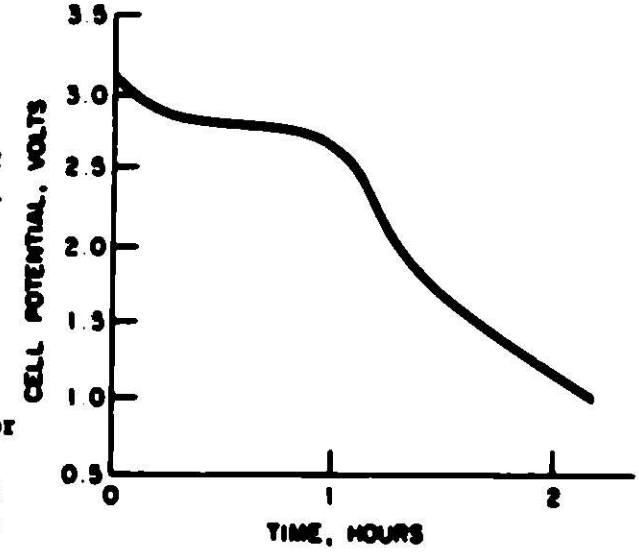

Fig. 9. Voltage-capacity curve for a Li-Al/C-$TeCl_4$ cell.[32] Discharge current: 6 A, area ~150 cm^2.

The problem areas for this cell are similar to those for other high-temperature cells: seals, feedthroughs, and materials, especially for the current collector of the positive electrode (where tungsten and graphite are now being used). An inherent difficulty for this system, because of the low capacity per unit weight of the positive electrode, is the low specific energy (45-60 W·h/kg); however, the high specific power capability is adequate (450 W/kg). It is expected that batteries of these cells will be constructed for testing in fork lift trucks in the future.[33]

LITHIUM/CHLORINE CELLS

Lithium/chlorine cells have been under investigation for over a decade, both as primary and as rechargeable cells. They make use of pure lithium held by capillary forces in a metallic current collector as the negative electrode, a molten LiCl or alkali halide mixture electrolyte, and a porous graphite chlorine electrode. Operating temperatures have been near 650°C, but have been reduced recently to 450°C.[34] The mixed alkali halide electrolyte which

has permitted the temperature reduction is 19 m/o LiF-66 m/o LiCl-15 m/o KCl.

The electrode reactions are very simple:

$$Li(\ell) \rightarrow Li^+ + e^-$$

$$\tfrac{1}{2}Cl_2(g) + e^- \rightarrow Cl^-$$

$$Li(\ell) + \tfrac{1}{2}Cl_2(g) \rightarrow LiCl(soln).$$

The cell potential is constant at about 3.6 V for the full capacity, in contrast to the situation for all other cells of this paper. The use of chlorine gas necessitates chlorine storage, which may be accomplished by adsorption on carbon.

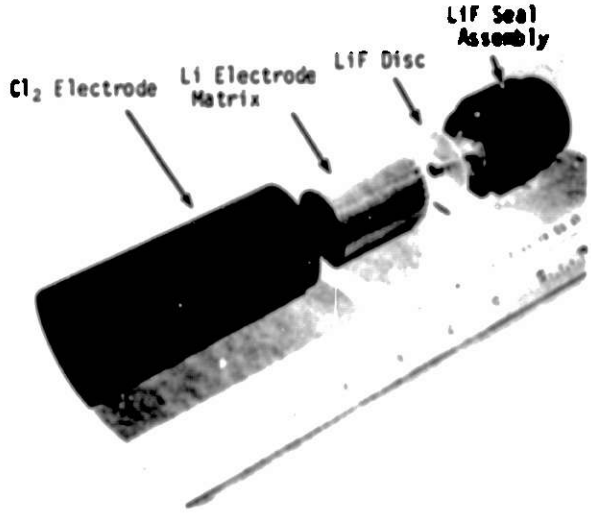

A recent cell is shown in Fig. 10. Cells of this type have operated for periods up to 668 h, and 210 cycles at a capacity density of 0.34 A·h/cm^2, corresponding to an impressive 277 W·h/kg, counting only the weight of the cell itself, without chlorine storage, insulation, etc.

The problem areas for the lithium/chlorine cell are largely materials-related, because of the corrosive nature of the chlorine. Reliable seals and conductors are needed, as well as a simple, compact, lightweight means for chlorine storage and handling. The chlorine electrode gradually floods with electrolyte, a life-limiting factor. Control of this problem is essential.

SUMMARY AND PROJECTIONS

The status of high-temperature cell performance and lifetime is summarized in the right-hand portion of Table I. The systems which have shown the most rapid progress are those receiving the most effort: sodium/sulfur, and lithium alloy/metal sulfide. Both cells show promise of achieving 200 W·h/kg in the not-too-distant future. Some difficulty will probably be experienced in attempting to achieve that specific energy at a specific power approaching 200 W/kg. Single cells are now showing lifetimes of several thousand hours, and cycle lives of hundreds, over practical composition ranges. Figure 11 shows the specific power *vs.* specific energy curves for a number of electrochemical cells and heat engines. The difficulties with regard to the simultaneous achievement of high specific energy and high specific power for Li-Al/FeS and Na/S cells are reflected by the leftward curvature of the solid lines in Fig. 11. The progress in the last seven or eight years has been very good. The projected curves (dashed) represent expectations for the next several years. The prospects for continued progress look bright, but during this period, the difficult materials and seals problems must be solved, and the cost problems must be squarely faced.

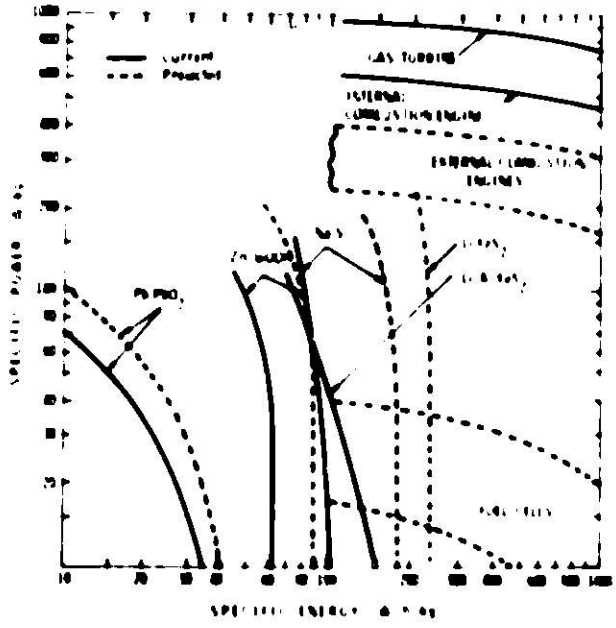

Fig. 11. Specific energy *vs.* specific power for various systems.

REFERENCES

1. E. J. Cairns and H. Shimotake, Science, 164, 1347 (1969.
2. H. Shimotake and E. J. Cairns, Abstract 206, Electrochemical Society Extended Abstracts, Spring Meeting, New York, N. Y., May, 1969; also Extended Abstracts of the Battery Division, 5, 520 (1969).
3. E. J. Cairns, *et al.*, "Lithium/Sulfur Secondary Cells," presented at the 23rd Meeting of the Inter. Soc. of Electrochem., Stockholm, Sweden, Aug. 27-Sept. 2, 1972; also Extended Abstracts, ISE, p. 432 (1972).
4. D. R. Vissers, Z. Tomczuk, and R. K. Steunenberg, J. Electrochem. Soc., 121, 665 (1974).
5. P. A. Nelson, E. C. Gay, and W. J. Walsh, in Proc. 26th Power Sources Symposium, PSC Publications Committee, Red Bank, N. J. (1974).
6. L. R. McCoy, *et al.*, in Proc. 26th Power Sources Symposium, PSC Publications Committee, Red Bank, N. J. (1974).
7. R. K. Steunenberg, *et al.*, in P. A. Nelson, *et al.*, "High Performance Batteries for Off-Peak Energy Storage, ANL-8057, Argonne National Laboratory (November 1974), p. 21 ff.
8. R. K. Steunenberg, *et al.*, in P. A. Nelson, *et al.*, "High Performance Batteries for Off-Peak Energy Storage, Jan.-June, 1974," ANL 8109, Argonne National Laboratory (January 1975), p. 77 ff.
9. P. A. Nelson, *et al.*, "High Performance Batteries for Off-Peak Energy Storage and Electric Vehicle Propulsion, July-Dec., 1974, ANL-75-1 (July 1975), p. 103 ff.
10. R. H. Seefurth and R. A. Sharma, J. Electrochem. Soc., 122, 1049 (1975)
11. W. J. Walsh, *et al.*, in Proc. 9th IECEC, Amer. Soc. of Mech. Eng'rs, New York, N. Y. (1974), p. 911.
12. E. C. Gay, F. J. Martino, and Z. Tomczuk, in Proc. 10th IECEC, Institute of Electrical and Electronics Engineers, New York, N. Y. (1975), p. 627.
13. S. Lai and L. R. McCoy, Abstract 21, Electrochemical Society Extended Abstracts, Fall Meeting, Dallas, Texas, October 1975.

14. S. D. James and L. E. DeVries, Abstract 22, Electrochemical Society Extended Abstracts, Fall Meeting, Dallas, Texas, October 1975.
15. C. C. McPheeters, W. W. Schertz, and N. P. Yao, Abstract 25, Electrochemical Society Extended Abstracts, Fall Meeting, Dallas, Texas, October 1975.
16. N. Koura, J. Kincinas, and N. P. Yao, Abstract 30, Electrochemical Society Extended Abstracts, Fall Meeting, Dallas, Texas, October 1975.
17. W. W. Schertz, *et al.*, in Proc. 10th IECEC, Institute of Electrical and Electronics Engineers, New York, N. Y. (1975), p. 634.
18. J. T. Kummer and N. Weber, Paper No. 670179, presented at the SAE Automotive Engineering Congress, Detroit, Mich., Jan. 9-13, 1967.
19. J. L. Sudworth, in Proc. 10th IECEC, Institute of Electrical and Electronics Engineers, New York, N. Y. (1975), p. 616.
20. R. P. Tischer and F. A. Ludwig, in "Advances in Electrochemistry and Electrochemical Engineering," V. 10, C. W. Tobias and H. Gerischer, editors, in press.
21. S. A. Weiner, *et al.*, "Research on Electrodes and Electrolyte for the Ford Sodium-Sulfur Battery," Ford Motor Co. Report to NSF, Annual Report for June, 1974 to June, 1975 (July, 1975).
22. J. Fally, *et al.*, J. Electrochem. Soc., 120, 1292 (1973).
23. C. A. Levine, in Proc. 10th IECEC, Institute of Electrical and Electronics Engineers, New York, N. Y. (1975), p. 621.
24. C. Levine, Proc. 25th Power Sources Symposium, PSC Publications Committee, Red Bank, N. J. (1972).
25. J. Fally, *et al.*, J. Electrochem. Soc., 120, 1296 (1973).
26. R. W. Powers, Report No. 73CRD289, General Electric Corp., Corporate R & D, October 1973.
27. R. W. Minck, Proc. 7th IECEC, Paper No. 729009, American Chemical Society, Washington, D.C. (September 1972).
28. "New Battery Will Double Range of Electrics," Commercial Motor, Nov. 10, 1972.
29. J. B. Bush, Jr., *et al.*, "Sodium-Sulfur Battery Development for Bulk Power Storage," Electric Power Research Institute, Research Report 128-2, September, 1975.
30. J. Werth, "Alkali Metal-Metal Chloride Battery," U.S. Patent 3,877,984, April 15, 1975.
31. J. J. Werth, "Sodium Chloride Battery Development Program for Load Leveling," Electric Power Research Institute, Research Report 109-2-1, June, 1975.
32. J. E. Metcalfe, E. J. Chaney, and R. A. Rightmire, in Proc. 1971 IECEC, Society of Automotive Engineers, New York, N. Y. (1971), p. 685.
33. J. C. Schaefer, *et al.*, in Proc. 10th IECEC, Institute of Electrical and Electronics Engineers, New York, N. Y. (1975), p. 649.
34. T. G. Bradley and R. A. Sharma, in Proc. 26th Annual Power Sources Symposium, PSC Publication Committee, Red Bank, N. J. (1974), p. 60.

STATE OF THE ART - METAL HALOGEN BATTERIES

David L. Douglas
Vice President-Contract Research
Gould, Inc.
Rolling Meadows, Illinois

While the category, metal halogen batteries, covers primaries capable of micro ampere drains to large secondary batteries with capacities in the tens of kilowatt hours, only secondary batteries such as might be used for vehicle propulsion or bulk energy storage will be discussed here.

The electrochemical couples which have been furthest developed toward practical hardware are (1) lithium/molten salt/chlorine, (2) zinc/zinc chloride (aq)/chlorine and (3) zinc/zinc bromide (aq)/bromine. The first, subject to corrosion incident to use of chlorine as well as high temperatures, will be limited to applications requiring high power for short periods of time. The latter two systems, involving near ambient temperatures, appear to have manageable materials problems. Activation polarization is minor, but the zinc electrode is subject to dendrite formation. Careful hydrodynamic design is required for optimum performance of both the zinc and halogen electrodes.

Substantial development effort is being directed toward halogen storage. Methods being investigated include storage as liquid, absorption in active carbon, halogen hydrate storage, separation and storage of quaternary ammonium polyhalide complexes, separation and storage by way of solvent extraction. Since some of the methods are in the early applied research stage, it is too early to conclude which will be useful in practical devices.

COMPARISON OF U.S. AND EUROPEAN HIGH-TEMPERATURE BATTERY PROGRAMS

Paul A. Nelson

Argonne National Laboratory
9700 South Cass Avenue
[illegible], Illinois 60439

ABSTRACT

Most of the present effort on high-temperature batteries, both in the U.S. and in Europe, is directed toward the development of sodium/sulfur and lithium/metal sulfide systems. This paper describes the major programs on both continents, and compares the economic incentives for battery development, the intended applications, the cell and battery designs, and the unsolved technical problems. Also discussed is the increased effort that is needed in the areas of battery design and development of low-cost components to produce batteries that are economically attractive for the intended applications.

INTRODUCTION

High-temperature batteries are being developed in the U.S. and Europe as power sources for electric vehicles; in the U.S. a second major application is the storage of energy on electric utilities. Energy storage devices for utilities must be compact and have low cost ($20-30/kW-hr). However, the specific energy is the most important criterion for electric vehicle batteries and the performance and cost requirements vary considerably with the type of vehicle. Because of differences in the economic incentive for developing batteries for the various applications in the U.S. and Europe, the performance and cost goals for the battery program on the two continents differ considerably. The selection of different goals has also resulted in somewhat different approaches to finding solutions to the major problems facing the battery developers.

GENERAL DESCRIPTION OF PROGRAMS

The high-temperature battery development programs in Europe and the U.S. are summarized in Table I. Almost all of the effort on high-temperature batteries in Europe is spent on sodium/sulfur systems. In the U.S., the lithium/metal sulfide system is receiving the greatest attention, but much effort is also being given to sodium/sulfur systems. The greater emphasis on the lithium/metal sulfide system in the U.S., as compared with that in Europe, probably results from the large lithium deposits in the U.S., and the lack of suitable deposits in Europe.

Most of the sodium/sulfur cells under development consist of a molten-sodium negative electrode, a molten-sulfur positive electrode, and a solid

Table I. High-Temperature Battery Development Programs in Europe and the United States

	Funding in 1975, $M	Battery Type	Applications	Cost Goal, $/kW-hr
France				
Laboratoires de Marcoussis, CGE	<0.5	Na/S	Exploratory Research	-
German Federal Republic				
Brown Boveri	1	Na/S	Load-Leveling	-
Subcontracts:				
Battelle Institute, Frankfurt				
Great Britain				
Admiralty Materials Laboratory	<0.5	Li(Al)/MS	Military	-
British Rail Technical Centre	1	Na/S	Trains	50
Chloride Silent Power Ltd.	2	Na/S	Buses and Vans	70
UKAEA, Harwell	0.5	Na/S	Buses and Trains	50-70
United States				
Argonne National Laboratory	4	Li(Al)/MS	Load-Leveling, Cars	20-30, 25-35
Major Subcontracts:				
Atomics International				
Catalyst Research Corp.				
Eagle-Picher Industries, Inc.				
Gould Inc.				
Atomics International	0.5	Li(Si)/MS	Load-Leveling	20-30
Dow Chemical Company	0.5-1	Na/Glass/S	Load-Leveling, Cars	15-30, 25-35
ESB	0.5	Na/MCl	Load-Leveling	15-30
ESB	0.5-1	Li(Al)/$TeCl_4$	Fork-Lift Trucks	75-100
Ford Motor Company	1-2	Na/S	Load-Leveling, Cars	15-30, 25-35
General Electric	1	Na/S	Load-Leveling	15-30
General Motors Corp.	0.5-1	Li(Al)/MS, Na/S	Vehicles	-
TRW	<0.5	Na/S	Load-Leveling	15-30

β-alumina electrolyte. The Dow cell uses a glass electrolyte in the form of fine capillary tubes and the ESB cell has a cathode of various metal chlorides of low stability, dissolved in $NaCl-AlCl_3$, instead of molten sulfur. The sodium electrode cells operate at 300-400°C, except for the ESB cell, which operates at 200°C. The main problems remaining to be solved for the sodium-electrode cells are (1) development of an inexpensive current collector for the positive electrode (this current collector usually serves as the cell container as well), (2) development of low-cost seals that are corrosion-resistant to sodium and to sodium polysulfide, (3) development of low-cost processes for producing β-alumina electrolyte having long life, and (4) design of low-cost batteries in configurations that can tolerate failure of a small percentage of the cell electrolytes without undue penalty to battery power and energy storage capacity.

In general, the lithium-type rechargeable batteries utilize Li-Al negative electrodes and FeS or FeS_2 positive electrodes. The electrical separator for the cells is porous and is constructed of boron nitride or other material resistant to attack by lithium. It may be in the form of a flexible fabric or paper, or a rigid ceramic structure. The electrolyte is the LiCl-KCl eutectic (mp, 352°C). It is distributed throughout the cell in the pores of the electrodes and the separator. The lithium-electrode cells operate between 425 and 500°C. Some exceptions to the general description of the lithium cells given above are the use of Li-Si alloys for negative electrodes at Atomics International and the use of $TeCl_4$ for a positive electrode at ESB.

COMPARISON OF PROGRAMS

Applications

In Europe, the application for advanced batteries which is being given the most attention is that of a power source for electric vehicles. The high cost of gasoline to consumers appears to be a strong incentive for developing electric vehicles. For example, in June 1975 the cost of gasoline to the consumer in England was $1.35/U.S. gal and in France, $1.75/gal, as compared to $0.55/gal in the U.S. These high costs in Europe result primarily from the very high tax which is imposed both to raise revenue and to restrict the use of gasoline. However, the use of electric vehicles would not necessarily circumvent the tax. In fact, until recently the annual registration tax on electric vehicles in Germany was much higher than that on gasoline-powered vehicles; however, the tax on electric vehicles has now been reduced. The political climate in Europe is now beginning to favor development of electric vehicles, not only to avoid an unfavorable balance of payments due to oil imports, but to reduce air pollution.

Although the uncertainty in the tax situation has diminished the incentive to develop electric vehicles in some European countries, the incentive has, nevertheless, been considerably greater than that in the U.S. As a result, there are 15,000 electric milk-delivery trucks and several experimental electric buses in England. In Germany, there are at least 20 electric buses, and operation of many more is planned. The fork lift equipment in Europe is almost entirely electrically driven.

It is apparent that the Europeans are placing greater emphasis on the development of large electric vehicles rather than urban cars. At British Rail Technical Centre, a program involving 22 personnel is under way to develop sodium/sulfur batteries for electric trains. Chloride Silent Power Ltd. in England is devoting the effort of 42 personnel to the development of sodium/sulfur batteries for urban buses. These programs, and the one at Harwell, are cooperating by exchanging information and avoiding unnecessary duplication of effort. European programs on ambient-temperature batteries also indicate the importance of developing improved batteries for vehicles. Varta Batterie, A.G. in Germany is developing lead-acid batteries for buses and already has such buses in operation. AGA of Sweden is developing nickel/zinc batteries for delivery vans, and delivery vans are secondary applications for the batteries being developed at Chloride Silent Power and Varta. The Swedish National Development Company is developing iron/air and iron/nickel batteries of relatively high specific energy for powering large mining vehicles. The use of these vehicles is expected to reduce air pollution within the mines. The presently used diesel-powered vehicles require a high rate of circulation of fresh air, and this air must be heated during winter months.

The technical and economic goals for development of batteries for urban buses are easier to meet than the development goals for batteries suitable for urban cars. High specific energy is not quite as important for these large vehicles as for urban cars, and the required discharge rates are not as high; urban cars must have batteries that can be discharged in about 2 hr and have peak power equivalent to a discharge rate of 0.5 hr, whereas the batteries for urban buses and delivery vans require discharge rates of 5 to 10 hr. The electric-train application, on the other hand, requires a high discharge rate similar to that for an urban car, but the peak power requirement is lower.

The high acceptable cost of batteries for the large electric vehicles is an important factor for directing attention in Europe to these vehicles, rather than urban cars. For instance, the cost goal at Chloride Silent Power for sodium/sulfur batteries for urban buses is $70/kW-hr, and the goal at British Rail for electric train batteries is $50/kW-hr. Costs in this same range are projected for batteries for vans and mining vehicles. If these cost goals can be met with batteries that also achieve the performance goals, the vehicles will be economically competitive with their gasoline- or diesel-powered counterparts. In contrast, an urban car battery would be much more difficult to develop than batteries for these large vehicles, and the cost would have to be about $25-35/kW-hr to be competitive with gasoline-powered cars.

There is little incentive in Europe to develop batteries for storage of off-peak power on electric utilities. Because of the many mountains and the short distances from the mountains to the electricity market, suitable sites on the continent for pumped-power storage units should be adequate for the storage capacity that will be needed through the year 2000. In Great Britain, low-cost storage batteries would be advantageous for use by electric utilities, but the general opinion there seems to be that the cost goals could probably not be met in the near future.

In the U.S., the advanced battery programs, for the long term, are directed toward achieving low-cost energy storage for utilities and urban

cars. The successful development of batteries for these two applications would contribute substantially toward conserving oil and reducing oil imports. Also, the U.S. has few suitable sites for pumped-storage units for utilities and must, at present, utilize the more expensive means of storage for generating peak power by means of oil- or gas-fired turbines.

As the development of the advanced batteries approaches technical success, the efforts must be focused on development of an economically viable product. In this regard, the programs in Great Britain on development of sodium/sulfur batteries are ahead of the programs in the U.S. The British programs are large, broad-based efforts, which are addressing engineering and economic problems, as well as the more basic technical problems of the cell systems. Until recently, the sodium/sulfur battery programs in the U.S. have been relatively small in scope, and the economic incentive for addressing some of the engineering and marketing problems has been lacking. Recent increases in funding to some of these programs by the U.S. Energy Research and Development Administration (ERDA) and the Electric Power Research Institute should improve this situation. The program at Argonne National Laboratory (ANL) on the lithium/sulfur system was not technically attractive until the development of iron sulfide positive electrodes in the spring of 1973. Since then ANL has spent much effort on engineering problems as well as on materials and cell chemistry.

The increase in the size and scope of the program at the Ford Motor Company on sodium/sulfur batteries and the involvement of industrial firms in the ANL program on lithium/metal sulfide batteries may result in a reevaluation of the near-term applications for these batteries. This reevaluation is expected because of the economic realities of initiating production of complex new products such as the high-temperature batteries. Both the sodium/sulfur and lithium/metal sulfide batteries show promise for meeting the long-range cost goals for urban car batteries and utility load-leveling batteries. However, to meet these cost goals, low-cost electrolyte tubes are required for the sodium/sulfur batteries, and a low-cost electrical separator of boron nitride paper or a similar material is required for the lithium/metal sulfide batteries. Production of these components at a moderate level will reduce costs significantly, but these reductions are not expected to be sufficient to meet the long-term cost goals. The facilities required to produce these items, alone, would cost several million dollars, even for a production rate equivalent to the production of only 100-200 MW-hr of batteries per year. Profitable marketing of the batteries at that level of production will require applications that can afford $50-100/kW-hr for a battery of high specific energy. Examples of such applications are power sources for electric buses, vans, mining equipment, military applications, deep diving submarines, and electric trains. Work will still continue on developing batteries to meet the long-term objectives of the programs being funded by ERDA and Electric Power Research Institute (EPRI); however, it is expected that the private sector will devote more attention to the near-term goals with some assistance from ERDA.

Cell Design

The acceptance of fairly high cost goals by the British in their sodium/sulfur battery programs has led to several differences in the approach to cell design between these programs and those in the U.S. For instance, in neither

of the large British programs is consideration being given at present to multiple-electrode cells. Also, all of the sodium in the cells is contained within the electrolyte tube; no provision is being made for a sodium reservoir above the cell. Thus, a gasketed mechanical seal at the top of the cell becomes feasible. For the usual cell design, in which the polysulfide is contained by the cell housing, the housing must be constructed of an expensive alloy or be coated on the interior with a corrosion resistant material. The method of preventing attack by the sodium polysulfide is proprietary, but the overall cost of these tubes is expected to be too high for use in the present applications for the batteries under development in the U.S. One method for reducing the overall cost with this design is to utilize the maximum feasible cell size. Both British Rail and Chloride Silent Power are developing large electrolyte tubes (3 cm in diameter, and 30 to 60 cm long). These are somewhat larger than the electrolyte tubes contemplated at the present time in the American programs. The British are designing cells for an upper temperature limit of 400°C. This temperature limit was chosen on the basis of considering the temperature variations expected under normal battery operating conditions. This temperature limit, which is higher than is normally used in laboratory tests of sodium/sulfur cells, would greatly accelerate corrosion at the cell casing, which also serves as the positive electrode current collector.

Most of the American programs on sodium/sulfur batteries are directed toward developing cell designs that have the potential for low cost in mass production. Several approaches are being considered. In some of the programs, the use of many electrolyte tubes within a single cell housing is being considered as a means of reducing the relative cost of the housing; this design will require the development of a ceramic manifold with effective glass seals between the tube sheet and the electrolyte tubes. The use of a sodium reservoir to minimize the electrolyte area per unit of battery capacity is also being considered; this will require an electrolyte of high ionic conductivity and thin cross sections. Restriction of the operating temperature of the cells to below 350°C or even lower may permit the use of aluminum housings with protective internal coatings. Whether such a low operating temperature limit will be practical remains to be seen. It is possible that the sodium/sulfur battery programs in the U.S. may adopt some of the approaches of the British programs, if near-term battery applications that permit higher cost goals are also adopted. Other innovations such as the reversal of the positions of the negative and positive electrodes (inside and outside the electrolyte tube) may also prove feasible.

In the large program at ANL on development of lithium/metal sulfide batteries, the engineering and manufacturing problems concerned with the battery have been under consideration for more than a year. In this respect, the ANL program is like the British programs on the development of sodium/sulfur batteries. Consideration of these engineering aspects has resulted in the development of large prismatic cells that could be easily connected to form batteries. In an effort to meet the low-cost goals for the applications of interest, the ANL program has attempted to reduce the near-term cost of all of the components of the cell except the separator. As noted above, the separator is expected to be costly, except at the very high battery production rates that would justify the construction of a sizable facility for fabricating boron nitride in the form of paper or fabric. The other lithium/metal sulfide battery programs, which are much smaller, have placed less emphasis

on engineering, but have made contributions in other areas. In the program at Admiralty Materials, a bipolar battery design was developed, initially for a primary thermal battery. However, tests have been conducted recently on secondary batteries of this design. Promising work on the use of molten lithium electrodes, aluminum nitride ceramic parts, electrolyte purification, and cell chemistry have been carried out at General Motors. Atomics International, which has an independent program in addition to its cooperative program with ANL, has developed a lithium-silicon negative electrode which may have higher specific energy than the lithium-aluminum electrode.

Battery Design

Considerably more effort must be devoted to battery design for both sodium/sulfur and lithium/metal sulfide batteries. This effort is needed to establish the cell design and to ensure that the appropriate problems are being addressed in cell development. A major problem in battery design is that of providing for the inevitable failure of individual cells without undue inconvenience to the battery operator. The two battery types have different failure mechanisms, which must be taken into account in designing batteries of cells. Sodium/sulfur cells usually fail by cracking of the electrolyte, which leads first to self-discharge of the cell and all cells in parallel with it, by means of a short circuit through the crack in the electrolyte. This short gradually heals by formation of sodium polysulfide; a permanent open circuit of very high resistance eventually develops. When this occurs, all cells in series with the failed cell become inoperative, unless there are other operating cells in parallel with the failed cell. The approach to this problem at Chloride Silent Power has been to design the batteries with large cells in series with the intention of removing individual cells as they fail. This approach would probably be impractical for a large load-leveling station. At British Rail, the approach is to connect some cells in parallel to permit operation with several failed cells in a large battery module; the battery maintenance procedure would be to replace modules.

Additional problems are imposed on the U.S. developers of sodium/sulfur batteries for urban cars because of the small capacity of the battery (30-40 kW-hr and 100 V). This small capacity, and the need to have several (5 to 10) electrolytes in parallel, limits the capacity of the electrodes associated with a single electrolyte tube to about 40-60 A-hr. The combination of small cell size and low cost ($25-35/kW-hr) is difficult to achieve.

The lithium/metal sulfide cells usually fail by a short circuit which causes the loss of all cells in parallel with the failed cell and a reduction in the overall voltage of the battery. In an automobile battery, in which all cells will probably be connected in series, several cells could fail without greatly reducing the capacity or power of the battery. In the load-leveling application, however, the cells will be connected in parallel, and some means must be found for disconnecting a cell that has developed a short circuit, to prevent the loss of all the cells.

CONCLUSIONS

Large-scale engineering efforts have been started on the sodium/sulfur battery programs in Great Britain, and these are considerably ahead of similar efforts in the U.S. The economic conditions in Europe favored the early development of batteries of high specific power and high specific energy, and moderately high production costs are not considered to be a major deterrent. The recent, significant increases in funding for the battery programs in the U.S., which resulted from increased emphasis on energy savings, are expected to cause a reevaluation of the near-term applications and goals for advanced batteries. Near-term programs are expected to be directed toward the development of high-performance batteries for applications that can afford relatively high cost, and these efforts will serve as a stepping stone to the long-range development of low-cost batteries for urban cars and energy storage by electric utilities. The higher cost goals for the near-term will permit the evaluation of approaches to cell and battery designs that would otherwise be impractical.

ACKNOWLEDGMENT

This work was conducted under the auspices of the U. S. Energy Research and Development Administration.

A-107

BATTERY DEVELOPMENT IN JAPAN

N. P. Yao

Argonne National Laboratory
9700 South Cass Avenue
Argonne, Illinois 60439

ABSTRACT

The main thrust of battery development in Japan is toward application in electric vehicles. Incentives to develop commercial-scale electric vehicles in Japan are the desires to improve the air and noise quality in big cities, and to secure an international position in the electric vehicle field and thereby expand Japan's economy. Development of advanced battery technology for electric vehicles has been in progress as a part of the National Electric Vehicle Research and Development Project, instituted early in 1971 by the Agency of Industrial Science and Technology, MITI, Japan. Three general types of advanced behicle batteries are being developed under the national project: lead-acid, metal/air, and sodium/sulfur. Progress has been made in each of the advanced batteries since 1971. Battery performance goals established for 1977, which also marks the conclusion of the national project, incorporated an increase of cycle life requirement with reduced specific energy goals. Performance demonstration of the advanced batteries in experimental electric vehicles is expected early in 1977.

INTRODUCTION

The main thrust of battery development in Japan is toward application for electric vehicle propulsion. The use of batteries to store off-peak energy for utility load-leveling or peak-shaving, as contemplated in this country,[1] is not being seriously considered by the Japanese electric utilities. The reasons for the current skepticism by the Japanese about the practicality of battery application in electric utilities stem from (1) the high cost and low reliability of present battery systems; (2) the strong technological background in pumped hydro storage,* and the availability of sufficient sites for pumped hydros by the year 2000; (3) the low credit for power transmission assignable to battery substations (a long power transmission network is not required because of the high population density in Japan); and (4) the lack of prime space for urban battery substations. However, because of increasing costs of new pumped hydro storage sites and strong environmental objections, the Japanese Central Electric Power Council is

---

*As of March 1975, the total installed hydro power capacity in Japan was 22,500 MW (about 24% of total power generation), of which 27% or 6000 MW was pumped storage hydro power. At present, the hydro power generating installation under construction is about 10,000 MW, of which 90% or 9000 MW accounts for pumped storage hydro.[2]

now taking an exploratory view to reassess battery technology, particularly the advanced technology, for this application.

Battery energy storage for electric load-leveling is not really a new application concept in Japan. In fact, three lead-acid battery plants, with power/capacity sizes of 2 MW (1000 V)/4 MW-hr, 1 MW (600 V)/2 MW-hr, and 1 MW (600 V)/2 MW-hr, were built in 1932 in the area of Kyoto-Osaka, Japan, by Keihan Electric Railroad Co. in collaboration with Yuasa Battery Co.[3] The plants were built to shave the peak load of the electric railway during the afternoon rush hours for the local electric utility. The battery plants operated very well for over nine years, with positive returns of investments to the Keihan Electric Railroad Co.[3] Unfortunately, the plants and the participating personnel are no longer available, and further details are not available.

Development of advanced electric vehicles, one of ten national research and development projects in Japan, has been under way since April 1971 by the Agency of Industrial Science and Technology (AIST), Ministry of International Trade and Industry (MITI). The project is directed toward research and development, and demonstration of advanced electric vehicle technology, which is urgently needed to implement commercial-scale introduction of electric vehicles. The major incentive for the development and commercialization of electric vehicles in Japan is the abatement particularly in big cities, of air and noise pollution, which is generated by the high density of gasoline-powered vehicles. Another incentive of the national project is the early development of electric vehicle technology as a means of securing an international position in this field and thereby expanding Japan's economy. Conservation of petroleum resources is not an applicable incentive, since Japan imports nearly all its petroleum from abroad. However, large-scale introduction of electric vehicles in Japan will indeed allow diversion of petroleum to other usages than motor-vehicle propulsion.

The Japanese National Electric Vehicle Project was initiated in 1971 and will be concluded in 1977. Under the leadership and full sponsorship of the Japanese Government, the project has been implemented with close cooperation from industrial and academic circles. Two government laboratories -- Osaka Government Industrial Research Institute and Tokyo Mechanical Engineering Laboratory -- have been entrusted with major roles in the planning and the implementation of the national project and the laboratories also have served as the national and international focal points for their test evaluation and specification of electric vehicle technology that have been developed under the national project.

This paper will discuss the Japanese battery development in the context of the National Electric Vehicle Project; specifically, the paper discusses the implementing arrangement of the project, the types of advanced electric vehicles, and the types of improved and advanced batteries. The developmental results for each are also summarized. Finally, an impression of the project status and its prospects are described from a view of a foreign observer.

IMPLEMENTING ARRANGEMENT OF JAPANESE NATIONAL ELECTRIC VEHICLE PROJECT

The national project is well coordinated under the central directorship of Mr. K. Ito, a senior officer of AIST, MITI. As shown in Table 1 for the project management structure, six separate working groups (those representing planning, vehicle test, vehicle body, battery, motor and control, and utilization system) report directly to a central R & D Committee chaired by Mr. Ito. Each working group comprises 8 to 13 members of relevant expertise to execute the group functions. The central R & D Committee comprises 29 members from government, government laboratories, universities, automotive industry, battery industry, and heavy electric machinery industry. The Committee serves essentially as an advisory board to Mr. Ito, the overall project manager. Dr. Y. Miyake and Mr. E. Kikuji of the two government laboratories serve, respectively, as the chairmen of the battery working group and the vehicle test and planning groups. Coordination between the working groups has been strongly encouraged by the project manager.

The development efforts of electric vehicle technologies have had the full blessing and participation of the major industries. Table 2 shows the contractual arrangement, under the national project, to develop three major component technologies: experimental vehicles, batteries, and motor and control systems. The software technology includes electric vehicle utilization systems and charging methods. As shown in the table, the effort of component development is well organized and well distributed among the major relevant industries. Furthermore, the contractors were selected for the development of specific experimental vehicles and battery systems on the basis of their background and expertise in the specific technology.

TYPES OF EXPERIMENTAL ELECTRIC VEHICLES

Five types of experimental electric vehicles[4] have been developed during the initial three years. They are lightweight passenger car, compact passenger car, lightweight truck, compact truck, and city route bus; these vehicles are shown in Figs. 1-5, respectively. The performances of these experimental vehicles were evaluated in 1974 for maximum speed, acceleration (0 - 30 km/hr), hill climbing ability (at 6° slope), and distance per battery charge (at 40 km/hr constant cruising speed). In the first experimental vehicles, improved lead-acid batteries of approximately 60 W-hr/kg specific energy were utilized. The lead-acid batteries, two of which are shown in Figs. 6 and 7, were developed and supplied by those battery firms listed in Table 2 as the battery subcontractors under the experimental vehicle R & D. The battery weights in these experimental vehicles were reported to be up to about 30% of the total vehicle weight.

The 1974 test performances of the experimental vehicles are also given in Figs. 1-5. The performance results essentially met the initial targeted performance goals. The impressive results obtained with the 1974 experimental vehicles are attributed to optimization of vehicle components and total system integration. Minimization of vehicle body weight was achieved by the development of new types of fiber-reinforced-plastic (FRP) materials and optimized chassis design. Highly compact and efficient motor and control systems were

Table 1. Management Structure of the National Electric Automobile Project

O R & D Committee

Chairman: K. Ito
Vice Chairman:
S.Kurosu

- **Planning Working Group**
  Chairman: E. Kikuji
  Vice Chairman: Y. Kuriyama
- **Test Vehicle Working Group**
  Chairman: E. Kikuji
  Vice Chairman: H. Fukuda
- **Vehicle Body Working Group**
  Chairman: A. Shimamura
  Vice Chairman: K. Ishine
- **Battery Working Group**
  Chairman: Y. Miyake
  Vice Chairman: S. Takahashi
- **Electric Motor and Control Device Working Group**
  Chairman: S. Miyairi
  Vice Chairman: T. Yata
- **Utilization System and Charging Method Working Group**
  Chairman: M. Iguchi
  Vice Chairman: M. Kitamura

Table 2. Contractual Arrangement of Japanese National Electric Vehicle Project (1971-1977)

● **EXPERIMENTAL VEHICLE R & D**

	Prime Contractor	Subcontractors: Battery	Subcontractors: Motor, Control
Lightweight Passenger	Daihatsu	Matsushita	Toshiba
Compact Passenger	Toyota	Japan Storage	Nihon-Denso
Lightweight Truck	Toyo Kogyo	Furukawa	Fuji Electric
Compact Truck	Nissan	Shin-Kobe Elect.	Hitachi Shinko Elect.
City Route Bus	Mitsubishi	Yuasa	Mitsubishi
Vehicle Body Material	Hitachi Kasei		

● **BATTERY R & D**

	Contractor
Pb/Acid	Japan Storage
Pb/Acid	Shin-Kobe Elect.
Pb/Acid	Yuasa
Zn/Air	Japan Storage
Zn/Air	Sanyo Elect.
Fe/Air	Matsushita
Na/S	Yuasa

● **EV UTILIZATION SYSTEM AND CHARGING METHOD**

Automotive Technology Committee

● **EV CHARGING METHOD**

Japan Electrical Council

● **MOTOR, CONTROL SYSTEM R & D**

	Contractor
Thyristor Chopper Control - DC Motor	Hitachi Seisaku
Transistor Chopper Control - Thyrister Motor	Toshiba Electric
Inverter Control - Induction Motor	Mitsubishi Electric Topi Industry

Passengers	4
Overall Length (mm)	3165
Gross Vehicle Weight (kg)	1132
Maximum Speed (km/hr)	89
Acceleration (sec), (0 - 30 km/hr)	2.4
Hill Climbing Ability (km/hr), (6° slope)	>40
Distance per Battery Charge (km) (40 km/hr constant speed	175

Fig. 1. Lightweight Electric Passenger Car (by Daihatsu)

Passengers	5
Overall Length (mm)	3350
Gross Vehicle Weight (kg)	1660
Maximum Speed (km/hr)	94
Acceleration (sec), (0 → 30 km/hr)	2.4
Hill Climbing Ability (km/hr), (6° slope)	>40
Distance per Battery Charge (km) (40 km/hr constant speed)	180

Fig. 2. Compact Electric Passenger Car (by Toyota)

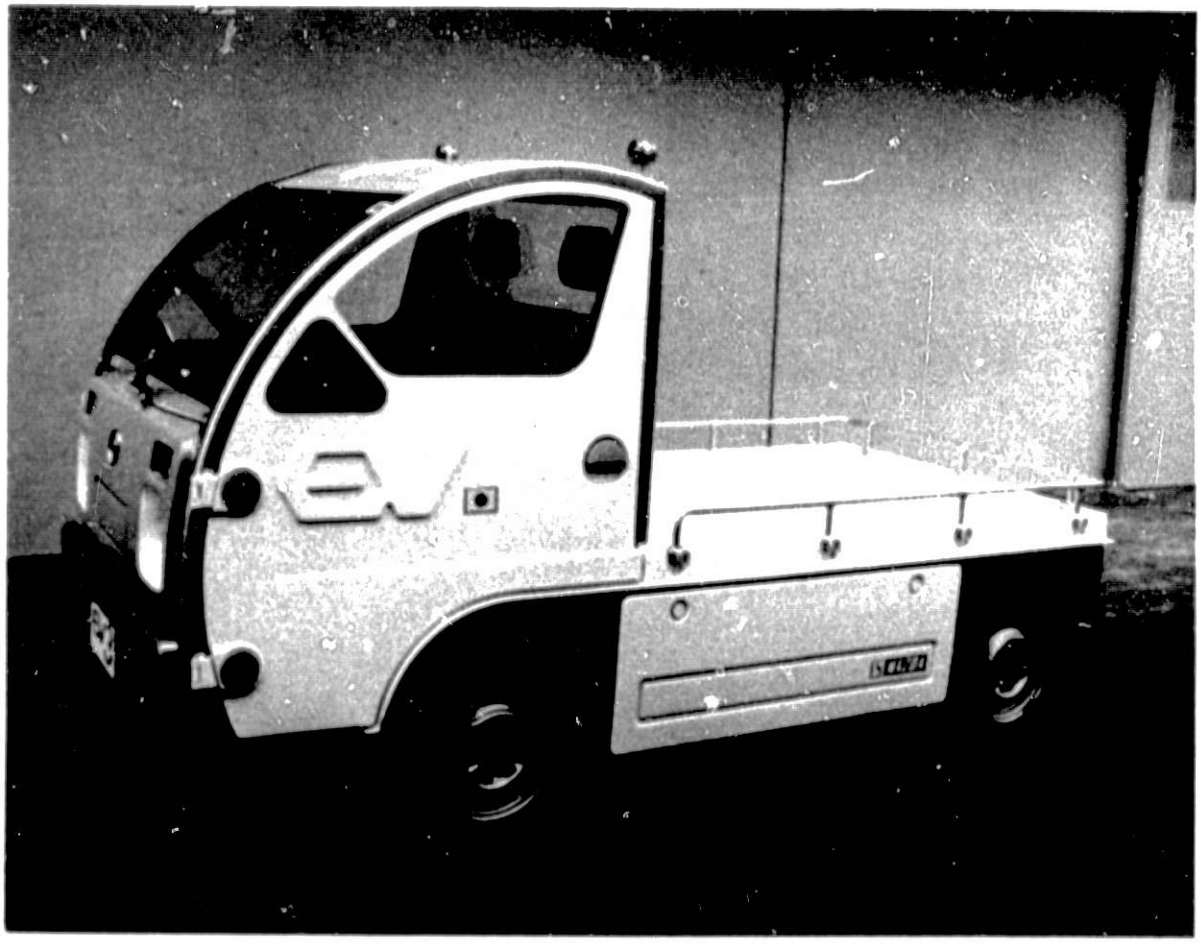

Passengers + Payload (kg)	2 + 200
Overall Length (mm)	2915
Gross Vehicle Weight (kg)	1090
Maximum Speed (km/hr)	73
Acceleration (sec), (0 - 30 km/hr)	4.1
Hill Climbing Ability (km/hr), (6° slope)	40
Distance per Battery Charge (km) (40 km/hr constant speed)	150

Fig. 3. Lightweight Electric Truck (by Toyo Kogyo)

Passengers + Payload (kg)	2 + 1000
Overall Length (mm)	4695
Gross Vehicle Weight (kg)	3550
Maximum Speed (km/hr)	85
Acceleration (sec), (0 → 30 km/hr)	3.5
Hill Climbing Ability (km/hr), (6° slope)	>40
Distance per Battery Charge (km) (40 km/hr constant speed)	220

Fig. 4. Compact Electric Truck (by Nissan)

Passenger Capacity (person)	70
Overall Length (mm)	9,380
Gross Vehicle Weight (kg)	13,640
Maximum Speed (km/hr)	68
Acceleration (sec), (0 → 30 km/hr)	6.2
Hill Climbing Ability (km/hr), (6° slope)	>29
Minimum Turning Radius (m)	8.1
Distance per Battery Charge (km) (40 km/hr constant speed)	330

Fig. 5. City Route Electric Bus (by Mitsubishi)

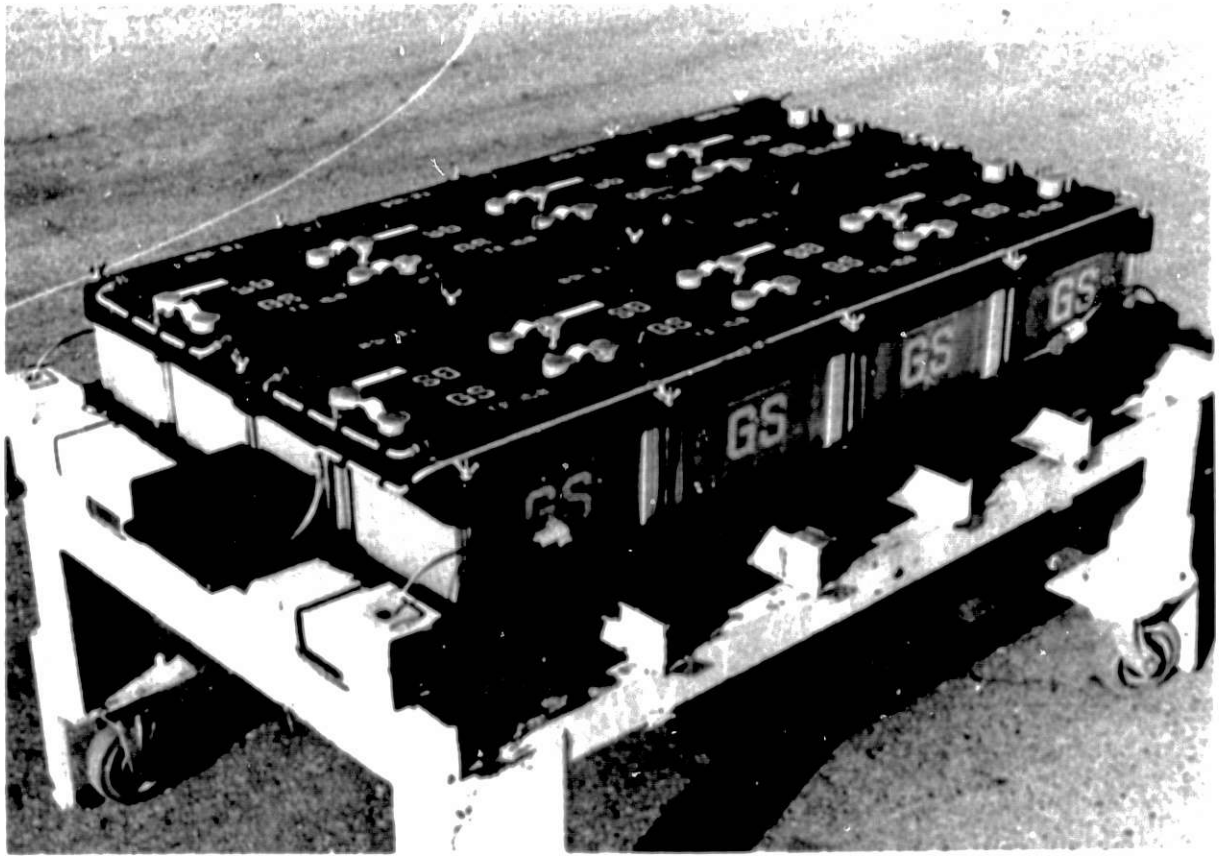

Nominal Voltage, V	192 (12 V x 16 modules)
Nominal Capacity, A-hr	158 (c/5 rate)
Specific Energy, Whr/kg	60

Fig. 6. Lead/Acid Battery for the Compact Electric Passenger Car (by Japan Storage)

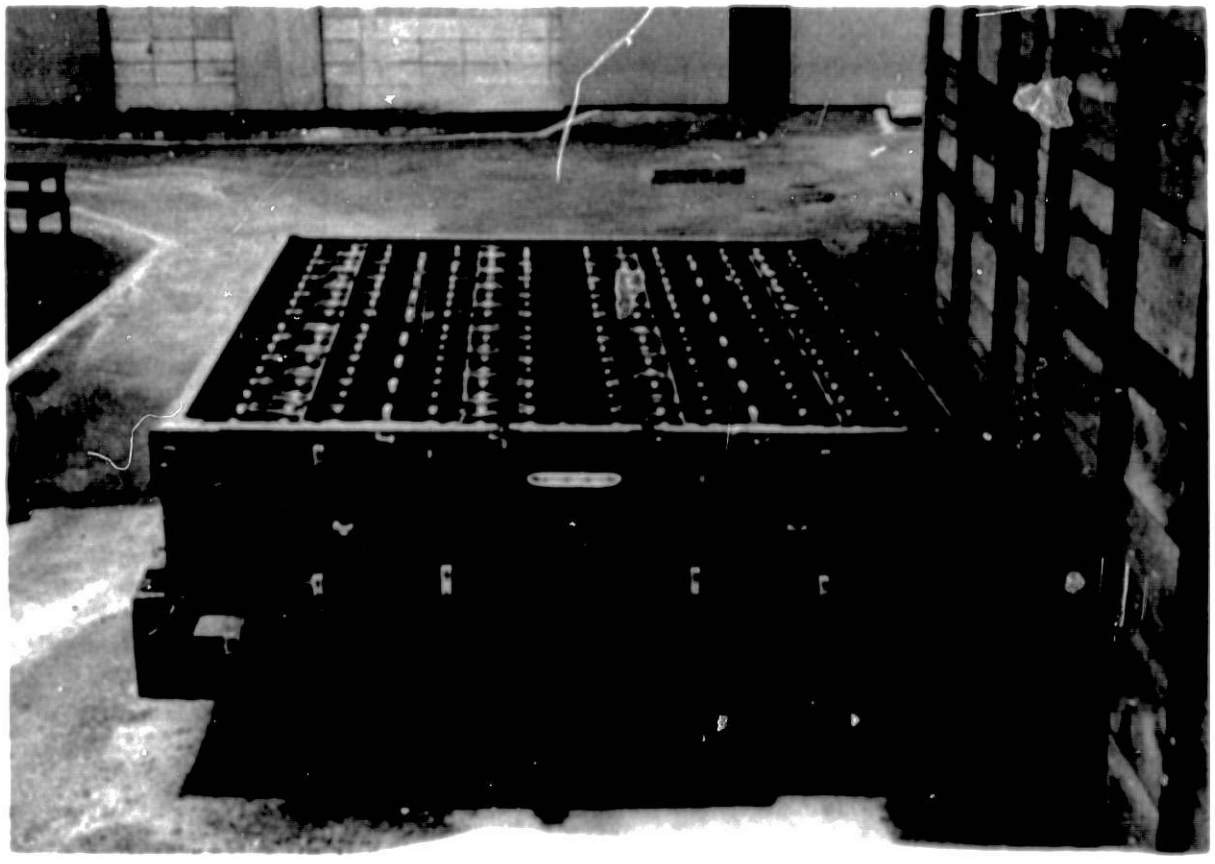

Nominal Voltage, V	432 (6 V x 72 modules)
Nominal Capacity, Ahr	460 (c/5 rate)
Dimension, mm	2010 W x 2360 L x 460 H

Fig. 7. A Complete Set of Lead-Acid Batteries for the City Route Electric Bus (by Yuasa)

also developed, which included (1) a dc motor and thyristor control system, (2) a thyristor motor and power transistor control system, and (3) an induction motor and inverter control system. Of the three motor and control systems, the thyristor motor (18 kW size) and transistor chopper control yielded the highest ratio of output power to motor weight (0.4 kW/kg at the 1-hr rate), as compared with 0.2 kW/kg for the conventional small-capacity motors.

Development of the component technology and the experimental vehicles is now being continued. The second-phase performance test, which is scheduled in 1977, will incorporate the advanced batteries (discussed in the next section) to meet the 1977 target performance goals shown in Table 3. It should be pointed out that the stringent vehicle performance goals were established in order to facilitate the adaptation of the vehicles into the present city traffic systems.

TYPES OF ADVANCED VEHICLE BATTERIES

At the very inception of the national electric vehicle project, development of advanced vehicle batteries was given an importance that was parallel to, but not greater than, the development of experimental vehicles. The development funding for the advanced batteries represented approximately 7 x 10⁷ U.S. dollars or about 47% of the total project funding over the past five years. As was the case for the experimental vehicles, the first performance evaluation of advanced batteries was conducted in bench tests in 1974. In the first-phase effort (1971 to 1974), the battery development goal was the attainment of the highest specific energy possible with each battery system. This again reflected the Japanese approach for achieving high-performance vehicles that are adaptable to existing transportation flow. Since the test evaluation in 1974, a set of new battery development goals were established for 1977 which incorporated a cycle-life requirement, but a cost goal has not yet been set. The second-phase evaluation will be conducted in experimental vehicles (except for the sodium/sulfur battery, which will likely be limited to bench tests). Concurrent with the development of advanced batteries and experimental vehicles was the development of battery system technology for quick battery replacement or exchange, and an automatic watering system for the lead-acid batteries. Both technologies appeared to have been fully developed.

Three general types of battery systems,[4] covering the intermediate and high specific energy systems, were selected for development; these are lead-acid, metal/air, and sodium/sulfur, as shown in Table 4. Within the three general types are three advanced lead-acid concepts, two zinc/air systems, one iron/air system, and one sodium/sulfur system. The respective battery developers, the battery module size that was developed, and the specific energy achieved for each battery module in 1974 are also summarized in Table 4. Three advanced concepts of lead oxide positive electrode have been developed: a multilayer structure by Japan Storage, a porous sheet structure by Shin-Kobe, and a bipolar, circulating system by Yuasa; these electrodes, coupled with the use of an optimized mixture of lead dioxide, a high corrison-resistant grid alloy, and a high-specific gravity electrolyte (~1.4) have resulted in lead-acid battery modules with specific energy exceeding 60 W-hr/kg (at a 5-hr rate). The zinc/air batteries have achieved specific energies of

Table 3.

TARGET PERFORMANCE OF EXPERIMENTAL ELECTRIC VEHICLES IN 1977

JAPANESE NATIONAL ELECTRIC VEHICLE PROJECT (1971-1977)

Vehicle Type	Vehicle Wt (kg)	Payload	Maximum Speed (km/hr)	Range[1] (km)	Acceleration[2] (sec)	Climbing Ability[3] (km/hr)
Lightweight Passenger	1,350	4(P)	80	>80	7	>40
Compact Passenger	1,500	4(P)	80	>250	6	>40
Lightweight Truck	1,400	2(P)+300 kg	70	>160	9	>40
Compact Truck	3,700	2(P)+1000 kg	70	>230	9	>40
City Route Bus[4]	9,900	70(P)	68	330	6.2 (0 → 30 km/hr)	>29 (6° slope)

1. Range per battery charge at a constant cruising speed of 40 km/hr.
2. Acceleration from 0 → 40 km/hr unless indicated otherwise.
3. For a 7% slope unless indicated otherwise.
4. Performance shown was achieved in 1974. Bus testing will not be conducted in 1977.

Table 4.

BATTERY DEVELOPMENT GOALS

JAPANESE NATIONAL ELECTRIC VEHICLE PROJECT (1971-1977)

Battery Type	Developer	Module Size (kW-hr)	1974 Achievement Sp. Energy* (W-hr/kg)	1977 Goal Sp. Energy* (W-hr/kg)	1977 Goal Cycle Life
Pb/Acid (Multilayer Electrode)	Japan Storage Battery	1.80	70	>50	>500
Pb/Acid (Porous Sheet Electrode)	Shin-Kobe Electric	1.68	64		
Pb/Acid (Bipolar, Circulating System)	Yuasa	2.00	61		
Zn/Air (Fixed Electrolyte)	Japan Storage Battery	1.25	123	>80	200-300
Zn/Air (Circulating Electrolyte)	Sanyo Electric	2.40	91		
Fe/Air	Matsushita	1.56	88	>70	200-300
Na/S	Yuasa (Toshiba)	2.81	90	NA	NA

*Specific Energy values correspond to C/5 rate for Pb/acid and Na/S batteries and C/7 rate for metal/air batteries.

123 W-hr/kg (for the fixed electrolyte type) and 91 W-hr/kg (for the circulating electrolyte type) at a 7-hr rate. The iron/air battery, which was developed by Matsushita and was the first of its kind in Japan, has also achieved a respectable specific energy of 88 W-hr/kg (at a 7-hr rate). The energy efficiencies of metal/air batteries are reported to be 30-35%. The sodium/sulfur battery is being developed at Yuasa Battery Co. in collaboration with Toshiba Electric Co. who supplies the β-alumina electrolyte tubes. A 2.8 kW-hr (560 W) module was assembled and tested in 1974. A specific energy of 90 W-hr/kg was achieved with the module at the 5-hr rate, but the cycle life was limited owing to the stress failures of the β-alumina joints. Problems related to the temperature control and cooling of the sodium/sulfur battery module are yet to be resolved, and the resolution may require total modification of the module design. Photographs of various types of battery modules are shown in Figs. 8-12.

The high specific energies achieved with the battery modules in 1974 were indeed impressive, but their cycle life, except for the lead-acid batteries, were quite limited, generally less than 100 cycles. As discussed previously, the new set of battery development goals that was established for 1977 tests (see Table 4), incorporates the cycle life requirement at reduced specific energy goals. The present indications are that these battery goals will be met in 1977.

The test results of metal/air batteries in 1974 indicated that these batteries could not sustain the required power density for the experimental vehicles. Consequently, the in-vehicle tests of the metal/air batteries which are planned for 1977 will assume a hybrid form, to be coupled with high-power-density lead-acid batteries. The planned couplings are as follows:

Zn/air (Japan Storage)-High Power Pb-acid (Japan Storage)

Zn/air (Sanyo Electric)-High Power Pb-acid (Shin-Kobe)

Fe/air (Matsushita)-High Power Pb-acid (Matsushita)

Second-phase experimental vehicles that will be powered by the hybrid battery sources and by the advanced lead-acid batteries are scheduled for test and demonstration early in 1977. The demonstration will also signify the conclusion of the Japanese national electric vehicle project, which has been a concerted and well-directed six-year effort. Further development and commercialization of the advanced electric vehicle technology that was developed under the Government's national project must then be undertaken by Japanese private industry.

UTILIZATION AND IMPACT OF ELECTRIC VEHICLES

Equally important to the electric vehicle hardware development is the software development. Software studies, such as (1) electric vehicle utilization systems, (2) considerations of safety and the secondary pollution resulting from electric vehicles, (3) electromagnetic interferences by electric vehicles, (4) standardization of batteries, electric vehicles and performances, and (5) development of new electric transportation systems, are under active assessment in Japan as a part of the strategy for implementing theuse of electric vehicles on a large scale. The development in this area will not be discussed here.

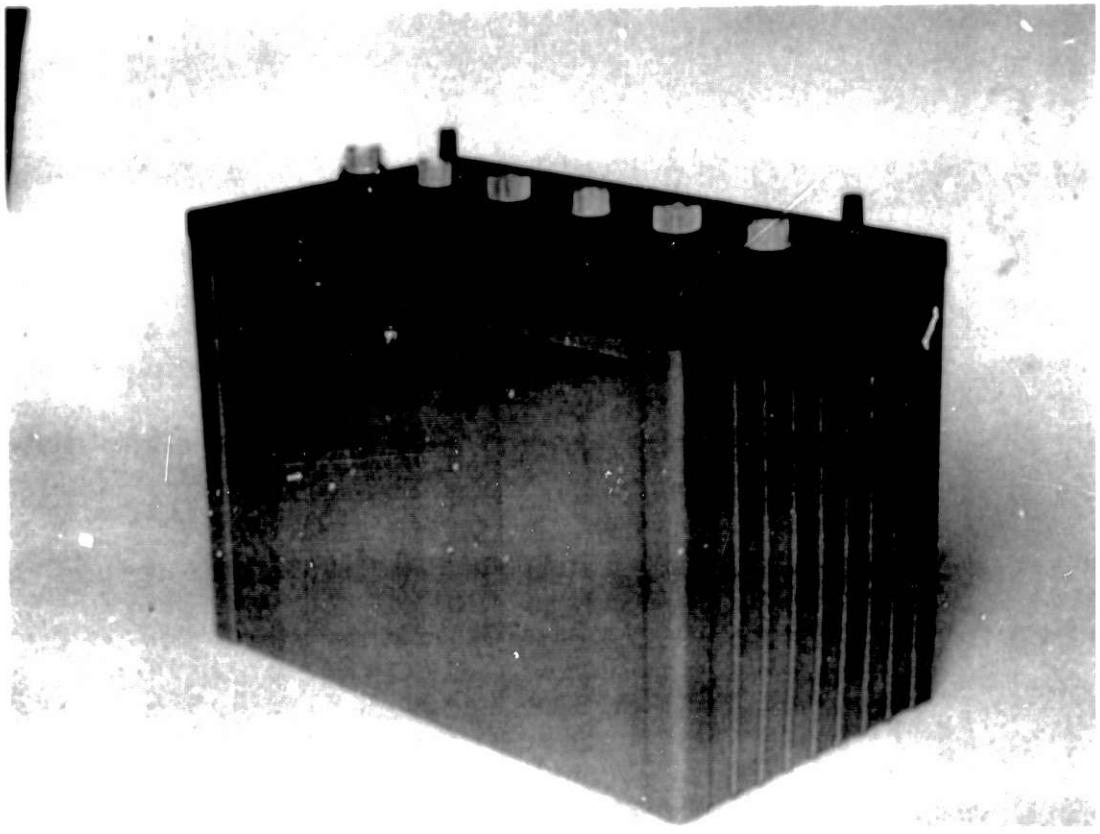

Nominal Voltage, V	12 (2 V x 6 cells)
Nominal Capacity, Ahr	150 (c/5 rate)
Module Weight, kg	28
Dimension, mm	318 L x 179 W x 234 H
Specific Energy, Whr/kg	70 (c/5 rate)

Fig. 8. Lead/Acid Battery Module with Multi-layer Positive Electrode (Japan Storage)

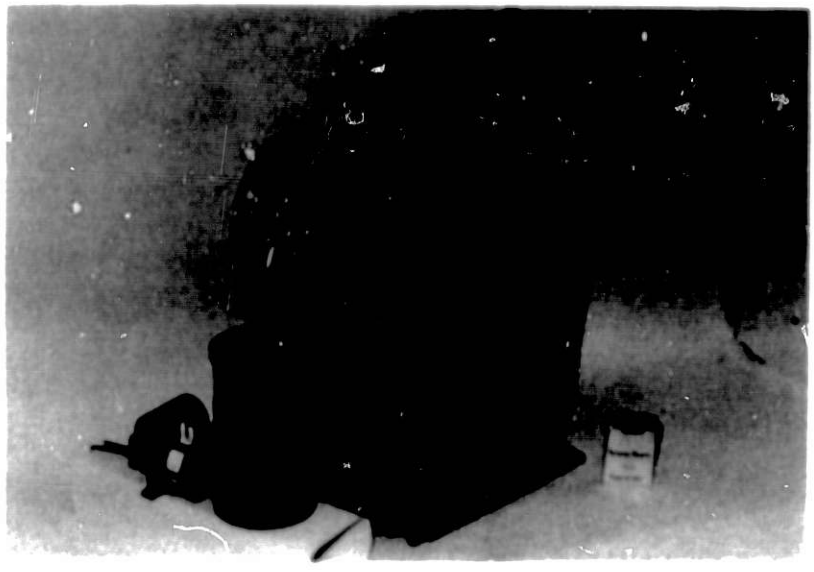

Nominal Voltage, V	40 (2V x 20 cells)
Nominal Capacity, Ahr	50 (c/5 rate)
Module Weight, kg	32
Dimension, mm	300 W x 200 L x 390 H
Specific Energy, Whr/kg	61 (c/5 rate)

Fig. 9. Bipolar Lead/Acid Battery Module with Circulating Electrolyte (Yuasa)

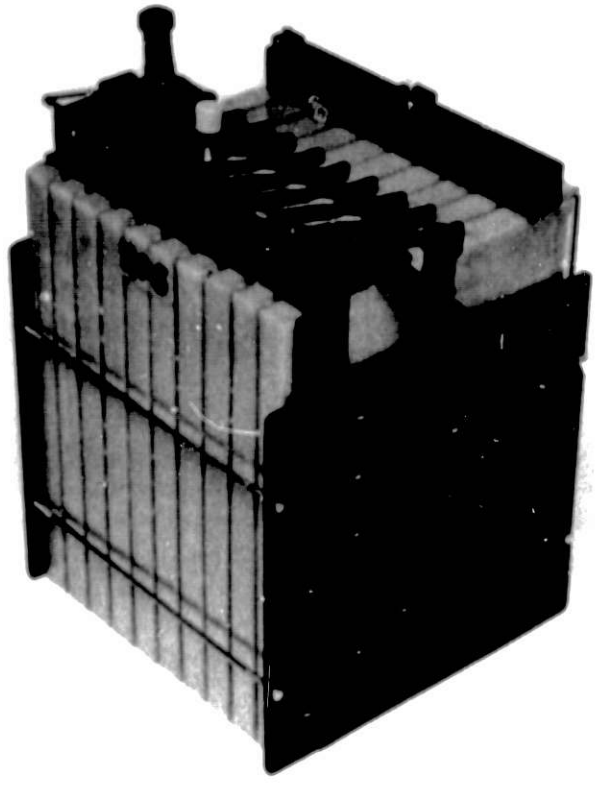

Nominal Voltage, V	10 (1 V x 10 cells)
Nominal Capacity, A-hr	125 (c/7 rate)
Module Weight, kg	11
Dimensions, mm	200 L x 200 W x 263 H
Specific Energy, W-hr/kg	123 (c/7 rate)

Fig. 10. Zinc/Air Battery Module with Fixed Electrolyte (Japan Storage)

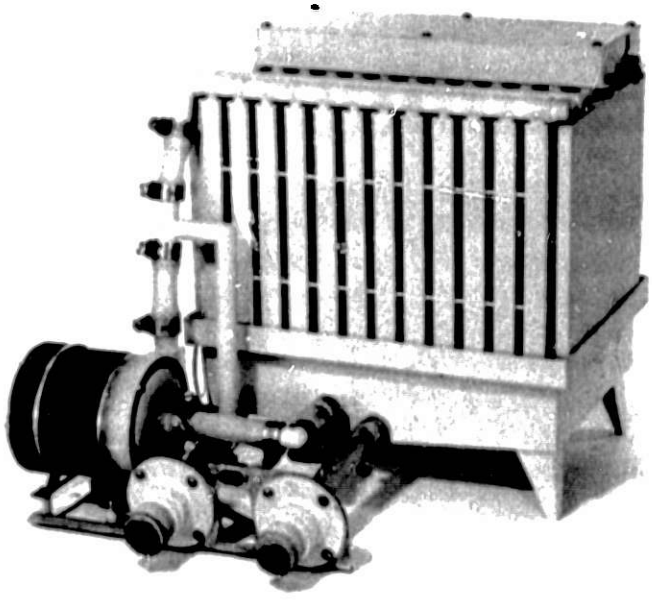

ZINC/AIR BATTERY MODULE WITH CIRCULATING
ELECTROLYTE (SANYO)

Nominal Voltage, V	:	12 (1 V x 12 cells)
Nominal Capacity, Ahr	:	200 (c/7 rate)
Module Weight, kg	:	28.4 (pump, others included)
Dimension, mm	:	460 L x 450 W x 375 H
Specific Energy, Whr/kg	:	91
Whr/ℓ	:	33

Fig. 11.

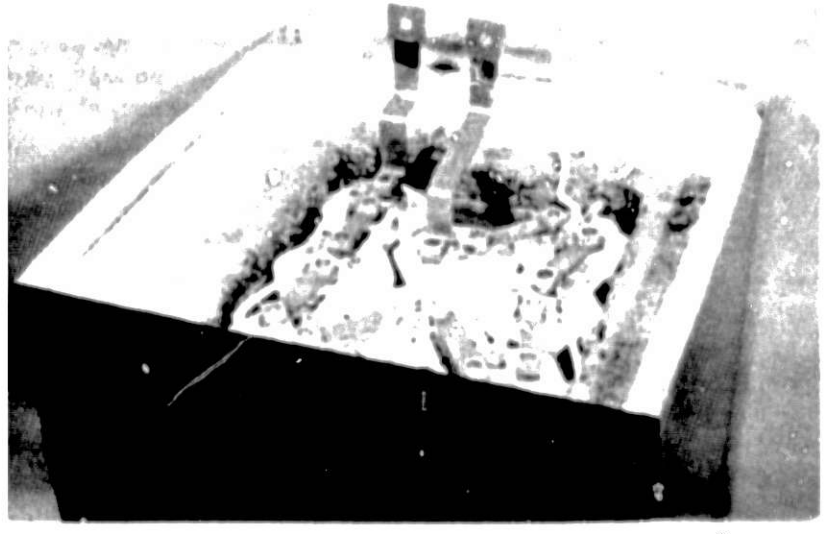

[illegible]

[illegible]		[illegible]
[illegible]		[illegible]
Number of Single Cells	:	66
Number of Volt Batteries	:	[illegible] (in series)
Specific Energy, W-hr/lb	:	93 (c/5 rate)

Fig. 12.

AN OVERVIEW OF JAPANESE NATIONAL ELECTRIC VEHICLE PROJECT

The National Electric Vehicle Project in Japan, which was initiated in 1971 and will be concluded in 1977, has been a well-planned and implemented national program that has been reflected by the full participation of private sectors involved in the electric vehicle technologies. Significant advancements have been made in vehicle component technologies and in total vehicle system integration. Advanced battery technology is yet to be emphasized and fully developed, but the engineering development of compact battery modules and their system integration to vehicles has indeed been impressive. The achievements are particularly noteworthy in view of the modest program size and the time element involved. The targeted 1977 performance goals for the advanced batteries and the experimental vehicles appear to be within the reach of their technology. However, development of the present electric vehicle technology into an economically viable enterprise is far from complete and will require extended efforts which the Japanese private industry must undertake.

ACKNOWLEDGMENTS

I wish to express my appreciation to the personnel of numerous Japanese organizations who kindly provided valuable information during my two visits to Japan in 1975. The organizations include all the advanced battery developers discussed in this paper as well as the automotive manufacturers Toyota, Daihatsu, and Mitsubishi. Above all, I would like to thank Mr. Kenichi Ito of AIST, MITI and Dr. Yoshizo Miyake of Osaka Government Industrial Research Institute who provided me with an overview of the Japanese Electric Vehicle Project and also the opportunity to visit the above organizations. I am grateful to the U. S. Energy Research and Development Administration for providing the travel funds.

REFERENCES

1. N. P. Yao and J. R. Birk, "Battery Energy Storage for Utility Load Leveling and Electric Vehicles: A Review of Advanced Secondary Batteries," *Proc. 10th Intersociety Energy Conversion Engineering Conference*, 1107 (1975).

2. K. Kanai and A. Azuma, Japan IERE Council, "Electric Energy Storage," presented at the 7th Annual Meeting, International Electric Research Exchange, Tokyo, Japan, May 14-16, 1975.

3. I. Kita, "The Usage Records of Lead-Acid Battery for Peak Shaving in Electric Utility Load," Yuasa News, 1944 (in Japanese).

4. "Development of Electric Vehicles in Japan," Agency of Industrial Science and Technology, Ministry of International Trade and Industry, Japan, December 1974 (in English).

METAL HYDROGEN BATTERIES

B. S. Baker
Energy Research Corporation
3 Great Pasture Rd.
Danbury, Conn. 06810

ABSTRACT

For the past few years Energy Research Corp. has been developing a family of special purpose metal-hydrogen batteries. Most of the work has been focused on the nickel-oxide hydrogen battery for use in communication satellities. More recently work on silver-hydrogen and lead-hydrogen batteries has been initiated.

The advantages of using a hydrogen fuel cell type electrode in a rechargeable battery are mainly with the low cost, long life and high degree of reversibility of the hydrogen fuel cell type electrode when operated under typical battery conditions. The latter are invariably dictated by positive plate design and usually result in a current density considered low by fuel cell design standards.

In addition to the basic operating advantages associated with hydrogen electrodes, metal-hydrogen batteries exhibit very attractive system characteristics for both overcharge and cell reversal.

Nickel-hydrogen test cells have undergone thousands of deep cycles without appreciable decay. Fifty amperehour cells delivering over 22 W-hr/lb are operating between 50 and 500 psi with negligible decay at our laboratories. Lead-hydrogen cells have also shown practical operating characteristics.

Nickel-hydrogen and lead-hydrogen batteries are candidate couples for load leveling applications. The former could be built at a $40/KWH cost and the latter for considerably less.

Hydrogen storage as a metal hydride or as a high pressure gas can be considered for these applications. Integrated hydride-nickel hydrogen test cells have been built and tested at ERC for hundreds of cycles.

In the paper the economics of nickel-hydrogen batteries for laod leveling will be discussed.

A-130

ALKALINE BATTERIES

Jack T. Brown
Westinghouse Research and Development Center
Pittsburgh, Pennsylvania 15235

ABSTRACT

Commercial secondary alkaline batteries include those based on the electrochemistry of the nickel-cadmium, silver-zinc, silver-cadmium, nickel iron, and manganese-zinc couples. From a market standpoint the most important of these is the nickel-cadmium type. However, the total market is less than $100 million per year, and less than 10% of that of the lead-acid battery.

These various cell types are manufactured in several construction technologies for various applications. For example, nickel-cadmium batteries are made as flat-plate pocket or sintered types, with the electrolyte flooding the cell, thus requiring a vent in the case, or retained only in the separators and plate pore volume, known as starved, and enabling the cell case to be sealed. Flat plates are stacked along side each other resulting in a rectangular shaped cell, or sintered plates can be spirally wound making a cylindrically shaped cell. Batteries with sintered, flooded, vented, rectangular cells are used for aircraft engine starting, and sintered spiral wound, starved, sealed, cylindrical cells are used in small calculators, etc. Some silver-zinc cells are manufactured in sizes up to 7000 ampere-hours capacity for underseas vehicle propulsion power sources.

In the near term, new secondary alkaline systems are being readied for market introduction. These are a technology modification called the iron-nickel system and the nickel-zinc and nickel-hydrogen batteries. The iron-nickel and nickel-zinc batteries are intended principally as candidates for reasonably low capital cost, high specific energy content ground transportation or underseas electric vehicle propulsion power sources. Nickel-hydrogen batteries are intended principally as an improved satellite battery.

For the longer term several groups of battery researchers and technology developers are intrigued with the combination of potential performance characteristics and low-cost of metal-air type systems. Here the prime candidates use alkaline electrolytes, and the air cathode in combination with either zinc or iron anodes. The technology opportunity is for perhaps doubling the specific energy content, and cutting the cost in half compared to the nickel electrode counterpart systems.

PART B

HIGH TEMPERATURE BATTERY

WORKSHOP

STRUCTURAL, THERMODYNAMIC, AND KINETIC PROPERTIES OF SOLID ELECTRODES

W. L. Worrell and A. S. Nagelberg

Department of Metallurgy and Materials Science
University of Pennsylvania, Philadelphia, Pennsylvania 19174

One major impediment to the development of useful reversible batteries is the lack of suitable solid electrode materials. After a brief review of electrochemical principles, the characteristics of an ideal solid electrode are summarized. Solid compounds which appear to possess many of these characteristics are the alkali metal intercalated dichalcogenides of the Group IV and V transition metals. The preparation and crystal structures of these intercalated compounds are reviewed. A method for estimating maximum values of the alkali metal chemical potential in these compounds is described. Knowledge of the compositional variation of the chemical potential and diffusivity of the alkali metal in these compounds is necessary to quantitatively assess their usefulness as cathode materials. Electrochemical cell techniques which can be used to obtain such data are briefly summarized.

INTRODUCTION

Within the past few years, there has been increased interest in developing reversible batteries and electrochemical cells. Much research has been directed toward the discovery of new solid ionic conductors having low resistivity.[1] Although a few solid electrolytes, for example the beta-aluminas, have unusually low resistivities, the most feasible electrolytes at ambient temperatures are liquids. Because of the inherent stability and other advantages of the solid-liquid interface, the use of a liquid electrolyte in a battery usually mandates the use of solid electrodes. The purpose of this paper is to summarize the characteristics of an ideal solid electrode and to describe the properties of one class of solids, intercalated dichalcogenides, which exhibit many of these characteristics.

ELECTROCHEMICAL PRINCIPLES

Before summarizing the characteristics of the ideal solid electrode, it is helpful to briefly review some basic electrochemical principles.[2] In a battery or electrochemical cell, the open circuit voltage (V) is established by the chemical potential difference across the electrolyte

$$V = \frac{1}{nF}(\mu_A' - \mu_A'') . \qquad (1)$$

In Eq.(1) n is the charge of ion A in the electrolyte, F is the Faraday constant, and μ_A' and μ_A'' are the chemical potentials of A in the anode and cathode, respectively. Under closed-circuit conditions, the cell voltage is equal to the $I\Omega$ drop across the electrolyte and the overvoltage (η).

$$V = I\Omega + \eta. \qquad (2)$$

For a useful and efficient battery, it is necessary to minimize the overvoltage and the resistance of the electrolyte. High overvoltages can be caused by slow electron transport at the electrode-electrolyte interface and slow transport in the solid electrodes. For reversible batteries in which an alkali metal ion, A^+, is transported across the electrolyte, only one electron is exchanged between A^+ and A at the electrolyte-electrode interface. Such a simple electron transfer reaction should be rapid and is unlikely to be rate-limiting. However, diffusion in solids is usually slow at ambient temperatures, and slow transport in the solid electrode is expected to be the most significant factor in establishing high overvoltages in alkali metal batteries.

When transport in the electrodes is rate-limiting, concentration or chemical potential gradients are established in the electrodes at each electrode-electrolyte interface. A schematic illustration of these chemical potential gradients is shown in Fig. 1(a), where the cell voltage (V-η) is less than the open circuit voltage established by Eq.(1). Indeed, one characteristic of ideal solid electrodes is a high diffusivity of A, so that chemical potential gradients in the electrodes are minimized. As shown in Fig. 1(b), the overvoltage is minimized in such cells, and the cell voltage is essentially equal to its open-circuit value.

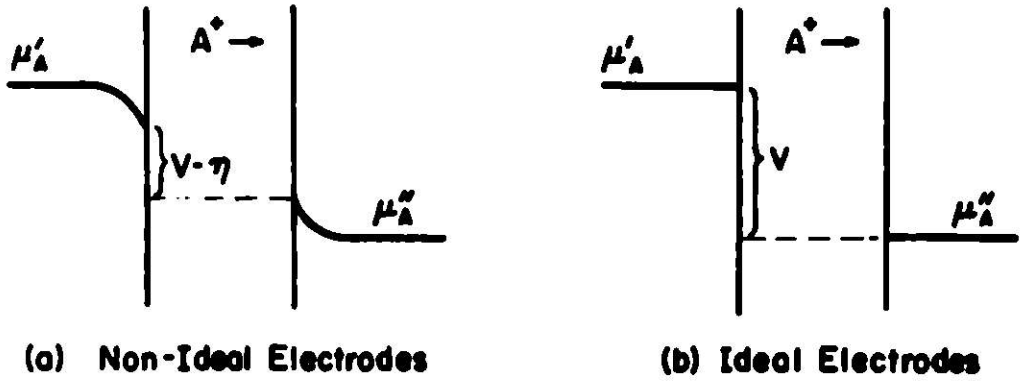

(a) Non-Ideal Electrodes (b) Ideal Electrodes

Fig. 1. Schematic picture of chemical potential gradients in electrodes during current flow.

IDEAL SOLID ELECTRODES

Besides a high diffusivity of the mobile species, ideal solid electrodes must have the other characteristics listed in Table I.

Table I

Characteristics of Ideal Solid Electrodes

1. Low value for μ_A in cathode and
   High value for μ_A in anode
2. Minimum compositional variation of μ_A
3. Reasonably wide compositional range
4. High Electronic Conductivity
5. High Diffusivity of A

The first characteristic listed in Table I is obvious from Eq.(1), in which the open-circuit voltage is directly related to the chemical potential difference across the electrolyte. In principle, the best anode material is pure A because μ_A is maximized and there is no possibility of a chemical potential gradient during current flow. However, other problems can arise with pure A nodes; for example, solution of A in the liquid electrolyte might be significant. Ideal cathode materials are highly stable solid compounds which have extremely low values for μ_A. A method for estimating μ_A in solid compounds will be described in a subsequent section.

During current flow the composition of A in the cathode increases. Thus, to avoid a significant decrease in cell voltage during operation, μ_A should be relatively constant with composition (c_A) at low values of μ_A. Curve (a) in Fig. 2 shows ideal cathode behavior in which μ_A is essentially constant at low values of μ_A. Curve (b) in Fig. 2 shows ideal anode behavior in which μ_A is essentially constant at high values of μ_A. The compositional range over which μ_A is constant must be extensive enough to permit significant charge transfer. To accomplish this, the electrode must also exhibit a reasonably wide compositional range (characteristic 3 in Table I), which eliminates from consideration many highly stable stoichiometric compounds.

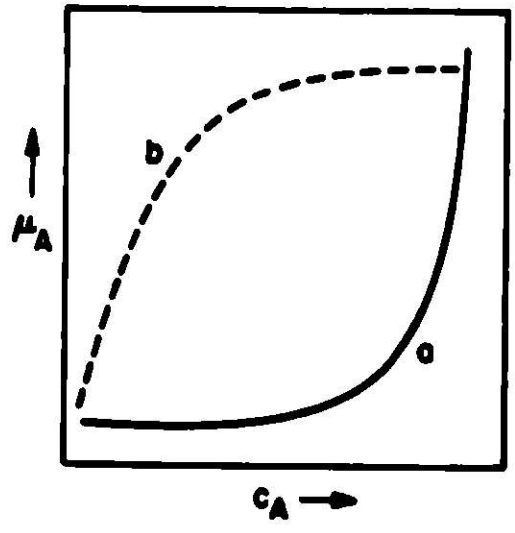

Fig. 2. Schematic picture of the variation of chemical potential (μ_A) with composition (c_A) in solids.
(a) ideal cathode behavior and (b) ideal anode behavior.

An ideal electrode should have high enough electronic conductivity to ensure that electrons are rapidly supplied or removed from the electrode-electrolyte interface. If electron transport in the electrode is too slow, the electrode resistance becomes significant, and the cell resistance is not simply equal to the resistance of the electrolyte. This problem can be eliminated by using a chemically inert current carrier to supply or remove electrons at the electrode-electrolyte interface. However, this restricts electron transfer reactions to one-dimensional lines of intersection of three phases (electrode, electrolyte, current carrier).

As indicated in Fig. 1, rapid transport of the mobile species in the electrodes is necessary to minimize cell overvoltages. Because diffusion in most solids is slow at ambient temperatures, characteristic 5 in Table I is one of the most difficult to achieve. However, solids with unique crystal structures can have abnormally high diffusivities. For example, alkali metals intercalated into dichalcogenides of the Group IV and V transition metals appear to have high chemical diffusivities in two dimensions.[3,4,5] Properties of these intercalated compounds are described in the next section.

ALAKLI METAL INTERCALATED DICHALCOGENIDES

Intercalated dichalcogenides are solids which possess many of the desirable characteristics listed in Table I. Before describing the intercalated dichalcogenides, the known electrical and structural properties of the disulfides and diselenides of the Group IV and V transition metals will be described. The ditellurides are not included because little inforamtion is available for the MTe_2 compounds.

Properties of the Dichalcogenides

Limited information concerning the electrical properties of the dichalcogenides is available. The Group IV and V compounds are usually low band-gap semiconductors or metallic conductors.[6] An exception is HfS_2, which has a room temperature resistivity greater than 10^5 ohm-cm[6]. In contrast, the resistivity of TaS_2 is $\approx 10^{-4}$ ohm-cm in the 'a' direction and $\approx 10^{-3}$ ohm-cm parallel to the 'c' direction.[7]

The outstanding structural characteristic of the Group IV and V transition metal dichalcogenides is their layer structure.[6] Figure 3(a) is a schematic picture of the stacking sequence of hexagonally packed M and X planes, where M is the transition metal and X is sulfur or selenium. The metal coordination is either trigonal prismatic or octahedral, as shown in Fig. 3(b). The coordination of X is unsymmetric, and weak van der Waals bonding exists between the adjacent sulfur (selenium) planes. These compounds exhibit marked cleavage perpendicular to the hexagonal c axis. There are a number of different polytypes of these compounds due to variations in the stacking sequence of the individual planes. For example, the 2-H polytype has a hexagonal unit cell with the c axis twice that of the simple structure, while the a parameter is unchanged. The 3-R polytype has a rhombohedral unit cell which, when indexed in the hexagonal system, gives a c parameter three times that of the simple structure; the a axis again remains unchanged.

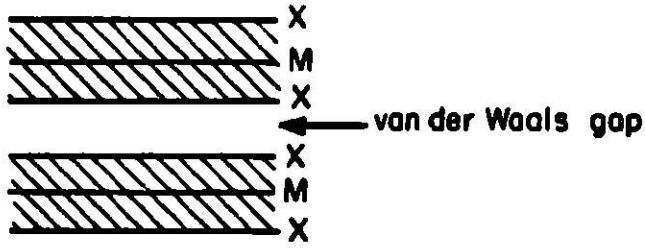

(a) Stacking Sequence of M and X Planes

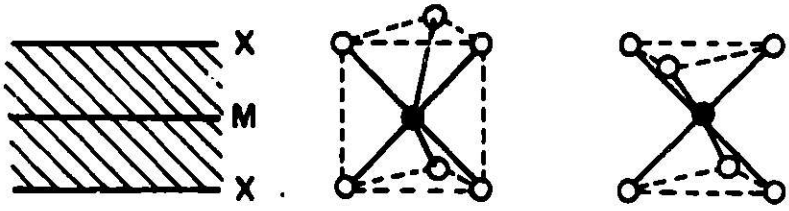

(b) Coordination Units for MX_2 Layer Structures

Fig. 3. Structural characteristics of the dichalcogenides of the Group IV and V transition metals.

Alkali Metal Intercalation

Rudorff first demonstrated that alkali metals could be intercalated into the van der Waals gaps of the transition metal dichalcogenides.[8] Even at liquid ammonia temperatures, the intercalation process was rapid. From magnetic measurements, Rudorff suggested that the intercalated compounds could be considered to be of the ionic form $A_x^+(MX_2)^{x-}$, where A is the alkali metal.

Alkali metal intercalation has been achieved by several methods.[3,8-15] One method is heating the dichalcogenide in an alkali metal vapor in quartz capsules.[9] However, at low temperature the alkali metal vapor pressure is too small; while at higher temperatures the vapor can react with the quartz capsule. Another method uses solutions of alkali metals in liquid ammonia.[3,8] Even though ammonia also intercalates, it apparently is removed by heating under vacuum. Aqueous solutions of alkali halides or hydroxides have been successfully used to intercalate the dichalcogenides.[10] Water molecules are also inserted into the van der Waals gap, but they can be removed in some cases by heating. Intercalation of dichalcogenide cathodes has also been achieved electrochemically by electrolysis of aqueous salt solutions.[11,12]

Recently solutions containing organometallic compounds of alkali metals have been used to intercalate transition metal dichalcogenides.[13-15] Lithium intercalation is achieved using n-butyllithium dissolved in hexane. For sodium intercalation, sodium naphthalide in tetrahydroforan is used.

Properties of A_xMX_2 Compounds

Alkali metal intercalated compounds have the chemical formula A_xMX_2, where x can vary between 0 and 1.0.[3,6] No conductivity measurements have been reported for the A_xMX_2 compounds, but a delocalization of the electrons could increase their conductivity above that of the original MX_2 compounds. Such electron delocalization has been observed in NMR studies,[3] which also supports the $A_x^+(MX_2)^{x-}$ formula first suggested by Rudorff.[8] The conclusion that the alkali metal exists as an ion in the van der Waals gap is also consistent with the observed linear variation of the c lattice parameter with ionic radius for a given composition x.[3]

Crystallographic investigations[3,8,13,14,16,17] of A_xMX_2 compounds have shown that intercalated alkali metal atoms cause an expansion of the c axis, which is proportional to their ionic radius. The a axis is essentially unchanged. The expansion of only the c axis is expected if the alkali metal atoms enter only the van der Waals gap between the adjacent x planes shown in Fig. 3(a). Lattice parameters determined for AMX_2 compounds of the Group IV transition metals[3,8,13,14] are tabulated in Table II. Similar data for the Group V transition metal compounds[14,16,18] are listed in Table III.

Table II. Lattice Parameters of Intercalated Compounds Formed Between Alkali Metals and the Group IV Dichalcogenides

Compound*	a (Å)	c (Å)**	Reference
TiS_2	3.407	5.696	13,14
$LiTiS_2$	3.454	6.187	13
$NaTiS_2$	3.469	3 × 6.86	3
$KTiS_2$	3.488	3 × 7.61	3
$RbTiS_2$	3.427	3 × 8.1	3
$CsTiS_2$	3.500	3 × 8.17	3
$TiSe_2$	3.535	6.004	14
$LiTiSe_2$	3.64	6.488	14
$Na_{0.98}TiSe_2$	---	3 × 6.9	8
ZrS_2	3.665	5.835	14
$LiZrS_2$	3.604	3 × 6.25	14
$NaZrS_2$	3.66	3 × 6.78	3
$KZrS_2$	3.718	3 × 7.4	3
$Rb_{0.75}ZrS_2$	3.657	3 × 8.01	3
$Cs_{0.64}ZrS_2$	3.644	3 × 8.41	3
$ZrSe_2$	3.776	6.160	14
$LiZrSe_2$	3.734	6.648	14
HfS_2	3.635	5.856	14
$LiHfS_2$	3.56	3 × 6.375	14
$HfSe_2$	3.742	6.160	14
$LiHfSe_2$	3.715	6.642	14

*All data are for x = 1.0 in the formula A_xMX_2, unless otherwise noted.

**To indicate the 2-H or 3-R polytype, some c lattice parameters are indicated as 2× or 3× the c axis of the simple hexagonal structure.

Table III. Lattice Parameters of Intercalated Compounds Formed Between Alkali Metals and the Group V Dichalcogenides

Compound*	a (Å)	c (Å)**	Reference
VSe_2	3.35	6.10	14
$LiVSe_2$	3.584	6.356	14
NbS_2	3.34	3 × 6.00	14
$LiNbS_2$	3.342	3 × 6.421	14
$Na_{0.67}NbS_2$	3.366	2 × 7.26	16
$K_{0.67}NbS_2$	3.345	2 × 8.11	16
$NbSe_2$	3.45	2 × 6.27	14
$LiNbSe_2$	3.436	2 × 6.772	14
$Na_{0.67}NbSe_2$	3.476	2 × 7.683	16
$K_{0.67}NbSe_2$	3.480	2 × 8.52	16
TaS_2	3.340	2 × 6.04	14
$LiTaS_2$	3.340	2 × 6.475	14
$Na_{0.8}TaS_2$	3.335	2 × 7.261	18
$K_{0.67}TaS_2$	3.345	2 × 8.11	16
$TaSe_2$	3.436	2 × 6.348	14
$LiTaSe_2$	3.477	2 × 6.817	14
$Na_{0.67}TaSe_2$	3.458	2 × 7.701	16
$K_{0.67}TaSe_2$	3.463	2 × 8.525	16

*All data are for x = 1.0 in the formula A_xMX_2, unless otherwise noted.

**To indicate the 2-H or 3-R polytype, some c lattice parameters are indicated as 2× or 3× the c axis of the simple hexagonal structure.

Because the alkali metal atoms are positioned in the van der Waals gaps of the A_xMX_2 compounds, one expects an unusually high mobility of these atoms perpendicular to the c axis. Rapid intercalation rates and NMR studies[3] provide qualitative support for such expectations. The only reported experimental measurements of the chemical diffusivity (D_A) of A in these A_xMX_2 compounds is the work of Winn and Steele.[4,5] They used electrochemical cells of the type

$$\text{Na} \mid \text{propylene carbonate (NaI)} \mid Na_xTi_{1+y}S_2 \qquad \text{(A)}$$

to measure D_{Na} as a function of x and y in the compound $Na_xTi_{1+y}S_2$. Values of D_{Na} ranged from 10^{-6} to 10^{-7} cm^2/sec for $Na_xTi_{1.0025}S_2$ at ambient temperatures when x was less than 0.45. Such diffusivity values are extremely high, particularly for solid compounds. When x was greater than 0.45 and the titanium concentration (y) was increased, the sodium diffusivity decreased to 10^{-9} cm^2/sec. Presumably titanium atoms in excess of the stoichiometric concentration reside in the van der Waals gaps and hinder the movement of the sodium atoms.

Winn and Steele[4,5] also measured the open-circuit voltages of cell (A). The cell voltage did not vary significantly with the titanium concentration (y) in $Na_xTi_{1+y}S_2$. When x was below 0.45, the cell voltage was approximately 2 volts. At higher values of x, the voltage dropped rapidly to about 1.4-1.5 volts at x = 1.0.

ESTIMATION OF μ_A IN AMX_2 COMPOUNDS

The A_xMX_2 compounds must have extremely low chemical potentials of A(μ_A) to function as useful cathode materials. With the exception of the Winn and Steele measurements[4,5] cited in the previous paragraph, there are no direct or indirect experimental measurements of μ_A in these compounds. Thus, it is useful to estimate μ_A from phase relationships in the ternary A-M-X system. Our method of estimation is applicable to the AMX_2 composition (x = 1) and thus yields a maximum value for μ_A. As an illustration of our method, consider the A-Ta-S system, where A is lithium, sodium or potassium. The isothermal ternary section for this system at 300 K is shown in Fig. 4. Figure 4 is obtained in the following manner. Phase data for the pertinent binary systems[19] are assembled. From the available thermodynamic data,[20,21] we conclude that reaction (3) must proceed to the right

$$2A + TaS \longrightarrow A_2S + Ta \ . \qquad (3)$$

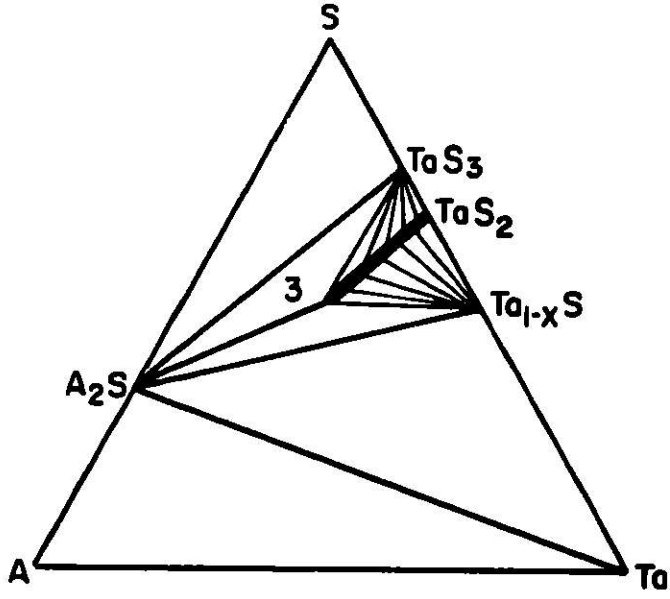

Fig. 4. Isothermal ternary section for the A-Ta-S system at 300 K, where A is Li, Na or K.

Thus, tantalum will not react with A_2S, and a two-phase tie line must exist between them as shown in Fig. 4. With the Ta-A_2S tie line established, the other two-phase tie lines must be as shown, because there are no other alternatives. The major uncertainty in Fig. 4 is the possible existence of ternary compounds, which would not be apparent in the binary phase diagrams. The existence of ternary compounds would not significantly affect our estimate for μ_A unless these compounds had unusually high thermodynamic stabilities. In Fig. 4 the compositional range of the A_xTaS_2 phase is shown as a narrow dark region projecting from TaS_2 into the ternary phase field. Non-stoichiometric ranges of the binary sulfides are not indicated, because such data are not necessary for our purpose.

Figure 4 implies that μ_A in A_xMX_2 must be extremely low, even in AMX_2 (x = 1), because AMX_2 is not in equilibrium with pure A. As indicated by the three-phase triangle marked 3 in Fig. 4, AMX_2 is in equilibrium with A_2S and TaS_3, which can be represented by

$$ATaS_2 + A_2S = TaS_3 + 3\underline{A} . \quad (4)$$

Thus,

$$\mu_A = \tfrac{1}{3}(\Delta G^\circ_{A_2S} + \Delta G^\circ_{ATaS_2} - \Delta G^\circ_{TaS_3}) , \quad (5)$$

where ΔG° represents the standard free energy of formation of the appropriate compounds. From thermodynamic equilibrium studies of TaS_2,[20] a value of -89.5 kcal/mole for $\Delta G^\circ_{TaS_2}$ at 300 K is obtained. In the tantalum-sulfur binary system, TaS_3 is a stable phase; thus, each of the following reactions must proceed toward the right

$$TaS_2 + \tfrac{1}{2}S_2(g) \rightarrow TaS_3 \quad (6)$$

$$TaS_3 + \tfrac{1}{2}Ta \rightarrow \tfrac{3}{2}TaS_2 . \quad (7)$$

Reaction (6) requires that $\Delta G^\circ_{TaS_3}$ is more negative than $\Delta G^\circ_{TaS_2}$, while reaction (7) requires that $\frac{3}{2}\Delta G^\circ_{TaS_3}$ is more negative than $\Delta G^\circ_{TaS_3}$. Thus, $\Delta G^\circ_{TaS_3}$ must have a value between -89.5 and -134.3 kcal/mole. The TaS_3 phase appears to be only slightly more stable than TaS_2,[19] thus, a value of -95 kcal/mole is estimated for $\Delta G^\circ_{TaS_3}$. A value of -108 kcal/mole for $\Delta G^\circ_{ATaS_2}$ is estimated from $\Delta G^\circ_{TaS_2}$ by assuming that the $ATaS_2$ compound is 20% more stable than TaS_2. Values for $\Delta G^\circ_{Na_2S}$ (-96 kcal/mole) and $\Delta G^\circ_{K_2S}$ (-95 kcal/mole) are available.[21] From these values, a reasonable estimate for $\Delta G^\circ_{Li_2S}$ is -94 kcal/mole. Using these free energy data and Eq.(5), one calculates the values of μ_A and the activity (a_A) of lithium, sodium, and potassium in $A_{1.0}TaS_2$ at 300 K which are tabulated in Table IV. Values of the open-circuit voltage (V) of cell (B), in which the cathode is $ATaS_2$ and the anode is pure A, are also tabulated in Table IV.

$$A \mid A^+ \text{ electrolyte} \mid ATaS_2 . \quad (B)$$

Table IV. Estimated Thermodynamic Properties of A in $ATaS_2$ at 300 K

A	Activity of A	μ_A (kcal/g atom)	V (volts)
Li	1.0×10^{-26}	-35.7	1.55
Na	3.4×10^{-27}	-36.3	1.57
K	5.9×10^{-27}	-36.0	1.56

The uncertainty in the calculated values of μ_A is estimated as ±10 kcal/gatom; thus, the uncertain in V is ±0.4 volts.

The chemical potential values tabulated in Table IV are maximum values, because μ_A in A_xTaS_2 must decrease with decreasing x. For this reason, calculated cell voltages are minimum values. For example, we have measured 1.7 volts for the open-circuit cell voltage using a $Li_{0.8}TaS_2$ cathode and a pure lithium anode.[22] If the compositional trend for μ_A in A_xTaS_2 is the same as that in Na_xTiS_2,[4,5] open-circuit cell voltages should increase to 2.0 to 2.5 volts when x is less than 0.5.

ELECTROCHEMICAL INVESTIGATIONS

Clearly more quantitative thermodynamic and kinetic data are required to assess potential cathode applications of the A_xMX_2 compounds. Knowledge of the compositional variation of the chemical potential and diffusivity of alkali metals in these compounds is particularly needed. Electrochemical cells with A_xMX_2 cathodes can be used to obtain such data. For example, open-circuit voltage measurements with cell (C) can be used to determine the variation of μ_A with composition x.

$$A \mid A^+ \text{ electrolyte} \mid A_xMX_2 \ . \qquad (C)$$

The composition of A in the A_xMX_2 electrodes can be precisely varied using coulometric titration techniques.[4,23]

Various methods of determining chemical diffusivities of alkali metals in the A_xMX_2 electrodes of cell (C) are available.[4,23] In the potentiostatic method, the concentration of the alkali metal at the A_xMX_2-electrolyte interface is suddenly raised by decreasing the steady-state cell voltage of cell (C). From measurements of the transient current and the appropriate solution to Fick's second law, accurate values of the alkali metal diffusivity in A_xMX_2 can be determined. Another method is the pulse-relaxation technique, in which a current pulse is applied to cell (C) and a known excess of alkali metal is deposited at the A_xMX_2-electrolyte interface. With small changes in cell voltage, the alkali metal diffusivity in A_xMX_2 can be determined from measurements of the transient voltage.

To our knowledge, the only electrochemical cell investigation using a A_xMX_2 cathode is the previously described study of Winn and Steele with Na_xTiS_2.[4,5] In our laboratory, we are currently using electrochemical cell techniques to study Li_xTaS_2 and Na_xTaS_2 electrodes.[18,22]

CONCLUSIONS

The characteristics of an ideal solid electrode listed in Table I are helpful guidelines for developing new useful electrodes. Because A_xMX_2 compounds possess many of these characteristics, they offer exciting possibilities as useful cathodes in alkali-metal batteries. However, the compositional variation of the chemical potential and diffusivity of alkali metals in these compounds is not yet known. Such information can be obtained using electrochemical cell techniques.

ACKNOWLEDGMENT

Our electrochemical cell investigations of solid electrodes has been supported by the Advanced Research Projects Agency of the Department of Defense through the Laboratory for Research on the Structure of Matter at the University of Pennsylvania.

REFERENCES

1. W. van Gool, Ed., Fast Ion Transport in Solids, Solid State Batteries, and Devices, North-Holland Publ. Co., Amsterdam (1973).
2. J. O'M. Bockris and A. K. N. Reddy, Modern Electrochemistry, Vols. 1 and 2, Plenum Press, New York (1970).
3. A. Leblanc-Soreu, M. Danot, L. Trichet, and J. Rouxel, Mat. Res. Bull. 9, 190 (1974).
4. D. A. Winn, Ph.D. Dissertation, Department of Materials Science, Imperial College, London (1975).
5. D. A. Winn and B. C. H. Steele, Abstract 22, J. Electrochem. Soc. 122, 68C, March (1975).
6. J. A. Wilson and A. D. Joffe, Adv. in Physics 18, 193 (1969).
7. A. H. Thompson, F. R. Gamble, and R. F. Koehler, Phys. Rev. B5, 2811 (1972).
8. V. W. Rüdorff, Chimia 19, 489 (1965).
9. F. R. Gamble, J. H. Osiecki and F. J. DiSalvo, J. Chem. Phys. 55, 3525 (1971).
10. M. S. Whittingham, Mat. Res. Bull. 9, 1981 (1974).
11. M. S. Whittingham, J. Chem. Soc. Chem. Comm 328 (1974).
12. G. V. Subba Rao and J. C. Tsang, Mat. Res. Bull. 9, 921 (1974).
13. M. S. Whittingham and A. H. Thompson, J. Chem. Phys. 62, 1588 (1975).
14. M. S. Whittingham and F. R. Gamble, Mat. Res. Bull. 10, 363 (1975).
15. M. B. Dines, Mat. Res. Bull. 10, 287 (1975).
16. W. P. F. A. M. Omloo and F. Jellinek, J. Less-Comm. Metals 20, 121 (1970).
17. R. B. Somoano, V. Hadek, and A. Rembaum, J. Chem. Phys. 58, 697 (1973).
18. A. S. Nagelberg and W. L. Worrell, University of Pennsylvania, unpublished research.
19. F. A. Shunk, Constitution of Binary Alloys, Second Supplement, McGraw-Hill Book Co., New York (1969).
20. H. R. Larson and J. F. Elliott, Trans. TMS-AIME 239, 1713 (1967).
21. J. F. Elliott and M. Gleiser, Thermochemistry for Steelmaking, Vol. 1 Addison-Wesley Press, Reading, Mass. (1960).
22. S. Basu and W. L. Worrell, University of Pennsylvania, unpublished research.
23. W. L. Worrell, Amer. Ceram. Soc. Bull. 53, 425 (1974).

SUBSTRUCTURE AND PROPERTIES OF SODIUM BETA ALUMINA SOLID ELECTROLYTES

L. C. De Jonghe and M. Y. Hsieh
Department of Materials Science and Engineering
Cornell University, Ithaca, New York 14853

ABSTRACT

In this work we attempt to clarify the microstructure and properties of sodium beta alumina solid electrolytes. Improved sinterability of commercial beta alumina powder was achieved by addition of small amounts of the Na_2O - Al_2O_3 eutectic. Complex crystallographic faults, and subgrain boundaries were found that can affect the microscopic homogeneity of the ionic current flow during d.c. ionic conduction. The effects of CaO and SiO_2 additions on microstructure and ionic conductivity are described.

1. INTRODUCTION

The performance and lifetime of sodium/sulphur solid electrolyte storage batteries is strongly affected by a variety of materials related problems. Some of these problems are related to corrosion of the cell containers, to failure of seals, and to the sulphur electrode design. Other limitations of lifetime and performance originate directly or indirectly from the failure of the β alumina type solid electrolytes themselves. We define direct failures as unsatisfactory electrolyte performance due to effects resulting from the preparation of the electrolyte (such as compositional, microstructural, and impurity effects), and indirect failures as those arising from the actual operation of the cell (i.e., the interaction of electrode derived impurities with the electrolyte during current passage). In this paper we are concerned with factors that can affect the direct failure of the sodium beta alumina solid electrolytes. We believe that the reason for electrolyte deterioration is connected with the impurities that were either introduced in the preparation of the electrolyte, or during its subsequent actual use, and does not reside in a chemically unstable nature of the electrolyte with respect to sodium or sodium polysulfides at its temperature of use.

We can distinguish roughly between a variety of impurities according to where they are located:

a - impurities in solid solution in the "spinel blocks" of the sodium beta alumina lattice
b - impurities leading to intergranular or intragranular second phase formation
c - impurities that lodge themselves in the Na^+ ion conduction planes.

In actuality, the impurities will be distributed in some way in these categories. Furthermore, they can affect the microstructure of the ceramic e.g. by promoting exaggerated grain growth. Both the distribution of the impurities and the concurrent microstructural changes are determined by the powder preparation methods and thermal and environment conditions during sinterings. It is clear then that a detailed quantitative study of impurity effects is a difficult task. It is, however, imperative to understand the detrimental

(or beneficial) nature of the most commonly encountered impurities (e.g., Ca and Si) and to estimate to what levels they can be tolerated, to determine whether cost-effective load leveling batteries with sodium β or β" alumina electrolytes are a realistic possibility. The object of our work is to acquire this understanding about the effect of impurities on properties of sodium beta alumina solid electrolytes.

2. ELECTROLYTE PREPARATION

2.1 Commercial Powders

Most of the work has been performed on commercial sodium β alumina powders prepared by Alcoa: XB-2 "superground". These powders have been prepared by a Bayer process, and are fairly clean. A typical analysis of this powder gives ∿7.3 wt.% Na_2O, 0.1 to 0.15 wt.% SiO_2, and a balance of Al_2O_3. Some other contaminants are also present in minor concentrations, such as CaO ∿0.02 wt.%, and Fe_2O_3 ∿0.03 wt.%. The average agglomerate size is 2∿3μ. A significant fraction of this powder consists of submicron particles. Fig. 1 shows the general appearance of the powder in the scanning electron microscope. The powder can be sintered to acceptable final densities (>3.15g/cm^2)

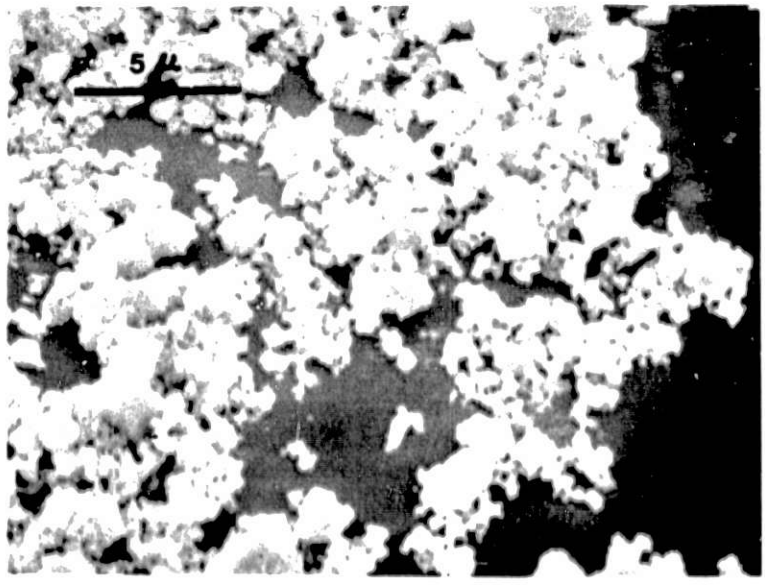

Fig. 1. Alcoa XB-2 "superground" powder as observed in the scanning electron microscope. The average agglomerate size is 2∿3μ; a significant fraction of the powder consists of submicron particles (0.2∿0.3 microns).

without further grinding. Impurities were introduced by dissolving the appropriate nitrates [e.g. $Ca(NO_3)_2$] in methanol, and stirring the powder, impurities and methanol while drying. This procedure insures intimate mixing, and avoids the introduction of additional impurities. If necessary, a binder could be added in this step. The green powders were then pressed into bar shaped samples at 20 ksi, to a green density of 1.8 to 1.9 g/cm^3 (∿55% of theoretical density).

2.2 Preparation from Laboratory Powders

Samples were also prepared from a variety of reagent grade chemicals in different ways:

a. decomposition of hydrated sulphates
b. decomposition of $NaNO_3$ + α Al_2O_3 (Meller, or Reynolds)
c. decomposition of $NaNO_3$ and $Al(NO_3)_3$ mixtures
d. preparation from polymer precursor.

Not all of these methods lead to satisfactory results. In Method C, for example, the decomposition of the nitrates has to be fast, since the molten nitrates have a sufficiently high vapor pressure and differential evaporation may lead to a total lack of control of the final composition. We found Method D (Union Carbide patent 3,385,915; May 28, 1968) unsatisfactory since extensive shrinkage of the polymer precursor (cellulose) prohibits the direct formation of electrolyte of any useful size or thickness. Moreover the yield of oxide from soaked polymer is so low ($\sim$15 g oxide from 100 g of dry cellulose) that the method is not practical.

An interesting observation was made on the powders prepared from nitrates mixed to give the β alumina composition. After rapid calcining at 850°C in air the resultant oxide shows only diffuse x-ray scattering indicating that the powder is either microcrystalline or amorphous. Sintering of such powder surprisingly led to low density electrolyte. We believe that the reason is that the intimately mixed oxides rapidly convert to crystalline particles about the size of the amorphous agglomerate, before the sintering temperature (1750°C) has been reached, thus trapping a lot of porosity. The absence of any transient liquid phases then makes this powder rather "unreactive". The importance of a transient liquid phase has been recognized for some time in the sintering of sodium β alumina solid electrolytes (see e.g. the Ford-Utah-RPI annual report on: "Research on electrodes and electrolyte for the Ford Sodium-Sulphur Battery", S.A. Weiner, project manager, July 1975[1]). We have specifically exploited such a liquid phase to improve the sintering behavior of the commercial sodium beta alumina powders.

2.3 Improving the Sintering Behavior of Commercial Sodium Beta Alumina Powders[2]

The method improves the densification of commercial sodium beta alumina powder and allows fabrication below the temperature where abnormal grain growth becomes rapid ($\sim$1720°C). In this method a sodium-aluminum oxide mixture (Na/Al:0.54), corresponding to the eutectic composition in the Na_2O-Al_2O_3 system[3] is added to the commercial powder up to 10 wt.%. The overall mixture is such that the overall composition of the electrolyte is still in the β alumina phase field. It is important that heating rates are high, to minimize reaction prior to reaching the actual sintering temperatures. We refer to Ref. 2 for additional details.

3. ELECTROLYTE CHARACTERIZATION

3.1 General Microstructural Features

The sodium beta alumina crystal structure can best be described as sodium conduction planes separated by spinel blocks[4,5]. It is well established that the sodium ion conduction normal to the conduction planes is orders of magnitude smaller than in the conduction planes[6]. This property should present problems in establishing microscopically homogeneous current transport in which the sodium ion diffusion rates parallel and through the grain boundaries can play a determining role. Point defects as discussed by Roth[7], dislocations in the basal plane described by Stevens[8], β-β" intergrowth examined by Bevan et al.[9], and complex faults normal to the basal planes as observed by De Jonghe[10], see Fig. 2, all are expected to affect the rapid, homogeneous flow of sodium ions.

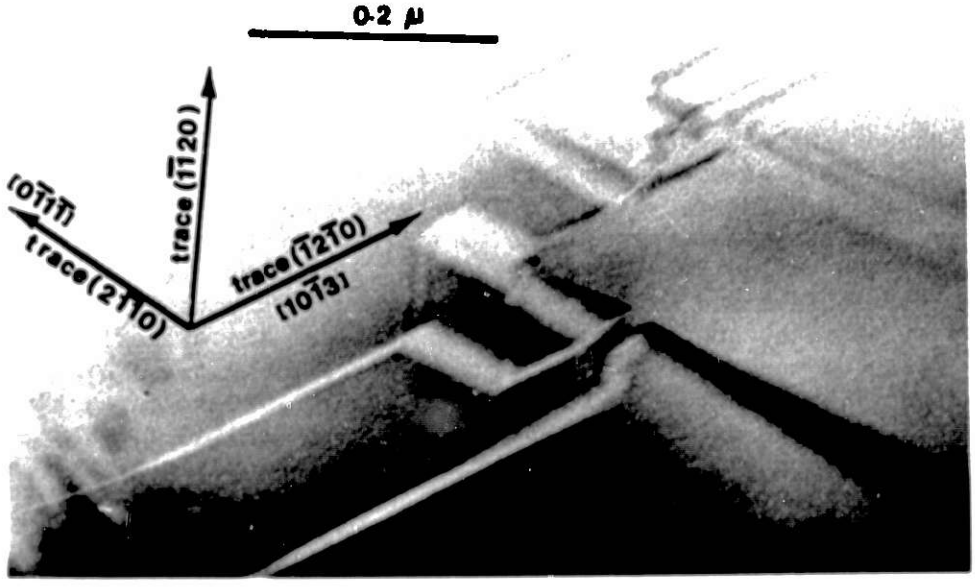

Fig. 2. Network of complex planar faults in sodium beta alumina. The faults are on {2̄1̄10} planes. In the spinel blocks they produce a cation fault only; where they intersect the conduction plane an oxygen stacking fault is produced[10].

Other features such as low angle boundaries, which can frequently be found in sodium beta alumina, may under certain conditions, give rise to current concentrations that might erode grain boundaries or thin grain boundary phases, initiating a failure mechanism as described by Richman and Tennehouse[11]. Fig. 3 shows a scanning electron micrograph of mechanically polished and etched sodium beta alumina, exhibiting micromorphological features that can be interpreted as low angle boundaries. Fig. 4 shows a transmission electron micrograph of some low angle tilt boundaries. Especially such [hk.0] tilt boundaries are thought to be susceptible to current concentrations. These features and their possible consequences have been discussed in more detail elsewhere by De Jonghe[12,13].

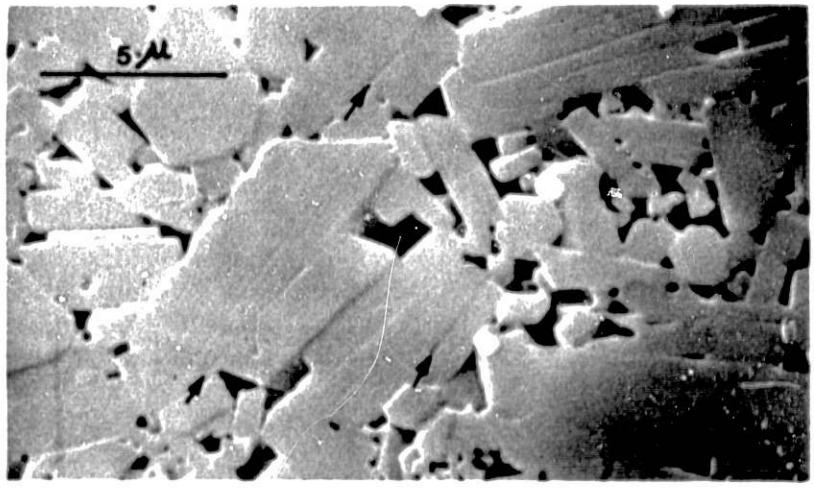

Fig. 3. Scanning electron micrograph of mechanically polished sodium beta alumina etched for 1 second in H_3PO_4 at ~300°C. Several low angle grain boundaries are indicated.

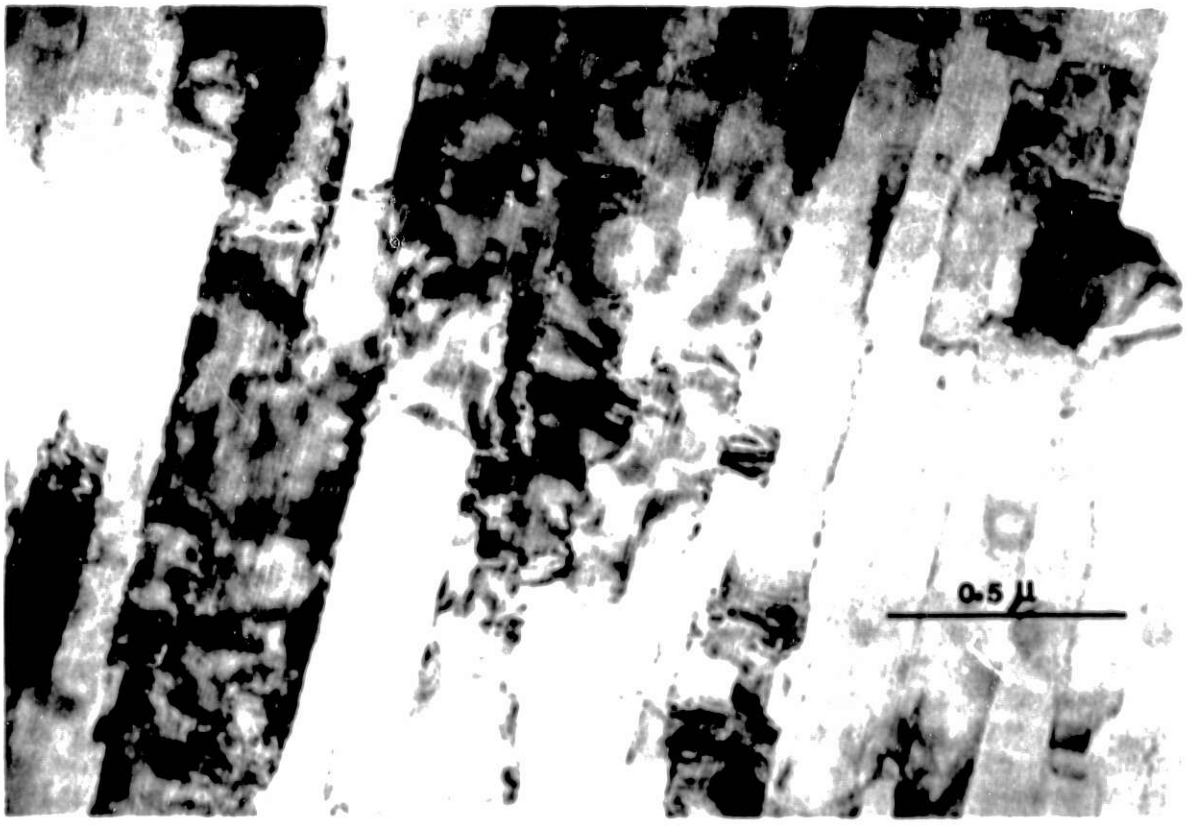

Fig. 4. Low angle [hk.0] tilt boundaries in sodium beta alumina. Such boundaries can give rise to localized ion current inhomogeneities. Detailed examination of the boundaries by means of lattice imaging revealed the presence of dislocations with a Burgers vector equal to $\frac{1}{2}C_o[00.1]$.[12,13]

3.2 Impurity Effects

Effects of calcium and silicon on the microstructure and ionic conductivity were examined. The ionic conductivity was determined from measurements of the impedance of the samples as a function of frequency and temperature, up to 10M Hz and 350°C. The method is equivalent to a measurement of the dielectric dispersion (for a review see Owen[14], and Bauerle[15]. The relevance of such measurements with regard to the substructure of sodium beta alumina was discussed by Powers and Mitoff[16], and was recently reviewed by Franklin[17]. It is sometimes useful to plot the data in the complex admittance plane (B-G plot). This procedure obscures somewhat the explicit frequency dependence of the impedance, but has the advantage of showing more clearly what the main characteristics of an equivalent circuit could be, and which are the electrode and the sample contributions to the dispersion. The interpretation of the dispersion measurements is, however, not always unambiguous, and the corresponding physical meaning of the equivalent circuit elements must be derived from a sufficiently detailed characterization of the sample's microstructure. In the complex admittance plane (B-G), or the complex impedance plane, the data rarely form a semicircle; instead, B-G plots more often approach circular arcs. This observation may be attributed to a physical process where sodium ions are diffusing in a field free region (Warburg type of impedance[17] which might e.g. arise when Na^+ is transported through a grain boundary phase that has a sizable electronic as well as ionic transport number), or to some statistical distribution of one type of ionic relaxation process[14] (e.g., purely ionic transport through a variety of grain boundaries). Although the dispersion measurements are relatively simple experimentally, and give significant information about ionic transport processes, they are not useful as substitutes for a direct microstructural characterization by means of electron optical or other techniques.

3.2.1 Effect of Calcium. Calcium was introduced into sodium beta alumina (Alcoa XB-2 "superground") as described in 2.1, up to 5 wt.% of CaO. Samples containing 5 wt.% of CaO showed evidence of partial melting at the sintering temperature (1700-1750°C), indicating the presence of a significant amount of a liquid phase. For lower CaO contents, the presence of liquid phases during sintering is indicated indirectly by a pronounced abnormal grain growth. Fig. 5A (optical) and Fig. 5B (scanning electron microscope) are micrographs of a sodium beta alumina sample, containing 0.5 wt.% CaO, prepared near 1750°C. They illustrate the extreme difference in average grain sizes of the bimodal distribution. The large grains are platelets with their largest dimensions between 300 and 500 micron, while the small grains have an average grain size of about 3 micron. The extreme abnormal grain growth results in a lower density, due to trapping of porosity. The rate of abnormal grain growth is, however, quite temperature dependent, perhaps due to the formation of different liquid phases. We have not yet identified the liquid phases that are active during sintering. A wide variety of liquid phases can occur in the $CaO-Na_2O-Al_2O_3$ system[18] with melting points ranging from ∿1400°C to ∿1720°C. Depending on the temperature cycle in the sintering process, a variety of non-equilibrium intergranular phases are then expected, which can dominate the low frequency a-c, or d-c ionic conductivity.

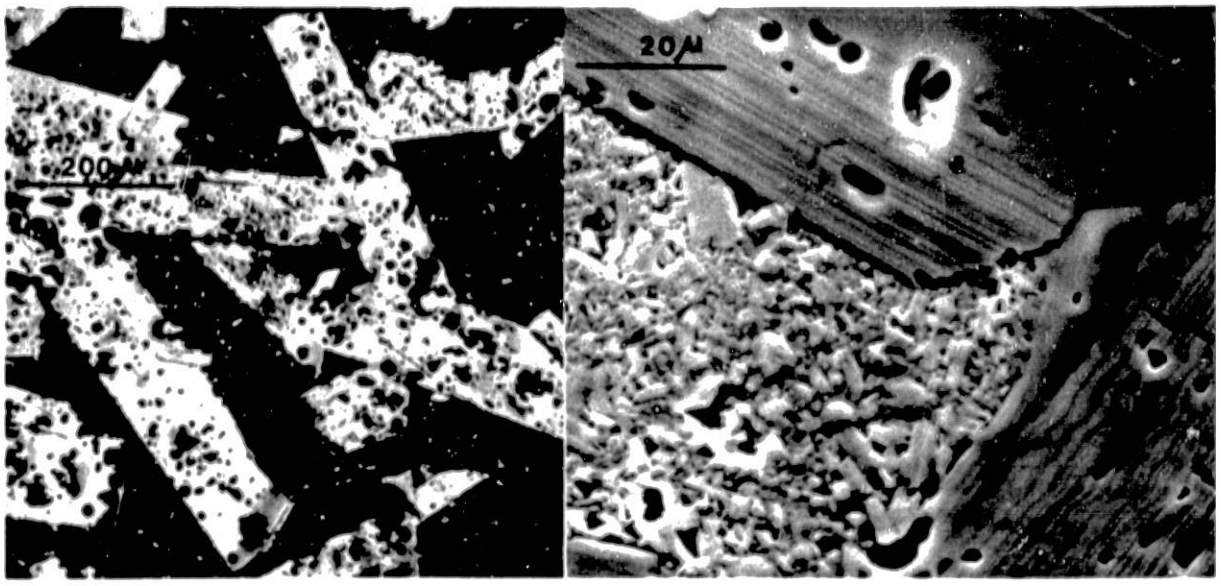

A B

Fig. 5. Optical (A) and scanning electron micrographs (B) of mechanically polished and etched (boiling H_3PO_4, 300°C, 1 sec) sodium beta alumina containing 0.5 wt.% CaO, sintered at 1750°C, 30 min, in air. The extreme biomdal grain size distribution is evident.

Dispersion measurements were performed on the doped samples between 150 and 350°C. Fig. 6 shows some B-G plots (susceptance-conductance) for the sample shown in Fig. 5. The dispersion due to the electrodes (evaporated gold), and the electrolyte are indicated. G_A can be interpreted as $G_A = (R_C + R_B)^{-1}$, where R_C = specific ionic resistivity of the grain bulk, and R_B = total specific ionic intergranular resistivity. $R_C + R_B$ should correspond to the d.c. ionic resistivity. G_B corresponds to R_C^{-1}. As can be observed from these plots, the B-G data lie approximately on a circular arc for which the center is below the G axis. The angle, α, between the radius connecting the center of the arc (between G_A and G_B) and G_A, and the G axis is approximately 30°. The angle α increases with decreasing temperature. From these data the grain bulk resistance R_C, and R_B can be determined. It is clear from an examination of the microstructures as shown in Fig. 5 that a physically meaningful equivalent circuit is not readily constructed. For this reason, we call R_B the intergranular resistance rather than the grain boundary resistance. Generally we find for calcium containing samples an activation energy for R_C between 3.8 and 4.2 kcal/mole, and for R_B an activation energy between 10 and 12 kcal/mole. The actual values for R_C and R_B are shown in Fig. 7. Very significant scatter in the data is observed, especially in R_B. The scatter is correlated with the microstructure, which in turn depends strongly on the sintering temperature for these doped samples. This is notably different from pure beta alumina where at 300°C the ionic conductivity is nearly insensitive to microstructure at densities above 3.0 g/cm³. For sinterings near 1700°C (30-45 min), a higher density (3.15 g/cm³), finer grain size, and higher R_B values are observed, while for sinterings near 1750°C, a lower density (~3.0 g/cm³), extreme bimodal grain distribution, and lower R_B values result. A quantitative relationship has not yet been established.

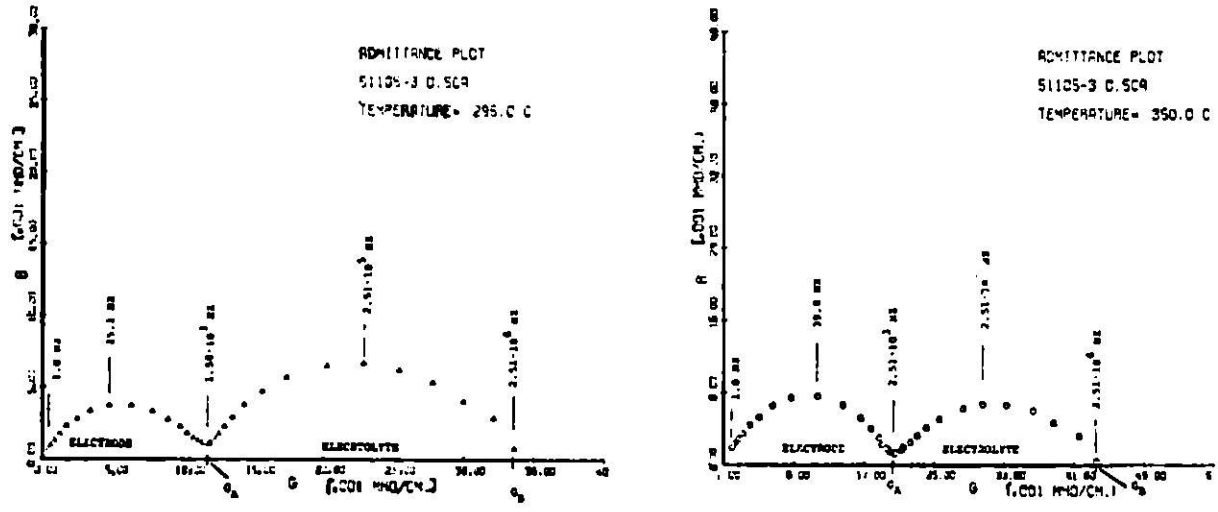

Fig. 6. B-G plots for a sample containing 0.5 wt.% CaO (see Fig. 5).

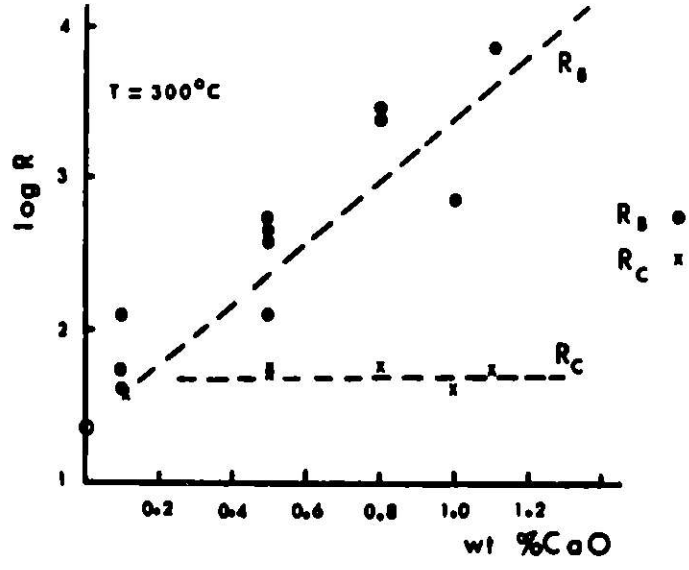

Fig. 7. Values of R_B and R_C as a function of weight % CaO for sodium beta alumina at 300°C. The scatter is due to difference in microstructures.

Due to the extreme scatter in the data it is not possible at this point to formulate the relation between R_B and [C] = wt.% CaO quantitatively. We can, however, express the trend as $\log(R_B/R_o) \propto \beta[C]$, where R_o is the specific ionic resistivity of undoped samples (which has no measurable intergranular contribution at 300°C). If [C] is expressed as wt.% CaO, we find $\beta \approx 2$. β

is a function of temperature, since the R_B and R_o have different activation energies. It is interesting to note that R_C is not as sensitive to preparation and substructure as R_B for calcium doped samples. We find $2<R_C/R_o<3$ when C>0.1 wt.% CaO. This indicates that Ca has not entered the grain bulks significantly beyond this level, regardless of the overall CaO content.

The sodium beta alumina samples were found to change from a transgranular to an intergranular fracture mode with increasing calcium content. For the intergranularly fractured samples it was possible to demonstrate the presence of Ca at the grain boundaries by means of Auger spectroscopy. This work is described in more detail in the paper by Unertl, De Jonghe, and Tu[19]. It is interesting to note in this work that excess sodium was observed for air fractured samples, but not for samples fractured in ultrahigh vacuum. It is thought that a reaction with atmospheric moisture produces a sodium rich layer on the sample surface.

3.2.2 Effect of Silica. Silica was added to commercial sodium beta alumina (Alcoa XB-2 "superground") as sodium silicate.* The samples were sintered, while packed in sodium beta alumina powder, for about 30 min. by passing them through the hot zone of a furnace. As in the case of calcium addition, the samples exhibited a bimodal grain size distribution, though the abnormal grain growth was not as rapid. Fig. 8A and 8B show an optical, and scanning electron micrograph of a sample containing 0.6 at.% SiO_2 that has been polished, and etched with boiling H_3PO_4. Fig. 8C and 8D show representative areas of samples containing 1.95 and 2.7 wt.% SiO_2.

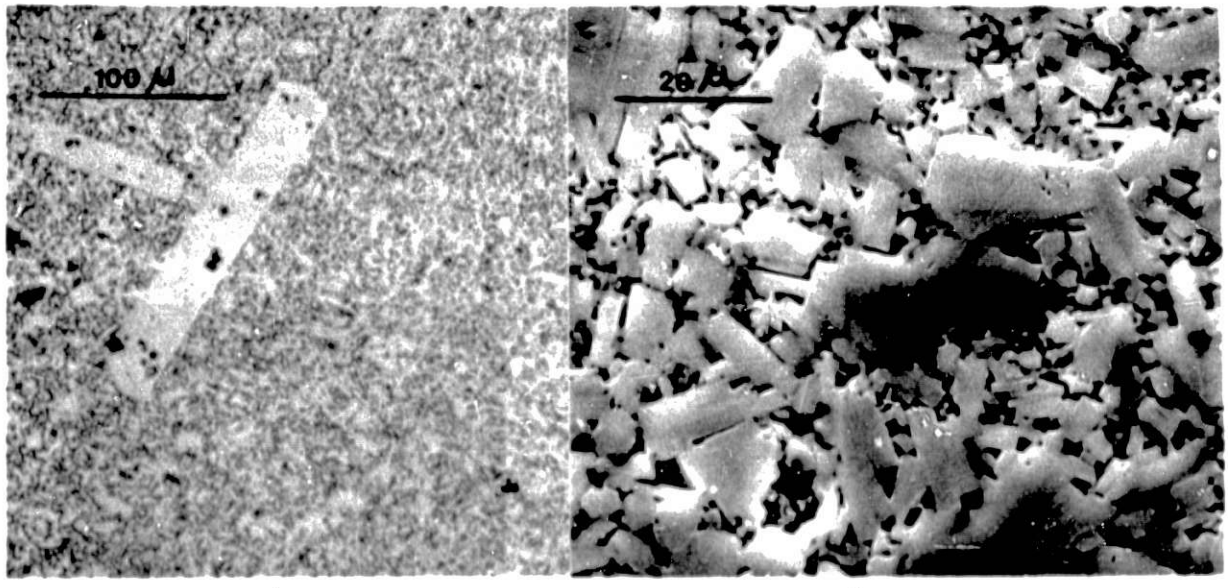

A B

Fig. 8. Sodium beta alumina containing SiO_2.
A: Optical micrograph 0.6 wt.% SiO_2.
B: Scanning electron micrograph 0.6 wt.% SiO_2.

* Al_2O_3 was added to compensate for the added Na

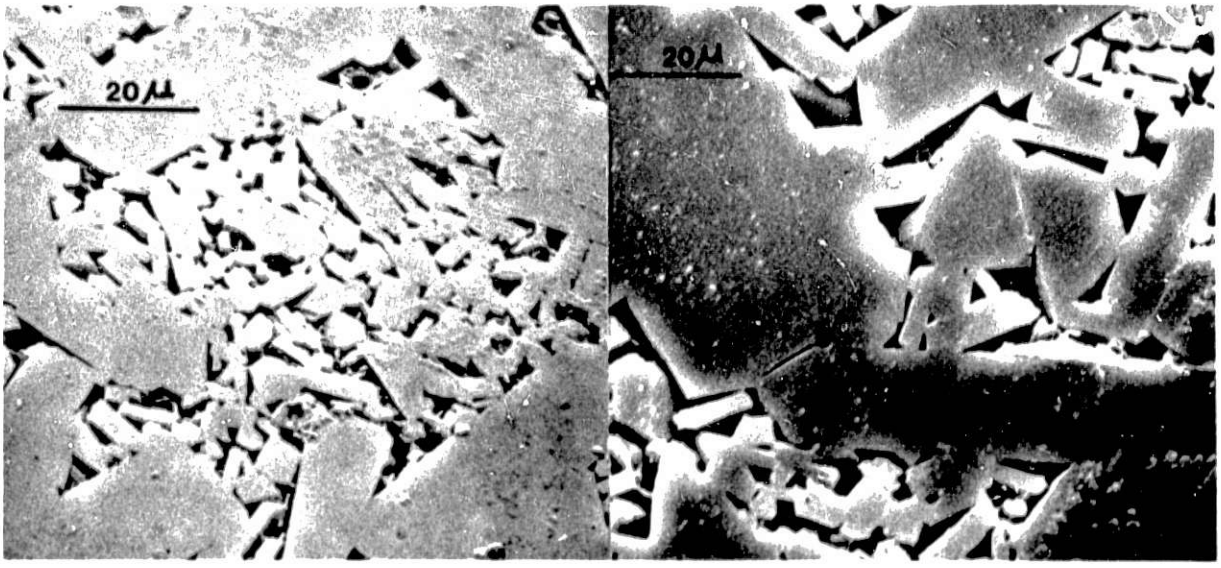

Fig. 8C: Scanning electron micrograph 1.95 wt.% SiO_2.
D: Scanning electron micrograph, 2.7 at.% SiO_2.

The presence of an intergranular phase could be demonstrated by direct observation with the electron microscope. This is shown in Fig. 9 for a sample containing 2.7 wt.% SiO_2. The selected area diffraction pattern of area A demonstrates that the intergranular material is amorphous. This is not surprising, since SiO_2 readily forms glasses with a variety of elements. The intergranular phase is affected by electron irradiation, and material is exuded during observation in much the same way as during the electron microscope observation of the crystalline beta alumina matrix. We have not directly identified this exuded material but its similarity in behavior during electron microscope observation suggests it is sodium. We tentatively conclude that the intergranular phase is a sodium alumino silicate glass.

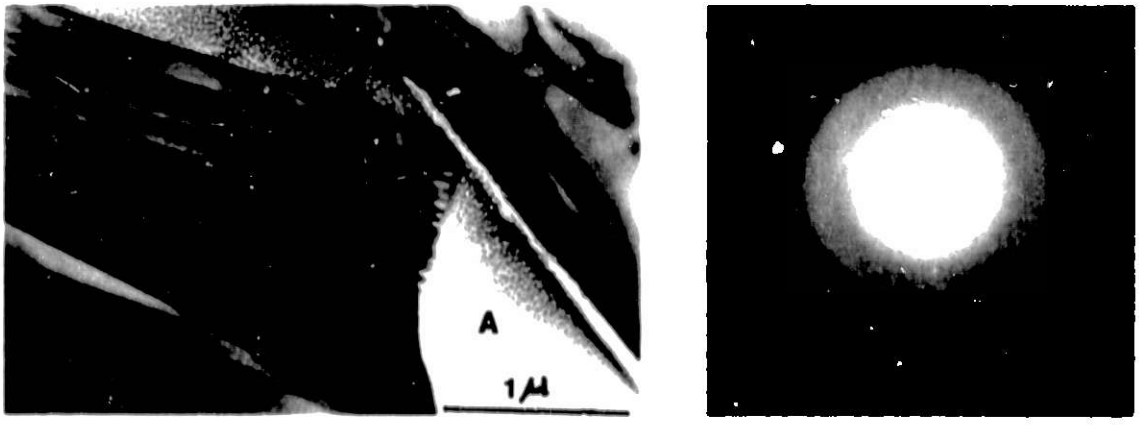

Fig. 9. Transmission electron micrograph of a sodium beta alumina sample containing 2.7 wt.% SiO_2. The diffraction pattern is from area A.

The ionic conductivity of the silica containing samples was determined from the dispersion measurements. It is interesting to note that the angle α (discussed in the previous section in connection with Fig. 6) now decreases with decreasing temperature. This suggests that in CaO and SiO_2 containing electrolytes different types of intergranular transport processes occur. We are currently exploring further the temperature dependence of α. The total specific resistance of the samples, R_T, at 300°C, is plotted versus the weight percent of SiO_2 in the sodium beta alumina samples in Fig. 10. Again, significant scatter is present due to some variation in microstructure, as was found for the CaO containing samples. As a trend, we put $\log(R_T/R_o) \approx \beta[C]$, where now [C] is the weight % of SiO_2, and R_o the resistance of the undoped beta alumina. We find $\beta \simeq 0.45$. Even though the data show a significant scatter, it can be concluded that SiO_2 is appreciably less detrimental than CaO for the ionic conductivity.

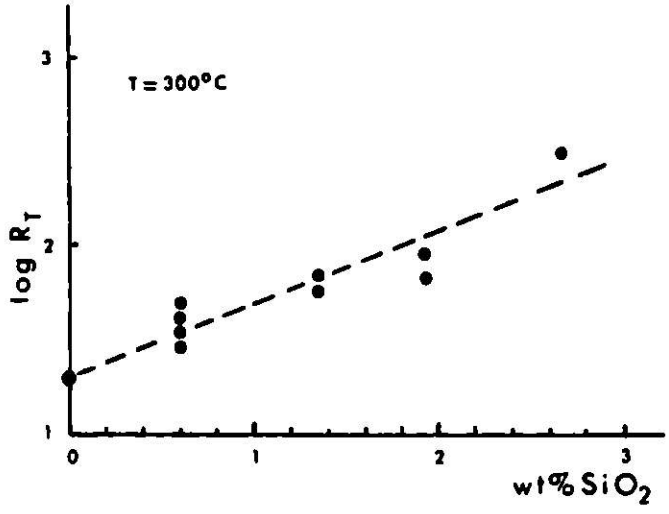

Fig. 10. Total specific ionic resistivity (extrapolated d.c.) at 300°C for sodium beta alumina samples containing SiO_2.

4. SUMMARY

In this work we attempt to clarify the microstructure and properties of sodium beta alumina solid electrolytes. Improved sinterability of commercial beta alumina powder was achieved by addition of small amounts of the Na_2O - Al_2O_3 eutectic. Complex crystallographic faults, and subgrain boundaries were found that can affect the microscopic homogeneity of the ionic current flow during d.c. ionic conduction. The effects of CaO and SiO_2 additions on microstructure and ionic conductivity were described. Pronounced abnormal grain growth occurs in both cases, due to the pressure of a liquid phase at the sintering temperature. It is concluded that CaO is more detrimental than SiO_2.

ACKNOWLEDGEMENTS

This work was supported by the Electric Power Research Institute. Additional funds were provided by the Advanced Research Projects Agency through the Materials Science Center at Cornell.

The contributions of A. Buechele, H. Chandan and B. Van Rees are gratefully acknowledged.

REFERENCES

1. S. A. Weiner, "Research on Electrodes and Electrolytes for the Ford Sodium-Sulphur Battery", Ford-Utah-RPI annual report, July 1975.
2. L. C. De Jonghe and H. Chandan, to be published in Bull. Amer. Ceram. Soc.
3. J. T. Kummer, "β Alumina Electrolytes", Prog. Solid State Chem. 11, 141 (1972).
4. W. L. Bragg, C. Gottfried and J. Wert, Z. Krist. 77, 255 (1931).
5. C. R. Peters, W. Bettman, J. W. Moore and M. D. Glick, Acta Cryst. B27, 1826 (1971).
6. J. T. Kummer, "β Alumina Electrolytes", Prog. Solid State Chem. 11, 141 (1972).
7. W. L. Roth, G.E. Technical Report No. 74, CRD054, March 1974.
8. R. Stevens, J. Mat. Sci. 9, 801 (1974).
9. J. M. Bevan, B. Hudson and P. T. Moseley, Mat. Res. Bull. 9, 1073 (1974).
10. L. C. De Jonghe, J. Mat. Sci. 10, 2173 (1975).
11. R. H. Richman and G. J. Tennehouse, J. Amer. Ceram. Soc. 58, 63 (1975).
12. L. C. De Jonghe, to be published, J. Mat. Sci.
13. L. C. De Jonghe, submitted to Scripta Met.
14. A. E. Owen, "Electric Conduction and Dielectric Relaxation in Glass", Prog. Ceram. Soc. 3, 77 (1963).
15. J. E. Bauerle, J. Phys. Chem. Solids 30, 2657 (1969).
16. R. Powers and S. Mitoff, G.E. Technical Report No. 74, CRD082, June 1974.
17. A. D. Franklin, J. Amer. Ceram. Soc. 58, 465 (1975).
18. L. T. Brownmiller and R. H. Bogue, Bur. Standards J. Research 8, 293 (1932).
19. W. N. Unertl, L. C. De Jonghe and Y. Y. Tu, submitted to J. Amer. Ceram. Soc.

OPTIMIZATION OF MgO DOPED β-Al_2O_3 WITH RESPECT TO ELECTRICAL CONDUCTIVITY

W. Haar, W. Fischer, H. Kleinschmager and G. Weddigen
Brown Boveri & Cie
Mannheim
Central Research Laboratory
Heidelberg, Germany

ABSTRACT

The composition of MgO stabilized β-Alumina has been varied in the following ranges

7.3	...	9.3	weight-% Na_2O
1	...	4	weight-% Na_2O
86.7	...	91.7	weight-% Al_2O_3

Rod shaped specimens were prepared from calcined and ballmilled powder, isostatically pressed and sintered at temperatures between 1550 and 1800°C.

A four electrode method has been applied to measure the electrical conductivity in the frequency range 100 Hz to 100 kHz using painted graphite electrodes contacted to platinum foils.

Both the conductivity and the β''-Al_2O_3 content increased with increasing Na_2O content. Furthermore at a constant Na_2O concentration the conductivity reaches a maximum at a certain MgO content depending on the Na_2O concentration. Conductivity values up to $0.3\ \Omega^{-1}cm^{-1}$ at 300°C have been obtained. Some preliminary results of life time tests will be given.

INTRODUCTION

In recent years there has been an increasing interest in superionic conductors. In particular polycrystalline sodium β-alumina which is a two dimensional ionic conductor , is of great importance for sodium/sulfur batteries.

The high ionic conductivity combined with negligibly low electronic conductivity and the fact that this material is corrosion resistant to liquid sodium and sulfur or sodium polysulfides at temperatures below 400°C makes it suitable as a separator in Na/S cells[1].

The term "β-alumina"[2] refers to a family of closely related structures and compositions with high ionic conductivity. In most publications, as in this paper, the term β-alumina is

used for the two block version with hexagonal symmetry and the ideal formula $Na_2O \cdot 11\ Al_2O_3$, whereas β''-alumina stands for the three block version with rhombohedral symmetry and the ideal formula $Na_2O\ 5Al_2O_3$. These two modifications are also obtained if the stoichiometry is varied within certain limits[3-6]. It has been shown by several authors[7-9] that the physical properties of β-alumina can be strongly influenced by mono- and divalent cations. Some of these dopants like Li^+, Mg^{2+}, Ni^{2+} are substituting Al^{3+} in the spinel blocks. In this way additional sodium is incorporated in the conduction planes and conductivity is increased.

When the development of a Na/S battery was started at Brown Boveri & Cie in 1973, little was published on the longterm stability of β-alumina. At this time, $\beta''\text{-}Al_2O_3$ seemed to be more favorable compared to $\beta\text{-}Al_2O_3$ because of its higher conductivity and lower sintering temperature. On the other hand $\beta\text{-}Al_2O_3$ seemed to be more stable under discharge. In order to get more information on this subject, a screening program was initiated in the course of which different compositions including β- and $\beta''\text{-}Al_2O_3$ were prepared and tested. MgO was chosen arbitrarily as stabilizing oxide. In fig. 1 the ternary system Na_2O - MgO - Al_2O_3 is shown, where results of Weber and Venero[1,2] are combined with those of Imai and Harata[9]. The Na_2O- and MgO-contents were varied in the ranges of 7 to 10 and 0 to 4.5 mass-% respectively as indicated by dots in fig. 1. In the following experiments, details and results of this program will be described.

POWDER PREPARATION

For the fabrication of a reproducible, dense and well conducting ceramic electrolyte, it is necessary to optimize a series of production parameters. Different sodium compounds (Na_2CO_3, $NaNO_3$, NaOH and $NaAlO_2$) were used for the powder preparation. The best results have been obtained by utilizing Na_2CO_3 together with MgO and $\gamma\text{-}Al_2O_3$ (Merck, Darmstadt). The $\gamma\text{-}Al_2O_3$ powder had to be converted to $\alpha\text{-}Al_2O_3$ at 1250°C for one hour. Without calcination only a low density was achieved. Good results were obtained when A16SG (ALCOA) was used as a source for $\alpha\text{-}Al_2O_3$. The starting products were mixed as a slurry for one hour in a ball mill provided with 500 ml cups (99.7 mass-% Al_2O_3). The cups were charged with an equivalent of 200 g β-alumina together with 240 ml of acetone. After the evaporation of acetone, the products were prefired at a temperature of 1230°C for one hour. The influence of this calcination temperature on the composition, density and conductivity can be seen in fig. 2. In the temperature range of 1000 to 1200°C the starting products are transformed to a mixture of β- and $\beta''\text{-}Al_2O_3$. Good apparent and geometrical fired bulk densities are obtained above a temperature of 1230°C. At higher calcination temperatures the BET surface

area and the reactivity of the powder decreases.

Milling of this powder has been carried out on centrifugal ball mills (Retsch, model S2) using 500 ml cups and three balls of 30 mm o.d. (both 99.7 mass-% Al_2O_3).

Charges of 200 g have been milled for 20 hours at 400 rpm using 0.5 mass-% ethylene-glycol as grinding aid. Fig. 3 shows that the density has not yet reached its maximum value after 22 h. Because of increasing ware of α-Al_2O_3 from the balls and the cup, grinding is terminated after 20 h.

After this process again 0.5 mass-% ethylene-glycol are added as pressing aid and milling is continued for 1 h. During this process the water content of the powder has to be controlled carefully in order to get an appropriate agglomerate size distribution for a reasonable flowability of the powder.

Powder prepared in this way exhibits BET surface areas of 8 - 10 m^2/g and a mean grain size below 1 µm.

Pressing of the powder

The powder is isostatically pressed with the aid of a silicone rubber bag (ERTV, Dow Corning). Close-ended tubes with lengths up to 250 mm, rods and discs have been pressed with this method. The influence of pressure on the fired bulk density is depicted in fig. 4. At pressures above 2 kbar, the density remains rather constant. A pressure of 1.5 kbar was chosen for the preparation of the test specimens. Green densities of 57% of the theoretical value have been achieved. A higher green density and strength was obtained with NH_4CO_3 carbowax and poly-ethylene-glycol. However, the flowability of the powder was better with 0.5 mass-% ethylene-glycol and as a consequence of this fired bulk density was higher. That is why ethylene glycol was chosen for this program.

Sintering

Sintering was carried out in a special furnace of low heat capacity with a graphite heater element. Heating and cooling rates were chosen to be 15°C/min. It is not yet clear whether these rates are optimal. Further experiments will be carried out on this subject. The specimens were kept at the sintering temperature for 30 minutes. An annealing period of 60 min at 1450°C followed sintering in order to improve the structural homogeneity and the conductivity of the ceramic.

During sintering the test specimens were embedded in unground β-Al_2O_3 powder in order to prevent sodium losses. This powder did not contain any MgO. The influence of the Na_2O content of this powder on the final Na_2O-content of the ceramic is

shown in fig. 5. The Na_2O content was determined by weight analysis of the specimens. Care was taken in order to prevent that the results were influenced by gain or loss of water. The final Na_2O content of the samples was nearly independent of the MgO content. This fact implies that the vapor pressure of β-Al_2O_3 is nearly independent of the MgO content. Consequently the Na_2O content of the specimens and of the embedding powder must be equal in order to keep the Na_2O content at a constant level during sintering.

ANALYSIS OF PHYSICAL PROPERTIES

For investigation of density and resistivity rods of 30 mm length and 7 mm o.d. were used. The fired bulk density was determined by measuring weight and buoyancy in toluene.

Resistivity was measured with two and four electrode techniques. In fig. 6 the two- and four-electrode resistivity is plotted against $1/\sqrt{f}$ (f = frequency) for different electrode materials at 300°C. For diffusion controlled transport processes at the electrodes a straight line is to be expected. In all cases using only two electrodes, essentially the same resistivity was obtained by extrapolating $f \to \infty$. Plotting the series impedance in the complex plane as in fig. 7 according to Armstrong[10] straight lines were obtained, which hit the real axis for $f \to \infty$ at the D.C. resistance value. The most reliable results were achieved by using two additional voltage electrodes, because of the frequency independence of ρ_{ab} (see fig. 6) in the frequency range from 100 Hz to 100 kHz. It was found that at 300°C up to 100 kHz a.c. current and voltage are in phase so that ρ can easily be determined by measuring the a.c. amplitudes. This is why this method was chosen for our investigation. Graphite contacts were used as current electrodes because they were easy to apply and gave reproducible results.

Life time tests were carried out in Na/Na-cells shown schematically in fig. 8. In these cells the sodium is pumped unidirectionally into the interior of small close-ended tubes from where it could drop out again across an isolating overflow collar made of potassium free glass. Current densities were arbitrarily chosen to be 0.9 A/cm^2, which is by a factor of 4 higher than those normally used in Na/S-cells.

The β''- to β-ration of the sintered specimens were measured by x-ray analysis of powdered samples using copper K_α-lines, ($2\Theta = 33.4^0$ or 44.4 for β-alumina and 34.6^0 or 46.0^0 for β''-alumina). Microstructure was made visible by polishing with 3 µm diamond paste and thermal etching at temperatures of 100°C below sintering temperature.

RESULTS AND DISCUSSION

For the different Na_2O-contents of the ceramics it was necessary to optimize the sintering temperature. Fig. 9 shows the temperature dependence of the fired bulk density of ceramics with Na_2O contents of 7.14, 7.8 and 8.4 mass-% respectively. The bars give the spread of values for different sintering charges and different MgO contents. The theoretical density is shown on the right hand scale assuming 3.256 g/cm^3 for the fully dense ceramic for all compositions. The sintering temperature is strongly dependent on Na_2O and only faibly on MgO content.

A longlife ceramic suitable for Na/S-battery application must have a density higher than 95% of the theoretical value (equivalent to 3.1 g/cm^3), in order to avoid open porosity. Otherwise a rapid degradation is found. On the other hand, very large grains, which mostly are found together with high densities, have to be avoided because of low fracture strength and low longterm stability of the ceramic. The microstructure can be influenced by many factors like grain size of the powder, temperature-time-profile during sintering and composition.

Fig. 10 shows the dependence of microstructure with sintering temperature of a ceramic containing 8.4 mass-% Na_2O, 2.5 mass-% MgO and Al_2O_3 rest. Small grains below 5 µm diameter occur at temperatures below 1595°C. At medium temperatures a duplex structure is found with some larger grains up to 100 µm in a matrix of small grains (5 µm). At even higher temperatures the larger grains grow at the expense of the small ones. Grain sizes of 300 µm diameter have been found at 1750°C.

The variation of MgO content has also an influence on the microstructure. For 8.4 mass-% Na_2O and temperatures below 1590°C small grains (5 µm) are found for MgO contents of 1 to 4.5 mass-%, but density is below 3.1 g/cm^3. At medium temperatures equiaxed grains of about 50 to 100 µm diameter are found for 1, and duplex structures for 1.5 to 4.5 mass-% MgO.

The MgO content also influences the density and resistivity of the electrolytes as shown in figs. 11 and 12 for 7.8 and 8.4 mass-% Na_2O respectively. Both have in common that the fired bulk density shows a flat maximum and that resistivity at a temperature of 300°C decreases with MgO content and reaches a minimum asymptotically. Values as low as 3 Ωcm have been obtained. The decrease in resistivity with MgO content is correlated with an increase in β''-content in the ceramic as can be seen in fig. 13. The position of the curves are dependent on the sintering temperature. At lower temperatures the curve is shifted to the left.

The occurrence of a maximum in the density is not yet understood. Whether this is an effect depending on production parameters, on eutectic liquid phases produced during an unknown stage of the sintering process or on other parameters is not yet clear and will be object of further investigation.

With 7.8 and 8.4 mass-% Na O we have entered the β''-Al_2O_3 region with increasing MgO content. This is in agreement with other investigations[9,12] as shown in fig. 1. At lower Na_2O contents β''-Al_2O_3 is not found anymore. For 7.14 mass-% Na_2O the sintering temperature has to be increased significantly in order to get high enough densities (conf. fig. 9). In this case, as shown in fig. 14, resistivity passes through a minimum near 2.0 mass-% MgO. The composition corresponding to this minimum agrees well with that reported by Kennedy and Sammels[13].

The life-testing of ceramics in Na/Na-cells caused several experimental troubles before reasonable results could be achieved. For example, when using metallic overflow devices, short circuits occurred near the open end of the tube by thin films of sodium between the overflow device and the ceramic. Another difficulty arose by using K_2O containing glass. In this case, as shown in fig. 15, at first a slow and then a rapid increase in resistance was observed before the ceramic failed. After dismantling, the ceramic showed several cracks and K_2O was found throughout the ceramic by microprobe analysis. Similar effects have been reported by Lazennec et al.[14] and Ford[15].

Good and reproducible results were obtained when a potassium free glass was used for the overflow device. Some of our preliminary results are given in table 1.

All the tests have been carried out at a temperature of 300°C and a current density of 0.9 A/cm^2. The densities of the ceramics fall in the range of 3.1 to 3.2 g/cm^3.

In the case of tubes 2, 4, 15 and 16 more than 1000 Ah/cm^2 were passed unidirectionally through the ceramic wall. Tubes 3, 5, 11, 12 showed clear evidence of electrolytic degradation. Tubes 3 and 5 were sintered at a temperature about 30°C higher than the optimum temperature. After cell termination cracks and black spots were found on the ceramic. Though density was high (3.21 g/cm^3) the ceramic failed because grain size was too high. Etched, polished surfaces showed a duplex structure with diameters of the large grains up to 200 µm.

Only tubes 1 to 5 were batch sintered according to the manner described above, all the others were zone sintered. Ceramics of tests number 6 to 8 and 15 to 19 were passed through the region of highest temperature within 25 minutes

whereas thos of 9 to 14 in half the time. Maximum heating and cooling rates have been measured to be 20 and 10^0C/min respectively.

Ceramics pulled through at a higher speed show rather high resistivities. This is due to the fact that the conversion to β'' is not yet complete, as was made obvious by x-ray analysis. By annealing one hour at a temperature of 1460^0C, resistivity dropped to the range given in fig. 11 and 12. Similar results were reported by Ford[15].

Ceramics pulled through at the lower speed but the same sintering temperature exhibit normal resistivity and density values and life times of more than 1000 Ah/cm^2. Those pulled through at the higher speed had poor densities (< 3.1 g/cm) and show no normal behavior: bad wettability, periodical short circuit or unstable resistance. Ceramics of cell tests number 11 and 12 failed and showed cracks after dismounting.

Some additional electrolytes with fine grained microstructures open porosity and densities below 3.1 g/cm^3 or coarse grained structures (300 µm) with densities above 3.2 g/cm^3 have been tested under the conditions listed in table 1 and in Na/S-cells. Both types showed rapid degradation from the beginning.

CONCLUSION

The screening program carried out so far on the ternary systems Na_2O-MgO-Al_2O_3 and Na_2O-Li_2O-Al_2O_3 has shown that by carefully optimizing the production parameters of the ceramic, high densities and low resistivities down to 3 Ωcm at 300^0C and good long term stability are achievable. Using the method of preparing the ceramics described above, only a small range of sintering temperatures (t ≤ 20 C) gives a stable ceramic. The best ceramics exhibit densities between 3.15 and 3.2 g/cm^3 and a duplex structure with a maximum grain size of about 100 µm. Preliminary results of life testing in Na/Na- and Na/S-cells show that one can expect MgO-stabilized β-aluminas to be suitable as diaphragms in Na/S-batteries. According to these results it is concluded that degradation seems to be more a question of optimizing the production parameters (in order to get a good microstructure and density) than of composition. The negative results obtained by other groups with MgO-stabilized electrolytes[14,16] could not be confirmed by our experiments. Whether the concentration of additives influences longterm stability on a larger time scale is not yet clear and is subject of further investigations.

References

1 Ford patent 3,719,531, March 6, 1973

2 J.T. Kummer, Progr. Solid State Chem. 1 (1972)141

3 R.C. DeVries and W.L. Roth
J. Amer.Ceram.Soc. 52(1969) 364

4 C.R. Peters, M. Bettman, J.W. Moore and M.D. Glick,
Acta Cryst. B27 (1971) 1826

5 M. Bettman and C.R. Peters, J. Phys. Chem.73 (1969)1774

6 W.L. Roth, J. Solid State Chem. 4 (1972)60

7 M.S. Whittingham, Electrochimica Acta 20 (1975) 575

8 L. Wynn Jones, L.J. Miles, Brit. Ceram. Soc. Proc. 19
(1971) 161

9 A. Imai and M. Harata, Jap. J. Apply. Phys. 11 (1972)180

10 R.D. Armstrong, T. Dickinson and P.M. Willis
Electroanal. Chem. and Interfacial Electrochemistry 53
(1974) 389-405

11 W. Bankal, R. Knoedler, J. Appl. Electrochem. 5(1975)105

12 N. Weber and A. Venero, ref. 47 in 2

13 J.H. Kennedy and A.F. Sammels, J. Electrochem. Soc.
119(1972)1609

14 Y. Larsennec, C. Lasne, P. Margotin and J. Fally
J. Electrochem. Soc. 122 (1975)734

15 Annual Report, June 30, 1974 to June 29, 1975
Ford Motor Comp. Dearborn, Mich., USA

16 W. Fischer and W. Haar, paper presented at the British
Ceram. Soc. Meeting "Mass Transport in Ceramic Materials"
London, Dec. 16-17, 1975

17 R.D. Armstrong, T. Dickinson, J. Turner
Electrochem. Acta 19 (1974) 187-192

Table 1

No	composition/mass-% Na_2O	MgO	Li_2O	Al_2O_3	Resistivity Ωcm	specific capacity Ah/cm²	Remarks
1	7.8	2.5	-	89.7	9.5	473*	periodical short circuit
2	7.8	-	0.5	91.7	6.8	1019*	
3	8.4	1.5	-	90.1	7.9	773	ceramic cracked; large grains
4	8.4	1.5	-	90.1	9.8	1397*	
5	8.4	1.5	-	90.1	8.5→5.7	572	failed; black spots, large grains
6	8.4	1.5	-	90.1	10.2	80	Na-short circuit across overflow device
7	8.4	1.5	-	90.1	9.3	504*	
8	8.4	1.5	-	90.1	8.0	66.3	Na-short circuit across overflow device
9	8.4	2.5	-	89.1	10.7	504*	bad wettability
10	8.4	3.0	-	88.6	10.9	504*	bad wettability
11	8.4	-	0.5	91.1	6.6	224	short circuit periodically
12	8.4	-	0.7	90.9	5.9	158	failed; cracks
13	8.4	-	0.9	90.7	8.2	504*	resistance not stable
14	8.4	-	1.1	90.5	7.9	504*	
15	9.3	1.0	-	89.7	9.3	1017*	
16	9.3	1.5	-	89.2	6.2	1049*	
17	9.3	1.5	-	89.2	8.0	504*	
18	9.3	3.3	-	87.4	4.6	1017*	
19	9.3	4.0	-	86.7	4.2	130	power failure

densities 3.1 to 3.2 g/cm³, current densities 0.9 A/cm²; temperature 300°C
* still on test, with ρ = constant after wetting

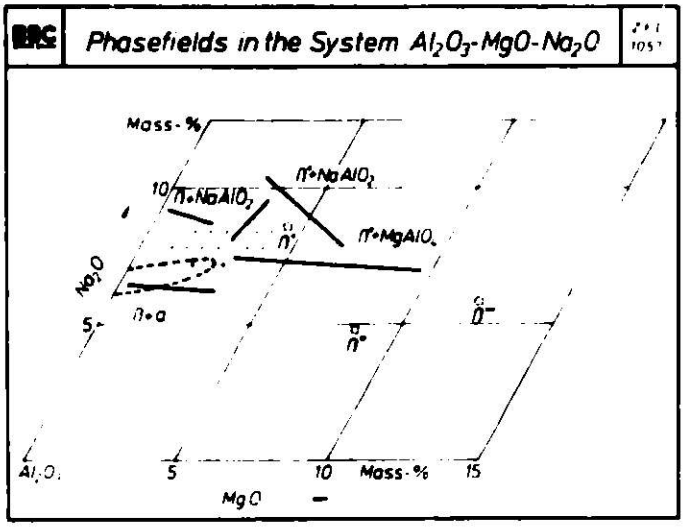

Fig. 1 Phase field of the ternary system Na_2O-MgO-Al_2O_3

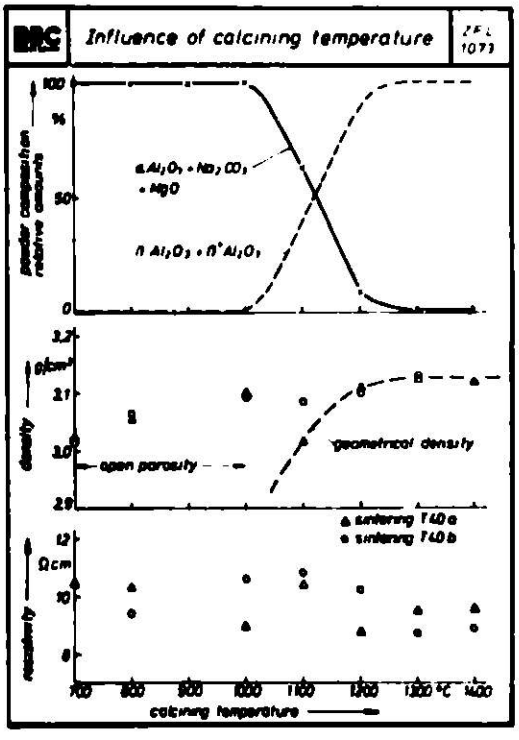

Fig. 2 Influence of calcining temperature on powder composition, density and resistivity (7.14 mass-% Na_2O, 2 mass-% MgO, Al_2O_3-rest)

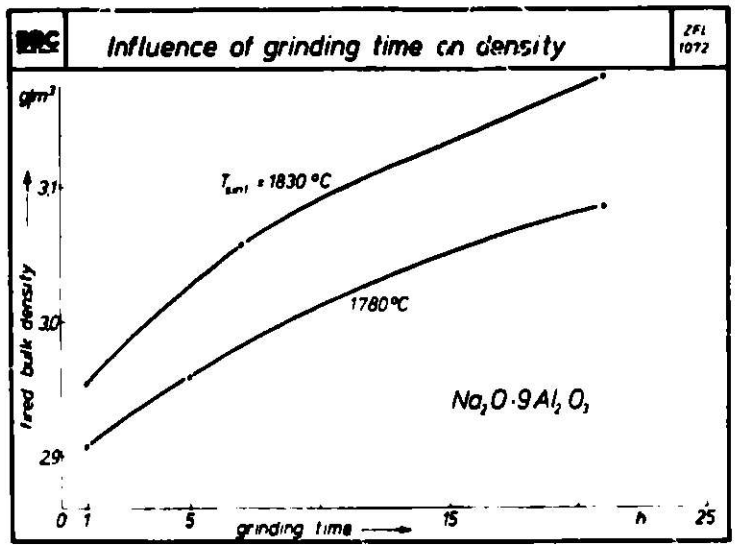

Fig. 3 Influence of grinding time on density

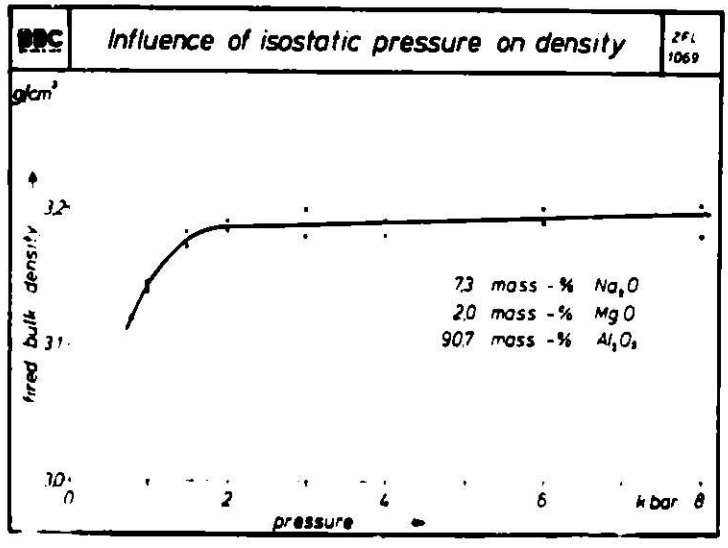

Fig. 4 Dependence of density on isostatic pressure

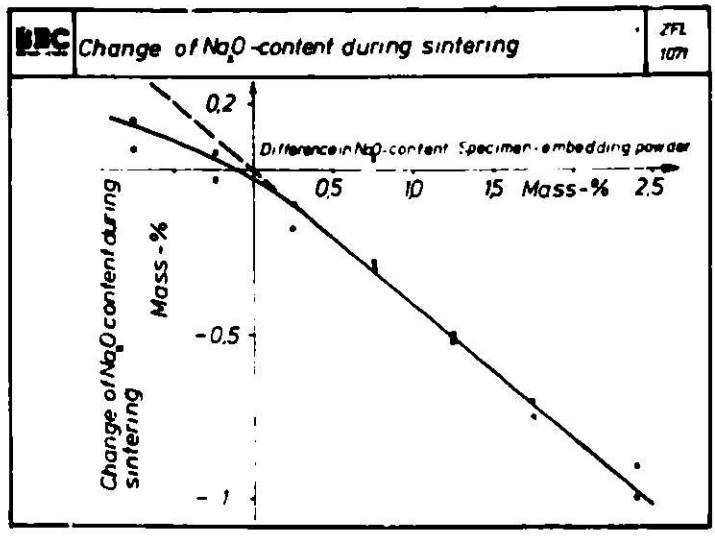

Fig. 5 Change of Na_2O content during sintering

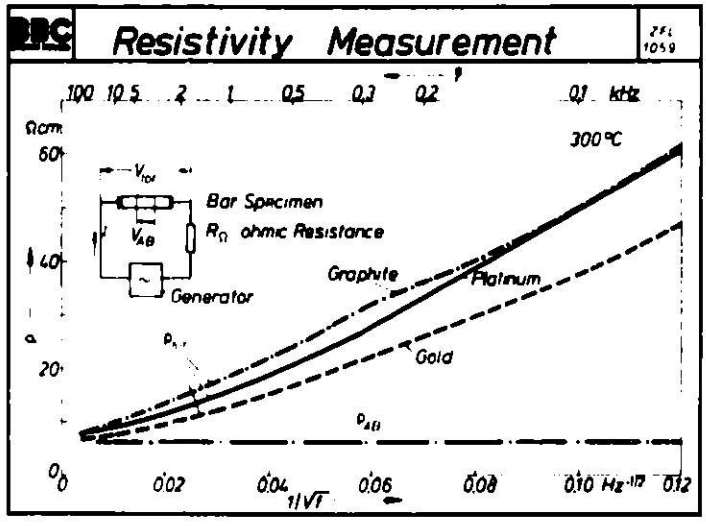

Fig. 6 Resistivity measurement

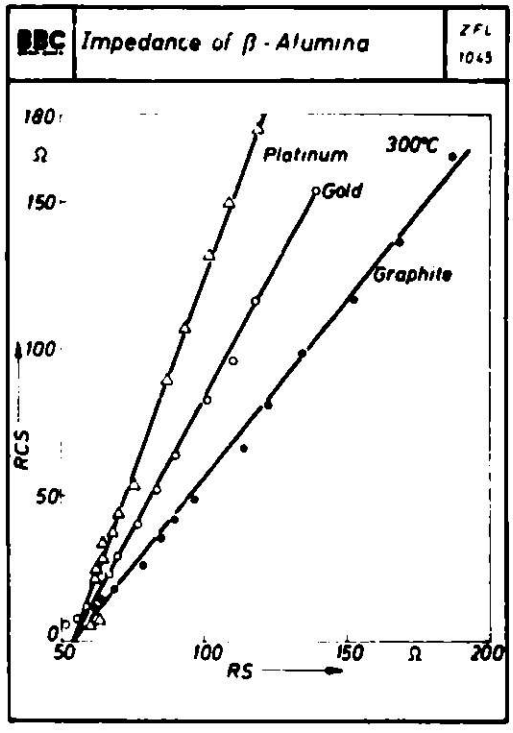

Fig. 7 Imaginary part RCS of the scrious resistivity of β-Al_2O_3as a function of the real part RS

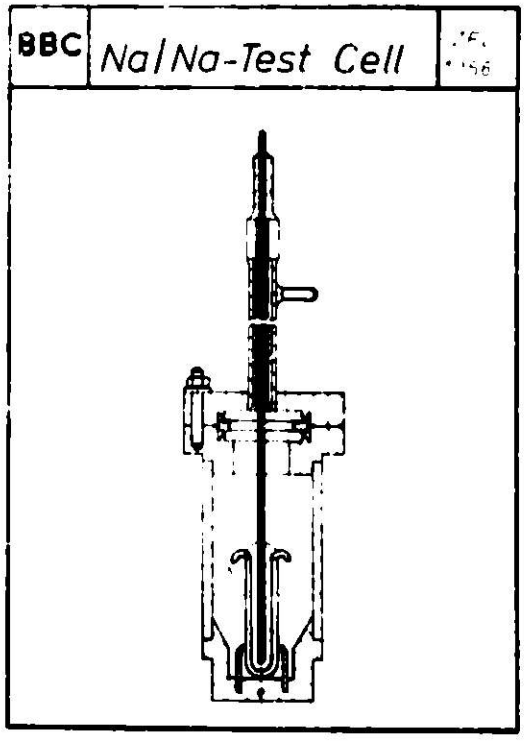

Fig. 8 Na/Na-test cell

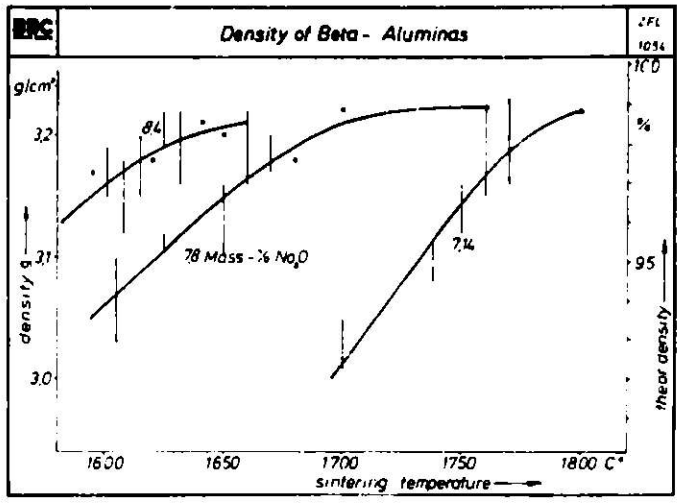

Fig. 9 Influence of sintering temperature on fired bulk density (sintering time 30 min)

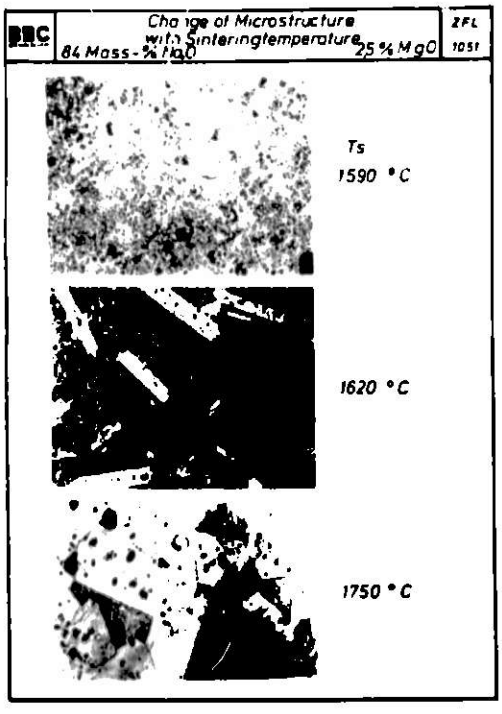

Fig. 10 Change of microstructure with sintering temperature

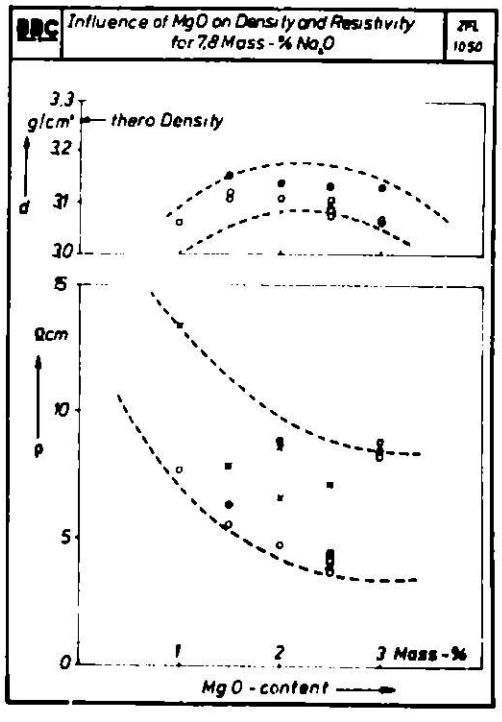

Fig.11 Influence of MgO-content on density and resistivity of β-Al_2O_3 containing 7.8 mass-% Na_2O

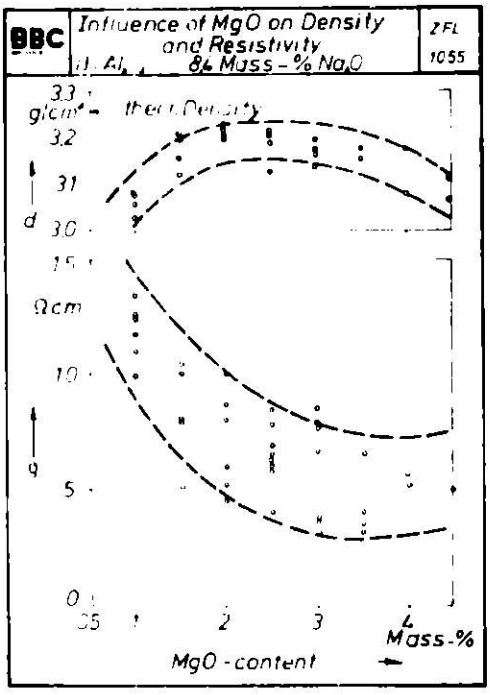

Fig. 12 Influence of MgO-content on density and resistivity of β-Al_2O_3 with 8.4 mass-% Na_2O

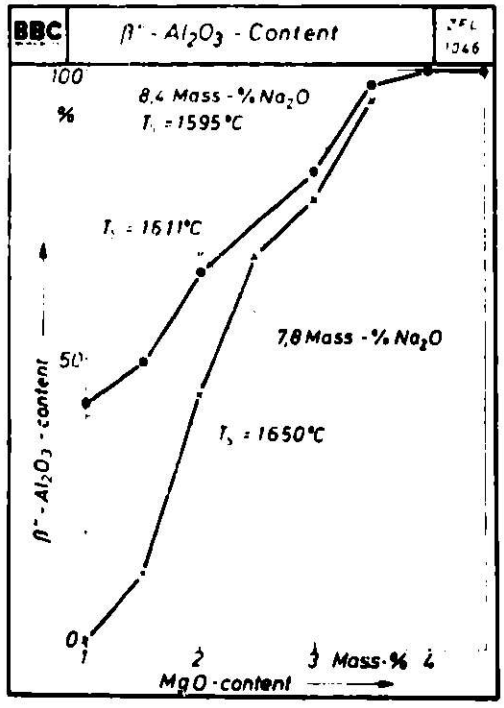

Fig. 13 Influence of MgO-content on β''-Al_2O_3

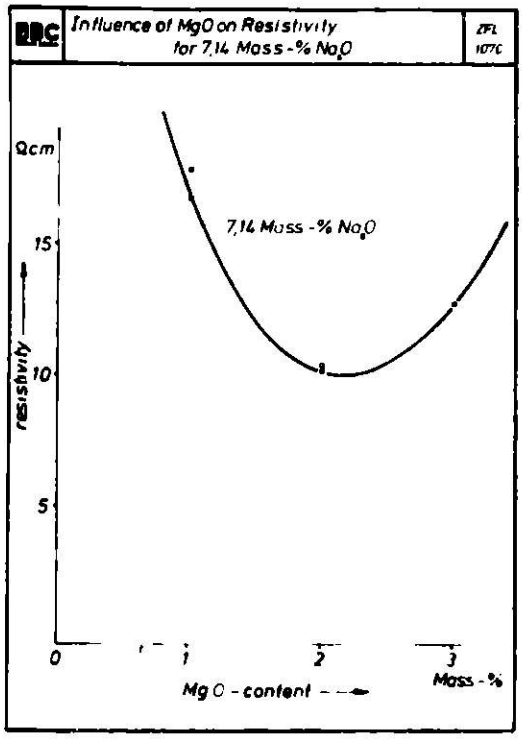

Fig. 14 Influence of MgO-content on resistivity of β-Al_2O_3

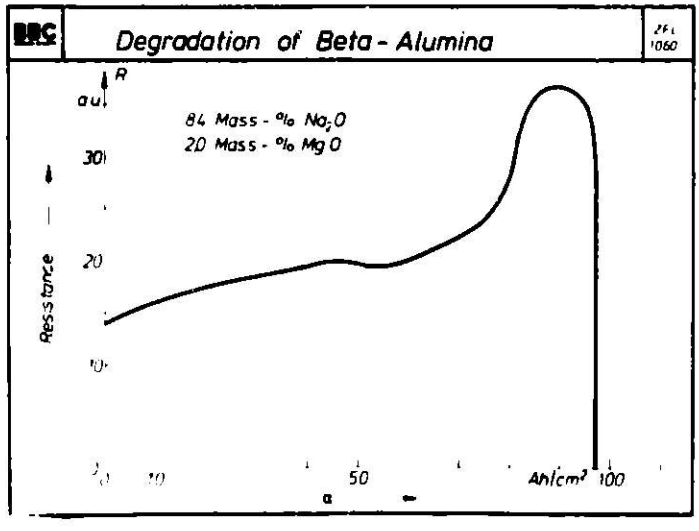

Fig. 15

Degradation of β-alumina by potassium

SEPARATORS FOR LITHIUM ALLOY-IRON SULFIDE FUSED SALT BATTERIES

Robert D. Walker, Jr. and C.C. Cheng
Department of Chemical Engineering
University of Florida
Gainesville, Florida 32611
and
James E. Battles and James P. Mathers
Chemical Engineering Division
Argonne National Laboratory
Argonne, Illinois 60439

ABSTRACT

Separators woven from boron nitride roving are reasonably satisfactory for these batteries, but they are expensive and somewhat limited as to their mechanical and electrical characteristics. Paper-like separators can be made from BN, Y_2O_3, or $LiAlO_2$ fibers or their mixtures, but they are very fragile and mechanically unstable. Organic and inorganic binders can overcome some of these limitations but they generally either react with the anode or they are thermally unstable at battery temperatures. The addition of chrysotile asbestos fibers in relatively small proportion increases strength and mechanical stability markedly, but the long-term stability of asbestos in the battery environment is somewhat in question. Preliminary cell tests suggest that the asbestos may disintegrate after a few cycles for reasons which are not clear at present. Strength and other properties can be further improved by adding substantial proportions of powders, such as BN, Y_2O_3, $LiAlO_2$, or MgO, to the fiber mixture. MgO produces very strong sheets but these tend to crack easily. A cell testing program is currently in progress.

INTRODUCTION

One of the principal materials problems in the development of Li-Al/LiCl-KCl/FeS_x batteries has been the separator. The separator must resist chemical attack by the highly reactive lithium of the alloy anode and it must be mechanically stable in fused LiCl-KCl for long periods. Moreover, since each of the electrodes undergoes very substantial volume changes on charge and discharge, the separator must withstand a good deal of movement during cycling.

One can, of course, form sintered ceramic separators from a number of these materials, but they are too brittle to yield separators having optimum characteristics. Flexible separators are desirable and these require mater-

ials in fibrous form, either for woven fabrics or for paper-like separator sheets. Economy and coworkers[1-4] have succeeded in preparing boron nitride fibers. As produced, these fibers are about 7 μm in diameter, very long (several inches), and reasonably flexible. Pure boron nitride is very resistant to attack by either the lithium-aluminum alloy or by the electrolyte.[5] On the other hand, these fibers are quite expensive and the fused electrolyte does not wet BN well. Moreover, the presence of only small amounts of B_2O_3 (from which the BN is made) is reported to markedly increase reactivity.[6] Economy and et al[1] have succeeded in producing BN roving from the fibers and this has been woven into a fabric which has proved to be a reasonably satisfactory separator material for these batteries.[5] However, the roving has a fairly large diameter, and the cloth is relatively rough, with substantial openings where the roving crosses. The roving diameter also sets a lower limit on the thickness of BN cloth separators.

Because of the limitations of woven separators and the possible limitations of BN, an investigation into the development of paper-like separators was undertaken at the Department of Chemical Engineering, University of Florida with the understanding that cell testing of promising materials would be carried out at the Argonne National Laboratory. This program has involved the study of several fibers including BN, Y_2O_3, $LiAlO_2$, and chrysotile asbestos; the incorporation of powders to act both as binders and fillers has also been explored to some degree. With the addition of relatively small amounts of asbestos, a number of compositions have been developed which possess excellent physical and electrical properties, and which show promise of performing satisfactorily in the cell environment. Testing of several of the more promising of these in cells at ANL is in progress, and the results of these tests will be reported as soon as practical.

MATERIALS

As noted earlier, both fibrous and powdered materials have been combined to make separators. In some cases mixtures of fibers alone have been used, but in most cases powders have been added to the fiber mixture. The fibers utilized were: boron nitride, yttria, lithium aluminate, and chrysotile asbestos. The powders explored to date include boron nitride, yttria, lithium aluminate, and magnesium oxide.

Boron Nitride Fibers

This material was made available to us by ANL in the form of roving; it originated at the Carborundum Company and is available from that organization. Scanning electron microscopy reveals the individual fibers to be very long (i.e., several inches) and relatively flexible rods having diameters between 5 and 10 μm. The surface of the fibers appears to be very smooth and this is borne out by the extreme difficulty of forming a paper-like sheet from the dispersed fibers. BN has a graphite-like structure and is known to exhibit very high lubricity.[2] Owing to its smoothness and high lubricity it is not surprising that its sheet-forming characteristics are poor. When pure, however, it possesses very good chemical resistance in the battery environment.[6]

Yttrium Oxide Fibers

These fibers were made available by ANL; they were procured from Zircar Products, Inc. Very cursory microscopic examination indicated that they are 5-10 μm in diameter and their length varies from a millimeter up to 5 mm. The bulk fibers contain an appreciable proportion of powder. The surface of the fibers appears quite smooth but the details of their structure are not available at the moment; electron microscopy is in progress and more details will be available later. Yttria has been shown to have good chemical resistance in the battery environment,[5] and these fibers are quite flexible. The fibers were very easily dispersed.

Lithium Aluminate Fibers

This material, too, was made available by ANL. The fibers are about 10 μm in diameter, rather short (about 2 mm), and very brittle. Some of the material seems to be bound together in fiber bundles somewhat like chrysotile asbestos, but most of the fibers appear to be short, single fibers, sometimes with powder particles attached to the surface. This particular batch of lithium aluminate fibers was so brittle that normal fiber dispersion procedures reduced the fibers to a powder. Very gentle dispersion techniques are required to produce a fiber dispersion. In spite of the apparent attachment of powder particles to the surface of the fibers the sheet-forming properties of these fibers was extremely poor.

Chrysotile Asbestos Fibers

The excellent sheet-forming properties of chrysotile asbestos are well-known. Asbestos occurs as veins in other rocks,[7] and must first be separated from them. Then the asbestos blocks must be broken into fiber bundles by milling procedures, and classified roughly by approximate fiber length. Asbestos dispersions for sheet-making are then made by breaking the fiber bundles into single fibers or small groups of fibers using any of a number of techniques. In the process of breaking the fiber bundles, the fibers are usually shortened to a considerable extent.

Chrysotile asbestos is a hydrous magnesium silicate having the general formula $Mg_3Si_2O_5(OH)_4$, but it never occurs absolutely pure.[8] Chrysotile asbestos fibrils have been shown to exist as hollow tubes with the outside diameter ranging from 20-30 nm and an effective inner diameter of 2-5 nm.[8] The aspect ratio, or length to diameter ratio, is very large, and the result of this structure is very high mechanical strength, and great flexibility. These permit the fibers to intertwine and produce sheets of excellent mechanical strength, as well as other desirable properties.

The asbestos fibers used in this investigation were fuel cell grade and were purchased from Johns-Manville. This asbestos has a very low iron content.

Powders: BN, Y_2O_3, $LiAlO_2$, and MgO

All of these powders were procured from commercial sources, except for one sample of BN, which was pretreated at ANL by heating at 1700°C in a stream of ammonia to improve the purity of the powder.

Scanning electron microscopy of the commercial BN powders revealed that they consist of roughly circular platelets having diameters ranging from about 0.5 to 10 μm but having relatively uniform thickness in the range of 10-20 nm.

Electron microscopy on the other powders has not yet been completed.

EXPERIMENTAL PROCEDURES

Fiber Dispersion

Several methods of fiber dispersion have been explored, and at least three of these yield generally similar fiber dispersions. The choice of one of these depends primarily on the amount of fiber to be dispersed. A Waring Blendor or Osterizer serves very well to disperse quantities of a few grams of fiber. For larger amounts of fiber in the range of 25 to 50 grams, the Gifford-Wood Homo-Mixer is suitable, while larger amounts of fiber are best dispersed in equipment such as a cycle beater of the type used in the pulp and paper industry. Generally speaking, however, the capacity of a cycle beater for efficient dispersion of inorganic fibers is considerably less than its capacity for cellulose pulp.

If one is preparing a mixture of fibers, it is often best to disperse them separately and then mix, or to begin with the most difficult to disperse, such as asbestos, and then add the more easily dispersed fibers and continue mixing until the desired dispersion has been obtained.

Low fiber concentrations, temperatures higher than room temperature, control of both the pH and the electrolyte content, and the addition of wetting or dispersing agents all contribute to improved fiber dispersion. Although most of our studies have been conducted with deionized water, isopropanol has also been noted to be a satisfactory dispersion medium. Wetting agents which cause foam require very careful handling.

In general fiber concentrations of about 5 grams/liter, temperatures of about 35°C, and deionized water have been found suitable. Small amounts of Triton X-100 (severe foamer), Quadraphos, an inorganic phosphatic dispersing agent, or substantial amounts of isopropanol have served adequately as wetting and dispersing agents. Mixing times of one to five minutes have given adequate fiber dispersions as judged by uniform appearance of the suspension and a lack of shreds or clots of undispersed fibers. Yttria disperses easily; asbestos requires the longest dispersion time because the principal process occurring with asbestos is the breaking of the fiber bundles.

The fibers of lithium aluminate available were so brittle that they could not be processed with the other fibers. They were generally placed in the Osterizer and the switch flicked on and off several times. Then this dispersion was added to the dispersion of the other fibers and the whole was mixed with a stirring rod.

If powders were incorporated in the mixture, these were added near the end of the fiber dispersion period.

Sheet Formation

The fiber-or fiber:powder slurry- was diluted to a solids content of about one gram per liter, stirred well to mix, and then poured onto a Buchner funnel modified to provide greater depth, or into a standard sheet mold (if 8" x 8" sheets were desired). Generally, sheets were formed in a 9 cm Buchner funnel, with either Millipore SC filter or Whatman filter papers as a filter base. The suspension was stirred gently and the convection currents allowed to subside, then vacuum was applied to speed filtration. Vacuum was continued until the sheet appeared dry, the vacuum was broken, and the sheet removed from the filter. It was placed between blotters on a flat plate and pressed at a total pressure of 100 lbs. to dewater the sheet further. The blotters were then removed and the sheet set aside to dry. In many cases it was possible to peel off the filter base before drying; in other cases the separator sheet which had been deposited on the filter base tended to stick to the filter base and the filter base was more readily removed from the separator after drying.

Separator Evaluation

Separator sheets have been evaluated by a series of tests which are either standard paper evaluation tests or modified to be suitable for these particular materials. The evaluation tests performed were: 1)Basis Weight, i.e., weight per unit area; 2)Thickness; 3)Mullen Burst Test; and 4)Flexibility. The average Density of the separator can be calculated from a knowledge of the component densities and the composition of the mixture. The Porosity can be calculated from a knowledge of the Basis Weight, the Thickness, and the average Density. In-cell separator evaluation is in progress.

Permeability, Effective Diffusion Coefficient, and Effective Electrolyte Conductivity tests are under development.

In practice, Mullen Burst Tests were run first because it was simpler to use the entire 9 cm. sheet for the Burst Test; then samples could be punched for determination of the Basis Weight and Thickness. For this reason, the Mullen Burst Test will be described first.

Mullen Burst Test: The apparatus consists of a ring resting on a rubber diaphragm, a clamp to hold the sample against the ring and diaphragm, and a hydraulic system by which the pressure on the diaphragm can be increased to cause it to bulge until the deformation of the adjacent sample

causes the sheet to burst. The pressure at which bursting occurs is noted; it is related to the tensile strength of the sample. Since the particular tester available was designed for measuring paper burst strength and the burst strength of the separators studied so far tends to be much less than that of paper, it was generally necessary to use two or more layers to produce pressures at bursting which were large enough to measure accurately. The data were converted to a basis of one thickness after it was demonstrated that a linear relation existed between thickness and pressure at bursting.

Basis Weight: Disks having a standard diameter were punched from separator sheets, they were dried at 110°C, and weighed. The mean weight per unit area and the standard deviation were calculated. The larger the sample area, the smaller the standard deviation. Sample areas of the order of 10 cm^2 yield Basis Weight data generally suggesting very uniform sheets, whereas sample areas of about one cm^2 usually give fairly considerable standard deviations. The standard sample diameter in our work is 0.500 inches or 1.27 cm, leading to an area of 1.27 cm^2. Basis Weight data are reported in units of mg/cm^2.

Thickness: This test employs a standard paper thickness gauge except that the spindle has been modified to accommodate a series of weights which enable one to measure the thickness of a sample at more than one pressure. This is especially important for compressible materials such as paper-like separators. The foot of the spindle has a diameter of 0.952 cm (0.367 in.), and the variability associated with small sample area-which reflects local variation in the properties of the sheet-tends to be relatively large, as is the case with Basis Weight measurements on small area samples. From thickness measurements at several pressures one can evaluate the compressibility of a sample and determine the actual thickness of the separator if confined under pressure in a battery.

Flexibility: The apparatus for this test consists of a series of rods having diameters ranging from 0.125 in. to 2 inches, in increments of 0.0625 in. (or 0.125 in. for the larger sizes). The test is conducted by bending a sheet around a rod, beginning with the largest one in the series and examining the sheet for evidence of cracking or separation, then proceeding to progressively smaller rods. The data are recorded as the smallest diameter rod at which cracking or separation did not occur.

In-Cell Separator Evaluation: Separator samples which have appeared to have promising physical and mechanical properties have been sent to ANL where they have been incorporated in cells and cycled. At the time of writing only a few data are available. Additional in-cell testing is in progress and some of these results will be reported at the meeting.

RESULTS AND DISCUSSION

Two quite different kinds of separators have been studied to date: 1)Composite Separators, in which fibers or a mixture of materials were deposited on a 10 mil asbestos base sheet, and 2)Homogeneous Separators, in which a mixture of fibers and/or powders was deposited on a filter base which is later stripped off.

Separators consisting entirely of fibers which are chemically resistant in the battery environment have proved too fragile to be of serious interest. Moreover, even when these fibers were deposited on an asbestos base sheet, the integrity of the resistant fiber layer was so poor that it did not seem worthwhile to explore this kind of mixture further. Therefore, attention was turned to the use of binders and the incorporation of materials with better sheet-forming properties.

Both organic (Teflon 30 emulsion) and inorganic (Alkaphos E) binders were explored in a small way. Although their addition to the mixture resulted in much improved sheets, obvious problems associated with their use suggested that other approaches would be more fruitful.

The incorporation of chrysotile asbestos in small to moderate amounts was found to markedly improve the physical properties of the sheets. Also, the addition of chemically resistant powders further improved the physical properties, whether composite or homogeneous separators are considered. Magnesium oxide powder was especially efficaceous in improving Burst Strength but it did so at the expense of Flexibility. Moreover, the addition of asbestos to the mixture is not without hazard. The lithium alloy anode reacts slowly with asbestos but does not appear to result in significant electrical shorting.[9] In addition, there is some preliminary evidence that asbestos will not be stable in the battery environment for long periods of time. This matter is being explored and the results will be reported as soon as they are available.

Selected physical test data are given in Tables 1 and 2. Though these are selected from a larger number of data, they are generally representative and they indicate some of the effects noted earlier. For example, Burst Strength tends to increase with asbestos content, Basis Weight, and Thickness; similarly the incorporation of moderate amounts of powder generally improves physical characteristics. The ability of MgO powder to improve Burst Strength while reducing Flexibility is very clearly illustrated.

In summary, it can be concluded that the production of paper-like battery separators from the chemically resistant fibers presently available is very difficult if not impractical. The incorporation of small to moderate amounts of chrysotile asbestos and certain powders, which act both as binders and fillers, improves the physical characteristics of the separator sheets, but in-cell evaluation will be required before one can include these materials in the separator with confidence that they will continue to exert their desirable influence for long periods in the battery environment.

REFERENCES

1. Economy, J., and R.V. Anderson, Textile Res. J., 36, 994 (1966).
2. Economy, J., and R.V. Anderson, J. Polymer Sci., Part C, No. 19, 283 (1967).
3. Economy, J., Research/Development, June, 1967.
4. Economy, J., W.D. Smith, and R.Y. Lin, Applied Polymer Symposium No. 21 131 (1973).

5. Battles, J.E., F.C. Mrazek, J.A. Smaga, and W.D. Tuohig, paper presented at the Electrochemical Society Meeting, Toronto, May, 1975; see Extended Abstracts, 75-1, 80 (1975).
6. Battles, J.E., private communication (1975).
7. Badollet, M.S., Asbestos, Symposium, Quebec Asbestos Mining Assn., p.1 (1961).
8. Martinez, E., Trans. Can. Min. & Met. Bull., LXIX, 414 (1966).
9. Battles, J.E., private communication.

Table 1

Physical Characteristics of Composite Separator Sheets

Composition, w/o AsbF*	BNF*	BNP*	Bas.Wt., mg/cm^2	Thickness, mils	ρ_{avg}, g/cm^3	Porosity	Burst; psi	Flexibility, 1/16 in.
2	8	90	41.8	17.9	1.82	0.50	0.50	3
2	18	80	38.7	17.6	1.82	0.51	0.65	8
10	40	50	41.4	20.7	1.88	0.64	1.21	10
AsbF	BNF	MgOP						
2	8	90	41.4	20.4	3.42	0.76	2.86	10
2	18	80	45.6	19.4	3.24	0.72	8.81	17
10	40	50	44.5	22.7	0.76	2.77	6.06	17
AsbF	BNF	$LiAlO_2P$						
2	8	90	38.2	13.5	2.48	0.42	0.75	4
2	18	80	40.5	15.0	2.42	0.48	0.57	10
10	40	50	37.3	17.4	2.25	0.67	1.05	17

Table 2

Physical Characteristics of Homogeneous Separator Sheets

Composition, w/o AsbF	BNF	BNP	Bas.Wt., mg/cm^2	Thickness, mils	ρ_{avg}, g/cm^3	Porosity	Burst; psi	Flexibility, 1/16 in.
2	8	90	69.3	37.3	1.93	0.62	0.34	17
4	16	80	70.3	36.2	1.83	0.58	0.59	17
10	40	50	68.3	37.5	1.88	0.62	0.16	17
AsbF	BNF	MgOP						
10	40	50	62.4	33.6	2.77	0.74	19.5	17

* F = fiber; P = powder

MATERIALS DEVELOPMENT IN THE LITHIUM-ALUMINUM/IRON SULFIDE BATTERY PROGRAM AT ARGONNE NATIONAL LABORATORY

K. M. Myles, F. C. Mrazek, J. A. Smaga, and J. L. Settle

Argonne National Laboratory
9700 South Cass Avenue
Argonne, Illinois 60439

ABSTRACT

The materials development effort in the lithium-aluminum/iron sulfide battery program at the Argonne National Laboratory traverses a spectrum of endeavors that includes design and fabrication, compatibility evaluation, and postoperative examination of various cell components. A brief historical overview of the effort is presented, but emphasis is placed on current areas of activity, with a mention of anticipated future plans. The major topics discussed are the development of electrical feedthroughs, the compatibility of negative- and positive-electrode components with the cell environment, the use of the postoperative examination as an aid in cell design, the study of the Li-Al phase diagram, and the development of positive-electrode current collectors.

INTRODUCTION

The Chemical Engineering Division of the Argonne National Laboratory (ANL) is engaged in a program on the development of high performance lithium-aluminum/iron sulfide batteries for powering electric vehicles and for storing off-peak electrical energy generated by electric utility power stations. The batteries consist of cells containing two negative electrodes of a lithium-aluminum alloy that are in electrical contact with the cell housing and a center positive electrode of iron sulfide, FeS or FeS_2, that is physically isolated from the negative electrode by a separator and electrically insulated from the cell housing by a feedthrough. The electrolyte is molten LiCl-KCl eutectic and, thus, requires a cell operating temperature between 400 and 450°C. The cells are prismatic, 13 cm wide, 13 cm high, and 2.0 to 3.8 cm thick, with the three electrodes vertically oriented. Cells containing FeS electrodes which appear attractive for the energy storage application, have achieved a capacity of about 90 A-hr at 1.2 V; and cells with FeS_2, suitable for vehicles, have demonstrated a capacity of about 120 A-hr at 1.5V. These values correspond to specific energy values of about 100 W-hr/kg and 150 W-hr/kg for the FeS and FeS_2 cells, respectively.

To assist in this effort, a materials development program was begun at ANL that has the broad responsibilities of identifying and specifying candidate construction materials, designing and fabricating materials into the various cell components, ascertaining the cell compatibility of the materials through corrosion testing, and performing postoperative examinations of cells to evaluate the behavior of the construction materials as well as the electrodes and separator. To a large extent, the actual cell design effort has been assumed by other programs at ANL and by outside commercial contractors, namely, Gould Inc., Eagle-Picher Industries, Inc., and Catalyst

Research Corp., with only technical assistance from the materials program. The emphasis of the materials development program has, as a result, centered on the areas of feedthrough development, separator development, corrosion testing, and postoperative examination, with some effort on the development of the negative electrode and the positive electrode current collector. Professor Walker in another paper to be presented at this workshop will discuss, to a large extent, the separator development effort and, thus, no further comment of this very important area of activity will be made in this paper. The bulk of this paper will describe the current status of the remaining areas with only brief mentions of past accomplishments, which have, in large, been reported elsewhere.

ELECTRICAL FEEDTHROUGH DEVELOPMENT

Significant progress has been achieved in the development of an electrical feedthrough, for the lithium-aluminum/iron sulfide cells. The many stringent, and often conflicting, design parameters have led to the development of several conceptually different prototypes that have sufficient merit to warrant in-cell testing. Among the parameters considered are the electrical conductivity of the conductor, the dielectric strength of the insulator, materials compatibility with the cell environment, relative cell and feedthrough sizes, cell assembly procedures, required leak-tightness, weight, and ultimate costs. Continued refinements in the cell design and assembly procedures as well as improvements in the feedthroughs themselves preclude the likelihood that a selection based on demonstrated superiority will be made in the near future. Nonetheless, data are being accumulated that indicate that the feedthrough costs will be consistent with other cell costs. Because the seal between the metal and ceramic members represents one of the more difficult problems, the feedthrough development program is keyed to whether the seal is strictly mechanical or whether a metallurgical or chemical bond is created.

Mechanical-Type Feedthrough

Two types of mechanical seals are being developed, namely, a compression type, wherein BN powder is compacted within a fairly heavy-walled metal fitting to effect the seal, and a ram type, wherein a thin-walled metal tube is forced over a high-strength BeO ceramic body to produce a seal. A preliminary effort was undertaken to produce a swaged type but failed to produce a compact, mechanically strong, leak-tight feedthrough.

The compression type is a modification of the commercially available Conax thermocouple seal. As currently designed, the upper insulator is made from high-purity Al_2O_3 and the lower insulator is machined from hot-pressed BN. This feedthrough has been successfully used in many ANL cells and will be installed in all of the commercial cells now being fabricated. The main advantage of the feedthrough are ruggedness, simplicity, and flexibility toward a variety of cell assembly procedures; the limitations are insufficient leak-tightness and excessive bulkiness. High strength insulators of BeO and Y_2O_3, which are being fabricated as replacements for the intrinsically weak BN lower insulator, are expected to permit more complete tightening of the feedthrough with resulting tighter seals. In an effort to reduce the bulkiness and cost of the feedthrough, the compacting nut on the Conax seal

was eliminated in favor of a retainer plug, which is held in place by crimping the feedthrough housing during assembly of the feedthorugh, and a housing that are tailored to automatic screw-machine fabrication methods. The internal components are quite similar to those used in the Conax seal and the method of introducing and compacting the BN powder is also the same. A schematic of the unassembled and assembled feedthrough is shown in Fig. 1. Cost quotations for the components of the redesigned feedthrough were solicited for 250 and 100,000 units to represent both immediate and anticipated future needs. The estimated cost of the feedthrough in large volume, without BN powder, is only $1.85 (the cost of BN powder, in limited-quantity purchases, is about $0.24).

The ram-type feedthrough, shown pictorically in Fig. 2, is being developed for ANL by Ceramaseal, Inc. Whereas design details are proprietary, the seal is formed by forcing (ramming) an internally plated, high-strength, thin-walled, metal sleeve over a carefully designed BeO ceramic body, thereby smearing the plate onto the ceramic. The sleeves in turn develop high hoop stresses that hold the ceramic in compression even at cell operating temperatures. Feedthroughs with leak rates down to about 1×10^{-9} cm^3 He (std)/sec under a sustained vacuum of about 1×10^{-9} torr have been delivered to ANL for evaluation. Future effort will be directed toward optimizing the feedthrough with regard to size and weight.

Brazed-Type Feedthrough

The electronics and ceramics industries have developed many different methods for bonding ceramic insulators to metal conductors and housings. Unfortunately, almost all of these methods employ brazes that are not compatible with the cell environment. The most common modes of failure are chemical oxidation of the braze upon charging, reaction of the braze with the sulfides in the positive electrode, and galvanic corrosion at the braze joint resulting from the electrochemical dissimilarity of the braze materials and the adjacent metal parts. Additional problems that must be resolved in designing a brazed-type feedthrough include intrinsically high cost, degradation upon thermal cycling and exposure, generally low mechanical strength, and mismatch of the thermal expansion coefficients of the braze and insulator.

Three independent efforts are under way to develop such a feedthrough each utilizing the technical expertise of a commercial feedthrough manufacturer. Feedthroughs with BeO insulators have been produced by the Technical Ceramic Products Division of 3M Company utilizing three different conventional brazing techniques, namely, molybdenum-manganese metallization, titanium active metal, and solution molybdenum metallizing. Because the brazes themselves were not expected to exhibit reasonable lifetimes, a coating of nickel or gold was subsequently plated on the braze joints in an attempt to protect them from the cell environment. Simulated cell-corrosion tests are being conducted at ANL to evaluate the effectiveness of this approach. ILC Technology has developed several Nb-base active metal brazes for BeO and has produced feedthroughs with Nb-Ni, Nb-Cu, Nb-Ag, and Nb-Au brazes. Niobium was selected as the base metal because it should not be oxidized to any extent at reasonable cell charge potentials, that is, 2 V (IR included). A schematic representation of these feedthroughs is shown in Fig. 3A. A more recent design, which closely resembles feedthroughs produced for the Eagle-

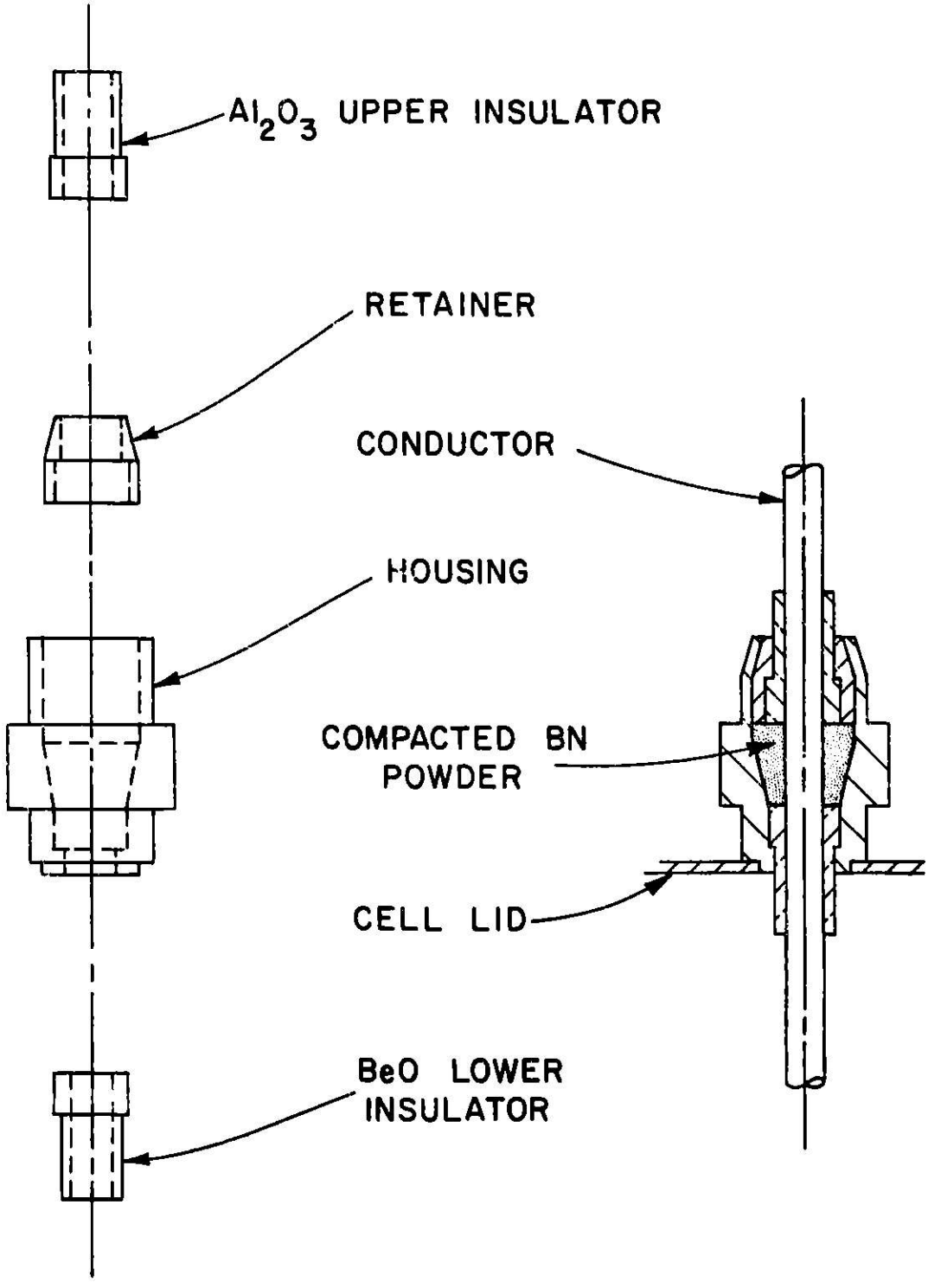

Fig. 1. Redesigned Compression-Type Feedthrough

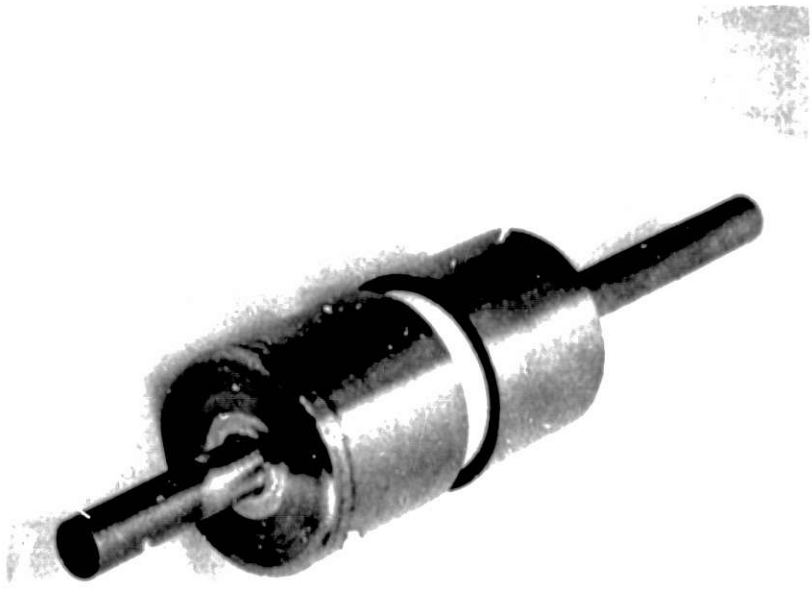

Fig. 2. Ceramaseal Ram-Type Feedthrough

Picher Industries, Inc. nickel-cadmium batteries, is drawn in Fig. 3B and appears ideally suited for use in the ANL prismatic cell because the housing configurations of the two batteries are similar. Plans are under way to purchase some of these feedthroughs for actual in-cell evaluation. A preliminary effort has been undertaken to further refine the design of the feedthrough, with an emphasis on minimizing the manufacturing costs. One such design is shown in Fig. 3C, where two of the three expensive BeO insulator rings are replaced with a single low-cost Al_2O_3 ring. Since BeO represents a large fraction of the total costs of the feedthrough, the substitution of Al_2O_3 yields a significant cost reduction. Some preliminary efforts to fabricate such a configuration have been encouraging. The most recently initiated program is with Coors Porcelain for the development of pressed-and-sintered Y_2O_3 ceramic bodies and a nonmetallic braze to bond the bodies to molybdenum metal. The development of Y_2O_3 is viewed only as a backup effort in case the use of the stronger but toxic BeO is restricted from use in electric vehicles. As a raw material, Y_2O_3 is somewhat more expensive and potentially in shorter supply than BeO, but the fabrication costs are lower, because special handling facilities are not required. ILC Technology has also been asked to consider developing brazes for Y_2O_3; however, this effort awaits the results of ongoing in-house compatibility tests on several unevaluated Y_2O_3-doped bodies produced by Ceradyne, Inc., which are required for the project.

Recently, equipment has been assembled for screening feedthroughs prior to in-cell testing. In brief, the feedthroughs are sealed into half-cells of 8 Li-Al/LiCl-KCl and held at 450°C. The variation in resistance across the ceramic insulators is determined by monitoring the current level under a

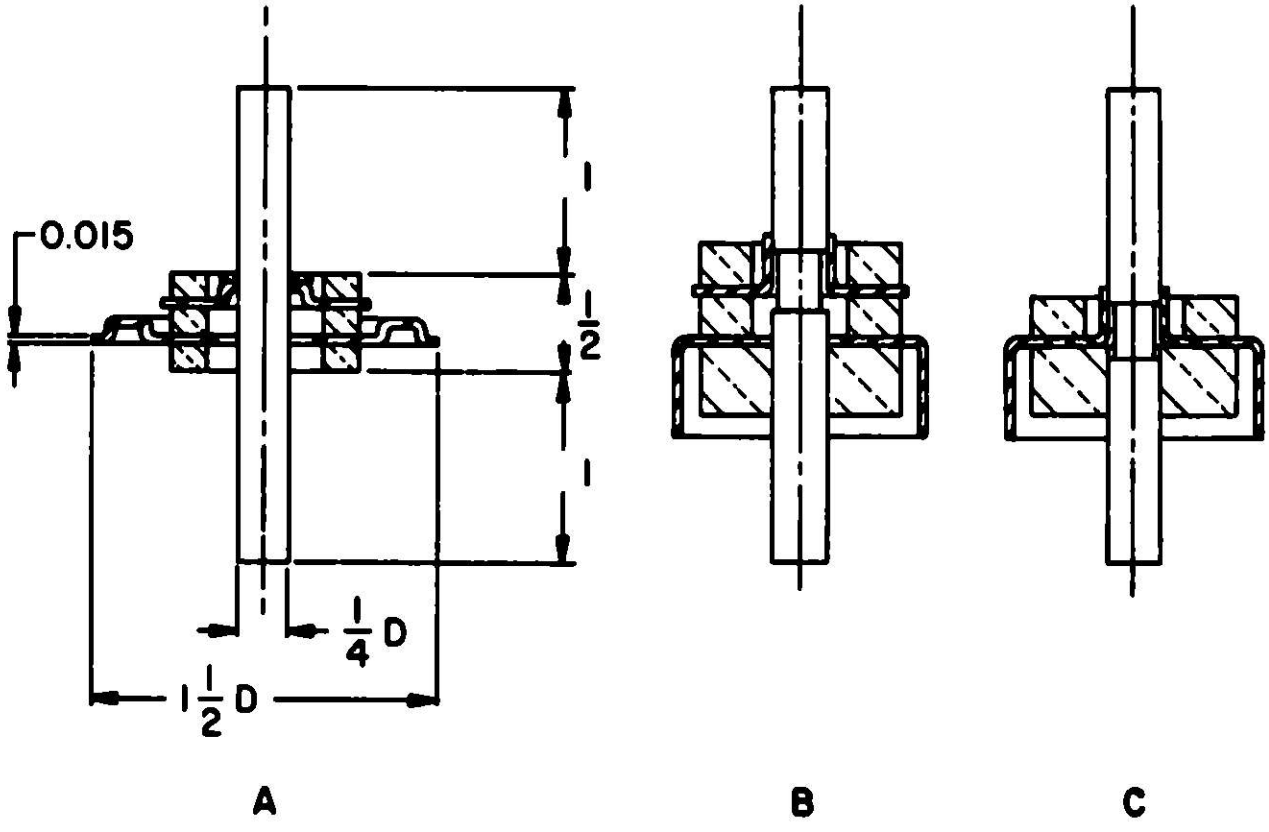

Fig. 3. Cross-Sections of ILC Brazed-Type Feedthroughs

constant applied potential of 2.0 V. The tested feedthroughs are subsequently examined using metallography and scanning electron microscopy.

Ceramic Insulator Development

A ceramic development effort has been under way for sometime at ANL in support of the feedthrough development program. Specimens of $CaZrO_3$, MgO, Al_2O_3, $MgAl_2O_4$, and Y_2O_3 were carefully prepared from high-purity raw materials and tested for corrosion resistance. Our current interest, however, is mainly in Y_2O_3 components for both the mechanical- and brazed-type feedthroughs.

The most promising Y_2O_3 bodies have been prepared according to the scheme outlined in Table I. The relatively high binder concentration, which necessitates additional concern during the initial sintering, can be reduced in all likelihood without adversely affecting the pressing characteristics. After attempts by slip casting were not successful, presumedly because Y_2O_3 powder tends to hydrate, prototype insulators for the mechanical-type feedthrough were prepared by an isostatic pressing technique; the mold and a pressed insulator are shown in Fig. 4. A preweighed charge of granulated powder, -60 to +170 mesh, is vibratorily loaded into the mold cavity that is then pressed at 170 MN/m^2 (25,000 psi). The green form is prefired at 1500°C, after which it can be readily machined to correct any dimensional transgressions. The part is finished by vacuum-firing at 1800°C followed by an oxidation-firing at 1500°C. Although the required dimensional tolerances

Table I. Preparation Scheme for Y_2O_3 Bodies

1.	Slip: mix in jar mill; Y_2O_3 powder, 4% stearic acid (die lubricant), 2% acrylic resin (binder), CCl_4 (solvent)
2.	Dry: vacuum at 100°C
3.	Crush and Granulate
4.	Size: screen to -60 +170 mesh
5.	Press

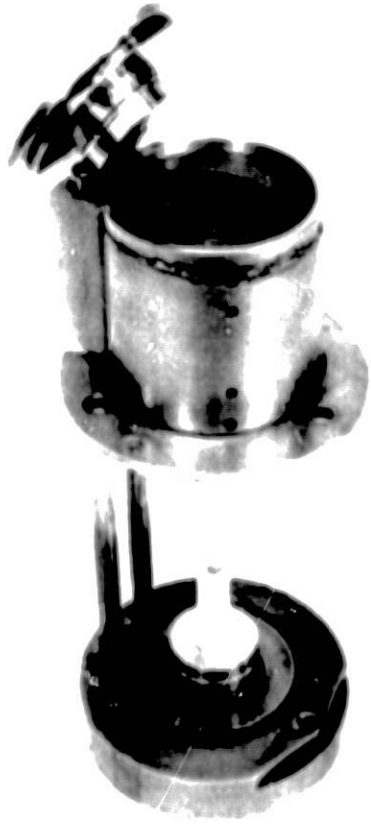

Fig. 4. Isostatic Mold Assembly for Pressing Y_2O_3 Feedthrough Insulators.

can be routinely obtained, the insulators are only about 90% of theoretical density and often contain fabrication flaws. In effort to eliminate these flaws, a number of rectangular test bars have been produced and these have been broken in a four-point bend test to determine the modulus of rupture. The strength and the microstructure are being correlated with observations of the fracture surfaces and the grain boundary morphology, to establish the allowable design stresses in the Y_2O_3 components.

CORROSION STUDIES

The high corrosiveness of the cell environment requires an extensive materials evaluation study of both metals and ceramics as an ongoing part of the materials program. Although it is recognized that the corrosion resistance of any given material can be fully evaluated only in operating cells, many candidate materials can be eliminated from further consideration by relatively simple static immersion in molten lithium, LiCl-KCl eutectic, 8 LiAl and LiCl-KCl eutectic, or FeS (or FeS_2) and LiCl-KCl eutectic baths. Experience has shown that materials behavior in these tests closely parallels the behavior in actual cells, as determined by postoperative examinations. Because the corrosive conditions in each electrode differs significantly, the following discussion will be presented according to the intended application.

Negative Electrode Environment

The recent postoperative examination of several cells operated near 500°C revealed that the aluminum from the Li-Al electrode had reacted with the low carbon steel (AISI 1008) cell-housing components to form a series of intermetallic-compound reaction layers; a typical series of electron microprobe scanning images is shown in Fig. 5. The intermetallic compounds were brittle and fractured under small applied stresses, and, undoubtedly, any prolonged development of the layers would have resulted in the premature failure of the cell. These observations were particularly surprising because no evidence of this reaction had been found in previously performed static immersion tests of the steel in 8 LiAl/LiCl-KCl electrolyte baths. Preliminary tests indicated that the reaction mechanism appeared to have resulted from the periodic formation of a galvanic couple between the lithium-depleted, discharged negative electrode and the cell housing. The corrosion reaction would be expected to accelerate with increasing temperature.

To test this hypothesis, a number of galvanic couples were assembled wherein high-purity aluminum, as the anode, was mechanically joined to various iron- and nickel-base alloys which served as the cathodes. The couples were inserted into quartz crucibles filled with LiCl-KCl eutectic salt for periods of 9 to 10 days at both 400 and 500°C. In all of the tests, it was observed that the weight loss of the aluminum was matched by a similar weight gain by the cathodic metals and that the weight change was one to two orders of magnitude larger at the higher temperature, as shown in Columns 2 and 3 of Table II; the variability in the data for a given couple is due to the simple experimental setup employed. The compositions of the reaction layers, determined from electron microprobe analyses, are listed in the last column of Table II.

PHOTOMICROGRAPH AND ELECTRON MICROPROBE SCANNING
IMAGES OF Li-Al REACTION WITH IRON (500X)
(PHOTOGRAPHICALLY REDUCED BY 40%)

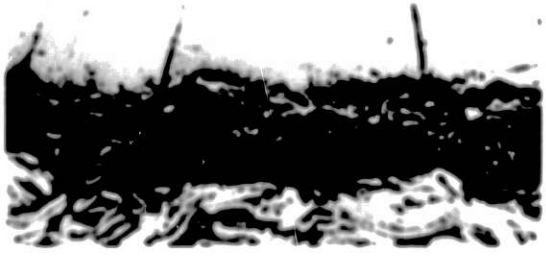

PHOTOMICROGRAPH 300X AS-POLISHED

SPECIMEN CURRENT IMAGE

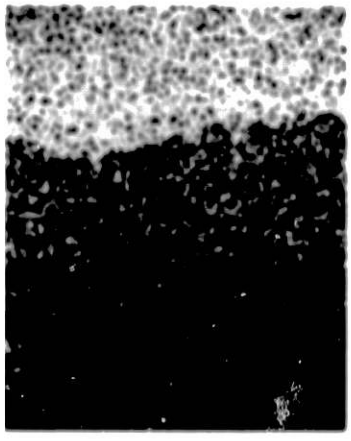

Fe K_α SCANNING IMAGE

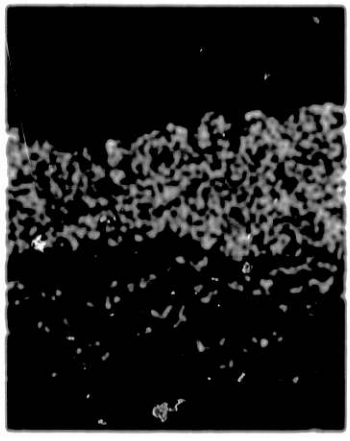

Al K_α SCANNING IMAGE

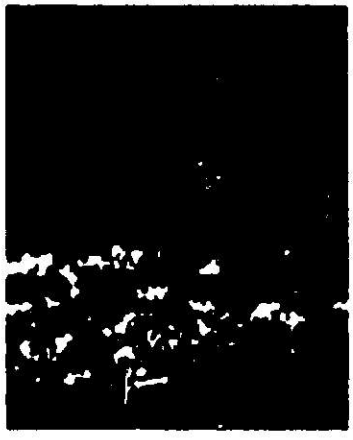

Mg K_α SCANNING IMAGE

Fig. 5. Photomicrograph and Electron Microprobe Scanning Images of Li-Al Reaction with Iron (500X) (Photographically reduced by 40%)

Table II. Reaction of Dissimilar Metal Couples in LiCl-KCl Electrolyte

Couple	Rate of Aluminum Pick-Up by the Cathodic Member, mg/cm²-yr				Intermetallic Compound[c]
	400°C APL[a]	500°C APL	400°C Lithcoa[b]	500°C Lithcoa	500°C, APL
Fe/Al	8, 30	95, 514	2	3, 14	$FeAl_2$
304 SS/Al	2, 8	55, 44	1	8	-
316 SS/Al	1	224	-	4	Inner layer, $Fe(Cr)Al_2$; Outer layer, $Fe(Cr, Ni)Al_2$
Ni/Al	5	337	-	11	Ni_2Al_3
E-Brite/Al	3	41	-	-	$FeCrAl_4$
1008/Al	55	90	-	-	-

[a] LiCl-KCl eutectic salt supplied by Anderson Physics Laboratories.

[b] LiCl-KCl eutectic salt supplied by Lithium Corporation of America.

[c] Compound formulations were estimated from linearized, relative X-ray intensity data.

During the course of these experiments, an alternative source for the electrolyte salt was found. Heretofore, the salt was procured from the Anderson Physics Laboratories (APL) and was quite expensive. The Lithium Corporation of America (Lithcoa), which utilizes the salt in the electrolytic refining of lithium, offered an abundant supply at considerably lower costs. As part of an effort to evaluate the salt for use in lithium-aluminum/iron sulfide cells, the Lithcoa salt was substituted for the APL in several of the test cells used in this study. The results were quite unexpected in that the weight gains of the cathodic metals were considerably smaller, particularly at 500°C, than previously observed, as shown in Columns 4 and 5

Table II. The obvious deduction was reached that an important chemical difference exists between the two salts that significantly affected the kinetics of the reaction. Voltammetry studies of the two LiCl-KCl salts showed that much high levels of OH^-, $O^=$, and possibly $(CO)_3^=$ anions are present in the Lithcoa salt. These anions are probably responsible for the observed high pH of the salt (about 10); the pH of the Anderson salt is about 6. It is hypothesized that the anionic impurities are involved in the formation of a passivating film on the aluminum anode surface that impedes further reaction. If one assumes that an increase in weight of less than 20 mg/cm^2 per year (the deposition of 3 mils of aluminum) is acceptable for cell housing materials, then none of the metals evaluated could be used in cells that are operated at 500°C with Anderson salt as the electrolyte Even at 400°C, AISI 1008 steel, the current cell housing construction material, and Armco iron may be unsatisfactory. On the other hand, if Lithcoa salt is used in the cells, any of the tested metals would be satisfactory even at 500°C.

Positive Electrode Environment

The fact that FeS and, in particular, FeS_2 are relatively unstable thermodynamically when compared with almost all other metal sulfides explains to a large extent the extreme difficulty in identifying a satisfactory metal for use in the current collector assembly of the positive electrode. The difficulty is further compounded because the generally specified charge cutoff potentials of approximately 1.6 and 2.0 V (relative to LiAl) for the FeS or FeS_2 electrode cells, respectively, cause a substantial number of metals to be chemically oxidized in the LiCl-KCl electrolyte at 450°C. To date, only molybdenum metal has been found to be resistant to sulfide attack and is not oxidized at the cell charge cutoff potentials. Unfortunately, pure molybdenum is costly and extremely difficult to fabricate into a current collector assembly. Alloys of molybdenum, particularly those of iron and nickel, are somewhat less costly and considerably easier to fabricate, but they are also more susceptible to sulfurization and chemical oxidation.

Nevertheless, because of the importance of developing an alternative to pure molybdenum, a number of metals were subjected to corrosion tests in both FeS and FeS_2 environments at 500°C. The commercially available metals tested were Armco electromagnet iron, nickel, molybdenum, niobium, Hastelloy B (65Ni-28Mo-5Fe-1Cr), and Hastelloy C (57Ni-17Mo-5Fe-16Cr-4W). Several iron-molybdenum and iron-molybdenum-nickel alloys that were prepared at ANL were also tested. Nickel was added to the iron-molybdenum alloy to increase the solubility of molybdenum in the alloy, with the aim of obtaining an alloy with corrosion properties more like molybdenum. The test specimens were immersed in molten, equal-volume mixtures of both FeS/LiCl-KCl and FeS_2/LiCl-KCl and removed for examination after 500 and 1000 hr. The results are summarized in Tables III and IV, which present both the corrosion rates and the metallographic observations for the FeS and FeS_2 environments, respectively.

The FeS corrosion study and subsequent electron microprobe and X-ray diffraction analyses indicate that the following materials have acceptable reaction rates at 500°C: nickel, molybdenum, niobium, Hastelloy B, Hastelloy C, Fe-10Mo-20Ni, Fe-15Mo-20Ni, and Fe-15Mo-30Ni. For both nickel and niobium, an adherent layer of iron developed on the surface of the samples; no metal sulfide layers were observed. In the two Hastelloys,

Table III. Results of Corrosion Tests in FeS/LiCl-KCl at 500°C

Material	Corrosion Rate,[a] μm/yr 500 hr	1000 hr	Comments
Armco iron	480	340	General attack, with intergranular penetration 1 to 2 grains deep.
Nickel	+58	+39	Iron-nickel reaction layer.
Molybdenum	8.7	11.6	Minor surface attack.
Niobium	+18	+30	Iron-niobium reaction layer.
Hastelloy B	+9	+12	Weakly adherent reaction layer consists of an internal molybdenum sulfide band and a plated iron layer. Localized areas of intergranular attack.
Hastelloy C	+26	+9	Similar to Hastelloy B but no apparent intergranular attack.
Fe-6Mo	110	130	Intergranular attack resulted in grain fallout.
Fe-6Mo-7Ni	25	79	Surface attack after 500 hr with intergranular penetration after 1000 hr.
Fe-6Mo-20Ni	74	90	Internal sulfidation of molybdenum resulted in a band of porosity 30 μm deep after 1000 hr.
Fe-10Mo-20Ni	17	+14	Localized areas of intergranular attack on 500-hr sample, but a reaction layer also developed on areas of the 1000 hr sample.
Fe-15Mo-20Ni	32	26	Intergranular attack resulted in grain fallout.
Fe-15Mo-30Ni	59	21	Intergranular attack was more severe for the 500-hr sample.

[a]Numerical values proceeded by a + sign indicate the formation rate of a reaction layer in μm/yr.

Table IV. Results of Corrosion Tests in FeS_2/LiCl-KCl at 500°C

Material	Corrosion Rate,[a] µm/yr 500 hr	1000 hr	Comments
Nickel	>6600	-	Completely reacted after 500 hr.
Molybdenum	+20	+11	Uniform but weakly adherent MoS_2 reaction layer.
Niobium	>4500	-	Completely reacted after 500 hr.
Hastelloy B	4100	>3900	General attack with some intergranular penetration left a porous reaction zone and an outer shell of NiS_{1+x}.
Hastelloy C	3000	3300	Similar to Hastelloy B, <10% of the 100-hr sample unreacted.
Fe-6Mo	>22000	-	Extensive reaction throughout entire thickness of sample.
Fe-6Mo-7Ni	>22000	-	External reaction shells consisted of various sulfides.
Fe-6Mo-20Ni	>22000	-	The porous substrates were depleted in iron and mechanically weak. Similar for all alloys in group.
Fe-10Mo-20Ni	>22000	-	
Fe-15Mo-20Ni	>22000	-	
Fe-15Mo-30Ni	11000	11000	Same form of attack as other iron-base alloys but at a lower rate (50% reaction after 500 hr, 90% reaction after 1000 hr). The reaction band has three distinct zones: an outer sulfide shell, a highly porous zone depleted in iron and nickel, and a less porous zone depleted in iron only.

[a]Numerical values preceded by a + sign indicate the formation rate of a reaction layer in µm/yr. Values preceded by > sign indicate the minimum corrosion rate based on the samples initial thickness.

see Fig. 6, the FeS reacted with the alloy to form a mixed molybdenum-iron sulfide surface layer. The iron freed from the FeS by the reaction deposited onto the outside surface of the sulfide layer forming an outer layer; nickel (and chromium in the case of Hastelloy C) diffused through the inner sulfide layer and into this iron layer without being appreciably retained in the sulfide. Armco electromagnet iron and the alloys Fe-6Mo and Fe-6Mo-7Ni, which are all body-centered-cubic structures, underwent extensive intergranular attack. The remaining ternary alloys, which are face-centered-cubic, underwent only shallow, localized intergranular attack, with the exception of Fe-6Mo-20Ni in which internal molybdenum sulfide particles formed.

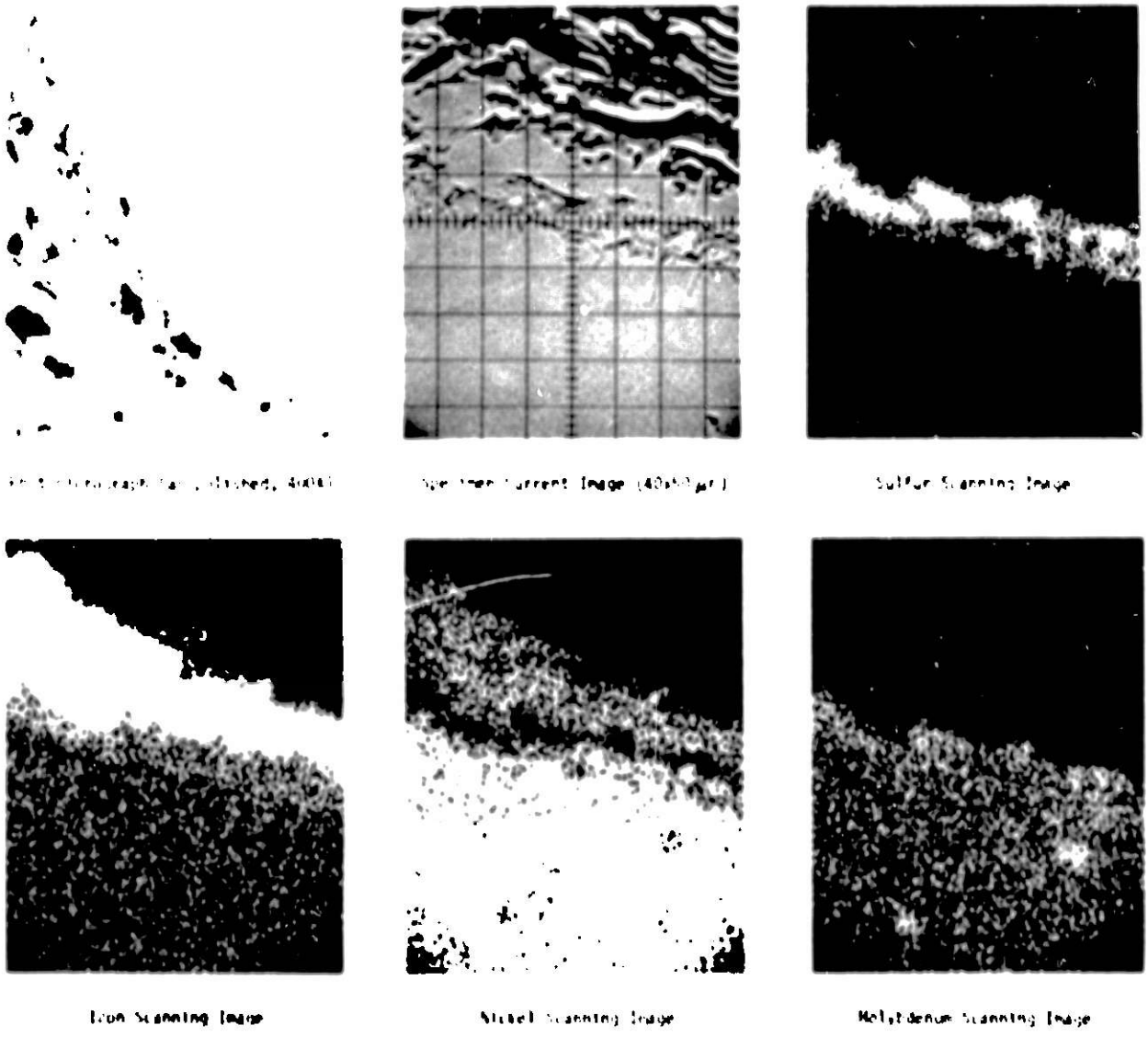

Fig. 6. Photomicrograph and Electron Microprobe Scanning Images of Hastelloy after Reaction with FeS/LiCl-KCl for 1000 hr at 500°C (2000X) (photographically reduced by 30%)

As expected, the corrosion rates of all the materials in the FeS_2/LiCl-KCl mixture at 500°C were much higher than those in FeS/LiCl-KCl. Molybdenum, the only material that showed an acceptably low reaction rate at both exposure times, formed a 5-μm-thick reaction layer of MoS_2 over the surface of the sample. Although the layer was quite uniform, it was not particularly adherent; thus, the role that MoS_2 performs in the corrosion resistance of molybdenum must be questioned. It should be noted that at 400°C in the same corrosive environment, molybdenum exhibits an average corrosion rate of only 2 μm/yr and that the MoS_2 layer is apparently too thin to be detected. At 500°C, all of the other metals and alloys underwent severe attack that was much higher than previously observed at 400°C; for example, the corrosion rates of the two Hastelloys were one to two orders of magnitude higher at 500°C than at 400°C. In general, the morphology of the corrosion-affected zones were similar for the Hastelloys and the iron-base alloys. Two distinctly separable reaction zones were observed. The outer zone consisted of three sulfide layers, and this zone formed at essentially the initial surface of the base metal. The innermost layer consisted of intermingled bands of mixed iron-nickel sulfides and molybdenum sulfide; the middle layer was a band of molybdenum sulfide; and the outer layer contained only mixed iron and nickel sulfides, which were weakly adherent, and presumedly higher in sulfur content than the other layers. The inner zone, which was adjacent to the unreacted base metal, was adherent, porous, and depleted of both iron and nickel. No sulfur was detected in this zone, which is believed to have been formed by the preferential outward diffusion of iron and nickel through the forming sulfide layers.

POSTOPERATIVE EXAMINATION

Postpoerative examinations are conducted on terminated test cells primarily to observe the compatibility of the various materials used in the construction of feedthroughs, current collectors, electrode separators, and cell hardware with the cell environment. In addition, however, the examinations provide important information on the performance and behavior of the electrodes, feedthroughs, and separators. In brief, the examination procedures generally consist of combinations of the following: radiography of the entire cell, sectioning for metallographic analyses and electrical resistance measurements, and preparation of samples for X-ray diffraction and chemical analyses. In some cases, further examinations with the electron and ion microprobes, the scanning electron microscope, and the image analyzing computer are undertaken. No attempt is made to describe the numerous postoperative examinations that have been performed; however, two series of examinations that clearly demonstrate the importance of this experimental technique will be discussed.

Examination of Cells PR-1, R-1, and R-2

Within the past several months, the first cells of the prismatic design, PR-1, R-1, and R-2 were examined. Cell PR-1, which had a hot-pressed FeS positive electrode and an electrochemically prepared negative electrode, was voluntarily terminated after 88 cycles and 1386 hr of operation; Cell R-1, which had an electrode of FeS_2 powder positive and electrochemical negative electrodes, developed an internal short and was terminated after 52 cycles

and 1010 hr of operation. Cell R-2 was similar in construction to R-1 but was assembled in the uncharged state, that is, the positive electrode was hot pressed Li_2S and Fe and the negative electrodes were porous plaques of aluminum fiber wire. This cell was terminated after 143 cycles and 1406 hr of operation because of internal shorting.

The most significant result of the macro examination of the vertical cross sections of all three cells was that no slumping of the vertically oriented electrodes was observed to have occurred. The observation is supported by the results of the sulfur and iron chemical analyses of the positive electrodes, see Table V, which indicate that both the sulfur and iron are distributed rather uniformly from the top to the bottom of the electrodes even after many hours of cell operation. Thus, the major concern that slumping would occur in the electrodes in prismatic design cells does

Table V. Spacial Distribution of Sulfur and Iron in Vertical Positive Electrodes (listed from top to bottom of each electrode)

Cell No.	Sulfur wt %	Iron,[a] wt %	S/Fe Ratio
PR-1	7.60	-	-
	11.55	-	-
	12.48	-	-
	11.33	-	-
	7.85	-	-
R-1	27.9	23.9	2.04
	25.8	22.7	1.98
	17.8	19.2	1.80
R-2	6.67	6.16	1.89
	19.73	17.87	1.92
	19.51	18.78	1.81
	17.89	17.75	1.76
	16.66	17.07	1.71
	15.84	13.98	1.98

[a]No iron analyses were made for Cell PR-1 because it had an iron current collector; Cells R-1 and R-2 had molybdenum current collectors.

not appear to be founded. The examination also revealed that the electrochemically prepared negative electrodes exhibited grossly nonuniform microstructures. Portions of the aluminum wire furthest removed from the positive electrode either had not reacted or had only partially reacted with lithium; lithium was typically more concentrated at the electrode-separator interface. The sizes of the particles at the interface were also smaller than those further away. This observation clearly indicates that most of the electrochemical reaction during cell cycling was occuring at the interfacial region in this type of electrode. It should be noted that, to a much less extent but in direct proportion to the thickness of the electrode, this phenomenon also occurs in pyrometallurgically prepared negative electrodes. Metallographic evidence of a reaction between the aluminum in the negative electrodes and the iron cell housings and current collectors was also found. The reaction product was typically $FeAl_2$ and was more extensive in the cells that were operated at temperatures greater than 450°C. At lower temperatures, the amount of reaction is negligible; but, presumably, longer cell lifetimes would increase the extent of the reaction.

Several maladies that were specific to individual cells were also observed. The large short present in Cell R-1 is clearly discernable in the photomicrograph shown in Fig. 7. Examination of Cell R-2 revealed that some of the active materials from the positive electrode had extruded out of the electrode and into an unintentional void space beneath the electrode, thereby forming an electrical short with the cell housing. The positive electrode of cell PR-1 underwent considerable swelling, probably the result of the formation of the compound $K_{2.8}Li_{0.4}Fe_{12}S_{13}$, identified as J phase at ANL, within the electrode; J phase does not form as readily in the FeS_2-type electrode.

Formation of J Phase

The other examination series to be discussed revealed the morphology of the formation of J phase during the discharge of cells with FeS-type positive electrodes. The photomicrograph in Fig. 8A shows the initial formation of an adherent dense layer of J phase on the surface of an FeS particle. The J phase is a product of a reaction between FeS and the LiCl-KCL electrolyte. With increased discharge, the layer breaks up as seen in Fig. 8B; the reaction at this point is undoubtedly no longer simply diffusion controlled. The irregular shape of the layer leads to an excessive volume expansion, or swelling of the electrode, when compared to the calculated volume increase of the J phase over the original FeS. In Fig. 8C, all of the FeS particles have been consumed; and the next step of the overall discharge reaction, namely the formation of Li_2S and Fe, has begun.

NEGATIVE ELECTRODE DEVELOPMENT

The configuration of the negative electrode of the lithium-aluminum/iron sulfide cell has evolved through a number of discernible designs. Always, a substantial effort has been undertaken to understand the metallurgy of the various electrodes. Examples are the elucidation of the phase relationships of the lithium-aluminum alloy system and the cell testing and postoperative examination of the exploratory, cast electrode plaques.

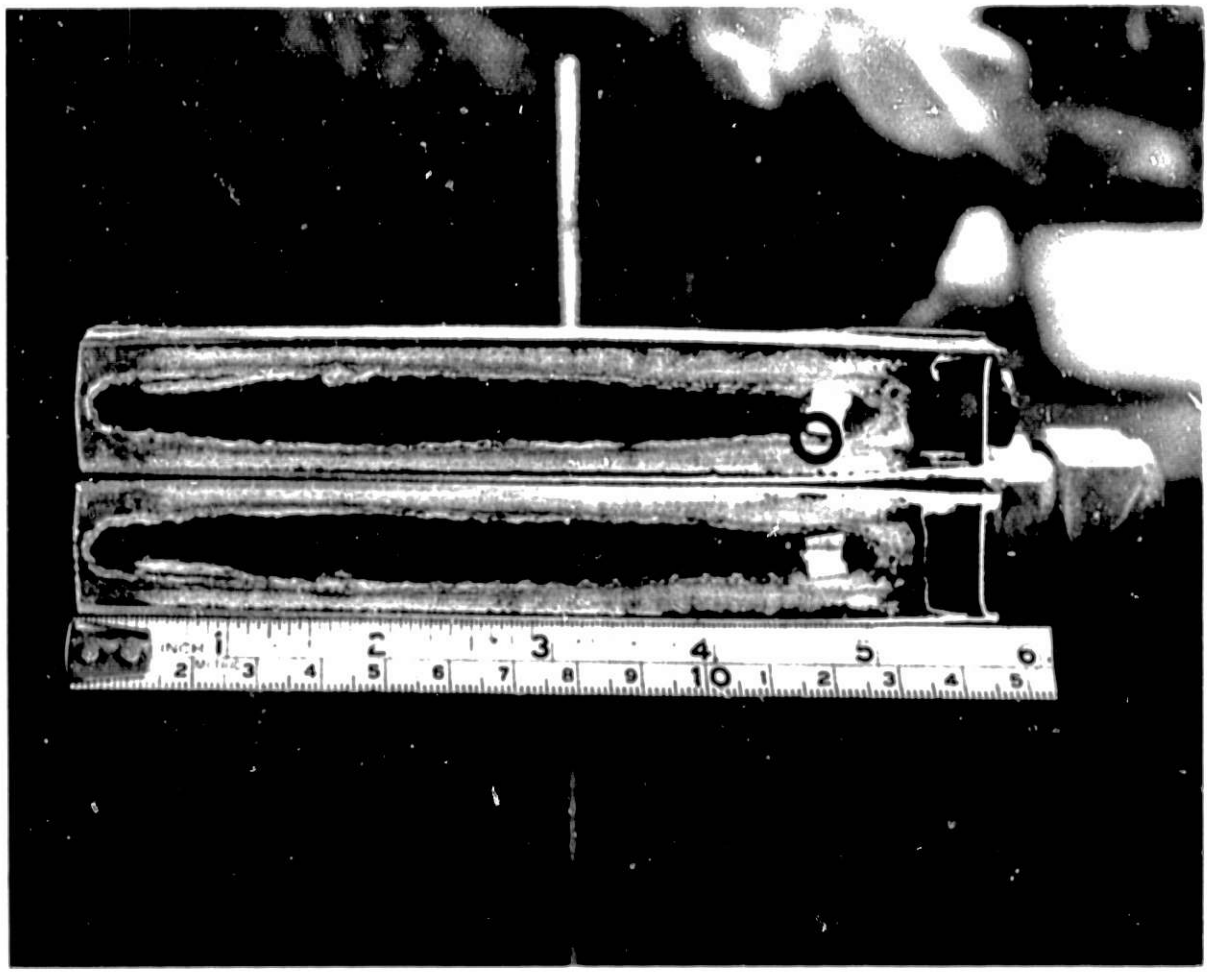

Fig. 7. Cross-section of Prismatic Cell R-1 (the short circuit is delineated by the circle)

Lithium-Aluminum Phase Diagram

The study of the lithium-aluminum phase diagram was undertaken when it became apparent that disparities existed between the accepted published diagram,[1] more recently published data,[2,3] and conclusions drawn from our early in-house efforts to produce lithium-aluminum alloys for electrodes. The alloys for the study were made in a tantalum crucible by dissolving pure aluminum into pure molten lithium at temperatures within 30°C of the liquidus. The alloys were stirred, splat cast, homogenized just below the solidus for about 3 hr, and requenched to room temperature. The three-phase-equilibrium, liquidus, and solidus temperatures were determined for each alloy with a differential thermal analyzer. The data were matched with the chemically analyzed compositions of the alloys and plotted to produce the various loci. The resultant phase diagram, which is shown in Fig. 9, was confirmed by metallographic and X-ray diffraction techniques. The saliently new features of the diagram are the peritectic formation and the polymorphic transition of Li_9Al_4 at 335°C and at 275°C, respectively. Other new details include the

A. Cell 5% Discharged.
Phases: FeS, J, Fe (white)

B. Cell 15% Discharged.
Phases: J, X_{Cu}, FeS, Fe (white);
(X_{Cu} is a modification of X phase in which Cu has been substituted for some Fe;
X = Li_2FeS_2)

C. Cell 35% Discharged.
Phases: J, Li_2S, Fe (white)

Fig. 8. Photomicrographs of J-phase Formation in Partially Discharged FeS Electrodes (as-polished, 500X; all phases determined by X-ray diffraction)

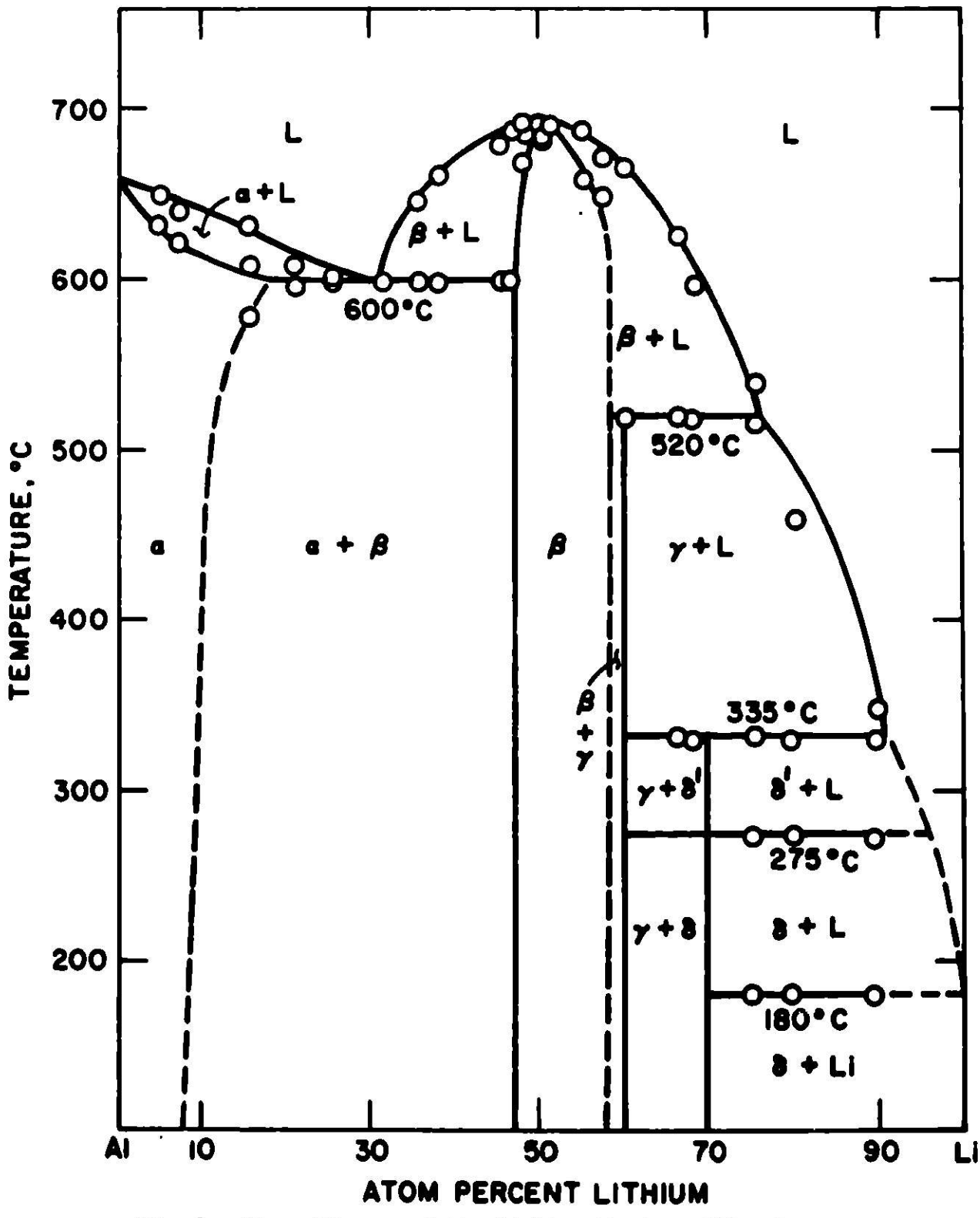

Fig. 9. Phase Diagram of the Lithium-Aluminum Alloy System (α = Al, β = LiAl, γ = Li_3Al_2, $\delta = \delta' = Li_9Al_4$)

location of the solubility limit of α Al into β LiAl at 48 at. % lithium and the confirmation of the formation of Li_3Al_2 rather than Li_2Al, as previously reported.

Future effort in this study will concentrate on establishing the solid solubility limit of β LiAl into α Li, the solubility of Li_3Al_2 into β LiAl, and the high temperature crystal structure of Li_9Al_4.

Solid Lithium-Aluminum Electrodes

The inherent advantage of a solid lithium-aluminum negative electrode over a conventional electrochemically or pyrometallurgically prepared electrode is the ease-in-handling of the electrode during fabrication of the cell. This is possible because the likelihood of internal oxidation and nitridation is tremendously decreased due to the elimination of the very large internal surface areas. To help ascertain the feasibility of the use of such electrodes in the lithium-aluminum/iron sulfide cell, several small electrodes were produced. The electrodes were first prepared by the direct casting of the lithium-aluminum alloy into molds of the desired shape; a plate was placed on the surface of the molten alloy to insure a flat surface after solidification. After in-cell testing, the postoperative examination revealed that the porosity of the electrode had been too small to permit adequate filling by the electrolyte and, as a result, most of the cell reaction had occurred at the electrode-separator interface. Nevertheless, the results were sufficiently encouraging that the electrode was redesigned to incorporate a metal current collector. In this concept, sheets of a low-bulk-density, reticulated, cellular structure of nickel were immersed into and quickly removed, within 15 sec, from a bath of the molten alloy held near 700°C. Presumedly, because the nickel had been wet and because the solidification of the alloy had been so rapid the pores of the nickel sheet were almost completely filled, again creating an electrode without sufficient porosity. The postoperative examination revealed that the regions in these electrodes furthest from the positive electrode also were relatively unreacted, and that the regions nearest the positive electrode were well broken up and had a uniformly dispersed microstructure similar to that found in a well cycled, conventionally prepared electrode. It was also observed that the nickel and aluminum had reacted to form the intermetallic compounds $NiAl_3$ and Ni_2Al_3. Nevertheless, because a solid negative electrode offers such promising advantages, development work on this type electrode is continuing.

POSITIVE-ELECTRODE CURRENT COLLECTOR DEVELOPMENT

One of the more perplexing materials problems has been the development of a current collector for the FeS_2-type positive electrode. Molybdenum thus far has proved to be the only conductive construction material that withstands the highly corrosive environment of the electrode.* The

*A variety of coating materials, including TiN and TaC, have been tried; but, unfortunately, none sufficiently protected the underlying metal substrate to warrant the large development effort that would probably be required to overcome this deficiency.

disadvantage of molybdenum, aside from the relatively high cost of the fabricated metal, is the impossibility of producing ductile welds. The reason for this is that during the weld-fusion process the semiductile fibrous grain structure of the molybdenum part is recrystallized into a brittle equiaxial structure. It is believed that impurities within the grain boundaries are responsible for the detrimental response to recrystallization, but the particular elements involved have not been unequivocally identified. Metallurgical bonds, such as those produced by welding, within the current collector structure are essential to maintain low electrical IR losses in the current collector assembly. Two solutions to the problem will be presented that typify the effort that so far has been undertaken.

In the first, an attempt is made to physically displace the brittle heat-affected zone of the weld away from the regions of high mechanical stress that occur during the assembly and operation of the cell. An example of this type design is shown in Fig. 10, where the molybdenum collector sheet has been pressed into a door-hinge configuration. The conductor, or hinge pin, is then forced through the hinge, creating a very tight and strong mechanical connection. Additional strength is achieved by hot-riveting the collector and conductor together. A metallurgical bond is subsequently added by either spot-welding or stitch, electron-beam welding along the length of the conductor through the collector.

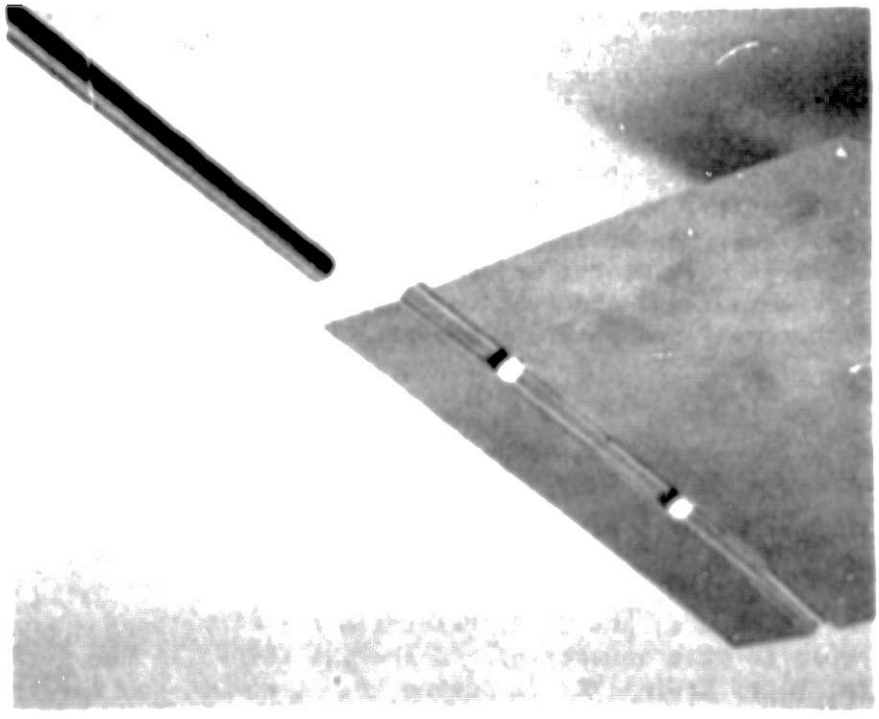

Fig. 10. Molybdenum Current Collector-Conductor Assembly

The second solution involves the use of brazes that have been carefully selected for compatibility with the cell environment. Since no existing braze would be expected to be compatible with the active materials of the FeS_2 electrode, the braze joint is removed from the electrode proper and possibly even from the electrolyte. Furthermore, only brazes with flow temperatures below the recrystallization temperature of molybdenum, which is between 1100 and 1200°C are considered. The alloy currently being evaluated has the composition Ag-7.3Cu-0.2Li. The alloy was selected because silver is not oxidized upon cell charging, forms only a weakly stable sulfide, has an electromotive force in LiCl-KCl sufficiently close to that of molybdenum so as to preclude the onset of galvanic corrosion, and flows well below the recrystallization temperature of molybdenum. Concern exists that the problems associated with "silver migration,"[4] experienced throughout the electronics industry, and high sulfureting rates might be detrimental to the life of the brazed joint. Alternative brazes include gold and Hastelloy B.

SUMMARY

The electrochemical coupling of lithium and sulfur results in a high-performance battery primarily because of the mutually high chemical affinity of the elements. Unfortunately, lithium and sulfur are also highly reactive with most of the other elements; and, thus, serious problems are encountered in developing materials for use as cell housings, current collectors, separators, feedthroughs, etc. The search for solutions is often complicated by the need to minimize the overall cost of the battery, thus restricting the selection to the more basic construction materials. Often solutions that seem to be technically logical cannot be utilized simply because the materials are not commercially available, and the development of the required commercial sources is unpredictable and costly. This paper presents a summary of the effort being expended at ANL to cope with these serious materials problems. An attempt is made to provide an insight into the level of involvement in each of the major current areas of activity rather than to mention every detail and observation. Additional information can be found in the publications[5] and periodic reports[6-8] of the materials development program.

ACKNOWLEDGMENTS

The authors wish to acknowledge the administrative support of L. Burris, D. S. Webster, P. A. Nelson, and R. O. Ivins. We are indebted to our co-workers, J. E. Battles, W. D. Tuohig, T. W. Olszanski, Z. Tomczuk, E. Chaney, W. E. Miller, N. Koura, and C. A. Melendres for contributing portions of their own work to this manuscript. A special thanks is due B. S. Tani, C. A. Seils, D. V. Steidl, K. J. Jensen, D. J. Rokop, and J. P. Faris who ran the X-ray, electron and ion microprobe, and chemical analyses. Finally, we express our appreciation to G. M. Kesser for editorial assistance.

REFERENCES

1. M. Hansen and K. Anderko, *Constitution of Binary Alloys*, p. 104, McGraw-Hill Book Co., New York (1958).

2. D. A. Hansen and J. F. Smith, Acta Cryst. *B24*, 913 (1968).

3. K. F. Tebbe, H. G. von Schnering, B. Rüter, and G. Rabeneck, Z. Naturforsch. *28B*, 600 (1973).

4. W. H. Kohl, *Handbook of Materials and Techniques for Vacuum Devices*, p. 232, Reinhold Publishing Co., New York (1967).

5. J. E. Battles, F. C. Mrazek, W. D. Tuohig, and K. M. Myles, "Materials Corrosion in Molten-Salt Lithium/Sulfur Cell," *Corrosion Problems in Energy Conversion and Generation*, pp. 20-31, C. S. Tedmon, Jr. (ed), The Electrochemical Society (1974).

6. P. A. Nelson *et al.*, *High-Performance Batteries for Off-Peak Energy Storage and Electric-Vehicle Propulsion*: Progress Report for the Period July-December 1975, ANL-76-9, Argonne National Laboratory (in preparation), Progress Report for the Period January-June 1975, ANL-75-36 (in press); Progress Report for the Period July-December 1974, ANL-75-1 (1975); Progress Report for the Period January-June 1974, ANL-8109 (1974).

7. P. A. Nelson *et al.*, *High-Performance Batteries for Off-Peak Energy Storage*: Progress Report for Period July-December 1973, ANL-8057, Argonne National Laboratory (1974); Progress Report for the Period January-June 1973, ANL-8038, (1974).

8. P. A. Nelson *et al.*, *Development of High-Specific-Energy Batteries for Electric Vehicles*: Progress Report for the Period August 1973-January 1974, ANL-8058, Argonne National Laboratory (1974); Progress Report for the Period February 1973-July 1973, ANL-8039 (1973). Also, E. J. Cairns *et al.*, Progress Report for the Period August 1972-January 1973, ANL-7998, (1973); Progress Report for the Period February 1972-July 1972, ANL-7953 (1972).

THE WETTABILITY OF HIGH-TEMPERATURE CELL SEPARATORS BY MOLTEN SALT

J. G. Eberhart

Argonne National Laboratory
9700 South Cass Avenue
Argonne, Illinois 60439

ABSTRACT

In lithium-aluminum/iron sulfide cells, the ceramic separator and particle retainer materials must be wet and penetrated by the molten LiCl-KCl electrolyte so that lithium ions can easily pass through these porous materials during discharge and charge. Measurements have been made of the wettability of solid surfaces of these materials. Molten-salt contact angles were observed to be nonwetting while advancing and wetting while receding. The hysteresis is quite large. Determinations have also been made of the molten salt penetrability of various fabrics and papers composed of these materials. These studies have suggested procedures which assure salt penetration and permeation through the materials that are difficult to wet.

INTRODUCTION

Wettability is an important factor in obtaining optimum performance and longevity from high-temperature cells. For example, the cell electrolyte must wet and penetrate the porous separator and particle retainer materials to permit easy passage of ions through the pores of these materials during discharge and charge. If either electrode material is a liquid, which must be held in a porous solid current collector, then the porous solid should be wet by the liquid in the environment in which the solid structure is first filled. Also, this same porous solid should be wettable by the liquid electrode material in the presence of the electrolyte. If the electrode material does not wet the solid preferentially over the electrolyte, the electrolyte will displace the electrode material. Finally, at the cell container or the electrical feedthrough surfaces it is desirable to have nonwetting by the electrolyte. This will prevent the creeping of thin liquid films of electrolyte along these surfaces with subsequent loss of electrolyte or electrical shorting.

This paper reports a study of the wettability and penetrability of various materials used as separators or particle retainers by molten LiCl-KCl, the electrolyte used in the Argonne lithium-aluminum/iron sulfide cells.[1,2] Molten salt wetting and penetration are important for these ceramic materials so that lithium ions can easily pass through the pores of these materials. The separators investigated were boron nitride fabric and paper, while the particle retainers studies were zirconia and carbon fabrics. Contact-angle measurements were made on solid surfaces of ceramic materials. Penetration tests were also performed with fabrics and papers made from fibers of these same ceramics. These studies have yielded procedures for assuring penetration of fabrics that are difficult to wet by the molten salt.

THEORY

The wettability of a solid surface is defined in terms of the contact angle, θ, of the liquid, which is shown for the sessile drop pictured in Fig. 1. If $\theta > 90°$, the liquid is said to be nonwetting on that solid; if $\theta < 90°$, it is wetting. If $\theta = 0$, then the liquid spreads on the solid.

If the solid surface is idealized as flat, smooth, uniform, isotropic, and nondeformable, then there is only one stable, equilibrium contact angle, which is given by Young's equation[3,4]

$$\gamma_{LV} \cos \theta = \gamma_{SV} - \gamma_{SL}$$

where γ_{LV}, γ_{SV}, and γ_{SL} are the interfacial tensions at the liquid-vapor, solid-vapor, and solid-liquid interfaces, respectively.

The surfaces of interest in high-temperature batteries are those of: theoretically dense rough solids, porous solids, powders, fabrics, papers, and screens. These surfaces are rough, heterogeneous, anisotropic, and deformable. Systems with these more realistic solid surfaces show a range of possible contact angles for a given liquid, because they possess a range of closely-spaced, metastable states.[5,6] In these systems the macroscopic contact angle, θ_M, may be different from that given by Young's equation, but the intrinsic or local contact angle, θ, which is measured relative to the local solid surface contour, does obey Young's equation. The largest and the smallest contact angles are relatively reproducible and are called the advancing contact angle, θ_A, and the receding contact angle, θ_R. These angles can be produced by increasing or decreasing the volume of a sessile drop. The difference between these two angles, $\theta_A - \theta_R$, is called the contact angle hysteresis. The magnitude of this difference is a measure of the physical roughness and/or chemical heterogeneity of the surface.

The penetration behavior of a fabric structure by a liquid is governed by the advancing and receding contact angles. If $\theta_A < 90°$ and $\theta_R < 90°$, then the fabric is *easy to wet* and the liquid will spontaneously penetrate the fabric,[7] filling the larger holes and notches between the yarns and the smaller spaces between the fibers which make up a yarn. If only one part of this fabric is contacted with the liquid, then the liquid will wick (laterally)

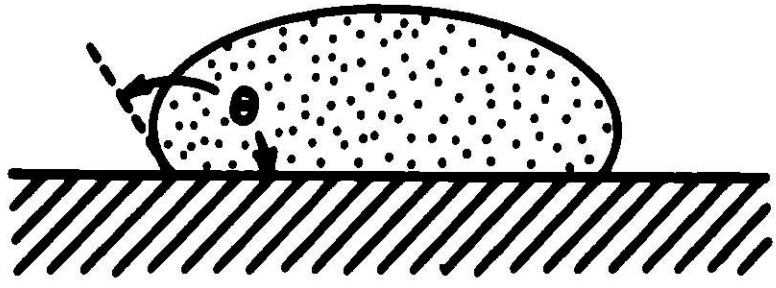

Fig. 1. Sessile Liquid Drop on a Solid Surface, Showing the Contact Angle, θ.

to other regions of the fabric. If $\theta_A > 90°$ and $\theta_R < 90°$, the fabric is *difficult to wet* and it will not be penetrated spontaneously by the liquid. However, if the liquid is forced into the fabric, *e.g.*, with a hydrostatic pressure, it will stay in place or move only slightly. If $\theta_A > 90°$ and $\theta_R > 90°$, then the fabric is *impossible to wet*, *i.e.*, it is completely repellent to the liquid. If the liquid is forced into the fabric, it will move out spontaneously when the force is removed.

It should also be possible, in principle, to specify whether a liquid will penetrate a fabric in terms of the cloth geometry and the intrinsic contact angle, θ, of the liquid on one of the fibers. Because of the geometric complexity of a fabric structure, this problem is as yet unsolved.

WETTABILITY OF SOLID SURFACES

Because the fabrics of major interest were zirconia, carbon, and boron nitride, contact angle measurements were first made on solid plaques of these ceramics to provide approximate comparisons of their wettability. The molten salt used to make the contact angle determinations was the LiCl-KCl eutectic (melting point of 352°C), which was obtained from the Anderson Physics Laboratory, Champaign, Illinois. The wettability determinations were made in a helium-atmosphere glovebox which contained a horizontal tube furnace. The outline of the molten-salt sessile drop was observed with a telescope that was mounted outside the glove box window. The droplet was back-lighted with a microscope illuminator. The contact angle was measured using the telescope crosshairs and a goniometer which was attached to the telescope body.

The procedure used to obtain advancing and receding drops of molten salt on the solid ceramic surface is shown in Fig. 2. A tall chunk of salt was placed on a substrate located in the horizontal tube furnace, Fig. 2a. The temperature, which was monitored continually with a chromel-alumel thermocouple, was 375°C in the neighborhood of the substrate. As the salt began to melt, Fig. 2b, it slumped downward and advanced over regions of the solid surface which had never before contacted the salt. The final configuration of the advancing salt drop is shown in Fig. 2c. The advancing contact angle, θ_A, was determined from this drop. (When additional small chunks of salt were added to this drop, it advanced further and the contact angle remainded the same.) To obtain the receding drop configuration, a cold nickel rod was repeatedly touched to drop, as shown in Fig. 2d. The salt wet the nickel and condensed on it, permitting the easy removal of a small portion of the drop volume. As this process was repeated the contact angle decreased and eventually reached a constant value, which was the receding contact angle, θ_R, shown in Fig. 2e. Further salt removal decreased the circular area of contact between the molten salt and the ceramic surface, but did not change the contact angle.

The molten salt contact angles on solid surfaces of zirconia, glassy carbon, and boron nitride are shown in Table I. For all of the surfaces, $\theta_A > 90°$, while $\theta_R < 90°$. Although these solid surfaces are somewhat rough and porous, the corresponding fabric surface is expected to have even greater roughness and porosity. Thus, if macroscopic contact angles were determined on fabrics of the same chemical constitution as the materials

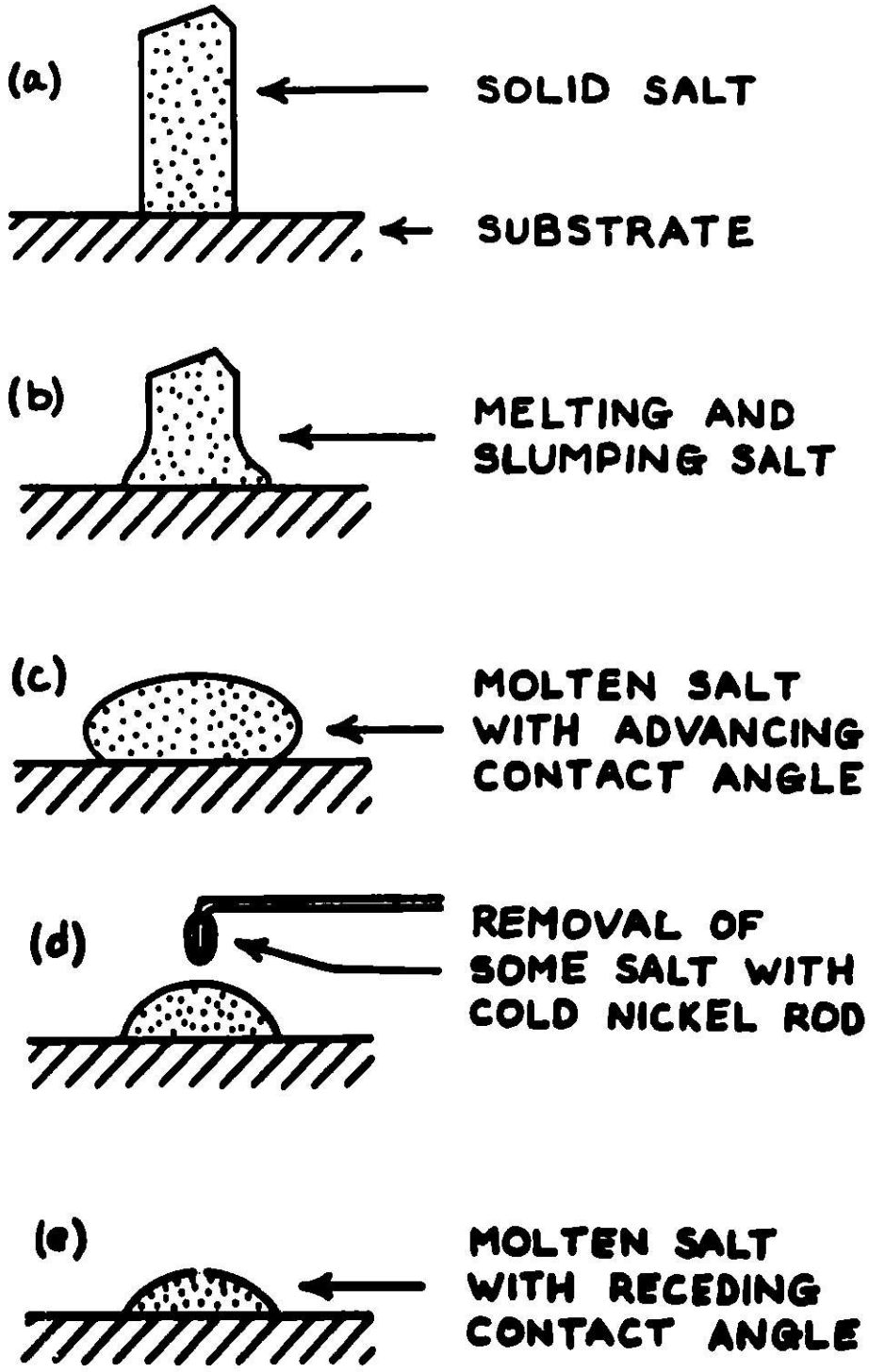

Fig. 2. Experimental Sequence for Producing Advancing and Receding Molten Salt Droplets.

Table I. Contact Angles of Molten LiCl-KCl on Solid Ceramic Surfaces

Solid Surface	Contact Angles	
	Advancing	Receding
zirconia	105°	45°
glassy carbon	117°	55°
boron nitride	138°	54°

described above, the fabrics would probably show an even larger hysteresis. Based on these contact angle measurements it is also expected that: some of the fabrics will be in the difficult-to-wet class, zirconia cloth will be the easiest of the three to penetrate with molten salt, carbon the next easiest, and boron nitride the most difficult. These predictions are borne out in the penetration studies described next.

PENETRABILITY OF FABRICS AND PAPERS

Penetration tests were performed on zirconia,* carbon,** and boron nitride† fabrics and on boron nitride papers.†† The stronger fabrics were studied with the apparatus shown in Fig. 3. Here the fabric was attached to the lower end of a vertical, boron nitride tube in drumhead fashion. A vertical rod was fastened to the fabric-and-tube assembly so that the assembly could be lowered into a crucible containing molten salt. The assembly and the salt crucible were located in a furnace well in the bottom of the helium-atmosphere glovebox and maintained at 400°C during the tests. The upper end of the vertical rod passed through a quick connect vacuum coupling which was mounted in the center of a Lucite furnace well cover. The furnace well could either be evacuated (to a minimum pressure of 5×10^{-3} Torr) or pressurized with glove box helium (to a maximum of 1 atm). When the assembly was lowered into the molten salt, the inside of the boron nitride tube could be easily observed from above through the transparent furnace well lid. A microscope illuminator was used to aid observation. The fabric was always lowered about 1 inch below the molten salt meniscus to provide a constant hydrostatic head in the

*Type ZYW-30A, satin-weave, yttria-stabilized zirconia fabric, from Zircar Products, Inc., Florida, New York.

**No. CCA-1 (1641), type G1550, satin-weave, high-purity carbon fabric, from Hitco Materials Div., Gardena, California.

†Twill-weave, 30-mil-diameter, 2-ply-yarn boron nitride fabric, from Carborundum Co., Niagara Falls, New York.

††Type C-715-95 boron nitride paper, from Carborundum Co., Niagara Falls, New York.

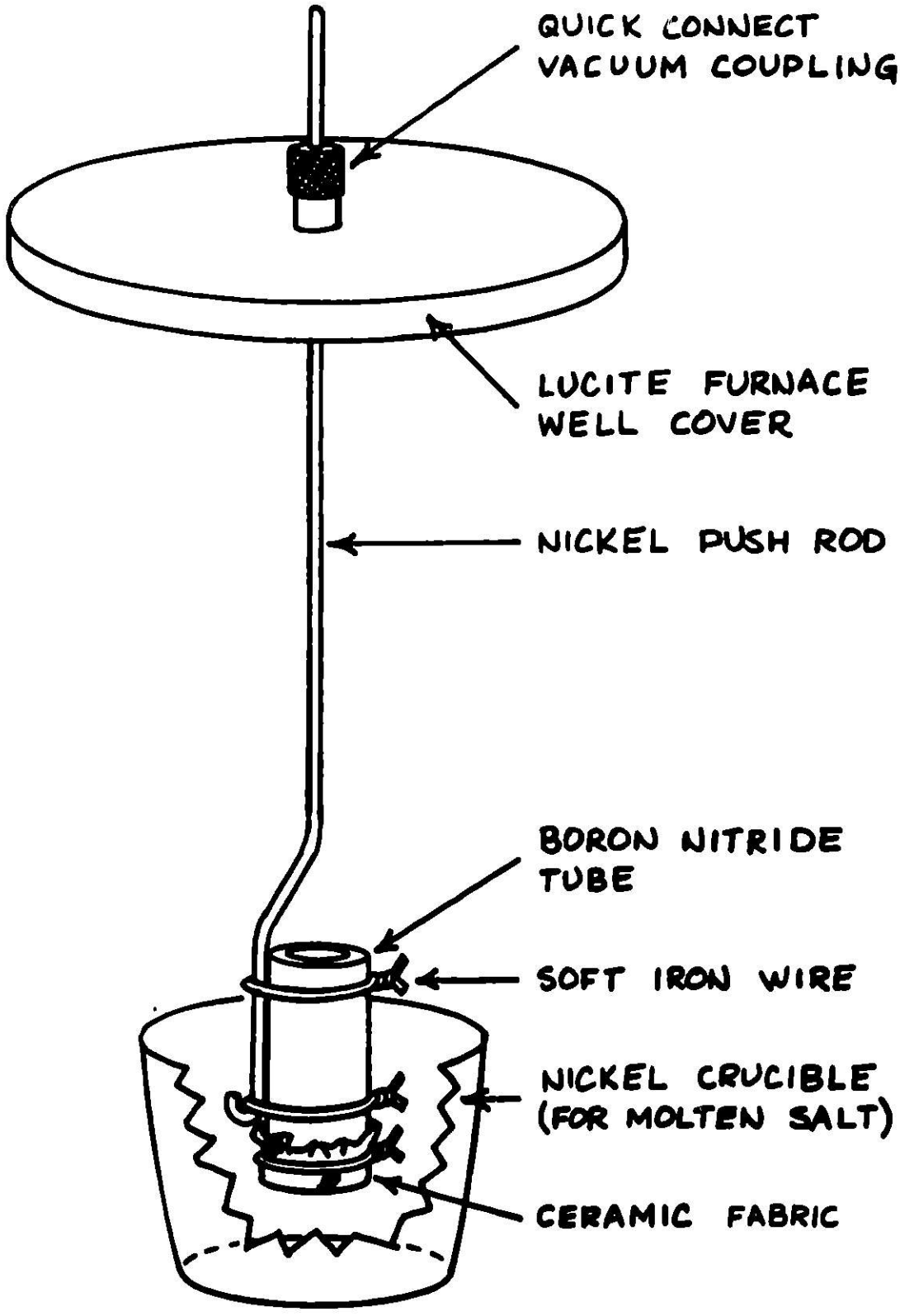

Fig. 3. Apparatus for Determining the Penetrability of Ceramic Fabrics by Molten Salt.

direction that favored penetration of salt from the outside of the assembly to the inside.

Because some of the fabrics and all of the papers were too fragile to be tied around the end of the boron nitride tube, a second appartus, which is shown in Fig. 4, was constructed for these materials. It differs from the first only in the nature of the boron nitride assembly, which snugly holds a disk of fabric or paper. As with the first apparatus, a hydrostatic head of 1 inch of molten salt was used.

Two of the three possible types of penetration behavior were observed in tests with the various fabrics and papers. The easy-to-wet behavior was observed only with zirconia fabric. This behavior is illustrated in Fig. 5. The dry fabric-and-tube assembly was initially suspended above the the molten salt in a helium atmosphere, Fig. 5a. The assembly was then immersed in the molten salt, Fig. 5b, which penetrated the zirconia fabric within several seconds to a minute. The salt level rose inside the tube and dropped outside the tube until the two levels were equal, Fig. 5c. When the assembly was lifted upward the salt easily drained through the fabric and back into the crucible, Fig. 5d, again within a minute. The entire procedure was carried out in a helium atmosphere. After the test, when the zirconia cloth was removed from the boron nitride tube, the entire cloth had become rigid as a result of solidification of the permeated salt. The salt had also wicked from the circular region that it had passed through to the entire cloth.

The difficult-to-wet behavior was observed in tests of carbon and boron nitride fabrics and boron nitride paper, and is illustrated in Fig. 6. Again the test was begun with the dry assembly suspended above the molten salt in a helium atmosphere, Fig. 6a. The assembly was then immersed in the molten salt, Fig. 6b. None of these difficult-to-wet fabrics or papers would permit the passage of molten salt in this configuration. This was observed even when the assembly was kept in this configuration for times as long as 10 days. Two conditions were found necessary to cause molten salt penetration of these difficult-to-wet fabrics and papers. First a chunk of salt was placed inside the assembly while the assembly was not in contact with the molten salt in the crucible. The salt chunk then melted, producing a layer of molten salt on the "upper surface" of the fabric or paper, Fig. 6c. The assembly was then lowered into the crucible, Fig. 6d, so that molten salt was now in contact with both the upper and the lower surfaces. The system was next evacuated to a pressure of about 10^{-2} Torr and then repressurized to 1 atm of helium. During the repressurization step the molten salt penetrated the separator or particle retainer, and the salt level inside the tube rose to the level outside, Fig. 6e. Once this penetration had been accomplished, the salt would pass easily through the material, such as when the assembly was raised and drained, Fig. 6f. Both of the key operations of (1) molten salt contact with both surfaces, and (2) evacuation and repressurization, are required. Neither operation by itself will produce penetration. Upon removal of a boron nitride or carbon fabric from the tube only the circular region of the fabric that originally had molten salt in contact with both surfaces was rigid from salt penetration. The remainder of the fabric was still dry and flexible. Thus, no lateral salt wicking had occurred to fabric outside this circular region. It is thought that repressurizing the evacuated system provides a force or push perpendicular to

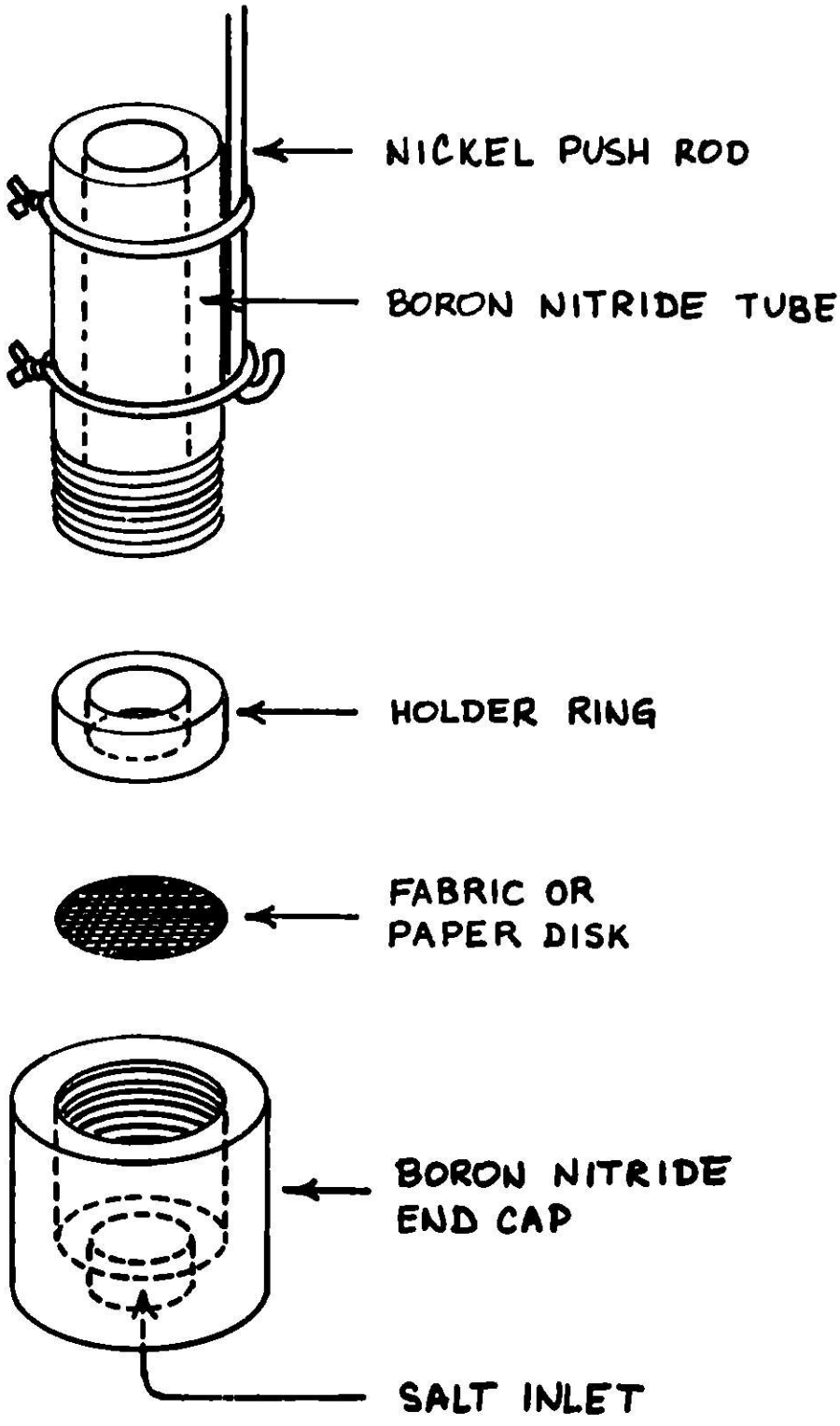

Fig. 4. Apparatus for Determing the Penetrability of Ceramic Fabrics or Papers by Molten Salt.

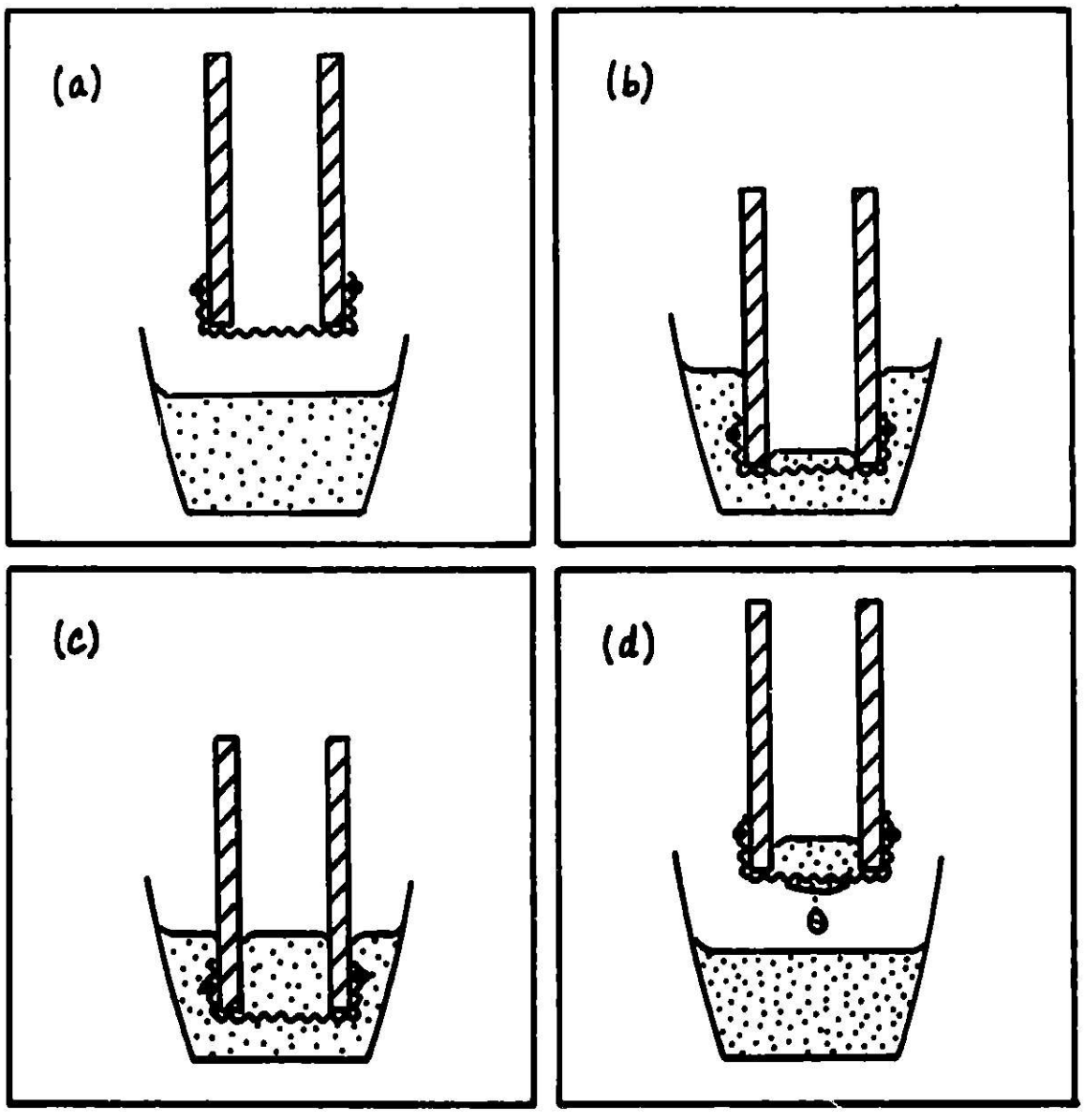

Fig. 5. Experimental Observations of the Penetration of Easy-to-Wet Fabric.

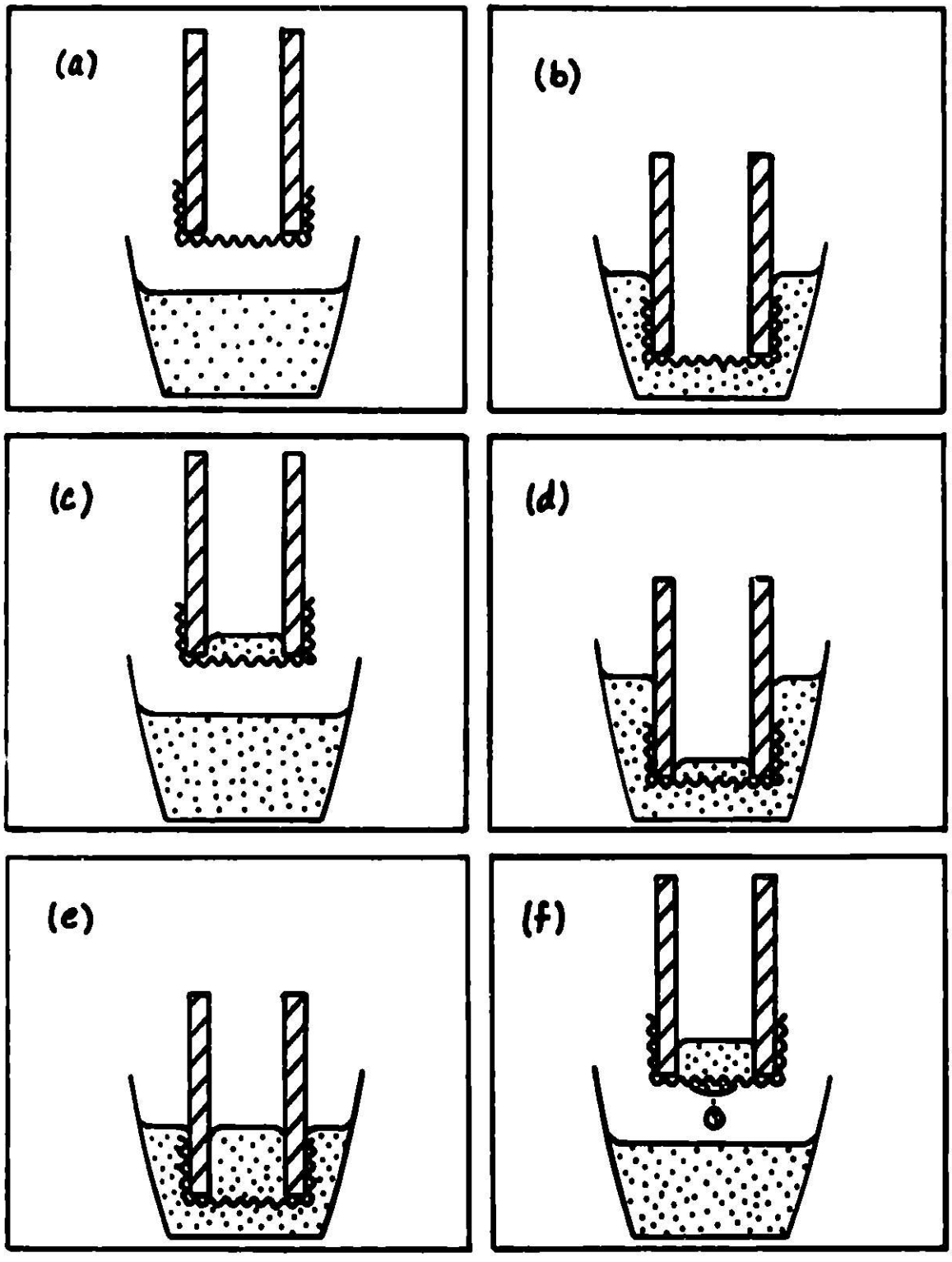

Fig. 6. Experimental Observations of the Penetration of Difficult-to-Wet Fabrics or Papers.

the fabric and produces wetting and penetration in the region of cloth which contacts salt at both surfaces. However, the procedure provides no force parallel to the fabric and thus does not promote lateral wicking.

No fabrics or papers have been found so far which exhibit impossible-to-wet behavior or molten salt repellency.

CONCLUSIONS

Molten salt wetting and penetration tests were performed on solids, fabrics, and papers made of materials used in separators or particle retainers in the Argonne lithium-aluminum/iron sulfide cells. Zirconia surfaces were found to be the most wettable and displayed a large contact-angle hysteresis. Zirconia fabric was easy to penetrate. Carbon and boron nitride surfaces were less wettable than zirconia and also displayed a large hysteresis. Carbon fabric and boron nitride fabric and paper were difficult to penetrate. However, these materials could be penetrated when the system was evacuated and repressurized while molten salt was in contact with both surfaces.

ACKNOWLEDGEMENTS

I wish to express my appreciation to R. K. Steunenberg, Z. Tomczuk, and C. M. Kasser of Argonne National Laboratory for helpful discussions during the course of this study and for their editorial suggestions on this manuscript.

This work was supported by the U.S. Energy Research and Development Administration.

REFERENCES

1. D. R. Vissers, Z. Tomczuk, and R. K. Steunenberg, J. Electrochem. Soc., *121*, 665 (1974).

2. W. J. Walsh, A. A. Chilenskas, E. J. Cairns, and P. A. Nelson, U.S. Patent No. 3,887,396 (1975).

3. T. Young, Phil. Trans. Roy. Soc., *95*, 65 (1805).

4. J. Willard Gibbs, "The Collected Works of J. Willard Gibbs," Vol. 1, "Thermodynamics," Yale University Press, New Haven, 1928, p. 326.

5. R. E. Johnson, Jr. and R. H. Dettre, "Wettability and Contact Angles," Vol. 2. "Surface and Colloid Science," ed., E. Matijevic, Wiley-Interscience, 1969, pp. 85-153.

6. A. W. Neumann and R. J. Good, J. Colloid Interface Sci., *38*, 341 (1972).

7. A. M. Schwartz, Ind. Eng. Chem., *61*, 10 (1968).

ELECTROCHEMICAL STUDIES OF MASS TRANSPORT IN HIGH TEMPERATURE ELECTROLYTES*

J. Braunstein
Chemistry Division
Oak Ridge National Laboratory
Oak Ridge, Tennessee 37830, USA

and

C. E. Vallet
Laboratoire de Thermodynamique des Sels Fondus
Universite de Provence
13397 Marseille, France

ABSTRACT

Since electrode kinetics are rapid for proposed high temperature batteries, and since the electrolytes are frequently complex or polymeric, mass transfer polarization becomes a limiting factor in recharge rates. Transport parameters needed for design and modeling studies include interdiffusion coefficients and transference numbers. Methods such as chronopotentiometry have been applied almost exclusively to self-diffusion coefficients of dilute constituents. We have developed the chronopotentiometric method to provide interdiffusion coefficients over broad ranges of concentration, and will illustrate the application in two kinds of melts: alkali fluoride-beryllium fluoride melts having a polymeric structure, and alkali chloride-aluminum chloride melts having a complex structure.

INTRODUCTION

A number of proposed high temperature battery systems employ electrolytes which are complex or polymeric, or in which complex or polymeric species are formed. In such systems appreciable changes of mass transport properties occur during charge or discharge. With increasing temperature, electrode kinetics become more rapid, and activation polarization is small for a number of high temperature electrodes. Mass transfer polarization is a significant factor in the rate of charge and discharge of high temperature batteries. Consequently, reliable values of transport parameters are needed for design and modeling studies. Among the needed transport coefficients are the interdiffusion coefficients, which may undergo considerable changes of magnitude

*Research sponsored by the Energy Research and Development Administration under contract with Union Carbide Corporation.

with electrolyte composition change, and which are difficult to determine in electrolytes at high temperatures, particularly in viscous melts. The classical methods for determination of diffusion coefficients in liquids, such as the capillary, diaphragm and NMR spin-echo measurements, are difficult to apply at elevated temperatures and in viscous systems. While pulsed spin-echo measurements may extend the applicability of the NMR method, this method requires nuclei of appropriate spin and, in any case, leads to self-diffusion coefficients rather than interdiffusion coefficients. Electrochemical scanning methods such as polarography, chronopotentiometry and linear sweep voltammetry have been employed frequently to obtain diffusion coefficients in electrolytes, both at room temperature and at elevated temperatures. With few exceptions, however, these methods are employed with low concentrations of solute ions under conditions such that electrical migration of the electroactive species is suppressed, thus providing only the limiting interdiffusion coefficient at vanishing solute concentration, which is the solute self-diffusion coefficient.

We have shown[1,2] that the restriction to dilute solute ions is not necessary, and we have employed anodic chronopotentiometry with beryllium electrodes in molten beryllium fluoride - lithium fluoride mixtures containing between 5 and 22 mole percent lithium fluoride. Equations have been developed, with the thermodynamics of irreversible processes, to identify the interdiffusion coefficient in this binary system under conditions of simultaneous diffusion and electrical migration. Computations have been developed to obtain mean values of interdiffusion coefficients and to resolve the composition dependent interdiffusion coefficients. The method, with suitable modification for specific systems, should be useful for other high temperature electrolytes, solid and liquid, including many of importance in battery systems.

We have used the term electromigrational depletion (ED) chronopotentiometry to describe the application of chronopotentiometry to binary melts such as $LiF-BeF_2$ since the anodic chronopotentiometric transition time with an electrode such as beryllium could be attributed to depletion of Li^+ from the anode region via migration, rather than to depletion of an electroactive constituent via the faradaic process, which is responsible for the transition in ordinary chronopotentiometry. We have shown the transference number of Be^{2+} relative to fluoride ions to be zero (and consequently that of Li^+ to be unity) over the composition range between 20 and 80 mole percent BeF_2 [3]. Our previous measurements have been mainly at higher BeF_2 concentrations, where it was presumed that the transference number remained constant and equal to unity. However, it could not be ascertained that the apparent composition dependence of the diffusion coefficients did not include also some concentration dependence of transference numbers. In this paper we present the results of chronopotentiometric measurements in $LiF-BeF_2$ melts of composition 53, 65 and 70 mole percent BeF_2, for which the transference number of Li^+ is known to be constant and equal to unity; these measurements therefore constitute a valid application of ED chronopotentiometry. We show that, although the chronopotentiograms reflect the variation of the interdiffusion coefficient with concentration from the bulk composition to pure BeF_2, analysis of the early portions of the chronopotentiograms, corresponding to melts of compositions close to the bulk composition, yields the interdiffusion

coefficient in the bulk melt. In addition to this application of chronopotentiometry to the polymeric melt, BeF_2-LiF, we discuss its application to the complex melt NaCl-$AlCl_3$.

EXPERIMENTAL

The cells, electrodes, purification of materials and the experimental procedure have been described previously [1]. Chronopotentiograms in the 70 m% BeF_2, 65 m% BeF_2 and 53 m% BeF_2 LiF-BeF_2 melts were recorded with a Hewlett-Packard 141A storage oscilloscope and photographed with a Polaroid camera, rather than recorded on a chart recorder. In these mixtures all of the chronopotentiograms were shorter than 10 seconds and some were shorter than 1 second. In order to avoid convection, faster chronopotentiograms were required than in our previous measurements in the more viscous BeF_2-rich melts.

Figure 1 shows a typical chronopotentiogram, obtained in 53 mole percent BeF_2 at 380°C. The initial increase of potential is very fast and has been shown [1,2] to correspond to the IR drop for melt of the bulk composition. Because the electrode configuration was not designed to provide a suitable conductance cell, the measurements provide only a relative electrical conductance. However, as shown previously [2], the temperature dependence of the relative conductance, I/(IR), leads to activation energies for conductance consistent with those obtained from directly measured electrical conductance in these melts [4].

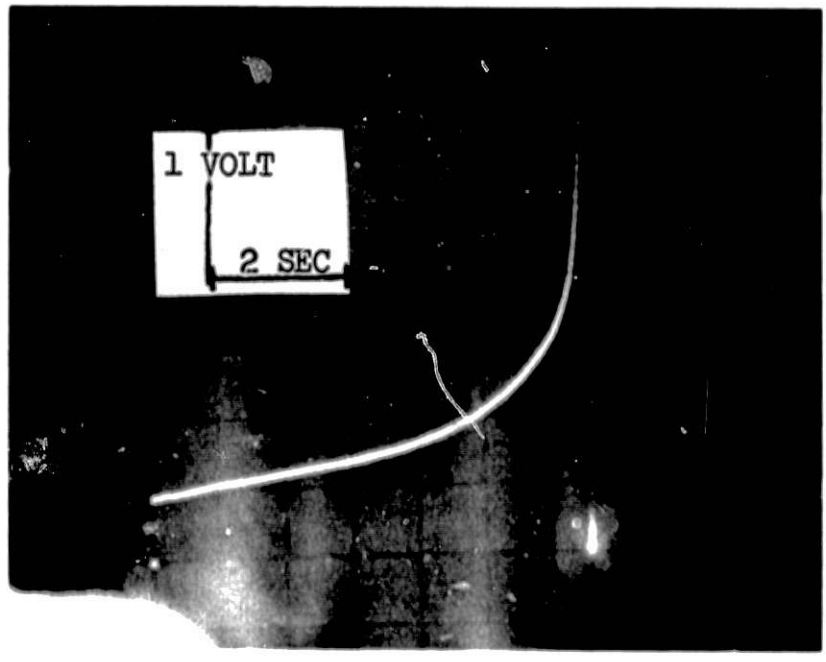

Figure 1. Typical chronopotentiogram, in 53 mole percent BeF_2 melt at 380°C with current density of 1.26 A/cm^2. EMF at working electrode versus time.

The final portion of the chronopotentiogram appears to rise sharply. As will be seen from the discussion to follow, however, the apparent sharpness of the transition may be deceptive. In any case, since the transition corresponds to the composition of almost pure BeF_2, this transition time does not represent the diffusion coefficient in the melt of bulk composition, but rather a mean diffusion coefficient. This mean diffusion coefficient contains a weighting function whose form depends ultimately on the composition dependence of diffusion.

At the lowest temperature (380°C), noisy chronopotentiograms such as the one in Figure 2 were sometimes obtained when low current densities were used. At higher temperatures, even with chronopotentiograms of similar duration (10 seconds) to those in the more viscous melts at 380°C, the chronopotentiograms are reproducible and not noisy. Therefore convection probably is not the cause of the noise. The appearance of the noise rather seems related to the slow scanning of composition at low temperature. As the concentration of BeF_2 near the anode increases, the liquidus temperature of the mixture becomes much higher than the temperature of the melt, and solid BeF_2 may precipitate in the vicinity of the working electrode. Similar behavior has been reported by Gilbert et al.[5] for anodic chronopotentiometry at an Al electrode in $AlCl_3$-NaCl mixtures. This behavior has not been further investigated, but could prove useful in studies of nucleation and precipitation kinetics.

Figure 2. Noisy chronopotentiogram at slow scan rate in 53 mole percent BeF_2 melt at 380°C with current density of 0.72 A/cm^2.

ANALYSIS OF CHRONOPOTENTIOGRAMS

The analysis of the experimental results must differ from that of ordinary chronopotentiometry. Ordinary chronopotentiometry applies to very dilute solutions and consequently leads to the self-diffusion coefficient of the dilute species. As we have shown previously in ED chronopotentiometry of LiF-BeF_2 mixtures [1,2] and NaF-BeF_2 mixtures [6], a large range of concentration is scanned and the measurements lead to the mutual diffusion coefficient. At long times there is a greater difference between the properties of the melt at the indicator electrode and the properties of melt of bulk composition in ED than in ordinary chronopotentiometry. Thus in ED chronopotentiometry of a 50 m% BeF_2 melt, the composition changes to nearly pure BeF_2 at the indicator electrode. The viscosities [7] change from 0.27 P to 7.63×10^5 P at 600°C and there are comparable differences in electrical conductance. Since the equations have been derived previously, we here give only the essential results.

The e.m.f. between the reference and working or indicator electrodes may be broken into two parts: a constant resistive term (IR) and the e.m.f. of a concentration cell. In a melt MA-M'A_n where M'^{n+} is the cation produced by the faradaic process at the indicator electrode, the e.m.f., E of the cell

$$M\,|MA, M'A_n\,|\,MA, M'A_n\,|M$$

may be written [1,2]

$$E = (IR) + \frac{1}{nF}\int_{y_o}^{y} t_M^A \frac{1 + (n-1)\,y}{1-y}\, d\mu_{M'A_n} \qquad (1)$$

where F is the Faraday, y_o the mole fraction of M'A_n in the bulk melt, y the mole fraction of M'A_n at the anode surface, $\mu_{M'A_n}$ the chemical potential of M'A_n and t_M^A the transference number of M relative to A. As M'A_n accumulates at the electrode, the e.m.f. rises and would theoretically become infinite (although of course another electrode process would occur instead) for nearly pure M'A_n (except in the unlikely event that the transference number of the alkali ion constituent falls to zero more rapidly than its mole fraction). The chronopotentiometric transition is thus a consequence of the thermodynamics of the system, as in classical chronopotentiometry, rather than of the buildup of a resistive layer.

The diffusion equation and boundary conditions have been derived [1] from the flux equation incorporating the coupling between diffusional and electromigrational flows. The thermodynamics of irreversible processes previously applied [1] leads to the following expression for the flow of cations, M, relative to the common anions taken as frame of reference.

$$J_M^A = -D_{M-M'}\frac{\partial c_M}{\partial \xi} + t_M^A\, I/F \qquad (2)$$

where $D_{M-M'}$ is the mutual diffusion coefficient of cations, M and M'

t_M^A is the transference number of cation M relative to anions A
c_M is the concentration of M in equivalents per volume unit
I is the current density at the working electrode
F is the Faraday
and ξ is a distance variable such that equal increments of ξ contain equal numbers of anions A. If x is the distance from a plane electrode, $d\xi = \bar{v}_{M'}/\bar{v}_A \, dx$, where $\bar{v}_A$ and $\bar{v}_{M'}$ are the partial equivalent volumes of A and M'. This transformation accounts for the effects of volume changes with composition on the reference frame for diffusion. If the equivalent volumes of M and M' are equal then $\bar{v}_{M'} = \bar{v}_M = \bar{v}_A$ and $d\xi = dx$.

The equation of diffusion may be derived by differentiation of (Eq. 2) with respect to the distance variable, leading to:

$$\frac{\partial c_M}{\partial t} = \frac{\partial}{\partial \xi}\left(\eta_{M-M'} \frac{\partial c_M}{\partial \xi}\right) - \frac{\partial}{\partial \xi}\left(t_M^A \frac{I}{F}\right)$$

$$= D_{M-M'} \frac{\partial^2 c_M}{\partial \xi^2} + \frac{dD_{M-M'}}{dc_M}\left(\frac{\partial c_M}{\partial \xi}\right)^2 - I/F \frac{dt_M^A}{dc_M}\left(\frac{\partial c_M}{\partial \xi}\right). \qquad (3)$$

Since at the electrode surface the flux of cations M is zero because no M ions cross it, Eq. 2 provides one of the boundary conditions,

$$\frac{I}{F} = \frac{D_{M-M'}}{t_M^A} \frac{\partial c_M}{\partial \xi}; \quad \xi = o, \; t \geq o \qquad (4a)$$

The other boundary condition and the initial condition are the usual ones of chronopotentiometry for semi-infinite diffusion to a plane electrode

$$c_M (t) = c_o; \; t \geq o, \; \xi \to \infty \qquad (4b)$$

$$c_M (\xi) = c_o; \; t = o, \; \xi \geq o \qquad (4c)$$

where c_o is the bulk concentration of M in equivalents per volume unit.

The general second order non-linear differential equation (Eq. 3) is not amenable to analytical solution. With constant diffusion coefficient and unity transference number the diffusion equation and boundary conditions are identical to those of ordinary chronopotentiometry, and the solution is of the same form as the Sand equation, although D is an interdiffusion coefficient rather than a self-diffusion coefficient. However, a useful result can be derived also for the slightly less restrictive assumption of a constant although non-unity transference number, although again considering a constant diffusion coefficient, which could apply over only a small range of composition. Under these assumptions, Eqs. (3) and (4a) may be written:

$$\frac{\partial c_M}{\partial t} = D_{M-M'} \frac{\partial^2 c_M}{\partial \xi^2} = D_{M-M'}/(t_M^A)^2 \left(\frac{\partial^2 c_M}{\partial (\xi/t_M^A)^2}\right) \qquad (5)$$

$$I/F = \left(D_{M-M'}/t_M^A\right)\frac{\partial c_M}{\partial \xi} = \left(D_{M-M'}/(t_M^A)^2\right)\frac{\partial c_M}{\partial(\xi/t_M^A)} \qquad (6)$$

Under these assumptions, the transformations

$$D' = D_{M-M'}/(t_M^A)^2$$

$$\xi' = \xi/t_M^A$$

lead to equations of the same form as for ordinary chronopotentiometry for the concentrations at the electrode surface as a function of time

$$c_M(\xi=0) = c_o - \frac{2\,I}{F\sqrt{\pi\,\frac{D_{M-M'}}{t_M^{A\,2}}}}\sqrt{t} \qquad (7)$$

Because the assumption of a constant interdiffusion coefficient is unrealistic, relation 7 does not apply rigorously over a wide range of concentration. However, as a first approximation, we have used it previously for calculating weighted mean interdiffusion coefficients at times along a chronopotentiogram [1,2]. In the present work, the three bulk compositions are melts where independent measurements[3] have demonstrated unicationic conduction by lithium ions. As before, by using equation 1, including the activity coefficient term, the time dependence of concentration at the electrode surface is calculated from the time dependence of the e.m.f. along the experimental chronopotentiograms. Eq. 7 is reminiscent of the Cottrell equation for the time dependence of current in chronoamperometry. Setting the concentration of M at the electrode surface equal to zero gives the analog of the Sand equation, but as pointed earlier, a diffusion coefficient calculated from a transition time may be difficult to interpret. Eq. 7 may be put in a useful form for graphical analysis

$$(1 - c_M/c_o)/I = \frac{2}{c_o\,F\sqrt{\pi\,D_{M-M'}/(t_M^A)^2}}\sqrt{t} \qquad (8)$$

In the hypothetical case of diffusion coefficient and transference number independent of composition over the entire composition range, plots of the left hand side of Eq. 7 vs the square root of time would be linear, with slope inversely proportional to $\sqrt{D_{M-M'}/(t_M^A)^2}$, up to the transition time, at which $c_M = o$. The limiting value of the ordinate is then equal to the reciprocal of the current density. Applying such plots to LiF-BeF_2 mixtures in the composition range in which $t_{Li^+}^F$ is known to be unity (20-80 mole percent BeF_2), deviations from linearity result from composition dependence of the diffusion coefficient, providing a useful diagnostic. The limiting ordinate still should be 1/I, and the plots at different current densities should be superimposed for values of the ordinate not too close to 1/I. This provides a test for consistency of the diffusion coefficients from measurements at different current densities, and is the analog of the constancy of $I\tau^{1/2}$ in classical chronopotentiometry.

RESULTS

ED chronopotentiometric measurements were made in the three bulk compositions of 53, 65, and 70 mole percent BeF_2 at several temperatures. At each temperature and composition chronopotentiograms with different current densities were obtained. Figure 3 shows typical plots of Equation 8 at 570°C in the melt of bulk composition 53 mole percent BeF_2. The different symbols refer to different current densities at the working electrode, and the mole fractions of BeF_2 at the indicator electrode are indicated. The three plots are obviously sigmoid in shape, indicating the variation of the interdiffusion coefficients. However the ordinates calculated from the early parts of the chronopotentiograms at differing current densities are superimposed on one another and lie on a straight line through the origin. Over a short concentration range the composition dependence of the interdiffusion coefficient may well be neglected and the slope, using equation 8, gives the value 1.52×10^{-5} cm^2/s for the mutual diffusion coefficient of lithium and beryllium in the 53 mole percent BeF_2 melt at 570°C. As the concentration of BeF_2 increases beyond 60 mole percent BeF_2, a sharp departure from linearity appears, and as the curves approach their limiting values the plots are no longer exactly superimposable. Up to 80 mole percent BeF_2 the curvature arises from the composition dependence of the mutual diffusion coefficient. If mean values of the diffusion coefficient are calculated from equation 8, the apparent anomaly of decreasing mean values of interdiffusion coefficient with increasing BeF_2 content is found, because of the weighting function. When the concentration of BeF_2 exceeds 80 mole percent BeF_2, the transference number of lithium relative to fluoride may decrease; at all three current densities a rapid decrease of slope occurs at about 90 mole percent BeF_2. The final parts of plots are plateaus as $(1-C_L/C_o)/I$ attains slowly its expected value of $1/I$. The corresponding compositions are very close to pure BeF_2 and very likely in this concentration range both interdiffusion coefficient and transference number decrease. In the absence of an analytical solution of the diffusion equation with a concentration dependent diffusion coefficient, the most reliable results probably are those from the very early parts of chronopotentiograms. However the current densities must be chosen low enough to provide compositions not too far removed from the bulk composition in the early part of the chronopotentiograms. In our previous measurements[1,2] at higher BeF_2 contents, the initial composition change was too rapid to provide data as close to the bulk composition as in the present work, and the plots probably correspond to the second, or rising portion of the sigmoid curve. However it was possible to resolve the weighted mean diffusion coefficients into composition dependent values which were mutually consistent when the values calculated for a given composition at the electrode surface in melts of differing initial compositions were compared. In the present work, the composition undergoes too large a change for convenient resolution of the weighted mean. Table I gives values of the mutual diffusion coefficient in melts of three compositions, together with the concentration interval over which the value is averaged. Temperature dependence of the mutual diffusion coefficient in the eutectic melt between 380°C and 600°C leads to an activation energy for diffusivity of 9 kcal/mol compared to a value of about 15 kcal/mol for the activation energy for viscous flow[7].

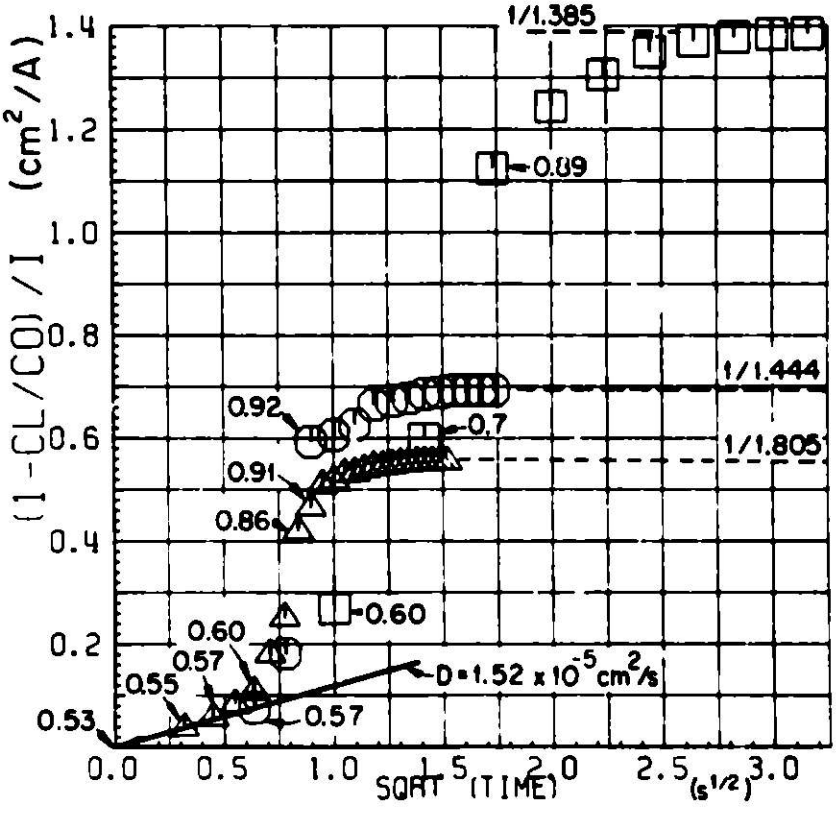

Figure 3. Dependence of composition at the Bc anode on square root of time (Eq. 8) for the 53 mole percent BeF_2 melt at 570°C and with different current densities (mA)

500; △ 400; ○ 200 □

Area of the working electrode: 0.277 cm^2. The compositions in mole fraction of BeF_2 are indicated, as is the diffusion coefficient calculated from the initial slope. Horizontal dashed lines are the plateaus calculated as the reciprocal current densities.

Table I. Mutual Diffusion Coefficient (cm^2/s) of Lithium and Beryllium in LiF-BeF_2 Melts

Melt Composition mole percent BeF_2	Temperature / °C			
	380	570	600	700
70				1.5×10^{-6} (70-85)
65			4.6×10^{-6} (65-74)	
53	3.4×10^{-6} (53-55)	1.52×10^{-5} (53-55)	1.6×10^{-5} (53-60)	

DISCUSSION

The magnitudes of the interdiffusion coefficients in 53-70 mole percent BeF_2 mixtures, shown in Table I, and the activation energy for diffusion, indicate the approach to values expected in ionic liquids with increasing alkali ion concentration and the breakdown of the network structure of BeF_2. Our previous measurements in mixtures containing 78-95 mole percent BeF_2 led to estimated interdiffusion coefficients in the range 10^{-6} to 10^{-8} cm^2/sec. Solute self-diffusion coefficients of the order of 10^{-6} cm^2/sec. have been reported[8] in 30 mole percent BeF_2 melts.

In plots such as Fig. 3, the slope of the chord between the origin and a point on the curve corresponds to a mean interdiffusion coefficient for compositions between the bulk or initial composition and the composition at the electrode surface at the corresponding time along the chronopotentiogram. It is clear from the sigmoid slope that these weighted mean values will first decrease with time (increasing chord slope) and then increase with time (decreasing chord slope) as the plateau is approached. In our previous work[1,2] at higher BeF_2 concentrations, assumption of a weighting function proportional to the alkali ion concentration led to consistency between diffusion coefficients calculated at differing times and concentrations along an individual chronopotentiogram, and diffusion coefficients calculated at the same concentration but different time from chronopotentiograms in melts of differing initial composition. Such a weighting function reflects the fact that in a system in which the diffusion coefficient is decreasing with time, the compositions with higher alkali concentration (and hence higher diffusion coefficient) contribute longer times towards the attainment of a given e.m.f. than the compositions with low diffusion coefficient.

The sigmoid slope of the approach to the limiting plateau also indicates that the evaluation of a transition time may be rather difficult, and that apparent sharpness may be deceptive. If one applies the Sand equation to a 6 second apparent transition time in Fig. 1, the calculated apparent diffusion coefficient is 2×10^{-6}. The diffusion coefficient calculated from the initial slope of Eq. 8 would require a transition time of 9 seconds if the diffusion coefficient were constant.

ED chronopotentiometric measurements have been reported[5] in $NaCl-AlCl_3$ melts where unicationic conductance by sodium ions (relative to chloride) is expected[6] because of the complexity ($NaAlCl_4$-Al_2Cl_6) of the melts rather than a network structure as in BeF_2. However, the interdiffusion coefficient of sodium and aluminum probably does not vary as sharply with composition as does that for LiF and BeF_2, since the viscosity does not change as much. Since the diffusion coefficients in that study were calculated from apparently sharp transition times, it seemed of interest to investigate a possible composition dependence by calculations such as the ones we have presented above.

Figure 4 shows a plot $(1-c_M/c_o)/I$ derived from the published chronopotentiograms[5] with 0.2 and 0.15 A/cm^2 in the melt 63 mole percent $AlCl_3$ - 37 mole percent - NaCl at 140°C. The superposition of the two sets of points indicates excellent consistency of the data at the two different current densities. The two filled symbols in Figure 4 are obtained by taking $C_{Na} = Co$ at transition times of 6.6 and 12.1 s as graphically determined by the authors in reference 5. Although the plateaus are of lesser extent in this chloroaluminate melt than in $LiF-BeF_2$ mixtures, the assumption of both constant interdiffusion coefficient and transference number probably does not hold over the full composition range spanned during the chronopotentiograms. Because of difficulty in reading the e.m.f. at very short times, the initial points probably correspond to concentrations far enough from the bulk concentration to belong to the non-linear part of the plots, and extrapolation through the origin must assume curvature. This would lead to a lower initial slope and a slightly higher value of the diffusion coefficient (perhaps $1.5\text{-}1.8\times10^{-6}$ $cm^2/sec.$) than the value 1.2×10^{-5} calculated from the transition time. Since there is little variation of the interdiffusion coefficient in this system, the use of the transition time here does not lead to significant error, as it would in the case of the $LiF-BeF_2$ system, but it would appear advisable to use all of the e.m.f. time data along the chronopotentiogram rather than a single point, the transition time, in the calculation.

CONCLUSIONS

Interdiffusion coefficients may be evaluated from chronopotentiometric measurements over much broader ranges of concentration than in the classical application of this method. Development of the method has passed through three stages. Initially[1] it was applied to a relatively narrow composition range, 95-100 mole percent BeF_2, providing mean interdiffusion coefficients approaching the self-diffusion coefficient of Li^+. Next[2] it was applied to melts in which the composition swept through the range 78-100 mole percent BeF_2, and a method was developed for resolving the weighted mean diffusion coefficients into composition dependent values. Extending the method to mixtures containing 53 mole percent BeF_2, in which the composition change is too large to use the weighted mean resolution, we have in this paper shown that it is possible to obtain interdiffusion coefficients for compositions close to the initial or bulk composition. These estimates of the composition dependence of the interdiffusion coefficients are needed as preliminary values in the development of numerical solution of the flux equations. Although the method has been applied to chronopotentiometry, it should be applicable to other kinds of electrochemical scanning programs, e.g. linear sweep voltammetry and chronoamperometry. In fact, other types of scanning function

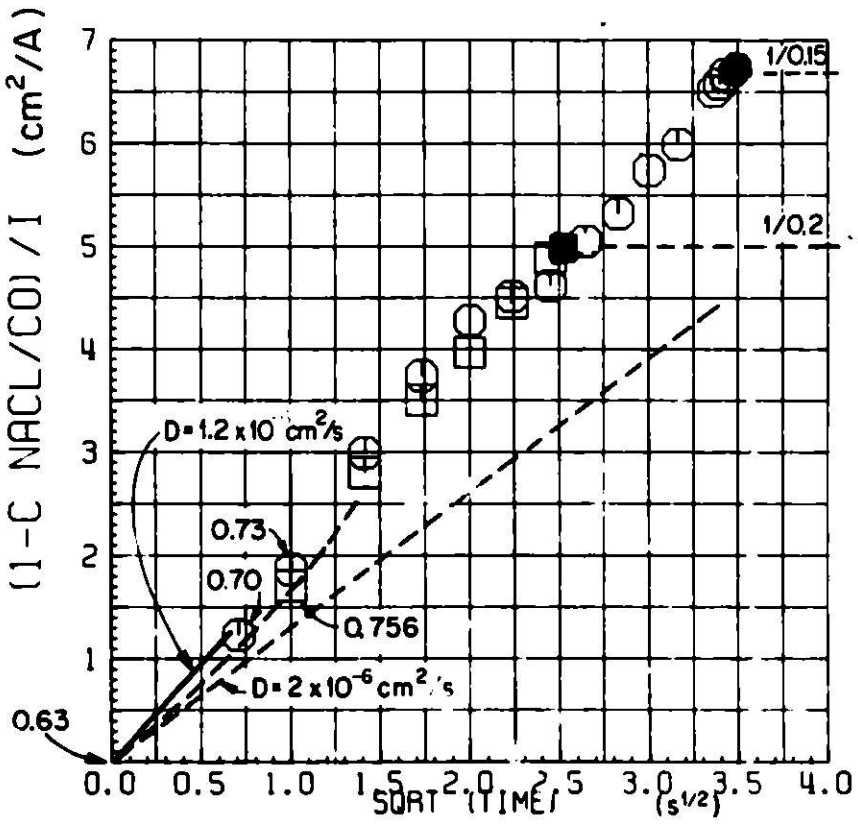

Figure 4. Dependence of composition at Al anode surface o square root of time in 63 mole percent $AlCl_3$ - 37 mole percent - NaCl melt from experimental data of reference (5) with different current densities (mA) at 140°C

□ 10; ○ 30

Area of the working electrode: 0.2 cm^2. The filled symbols correspond to the reported graphical transition times[5]: 6.0 s; 12.1 s.

The compositions in mole fraction of $AlCl_3$ at the aluminum anode surface are indicated. The slope of the solid line corresponds to the reported[5] diffusion coefficient, that of the dashed line to be a limit slope of the curve. The plateaus are calculated from the reciprocal current densities.

may prove more useful than chronopotentiometry for resolving diffusion coefficients at compositions near the bulk composition, i.e., at short times. The method has been applied to binary polymeric melts and binary complex melts, but should be applicable to the evaluation of transport parameters in high temperature electrolytes of proposed battery systems. The analysis should prove useful in systems where composition dependent diffusion coefficients may be expected, as in silicates[9] and in the anodic dissolution of metals[10].

LIST OF SYMBOLS

A	common anion
C_M	concentration of MA (moles/cm^3); (L for LiF, Na for NaCl)
Co	concentration of alkali halide in the bulk (moles/cm^3)
$D_{M-M'}$	mutual diffusion coefficient of M and M' (cm^2/s)
D'	transformed mutual diffusion coefficient, $D/(t_M^A)^2$
E	e.m.f. between reference and indicator electrodes (Volt)
F	the Faraday (96,487 coulombs)
I	current density (A/cm^2)
J_M^A	flow of M relative to A (common anion), equiv./(cm^2/s)
(IR)	IR drop (Volt)
M	alkali cation
M'	cation Be or Al
n	charge number of cation
t	time (seconds)
t_M^A	transference number of cation M relative to anion A
x	distance from electrode surface
y	mole fraction of MA
y_o	mole fraction of MA in the bulk
$\mu_{M'A_n}$	molar chemical potential of $M'A_n$
ξ	distance variable
ξ'	transformed distance variable, ξ/t_M^A

ACKNOWLEDGMENT

We are pleased to acknowledge discussion of the manuscript with Dr. S. Canton.

REFERENCES

1. C. E. Vallet, H. R. Bronstein and J. Braunstein, "Electromigrational Depletion (ED) Chronopotentiometry. Temperature Dependence of Diffusion in Molten BeF_2-LiF," J. Electrochem. Soc. 121, (11), 1429-39 (1974).

2. C. E. Vallet and J. Braunstein, "Concentration and Temperature Dependence of Diffusion and Conductance in Molten BeF_2-LiF Mixtures," J. Amer. Ceram. Soc. 58, (5-6), 209-14 (1975).

3. K. A. Romberger and J. Braunstein, "Transference Numbers and Mobilities in Molten Mixtures of Beryllium Fluoride and Lithium Fluoride," Inorg. Chem. 9, (5), 1273-5 (1970).

4. G. D. Robbins and J. Braunstein; pp. 156-9 in Molten Salt Reactor Program Semi-annual Progress Report for Period Ending Feb. 28, 1970. Tech. Report ORNL-4548, Aug. 1970.

5. B. Gilbert, D. L. Brotherton and G. Mamantov, "Chronopotentiometric Investigation of the Oxidation of Aluminum in Chloroaluminate Melts," J. Electrochem. Soc. 121, (6), 773-6 (1974).

6. J. Braunstein, H. R. Bronstein and J. Truitt, "Chronopotentiometry Based on Diffusion of Mobile Nonelectroactive Species," J. Electroanal. Chem. 44, (3), 463-8 (1973).

7. S. Cantor, W. T. Ward and C. T. Moynihan, "Viscosity and Density in Molten BeF_2-LiF Solutions," J. Chem. Phys. 50, (7), 2874-9 (1969).

8. G. Mamantov and D. L. Manning, "Voltammetry and Related Studies of Uranium in Molten Lithium Fluoride-Beryllium Fluoride-Zirconium Fluoride," Anal. Chem. 38, (11), 1494-8 (1966).

9. K. Nagata, M. Kawakami and K. S. Goto, "Electrochemical Determination of Rate Controlling Step of Silicon and Aluminum Transfer Between Molten Slag and Metal, and Estimation of Interdiffusivity of SiO_2 and CaO, Al_2O_3 and CaO in the Slag;" pp. 183-98 in "Metal-Slag-Gas Reactions and Processes," edited by Z. A. Foroulis and W. W. Smeltzer, The Electrochemical Society, Princeton, J., 1975.

10. D. L. Piron, "A Critical Discussion of Chronopotentiometric Measurement of Diffusion Coefficients in Molten Salts," Corrosion Sci. 15, 383-92 (1975).

OVERCHARGE STUDIES OF THE FeS_2 ELECTRODE IN Li/FeS_2 CELLS

Z. Tomczuk, R. E. Hollins*, and R. K. Steunenberg

Argonne National Laboratory
9700 South Cass Avenue
Argonne, Illinois 60439

ABSTRACT

The overcharge reaction of the FeS_2 electrode in Li/FeS_2 cells has been studied by operating five cells to successfully higher charge cutoff voltages and also by cyclic voltammetry. The results indicate that increasing the charge cutoff voltage increases the porosity in the FeS_2 electrode while decreasing the coulombic efficiency. The products of the overcharge have been identified as ferrous chloride and sulfur. The cyclic voltammetry results indicate that the reaction is irreversible and diffusion-limited. A reduction mechanism consistent with experimental data is proposed.

INTRODUCTION

The present program on Li-Al/FeS batteries at Argonne National Laboratory is an extension of the work started in 1967 on lithium/chalcogen electrochemical cells.[1] The previous experimental work indicated that power densities in excess of 3 W/cm^2, current densities over 1 A/cm^2, and discharge voltages in excess of 1.5 V could be obtained using low-melting halide electrolytes. These results were obtained with lithium negative electrodes and tellurium or selenium positive electrodes.

The use of these elements as positive electrodes is impractical because the elements are not in plentiful supply and their compounds are extremely toxic. This leaves sulfur as the most suitable positive electrode material. Lithium is ideally suited for use as the anode material because it is a liquid at cell operating temperatures, and has a high electrochemical reactivity and a low equivalent weight. Sulfur is also well suited as the positive electrode material because it is a liquid at cell operating temperatures, and has a high electronegativity value and a reasonably low equivalent weight. However, it became apparent that materials corrosion problems and the loss of sulfur from the positive electrode would make Li/S cells impractical. The loss of sulfur from the cells can occur by several pathways: (1) vaporization (the vapor pressure of sulfur at about 400°C is about 400 Torr), (2) solubility of sulfur species such as S_2^-, S_2^{2-}, and S^{3-} in the electrolyte, and (3) physical entrainment in the electrolyte. Of these, (2) is considered dominant. Efforts to reduce the sulfur loss by the use of additives such as thallium or arsenic were of limited success.[2] The problems associated with the use of liquid lithium at temperatures near 400°C presents

---

*Roosevelt University, Chicago, Illinois

a materials problem that still remains unsolved. This problem can be avoided by using a solid lithium-aluminum alloy rather than the liquid lithium.

In 1973, preliminary cell test data were obtained that indicated that the use of iron sulfides, FeS_2 and FeS, could prevent or reduce the loss of sulfur from the positive electrode. These results[3] were so encouraging that an immediate large-scale engineering effort was undertaken using both FeS_2 and FeS as positive electrode materials. To date, large engineering-scale cells have demonstrated that cell operating times in excess of 3000 hr and 100 cycles can be achieved.

From early results of laboratory-scale Li/FeS_2 cells, it became apparent that discharge-charge cycling produced phases (initially believed to be FeS_2, FeS, and Fe plus Li_2S) that were complex and could not be identified by X-ray diffraction. A study[4] was then initiated using laboratory-scale tests to help identify the phases present in the FeS_2 electrode and also to determine the voltage range at which these phases were found on charging. The general progression was as follows:

Li_2S and Fe (fully discharged condition), "X" phase, "Z" and FeS phases, and FeS_2 (fully charged condition). The X phase has been clearly identified as Li_2FeS_2; the Z phase was originally thought to have the empirical formula $Li_4Fe_2S_5$, but it appears now that this formula is only an approximation of the true stoichiometry. The presence of a third Li-Fe-S compound has been suggested by results obtained in several different synthesis procedures; however, the formula has not yet been determined. The composition of this phase is believed to lie somewhere between those of Z and FeS_2.

The X phase was formed below 1.95 V *vs.* Li; the Z and FeS phases were formed between 1.95 and 2.15 V ; the Z, FeS, and FeS_2 phases were formed between 2.15 and 2.25 V. Charging cells to 2.50 V yielded only FeS_2, but with an indication that an electrolyte-FeS_2 reaction was taking place. The phase or phases found in cells charged to voltages in excess of 2.5 V *vs.* Li were not investigated.

It is obvious from the above discussion that complex phases are to be found in cells charged to 2.5 V *vs.* Li and lower. These are the charge cutoff voltages normally used in cell testing. However, in a real battery there will be considerable voltage variations between cells. This results in part from electrode capacity mismatch and poor current distribution. As a result, some cells will be charged to values in excess of 2.5 *vs.* Li. It is of practical importance, therefore, to know what the products are and at what potential they form, which was the purpose of this study.

The only previous electrochemical study of FeS_2 was reported by Peters and Maitra[5]. However, their work was done with aqueous solutions. Their results indicate that the oxidation of FeS_2 proceeds by the reaction

$$FeS_2 + 8H_2O \rightarrow Fe^{3+} + 2SO_4^{2-} + 16H^+ + 15e^- \quad (1)$$

while the cathodic reduction proceeds by

$$2e^- + FeS_2 + 4H^+ \rightarrow Fe^{2+} + 2H_2S \quad (2)$$

The present study was approached in two different ways, namely, by electrochemical cell studies and by cyclic voltammetry. The former were undertaken to determine the effect of charge cutoff voltage on cell performance, whereas the latter was used to help identify the reaction mechanism. In the cell studies, liquid lithium was used in the negative electrode because of the ease of electrode preparation. Solid Li-Al alloy was used in the cyclic voltammetry studies to decrease the solubility of lithium in the electrolyte,[6] which might affect the reaction at the positive electrode.

EXPERIMENTAL

Electrochemical Cell Studies

All the cells tested were of a design described earlier.[3] The positive electrode (FeS_2) rested at the bottom of an Al_2O_3 crucible, and the negative electrode (Li) was positioned ~1 cm above the FeS_2 electrode. Typically, the negative electrode consisted of a disk of Type 302 stainless steel Feltmetal* (90% porosity, 27 μm pore size) that was prewet with liquid lithium at about 600°C in a helium-atomosphere glovebox. The LiCl-KCl eutectic (mp, 352°C) that was used as the electrolyte, was obtained from the Anderson Physics Laboratories, Inc., Champaign, Illinois, and was used as received. At the authors' request, this eutectic electrolyte was contacted with lithium by the manufacturer before delivery. The purpose of this step was to reduce and eliminate any metallic ions present as impurities in the eutectic. The FeS_2 used in this study was single-crystal material that was obtained from the Atomics International Dividion of Rockewell International, and was ground and only the -60 +100 mesh size fraction was used. The stated purity of the FeS_2 was 99%. Chemical analysis of this material confirmed the stated purity. Metallographic and X-ray diffraction analysis showed that the material was single phase.

The cells were open and were operated in a furnace well (3-in. ID) located in the floor of a high-purity helium atmosphere glovebox. The physical characteristics of the cells are given in Table I. The positive electrode materials were contained in a cavity within a disk-shaped ATJ** graphite cup. A PG-60** porous graphite diffusion barrier, 0.63 cm thick, was graphite-cemented to the ATJ graphite cup to confine the FeS_2. The amount of FeS_2 used (1.12 g) was that necessary for 1 A-hr capacity. The geometric active area of all positive electrodes was 4.8 cm^2. Vacuum impregnation of the positive electrodes by the LiCl-KCl eutectic was necessary to ensure electrolyte contact.

The cell temperature was monitored by a calibrated chromel-alumel thermocouple fixed to the Al_2O_3 crucible by wire mesh. The resulting output signals were corrected by the use of an Ice Point Reference Standard,† and recorded on a Honeywell recorder having a 1-mV span.

---

*
**A product of the Brunswick Corporation
**Products of Union Carbide.
†A product of Kaye Instruments, Inc.

TABLE 1. Physical Characteristics of Li/FeS_2 Cells

Positive Electrode	
Area, cm^2	4.8
Active Material	FeS_2
Weight of Material, g	1.12
Theoretical Capacity, A-hr	1.0
Theoretical Capacity Density, A-hr/cm^2	0.22
Lithium Electrode	
Area, cm^2	5.0
Weight of Lithium, g	1.5
Current Collector	Type 302 S.S. Feltmetal
Theoretical Capacity, A-hr	5.8
Electrolyte	LiCl-KCl Eutectic
Weight of Electrolyte, g	95.7-117
Interelectrode Distance, cm	~1
Operating Temperature	381-407

Discharge and charge cycling was conducted at constant current using a Hewlett-Packard Model 6201 Model 6201B constant-current power supply which was connected to a meter relay that automatically reversed the polarity of the power supply when a present voltage was reached. The discharge cutoff voltage for each cell was set a ~1.0 V to avoid a lithium-graphite reaction. At the end of each cell test, the electrodes were rapidly removed from the cell for post-test characterization. Sections of each sulfide electrode were examined metallographically and by X-ray diffraction.

Cyclic Voltammetry Studies

The cell design for the cyclic voltammetry is shown in Fig. 1. The electrodes (an FeS_2 working electrode and Li-Al working and reference electrodes) were positioned vertically, and the distance between the Li-Al reference electrode and the FeS_2 electrode was kept as close as possible. The Li-Al reference electrode was isolated by jacketing it with an Al_2O_3 tube (~10 cm long, ~2 cm ID) which had a porous Al_2O_3 frit (estimated pore size, 50 μm) at the bottom. The choice of Li-Al as the reference electrode was based on the work of Yao *et al*,[7] who showed that, over composition range from 7 to 47 at. % Li, the electrode emf is constant for a fixed temperature.

The Li-Al alloy (40 at. % Li) used in all the Li-Al electrodes was prepared in a helium-atmosphere glovebox by heating elemental lithium and aluminum to a temperature of about 720°C, to prepare a homogeneous alloy. At this temperature and composition, the alloy is liquid. The resulting alloy was annealed at a temperature of about 550°C for 1.5 hr to insure complete formation of the Li-Al phase.

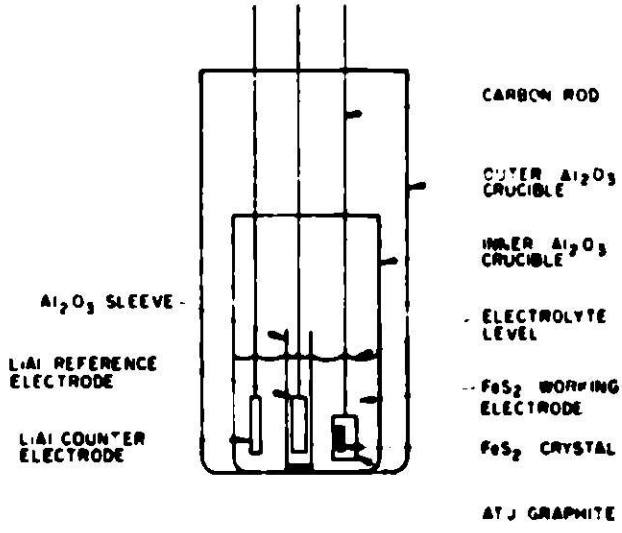

Fig. 1. Cell Design for Cyclic Voltammetry Studies

The positive working electrodes were prepared by placing single crystals of FeS_2, obtained from the Lizzadro Museum of Lapidary Art, Elmhurst, Illinois, into cavities drilled in the ATJ graphite housing and then graphite-cementing them into place. A carbon rod was also graphite-cemented onto the ATJ housing. The geometric area of each of the four FeS_2 electrodes prepared was about 0.6 cm^2.

Cycling studies were initiated under the experimental conditions shown in Table 2 by placing the three electrodes in the Al_2O_3 crucible containing 130 g LiCl-KCl and making the necessary external electrical connections to a Wenking potentiostat Model VSG 72 and a Hewlett-Packard Model 7001 AM X-Y recorder. When the cell temperature equilibration was completed, voltammetric scanning was begun. In no case was the temperature equilibration time less

TABLE 2. Experimental Conditions for Cyclic Voltammetry Studies

Cell Container	Two Al_2O_3 crucibles
Electrodes	
Working	FeS_2
Counter	40 at. % Li-Al weighing 10.8 g
Reference	40 at. % Li-Al weighing 11.4 g
Working Electrode Area	~0.6 cm^2
Electrolyte	130 g LiCl-KCl
Temperature Region Studied	372-453°C
Instrumentation Used	Wenking potentiostat and Wenking voltage scan generator

than 2 hr. The scan region was started at 1.70 V *vs.* Li-Al and was increased in increments until peaks could be observed on the X-Y recorder. The scan range was increased until a maximum value of 2.75 V *vs.* Li-Al was reached. Multiscans at a fixed sweep rate were made to ensure that the recorded results were reproducible. Various sweep rates were also used at a fixed temperature. Additional tests were made by adding solid Li_2S to the melt and recording the voltammograms to determine whether any of the observed peaks could be attributed to the oxidation of sulfide ion, S^{2-}.

Cyclic voltammetry studies were also made briefly with X phase (Li_2FeS_2) to see whether it could be responsible for some of the observed peaks. This was accomplished by using the same cell design, but by using fresh electrolyte and removing the FeS_2 working electrode. The working electrode structure was jacketed by an Al_2O_3 tube identical to that used for the reference electrode, but without a frit at the bottom. the X phase was introduced into the compartment and cycling was again initiated.

A brief test was also made to identify the gas evolved at a potential of 2.72 V *vs.* Li-Al using the potentiostat as a constant voltage source. The cell arrangement was again similar to that used with the X-phase study, but with two notable exceptions: the length of the Al_2O_3 tube was increased to ~30 cm, and the tube was lined with 5-mil-thick copper foil ~7 cm above the melt. The FeS_2 electrode was then electrolyzed at a potential of 2.72 V *vs.* Li-Al for a period of 1 hr. During this time, approximately 0.1 A-hr of the FeS_2 was electrolyzed. At the end of electrolysis, the FeS_2 electrode and the copper foil were removed rapidly. Visual inspection indicated that considerable attack of the copper foil had taken place. A section of the reacted portion was submitted for X-ray analysis to determine the identity of the product resulting from the reaction of copper with the evolved gas.

RESULTS AND DISCUSSION

Electrochemical Cell Studies

Five Li/FeS_2 cells were operated to successively higher charge cutoff voltages.* The first cell test was terminated at 2.52 V and the last was terminated at 2.88 V.

A description of the electrical performance of each cell test is given below.

Cell RU-1. The purpose of this cell test was to determine the electrochemical behavior when a charge cutoff voltage of 2.52 V was used. This value was chosen for a baseline because previous phase studies were conducted on FeS_2 electrodes that had been charged to the 2.5-V value. The cell was operated at a temperature of 400°C for 15 discharge-charge cycles at current densities varying from 25 to 83 mA/cm^2. At the end of the last charge cycle, the cell was trickle-charged to ensure uniform reaction. The electrical performance of the cell was excellent. The coulombic efficiency was close to 90% and the FeS_2 utilization was close to 80% of the theoretical value.

* All voltages in this paper are IR-free unless otherwise designated.

Cell RU-2. This cell was operated with the objective of determining the electrical performance of a Li/FeS_2 cell charged to a 2.65-V cutoff, as well as establishing the phases present in the sulfide electrode at this higher charge cutoff voltage. The cell was cycled at constant current densities varying between 19 and 50 mA/cm^2 for 13 cycles at a temperature of 400°C. The cell was again trickle-charged near the end of the cell test.

The electrical performance data indicated that there were no deleterious effects on cell performance using this higher cutoff voltage. The coulombic efficiency was near 90% and the FeS_2 utilization was close to 80%. X-ray analysis and metallographic examination of the sulfide electrode at the end of the cell test again showed that FeS_2 was the dominant sulfide phase present. The metallographic examination also showed the presence of the Z phase in the region farthest away from the ATJ graphite current collector, indicating again the need for good current collection in cells of this type. In addition, the metallographic examination showed that the reaction layer, which was barely noticeable in Cell RU-1, had increased in height. However, this layer still could not be identified.

Cell RU-3. The purpose of this cell test was to determine the effect of charging a Li/FeS_2 cell to a 2.74-V charge cutoff. On the basis of the results obtained for Cell RU-2, it was thought that an additional 0.1-V higher charge cutoff might be sufficient to produce a significant amount of the overcharge layer observed with the first two cells, so that the overcharge products could be identified. The cell was cycled at constant current densities varying from 19 to 37 mA/cm^2 for twelve cycles at a temperature of 404°C. The initial cycles employed a cutoff voltage (2.54 V) that would ensure conditioning of the FeS_2 electrode. From the seventh cycle through the final cycle, the charge cutoff was 2.74 V.

The cell behaved satisfactorily at this high cutoff voltage but began to deteriorate gradually as evidenced by the decreasing coulombic efficiency. On the last cycle, the cell could no longer be recharged to this 2.74-V cutoff.

Because of the difficulties encountered on the twelfth charge cycle, operation of the cell was terminated. Examination of the sulfide electrode products by X-ray diffraction analysis and metallographic examination showed that FeS_2 was still present. Moreover, the X-ray analysis indicated the presence of either $KFeCl_3$ or K_2FeCl_4 (it is difficult to distinguish these two compounds when they are present in low concentrations). The metallographic examination showed also that the degree of porosity was much higher than that in the first two electrodes, giving further indication that the overcharge reaction involved gas formation.

Cell RU-5. The purpose of this cell test was to determine the electrical performance of a Li/FeS_2 cell charged to a 2.79-V cutoff. The three previous cell tests had indicated that the degree of porosity in the FeS_2 electrode and the reaction of the LiCl-KCl electrolyte with the FeS_2 increased with increasing cutoff voltage. To ensure that the FeS_2 electrode was properly conditioned, the cell was cycled between 1.00 and 2.57 V for the first four cycles, and the charge cutoff voltage was then increased to 2.79 V. The cell was operated for five additional discharge-charge cycles at a constant current

density of 38 mA/cm^2 at an operating temperature of 407°C before the test was terminated. At the end of the last charge cycle, the cell was trickle-charged to ensure uniform reaction of the FeS_2 electrode.

The electrical performance of this cell was not entirely satisfactory. The percent FeS_2 utilization was still high (80%), but the coulombic efficiency had dropped below that of the first three cells.

The X-ray analysis and metallographic examination of the sulfide product electrode revealed that the overcharge reaction was more extensive than with the previous three cells. However, FeS_2 particles were still present. Moreover, the metallographic examination showed that the $KFeCl_3$ (identified by X-ray diffraction) present in the electrode was apparently in solution at cell operating temperatures.

Cell RU-6. The purpose of operating this cell was to see whether a still higher cutoff voltage than that used for Cell RU-5 would yield any other information on the overcharge products. An additional purpose was to determine the effect of a 2.88-V charge cutoff on electrical performance. The cell was operated for twelve full discharge-charge cycles at 422°C with current densities varying between 25 and 50 mA/cm^2. The cell performed erratically for the first two cycles, but the performance improved after the lithium electrode was repositioned. This erratic behavior apparently resulted from the formation of a conductive phase on the Al_2O_3 crucible through an interaction of the lithium with Al_2O_3. Placing the lithium electrode away from this conductive phase eliminated the short circuit.

X-ray diffraction analysis and metallographic examination of the product sulfide electrode revealed that the degree of overcharge was less than that observed for Cell RU-5. The amount of FeS_2 present was greater, but, surprisingly, the porosity was less. These results were totally unexpected in light of the higher charge cutoff voltage used.

The major findings from the operation of the five Li/FeS_2 cells are summarized in Table 3. The data clearly show that the major impact of higher charge cutoff voltage is on coulombic efficiency and FeS_2 electrode porosity.

TABLE 3. Results of Charging Li/FeS Cells to Successively Higher Cutoff Voltages

Cell No.	Charge Cutoff Voltage, V	Average Coulombic Efficiency	Porosity of Sulfide Electrode	Phases Found by X-ray
Ru-1	2.52	0.92	Very Low	FeS_2
RU-2	2.65	0.91	Low	FeS_2, Z Phase
RU-3	2.74	0.87	Medium	FeS_2, $KFeCl_3$ or K_2FeCl_4
Ru-5	2.79	0.84	High	FeS_2, $KFeCl_3$ or K_2FeCl_4
RU-6	2.88	0.83	Medium High	FeS_2, $KFeCl_3$ or K_2FeCl_4

As the cutoff voltage was increased, the porosity of the FeS_2 electrode increased and the cell current efficiency decreased. This increase in porosity can be seen in Fig. 2. In this figure, the FeS_2 particles are white in a grayish electrolyte background. The fine needle-like material is the overcharge product. The porosity is apparently related to the degree of overcharge and it suggests that one of the overcharge products is a gas. The decrease in coulombic efficiency with increased cutoff voltage is consistent with the observation that the overcharge reactions are not entirely reversible; otherwise, there would not be any effect on coulombic efficiency.

The discharge-charge curves for these cells such as those shown in Fig. 3 for Cell RU-6, are remarkably similar to those obtained using lower charge cutoff voltages; the only exception is the marked upsweep of the voltage vs. time curve as the charge cutoff voltage is increased.

The presence of $KFeCl_3$ in the sulfide electrode product is consistent with the conclusion that iron chloride ($FeCl_2$) is one of the overcharge products. Beusman,[7] in his study of the KCl-$FeCl_2$ and $LiCl$-$FeCl_2$ systems, found that $FeCl_2$ reacts with KCl to form two compounds--$KFeCl_3$ and K_2FeCl_4. No analogous $LiCl$-$FeCl_2$ compounds were found. The metallographic observation that the $KFeCl_3$ present in the sulfide electrode from Cell RU-5 was in solution at the cell operating temperature is consistent with the finding of $FeCl_2$ in the bulk electrolyte.

Cyclic Voltammetry Studies

These cell results, discussed above, indicated that perhaps a gaseous product was being formed in the FeS_2 electrode when charge cutoff voltages in excess of 2.65 V were used. Cyclic voltammetry studies were therefore undertaken in an attempt to define the product and also to elucidate the reaction mechanism.

The three experimental variables in the cyclic voltammetry studies of the FeS_2 electrode were the following: the effect of temperature on peak positions, the effect of scan rate on peak positions, and the effect of voltage on peak positions. The results obtained and the species identified are described below.

Effect of Temperature on Peak Positions. A typical voltammogram obtained at a temperature of 372°C and a scan rate of 10 mV/sec is shown in Fig. 4. Additional voltammorgrams were obtained over the temperature range from 372 to 453°C. These results are summarized in Table 4, where it is apparent that one of the cathodic peaks at 372°C was absent when the temperature was raised to 397°C. The peaks were also shifted to higher voltages as the temperature was increased. Also, less structural detail was observed as the temperature was increased to 450°C. This suggests the formation of soluble products which were able to diffuse into the bulk electrolyte at a rate faster than that used to scan the voltage region.

These results indicate that at least one chemical reaction must have been taking place at temperatures in excess of 397°C. Otherwise, the effect of temperature on peak position appears to be negligible.

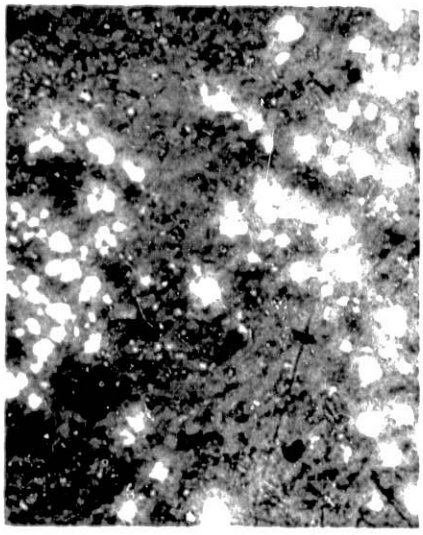

Cell RU-1

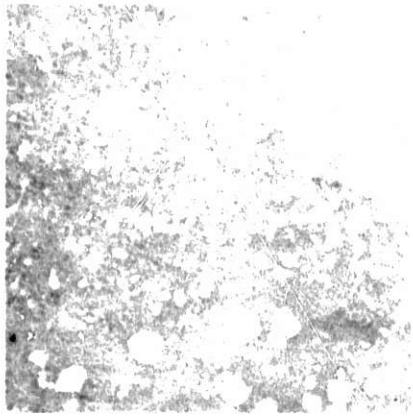

Cell RU-2

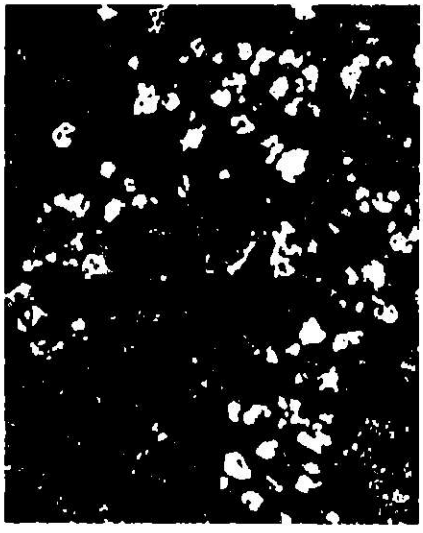

Cell RU-3

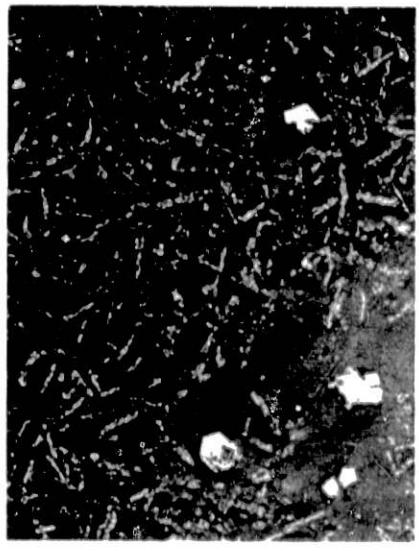

Cell RU-5

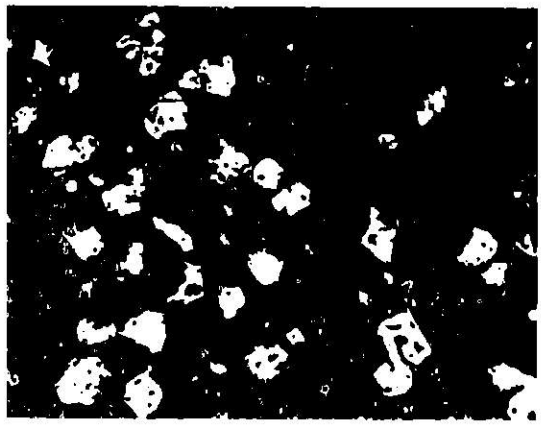

Cell RU-6

Fig. 2. Photomicrographs of Sulfide Electrodes (500X)

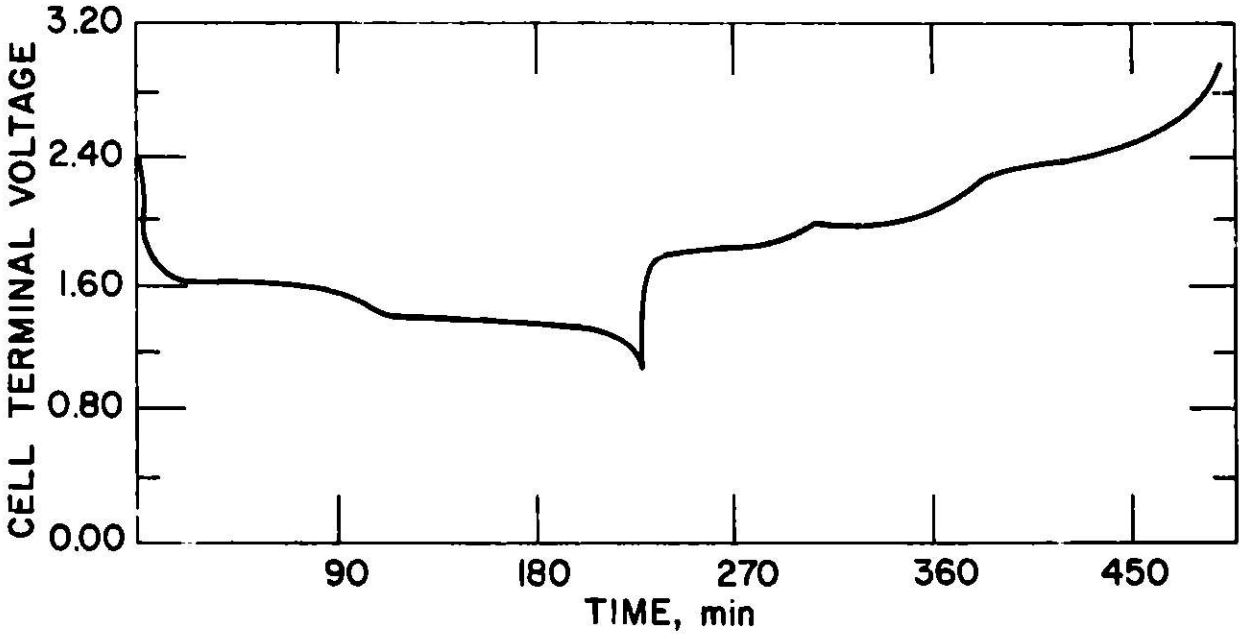

Fig. 3. Typical Discharge-Charge Curves for Cell RU-6

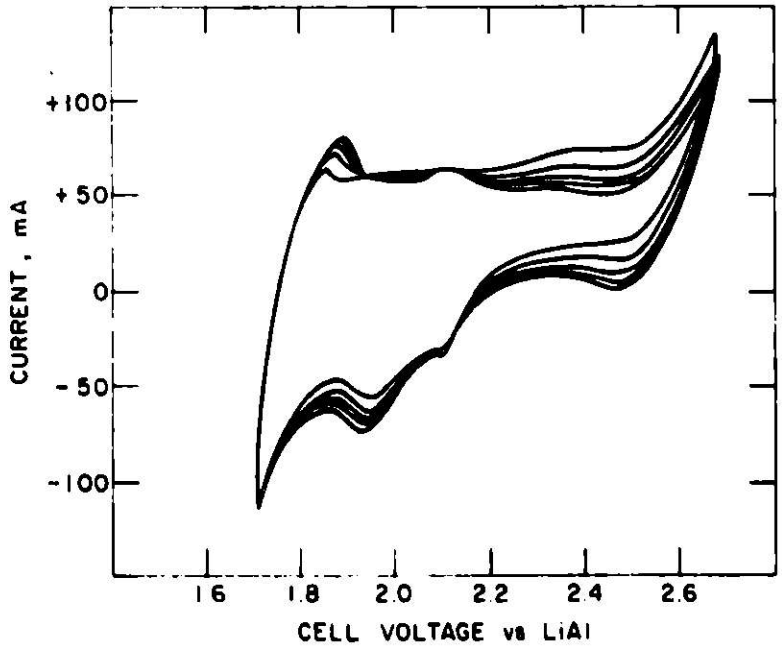

Fig. 4. Typical Voltammogram at 372°C

TABLE 4. Summary of Cyclic Voltammetry Data

Scan Rate, mV/sec	Voltage Range, V	Temp °C	Peak Potentials *vs.* Li-Al, V					
			Anodic			Cathodic[a]		
			1	2	3	1	2	3
3	1.70 - 2.69	372	1.88	2.09	2.46[b]	2.49	2.12[c]	1.94
6	1.70 - 2.69	372	1.89	2.10	2.42[b]	2.47	2.10	1.93
10	1.70 - 2.69	372	1.89	2.12	2.45[b]	2.47	2.10	1.93
20	1.70 - 2.69	372	1.89	2.15	2.46[b]	2.42	2.08[c]	1.95[c]
10	1.70 - 2.30	372	-	-	-	-	-	-
10	1.70 - 2.400	372	1.82[b]	2.06	-	-	-	-
10	1.70 - 2.50	372	1.83	2.06	2.40[b]	-	2.10[c]	-
10	1.70 - 2.60	372	1.83	2.06	2.38[b]	2.42	2.13	-
10	1.70 - 2.70	372	1.87	2.14	2.39[b]	2.37	2.12	1.96
10	1.70 - 2.70	372	1.89	2.12	2.45[b]	2.47	2.10	1.93
10	1.70 - 2.70	385	1.84	2.12	2.40[b]	2.43	2.15	1.97
10	1.70 - 2.70	391	1.87	2.14	2.39[b]	2.37	2.12	1.96
10	1.70 - 2.70	397	1.86	2.12	2.40[b]	2.42	-	1.96
10	1.70 - 2.70	403	1.85	2.12	2.40[b]	2.42	-	1.97
10	1.70 - 2.70	429	1.83	2.14	2.40[b]	2.39	-	1.95
10	1.70 - 2.70	430	1.84	2.12	2.35[b]	2.40	-	1.98
10	1.70 - 2.70	453	1.80[c]	-	2.35[b]	-	-	-

[a] A fourth cathodic peak, unrelated to overcharging of the FeS_2 electrode, is not listed.

[b] Onset of peak.

[c] Only a hint of a peak.

Effect of Scan Rate on Peak Positions. It became immediately obvious that scan rates of 100 mV/sec and higher would yield very little useful information. However, this fact alone establishes that a diffusion-limited process was occurring. Scan rates of 30, 20, 10, 6, and 3 mV/sec were also used at various temperatures. Scan rates greater than 10 mV/sec for a fixed temperature caused some peaks to be absent; scan rates below 10 mV/sec did not provide any additional details.

Increases in scan rate, as summarized in Table 4. had the effect of increasing the peak voltage *vs.* Li-Al on the anodic portions of the voltammograms, while decreasing the peak voltage *vs.* Li-Al on the cathodic portions. This effect was partially due to higher peak currents at the higher scan rates, and therefore, to a slightly higher ohmic voltage contribution. When this ohmic voltage contribution is eliminated, the effect of scan rate on peak position becomes negligible (for scan rates of less than 20 mV/sec).

Effect of Voltage Range on Peak Position. It became very obvious, at a fixed temperature and scan rate, that the voltage range had the most important effect on the FeS_2 electrode. Peaks could be made to appear or disappear by merely increasing or decreasing the voltage range scanned. The results, also shown in Table 4, indicate that peaks were absent until the voltage range scanned was between 1.70 and 2.40 V *vs.* Li-Al. Even in this voltage region, only two small anodic peaks could be observed. The corresponding cathodic peaks were still absent. It was only when the voltage range was between 1.70 and 2.70 V *vs.* Li-Al that all three cathodic and anodic peaks were observed. This result indicates that the two anodic peaks and the three cathodic peaks resulted from the main anodic reaction occurring close to 2.4 V *vs.* Li-Al. This effect of voltage range is shown in Fig. 5.

Species Responsible for Observed Peaks. The four cathodic peaks observed at the lower temperature (372°C) are identified in Fig. 6 and described below.

(1) The peak close to 1.74 V *vs.* Li-Al is not at all realted to overcharging the FeS_2 discharge electrode. It is merely the onset of the normal cell reaction

$$LiAl + FeS_2 \rightarrow Li_2S + Z$$

(2) The peak at about 1.95 V corresponds to the reduction of S_2^{2-} to S^{2-}.

(3) The peak at about 2.0 V corresponds to $2S + 2e^- \rightarrow S_2^{2-}$.

(4) The peak at about 2.4 V is a partial reversal of the overcharge reaction, *i.e.*, the reverse of $FeS_2 + 2Cl^- \rightarrow FeCl_2 + 2S + 2e^-$.

The three anodic peaks are identified as the following:

(1) The peak at about 2.4 V corresponds to the oxidation of FeS_2 by the reaction $FeS_2 + 2Cl^- \rightarrow FeCl_2 + 2S + 2e^-$.

(2) The peak at about 1.87 V corresponds to the oxidation of sulfide, S^{2-}, probably to S_2^{2-}.

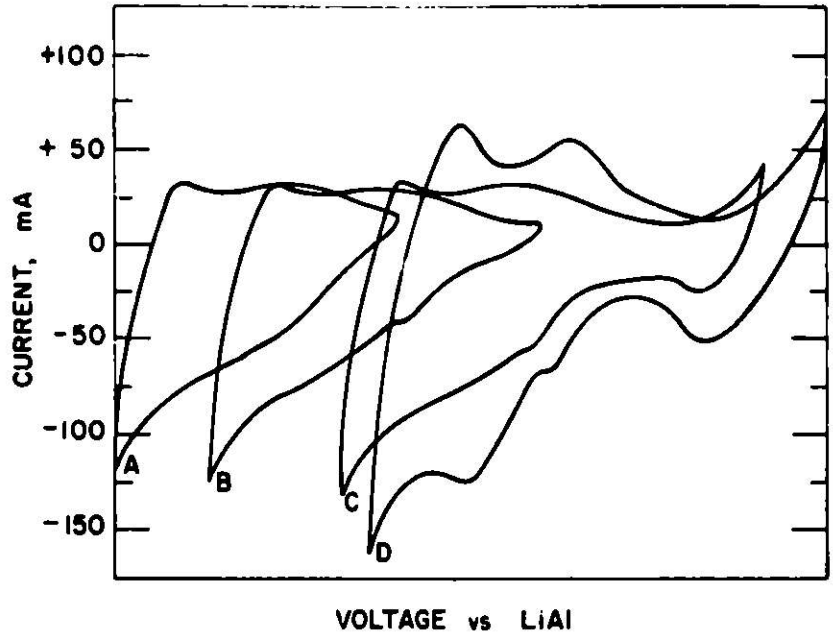

Fig. 5. Effect of Voltage Range on Peak Position (temperature, 372°C; scan rate, 10 mV/sec)

A = 1.70 - 2.30 V
B = 1.70 - 2.39 V
C = 1.70 - 2.59 V
D = 1.70 - 2.70 V

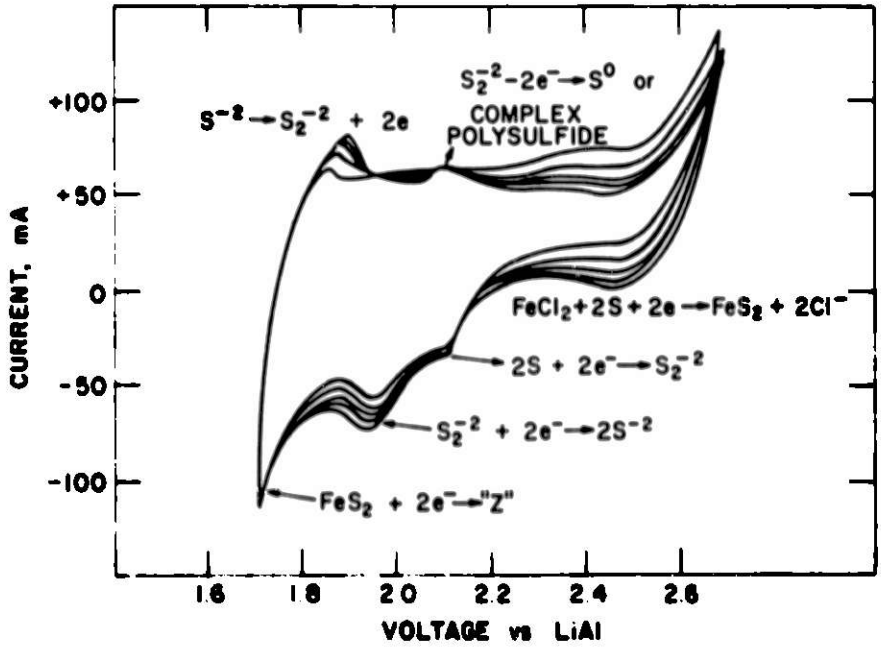

Fig. 6. Identification of Species Responsible for Observed Peaks

(3) The peak at about 2.15 V corresponds to the oxidation of S_2^{2-}, probably to sulfur or to a complex polysulfide of FeS_2.

The evidence for these assignments is the following:

The cell data have identified $FeCl_2$ as one of the products of overcharging the FeS_2 electrode. The formation of $FeCl_2$ at potentials is excess of 2.6 V *vs.* Li by the reaction

$$FeS_2 + 2Cl^- \rightarrow FeCl_2 + 2S \qquad (3)$$

is predicted by thermodynamic calculations.[8]

Controlled-potential electrolysis of the FeS electrode at a potential of about 2.72 V *vs.* Li-Al evolved a gaseous product. This gas was trapped by allowing it to react with 5-mil copper foil. Positive identification was obtained by X-ray that the reaction product was a sulfide of copper. Therefore, the evolved gas was deduced to be sulfur.

The cyclic voltammograms indicate that the anodic overcharge reaction is partially reversible, *i.e.*, the number of anodic coulombs is greater than the corresponding coulombs on the cathodic side (for the 2.4 V peak). This finding is consistent with the cell results in which a decrease in current efficiency was observed but the major sulfide phase was still FeS_2.

The cathodic peak at about 2.1 V *vs.* Li-Al cannot result from the reduction of $FeCl_2$. The potential for the reaction

$$FeCl_2 + 2e^- \rightarrow Fe + 2Cl^- \qquad (4)$$

is lower by about 0.3 V.[9] Therefore, the only species capable of being reduced at this potential must be sulfur. Additional evidence is that the open-circuit voltage of a LiAl/S cell is about 2.1 V. The likely species formed is S_2^{2-}, as determined by several workers.[10,11]

The cathodic peak at about 1.95 V must involve the reduction of the species formed above to form sulfide, S^{2-}. This conclusion was verified by an experiment in which solid Li_2S was added to the melt while the FeS_2 electrode was present. The effect of the Li_2S is shown in Fig. 7.

The anodic peak at about 1.87 V must represent the oxidation of sulfide, S^{2-}, because this peak also increased when Li_2S was added. The 1.87-V peak cannot be due to the X → Z transition because the cyclic voltammogram of the X phase, Li_2FeS_2, does not show this transition at this voltage (see Fig 8).

The anodic peak at about 2.1 V must involve the further oxidation of the species, probably S_2^{2-}, mentioned above. The most probably product is either free sulfur or a complex polysulfide described by previous authors.

A complex polysulfide of FeS_2 is likely. This conclusion is based on the experimental observation that, after the cycling studies had been completed, the electrolyte was extremely yellow. This could have only occurred if a complex species was being formed, since an additional out-of-cell test

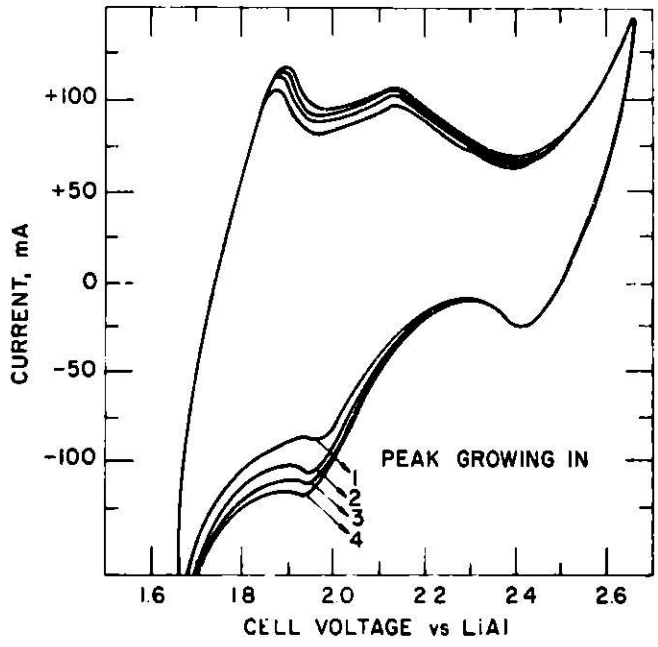

Fig. 7. Effect of Li_2S Addition to FeS_2 Electrode (temperature, 392°C; scan rate, 10 mV/sec)

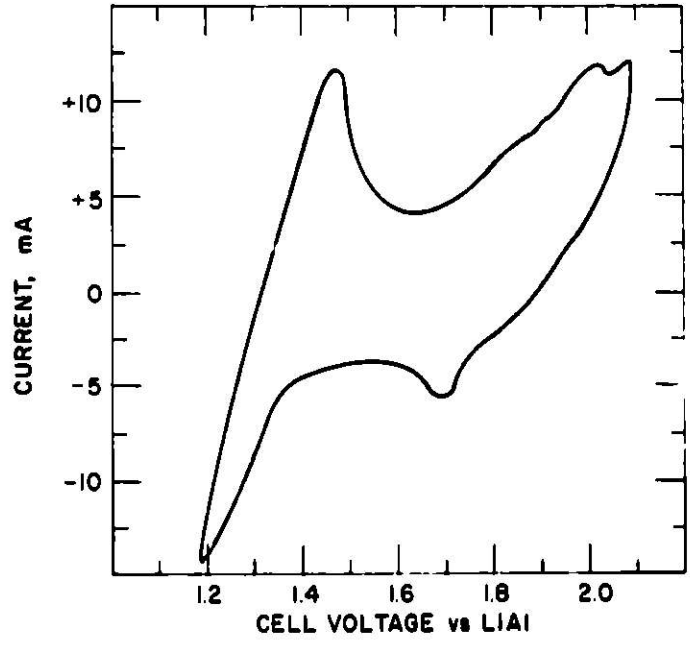

Fig. 8. Typical Voltammogram of X Phase (Temperature, 416°C; scan rate, 10 mV/sec)

to produce this color by heating FeS_2 plus the LiCl-KCl electrolyte failed to yield this color, but this same test did yield a highly yellow-orange solution when Li_2S was added.

The results of cyclic voltammetry and the cell studies indicate that the overcharge mechanism is, therefore, the oxidation of FeS_2 by the following reaction:

$$FeS_2 + 2Cl^- \rightarrow FeCl_2 + 2S + 2e^- \quad (5)$$

The reduction mechanism then becomes

$$FeCl_2 + 2S + 2e^- \rightarrow FeS_2 + 2Cl^- \quad (6)$$

$$2S + 2e^- \rightarrow S_2^{2-} \quad (7)$$

$$S_2^{2-} + 2e^- \rightarrow 2S^{2-} \quad (8)$$

SUMMARY AND CONCLUSION

The Li/LiCl-KCl/FeS electrochemical cell studies indicate that ferrous chloride and sulfur are formed at potentials in excess of 2.65 V *vs.* Li (2.35 V *vs.* Li-Al). In addition, these studies indicate that the effect of increasing the charge cutoff voltage resulted in an increase in the porosity of the sulfide electrode and an accompanying decrease in cell coulombic efficiency.

The cyclic voltammetry studies indicate the presence of three cathodic (reduction) peaks, one of which disappeared at temperatures in excess of 392°C. These studies also indicate that the overcharge reactions of the FeS_2 electrode are irreversible and are diffusion-limited.

The main cinclusion from these studies is that cell charging voltages in excess of 2.65 V *vs.* Li (2.35 V *vs.* Li-Al) cannot be used without overcharging the FeS_2 electrode. Occasional overcharge may not be extremely harmful; however, consistent overcharge will probably result in a marked decline in cell performance owing to the migration of both of the overcharge products to the Li (or Li-Al) electrode.

ACKNOWLEDGMENT

The authors would like to express their appreciation to Dr. J. R. Selman for fruitful discussion of the cyclic voltammetry results. Thanks are extended to B. S. Tani for performing the X-ray diffraction analyses and to T. W. Olszanski for help with the preparation of the Li-Al electrodes. Special thanks are extended to Dr. A. E. Martin for performing the metallographic examinations and for supplying the sample of the X phase.

The work reported in this paper was supported by the Energy Research and Development Administration (ERDA).

REFERENCES

1. E. J. Cairns *et al.*, *Galvanic Cells with Fused Salt Electrolytes*, ANL-7316, Argonne National Laboratory (1967).

2. H. Shimotake *et al.*, "Development of a Sulfur-Arsenic-Carbon Electrode for Lithium-Sulfur Cells," Electrochem. Soc. Meeting, Boston, Mass., Oct. 7-12, 1973, Abstract 13; Extended Abstracts, Vol. *73-2*, 38 (1973).

3. D. R. Vissers, Z. Tomczuk, and R. K. Steunenberg, J. Electrochem. Soc. *121*, 665 (1974).

4. A. E. Martin, Z. Tomczuk, and R. K. Steunenberg, "Changes in the Composition of FeS_2 Electrodes of Li/LiCl-KCl/FeS_2 Cells During Cycling," Electrochem. Soc. Meeting, New York, N. Y., Oct. 13-17, 1974, Abstract 54; Extended Abstracts of Battery Division, Vol. *74-2*, 132 (1974).

5. E. Peters and H. Majima, Can. Met. Quart. *7*, 111 (1968).

6. M. V. Smirnov and N. P. Podlesnyak, Zhur. Priklad. Khim. *43*, 1463 (1970).

7. C. Beusman, *Activity in the KCl-$FeCl_2$ and $LiCl$-$FeCl_2$ Systems*, ORNL-2323, Oak Ridge National Laboratory (1957).

8. *High Performance Batteries for Off-Peak Energy Storage and Electric Vehicle Propulsion, Progress Report for the Period January-June 1974*, ANL-8109, pp. 89-91, Argonne National Laboratory (1975).

9. J. Plambeck, J. Chem. Eng. Data *12*, 77 (1967).

10. J. R. Kennedy and F. Adamo, J. Electrochem. Soc. *119*, 1518 (1972).

11. J. R. Birk and R. K. Steunenberg, "Chemical Investigations of Lithium-Sulfur Cells," in *New Uses of Sulfur*, J. R. West, ed., Advances in Chemistry Ser. 140, pp. 186-202, Am. Chem. Soc., Washington, D. C., (1975).

A REVIEW OF THE KINETICS OF THE SULFUR ELECTRODE IN MOLTEN SODIUM POLYSULFIDE

Frank A. Ludwig
Research Staff, Ford Motor Company
Dearborn, Michigan 48121

Most investigations of electrode kinetics have been carried out in dilute solutions of the reacting species containing a supporting electrolyte, rather than from a pure melt of a salt of the redox system. However, for the sulfur/sulfide system there was strong interest in knowing the electrode kinetics in such a pure melt in conjunction with the development of the sodium-sulfur battery.

Some preliminary discussion of the pure melt as an electrochemical system is needed prior to an examination of the experimental data. These arguments are a further development of those previously proposed by Ludwig (1). It will be shown later in this review that a Na_2S_4 melt consists primarily of Na^+ and $S_4^=$ ions, that the entire anion concentration is electroactive, that $S_2^=$ ion is the product of reduction at the electrode, and that there is no chemical reaction prior to this charge transfer reaction. It will be further shown that the usual electroanalytical equations for diffusion control are obeyed within a few percent; and that the experimental errors of the measurements are within a few percent. How, then, do we perceive of diffusion in a pure binary salt? Furthermore, is it possible to prove that the usual electroanalytical diffusion equations should, indeed, apply to our special case?

With the constraints established so far, diffusion can occur only if the electrode reaction product and the reactant inter-diffuse. For a quantitative study of the nature of the diffusion coefficients of the reactant and product with respect to the electrode as a frame of reference, the methods of the thermodynamics of irreversible processes would have to be used (2). However, there is adequate justification for the direct application of the usual electroanalytical equations.

Crank (3) and others (4) have shown that interdiffusion in a two-component liquid, in which there is no volume change on mixing, yields $D_O = D_R = D_{OR}$ where O and R are the two components. Furthermore, the volume-fixed frame of reference is identical to the cell-fixed frame of reference. However, in the experiment under consideration, we are eliminating O and creating R in a reaction $O + 2e^- \rightarrow 2R$ ($S_4^= + 2e^- \rightarrow 2S_2^=$) at the electrode. The molar volume of Na_2S_4 is 1.5 times that of Na_2S_2. Therefore, we do not have a constant total volume and the volume-fixed frame (V) is moving with respect to the cell-fixed frame of reference (c). However, Sundheim (2) has pointed out that, under these conditions, $D^V_{OR} = D^c_{OR}$, and Dullien and Shemilt (4) have shown that using the diffusion equations without corrections for volume changes introduces small errors only. Laity (5) and Wagner (6) hold that interdiffusion in a mixture of two binary salts with a common ion in the presence of a potential gradient as well as a concentration gradient can still be expressed in terms of $D'_{OR} = D'_O = D'_R$ where D' values are "effective diffusion coefficients" containing averaged mobility terms.

The general theory of diffusion limited charge-transfer processes in electroanalytical techniques (7,8) assumes Fick's second law to be applicable to both species O and R, the effects of modes of mass transfer other than diffusion, e.g. electrical migration, to be negligible, and D_O and D_R to be independent of distance x from the electrode or time t. The polysulfide anions are similar enough so that ideality may be expected. Therefore, assuming ideality in conjunction with the preceding arguments regarding volume changes, D_O and D_R should be nearly independent of x and t. The essence of the interdiffusion

coefficient is that Fick's law applies to both species. It may seem that the requirement above of the independent applicability of Fick's second law to O and R is more general than it is in the pure melt case, where the concentrations of O and R are rigorously interdependent because of electroneutrality requirements. However, in both cases the forcing boundary condition is given by the charge transfer at the electrode where the rates of arrival and removal of diffusing ions are fixed (7,8). Therefore, we can treat the pure melt case like the general case with the influence of migration included in the effective diffusion coefficient.

Thus, the electroanalytical equations based on the simple Fick diffusion equations should be applicable to an electrochemically reacting pure binary salt. Small errors are expected. A rigorous mathematical treatment is called for in light of the surprisingly close fit of experimental data to the curves predicted by the general theory of diffusion limited charge transfer.

For an investigation of electrode kinetics, it is quite essential to know the ionic species present in the electrolyte. The DTA and x-ray diffraction results of Oei (9) and more recently, the laser-Raman spectroscopic results of Janz (10) indicate that $S_3^=$ in sodium polysulfide is not stable in the solid above 106 °C and, therefore, it is probably not stable at the higher temperatures of the molten state. Oei and Janz ascertained that above 106 °C Na_2S_3 disproprotionates into Na_2S_2 and Na_2S_4. The dissociation of polysulfide ions into ion radicals (S_2^- or S_3^-) in solutions in molten salts (11,12,13,14) and aprotic solvents (15,16,11,12) has been well documented. Preliminary e.s.r. measurements in molten sodium polysulfides show only very weak signals (17) between 300 and 400 °C. This and the mounting repression of this dissociation with increasing concentration make it most probable that the concentration of ion radicals in the undiluted polysulfide melt is extremely small.

Transference experiments by Cleaver and Davies (18) have shown that there is no free elemental sulfur in the melt, i.e., the melt contains Na^+ and polysulfide ions only. Thus the undiluted sodium polysulfide melts in the 300 °C-400 °C range contain mainly $S_2^=$, $S_4^=$, $S_5^=$ and some $S_6^=$, the relative amount of each depending on the overall composition. This assignment of distinct species to the melt is generally in accord with the results of Rosen and Tegman (19) and Cleaver and Davies (14). Tegman (19) relates sulfur vapor pressures to the relative amounts of the various polysulfide anions. However, the existance of the various anion species is hypothesized and the distribution curves for the amounts of the various species are empirically fitted to the pressure data. Tegman postulates that $S_3^=$ is present in appreciable amounts. Cleaver and Davies (14) determine the number of ions in dilute solution in KCNS by freezing point depression measurements.

The above conclusions concerning the species present in undiluted sodium polysulfide melts are fairly well founded. However, it would be desirable to obtain more direct evidence. The following discussion on sweep voltammetry does lead to some direct evidence in support of the above arguments.

Weber and Kummer (20) demonstrated that stable, steady state potentials are obtained at graphite electrodes in sodium polysulfide melts. Three separate groups have studied kinetics in the pure sodium polysulfide melts: Selis (21) South et al. (22) and Ludwig et al. (23). Selis worked on platinum and graphite electrodes, whereas the latter two groups worked at vitreous carbon electrodes. The experimental results, however, are quite similar and also do not seem to be influenced by origin or preparation method of the melt. The work of Selis (21) and of the other groups is clear evidence that the results of investigations with transient methods are independent of the electrode material used (graphite,

vitreous carbon, platinum) for reduction of the melt. As will be discussed, the kinetics of oxidation of the melt differs substantially at metal and carbon electrodes.

The salient feature of all voltage sweep diagrams is a clear distinction between the $S/S_x^=$, the $S_x^=/S_2^=$ and the $S_x^=/S^=$ reactions. In addition, the diagrams always show a final rise of current at large polarizations. Cathodically this rise represents the deposition of sodium (22). The final rise on the anodic side is more difficult to interpret. For lack of any other possibility and since the carbon electrodes do not seem to take part in the reaction, we can safely conclude that it is sulfur that is oxidized in this region to positive sulfur ions.

It is difficult to determine the kinetics of a process without knowing the concentrations of the diffusing species involved in the electrode reaction. Owing to our current inability to measure concentrations of individual ions in the melt, indirect means must be used to obtain the concentrations. In most electroanalytical techniques, the current is proportional to $CD^{1/2}$ (C is concentration and D is diffusion coefficient). The $CD^{1/2}$ values can be combined with $CD^{2/3}$ values from the rotating disc technique to separate C and D. South et al. (22) have combined chronopotentiometric and linear sweep voltammetric data to eliminate the $CD^{1/2}$ dependence and obtain an experimental value of the linear sweep current function for the primary reduction wave in Na_2S_3, Na_2S_4 and Na_2S_5 melts. They assumed a value of n = 2 for the number of electrons for the reaction. Rather than making this assumption, Ludwig uses their experimental value of $n^{1/2}\chi(at)$, where $\chi(at)$ is the current function in the sweep equation:

$$i = nFAC_o^b D_o^{1/2} v^{1/2} \left(\frac{F}{RT}\right)^{1/2} \pi^{1/2} n^{1/2} \chi(at)$$

$$\text{where} \qquad a = \frac{nFv}{RT} \ ,$$

v is the sweep rate, and C_o^b is the bulk concentration of the diffusing species. By using the experimental value $n^{1/2}\chi(at)$ and eliminating D by combining linear sweep (24)* and rotating disc (25) data for an Na_2S_4 melt at 300 °C, a value of nC_o^b = 30 moles/liter is obtained (24). Since the concentration of $S_4^=$ is only 11 moles/liter, we state that the reaction is a two electron reaction in which the entire concentration of $S_4^=$ in the melt is reacting. The choice of n = 2 rather than n = 3 and the claim that $S_4^=$ is the reacting species rather than a disproportionation product of $S_4^=$ will be supported later in this review. First some additional experimental details should be examined. The determination of nC permits a calculation of an effective D; this value is 3×10^{-7} cm^2/sec (24). This value seems low for fused salts, however the viscosity of the melt of 40 cp is much larger than the range of 0.5-5.0 cp for most fused salts (26), and the size of the $S_4^=$ ion is larger than that of most fused salt ions (27). The D can be estimated from the equivalent conductance of the melt using the Nernst-Einstein equation. A 10-50% increase of D over that calculated is usually required in the application of this equation for molten salts (2); a value of $D = 7\text{-}9 \times 10^{-7}$ cm^2/sec is obtained (24). The equivalent ionic conductivity used in the equation was calculated from the equivalent conductance of the melt (28) and the estimated ionic radii of Na^+ and $S_4^=$ (27). The calculated D is in good agreement with the experimentally determined effective D.

---

* It would be advantageous to combine chronopotentiometric data directly with rotating disc data to determine nC and D. The chronopotentiometric equation:

$$i\tau^{1/2} = 1/2\ \pi^{1/2} nFCD^{1/2}$$

The n, D and C values given above were for the reduction of an Na_2S_4 melt at 300 °C. The reduction reaction is designated by peak A in the cyclic sweep shown in Figure 1 (23). The sweep begins in the cathodic direction from the rest potential at a vitreous carbon (VC) electrode of 0.00407 cm^2 area. All sweep curves which will be discussed begin from the rest potential. Those cases in which diagnostic information is gained by starting a sweep at a potential other than the rest potential or holding a sweep at a certain potential will be specified. Because of the very high current densities involved, care was taken to surround the working electrode with the counter electrode to insure uniform current distribution over the working electrode. Differential conductance measurements were taken during the sweep as shown in Figure 1 by superimposing a small amplitude a.c. signal on the triangular sweep, at frequencies between 1592-10,000 Hz. The faradaic impedance has dropped to about 1% of the melt resistance at 1592 Hz (24). We will later return to these differential melt conductance data; at this time we point out the constancy of the conductance from the beginning of the wave to the wave peak A. The melt resistance remains constant during the sweep. This is an important point because of the desirability of having a truly constant sweep rate in order to obtain good quantitative data. The increase of current in Figure 1 is seen to be nearly linear with potential for wave A. Thus di/dt as well as dE/dt are constant and the iR drop can be used directly to correct the sweep rate. Because of the high current densities observed, this iR drop correction must be extremely accurate, since a Luggin capillary cannot be brought close enough to the electrode to make the correction small. The counter-electrode was large enough that it did not polarize, and it was therefore also used as the reference electrode. Both current interruption and a.c. impedance techniques were used to measure the resistance. The values agreed within a few percent. However, the exchange current for the reduction process was determined by an independent transient technique and found to be very rapid (30). Since the peak potential for a reversible wave is independent of sweep rate, observed peak potential was plotted against peak current, as shown in Figure 2, and the slope was interpreted as the resistance of the melt, with the intercept being the true peak potential, E_p. This resistance was in close agreement with the interrupt values and slightly higher than the a.c. impedance values. Using the value of the resistance from Figure 2 to obtain a corrected sweep rate, the plot of Figure 3 was obtained (23). The linearity of the plot is indicative of simple diffusion control without any complications from coupled chemical reactions. The data of South et al. (22) shown in Figure 4 were taken over a much more limited sweep rate range and show an upturn at low sweep rates for Na_2S_4 and Na_2S_5. They interpret this increase in current function as indication of a following chemical reaction in which sulfur in the melt reacts with the reduction product, Na_2S_2 to reform the original polysulfide (for the sequence $O + e^- \rightarrow R$, $R + Z \rightarrow O$, Nicholson and Shain (8) term the chemical reaction "catalytic" since the rate of reaction is enhanced because of the regeneration of O). Our data in Figure 3 do not indicate an upturn at low sweep rates. Indeed, South et al. also mention that below 0.01 V/sec the major portion of the cathodic curve no longer decreases in current. This strongly suggests that at these slow rates, the onset of convection could easily account for the

---

does not contain a separate proportionality constant, as does the linear sweep equation. At the time of writing, chronopotentiometric data were available only at 350 °C, rotating disc data only at 300 °C, whereas linear sweep data existed at both temperatures. Very recently, rotating disc data by Armstrong, et al. (29) at 305° and 350 °C has been published. The effect of their data on the above calculations will be discussed in the talk.

constant current, and the apparent increase in current function for Na_2S_4. The steeper rise for Na_2S_5, we feel, is partly due to convection but also in accord with the criteria for a catalytic step (8). We ascribe the catalytic reaction to: $Na_2S_2 + 2Na_2S_5 \rightarrow 3Na_2S_4$. As will be shown, both Na_2S_4 and Na_2S_5 give very similar reduction waves. In other words, Na_2S_5 can react with Na_2S_2 to regenerate more reactant, but Na_2S_4 and Na_2S_2 could only give Na_2S_3, whose existence in the melt is doubtful; therefore, we would not expect a catalytic step for Na_2S_4. South et al. (22) conclude that Na_2S_2 reacts with elemental sulfur because they measured sulfur activities in the melt of 0.9 in Na_2S_5, 0.2 in Na_2S_4, and 0.04 in Na_2S_3, based on unit activity for pure sulfur, which is in equilibrium with a composition of approximately $Na_2S_{5.2}$ at 350 °C. However, these activities do not necessarily mean that the sulfur exists as a free element in the melt. According to the previously mentioned transference experiments of Cleaver and Davies (18) it does not.

South et al. also suggest that the reduction wave represents the reduction of polysulfide rather than sulfur, because the heights of the waves in the three melts are nearly the same, whereas the activities of sulfur vary significantly.

The i_L^{-1} vs. $\omega^{-1/2}$ linearity of the rotating disc data shown in Figure 5 is specific to a first order reaction. The zero intercept is confirmation that the charge transfer rate is very high. The data in Figures 3, 4 and 5 have been shown to indicate the close experimental agreement with theory and the apparently high experimental accuracy that can be attained in the measurements. Thus, even though the $CD^{1/2}$ vs. $CD^{2/3}$ comparison involves a 1/6 power dependence, the data seems reliable enough to yield a value of D and C which should not exceed the error implied in the C = 11 vs. C = 15 moles/liter comparison made earlier. With constant use of the vitreous carbon electrode for either anodic or cathodic sweeps, a slow change in the availability of surface sites for reaction is obtained. This available area is very easily ascertained by conductance measurements (as illustrated in Figure 1) at the open circuit potential (OCV). The original conductance can be regained by holding the potential at voltages more negative than 0.9 V vs. the OCV for approximately one minute. During this time, the current increases rather than decreases. The reduction at these more negative voltages in KCNS solutions has been shown (31) to be reduction to Na_2S. Probably the tetrasulfide is reduced in steps to $S^=$ with the $S_2^=$ existing as an intermediate. South et al. (22) have also found a decrease in film resistance at these negative potentials and attribute this to a more rapid dissolution of Na_2S than Na_2S_2 in the bulk melt (however, see text accompanying Figure 9). If quantitative kinetic data are being sought, great care must be taken to renew the surface periodically as described, and to keep the conductance between 85-95% of the fresh surface value.

So far, it has been proposed that wave A in Figure 1 is due to a reversible, two-electron reduction of first order, uncomplicated by chemical reactions. At 300 °C, $E_p - E_{1/2}$ for a two electron reaction should be only 0.027 volts (8). An $E_p - E_{1/2}$ of 0.059 volts is observed. This strongly suggests a two step charge transfer process with superposition of two reversible waves (36). The reverse oxidation wave labeled D in Figure 1 extends over the same voltage range (-0.25 to 0 volts) and is of the same peak height as wave A. If the potential is held constant for 30-60 seconds at values between -0.25 and -0.35 V the peak current, i_p, of wave D is not altered; thus the oxidation process is not coupled with a chemical reaction. Double-pulse galvanostatic (32) and current impulse relaxation techniques (33) gave very high values for the exchange current for the first reduction wave (34) (Figure 6). Chronocoulometric experiments gave a value of

1 A/cm^2 for the total two-step charge transfer at 300 °C (30). The results for the first reduction wave were based on potential excursions of a few millivolts, whereas the result for the total two-step charge transfer came from cathodic potential steps up to 400 mV.

As shown in Figure 1, the differential conductance remained quite constant on the cathodic sweep until after peak A. The abrupt drop is interpreted as resulting from the formation of an insoluble, partially blocking layer of Na_2S_2. Calculations based on experimental values of the faradaic capacitance and faradaic resistance show that neither the Warburg nor the charge transfer resistance change abruptly enough with potential to account for the sudden decrease in conductance (24). There is no evidence to date from any of the experimental techniques of the extent of monolayer adsorption, and therefore the nature of the blocking layer cannot be specified. As shown in Figure 1, when the cathodic sweep is reversed, a potential is reached at which the Na_2S_2 redissolves, the conductance increases, and a cathodic spike occurs due to reduction of Na_2S_4 at the more negative potential suddenly imposed on the electrode by the absence of the blocking layer. As the sweep continues in the positive direction, a rapid change from reduction to oxidation occurs as the material which was precipitated is oxidized. A current akin to a stripping current is obtained. The potential at which the Na_2S_2 begins to be oxidized coincides with the equilibrium potential for the saturated melt, further identifying the solid phase as Na_2S_2. This can be clearly seen by comparing data from Figures 7 and 8. The potential difference between (solid Na_2S_2/liquid melt) and (liquid S/$Na_2S_{5.2}$ liquid melt) is 0.32V at 340 °C, as shown by the potential difference between the horizontal lines in Figure 7 (35). An iR corrected plot of sweep curves for compositions $Na_2S_{3.0}$, $Na_2S_{4.0}$ and $Na_2S_{5.2}$ is shown in Figure 8 (23). The three curves all superpose on the reverse sweeps at -0.3 volt vs. $Na_2S_{5.2}$, indicating that the precipitated Na_2S_2 from the three reduction processes redissolves at the potential of the Na_2S_2-saturated melt. Peak A occurs at about the same potential in the three melts, suggesting a common reduction process. The $Na_2S_{3.0}$ wave occurs over a narrower potential range. The rest potential in Na_2S_3 is negative enough so that only the second wave of the two-step reduction occurs. And, in fact, the current function for a two-electron reversible $Na_2S_{3.0}$ reduction agrees with the theoretical value within a few percent, as shown by South et al. (22). It now becomes clear why the experimental values of the current funcation for Na_2S_4 and Na_2S_5 found by South et al. are less than the theoretical value for a two-electron wave; namely, the theoretical current function for superposed waves for two consecutive one-electron steps separated by -90 millivolts is 0.75 (sign according to Polcyn and Shain (36)). This value compares with the 1.26 value for a two-electron single step wave with the $n^{3/2}$ factor included. The experimental value of the separation for the two waves for Na_2S_2 and Na_2S_5 is about -90 millivolts (24) when reduced to 25 °C, and therefore the current function should be about 0.75. Using the data of South et al. (22) the value for Na_2S_5 is 0.67 and for Na_2S_4, 0.87. The fact that the Na_2S_3 is proposed to by an equimolar mixture of Na_2S_2 and Na_2S_4 is well supported by the data in Figure 8. The wave occurs at the same peak potential as the Na_2S_4 wave, and its peak current is less.

It is because of the two-step nature of the reduction wave that we can be quite certain that the chemical disproportionation, $S_4^= \rightarrow 2S_2^-$ followed by the one step reduction of S_2^- to $S_2^=$, is not the reaction mechanism. In the mechanism proposed below, $S_4^=$ is written as $^-S_2$-S_2^- for convenience only. The reader is referred to Giggenbach (37) and Allen (38) for a discussion of the various resonance forms, electronic configurations and bond energies of the

tetrasulfide ion. The reaction proposed may proceed as a concerted reaction as written, or the bond may break forming $S_2^{=}$ and S_2^{-} with the second electron then adding to the radical anion:

For Na_2S_4 and Na_2S_3

$$^{-}S_2 - S_2^{-} + e^{-} \rightleftarrows {}^{-}S_2 \cdots S_2^{=}$$

$$^{=}S_2 \cdots S_2^{-} + e^{-} \rightleftarrows 2S_2^{=}$$

For Na_2S_5

$$^{-}S_3 - S_2^{-} + e^{-} \rightleftarrows {}^{-}S_3 \cdots S_2^{=}$$

$$^{=}S_2 \cdots S_3^{-} + e^{-} \rightleftarrows S_2^{=} + S_3^{=}$$

$$2S_3^{=} \rightarrow S_2^{=} + S_4^{=}$$

The cathodic peak B in Figure 1 does not appear to be due to a separate reaction. If the cathodic sweep is stopped in the trough after peak A and before peak B, the current rises to the level of peak B and then slowly falls. Apparently, wave B is produced by a reorganization in the blocking Na_2S_2 layer, which causes a temporary decrease in resistance. This is not apparent in the slower response of the autobalancing technique used with the a.c. bridge differential conductance measurements shown in Figure 1, but becomes quite clear with the faster response obtained when a lock-in amplifier was used to make differential conductance measurements, as shown in Figures 9 and 10 (23). The rise in conductance at -1.0 volt represents the reduction to Na_2S discussed previously.

Occasionally at 0.01 V/sec sweep rate a wave C would begin at -1.0 volt in agreement with the data of South et al. (22). It obviously is involved with the reduction to Na_2S. In Figure 9 the conductance but not the sweep data show the effect of the reduction. Apparently the reduction is occurring without the formation of a wave; instead of the current decreasing in the cathodic direction because of the thickening Na_2S_2 layer blocking the access of Na_2S_4, the current remains fairly constant due to the reduction to Na_2S. The expected chemical reaction, $2S^{=} + S_4^{=} \rightarrow 3S_2^{=}$ apparently results in a precipitation of Na_2S_2. The chemically produced Na_2S_2 probably does not block the electrode as effectively as the electrochemically produced Na_2S_2.

The data in Figure 10 for $Na_2S_{5.2}$ are similar to those of Figure 9, except that the differential conductance does not decrease very much after the reduction peak, probably because of the reaction $S_2^{=} + 2S_5^{=} \rightarrow 3S_4^{=}$ discussed previously.

The anodic wave producing peak E in Figure 1 represents the oxidation of tetrasulfide to sulfur. The differential conductance data indicate the formation of a blocking sulfur layer (see also Figures 9 and 10). The height of the peak compared to peak A is in excess of that expected for a two electron wave with a normal current function. However, the value of the current function (i.e., $i_p/v^{1/2}$) falls with increasing sweep rate. This suggests a following chemical reaction based on the removal of sulfur from the electrode. The net electrochemical and chemical reactions are postulated to be (23):

$$S_4^{=} \rightleftarrows S_4 + 2e^{-}$$

$$S_4 + 2S_4^{=} \rightarrow 2S_6^{=}$$

$$S_4 + 4S_4^{=} \rightarrow 4S_5^{=}$$

The $S_5^=$ can be further electro-oxidized and in this respect the reaction is partially catalytic (8). However, the two chemical reactions and the electro-oxidation of $S_5^=$ can proceed only to an overall composition of $Na_2S_{5.2}$, the composition of polysulfide phase in equilibrium with a separate liquid sulfur phase in the temperature range of interest. The species S_4 and $S_6^=$ were chosen because of their proposed existance in liquid sulfur (39) and polysulfides (40), respectively. The length of the sulfur and polysulfide chains could just as well remain unspecified (e.g., S_2 is known to exist in the liquid state) without altering the kinetic interpretations.

The important aspect of the anodic reaction is not the catalytic part, but the removal of the sulfur by chemical reaction. At faster sweep rates, the slower chemical reactions cannot remove the sulfur and therefore $i_p/v^{1/2}$ decreases with sweep rate. Thus the peak current does not represent a diffusion controlled process but a process of a chemical reaction removing a blocking layer. This is why peak E shows erratic current flow. Furthermore, at fast sweep rates, where the chemical reaction is too slow to remove the sulfur and form soluble ions, little diffusion can occur. The reaction product, sulfur, is immiscible in the melt, and the product cannot dilute the reactant. Therefore the current increases with little concentration polarization, the slope of the i/E curve being nearly equal to the conductance of the melt. The current peak is determined by the blocking of the electrode by sulfur. On the reverse sweep, the sulfur layer disappears at +0.4V and the trace nearly superimposes over the forward trace (23) (Figure 11). A possible explanation of the slight separation of the forward and reverse trace is that some diffusion is taking place. This diffusion may be due to a small amount of chemical reaction with the sulfur, as discussed previously.

In Figure 12 (23), a partial pre-oxidation of lower polysulfides to higher polysulfides is observed prior to the oxidation to sulfur. The quantity of charge should increase from Na_2S_5 to Na_2S_3, as evident in Figure 12. The difference in the peak currents at the slower sweep rate shown in Figure 12 is an indication of the difference in chemical reaction rate of sulfur with $S_2^=$ (in Na_2S_3), $S_4^=$ and $S_5^=$ (23). In support of this rate sequence is the observation that if the sweep is stopped at the anodic limit, then the sulfur layer covering the electrode is removed only slowly in Na_2S_5 (determined by the slow drift of the OCV back to the original OCV). The drift rate back to the original OCV varies in the order $S_2^= > S_4^= > S_5^=$. Note also that the current in the return sweep in the sulfur saturated Na_2S_5 melt exceeds the current in the forward sweep in Figure 12. This is probably due to convective flow, the density of sulfur being less than the density of Na_2S_3, Na_2S_4 or Na_2S_5. Finally, at the intermediate sweep rate of 0.1 V/sec of Figure 12, the conductance data clearly show that, when the electrode is suddenly blocked by sulfur, the current falls (Figures 9 and 10); the current for Na_2S_3 remains high for a long time (Figure 12) and the conductance does not fall until the current begins to drop. At high sweep rates when the sweep is in the cathodic direction first or the potential is held at the cathodic potential of peak A prior to the anodic sweep, a new peak F appears (23,24) shown in Figure 13 (compare with Figure 11). The oxidation peak of Na_2S_2 is absent, probably because the sweep rate is in excess of the dissolution rate of Na_2S_2 in the melt. However in keeping with the same sequence of chemical reaction rates noted above for sulfur with the polysulfides, we would expect solid Na_2S_2 or Na_2S on the electrode surface to react very rapidly with the sulfur formed on the electrode. Thus peaks E and F may be postulated to be like an ECE mechanism, with $S_4^=$ remaining adsorbed on the electrode:

$$S_4^{=} \rightleftharpoons S_4 + 2e^-$$

$$2S_2^{=}(ads) + S_4 \rightarrow 2S_4^{=}(ads)$$

$$S_4^{=}(ads) \rightarrow S_4 + 2e^-$$

South et al. (22) state the $i_p/v^{1/2}$ was constant with sweep rate for their anodic peaks, whereas we found $i_p/v^{1/2}$ decreased. They state that in Na_2S_4 $i_p/v^{1/2}$ was more than twice the value obtained for the cathodic results, and in Na_2S_5 it was less than half the corresponding cathodic value. We suggest their sweep rate range, 10 mv/sec to 50 mv/sec, was too limited for a good conclusion concerning the constancy of $i_p/v^{1/2}$ with sweep rate; also that their observations on the $i_p/v^{1/2}$ comparisons to the cathodic values are a proof of the chemical reaction rates we proposed, since if the anodic process were diffusion controlled, the $i_p/v^{1/2}$ values would be in closer agreement for Na_2S_4 and Na_2S_5 and would also agree more closely with the cathodic values; and finally that an electrode surface which was not restored to its virgin state and remained coated with Na_2S_2, for example, would show the effect of the more rapid chemical reaction of sulfur with Na_2S_2, and $i_p/v^{1/2}$ would not drop as rapidly with increasing sweep rate. The only high sweep rate data obtained by South et al. were a few cyclic sweeps. These data were not used in their $i_p/v^{1/2}$ plots, but do show a large decrease in $i_p/v^{1/2}$ for the anodic peak (22). They also mention that their anodic chronopotentiometric results were not in accord with the Sand equation.

If sulfur is deposited on the electrode anodically, in the following cathodic sweep (Figure 14) a wave suggesting a catalytic mechanism is obtained (1,23):

$$S_4^{=} + 2e^- \rightleftharpoons 2S_2^{=}$$

$$2S_2^{=} + S_4 \rightarrow 2S_4^{=}$$

where the first reaction is the two step charge transfer discussed previously. The second step, identical to that discussed for the anodic peaks, is a pseudo-first order reaction in which the activity of sulfur is constant because of its presence as a separate phase. The cathodic wave in Figure 14 is in accord with the Nicholson-Shain criteria (8) for a catalytic reaction. The main features are the increased cathodic current, the presence of a limiting current rather than a current peak, the lack of hysteresis on the reverse sweep, and the return to the normal peak A at fast sweep rates. The breakup of the blocking sulfur layer can be seen as a small blip at -0.1 volt (confirmed also by a rise in conductance to about half the value at the virgin electrode). The first order rate constant is 0.2 sec^{-1}, calculated on the basis of the ratio of the limiting kinetic current to the pure diffusion current (8) for peak A. The value of this rate constant can be of direct importance to the understanding and designing of the sulfur electrode in the sodium-sulfur cell. Sixty percent of the discharge capacity of the cell involves discharge from a two phase $S/Na_2S_{5.2}$ melt, therefore the catalytic reduction mechanism just described is operative.

In order to determine the conditions under which cell electrodes might become blocked with sulfur layers, a vertical graphite rod electrode suspended

in a large volume of $Na_2S_{5.2}$ melt at 320° was operated at various anodic constant current levels (24). The experiment was repeated in an $Na_2S_{4.7}$ melt. The results are shown in Table I.

TABLE I
DURATION OF LOW POLARIZATION. CONSTANT CURRENT AT 320 °C
ON GRAPHITE (ULTRA CARBON CORP. UF4S)

$Na_2S_{5.2}$ + S		$Na_2S_{4.7}$	
Current (ma/cm^2)	Time (minutes)	Current (ma/cm^2)	Time (minutes)
5.0	1230	17.5	1188
10.0	25	25.0	84
15.0	12	63.5	4

The polarization was negligible at the graphite electrodes for the time periods shown. Then within seconds the polarization increased to 15 volts, the limit of the constant current power supply. On some of the voltage traces, the final period before the blocking layer formed showed small irregular blips, indicating convective removal of sulfur. The initial negligible polarization in both melts and the higher current levels in the $Na_2S_{4.7}$ as compared with those in $Na_2S_{5.2}$ are in accord with the kinetic observations made with respect to Figure 12. The sudden blocking of the electrode is in accord with the observation previously mentioned that the electrode surface slowly becomes less active. At OCV the blocking sulfur layer disappeared in minutes, but it took many hours before the graphite recovered its activity. If the constant current experiments were repeated before full recovery of activity, the time period prior to the sudden blocking was considerably shortened. Polarizations approaching -1.0 volt tended to hasten the recovery of the electrode but the effect was not nearly as dramatic as that at the vitreous carbon microelectrode discussed previously.

A vertical stainless steel rod electrode under the same experimental conditions in $Na_2S_{5.2}$ at 320 °C was operated at 500 ma/cm^2 for 20 hours at negligible electrode polarization (24). No blocking layer developed, nor did the electrode corrode. Stainless steel appears to be anodically protected in the polysulfide melts rich in sulfur; just as stainless steels can be anodically protected in aqueous media.

A preliminary explanation for the anodic results at stainless steel compared with graphite in the two-phase region may be found in the different wicking and wetting characteristics of the two materials. Contact angles were measured for molten sulfur and Na_2S_4 on graphite, vitreous carbon and AISI 446 stainless steel (24). The results on the metal surface were independent of the surface preparation of the metal (i.e., etched in HCl, oxidized in air at 800 °C, untreated or freshly abraded). In a helium atmosphere at 318 °C, the contact angles for Na_2S_4 were approximately: on graphite, 100°; on vitreous carbon, 100°; on stainless steel, 0-5°; in helium at 282 °C, the contact angle for sulfur on all three materials was 20-30°. Over the period of 45 min., the contact angle for Na_2S_4 changed only on the vitreous carbon, going from 100° to 70°. These data are preliminary estimates, since the molten materials were not in equilibrium with their vapors and since no attempt was made to clearly define the difference between advancing and receding contact angles. Furthermore, the effect of potential on contact angle was not obtained. However, the difference in wetting of the metal and the graphite by Na_2S_4 is so extreme, that it is likely that the metal does not become blocked by sulfur at anodic potentials because

it is not preferentially wetted by sulfur.

More work is needed on the nature of the sulfur/carbon interaction. It is hoped that further experimental work will yield values for the extent of surface coverage θ by sulfur on graphite and vitreous carbon electrodes. The observed time-dependent blocking of the electrode is reminiscent of passivation effects observed in other systems. The adsorption-desorption kinetics of sulfur on various electrode surfaces are undoubtedly complex. The wetting observations made above provide only a preliminary approach to the problem.

The author gratefully acknowledges the support of NSF-RANN for this work and the encouragement given by S. A. Weiner; also the helpful discussions with D. A. Aikens of Rensselaer Polytechnic Institute and with my colleagues R. W. Minck and especially R. P. Tischer.

1. "Research on Electrodes and Electrolyte for the Ford Sodium-Sulfur Battery," Annual Report for Period June 30, 1973 to June 29, 1974, (July, 1974), National Science Foundation, Contract #NSF C-805 (AER-73-07199).
2. B. R. Sundheim, "Fused Salts," McGraw-Hill, New York (1964).
3. J. Crank, "The Mathematics of Diffusion," Oxford University Press, New York (1956).
4. F. A. L. Dullien and L. W. Shemilt, Trans. Farad. Soc. 58, 244 (1962).
5. R. W. Laity, J. Phys. Chem. 67, 671 (1963).
6. C. Wagner, in W. Jost, "Diffusion in Solids, Liquids, Gases," Academic Press, New York (1952).
7. W. H. Reinmuth, Anal. Chem. 34, 1446 (1962).
8. R. S. Nicholson, I. Shain, Anal. Chem. 36, 706 (1964).
9. D. G. Oei, Inorg. Chem. 12, 438 (1973).
10. G. J. Janz in "Research on Electrodes and Electrolyte for the Ford Sodium-Sulfur Battery," Annual Report for Period June 30, 1974 to June 29, 1975 (July 1975), National Science Foundation, Contract NSF C-805; to be published in Inorg. Chem.
11. T. Chivers, Nature 252, 32 (1974).
12. T. Chivers and I. Drummond, Chem. Soc. Rev. 2, 233 (1973).
13. J. Greenberg, B. R. Sundheim and D. M. Gruen, J. Chem. Phys. 29, 461 (1958); cf. also D. M. Gruen, R. L. McBeth and A. J. Zielan, J. Am. Chem Soc. 93, 6691 (1971).
14. B. Cleaver, A. J. Davies, Electrochimica Acta, 18 741 (1973).
15. T. Chivers and I. Drummond, Inorg. Chem. 11, 2525 (1972); J. Chem. Soc., Dalton, 1974, 631.
16. F. Seel and H. J. Güttler, Angew. Chem. 85, 416 (1973); Angew. Chem. Internat. Edit. 12, 420 (1973).
17. J. Gerlock, Ford Motor Co. personal communication. See also W. Giggenbach, Inorg. Chem. 10, 1308 (1971), and T. Chivers, I. Drummond, Chem. Soc. Rev. 2, pp. 239, 240, 242 and 244 (1973).
18. B. Cleaver and A. J. Davies, Electrochimica Acta 18, 733 (1973).
19. E. Rosen, R. Tegman, Chemica Scripta 2, 63 (1972).
20. N. Weber, J. T. Kummer, "Advances in Energy Conversion Engineering," Am. Soc. Mech. Eng., New York (1967).
21. S. M. Selis, Electrochimica Acta 15, 1285 (1970).
22. K. D. South, J. L. Sudworth, J. G. Gibson, J. Electrochem. Soc. 119 554 (1972).
23. F. A. Ludwig, R. P. Tischer, D. A. Aikens, K. W. Fung, Extended Abstracts #386, 147th Meeting, The Electrochem. Soc., May (1975).
24. F. A. Ludwig, unpublished data.
25. M. A. Dzieciuch, Ford Motor Co., personal communication.

26. B. Cleaver, A. J. Davies, Electrochimica Acta 18, 727 (1973).
27. S. C. Abrahams, J. L. Bernstein, Acta. Cryst. B25, 2365 (1969).
28. B. Cleaver, A. J. Davies, M. D. Hames, Electrochimica Acta 18, 719 (1973).
29. R. D. Armstrong, T. Dickinson, M. Reid, Electrochimica Acta 20, 709 (1975).
30. K. W. Fung, D. A. Aikens, F. A. Ludwig, R. P. Tischer, unpublished data.
31. D. A. Aikens, K. W. Fung, F. A. Ludwig, R. P. Tischer, unpublished data.
32. H. Gerischer and M. O. Krause, Z. Phys. Chem. N.F., 10, 264 (1957); 14, 184 (1958); H. Matsuda, S. Oka, P. Delahay, J. Am. Chem. Soc. 81, 5077 (1959).
33. W. D. Weir, C. G. Enke, J. Phys. Chem. 71, 275 (1967).
34. N. K. Gupta and R. P. Tischer, unpublished data.
35. N. K. Gupta and R. P. Tischer, J. Electrochem. Soc. 119, 1033 (1972).
36. D. S. Polcyn, I. Shain, Anal. Chem. 38, 370 (1966).
37. W. Giggenbach, J. Inorg. Nucl. Chem. 30, 3189 (1968); J. Chem. Soc., Dalton, 729 (1973).
38. T. L. Allen, J. Chem. Phys. 31, 1039 (1959).
39. B. Meyer, T. Strayer-Hansen, D. Jensen, T. V. Oommen, J. Amer. Chem. Soc. 93, 1034 (1971); B. Meyer, T. V. Oommen, D. Jensen, J. Phys. Chem. 75 912 (1971).
40. R. Bonnaterre and G. Cauquis, J. Chem. Soc., Chem. Commun. 293 (1972).

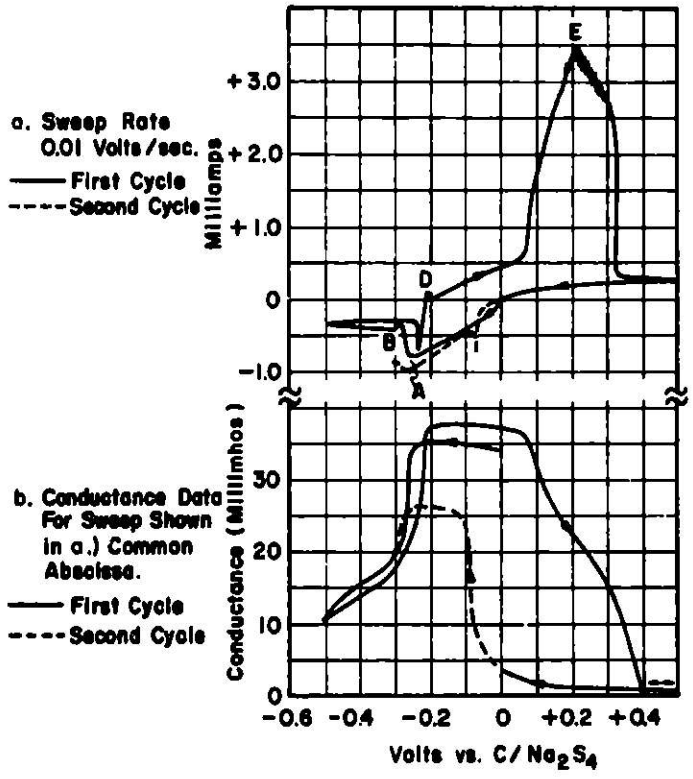

Fig. 1. Cyclic Sweep and Melt Conductance in $Na_2S_{4.0}$ at 300°C. Vitreous Carbon Electrode Area is 0.00407 cm^2. Sweep is iR Uncorrected (from Ludwig (1)).

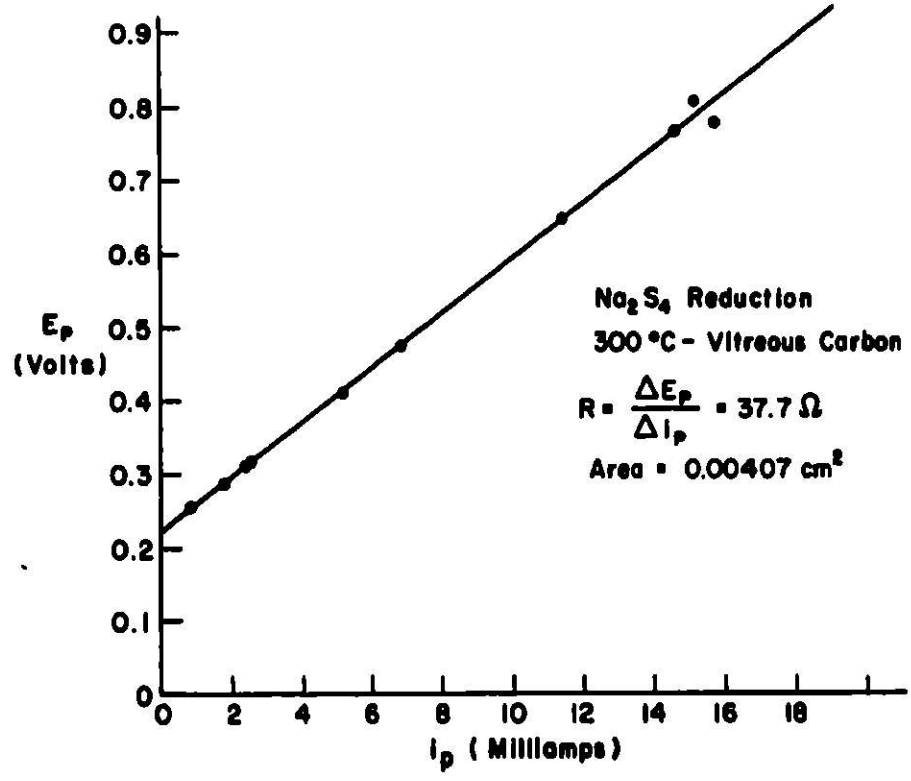

Fig. 2. Peak Potential *vs.* Peak Current For Wave A (from Ludwig (24)).

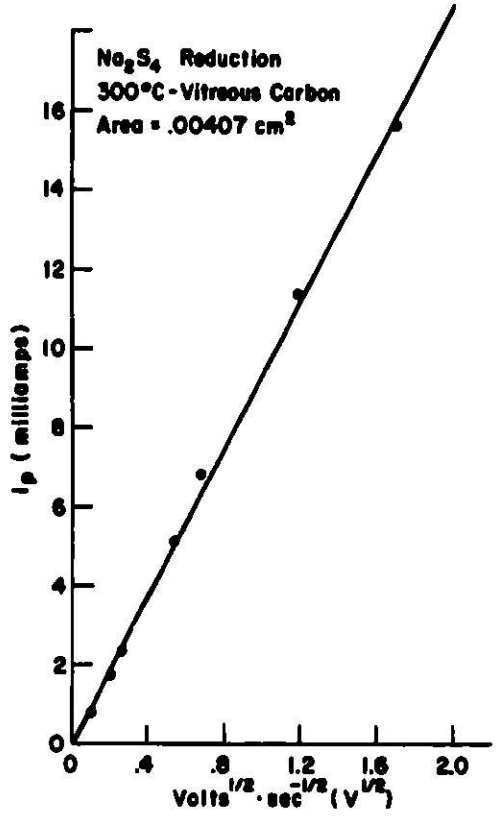

Fig. 3. Peak Current *vs.* Sweep Rate, iR Corrected, for Wave A (from Ludwig (24)).

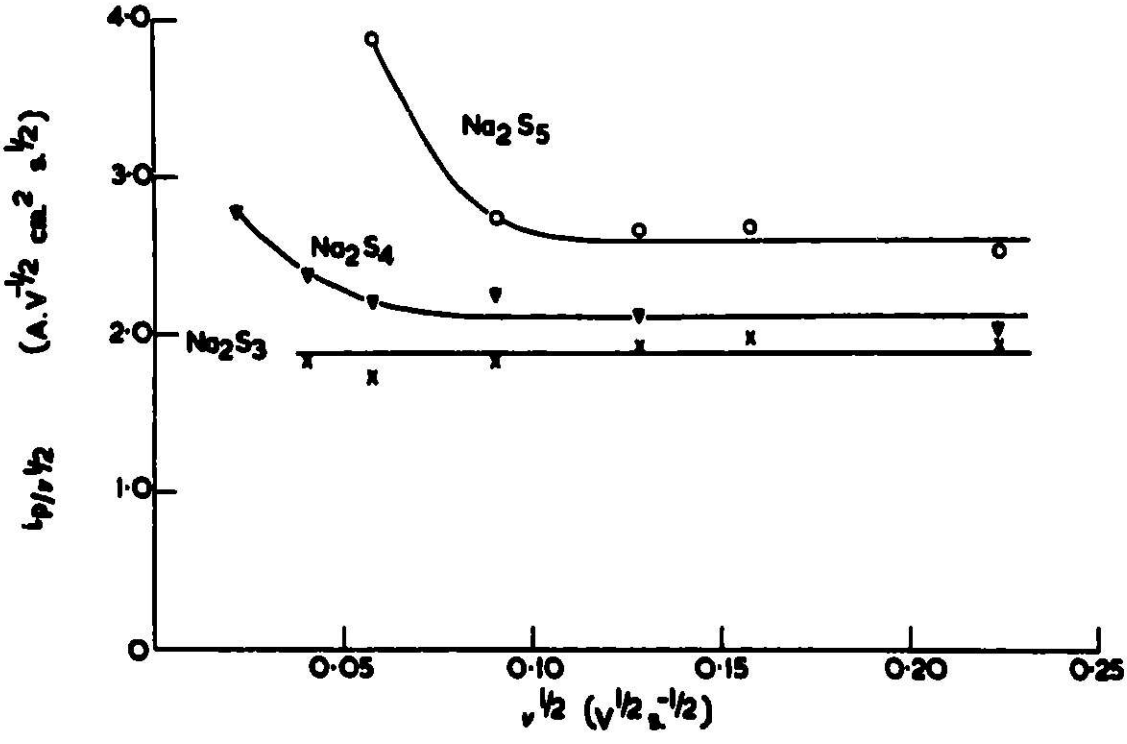

Fig. 4. Current Function, $i_p/v^{1/2}$, *vs.* $v^{1/2}$ for Wave A in Different Melt Compositions at 350°C (from South et al. (22)).

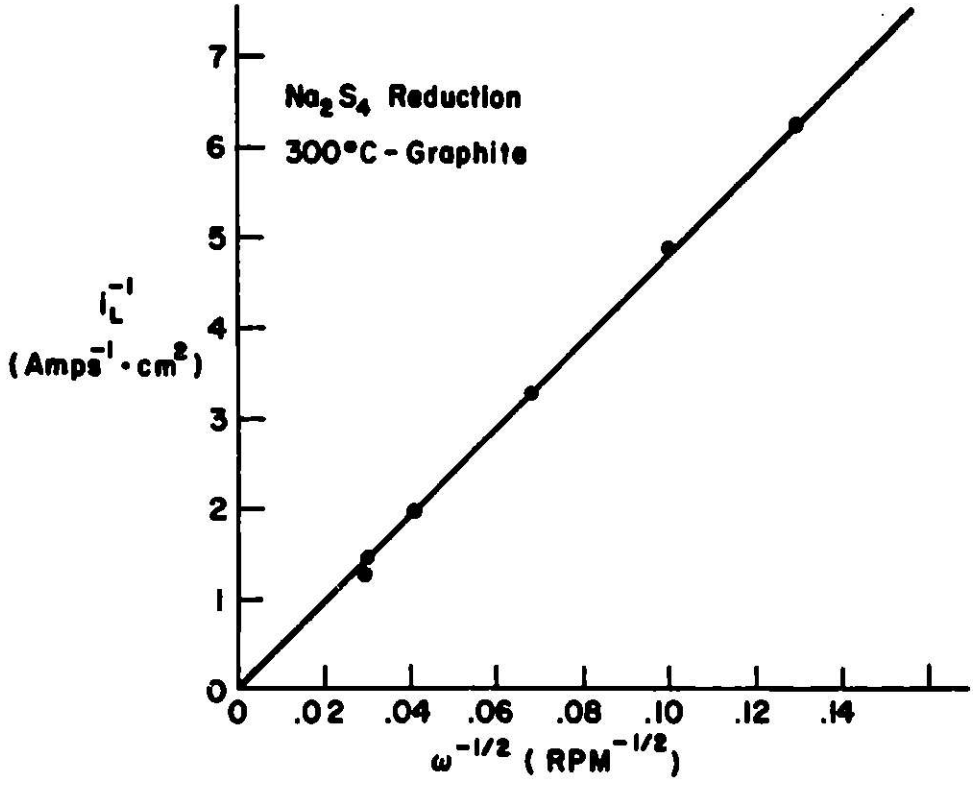

Fig. 5. Rotating Disc Diffusion Limited Current *vs.* Rotation Rate (from Dzieciuch (25)).

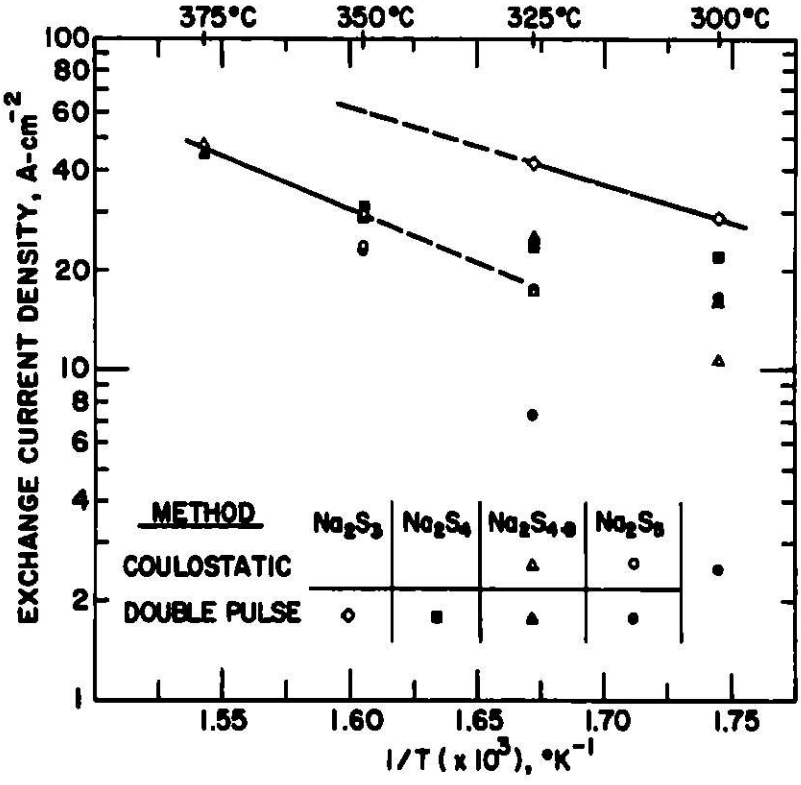

Fig. 6. Exchange Currents for the First Reduction Wave as a Function of Temperature, Determined by Two Different Methods. The Wide Scatter at Lower Temperature Shows the Difficulty of Measuring Exchange Currents of Very Fast Reactions in a Viscous Medium with Low Diffusion Coefficient and Correspondingly Fast Buildup of Diffusion Polarization (from Gupta and Tischer (34)).

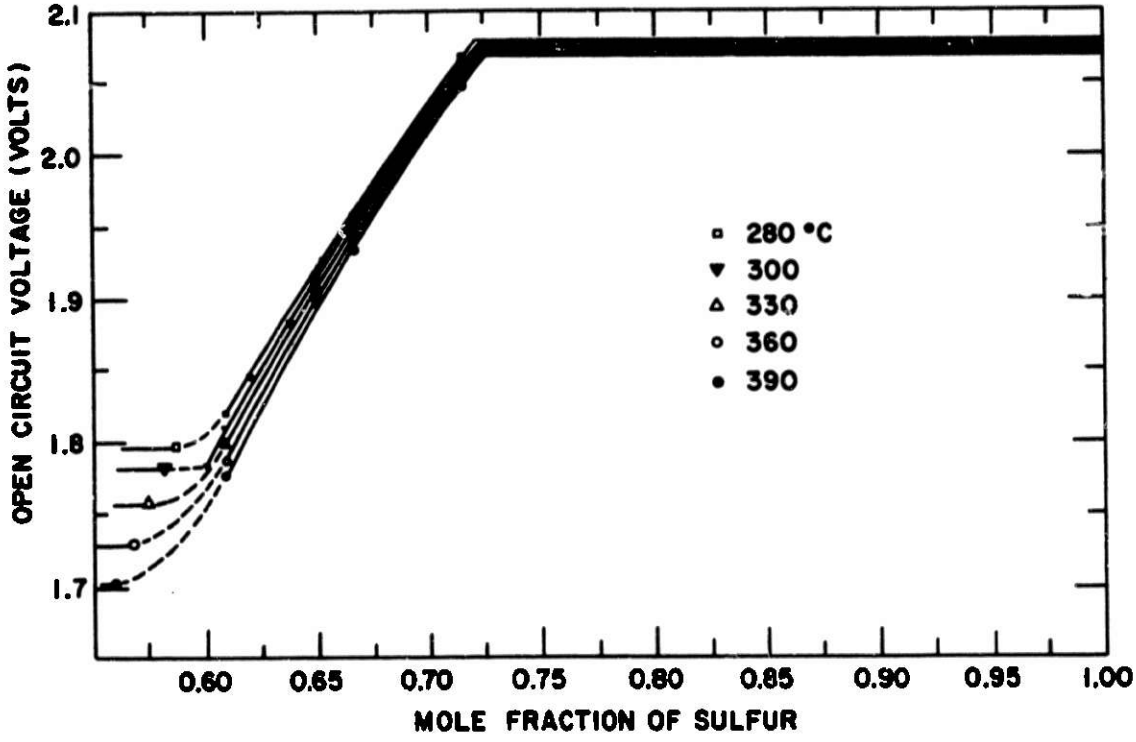

Fig. 7. Equilibrium Potentials (*vs.* Na/Na^+) *vs.* Sodium Polysulfide Composition (from Gupta and Tischer (35)).

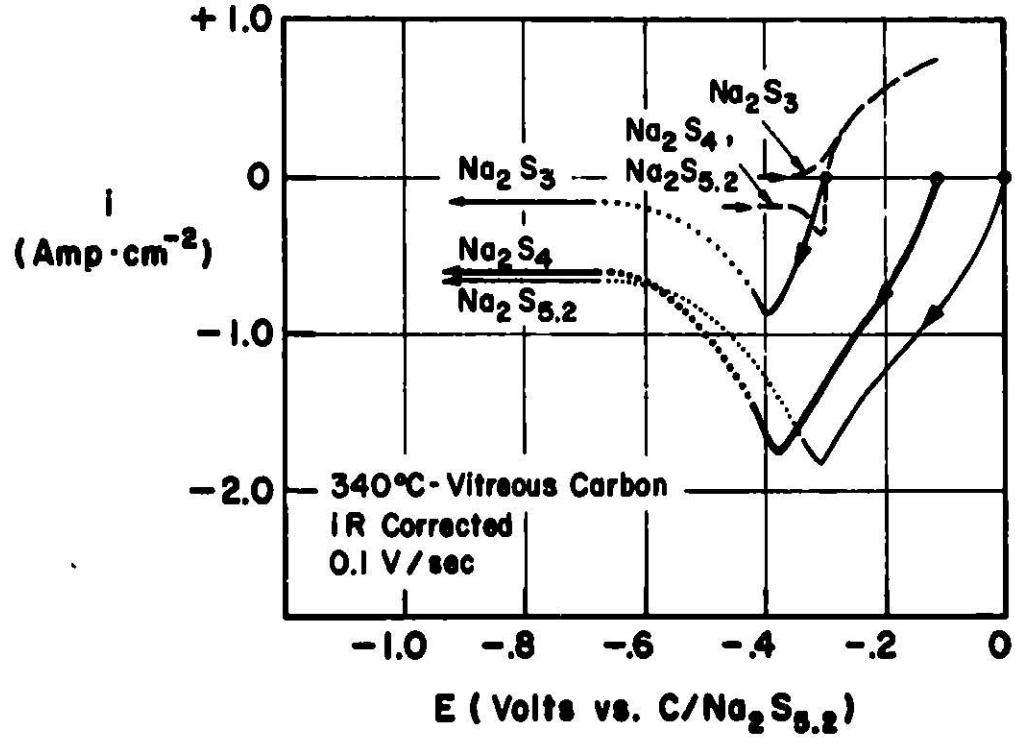

Fig. 8. Cyclic Sweeps Cathodic of Rest Potentials. Reverse Sweeps Partially Shown (from Ludwig et al. (23)).

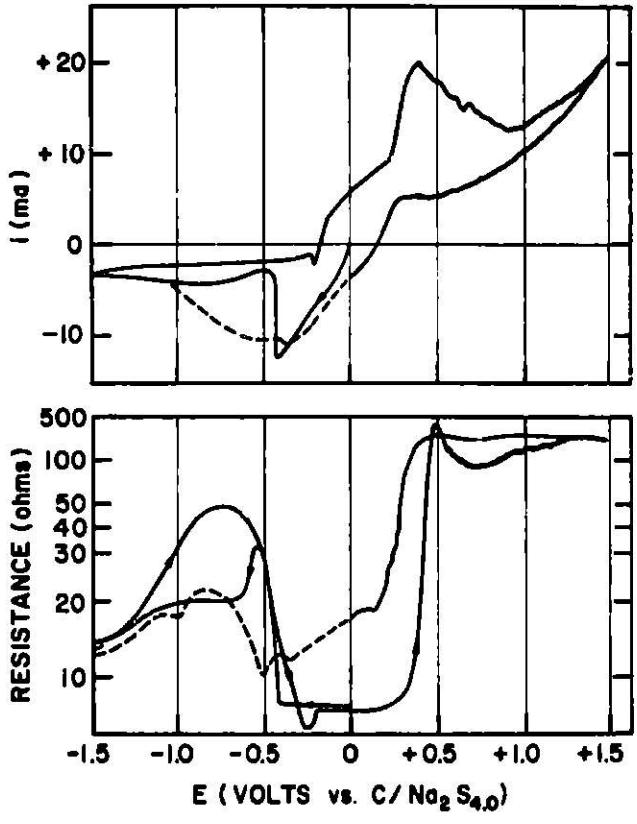

Fig. 9. Cyclic Sweep, 0.1 V/sec, and Melt Resistance in $Na_2S_{4.0}$ at 340°C. Resistance Measured With 5 kHz, 5 mV p-p Signal. Sweep Data is iR Uncorrected (from Ludwig et al. (23)).

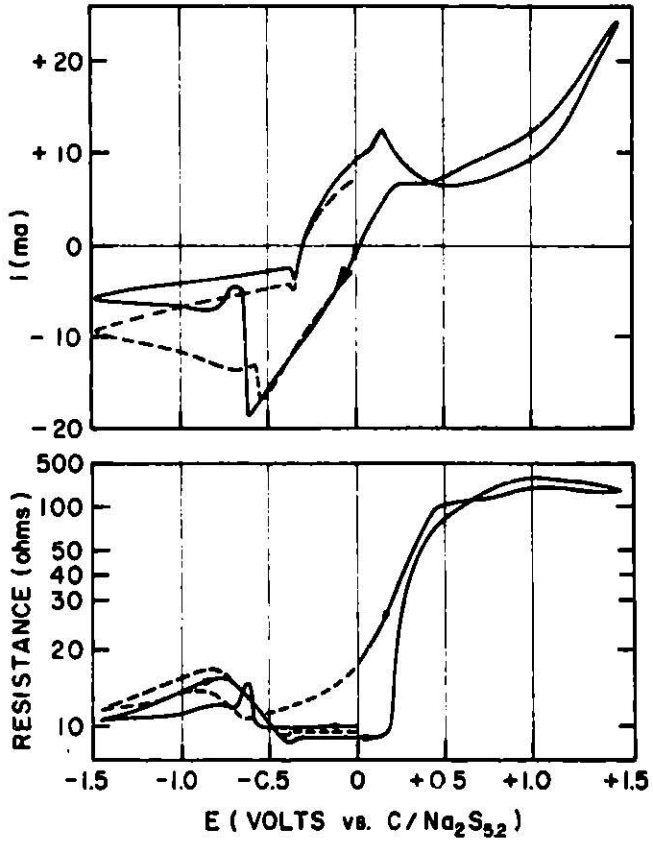

Fig. 10. Cyclic Sweep, 0.1 V/sec, and Melt Resistance in $Na_2S_{5.2}$ at 340°C. Resistance Measured With 5 kHz, 5 mV p-p Signal. Sweep Data is iR Uncorrected (from Ludwig et al. (23)).

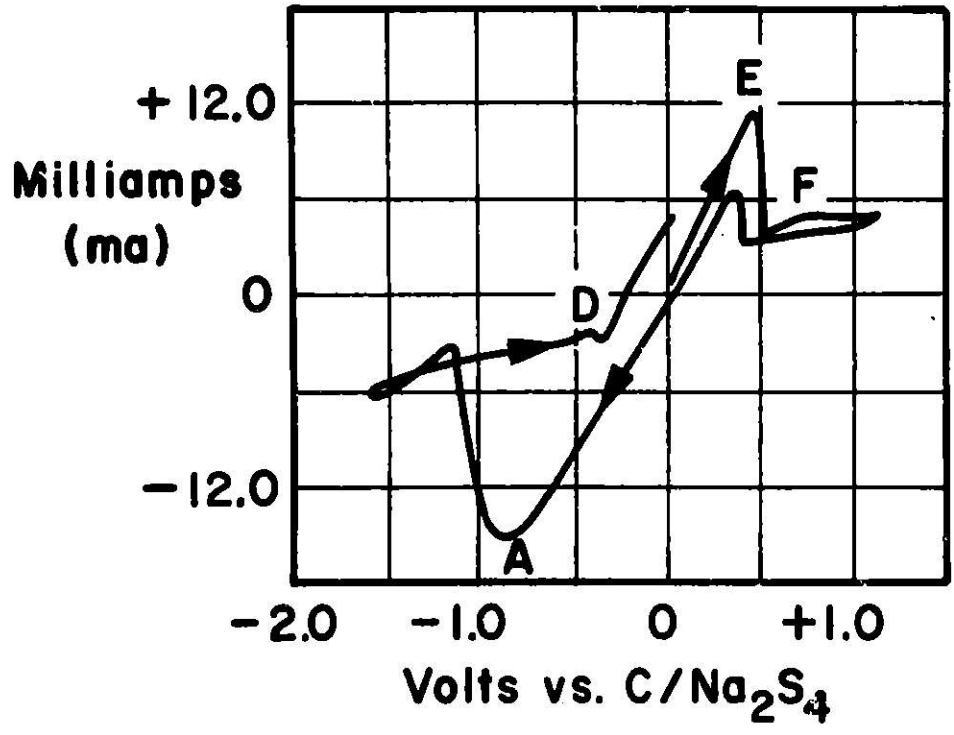

Fig. 11. Cyclic Sweep, 11.7 V/sec, iR Uncorrected, $Na_2S_{4.0}$ at 300°C, Vitreous Carbon Electrode Area is 0.00407 cm^2 (from Ludwig (1)).

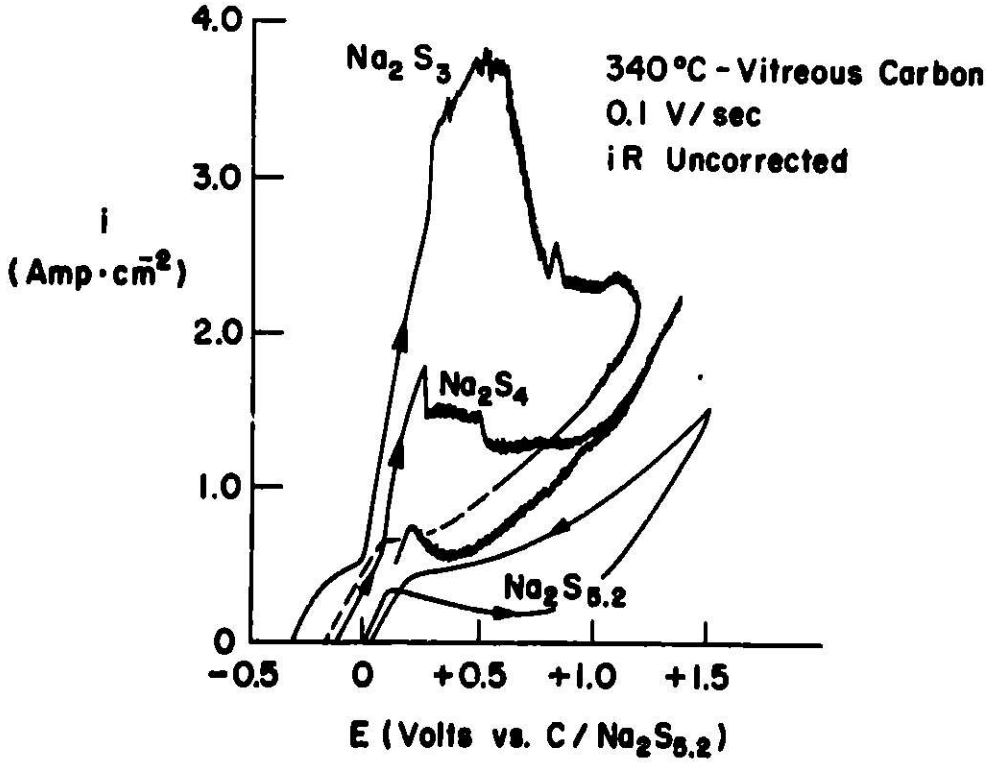

Fig. 12. Cyclic Sweeps Anodic of Rest Potentials (from Ludwig et al., (23)).

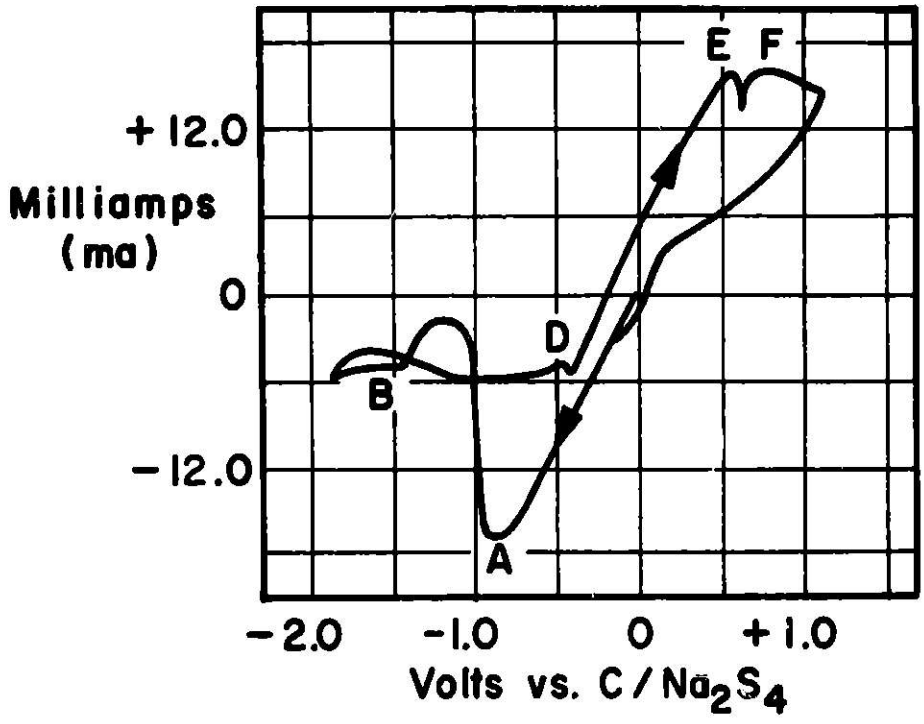

Fig. 13. Cyclic Sweep, 13.2 V/sec, iR Uncorrected, $Na_2S_{4.0}$ at 300°C, Vitreous Carbon Electrode Area is 0.00407 cm^2 (from Ludwig (1)).

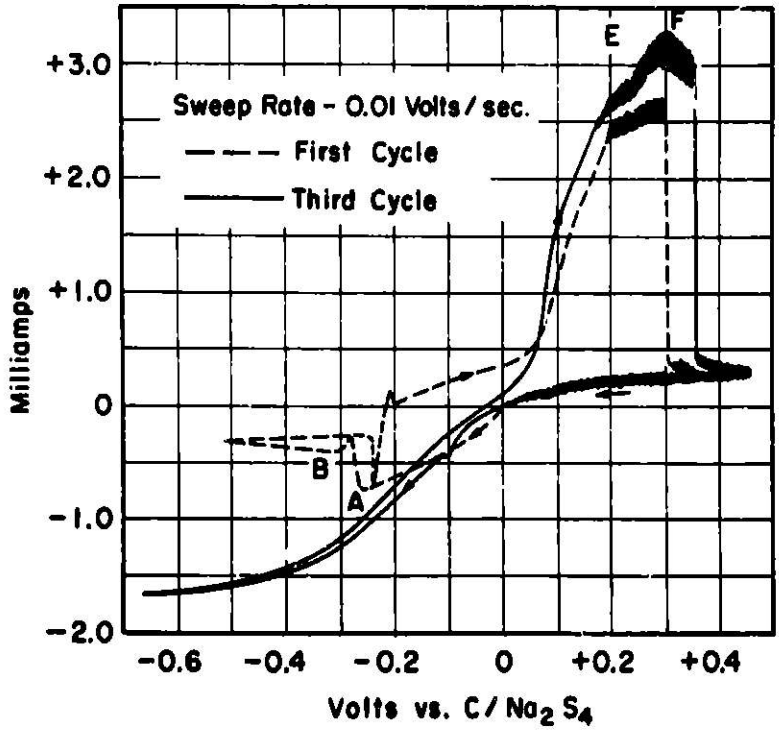

Fig. 14. Cyclic Sweeps in $Na_2S_{4.0}$ at 300°C, iR Uncorrected, Vitreous Carbon Electrode Area is 0.00407 cm^2 (from Ludwig (1)).

RECHARGEABLE CALCIUM HIGH-TEMPERATURE CELLS

S. J. Preto, L. E. Ross, A. E. Martin, M. F. Roche

Argonne National Laboratory
9700 South Cass Avenue
Argonne, Illinois 60439

ABSTRACT

Calcium is an attractive negative electrode material for use in secondary cells because of its great abundance, low equivalent weight, and high reaction energy. In this study, a number of secondary, molten-salt calcium cells having capacities of up to 20 A-hr were evaluated in terms of their charge-discharge characteristics. The negative electrodes were compounds of calcium and either aluminum or silicon, the electrolytes were mixtures of calcium chloride and alkali halides and the positive electrodes were iron sulfide (FeS). These cells generally exhibited high ampere-hour efficiency, good electrode utilization, and a voltage slightly higher than that of comparable lithium cells.

INTRODUCTION

A wide variety of secondary electrochemical cells are under development for application to utility load-leveling and electric-vehicle propulsion. These applications place stringent demands on battery cost, power, and cycle life. The trend has been toward high-temperature, alkali-metal cells which are expected ultimately to be capable of long cycle life and of delivering high specific energy (up to 200 W-hr/kg) and power (up to 100 W/kg) at operating temperatures ranging from 350 to 500°C. These and other more conventional cells under development at laboratories in the U.S. and abroad are the subject of recent reviews[1-3] and of many of the papers in this symposium. Secondary alkali metal/sulfur cells that employ either a solid electrolyte, *e.g.*, Na/β-alumina/sulfur, or a liquid electrolyte, *e.g.*, Li-Al/LiCl-KCl/iron sulfide, are at advanced stages of development, with studies now directed toward improvements in cycle life and cost. However, the relatively high fabrication cost and fragile nature of β-alumina and the low abundance of lithium, and thus its relatively high cost, may ultimately impose a limit on widespread application of these devices. Consequently, second-generation systems are being sought that circumvent the potential problems. The search, which focused on molten-salt/solid-electrode combinations for good electrochemical characteristics and ease of fabrication, led to the present investigation of rechargeable calcium high-temperature cells.

Calcium, an alkaline-earth element, has high abundance, relatively low equivalent weight, and high reaction energy with common positive electrode materials. Its properties, which are compared with those of lithium and sodium in Table I, appear to make calcium a very attractive electrode material. However, it has found application in the past only in the so-called thermal batteries which contain LiCl-KCl electrolyte and are designed to provide high power for a brief time after the electrolyte is melted.[1,4]

Table I. Selected Properties of Calcium, Lithium, and Sodium

	Ca	Li	Na
Abundance, wt % of earth's crust	3.63	0.0065	2.83
Equivalent Wt., g/g-equiv.	20	6.94	23
Melting Point, °C	842-848	179	97.81
Boiling Point, °C	1487	1317	892
Density, g/cm^3	1.54	0.534	0.97
Emf *vs.* FeS at 500°C,[a]	1.86	1.65	1.19
Specific Energy for Cell with FeS at 500°C[a]	780	870	480
Decomposition Voltage of Chloride at 500°C[b]	3.534	3.646	3.519

[a]Calculated for reaction to form Fe + MS, where M = 2 Li, 2 Na or Ca; Refs. 7-9.
[b]Ref. 10

For this specialized application, rechargeability is not a requirement, and the cells, as designed, are definitely not rechargeable. A major impediment to rechargeability is the tendency for calcium to form a liquid-metal Li-Ca alloy by reaction with the cell electrolyte, LiCl-KCl. The liquid metal thus formed tends to flow out of the negative electrode structure and short the cell. In sodium/sulfur cells, where liquid metal is unavoidable, shorting is prevented through use of a solid electrolyte, whereas in lithium cells, the problem is circumvented by formation of solid intermetallic compounds of lithium with aluminum[5] or silicon[6]--at some cost in cell voltage and specific energy.

Calcium, like lithium and in contrast to sodium, forms compounds with aluminum[11] ($CaAl_2$ and $CaAl_4$) and silicon[12] (Ca_2Si, CaSi and $CaSi_2$) that are stable solids at cell operating temperature. The use of these compounds eliminates liquid-metal formation and makes the calcium cells rechargeable (even in $CaCl_2$-NaCl electrolyte, where calcium alone converts almost entirely to sodium). Examples are given of rechargeable Ca-Al/FeS and Ca-Si/FeS cells operated in 5 mol % $CaCl_2$, 55 mol % LiCl, 40 mol % KCl electrolyte (mp, 345°C) and in the Downs-cell electrolyte,[13] 53 mol % $CaCl_2$, 47 mol % NaCl (mp, 506°C).* The $CaCl_2$-LiCl-KCl electrolyte offers the advantages of a much lower melting point, but contains an expensive ingredient, LiCl, that may also complicate the cell chemistry through the added participation of lithium in electrode reactions. The use of calcium-alloy electrodes instead of lithium-alloy electrodes in this electrolyte may be viewed as a means of extending available lithium supplies by a factor of two. The $CaCl_2$-NaCl electrolyte contains only low-cost ingredients (and has a much higher mole fraction of calcium), but its high melting point poses serious materials problems. A variety of other eutectic compositions, melting at 425-460°C, are known for mixtures of

*This salt is normally used for electrolytic production of sodium, but preferential calcium-compound formation (*e.g.*, $CaAl_4$) causes calcium to be reduced at a voltage much lower than that required for sodium reduction. Liquid sodium formation is thus avoided.

calcium chloride with lithium, potassium, and sodium chlorides,[14] and various low-melting mixtures containing fluoride and bromide ion are also possible. For example, a salt of the composition 53 mol % $CaCl_2$, 42 mol % NaBr, 5 mol % KF melts at 457°C, a melting point that is fifty degrees lower than that of the Downs-cell electrolyte. These alternative electrolytes provide a spectrum of calcium-ion and lithium-ion contents and can be used to modify cell performance and cost.

The primary objectives of this first investigation of secondary calcium cells were to demonstrate their rechargeability and to obtain preliminary data on cell performance characteristics for comparison with Li-Al/LiCl-KCl/FeS cells.[15] The cells described were not optimized with respect to positive electrode composition (possible substitutes for FeS include Fe_3O_4 and FeS_2), electrolyte composition (as noted above), or electrode thicknesses and loadings. Experience with lithium-cell systems[15,16] indicates that major improvments in performance can be expected upon optimization of the various cell components and cell design.

EXPERIMENTAL

The cell electrolytes were prepared from reagent-grade anhydrous chemicals in the case of $CaCl_2$-NaCl mixtures or from reagent-grade $CaCl_2$ and high-purity LiCl-KCl of eutectic composition obtained from Anderson Physics Laboratories, Incorporated, Champaign, Illinois. The reagent-grade chemicals were vacuum-dried at temperatures of 300 to 500°C to eliminate water, and the $CaCl_2$-NaCl melts were treated with sodium, Ca_2Si, or $CaAl_2$ at 550°C under a helium atmosphere to remove reducible impurities (principally hydroxide, which evolved hydrogen on chemical reduction). The electrolytes, which were clear and free of suspended particulates, were used without further treatment. Electrolysis with a glassy-carbon positive electrode and a stainless steel negative electrode was shown to be an effective means of freeing the $CaCl_2$-NaCl electrolyte from impurities. However, this time-consuming procedure was not routinely used, since it did not appear to be necessary. (For long-term cell operation, electrolyte purified by the electrolysis method may be required.)

The electrodes had thicknesses of 0.7-0.9 cm and areas of 7-25 cm^2. Negative electrode compounds ($CaAl_2$ and Ca_2Si powders) were either prepared pyrometallurgically or generated within the cell by starting the cell in an uncharged state using Al, Si, or $CaSi_2$ powders. The positive electrodes were prepared either from FeS or, in the case of uncharged cells, from CaS and iron powders. The electrode materials were checked for impurities by metallographic and X-ray methods. Generally, only minor levels of impurities (mainly Al_2O_3, CaO, SiO_2) were found.

Electrode ingredients were usually dispersed in a small amount of molten electrolyte, and this mixture was frozen and reground. The resulting powder was vibrated into an iron Retimet* structure, which served as a current collector, and this assembly was welded into an electrode housing. The electrode faces were covered with zirconia fabric, and iron or stainless steel screens were welded on for particle retention. The positive electrode was sewn within a BN fabric separator. In some of the early cells (SC-1, SC-2, SP-2, LR-1),

*A foam-like material of 95% porosity manufactured by Dunlop Ltd., England.

the salt dispersal step was omitted, and the electrode was infiltrated with electrolyte during cell startup. However, this procedure led to a distribution of active materials that was less uniform than the salt-dispersal method. In one of the cells (SP-2), the positive electrode housing and current collector were an alumina cup and molybdenum screens, respectively, instead of the usual iron housing and Retimet collector (this construction was not used in later cells because of fabrication difficulties). All of the electrolyte- and electrode-preparation steps were conducted in helium-atmosphere gloveboxes maintained at high purity by a combination of molecular sieves and a liquid-nitrogen-cooled charcoal absorber.

A schematic of a typical cell assembly is shown in Fig. 1. In this configuration the positive electrode is at the bottom of the cell. The assembled cells were operated in wells attached to the helium boxes and heated by external furnaces. The wells could be sealed and were equipped with baffles for temperature control and with a vacuum pump for removal of residual gases from the cells. The ability to alternately evacuate and backfill the furnace wells with helium proved to be quite important because this procedure was needed to cause electrolyte penetration through the BN fabric separator and to remove occluded gases from the electrodes. The cells were driven at constant, preselected charge-discharge currents with a regulated direct-current power supply equipped with a meter relay that automatically reversed the power-supply polarity at preset charge and discharge cutoff voltages. Cell voltage and current were monitored with dual-pen, strip-chart recorders and with digital voltmeters, and current was integrated electronically for each half-cycle for determination of ampere-hour efficiency. Electrodes from terminated cells were cross-sectioned and examined by metallographic and X-ray methods to determine the compounds that had formed and the distribution of active material.

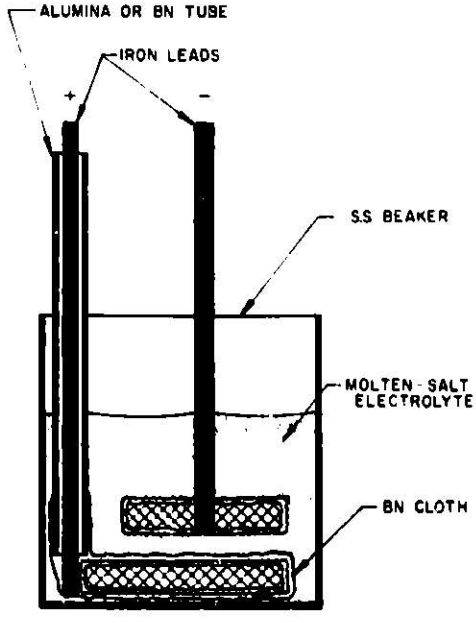

Fig. 1. Typical Cell Design (bottom electrode, with BN wrapping, is the FeS positive electrode).

Aluminum and silicon electrodes were also tested in the special cell, shown in Fig. 2, which had a counter electrode consisting of a pool of Na-5 wt % Ca. The apparatus was intended to provide a means of obtaining both emf and extended cycling data for the Ca-Al and Ca-Si compounds. However, these tests had to be terminated after only a few cycles because the Na-Ca pool electrode slowly wet and reduced the surface of the alumina tube causing shorting. Degradation of the BN fabric wrapper on the test electrode was also observed; therefore, this method of testing electrodes was not pursued further. However, preliminary information was obtained on electrode voltage and cycling characteristics in $CaCl_2$-NaCl electrolyte during these tests.

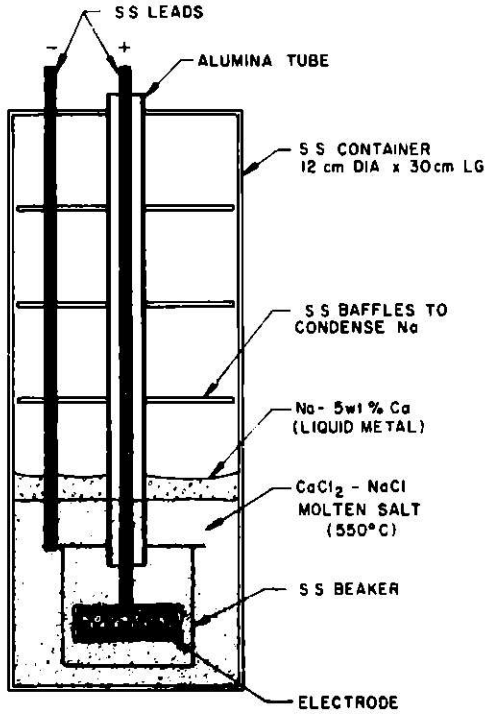

Fig. 2. Negative-Electrode Test Cell (the Na-Ca pool is the counter electrode).

RESULTS AND DISCUSSION

A summary of cycling data for the calcium alloy/FeS cells is given in Table II. Except for Cell SP-5, the calcium alloy/FeS cells had high ampere-hour efficiencies and exhibited little decline in available capacity during cycling. The characteristics of the cells with $CaCl_2$-NaCl as the electrolyte are described first and in some detail because they represent a new class of cells and thus pose more difficult problems.

Cells with $CaCl_2$-NaCl Electrolyte

Cell SP-2 was started with a $CaAl_2$ negative electrode of 6 A-hr capacity. However, after the first discharge, which yielded 4 A-hr, the cell proved to be rechargeable only to 3 A-hr, which is equivalent to the compound $CaAl_4$.

Table II. Cycling Data for Ca-Al/FeS and Ca-Si/FeS Cells

Cell No.[a]	Composition and Capacity	Cycles[b]	A-hr Eff., %	Total A-hr Discharged
	$CaCl_2$-NaCl Electrolyte (550°C			
SP-2	$CaAl_4$ (3 A-hr)/FeS (11 A-hr)	14	98	38
SP-5	Ca_2Si (11 A-hr)/FeS (9 A-hr)	8	85	32
	$CaCl_2$-LiCl-KCl Electrolyte (460°C)			
LR-1	$CaAl_2$ (15 A-hr)/FeS (15 A-hr)	36	99+	253
LR-2	Ca_2Si (20 A-hr)/FeS (15 A-hr)	15	99+	130
LR-3	Ca_2Si (20 A-hr)/FeS (15 A-hr)	33	96	270

[a]All cells assembled in charged state except LR-3 (uncharged).

[b]All cells terminated voluntarily for metallographic examination except SP-5, which showed a marked decline in capacity.

Consequently, the cell was operated on the $CaAl_4$ plateau, which had an emf of 1.40 V. Figure 3 shows, in addition to a normal cycle D8-C8, the result of an attempt to charge the upper plateau (equivalent to $CaAl_2$) by increasing the ampere-hour charged to 4.0. This led to a high initial voltage region in the following discharge (D-10), but no increase in cell capacity. Thus the ampere-hour efficiency on this overcharge cycle was poor (75%). Subsequent cycles with normal charges exhibited a decreased, but stable, capacity of 2 A-hr as a consequence of the overcharge. Cell SC-1, which consisted of an aluminum test electrode and a sodium-calcium pool electrode, complemented Cell SP-2; Cell SC-1 showed only a single plateau, at an emf of 0.40 V *vs.* sodium (see Fig. 4), rather than the two plateaus expected for successive formation of $CaAl_4$ and $CaAl_2$. A $CaAl_4$/FeS cell, designated SP-4, of 10 A-hr capacity was constructed using pyrometallurgically prepared $CaAl_4$ rather than $CaAl_2$. This cell had a single, 1.40-V plateau, and thus confirmed the conclusions drawn from Cell SP-2. However, the cell was operated for only two

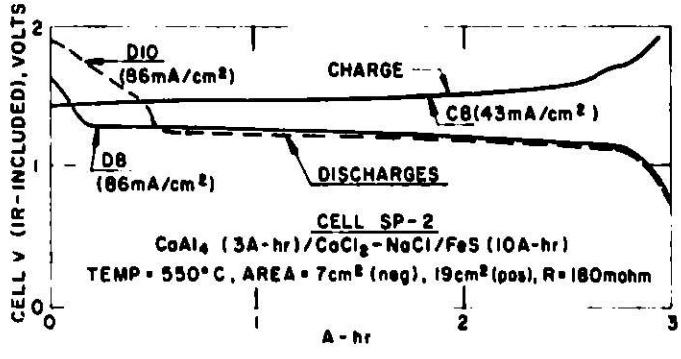

Fig. 3. Cell SP-2 Voltage Curves (dashed curve followed an overcharge; current density calculated from negative electrode area).

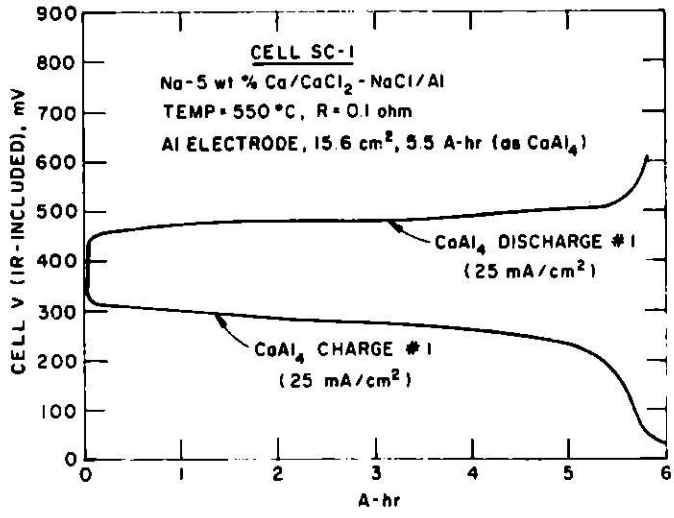

Fig. 4. Formation and Discharge of $CaAl_4$.

cycles (6 A-hr and 10 A-hr cycles at 93% ampere-hour efficiency) before developing a short. Its operation was thus less satisfactory than that of Cell SP-2.

An interesting thermodynamic calculation can be made from the cell emfs and the voltages in Table I, recalculated for 550°C. The sum of the emfs of Cells SP-2 ($CaAl_4$/FeS) and SC-1 (Na-Ca/Al) is 1.80 V, and a calcium metal electrode is expected to be 0.03 V more negative than the sodium pool electrode (from the metal chloride decomposition potentials). Thus, the emf of a hypothetical Ca/FeS cell in $CaCl_2$-NaCl electrolyte is 1.83 V, in good agreement with a calculated value at 550°C of 1.834 V. Also, the emf of a Ca/$CaAl_4$ cell is 0.40 + 0.03 V, and thus the calculated free energy of formation of $CaAl_4$ at 550°C is -20 kcal.

The $CaAl_4$/FeS cells were terminated near full charge, and the electrodes were examined metallographically. The SP-2 positive electrode, which contained excess FeS, had a sharp boundary between finely divided, well-reacted FeS and coarser, unreacted FeS. The reacted region was closest to the negative electrode. The major phase found in the negative electrodes was $CaAl_4$, which was readily distinguished by its reddish tint. Only minor isolated zones of another phase were found; this phase was present at electrolyte/$CaAl_4$ interfaces and appeared to be $CaAl_2$. It was concluded that electrochemical formation of $CaAl_2$ in these $CaCl_2$-NaCl cells either was kinetically hindered or occurred at a potential too close to sodium potential for the electrode to be easily charged. This result was disappointing because the $CaAl_2$ compound has a much lower equivalent weight than does $CaAl_4$. The theoretical specific energy of the 1.40-V $CaAl_4$/FeS (550°C) cell is a modest 320 W-hr/kg. Comparable figures for the 2-V lead-acid cell and the 1.33-V Li-Al/FeS (450°C) cell are 160 and 460 W-hr/kg, respectively.

The Ca_2Si/FeS cell has a theoretical specific energy of about 560 W-hr/kg. This value was calculated from the emfs of the three plateaus for Cell SP-5, shown in Fig. 5, and an assumption that the negative-electrode discharge reactions corresponded to the reaction sequence:

$$Ca_2Si \rightarrow CaSi \rightarrow CaSi_2 \rightarrow Si$$

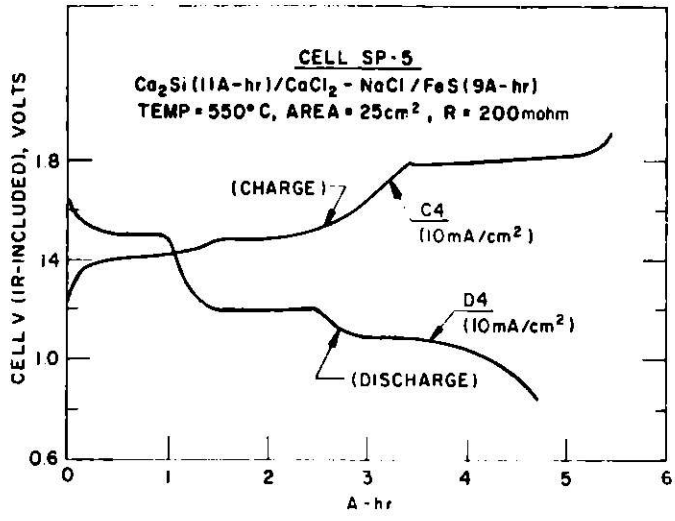

Fig. 5. Cell SP-5 Voltage Curves.

The poor behavior of the pool-electrode Na-Ca/Si cell (Fig. 6) prevented coulometric measurement of the capacities of the compounds formed and measurement of thermodynamic properties. However, the discharge curve in Fig. 6 showed that the Ca-Si electrode had three plateaus and gave an indication of the plateau voltages to be expected from operation of a Ca_2Si/FeS cell. In such a cell (SP-5), plateau emfs were determined from open-circuit measurements. These plateau emfs (1.65, 1.35, and 1.28 V) and the calculated emf of Ca/FeS (1.834 V at 550°C) permitted an approximate determination of the free energy of formation of the compounds, Ca_2Si (-32 kcal), CaSi (-24 kcal) and $CaSi_2$ (-25 kcal), from their elements at 550°C. Enthalpies of these compounds have been reported as follows: Ca_2Si (-50 kcal), CaSi (-36 kcal) and $CaSi_2$ (-36 kcal).[17] Thus, large, positive entropies appear to be involved, as is the case with lithium silicides.[18]

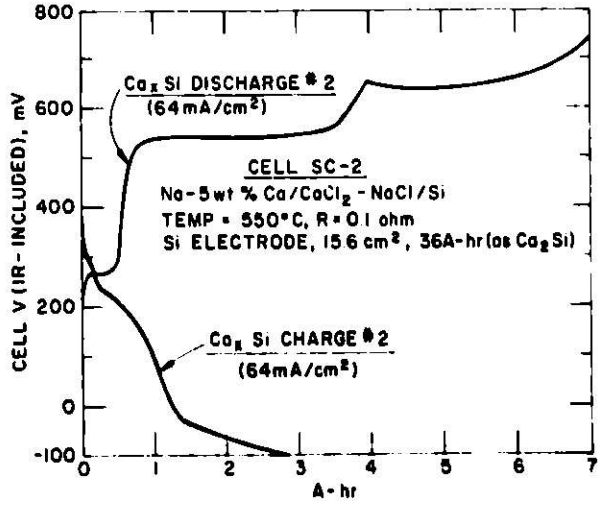

Fig. 6. Formation and Discharge of Ca-Si Compounds.

Cell SP-5 exhibited a rather poor ampere-hour efficiency and its available capacity declined from 6 to 3 A-hr in eight cycles. Another cell of the same type gave almost identical results (an ampere-hour efficiency of 86% and a decline in available capacity from 8 to 3 A-hr in six cycles). A metallic deposit noted on the cooler portions of the furnace well during operation of these cells appeared to be condensed sodium vapor, and, after a few cycles of successful cell operation, the normally smooth cell voltage curves exhibited occasional steps of 10 to 30 mV. Thus, a variety of problems were encountered. Two possible causes were found through postoperative examinations of the cells and a calculation of the sodium vapor pressure. Metallographic examination of the negative electrode showed that the Ca-Si compounds were present as small ($\leq$100 μm), individual crystallites in relatively poor contact with the Retimet current collector. (The active materials in other negative electrodes examined were in the form of interconnected, porous masses in good contact with the Retimet.) The value calculated for the activity of Na in equilibrium with Ca_2Si, from the 150-mV difference in emf between Ca_2Si and a sodium pool, was 0.12, and the sodium vapor pressure (11.5 mm for pure sodium) was thus 1.4 mm. The combination of poor electrode morphology and capacity loss through sodium vaporization may well account for the poor cell behavior. Steady-state polarization characteristics of these cells were also poor (about 15 Ω-cm^2 at mid-discharge), but these may be improved markedly when the other problems are corrected through development of a better negative electrode design and construction of sealed cells. (Development of engineering-scale cells was beyond the scope of this study.)

None of the cells in $CaCl_2$-NaCl electrolyte were studied from the standpoint of the effect of current-density increases on discharge capacity because, at this early stage of development, observation of possible mechanisms for decline in capacity (at constant current) were considered to be of more importance. However, data obtained when occasional changes in current density were made during cycling showed that the cell polarization increased linearly with current density; moreover, cell resistances, which were obtained by current interruption measurements and are given in each figure, remain nearly constant once the cells were well outgassed. Thus, the polarization behavior of these cells is similar to that observed[12] in Li-Al/metal sulfide cells.

Cells with $CaCl_2$-LiCl-KCl Electrolyte

The calcium alloy cells performed reasonably well in $CaCl_2$-LiCl-KCl electrolyte, as shown by the cell data in Table II. Discharge curves of voltage *vs.* capacity obtained at current densities up to 160 mA/cm^2, are shown in Figs. 7-10. A 20 mA/cm^2 charge curve is also plotted in each of the figures, and the beginning of charge is aligned with the end of the corresponding 20 mA/cm^2 discharge for purposes of charge-discharge comparisons. Note that two of the cells, LR-2 and LR-3, have the same active materials and electrode capacities, but were started in a charged and an uncharged state, respectively. The major difference, however, was not the initial state of charge, but the inclusion of 100-mesh stainless steel retainer screens inside the Ca_2Si electrode of Cell LR-3 to prevent migration of Ca_2Si out of the Retimet current collector. Postoperative metallographic examination of the cells showed that the screens were effective retainers. In Cell LR-2, much of the negative-electrode active material was located between the retimet and zirconia-cloth retainer furthest from the positive electrode, whereas in Cell LR-3, the active material was well-contained inside the Retimet. The polarization of

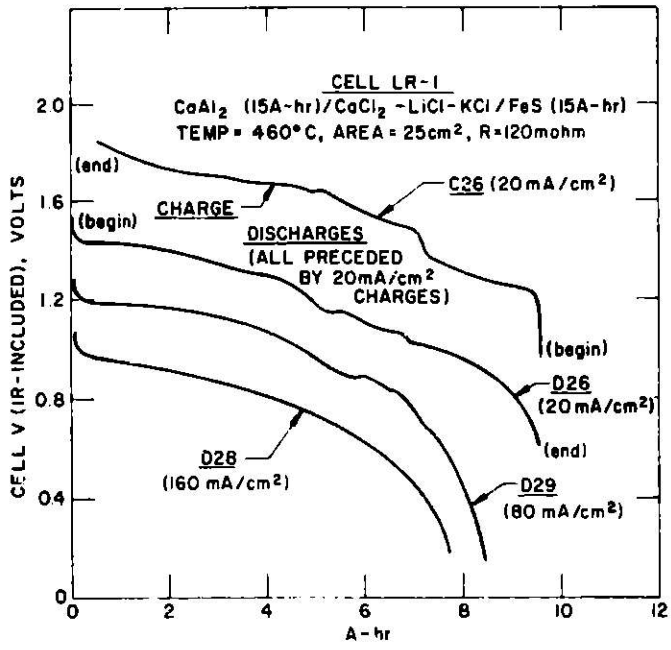

Fig. 7. Cell LR-1 Voltage Curves at Various Current Densities.

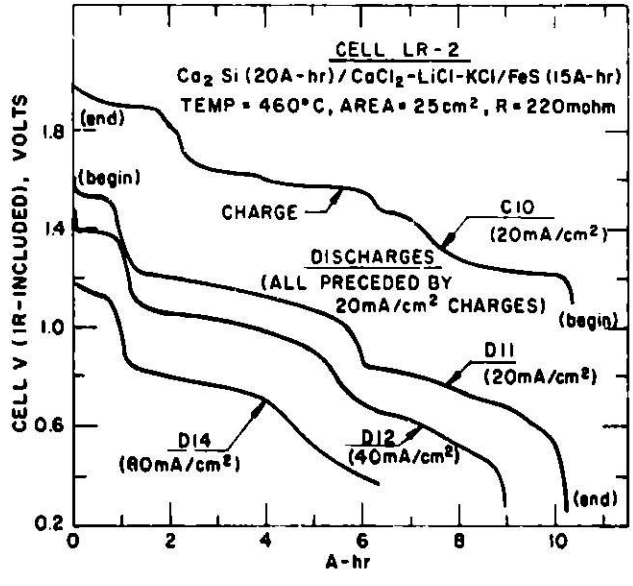

Fig. 8. Cell LR-2 Voltage Curves at Various Current Densities.

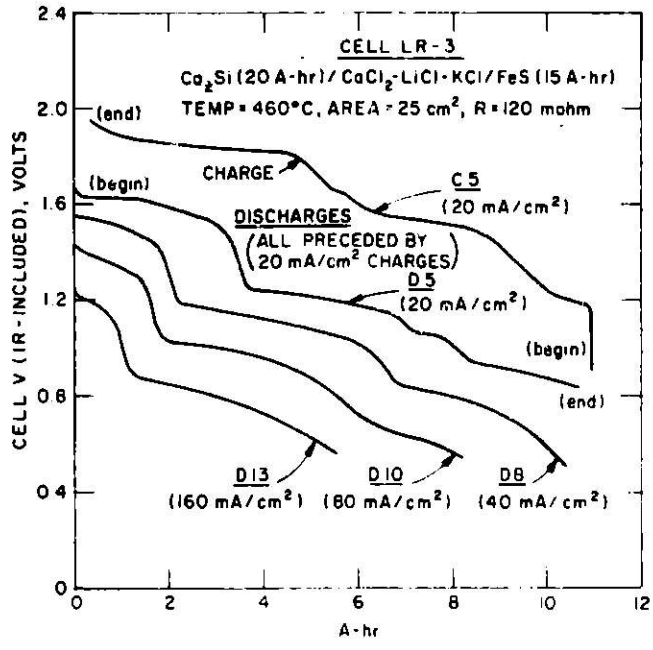

Fig. 9. Cell LR-3 Voltage Curves at Various Current Densities.

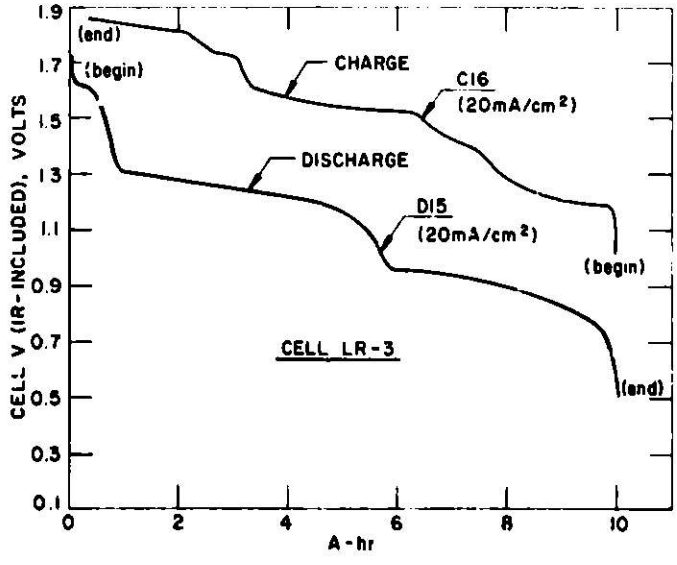

Fig. 10. Cell LR-3 Voltage Curves for Cycle Following High-Current Discharges.

Cell LR-3 was only half that of Cell LR-2, as can be seen by comparing Figs. 8 and 9. Thus, this very simple modification in design has produced a significant improvement in cell performance. Metallographic examination showed that Cell LR-1 would also have benefited from addition of internal screens. The negative electrode material was well attached to the Retimet, but was located in zones above and below the 6-mm thick Retimet.

Cell LR-1 was terminated at 50% charge, and portions of the metallographic samples were submitted for X-ray examination. The examination showed $CaAl_4$ in the lower zone of the negative electrode (close to the positive electrode) and a mixture of $CaAl_4$ and Al in the upper zone. The LR-1 positive electrode contained CaS, Fe and FeS. In Cell LR-2, which employed a Ca-Si negative electrode, CaSi was identified. However, it had lattice parameters that were slightly smaller than normal, which suggests that lithium was incorporated in the compound. Involvement of both lithium and calcium in the negative-electrode reactions is a strong possibility. Three Ca-Li-Si compounds ($CaLiSi_2$, Ca_2LiSi_3, and $Ca_{1.65}Li_{1.85}Si_{4.0}$) have been reported.[19] These particular silicides, which are rich in silicon, were not detected, of course, since Cells LR-2 and LR-3 were terminated at full charge.

The cell-voltage curves in Figs. 7-10 also suggest involvement of both lithium and calcium in electrode reactions. Cell LR-1, for example, had an open-circuit potential that varied gradually from about 1.6 to 1.1 V with the state of charge, and no easily recognized voltage plateaus were present (Li-Al/LiCl-KCl/FeS cells have a constant emf of 1.33 V,[15] and the $CaAl_4$/$CaCl_2$-NaCl/FeS cell, SP-2, had a well-defined plateau at 1.40 V). Cell LR-1, unlike Cell SP-2, was fully rechargeable, which also suggested involvement of lithium in the negative electrode reaction. Nonlinear changes in polarization with current density were yet another indication of mixed reactions. Again using Cell LR-1 (Fig. 7) as an example, the 20 mA/cm^2 discharge exhibited a total polarization equivalent to approximately 8 Ω-cm^2 at 50% discharge, but the voltage difference between the higher current density curves indicates a value of 3 Ω-cm^2. Values for LR-3 were about 7 Ω-cm^2 at low currents, 4 to 5 Ω-cm^2 at intermediate currents, and 2 to 3 Ω-cm^2 at the highest currents. (Similarly constructed LiAl/FeS cells exhibit a polarization equivalent to about 3 Ω-cm^2.[15] The high polarization at low currents leads to an undesirably large gap between the low-current charge and discharge curves. Watt-hour efficiencies were 80%, 65%, and 75% for the 20 mA/cm^2 cycles of Cells LR-1, -2, -3, respectively.

There are, however, indications that calcium is a major contributor to the cell reactions, aside from the X-ray identification of calcium compounds in the electrodes. The high cell voltage of Cell LR-1 and the presence of three more-or-less distinct plateaus in Cells LR-2 and LR-3 (rather than four as in Li-Si systems[6,14]) indicate strong calcium participation at low currents. The relatively low percentage of calcium ion (5 mol % $CaCl_2$) and high percentage of lithium ion (55 mol % LiCl) in the electrolyte tend to promote lithium participation at higher currents and may be the reason for polarization nonlinearities. (Adjustments in the Ca^{++}/Li^{+} ratio represent one area of future cell modifications.)

One final aspect of the operation of Cell LR-3 is of note. The curves in Fig. 10 show the 20 mA/cm^2 cycle that followed the high-current cycles. It can be seen by comparing Figs. 9 and 10 that the high-voltage plateau

decreased in capacity, and the cell, except for its better resistance, was then similar to Cell LR-2 (Fig. 8). Thus, the highest voltage plateau appears to be difficult to maintain in the present system. The plateau collapse can be seen directly in Fig. 9, which suggests that the high currents caused the collapse, but the return to low currents established the decline more definitely. The cell performed in a stable manner following the drop in high-voltage capacity. This high-voltage-plateau problem may also be a consequence of insufficient calcium ion, since calcium is needed for formation of the higher voltage compounds.

CONCLUSIONS

Rechargeability of calcium-alloy/FeS cells was demonstrated in two molten-salt electrolytes, namely, $CaCl_2$-NaCl and $CaCl_2$-LiCl-KCl. Some problems were encountered in maintaining capacities at the high-voltage plateaus, but the cells generally operated quite well. Further studies to optimize the cell-electrode design and the electrolyte composition thus appear justified. This optimization is expected to lead to relatively inexpensive cells for use in load-leveling and electric-vehicle applications.

ACKNOWLEDGMENTS

The authors express their appreciation to J. W. Allen, L. G. Bartholme, B. S. Tani and H. Shimotake for experimental assistance and to R. K. Steunenberg, P. A. Nelson and L. Burris for their guidance and helpful discussions.

This work was performed under the auspices of the U. S. Energy Research and Development Administration.

REFERENCES

1. E. J. Cairns and R. K. Steunenberg, "High-Temperature Batteries," in *Progress in High Temperature Physics and Chemistry*, Vol. 5, p. 63, C. A. Rause, Ed., Pergamon Press, New York (1973).

2. N. P. Yao and J. R. Birk, "Battery Energy Storage for Utility Load Leveling and Electric Vehicles: A Review of Advanced Secondary Batteries," *Proc. Tenth IECEC*, p. 1107 (1975).

3. P. A. Nelson, A. A. Chilenskas, and R. K. Steunenberg, *The Need for Development of High-Energy Batteries for Electric Automobiles*, USAEC Report ANL-8075, Argonne National Laboratory (1974).

4. R. Jasinski, *High Energy Batteries*, Plenum Press, New York (1967).

5. N. P. Yao, L. A. Heredy, R. C. Saunders, J. Electrochem. Soc. *118*, 1039 (1971).

6. S. Lai and L. R. McCoy, "Lithium Silicon Electrodes," Extended Abstracts of the Electrochemical Society Meeting, Dallas, October 5-10, 1975, Vol. 75-2, pp. 56-57 (1975).

7. J. F. Elliott and M. Gleiser, *Thermochemistry for Steelmaking*, Vol. 1, Addison-Wesley Publ. Co., Inc., Reading, Mass. (1960).

8. O. Kubaschewski, E. Evans, and C. Alcock, *Metallurgical Thermochemistry*, 4th Ed., Pergamon Press, London (1967).

9. D. R. Stull, H. Prophet, *JANAF Thermochemical Tables - 2nd Ed.*, NSRDS-NBS37, U.S. Gov. Printing Office, Washington, D.C. (1971).

10. *The Encyclopedia of Electrochemistry*, C. A. Hampel, Ed., Reinhold Publ. Corp., New York, N.Y., p. 645 (1964).

11. M. Hansen and K. Anderko, *Constitution of Binary Alloys*, McGraw-Hill Book Co., New York (1969).

12. E. Schurmann, C. Zellerford, H. Littersheidt and P. Funders, Arch. Eisenhuttenw. *45*, 367 (1974).

13. *The Encyclopedia of Electrochemistry*, C. A. Hampel, Ed., Reinhold Publishing Corp., New York, pp. 1063-4 (1964).

14. E. M. Levin, C. R. Robbins, H. F. McMurdie, *Phase Diagrams for Ceramists*, American Ceramic Soc., Columbus, Ohio (1964 and 1969 suppl.).

15. P. A. Nelson *et al.*, *High-Performance Batteries for Off-Peak Energy Storage and Electric-Vehicle Propulsion*, USERDA Report ANL-75-1, Argonne National Laboratory (1975).

16. P. A. Nelson *et al.*, *High-Performance Batteries for Off-Peak Energy Storage and Electric-Vehicle Propulsion*, USERDA Report ANL-8109, Argonne National Laboratory (1975).

17. O. Kubaschewski, E. Evans, and C. Alcock, *Metallurgical Thermochemistry*, 4th Ed., Pergamon Press, London (1967).

18. W. R. Frost, D. R. Vissers, M. F. Roche, K. E. Anderson, "Characteristics of Li-Al and Li-Si Alloys as the Negative Electrode Materials in Li/LiCl-KCl/Li-M Cells," to be presented at the Washington Meeting of the Electrochemical Society, May 2-7, 1976.

19. W. Muller, H. Schafer, A. Weiss, Z. Naturforsch. *26b*, 534 (1971) and *25b*, 1371 (1970).

CATHODE SYSTEMS FOR ALUMINUM - MOLTEN CHLOROALUMINATE BATTERIES

G. Mamantov, R. Marassi,* and J. Q. Chambers

Department of Chemistry, The University of Tennessee
Knoxville, Tennessee 37916

We have been concerned with the electrochemical characterization of several potential cathode systems for batteries using low-melting (<200°C) molten chloroaluminate ($AlCl_3$-NaCl mixtures) solvents. These melts offer several advantages for molten salt battery applications,[1,2] such as the low liquidus temperatures (for example, the ternary eutectic $AlCl_3$-NaCl-KCl (63.5-20-16.5 mole %) has a liquidus temperature of 89°C[3]) and high conductivity (for ex., $AlCl_3$-LiCl (55-45 mole %) has a specific conductivity of 0.317 ohm^{-1} cm^{-1} at 200°C)[4]. The use of solid aluminum as anode is a potential advantage since aluminum is relatively inexpensive and has a small equivalent weight. In a secondary battery, the problems associated with formation of aluminum dendrites upon charging remain to be solved although some progress in this area has been recently reported.[5]

The aluminum-chlorine battery utilizing molten chloroaluminates has been investigated at Tyco Laboratories.[6] It has a high theoretical energy density (~1400 Whr/kg) and reasonable EMF's (open circuit voltage, OCV, ~2.1V). Problems associated with the use of the gaseous chlorine make the above battery, however, somewhat less desirable. Therefore, continuing needs exist for other cathode systems suitable for chloroaluminate melts.

We have investigated the following potential cathode systems in these melts: fluorinated graphite with different fluorine content ($CF_{0.85-1}$), binary and ternary intercalation compounds, such as C-WCl_6 and C-$AlCl_3$-Cl, several quinones, and positive iodine and sulfur cations. The latter, involving positive oxidation state(s) of sulfur, is the most promising cathode system of those studied. High OCV's (~2.1V) and significant current densities (~20mA/cm^2) were obtained with the preliminary design of a cell involving the system S_n^{m+} /Al.

In order to arrive at a better understanding of the electrode reactions occurring in charge/discharge processes in this cathode system, the electrochemical behavior of sulfur and sulfide in molten $NaAlCl_4$ saturated with NaCl was investigated at different temperatures and with different electrode materials. In melts containing sulfur one reduction and one oxidation wave are seen at tungsten and glassy carbon electrodes. At platinum two reduction waves are observed. The oxidation waves are similar for all three electrode materials.

Reduction of sulfur leads to the formation of sulfide; the oxidation leads to S(I) or S(II) depending upon the temperature, the higher oxidation state being formed at higher temperatures. The data obtained in sulfur solutions have been confirmed by the results obtained in melts containing Na_2S.

The mechanism for the electrochemical oxidation of sulfur apparently involves a complex set of charge transfer and chemical steps.

*Presently at Istituto Chimico, Universita di Camerino, 62032 Camerino, Italy

References

1. D. A. J. Swinkels in "Advances in Molten Salt Chemistry", Vol. 1, J. Braunstein, G. Mamantov, and G. P. Smith, Eds., Plenum Press, New York, 1971, pp. 165-223.

2. E. J. Cairns and R. K. Steunenberg in "Progress in High Temperature Physics and Chemistry", Vol. 5, C. A. Rouse, Ed., Pergamon Press, 1973, pp. 63-124.

3. B. G. Korshunov, " V. Safonov, and D. V. Drobot "Diagrammy Plavkosti Khloridnykh Sistem", Khimiya, 1972, p. 270.

4. P. V. Clark, "Fused Salt Mixtures - Specific Conductivity Tables", Report SC-R-69-1386, National Bureau of Standards, U.S. Dept. of Commerce, October 1969, p. 58.

5. R. C. Howie and D. W. MacMillan, J. Appl. Electrochem., 2, 217 (1972).

6. J. Giner and G. L. Holleck, NASA Report CR 1541, March 1970.

Acknowledgements

Our exploratory work on new cathode systems in chloroaluminate melts was supported by the U.S. Army Electronics Command, Contract DAAB-07-73-C-0060. A patent application covering the use of positive oxidation states of electronegative elements in chloroaluminate melts in high energy batteries has been filed by the Army Electronics Command. Our current work in this area is being supported by the Energy Research and Development Administration, Contract E-(40-1)-5053.

STUDIES ON THE NEGATIVE ALLOY ELECTRODE

Yasuhiko Ito*, Morio Matsunaga**, and Shiro Yoshizawa**
* Department of Chemistry, College of Liberal Arts and Sciences, Kyoto University, Sakyo, Kyoto, Japan
** Department of Industrial Chemistry, Faculty of Engineering, Kyoto University, Sakyo, Kyoto, Japan

ABSTRACT

Alkali metal alloy is a promising negative electrode for a high performance battery. Energy density and power density of such alloy electrodes can be discussed in relation to the phase diagram. Liquid alloy is preferable when cycle life is exaggerated, and solid alloy is preferable from the cell disign aspect. Experimental data to support such conclusions are shown in this paper.

INTRODUCTION

High temperature battery using molten salt electrolyte is very promising for a load leveling device. One of the reasons is its low polarization, and the other is that we can use alkali metal for a negative electrode active mass, which shows high electromotive force. But when we try to use alkali metal, some technical difficulties occur, such as metal fog formation and corrosion of the cell materials. Further difficulty is its low density. Because of it, alkali metal floats up to the upper part of the cell, and hence, the cell construction should be rather complex. To avoid such difficulties, the use of solid electrolyte or the paste type electrolyte, or the wick electrode etc. are proposed and developed elsewhere.

Another possible solution to such difficulties is to use alkali metal alloy, by which we can avoid metal fog formation and can design a simple cell construction. This paper concerns with a detailed study of alkali metal alloy electrode, by which basic concept in selecting high performance alloy electrode can be established. As an example, alkali metal-chlorine battery using such an alkali metal alloy electrode is discussed here, which reaction can be written as follows.

$$\begin{cases} \text{Positive electrode} & Cl_2 + 2e^- \underset{\text{Charge}}{\overset{\text{Discharge}}{\rightleftharpoons}} 2Cl^- \\ \text{Negative electrode} & Li(Me) \underset{\text{Charge}}{\overset{\text{Discharge}}{\rightleftharpoons}} Li^+ + e^- + Me \end{cases}$$

EXPERIMENTAL METHOD AND APPARATUS

Fig. 1 (a) shows an experimental cell used to examine solid alloy electrode. For a liquid alloy electrode, similar arrangement as shown in Fig. 1 (b) was used, too. Cell and cell holder is made of pyrex glass and when we needed long term operation, corundum cruicible was used for the cell. As

electrolytes, LiCl-KCl eutectic or LiCl-KCl-NaCl molten mixtures were used depending on the situation. All reagents used were chemically pure grade, which were dehydrated before use in a conventional manner (1). If necessary, further pre-electrolysis was done to eliminate residual water and other unknown contaminants. All experiments were carried out in a dried argon atmosphere. As a substrate metal of working electrode, zinc plate or aluminum plate was used for a solid electrode and lead or tin was used for a liquid electrode. To insulate molibdenum lead of negative electrode, alumina pipe covered it. As a counter electrode, Sn-Zn-Li liquid alloy or chlorine electrode war used depending on the situation. As a reference electrode, Li-Al alloy reported by Yao (2) or chlorine electrode was used, also depending on the situation. The Li-Al electrode was prepared by the electrolysis of LiCl-KCl eutectic melt.

CLASSIFICATION OF ALLOY ELECTRODES

Alloy electrodes are devided into two categories, that is, liquid alloy and solid alloy. As an example, let us consider Li-Zn alloy. Fig. 2 shows a phase diagram of it, given by Hansen. When we start charging it from pure Zn at 400°C, solid state is maintained until the Li concentration of 47 atomic %. And when we start it at 450°C, liquid state is maintained until 10 atomic %. Table 1 shows states of alloys at 450°C, expected from phase diagrams. Liquid $\rightleftharpoons$ Solid in this table means the alloy which can be used as a liquid at low concentration and can be used as solid at higher concentration.

EXPERIMENTAL RESULTS AND DISCUSSIONS OF SOLID ALLOY ELECTRODES

Effect of the number of charge-discharge cycles

Fig. 3 shows typical behavior of the negative electrode when zinc plate was used as a substrate. After charging with 100 mA/cm^2 for a certain minutes, this electrode was discharged with 100 mA/cm^2 until abrupt potential rising was observed. After that, discharging current was decreased to 50 mA/cm^2, by which potential went back to its proper position. When abrupt potential rising appeared again at this current density, discharging current was decreased further. These procedures were repeated until discharging current reached some hundreds μA/cm^2 . During these procedures, care was paid to keep the potential more negative than the dissolution potential of zinc plate itself. During the repetition of such procedures, charge-discharge current efficiencies and charge-discharge curves change with the number of charge-discharge cycles.

Fig. 4 shows current efficiencies as a function of the number of cycles. In this experiment, 20 atomic percent (Li and K) containing alloy prepared by the charging of 50 mA/cm^2 was discharged in the same way as above. Change of charging curve with a number of runs and that of discharging curve with it obtained by a maximum current density discharging are shown in Fig. 5 and Fig. 6, respectively. In Fig. 4, total current efficiency rises from 50 % to 90 % after several charge-discharge cycles. At the same time, discharging electric quantity obtained by a 50 mA/cm^2 discharging increased from 15 % to 85 %, too. On the other hand, electric quantity obtained by a discharge of 20 mA/cm^2 decreases from the third run and becomes to contribute only few %, at last. In Fig. 5, as the number of runs increases, potential plateaux at

+0.27 V, +0.05 V, and -0.06 V (vs. Li/Li-Al) appear more definitely and a figure of curves becomes more smooth. In a discharging cruve of Fig. 6, similar tendency can be observed. These might be explained by a slow mass transfer from the bulk to the surface of the solid electrode, which is accelerated by the structure change caused by a repetition of charge-discharge cycles. After more than three times' repetition of them, remarkable current efficiency change was not observed any more, and it stayed around 90 % as can be seen in Fig. 4. As an explanation of it, recombination of the produced alkali metal with chlorine, redissolution of the deposited K into electrolyte, and/or the trap of alkali metal inside the electrode etc. might be possible. But the third one can not be regarded as a main reason, because, by it, Fig. 5 can not be explained. As mentioned above, repetition of the charge-discharge cycle makes an active electrode, which is caused by an electrode structure change. But by it, expansion or degradation of the electrode is anticipated, which is not desirable from the viewpoint of cycle life. Then in a practical cell, it might be necessary to use some kind of matrix to buffer this structure change.

Fast discharge of the solid electrode

Fig. 9 shows discharging curves obtained at various current densities. The used electrode was pre-treated by repeating several charge-discharge cycles before obtaining these curves. Initial Li concentration of this electrode was 10 atomic %. Current efficiency stayed within 50 - 70 % in each discharging, and this means rapid mass transfer rate in the electrode, as has been expected. At 2 A/cm^2, however, abrupt potential change was observed even at the begining. But at 1 A/cm^2, fairly stable potential could be obtained. And for example, when we discharged it from the initial Li concentration of 40 atomic %, ten minutes' discharge of 1 A/cm^2 was possible. Table 2 summarizes the data read from Fig. 9. Power density was calculated by assuming the electrode thickness of 1 mm. This result shows high feasibility of this type of cell.

EXPERIMENTAL RESULTS AND DISCUSSIONS OF LIQUID ALLOY ELECTRODE

Concerning with a cycle life, liquid alloy electrode seems more preferable. Because, it does not change its structure at all by charge-discharge cycles. And hence, it is worth examining liquid alloy electrode more detailedly in a practical sense.

Behavior of liquid alloy electrodes in LiCl-KCl

As mentioned above, concentration range to be used in a liquid state can be anticipated from the phase diagram. For example, Li-Zn system can be used as a liquid until 10 atomic % Li at 450°C, but this liquid phase region is rather narrow. Then it is necessary to seek for the other system that has a wide liquid phase region. Li-Sn and Li-Pb systems are interesting in this sense, which diagrams are shown in Fig. 10. Fig. 11 shows charge-discharge curves obtained by the use of Li-Pb system in LiCl-KCl. As can be seen in this figure, behavior of the liquid alloy differs from that of solid alloy electrode. That is, in the case of liquid alloy, electrode potential shifts gradually towards the negative potential as the charging electric quantity increases, until -3.18 V. This final potential of -3.18 V corresponds to the liquid-solid two phase co-existing region. Current efficiency of liquid electrode is usually more than 95 % and effect of the repetition of charge-

discharge cycles was not observed in this case. Hence liquid metal electrode is more preferable from the cycle life vierpoints as mentioned at the top of this chapter.

Behavior of liquid electrodes in LiCl-KCl-NaCl

From an economical viewpoint, possibly small amount of LiCl should be used, because it is rather expensive. In addition to this, an expectation to find new suitable electrolyte for getting high performance battery, let us try the addition of NaCl into LiCl-KCl system. Fig. 12 shows charge-discharge curves obtained by the use of LiCl-KCl-NaCl electrolyte and liquid lead substrate. The reason of using lead as a substrate is its feasibility of making liquid phase both with Li and K in a fairly wide concentration range, and with Na in a whole concentration range. From Fig. 12, solid formation of this alloy electrode is suggested at the potential of -3.16 V. That is, this potential suggests solid-liquid equilibrium. Comparing this result with that of Fig. 11, increase of charging capacity by the addition of NaCl is confirmed. Both liquid and liquid-solid equilibrium phases are included in the discussion. Fig. 13 shows more remarkable effect of NaCl addition, which was obtained by a potentiostatic charging and subsequent constant current discharging. Detailed study of such effect is necessary in future.

UTILIZATION OF BOTH LIQUID AND SOLID PHASE AS AN ALLOY ELECTRODE

If we can use both liquid and solid phase as an active mass, capacity of this electrode will increase very much. For example, with Li-Sn system, electric quantity obtained from the alloy containing Li of 80 atomic % is four times more than that obtained from the liquid alloy containing maximum Li concentration of 50 atomic %. To confirm such an idea, Li-Sn system was examined in LiCl-KCl. Fig. 14 shows charge and discharge curve for this electrode. Unfortunately, maximum charge capacity was only 50 % of the theoretically expected, when we charged at 100 mA/cm^2, which is probably due to the slow mass transfer in the solid electrode. At discharging, potential plateau at -3.24 V was observed, that is probably due to the solid alloy discharge in a two phase co-existing region. Fig. 15 shows discharge curve obtained by the same electrode at different current densities. Initial concentration was 67 atomic %. Violent potential disturbance was observed at the current density of 1 A/cm^2, but otherwise, fairly high current efficiency was obtained. Table 3 summarizes the results obtained from Fig. 15. Power density of it is only about 10 % of that of Li-Zn system. It mainly comes from the fact that the thickness of at least 3 mm was necessary in stead of 1 mm for solid electrode, to keep liquid electrode on the substrate. By the way, the current efficiency was more than 90 % in each case.

CONCLUDING REMARKS

From a viewpoint of high current density and stable potential, solid electrode is preferable and from that of cycle life, liquid alloy electrode is more preferable. Utilization of both liquid and solid phase is also possible. Concerning with the electrolyte, lowering of the cost by an addition of NaCl or other electrolyte will be an interesting subject in future.

REFERENCES

(1) H.A. Laitinen et al, J. Electrochem. Soc., 104, 516 (1957)
(2) N.P. Yao, J. Electrochem. Soc., 118, 1039 (1971)
(3) M. Hansen, K. Anderko, " Constitution of Binary Alloys ", Mcgraw-Hill, N.Y. (1958)

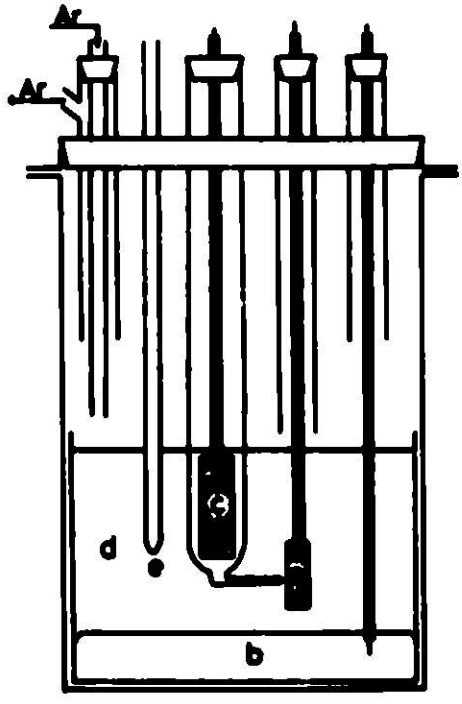

Fig.1 (a)

a: solid Li-Zn/Li⁺ electrode(W.E.)
b: liquid Li-Sn-Zn/Li⁺ electrode(C.E.)
c: solid Li-Al/ Li⁺ electrode(R.E.)
d: electrolyte (LiCl-KCl melt)
e: thermocouple

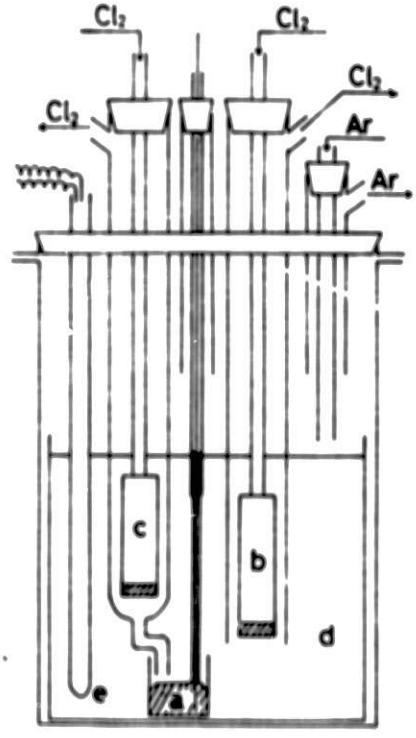

Fig.1 (b)

a : liq. alloy electrode
b : Cl_2-gas electrode(C.E)
c : Cl_2-gas electrode(R.E)
d : electrolyte
e : thermocouple

Fig. 2

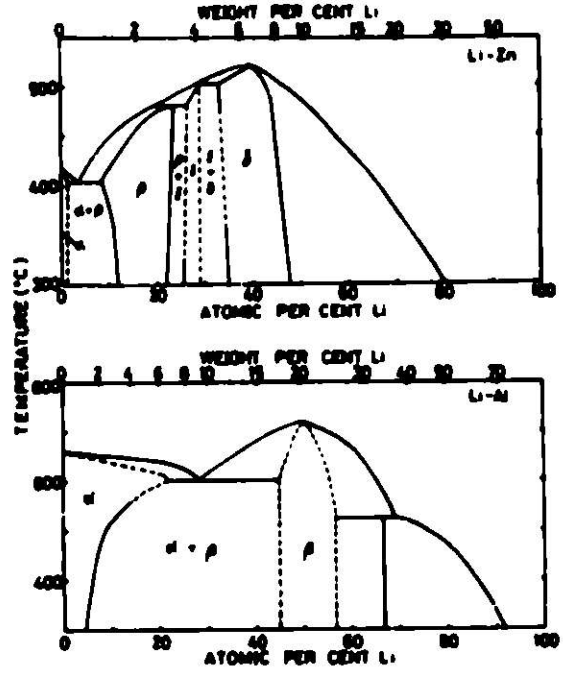

Table 1

STATE OF ALLOY	EXAMPLE
LIQUID	Sn-Li, Pb-Li, Bi-Li, Zn-Li (450°C), Na-Pb.
SOLID	Zn-Li (400°C), Al-Li
LIQUID⇌SOLID	Li-Sn, Li-Pb.

Fig. 3

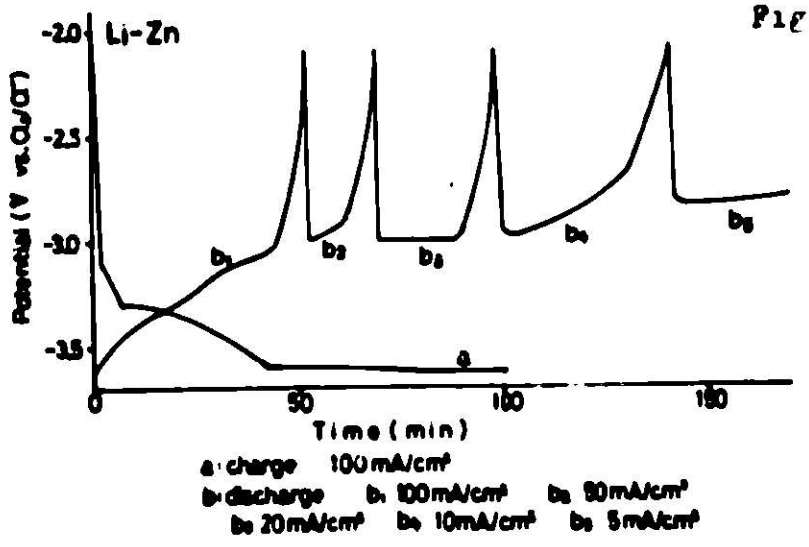

a: charge 100 mA/cm²
b: discharge b₁ 100 mA/cm² b₂ 50 mA/cm²
b₃ 20 mA/cm² b₄ 10 mA/cm² b₅ 5 mA/cm²

Fig.4

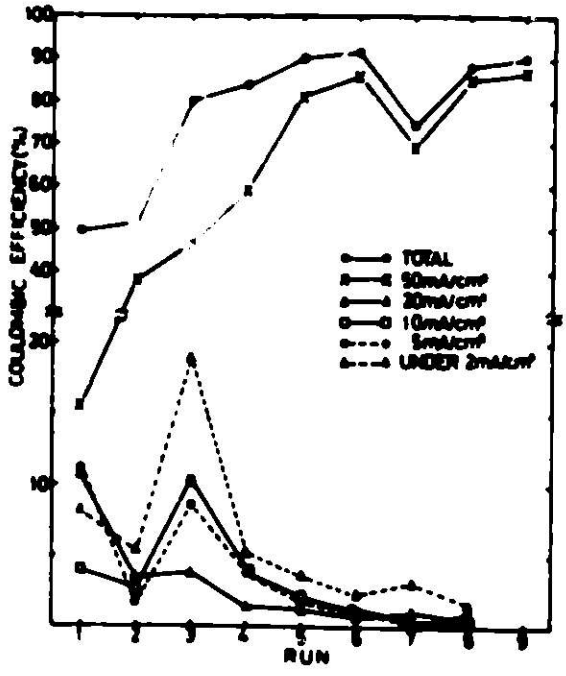

Fig.5

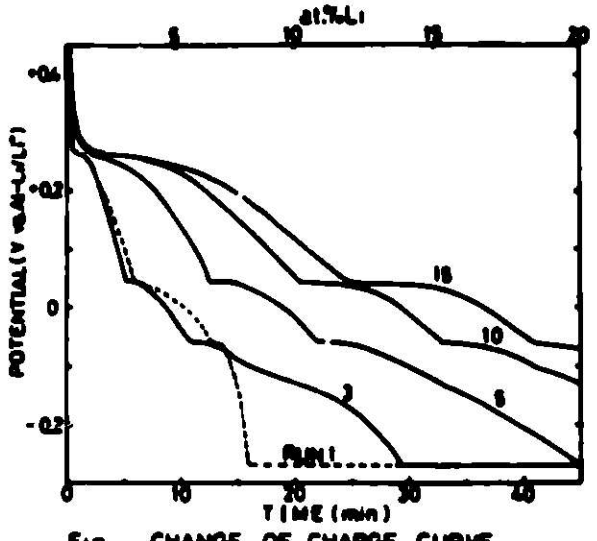

Fig CHANGE OF CHARGE CURVE
(current density 50mA/cm²; tem 380°C)

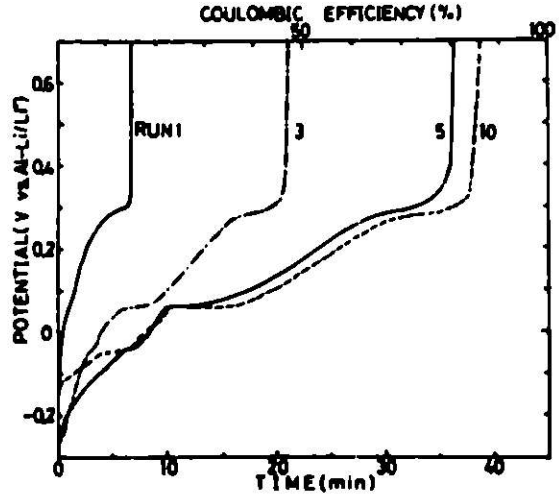

Fig.6

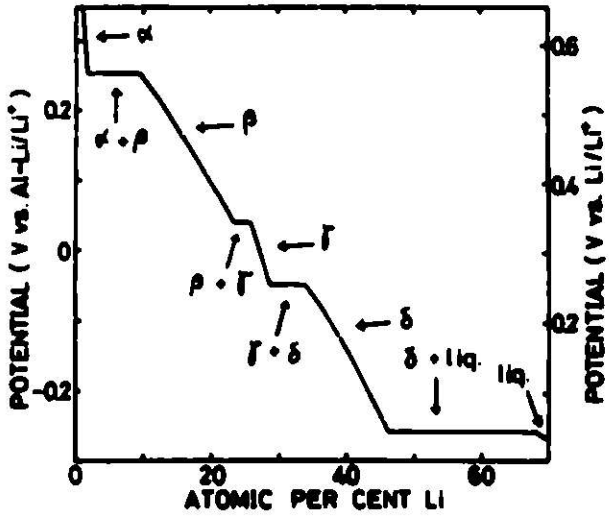

Fig.7

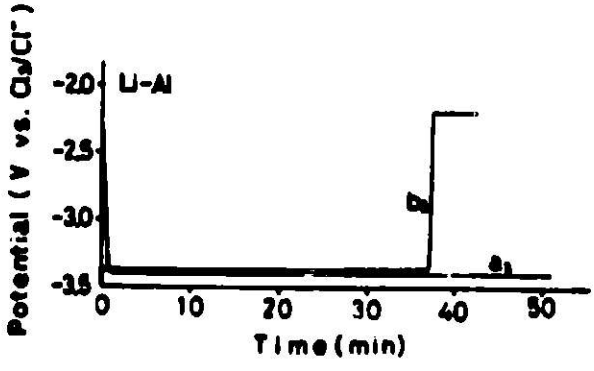

Fig.8

charge 50 mA/cm²
discharge 50 mA/cm²

Fig. 9

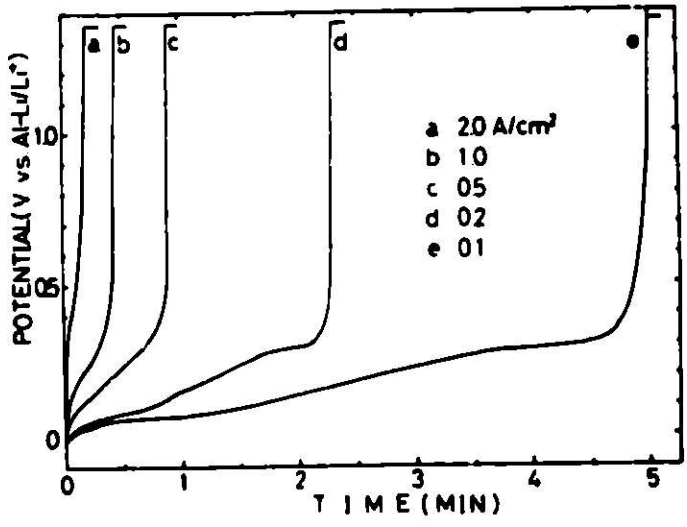

Table 2

Current density (amp/cm²)	Potential range (volt)	Duration (min)	Power density (kw/kg)	Utilization (%)
2.000	-3.35~-2.70	0.16	19.1	47.1
1.000	-3.35~-295	0.36	9.88	55.9
0.500	-3.35~-3.02	0.80	5.00	58.8
0.200	-3.36~-3.05	2.15	2.02	63.2
0.100	-3.38~-3.05	4.60	1.01	67.6

Fig.10

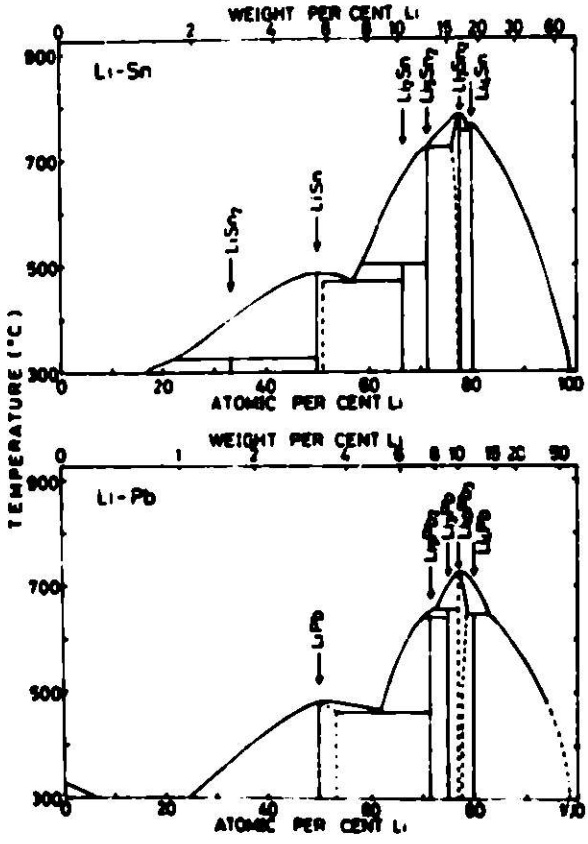
WEIGHT PER CENT Li
Li-Sn
Li-Pb
TEMPERATURE (°C)
ATOMIC PER CENT Li

Fig.11

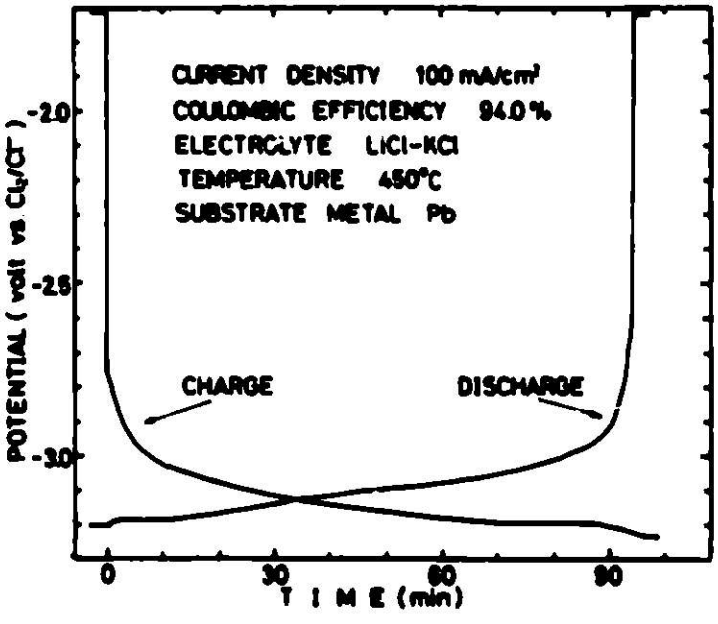
CURRENT DENSITY 100 mA/cm²
COULOMBIC EFFICIENCY 94.0 %
ELECTROLYTE LiCl-KCl
TEMPERATURE 450°C
SUBSTRATE METAL Pb
CHARGE
DISCHARGE
POTENTIAL (volt vs. Cl₂/Cl⁻)
T I M E (min)

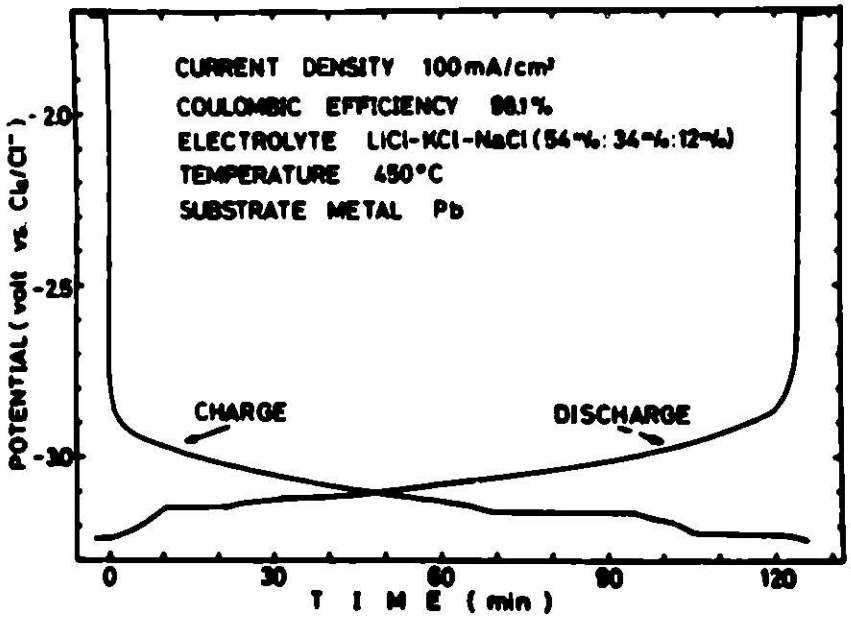
CURRENT DENSITY 100mA/cm²
COULOMBIC EFFICIENCY 98.1%
ELECTROLYTE LiCl-KCl-NaCl (54~%: 34~%: 12~%)
TEMPERATURE 450°C
SUBSTRATE METAL Pb
CHARGE
DISCHARGE
POTENTIAL (volt vs. Cl₂/Cl⁻)
-2.0
-2.5
-3.0
0
30
60
90
120
T I M E (min)

Fig. 12

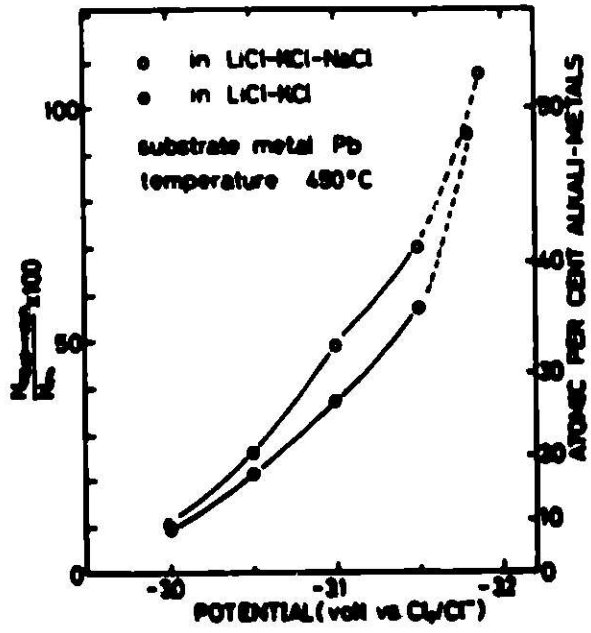
in LiCl-KCl-NaCl
in LiCl-KCl
substrate metal Pb
temperature 450°C
100
50
0
-30
-31
-32
POTENTIAL (volt vs. Cl₂/Cl⁻)
ATOMIC PER CENT ALKALI-METALS
40
30
20
10
0

Fig. 13

Fig. 14

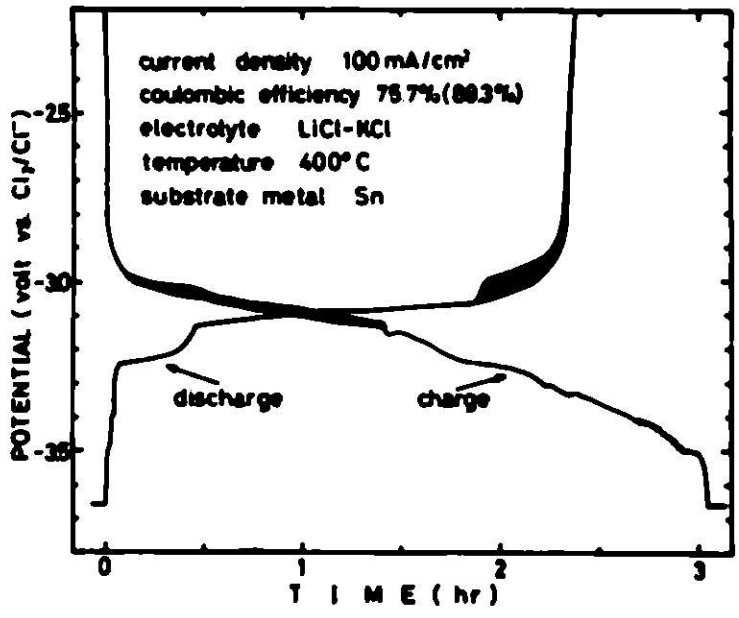

Fig. 15

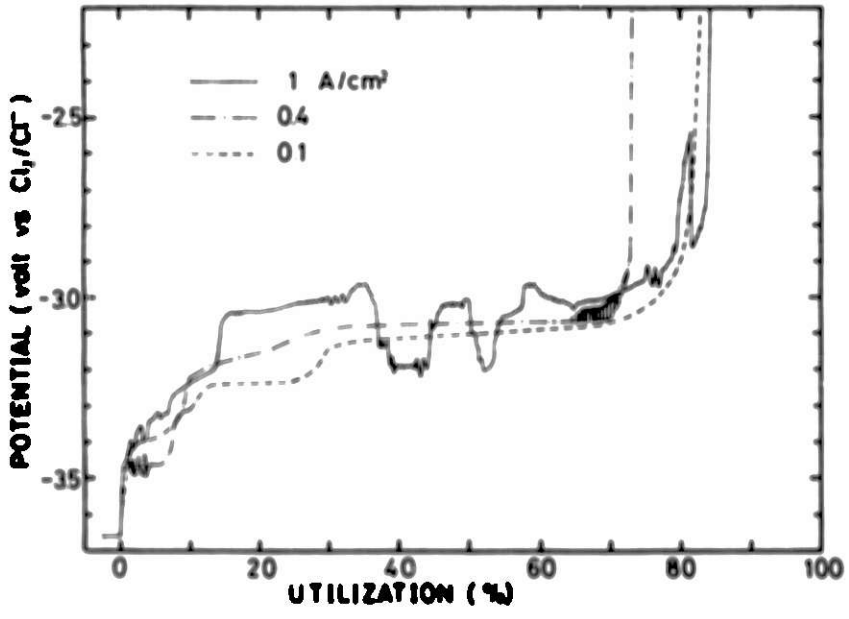

Table 3

CURRENT DENSITY (amp/cm²)	POTENTIAL RANGE (volt)	POWER DENSITY (W/kg Sn)	UTILIZATION (%)
1.000	-347 ~ -255	907	83.9
0.400	-347 ~ -290	369	72.8
0.100	-350 ~ -290	92.2	80.2

LITHIUM-SILICON ELECTRODES FOR THE LITHIUM – IRON SULFIDE BATTERY*

L. R. McCoy and S. Lai
Rockwell International
Atomics International Division
Canoga Park, Calif.

ABSTRACT

Lithium- ilicon negative electrodes are being developed at Atomics International for use in high temperature (400°C) lithium-iron sulfide load-leveling batteries. These electrodes discharge in a series of voltage plateaus with an average open-circuit potential of 230 mv positive to lithium. Four alloy compositions, solid at temperatures below ~600°C, have been identified. Thermodynamic data for the formation of each composition has been calculated. Light weight structures providing current collection as well as support and containment for the alloys have been found. These electrodes have specific capacities in excess of 0.80 amp-hr/cm^3 and 80% or more utilization of the theoretical capacity of the active material has been obtained at current densities (40 ma/cm^2) of interest to load-leveling service with electrodes 0.64 cm thick. Optimization studies are being made to determine the effect of structural variables and specific capacity loading on electrode performance.

INTRODUCTION

High temperature lithium-iron sulfide batteries are presently under development at Argonne National Laboratory (ANL) and at the Atomics International (AI) Division of Rockwell International for use in electric utility load-leveling plants and electric vehicles.[1,2] These batteries use a molten KCℓ-LiCℓ electrolyte and, therefore, operate at temperatures of 400°C or higher. The cell designs under study at both locations utilize iron sulfide positive electrodes and porous ceramic separators resistant to attack by the electrolyte and lithium.

Different approaches have, however, been taken with the lithium electrode. ANL cells use a lithium-aluminum alloy with a potential, 303 mv positive to lithium metal at 400°C. Until last year, work at AI emphasized the development of liquid lithium negative electrodes as these would provide higher energy densities and very low negative electrode polarization, even at high rates of charge and discharge. These electrodes used a porous Feltmetal support with the liquid lithium retained in this structure by capillary forces. Despite significant advances in extending the life of these electrodes by the use of "wetting" alloying additives such as copper and zinc, slow capacity losses were experienced due to escape of lithium metal in dispersed form during charge.

*Work performed under Rockwell International sponsored program.

Because of this difficulty, a search was made to find solid alloys which would provide more reliable containment of lithium but which would have a more favorable potential vs lithium than does the lithium-aluminum alloy. This work has resulted in the discovery of the lithium-silicon alloy electrode at Al. This paper will describe the properties of this electrode and the current status of the development effort.

MATERIALS

Lithium metal from Foote Mineral Division of Newmont Mining Company was used in all experiments. Silicon, 97% pure, purchased from MCB was used in the preparation of the alloys. Highly purified electrolyte salts were purchased from Anderson Laboratories for the tests described below. Feltmetals, used as porous electrode supports, are compacted and sintered metal fiber materials produced by the Brunswick Corporation under that trade name. Other metal supporting structures used in these investigations are described below.

PROPERTIES OF LITHIUM-SILICON ALLOYS

Discharge of small electrodes prepared using alloy compositions containing 60 wt % lithium disclosed the existence of four distinct voltage plateaus corresponding to alloys solid at temperatures above 600°C. A series of measurements were made to characterize these voltage plateaus and to identify the alloy compositions corresponding to each.

A lithium-silicon electrode was prepared by impregnating a titanium fiber mat (100-μ wires, 70% porous, obtained from Gould, Inc.) with a molten alloy containing 60 wt % of lithium and 40 wt % of silicon at 700°C. Titanium was chosen for the supporting structure because the solubility of this metal in lithium is low and it therefore resists attack by the molten alloy during the impregnation process. A copper Feltmetal panel, impregnated with pure lithium metal, was used as the counter-electrode. A nickel Feltmetal panel, impregnated with pure lithium, was used as the reference electrode. The electrode leads were mounted through insulated feedthroughs brazed to a close-fitting cover for a beaker containing the KCl-LiCl eutectic salt electrolyte. A thermocouple well permitted the temperature of the electrolyte to be monitored.

The electrode was discharged through the successive voltage plateaus, disregarding the first, substantially at the lithium potential. From the known weight of the alloy in the electrode, and the quantity of charge passed at each transition point, it was possible to calculate the alloy compositions with fair precision. The variation in potential at each voltage plateau was also measured over the range of 360 to 440°C. The variation of potential with temperature was sufficiently linear that a straight line formula could be written for each plateau using the least squares method. The voltage-temperature relationship derived in this manner is shown in Table 1.

TABLE 1

EMF OF LITHIUM-SILICON ALLOYS VS LITHIUM METAL

Voltage Plateau at 400°C (mv)	Temperature Dependence (mv vs °K)
+ 48	137.7 - 0.1336T
+158	276.5 - 0.1761T
+280	332.1 - 0.0771T
+336	430.7 - 0.1402T

The experimentally determined compositions are shown in Figure 1 together with alloy compositions described in literature.[3,4] The compositions, Li_5Si and Li_2Si, have been established with some certainty. The empirical formula, $Li_{4.1}Si$, is more likely to be Li_4Si. More precise tests will be required to establish the exact stoichiometric ratio. No reference has yet been found to a composition even approximating that of $Li_{2.8}Si$.

From the temperature dependence of the electrode potentials shown in Table 1, it is possible to calculate ΔS_f° and, in turn, ΔH_f° and ΔG_f° using the usual well-known thermodynamic relationships. The results of such calculations appear in Table 2.

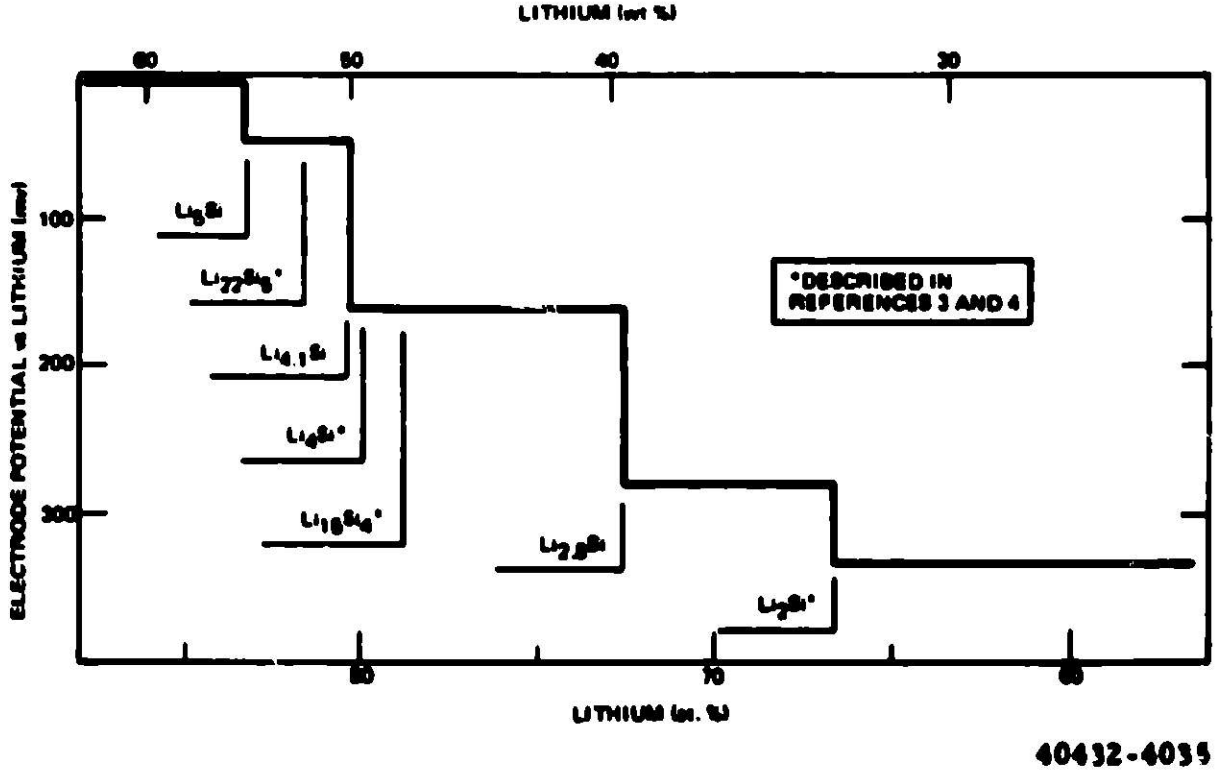

40432-4035

Figure 1. Lithium-Silicon Alloy Compositions

TABLE 2

THERMODYNAMIC DATA FOR LITHIUM-SILICON ALLOYS AT 400°C

Alloy	ΔG_f° (Kcal/mole)	ΔS_f° (eu)	ΔH_f° (Kcal/mole)
Li_5Si	-26.4	-15.9	-37.1
$Li_{4.1}Si$	-25.4	-13.2	-34.3
$Li_{2.8}Si$	-20.7	- 7.9	-26.0
Li_2Si	-15.5	- 6.5	-19.9

From Figure 1, it can be seen that the more lithium-rich alloy, Li_5Si, contains 55 wt % of lithium, establishing the maximum capacity for solid alloys of this type at 2.12 amp-hr/gm of Li_5Si. This is more than twice that achievable with lithium aluminum alloys solid at 520°C (~0.8 amp-hr/gm). The average voltage of all plateaus covered in the complete discharge of Li_5Si is 230 mv positive to lithium, vs 303 mv for lithium-aluminum. If some capacity in ampere-hour per gram is sacrificed by restricting discharge to only half of the 336-mv plateau, the electrode potential loss vs lithium can be reduced. Under this condition, the average potential is 170 mv positive to lithium, while the capacity is still 1.6 amp-hr/gm of the starting alloy Li_5Si.

These results, together with early experiments showing excellent capacity retention of alloys electrodes during cycling, provided a strong incentive to investigate lithium-silicon alloy electrodes thoroughly.

LITHIUM-SILICON ALLOY ELECTRODE STRUCTURES

Initial efforts to produce practical electrodes using lithium-silicon alloys as the active material followed earlier practices used with liquid lithium where porous metal substrates were impregnated with the molten metal at high temperatures. Feltmetal made from low carbon steel using 8-μ diameter wire was used as one of the first supports tested. These electrodes, measuring 2.5 cm by 2.5 cm by 0.31 cm, were cycled at 50 to 100 ma/cm^2 against high capacity liquid lithium electrodes in the KCl-LiCl electrolyte without detectable loss of capacity. It was subsequently found, however, that on extended cycling, the electrode volume increased noticeably and the electrode slowly disintegrated due to disruption of the relatively weak supporting structure by the swelling forces generated by the alloy when charged and discharged repetitively. Complete discharge of these electrodes also led to physical loss of small quantities of silicon with the obvious inference that capacity could be lost in this manner.

It was realized from these early investigations that physically stronger supporting structures were required, and that the full volumetric capacity of the alloy (~2.3 amp-hr/cm^3) could not be utilized in practical electrodes. Sintered titanium plaques (35% dense) and stronger Feltmetal structures

(20% dense, Type 430 stainless steel, 46-μ diameter wire) were impregnated with molten lithium-silicon alloys containing 60 wt % of lithium at 700°C and electrochemically stripped to 55 wt % lithium to reduce the specific capacity to 2.1 amp-hr/cm^3. These electrodes were cycled with greater success but evidence of swelling or cracking of the supporting structure was found also in these cases.

Further reductions in capacity were tested by the expedient of filling the porous substrates with more lithium-rich mixtures at high temperatures and then electrochemically stripping excess lithium in KCl-LiCl electrolyte to bring the alloy composition to the 55 wt % lithium content prior to use. It was established in this manner that a theoretical volumetric capacity of 1.5 amp-hr/cm^3 (based on void volume) could be entirely contained within the confines of the structure and that extended cycling could be conducted without evident change in the electrode dimensions. Losses of silicon, observed earlier after complete discharge, were also avoided in this manner.

The final evolutionary stage in structural investigations was reached when it was realized that the dense supporting structures previously described could be replaced with more open-pored materials with internal strength provided by concentration of the mass in fewer but heavier connecting members. At this time, supporting structures only about 6% dense are being used without difficulty. In this case, a covering of fine-pored material is required as a particle retainer. The weight of the supporting structures of this type is approximately equal to that of the active material. Stainless steel is presently used as the material of construction because of its ready availability in the required physical forms. Low carbon steel appears to be equally suitable and is preferred on the basis of cost and better electrical conductivity.

With the adoption of open-pored supporting elements, the electrode could be loaded directly with the powdered Li_5Si alloy, eliminating the need for the inefficient fill-and-strip operation described. It has also been found feasible to fill the pores with powdered silicon and charge the electrode electrochemically. This procedure provides the option of fabricating the electrode in the discharged condition.

EXPERIMENTAL RESULTS

Two types of tests with lithium-silicon alloy electrodes are currently in progress. In one case, the test electrode is cycled against a larger counter electrode with the working electrode potential monitored vs a liquid lithium reference electrode, as shown in Figure 2. These electrodes measure 5.1 cm by 5.1 cm by 0.64 cm thick. The porous internal support is housed within a stainless steel box, 0.64 cm deep to define the working area to the one exposed face. A fine-pored covering is used over the exposed electrode area. This test procedure is being used to determine the effects of variations in specific capacity loading and on structural parameters on electrode performance. Electrode resistance and polarization are measured as a function of current density at charge-discharge rates ranging from 20 to 100 ma/cm^2. Because of the large number of variables to be investigated,

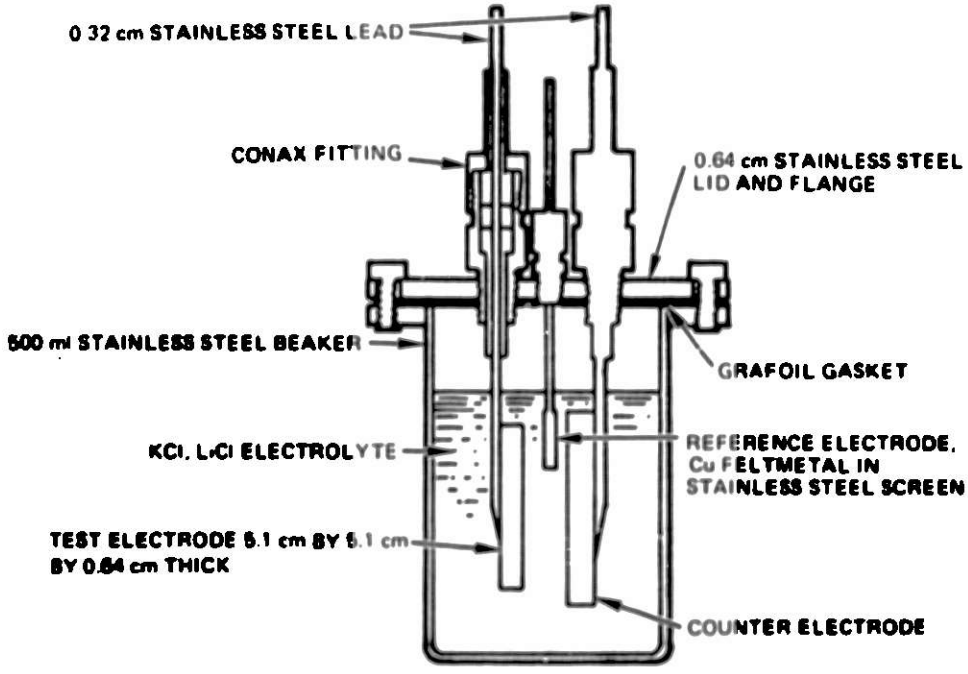

Figure 2. Lithium-Silicon Electrode Test Cell

these are necessarily short-term tests. Long-term tests of representative negative electrodes are presently being conducted in completed cells built and operated under associated programs funded by ANL and the Electric Power Research Institute (EPRI).

The effect of the internal supporting structure on electrode performance is shown in Figures 3 and 4. In these figures, the discharge curves are "folded back" under the charge curve to permit ready comparison. The data shown in Figure 3 were taken with an electrode using 20% dense Type 430 stainless steel Feltmetal with a median pore size of 0.2 mm as the internal supporting structure and having a specific capacity of 1.2 amp-hr/cm^3 of electrode void volume. The charge-discharge curves show little symmetry and the voltage plateaus are poorly defined in the charge mode. A recovered capacity about 60% of the theoretical value was reached under these conditions. The results shown in Figure 4 were obtained with an electrode with the same dimensions and about the same theoretical capacity based on void volume. In this case, however, the pore size of the internal support was more than ten times that of the other electrode and the greater reversibility is apparent. Electrodes of the latter type can be charged successfully at current densities up to 100 ma/cm^2, but at this point, the behavior on charge begins to approach that shown in Figure 3. At current densities of 40 and 80 ma/cm^2, capacities corresponding to 80 and 64% respectively of the theoretical values were reached. The values given for 40 ma/cm^2 correspond to a specific capacity of 0.85 amp-hr/cm^3.

Although little data are presently available to show the effect of electrode thickness on electrode performance, one experimental electrode, 0.26 cm thick has been tested at a current density of 35 ma/cm^2 and found

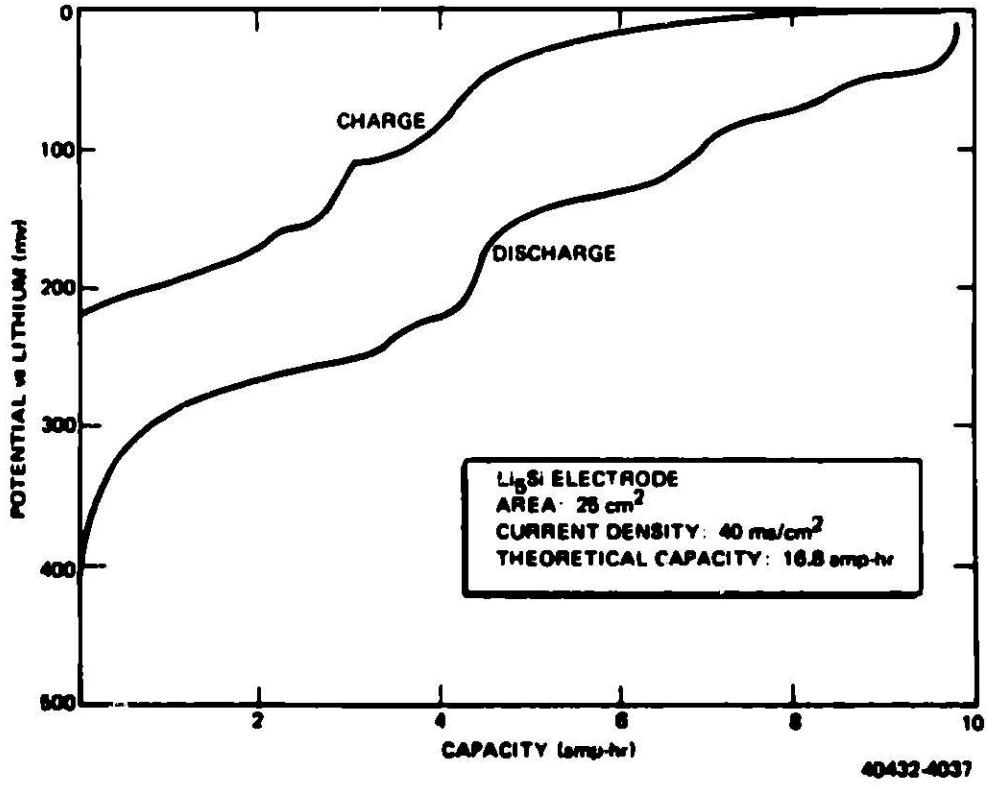

Figure 3. IR-Free Polarization, Feltmetal Structure

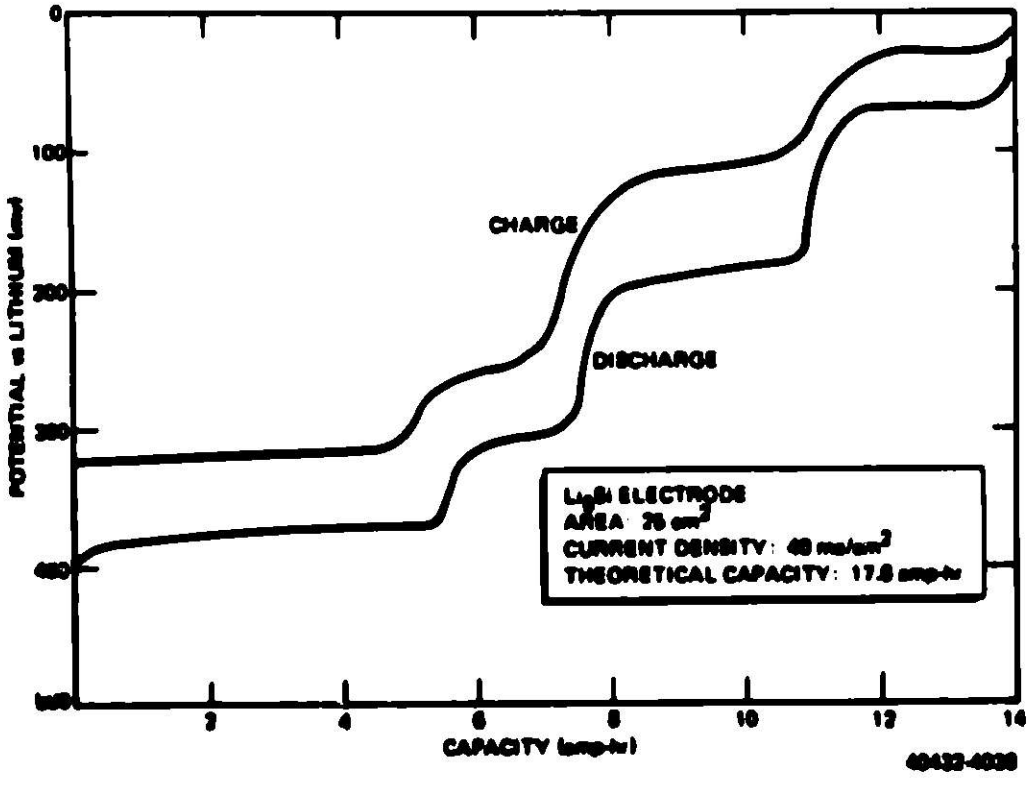

Figure 4. IR-Free Polarisation, Open-Pored Structure

to yield an active utilization of 91%. The specific capacity under these conditions was 1.06 amp-hr/cm^3.

Electrodes using the more open-pored structure described above are now in use in a 25 whr and a 150 whr cell built with EPRI and ERDA funds. These have sustained continued cycling at C/5 and C/10 rates for thousands of hours without evidence of physical deterioration or capacity loss in the sealed (150 whr) cell. A summary of several long-term tests of these electrodes is given in Table 3.

TABLE 3

LONG-TERM LITHIUM-SILICON ELECTRODE TESTS

Electrode	Electrode Area† (cm^2)	No. of Cycles	Time (hr)
LiSi/Li Cell*	8	300	2500
25 whr LiSi/$FeS_{1.5}$ Cell§	25	300	5040
150 whr LiSi/$FeS_{1.5}$ Cell**	100	390	5440

*Test electrode cycled against lithium counter-electrode, open cell.
†Area of one side of the electrode
§Open cell
**Sealed cell

CURRENT PROGRAM

Current investigations are concerned with optimizing lithium-silicon electrodes for use in load-leveling batteries. As discussed in the preceding text, the nature of the supporting structure has a profound effect on the performance of these electrodes and this matter is receiving first attention. This element of the electrode must not only satisfy performance needs but must be potentially inexpensive and long-lived in the cell environment. Optimum loading in terms of specific capacity is a second matter of importance and recent data show that this will be influenced by the active depth of the electrode. This aspect of electrode investigations is as yet in its earliest stages. Finally, although the feasibility of loading these electrodes in the discharged state, e. g., with silicon powder, has been well established, further work will be done with this method of electrode preparation.

REFERENCES

1. W. Schertz, A. Chilenskas, and V. Kolba, "Battery Design and Cell Testing for Electric-Vehicle Propulsion," Record of the Tenth Intersociety Energy Conversion Engineering Conference, Newark, Delaware, August 18-22, 1975, p 634

2. S. Sudar, L. McCoy, and L. Heredy, "Rechargeable Lithium/Iron Sulfide Battery," Record of the Tenth Intersociety Energy Conversion Engineering Conference, Newark, Delaware, August 18-22, 1975, p 642

3. F. A. Shunk, Constitution of Binary Alloys, Second Supplement, (McGraw-Hill, New York 1969), p 481

4. B. W. Mott, "Intermetallic Compounds and Alloys of the Alkali Metals," Special Publication No. 22, The Chemical Society, Burlington House, London, 1967, p 92

THE CHARACTERIZATION OF POROUS Li-Al ALLOY ELECTRODES

D. R. Vissers and K. E. Anderson

Argonne National Laboratory
9700 South Cass Avenue
Argonne, Illinois 60439

ABSTRACT

The effects of electrolyte void fraction (0.2, 0.4 and 0.7), electrode thickness (0.3 and 0.6 cm), and the type of current collector on the performance of porous Li-Al electrodes were investigated. The results of these studies, which were conducted at ~425°C, were as follows: (1) At moderate current densities (~100 mA/cm^2), the lithium utilization (fraction of the theoretical capacity of the Li-Al electrode) decreased markedly as the electrode thickness was increased from 0.32 to 0.64 cm. (2) The capacity densities of the 0.32-cm and 0.64-cm thick electrodes were higher with 0.2 volume fraction of the electrolyte than with a higher volume fraction of 0.7. (3) The Li-Al electrode performance was apparently limited by resistive polarization associated with the electrolyte, and with particle-to-particle contact of the Li-Al within the porous structure. (4) The addition of a porous metal current collector greatly improved the performance of the 0.64-cm-thick Li-Al electrode.

INTRODUCTION

Secondary batteries of high specific power and high specific energy are being developed at the Argonne National Laboratory (ANL) for application to off-peak energy storage on electric utility networks and to automobile propulsion. The present cells utilize positive electrodes of either iron sulfide (FeS) or iron pyrite (FeS_2),[1-5] negative electrodes of lithium-aluminum alloy,[6-10] and a molten salt electrolyte such as LiCl-KCl eutectic (mp, 352°C), and are operated at temperatures between approximately 400-450°C.

A 48 at. % lithium-aluminum alloy has shown excellent promise of meeting the performance requirements for negative electrodes in these cells.[11-14] Previous attempts to develop a negative electrode using liquid lithium as the active material for high-energy secondary cells have been extensive,[15-18] but generally unsuccessful. The primary problem in these cells has been cell shorting. This problem results from the high rates of corrosion of the ceramic separators and feedthroughs by liquid lithium and from the movement of liquid lithium from the negative electrode structure into the ceramic separator, with consequent decline in cell capacity with time. The problem can be avoided or alleviated by the use of a solid lithium-aluminum alloy as the negative electrode material.

The present electrodes utilize that portion of the lithium-aluminum phase diagram wherein both the β-phase of Li-Al and the lithium-saturated α-phase of aluminum are present. In going from this region, which at 425°C has a

potential of +0.3 V relative to liquid lithium* into the single-phase region of β-phase Li-Al, the potential of the Li-Al material decreases very rapidly as the lithium content increases, as shown by the studies of Selman *et al.*[9] These studies also indicated that the use of Li-Al electrodes containing more than 50 at. % lithium is not practical because of the high lithium activity at these concentrations.

This paper deals with studies that were carried out at ANL on the lithium-aluminum electrode system to gain a better understanding of the parameters that limit the performance of the electrode system. These investigations addressed the effects of electrode performance on the electrolyte volume fraction, the electrode thickness, and the type of current collector used in the electrode structure.

A liquid lithium electrode was chosen as the counter-electrode because this electrode is unpolarized at high current densities.[10] Thus, the liquid lithium electrode serves both as a working electrode and as a near-perfect reference electrode. Consequently, for measurements made during normal cycling, the electrochemical potential of the Li-Al electrode could be easily monitored. Current interruption and ac impedance measurements were made to examine the overpotential characteristics of the different electrodes.

EXPERIMENTAL

The general design of the cells is illustrated in Fig. 1. The lithium counter-electrodes consisted of 5 cm-dia by 0.64-cm-thick disks of Type 302

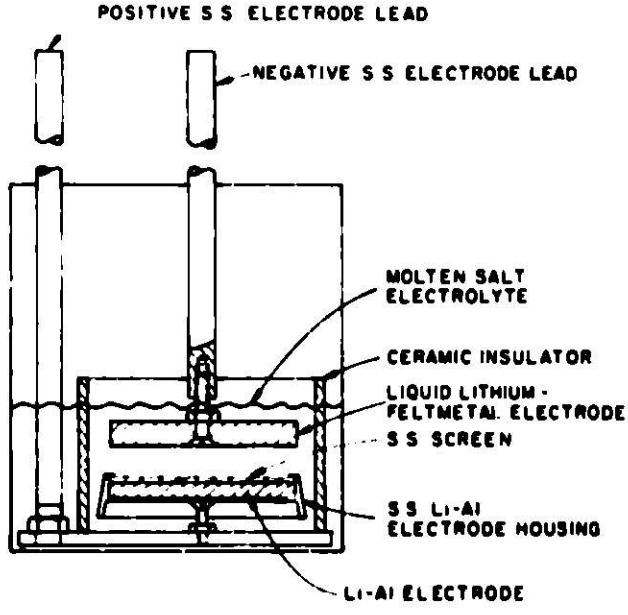

Fig. 1. Cell Design

*All potentials reported in this paper are relative to liquid lithium and are IR-free.

stainless steel Feltmetal (90% porosity, 27 μm ave. pore dia) that contained ∿6 g of lithium. Approximately 25 wt % copper was added to the liquid lithium to improve the lithium retention in the Feltmetal.

Most of the Li-Al electrodes were prepared electrochemically from pressed aluminum plaques. The plaques were formed by pressing aluminum York mesh (fabricated from 6-mil aluminum wire) to a thickness of either 0.32 or 0.64 cm. The weight of aluminum was chosen to give electrolyte volume fractions, in the charged electrodes, of 0.2, 0.4 and 0.7. Approximately 2 wt % stainless steel wire, 5 mil in diameter, was incorporated into each aluminum mesh structure before pressing to serve as a current collector. The plaques were contained in housings of Type 304 stainless steel. Two screens (16 and 24 mesh) across the face of the housing provided support for the electrodes, while a piece of zirconia fabric was inserted between the aluminum plaque and the screen to retain the Li-Al particles, which are formed during electrochemical cycling. Some electrodes were prepared electrochemically from aluminum powder that had been vibratorily loaded into a porous iron Retimet structure. The Retimet was obtained from the Hydro-jet Corporation, Rancho Santa Fe, Cal. In the uncharged Li-Al electrode design for Cell DK-19, two layers of Retimet ∿0.4 cm thick by 5 cm in diameter were employed. The Retimet was expected to provide improved current collection. All the Li-Al electrodes had areas of 15.6 cm^2.

The cell electrolyte was LiCl-KCl eutectic (mp, 352°C) obtained from the Anderson Physic Laboratories Inc., Urbana, Illinois, where it was prepared by a procedure outlined by Laitinen, Tischer, and Roe.[19] The cells, which were unsealed, were operated at temperatures between 400 and 500°C in a furnace well located in the floor of a high-purity (∿3 ppm O_2, ∿1 ppm H_2O) helium-atmosphere glovebox.

The cells were cycled at constant current with the aid of a regulated ac power supply. A meter relay automatically reversed the polarity of the power supply when a cell reached the preset cutoff voltage for either charge or discharge. In this way, the cells could be automatically charged and discharged at selected current densities. The total capacity (A-hr) for the charge and discharge half-cycles was measured electronically and the data were provided in print-out form. Current interrupter measurements of resistance and polarization relaxation were performed with the aid of a Biomation 1015 Waveform Recorder (Biomation Corp., Cupertine, Cal.).

A cutoff potential of either 0.4 or 0.7 V was used during Li-Al electrode discharge; for most of the measurements, the cutoff potential during Li-Al electrode charge was 0.15 V, but for some measurements it was 0.04 V. Under these conditions, the composition of the Li-Al electrode, at the end of charge, is in the lithium-rich region of β-phase of Li-Al and, toward the end of discharge, the composition is α-Al, only partially saturated with lithium.

In the charge-discharge terminology that is used here, lithium is loaded into the Li-Al electrode on charge and unloaded on discharge. This charge-discharge terminology, then, conforms with the conventional usage for a useful cell such as a Li-Al/metal sulfide cell, in which the Li-Al is the negative electrode.

The capacity densities (A-hr/cm^2) achieved by the Li-Al electrodes were used as a measure of the electrochemical performance of the electrodes. Capacity-density measurements were usually carried out at current densities of 0.025 to 0.10 A/cm^2 during charge and 0.025 to 0.30 A/cm^2 during discharge. These studies were made at a temperature of 425°C, unless stated otherwise.

RESULTS AND DISCUSSION

The performance of 0.32-cm-thick Li-Al electrodes with electrolyte volume fractions of 0.7 (Cell DK-3), 0.4 (Cell DK-6), and 0.2 (Cell DK-4) are shown in Figs. 2 to 4, respectively. All electrolyte volume fractions cited are for fully charged Li-Al electrodes.) The results of these studies indicate that lithium utilization is better for the Li-Al electrodes with the lower electrolyte void fractions (0.2 and 0.4). This suggests that the low electrolyte volume fraction in the Li-Al electrode does not impede utilization of the material in 0.32-cm-thick electrodes. The somewhat lower utilization found in Cell DK-3 (electrolyte volume fraction, 0.7) suggests that there may be an electronic conduction problem in the electrode, that is, many of the fine Li-Al and Al particles may not be in physical contact.

The effect of the charge cutoff potential on the achievable capacity density of the Li-Al electrode was investigated in Cell DK-4. The charge cutoff potential was reduced from 0.150 to 0.040 V, while the discharge cutoff potential was held constant at 0.40 V. Operation under these conditions produced an improvement in performance of about 25%. Since the Li-Al electrode is believed to become liquidus at 0.028 V, it is questionable whether

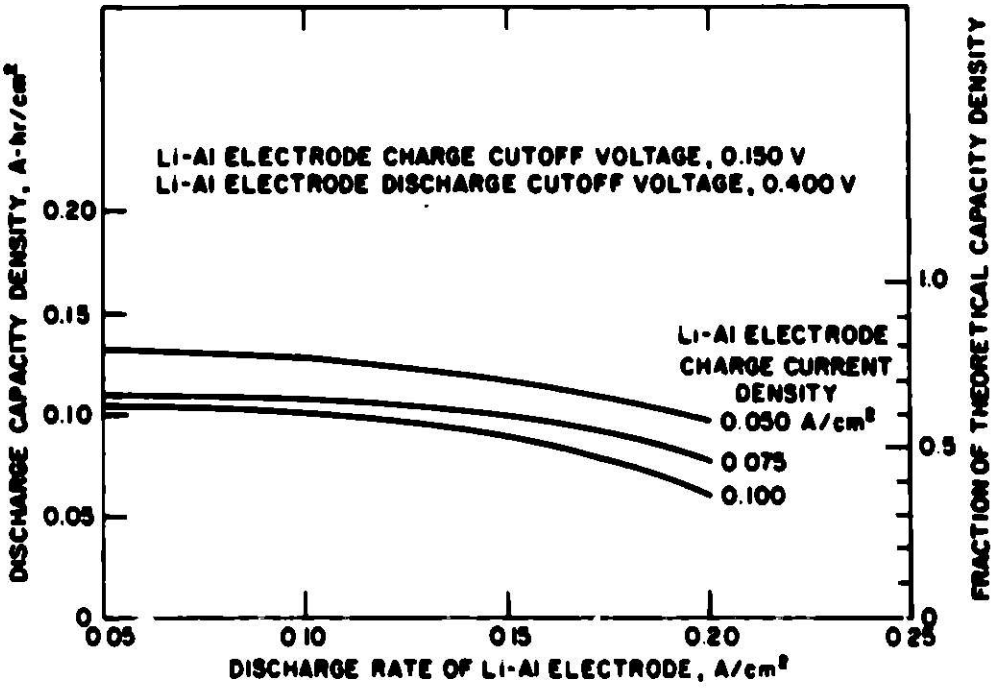

Fig. 2. Capacity Density of Cell DK-3 as a Function of Current Density

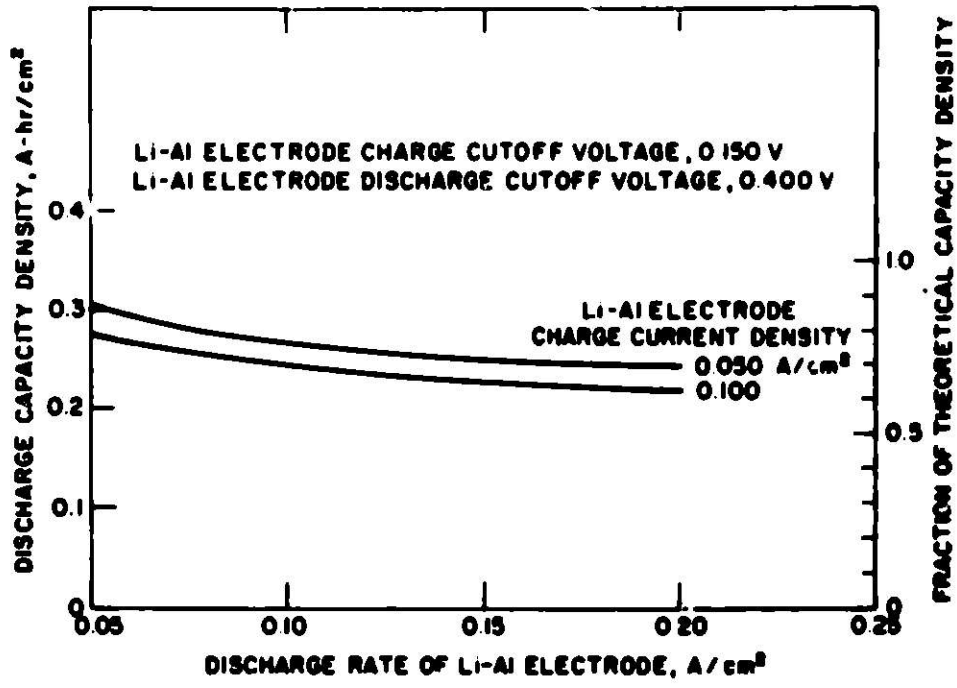

Fig. 3. Capacity Density of Cell DK-6 as a Function of Current Density

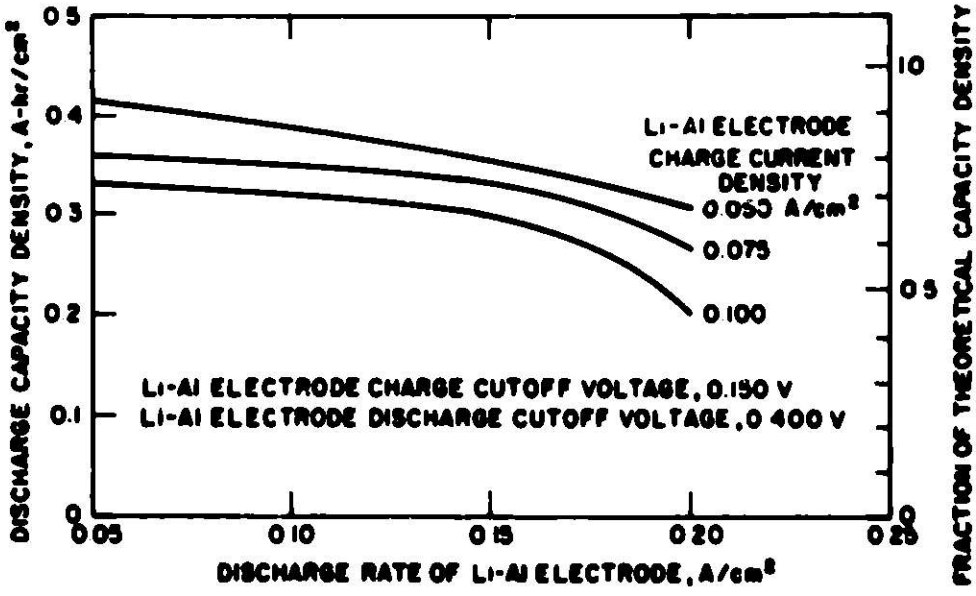

DISCHARGE CAPACITY DENSITY OF Li-Al ELECTRODE AS A FUNCTION OF CURRENT DENSITY AND DISCHARGE RATE

Fig. 4. Capacity Density of Cell DK-4 as a Function of Current Density

a charge cutoff as low as 0.040 V could be used successfully in a Li-Al/metal sulfide cell.

These results indicate that the highest capacity densities are achieved with these electrodes which have relatively low electrolyte volume fractions. The results further suggest that the ion-transport properties of the electrolyte probably do not limit the Li-Al electrode performance. The performance is probably limited by the physical and chemical properties of the solid constituents of the porous electrode, including electronic conduction, lithium transport in the solid, and perhaps other properties.

Because of the relatively poor performance of the Li-Al electrode with 0.7 volume fraction electrolyte (Cell DK-3), studies of 0.64-cm-thick electrodes examined the effect of electrolyte volume fractions of 0.2 and 0.4 (Cells DK-9 and DK-11A, respectively). These electrodes were also formed from pressed aluminum York mesh plaques.

The performance of Cells DK-9 and DK-11A, which had theoretical capacity densities of 0.693 and 0.904 A-hr/cm^2, respectively, are presented in Figs. 5-8. Because the 0.64-cm-thick electrodes are more seriously polarized than the 0.32-cm-thick electrodes, capacity density measurements were made at cutoff potentials of 0.7 V as well as at 0.4 V during the discharge of the electrodes. The achievable capacity density of Cell DK-9 (electrolyte volume fraction, 0.2) was superior to that of Cell DK-11A. These results are, therefore in general agreement with those for the 0.32-cm-thick electrodes. However, the achievable capacity density of the thicker electrode at high and intermediate discharge densities actually increased as the charge current

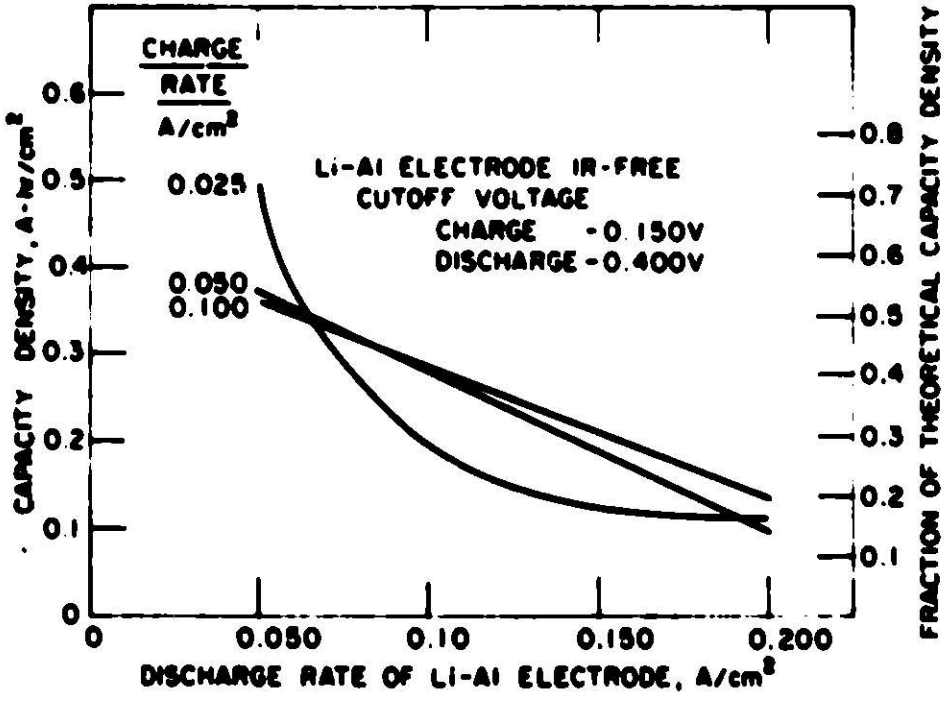

Fig. 5. Capacity Density of Cell DK-11A as a Function of Current Density (discharge cutoff voltage, 0.400)

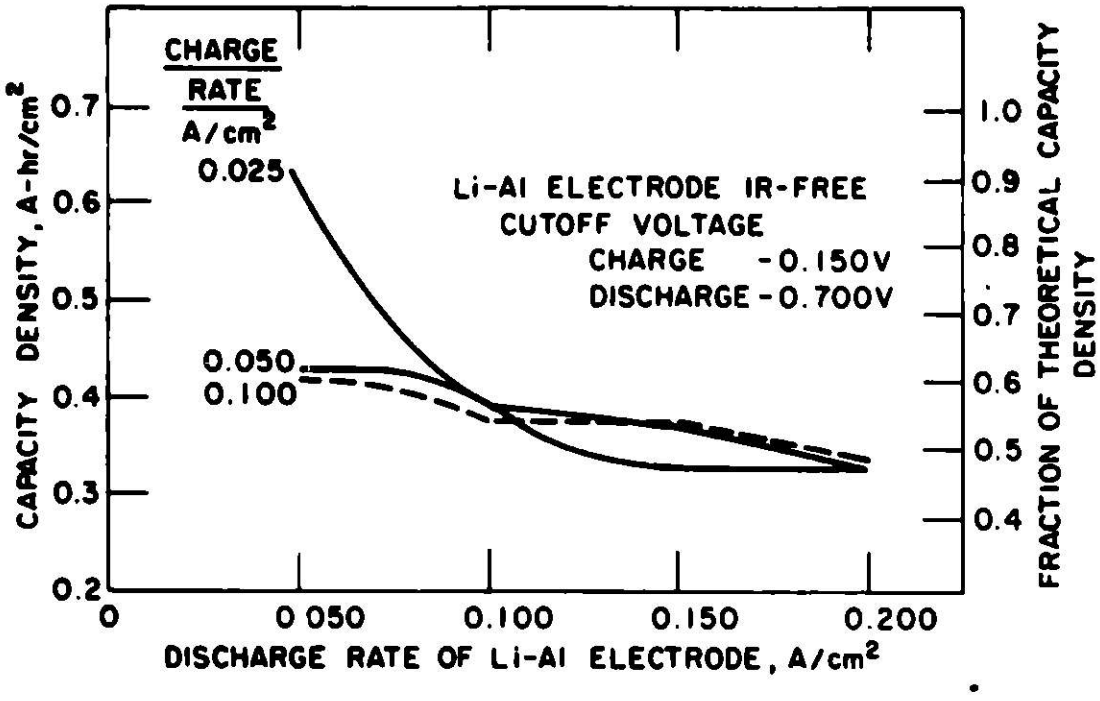

Fig. 6. Capacity Density of Cell DK-11A as a Function of Current Density (discharge cutoff voltage, 0.700)

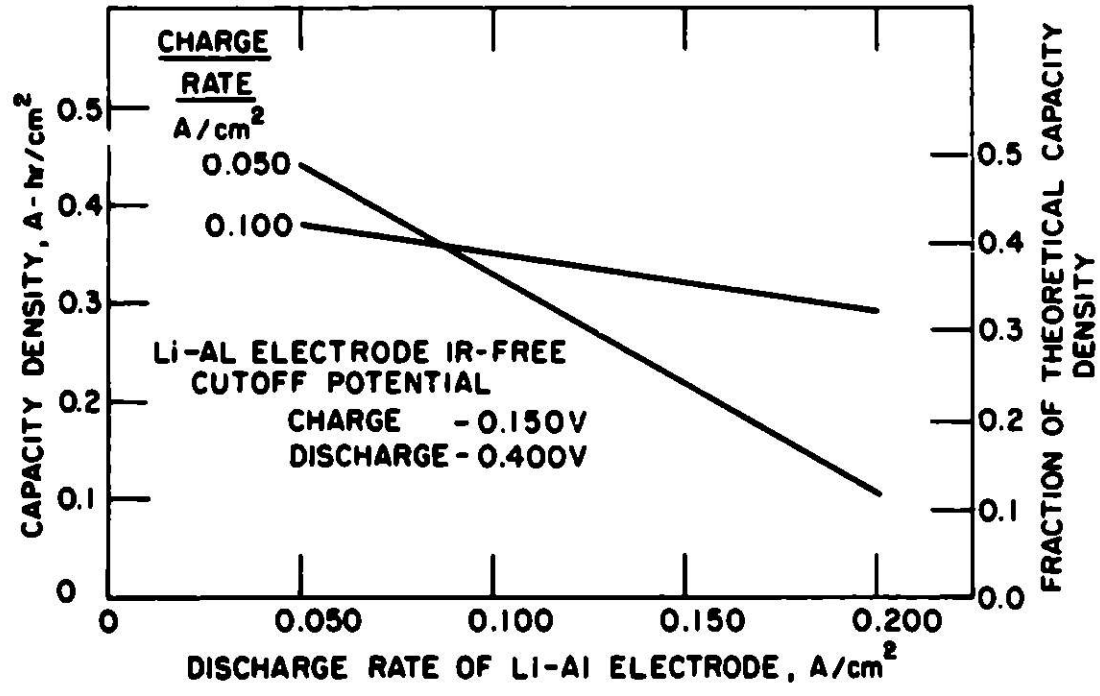

Fig. 7. Capacity Density of Cell DK-9 as a Function of Current Density (discharge cutoff voltage, 0.400)

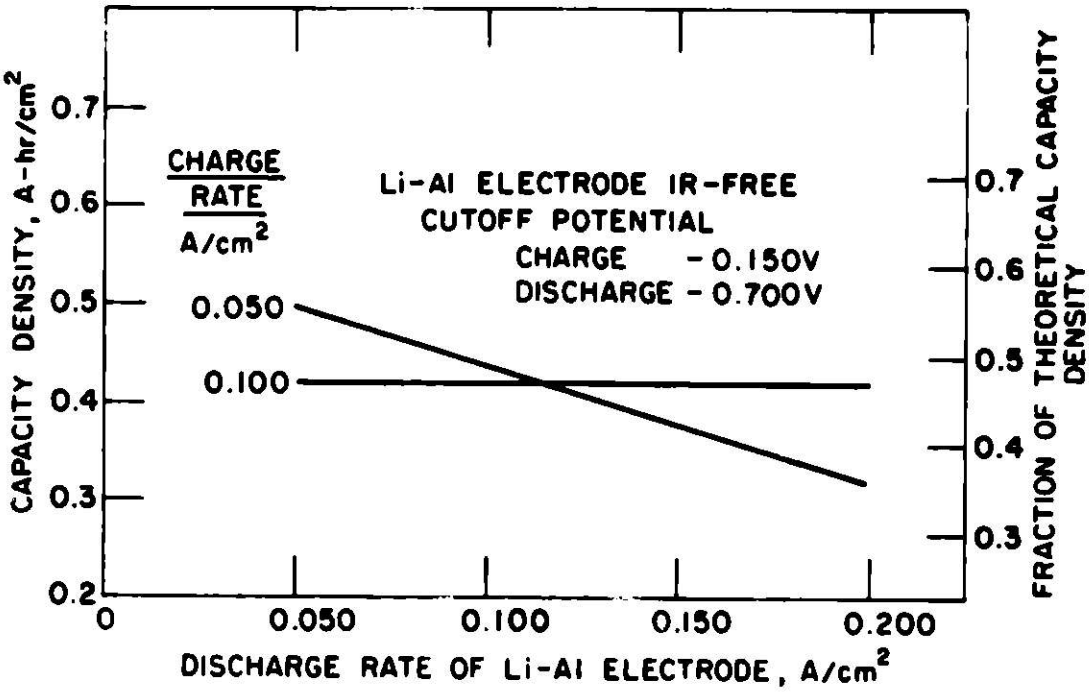

Fig. 8. Capacity Density of Cell DK-9 as a Function of Current Density (discharge cutoff voltage, 0.700)

density was increased, see Figs. 5-8. This increase, which was not observed with the 0.32-cm-thick electrodes, may result from morphology changes that are directly associated with the charge current densities, or may result from a nonuniform axial distribution of lithium in the Li-Al electrode. Examinations are being conducted by scanning electron microscopy on uncharged Li-Al electrodes after cycling to evaluate the effects of charge rate on the morphology of the Li-Al electrode. The results of these studies will be presented in a future paper.

The performance characteristics of 0.32- and 0.64-cm-thick electrodes of the same electrolyte volume fraction are compared in Figs. 9 and 10; achievable capacity densities of the electrodes are very similar when a discharge cutoff potential of 0.40 V is used. The achievable capacity density of Cell DK-6 is somewhat greater than that of Cell DK-11A, an electrode twice as thick. These results suggest there may be a serious problem associated with current collection in the 0.64 cm thick Li-Al electrodes.

An attempt was made in Cell DK-19 to improve performance of the thicker Li-Al electrode by the incorporation of a porous iron current collector structure. The uncharged electrode structure was prepared by loading aluminum powder into two layers of porous iron Retimet; the electrode, when fully charged, had an electrolyte volume fraction of 0.48, and a theoretical capacity density of 0.65 A-hr/cm^2. The performance of Cell DK-19, at charge cutoff potentials of 0.40 and 0.70 V, is shown in Figs. 11 and 12, respectively.

The data in Fig. 11 indicate that for a discharge cutoff potential of 0.4 V, the addition of the Retimet current collector (Cell DK-19) does not

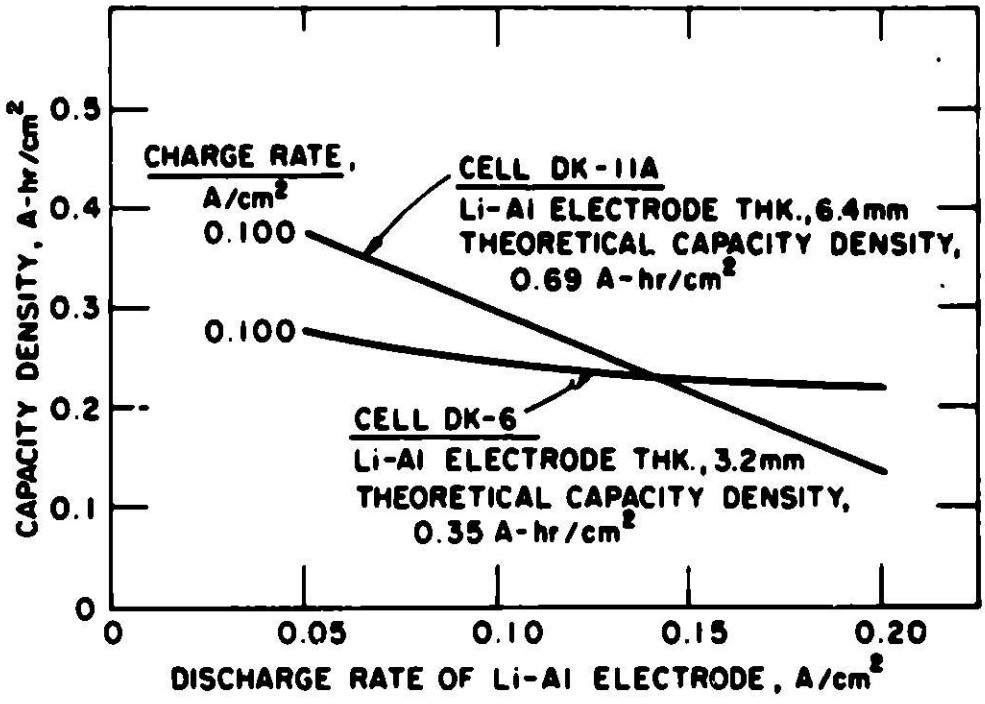

Fig. 9. Capacity Density of Cells DK-11A and DK-6 as a Function of Current Density

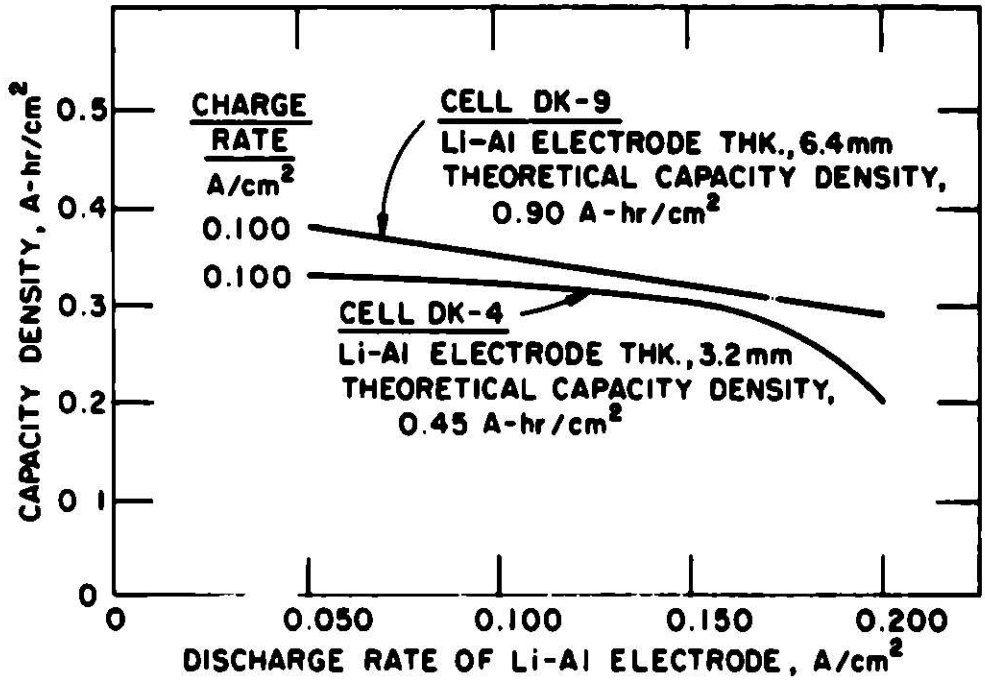

Fig. 10. Capacity Density of Cells DK-9 and DK-4 as a Function of Current Density

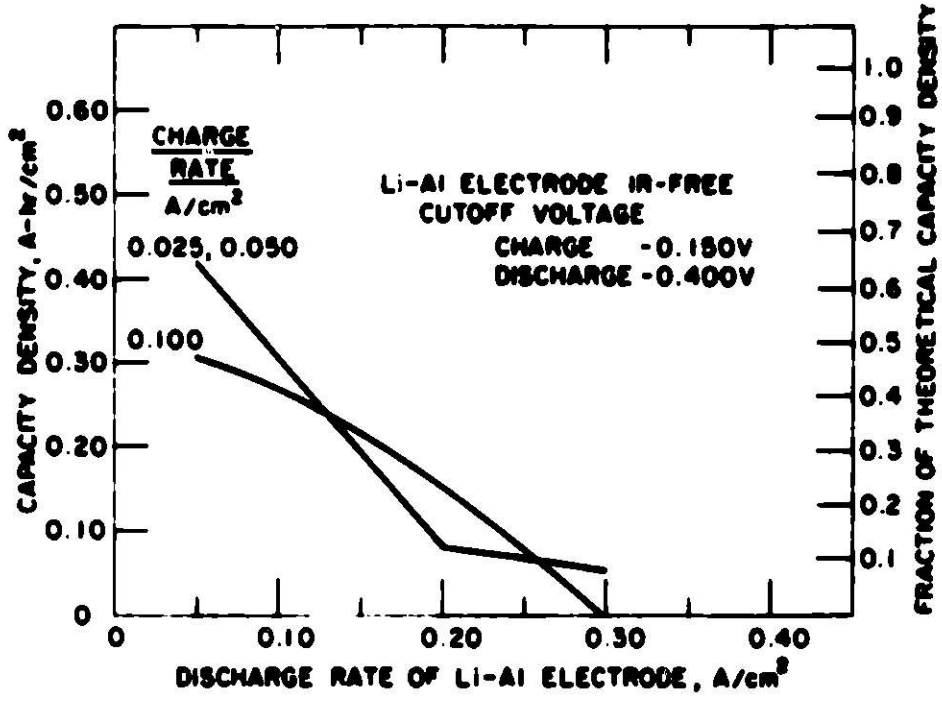

Fig. 11. Capacity Density of Cell DK-19 as a Function of Current Density (discharge cutoff voltage, 0.400)

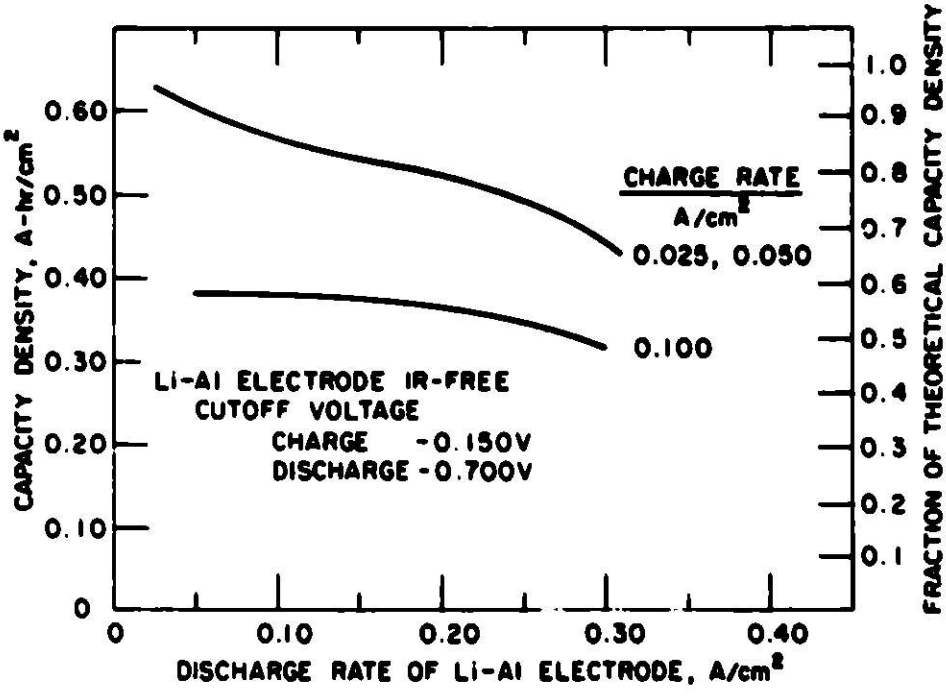

Fig. 12. Capacity Density of Cell DK-19 as a Function of Current Density (discharge cutoff voltage, 0.700)

improve electrode performance relative to an electrode which does not contain the Retimet (Cell DK-11A, Fig. 5). However, when the Li-Al electrode in Cell DK-19 is allowed to polarize by 0.40 V (0.70 V cutoff), the performance of the electrode is far superior to an Li-Al electrode of the type used in Cell DK-11A, as shown in Fig. 13. The results of the DK-19 cell studies are in agreement with earlier work carried out by Gay *et al*[20] using FeS_2 counter-electrodes. Thus, for Li-Al electrodes ≥0.64 cm thick, the performance of the Li-Al electrodes at high discharge current densities appears to be limited by the resistive nature of the electrode.

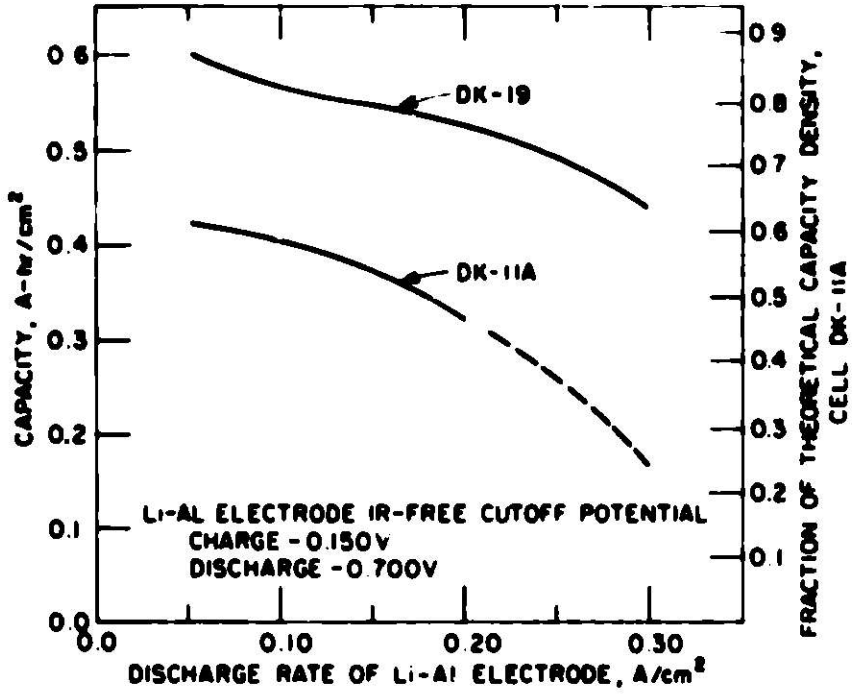

Fig. 13. Capacity Density of Cells DK-19 and DK-11A as a Function of Current Density

CONCLUSIONS

1. The lithium utilization (fraction of theoretical capacity density) of the Li-Al electrodes at moderate to high current densities (~0.100 A/cm²) decreases rapidly as the thickness of the electrode is increased from 0.32 to 0.64 cm.

2. For both thicknesses of electrochemically formed Li-Al electrodes, those with an electrolyte volume fraction of 0.2 have acceptable cycling characteristics and yield a higher capacity density than electrodes with the high electrolyte volume fractions.

3. The performance of the Li-Al electrode appears to be limited by a phenomenon associated with the physical characteristics of the active particles and not by the lithium-ion transport characteristics of the LiCl-KCl eutectic (mp, 352°C). This phenomenon may well be a resistive polarization associated with the electrolyte and with particle-to-particle contact within the porous structure.

4. The performance of Li-Al electrodes ≥0.64 cm thick is greatly improved by the addition of porous metal current collector to such electrodes when the Li-Al electrode is allowed to polarize by 0.4 V, that is, when a discharge cutoff potential of 0.7 V is used.

5. The achievable capacity density of 0.64-cm-thick electrodes at high discharge current densities increases with increasing charge current density. The polarization developed during discharge appears to be ohmic in nature.

ACKNOWLEDGMENTS

The authors are grateful to L. Burris, D. S. Webster, P. A. Nelson and E. C. Gay for support and encouragement.

This work was conducted under the auspices of the U. S. Energy Research and Development Administration.

REFERENCES

1. D. R. Vissers, Z. Tomczuk, and R. K. Steunenberg, Electrochem. Soc. *121*, 665 (1974).

2. Katsushi Abe and Takewo Chiku, ibid, *122*, 1322 (1975).

3. Z. Tomczuk, A. E. Martin, and R. K. Steunenberg, Extended Abstracts of Electrochemical Society Meeting, New York, October 13-17, 1974, *74-2*, 130-131 (1974).

4. A. E. Martin, R. K. Steunenberg, and Z. Tomczuk, ibid, *74-2*, 132-133 (1974).

5. L. C. McCoy, S. Lai, R. C. Saunders and L. A. Heredy, *Proc. 26th Annual Power Sources Conf.*, p. 68 (1974).

6. N. P. Yao, L. A. Heredy and R. C. Saunders, J. Electrochem. Soc. *118*, 1059 (1971).

7. S. D. James, *Preliminary Study of a Lithium Aluminum Electrode for Thermal Batteries*, Naval Ordinance Laboratory Report NOLTR 72-224 (Jan. 22, 1973).

8. R. A. Rightmore and A. L. Jones, *Proc. 21st Annual Power Sources Conf.*, p. 42 (1967).

9. J. R. Selman, D. K. DeNuccio, C. J. Cajigas and R. K. Steunenberg, Extended Abstracts of Battery-Electronics Divisions, Electrochemical Society Meeting, Toronto, Canada, May 11-16, 1975, Vol. 75-1, pp. 75-77 (1975).

10. D. R. Vissers, E. C. Gay, A. C. Sheth, F. J. Martino, and F. C. Mrazek, Extended Abstracts of Electrochemical Society Meeting, New York, October 13-17, 1974, Vol. 74-2, pp. 134-135 (1974).

11. P. A. Nelson *et al.*, *High-Performance Batteries for Off-Peak Energy Storage and Electric Vehicle Propulsion, Progress Report for the Period July-December 1974*, ANL-75-1, Argonne National Laboratory (1975).

12. E. C. Gay *et al.*, *Proc. 9th Intersoc. Energy Conversion Engineering Conf.*, pp. 862-867 (1974).

13. H. Shimotake *et al.*, *Proc. 11th IECEC*, Lake Tahoe, Nev., to be published (1976).

14. P. A. Nelson *et al.*, *Proc. 26th Annual Power Sources Conf.*, pp. 65-68 (1974).

15. D. A. Swinkels, J. Electrochem. Soc. *113*, 6 (1966).

16. T. G. Bradley and R. H. Sharma, *Proc. 26th Annual Power Sources Conf.*, pp. 60 (1974).

17. H. Shimotake *et al.*, *Proc. 1st Electric Vehicle Symp.*, p. 392, Electric Vehicle Council, New York (1969).

18. E. J. Cairns and R. K. Steunenberg, *Progress in High-Temperature Physics and Chemistry*, Vol. 5, p. 63, C. A. Rouse, Ed., Pergamon Press, New York (1973).

19. H. A. Laitinen, R. P. Tischen and D. K. Roe, J. Electrochem. Soc. *107*, 546 (1960).

20. E. C. Gay, F. J. Martino and J. Dorsey, in *High-Performance Batteries for Off-Peak Energy Storage and Electric Vehicle Propulsion, Progress Report for the Period July-December 1975*, ANL-75-1, pp. 36-42, Argonne National Laboratory (1975).

STUDIES ON THE BIPOLAR LIQUID METAL ELECTRODE

Yasuhiko Ito*, Mamoru Goto*, and Shiro Yoshizawa**

* Department of Chemistry, College of Liberal Arts and Sciences, Kyoto University, Sakyo, Kyoto, Japan
** Department of Industrial Chemistry, Faculty of Engineering, Kyoto University, Sakyo, Kyoto, Japan

ABSTRACT

This paper concerns with a new cell design, in which liquid layer acts as a bipolar electrode and as a current conducting by-path. In a molten salt battery system, increase of current efficiency and decrease of ohmic loss are usually the contradicting factors, but if we use liquid metal layer as an intermediate by-path of current, these factors are not in conflict any more. Principle of this method and experimental results are discussed in detail.

INTRODUCTION

High temperature battery using molten salt as an electrolyte seems promising, because of its high electromotive force and low polarization. But it is rather difficult to design delicate battery structure, mainly because of a material problem. Possibly simple structure by the use of corrosion resistant material is necessary for this purpose. For example, it is desirable if we can use ceramic skirt as a separator, instead of diaphragm. But in this case, if we want to keep current efficiency of more than 90 %, position of the skirt end should be set as low as possible, and then, ohmic loss increases very much. On the other hand, if we want to get high energy efficiency, its position should be set high and then current efficiency decreases very much. One possible way of avoiding such contradicting factors is to use bipolar liquid metal electrode, which details will be explained and discussed in the following.

PRINCIPLE OF BIPOLAR LIQUID METAL ELECTRODE

In order to explain the principle of bipolar liquid metal electrode, let us consider Li-Cl_2 battery as an example. Fig. 1 shows a scheme of a cell using bipolar liquid metal electrode. By charging, chlorine evolves from anode and lithium deposits on cathode. Charging current is now the sum of an ionic current which passes through molten salt electrolyte and an electronic current which passes through liquid metal alloy settled on the cell bottom. Let us explain concretely. Following reaction occurs on the right hand half of a liquid alloy surface.

$$Li^+ + e^- + Me \longrightarrow Li\text{-}Me\ (\text{alloy}) \qquad (1)$$

This deposited Li moves toward its left hand part, which then dissolves anodically into electrolyte, according to the following.

$$Li\text{-}Me\ (\text{alloy}) \longrightarrow Li^+ + e^- + Me \qquad (2)$$

That is, right half of a liquid electrode acts as a cathode and left half as an anode. Lithium moves from right to left both by diffusion and convection. This convection is mainly caused by an interfacial tension gradient, which will be explained in a following chapter. By discharging, reverse reaction occurs and high current can be drawn out from the cell.

Motive force and flow pattern of an interfacial convection

Fig. 2 shows an electrocapillary curve given by Karpachev[1]. In this figure, potential of a reference electrode is not defined so clearly, but by comparing the experimental immersion potential of lead electrode with chlorine electrode potential, electrocapillary maximum potential is estimated to be -2.3 V vs. Cl_2/Cl^-. Potential gradient along the liquid electrode surface is given by arranging cathode and anode asymmetrically as shown in Fig. 1. Then an interfacial tension gradient can be established easily, which will become to be a motive force of stirring. For example, if there is a potential gradient of 2.3 (mV/cm) along the electrode surface, there exists an interfacial tension gradient of 0.34 (dyne/cm^2), which is easily calculated from the electrocapillary curve. Flow pattern in the electrode can be obtained as follows[2]. Let us assume the electrode thickness δ not so large, compared to its length, as shown in Fig. 3. Then we can derive following equation for the horizontal velosity u.

$$u = \frac{3\tau_0}{4\mu\delta} Z\left(Z - \frac{2}{3}\delta\right) \qquad (3)$$

τ_0 : shear stress in a steady state
μ : viscosity of liquid metal

Flow pattern in the electrode is then drawn as shown in Fig. 4, according to the above equation. Interfacial tangential velocity u_δ is then given as follows.

$$u_\delta = \frac{\tau_0\delta}{4\mu}$$

Numerical estimation of current-voltage characteristics

Numerical calculations of current-voltage characteristics are given in Fig. 5, for three different types of cell model. Fig. 6 shown the three types used in calculation. Under part of cell C represents liquid alloy layer. κ is a conductivity. No remarkable change of current-voltage relation was observed at any κ values of liquid metal larger than 100 $cm^{-1} \cdot ohm^{-1}$ in case of cell C. Drastic effect of a presence of liquid alloy layer is clear from these figures. That is, current efficiency of cell C is nearly the same as that of cell A, and voltage required for a passage of the same current is much smaller in case of C, than in case of cell B and A. This suggests a priority of cell C compared with the other types of cell. Our consideration in this chapter is only limited to the primary current-voltage characteristics now,

and secondary one including mass transfer process might be necessary in future, but it is rather difficult to get a quantitative expression in the present stage.

PERFORMANCE OF Li-Cl_2 BATTERY

To confirm the possibility of a practical application of this principle mentioned above, experimental cell as shown in Fig. 7 was constructed and examined. Cell itself is an alumina cruicible and container is made of pyrex glass. As a positive electrode, porous carbon was used, through which chlorine gas was supplied in case of discharging. Stainless steel rod was used as a negative electrode. Skirt is also made of alumina. LiCl-KCl eutectic melt was used as an electrolyte, which has been dehydrated before use in a conventional manner. Liquid tin alloy layer thickness is about 1.0 cm, which contains 10 atomic % Li.

Comparison of a polarization characteristics

Fig. 8 shows current-polarization characteristics obtained by a constant current electrolysis by the use of two types of cell (cf. cell A and cell C in Fig. 6). Skirt end height from the cell bottom in the case of direct electrolysis (Corresponding to Cell A) and from the liquid metal electrode surface in case of liquid metal bipolar electrode (corresponding to Cell C) were set equal in each experiment. Priority of the latter is evident from this figure.

Charge-discharge characteristics

Charge-discharge characteristics of this bipolar type cell was obtained as shown in Fig. 9. Table 1 shows current efficiency obtained by this same experiment. After a series of experiment, composition of the liquid alloy was determined and no concentration change was observed, which shows the expected role of liquid alloy electrode as a bipolar electrode. From these data and considerations above, this type of Li-Cl_2 battery seems promising in a practical sense.

APPLICATION OF THE PRINCIPLE TO A HYDROGEN ENERGY SYSTEM

Hydrogen energy system, where water electrolysis for energy storage and water formation from hydrogen and oxygen by the use of fuel cell for energy supply are carried out in turn, is one of the interesting load leveling systems. But when we use aqueous solution for this purpose, high overvoltage makes it difficult to apply this system to a practical use. High temperature hydrogen system might give us one solution to such difficulties, in which small amount of water dissolved in a molten sodium hydroxide is electrolyzed or the water is formed in a molten sodium hydroxide from hydrogen gas and oxygen gas at a temperature of higher than 330°C. In this case, however, selection of a diaphragm material is very difficult because of high temperature and corrosive nature of the molten sodium hydroxide. Separation of hydrogen gas and oxygen gas is then very difficult. For such a situation, liquid metal bipolar electrode system gives us one of the useful cell designs indeed. Fig. 10 shows the principle of this type of cell. Explanation is

almost exactly the same as Fig. 1, except that negative electrode and positive electrode is the hydrogen electrode and oxygen electrode, respectively, and that sodium comes into and out from the liquid alloy electrode. Possible practical cell construction may be as shown in Fig. 11. To examine the possibility of such type of cell, experimental cell shown in Fig. 10 was constructed and examined. Table 2 shows the current efficiencies of water electrolysis, and Fig. 12 shows its polarization characteristics. From these data, expected role of this cell can be confirmed. To know the single electrode behaviors separately, experimental cell shown in Fig. 13 was constructed, where liquid sodium was used as a counter, and a reference electrode. And β-alumina tube was used as a diaphragm. Polarizations of oxygen evolution and hydrogen evolution reactions are very small as can be seen in Figs. 14 and 15, and polarization characteristics of oxygen reduction is fairly good as seen in Fig. 16, but the polarization characteristics of hydrogen oxidation is very bad by the use of such a plate electrode. Further engineering development of hydrogen electrode might be necessary for applying this design to a practical one, and this might be our future subject.

CONCLUSION

Usefulness of liquid metal bipolar electrode was confirmed by considering Li-Cl_2 battery and water electrolysis and hydrogen-oxygen fuel cell. The possibility of applying this principle to the other battery system is also expected in future.

REFERENCES

1. S. Karpachev and A. Stromberg, The Electrocapillary Phenomena in Molten Electrolytes, J. Phys. Chem. (USSR) 10:739-746 (1937).

2. Y. Ito and N. Ibl, in preparation, to be published.

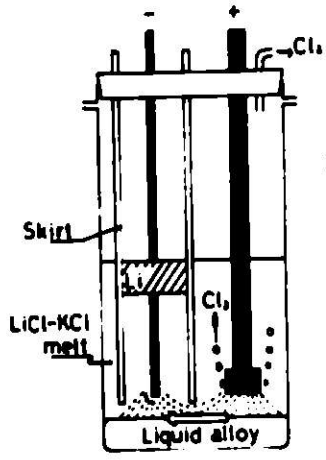

Fig. 1

$Li^+ + e + Metal \rightarrow Li + Metal$

$Li + Metal \rightarrow Li^+ + e + Metal$

$Cl^- \rightarrow 1/2\ Cl_2 + e$

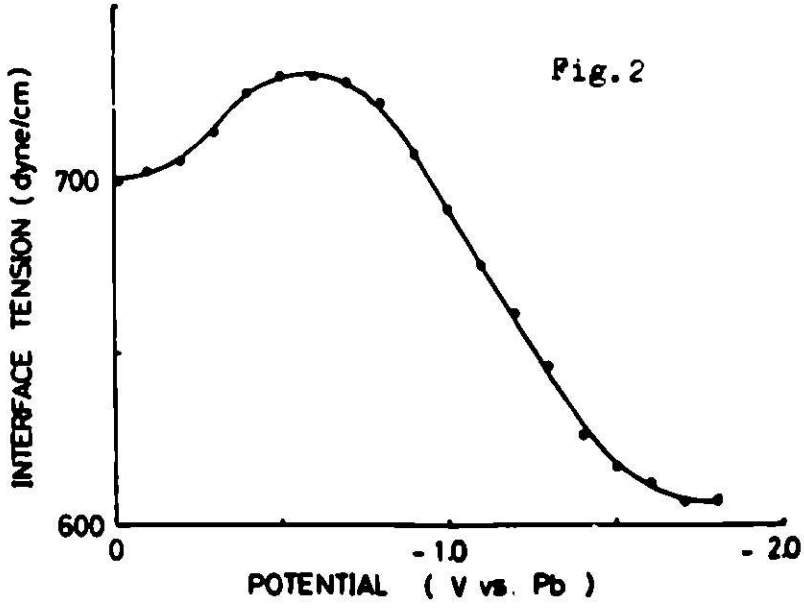

Fig. 2

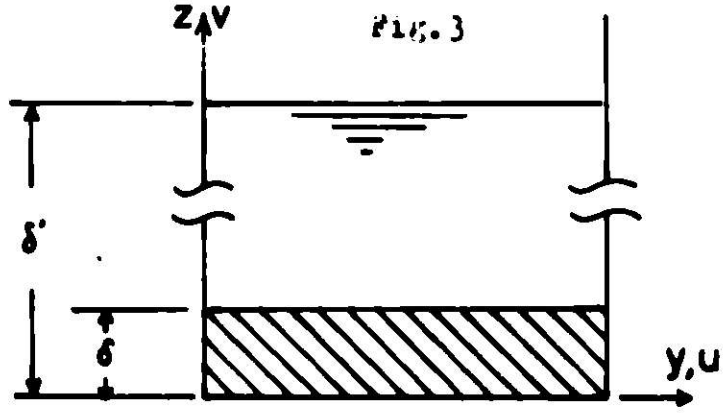

Fig. 3

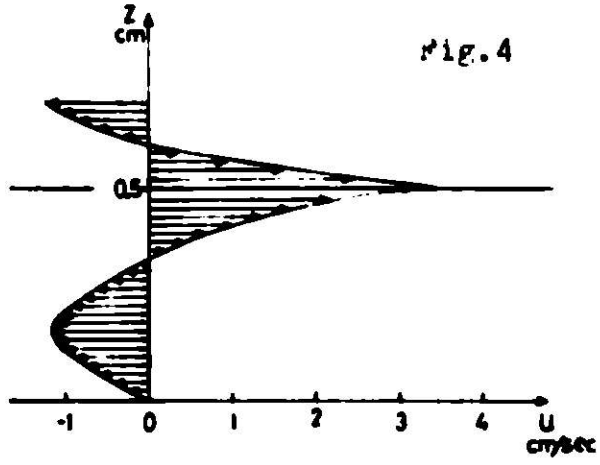

Fig.4

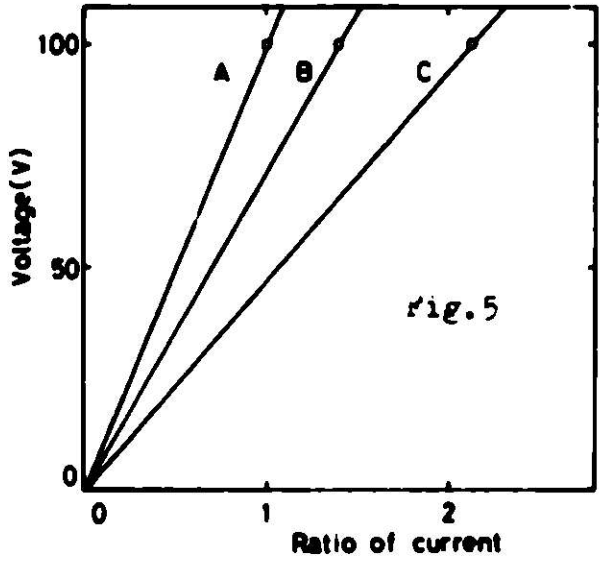

Fig.5

Fig.6

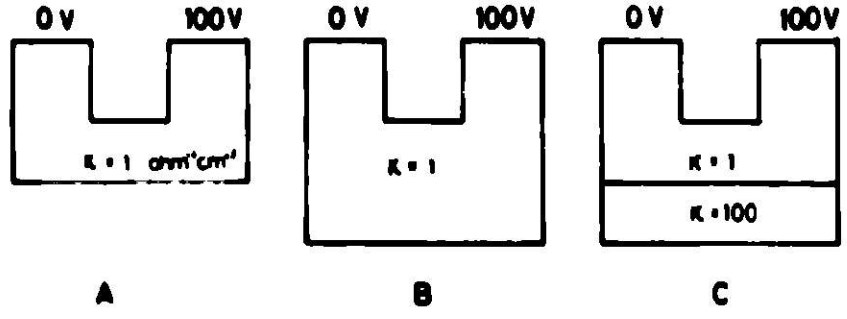

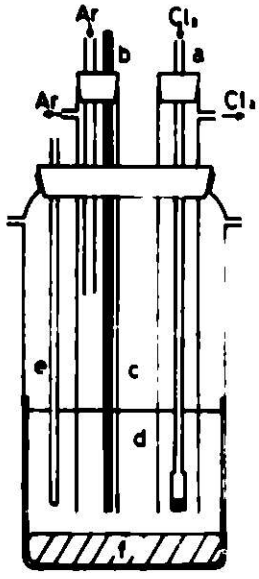

Fig.7

a Positive electrode
(Cl_2/Cl^- electrode)
b Negative electrode
(stainless steel rod)
c Skirt
d Electrolyte
(LiCl-KCl melt)
e Thermocouple
f Liquid alloy

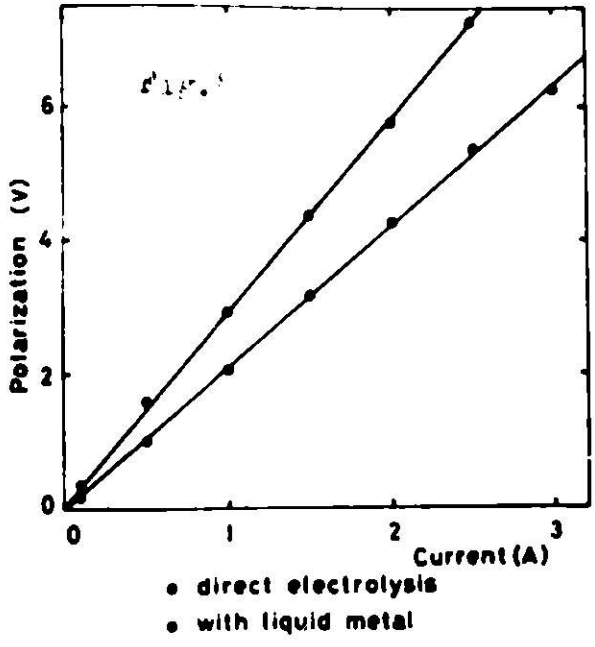

Table 1

Current density A/dm²	Current efficiency %
13	77.0
25	86.7
40	88.9
52	88.3

Fig.9

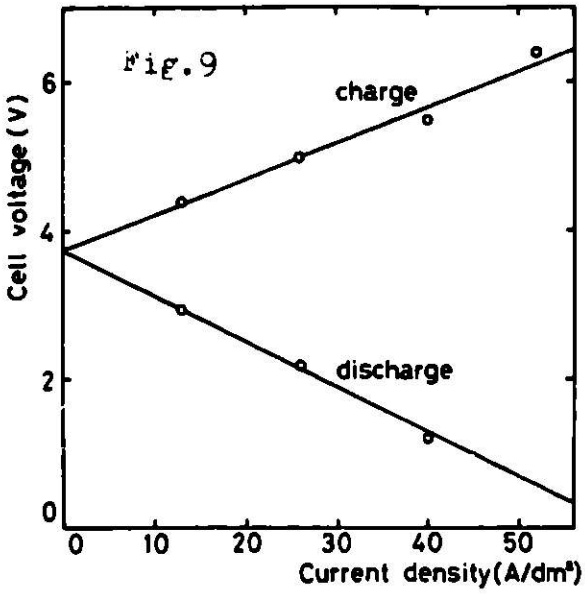

Fig.10

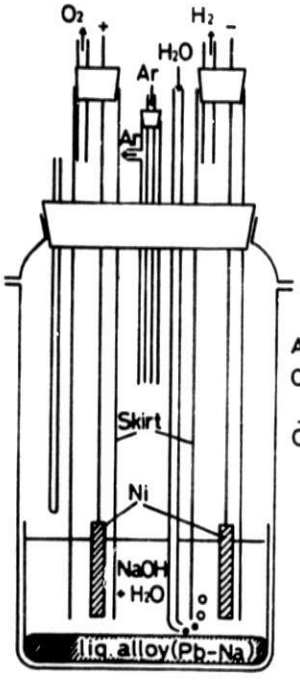

Anode: $OH^- \longrightarrow 1/4O_2 + 1/2H_2O + e$

Cathode:

$H_2O + e \longrightarrow OH^- + 1/2H_2$

Overall reaction

$1/2H_2O \longrightarrow 1/2H_2 + 1/4O_2$

in liquid alloy

$Na^+ + e + Metal \longrightarrow Na\text{-}(Metal)$

$Na\text{-}(Metal) \longrightarrow Na^+ + e + Metal$

Fig.11

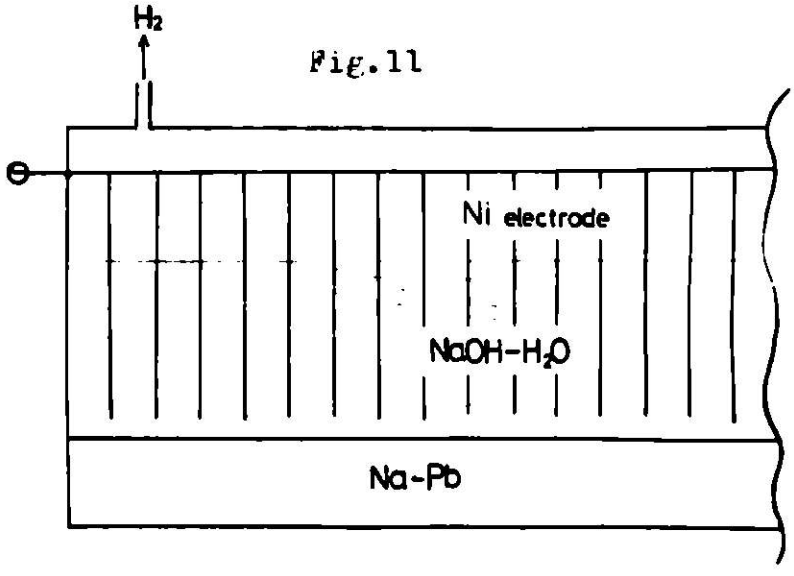

Table 2

	direct electrolysis	with liquid alloy
Anode C E(%)	118	112
Cathode C E(%)	92.8	85.2

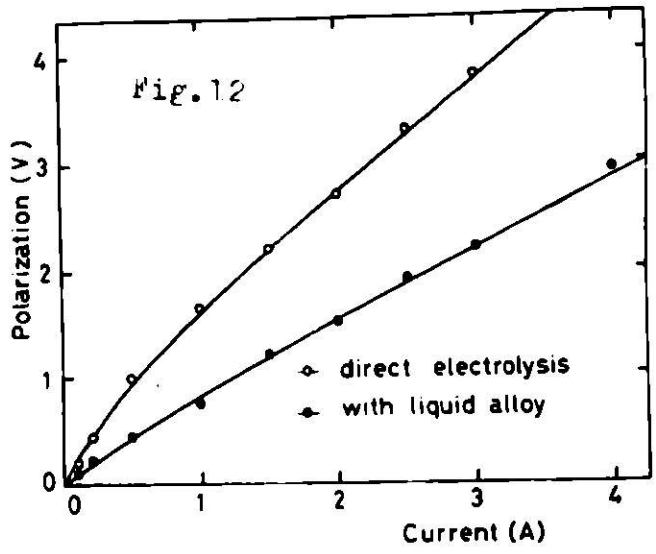

Fig. 12

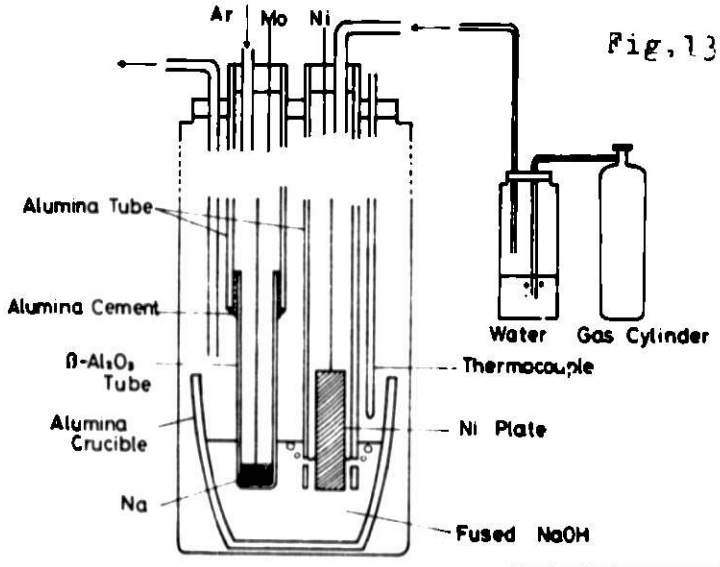

Fig. 13

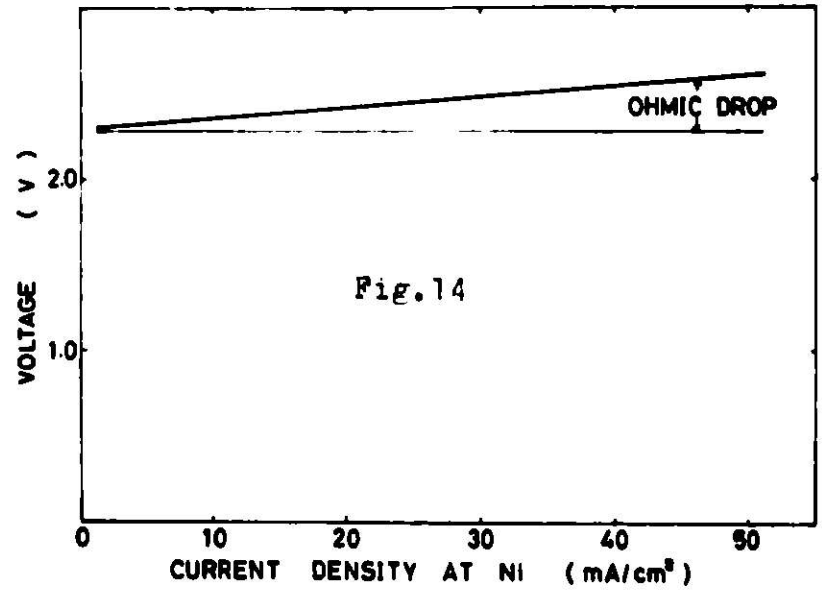

Fig. 14

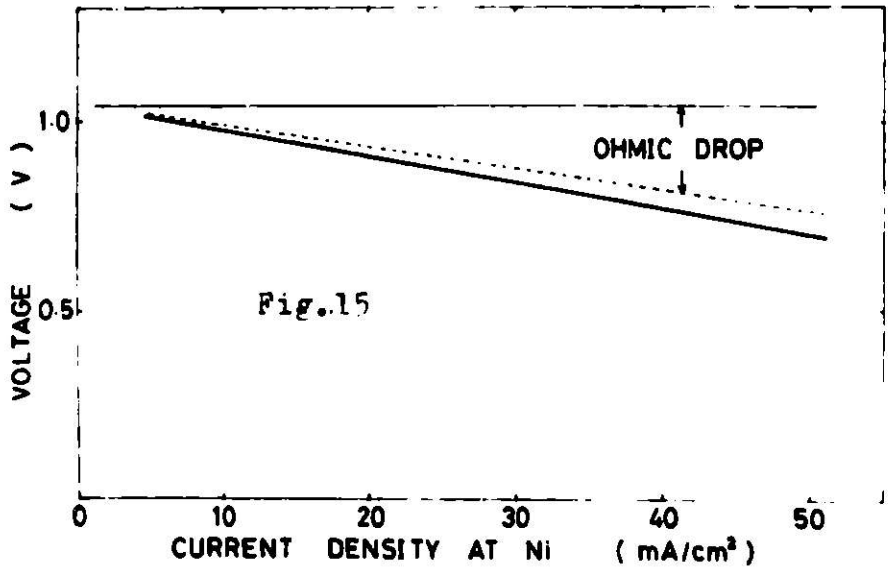
1.0
0.5
VOLTAGE (V)
OHMIC DROP
0
10
20
30
40
50
CURRENT DENSITY AT Ni (mA/cm²)

Fig.15

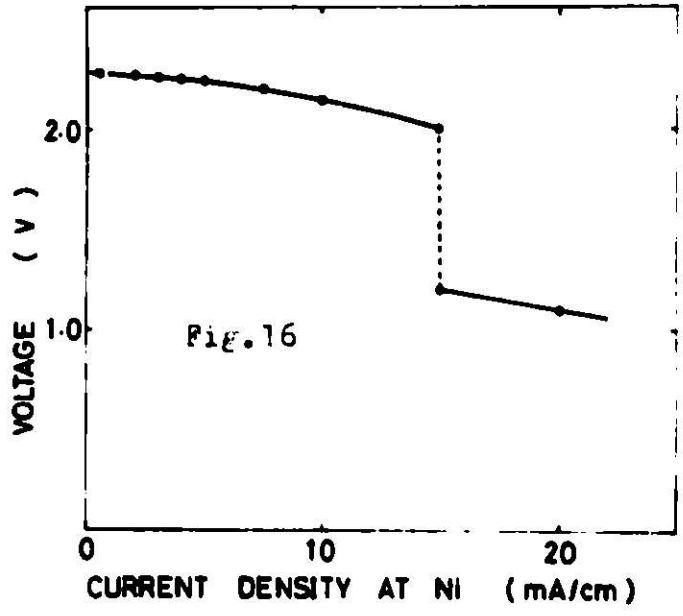
2.0
1.0
VOLTAGE (V)
0
10
20
CURRENT DENSITY AT Ni (mA/cm)

Fig.16

THE PERFORMANCE OF SHAPED GRAPHITE ELECTRODES IN SODIUM SULFUR CELLS

R. W. Minck
Chemistry Department, Research Staff
Ford Motor Company
P. O. Box 2053
Dearborn, Michigan 48121

ABSTRACT

This paper presents results obtained on testing a series of cells which incorporated differently shaped graphite electrodes. The results are interpreted in terms of mass transport processes.

The geometry of the electrode strongly influences cell performance. Generally, geometric changes enhance discharge performance at the expense of charge performance, or vice-versa. In contrast, changes in operating temperature affect both charge and discharge performance similarly.

INTRODUCTION

The understanding of the basic electrochemical processes which occur in the molten sodium polysulfides has been advanced greatly by the recent work of Ludwig and others.[1] Their findings are reported in the literature and in the reports prepared under the NSF-RANN contract, and therefore will not be repeated here.

These research studies deal with the charge transfer, chemical reactions, and mass transfer processes on a local scale near the electrode surface. Applying the findings to the complex geometry encountered in practical cells requires the consideration of the coupling of long-range mass transport to the behavior on the local level. It is this topic, and more particularly, the role of electrode shape on mass transfer, which forms the subject of this paper.

The sodium polysulfide-sulfur system contains several well known peculiarities. The phase diagram[2] contains a sizeable region in which two immiscible liquids coexist, one is sulfur-saturated pentasulfide, abbreviated as $Na_2S_{5.2}$ in this paper; the other is pentasulfide-saturated sulfur, taken as S since experiments failed to find any sodium in this phase. The physicochemical properties of these two liquid phases are vastly different. Their viscosity and electrical conductivity values differ by orders of magnitude; whereas their surface tension and density values differ by a factor of two or less.

The insulating and viscous nature of liquid sulfur makes its mass transfer particularly critical and difficult; and since the two-phase region corresponds to more than half of the potential ampere-hour capacity of the Na-S system, it is imperative that methods be found to overcome limitations introduced by its presence.

CELL OPERATION

The Na-S system employs a solid ion-conducting electrolyte, beta or beta" alumina, in conjunction with a liquid electrolyte, sodium polysulfide. Since the current density that can be supported on a planar graphite surface is far less than is allowed by the rest of the system,[3] an extended area, porous electrode structure is employed. Graphite felt is used commonly for this purpose. The liquid polysulfide electrolyte is then capable of providing ionic contact to this extended area electrode. The electronically conducting felt (ρ ~0.3 ohm-cm) makes contact to a current collector which is connected to the positive terminal of the cell.

It is convenient to discuss cell operation starting from a completely charged cell. To provide room for subsequent expansion of liquids as sulfur is converted to polysulfide, the sulfur compartment is filled initially with sulfur to 70% or less by volume. Because the felt is wetted by sulfur, sulfur is wicked more or less uniformly throughout the entire electrode causing the 30% void volume to be distributed throughout the electrode. Initially, only the triple interline of sulfur, graphite, and ceramic presents the requirements for reaction. As polysulfide is formed during discharge, an interfacial area develops between graphite and polysulfide which provides an increased active electrode surface area. On this surface, the $S_4^=$ ion is reduced to $S_2^=$, which chemically reacts with sulfur to reform $S_4^=$. The supply of sulfur may be by surface diffusion along the graphite fibers, or by convection and diffusion through the "bulk" electrolyte (in the ca. 100 μ spaces between fibers).

As the discharge continues, several fluid flow processes can compete. As more polysulfide is formed, the volume expansion builds a local pressure which may push the sulfur/polysulfide interface uniformly away from the ceramic. Because an enormous viscous drag would be associated with the motion of sulfur (1500 cp) through a porous media, it is more likely that the polysulfide (30 cp) will find a less restrictive channel and escape outward through openings between or within the felt, or axially along the ceramic tube surface.

If one presumes that the sulfur is essentially stationary, the sulfur/polysulfide front advances away from the ceramic by consumption of sulfur, thereby forming an expanding cylindrical region of polysulfide. Within this cylindrical region, the electrode reactions are distributed on the surface of the felt fibers so as to be consistent with the distributions of potential and composition in this region. The performance of porous electrodes has been studied extensively both experimentally and by analytic modeling by workers such as Newman and coworkers.[4] Such work on undiluted fused salts is however, very limited. Preliminary results[5] indicate that large concentration gradients can develop over distances of several millimeters in NaS cells. The existence of composition gradients substantially increases the sodium ion transport, but has with it an associated high concentration polarization.

The end of discharge occurs either when the sulfur/polysulfide front reaches the outer cell wall thereby consuming all sulfur, or when the continuing electrode reactions near the ceramic drive the local composition far into the region of the phase diagram where liquid ($\simeq Na_2S_{2.8}$) plus solid

(Na_2S_2) coexists. The graphite surface is likely to passivate under these conditions because of the limited availability of sulfur to remove the Na_2S_2 film, and because the ionic conductivity of the liquid phase plus solid phase is lowered. Both factors contribute to an increased cell resistance. At fixed discharge current, the cell voltage drops below a set limit, and the discharge cycle is considered complete.

On charging from a "fully discharged" condition, the following sequence is probable. The conductivity of the felt is 10 times that of the polysulfide. Therefore, the charging process occurs predominantly on the graphite fiber surfaces near the ceramic, where $S_4^=$ is oxidized to sulfur, which can then react with $S_2^=$ to reform $S_4^=$. As long as lower polysulfides are available to consume the sulfur formed by the charging process, the sulfur is removed by chemical reaction as well as by convection to maintain the electrode surface active. When diffusion from the outer regions can no longer supply $S_2^=$ at sufficient rate, the sulfur film will remain on the graphite and form an insulating layer which blocks further charging. Adding to this effect is the fact that sulfur prefers to wet the graphite. In addition, shrinkage of the liquid phase occurs when polysulfide is converted to sulfur, forming voids which further reduce the effects of diffusion.

Experimentally, we frequently have obtained cell performance in accord with this explanation when thick felt electrodes are employed. In the cell design shown in Figure 1, graphite felt fills the region between the 1 cm OD ceramic and the 1.8 cm ID hole in the graphite block. The performance is indicated in Figure 2. Cell operation is limited to the single phase region.

An approach, based on shaped electrodes, was tried to circumvent this problem. This idea was first tested in Na-S cells using a perforated metal screen to enclose the graphite felt, as shown in Figure 3. The metal screen was to act as a current collector while permitting the fluids to commute between the outer storage region and the inner active electrode area. The improvement in performance was very substantial, but we began to suspect the interpretation that the improvement was due to shaped electrodes when we learned that metal electrodes exhibit superior charging properties.[6] The concept was retested in a metal free cell construction, shown in Figure 4. This cell was designed to have an extremely high specific capacity -- over 2 ampere-hours per square centimeter of ceramic area. The performance of this cell, #89, was good, as indicated in Figure 5. The results were interpreted as follows: the polysulfide formed during discharge was able to flow through the thin portion of the felt and be removed by reaction and convection in the large open channels. Sulfur would be brought close to the active region by convection, and be able to diffuse and react, thereby providing high utilization of reactants on discharge as indicated by the data. On charge, the improved performance was attributed to the presence of a liquid column whose hydrostatic pressure would prevent void formation and improve diffusion. If phase separation occurred rapidly in the two phase region, the $Na_2S_{5.2}$ at the bottom of the cell would continue to feed into the electrode and be charged. Thus, the improvement of performance of cell 89 is attributed to the improved feeding and extraction of reactants through the thin regions of the electrode.

Because cell performance is thought to be limited by mass-transfer, one would expect marked improvement with increasing temperature as chemical reaction rates, diffusion, viscosity, and conductivity all improve with increas-

ing temperature. Data for cell 89 at various temperatures are presented in Figure 5. We have not ascertained which of the factors discussed is dominant, but it is clear that if corrosion and other life limiting processes can be suppressed, very substantial gains in cell performance can be obtained by an increase in operating temperature. Such improvements in performance with temperatures are common to the Na-S cells we have tested.

The role of shaped electrodes on cell performance was studied further with a series of cells, designed for about 1 Ah/cm^2 of ceramic, having electrodes as shown in Figure 6. In cell #93 having shape (a), a portion of the ceramic surface was not covered with felt. In cell #94, having shape (b), the electrode is similar to that used in cell #89 and covers all the ceramic surface. The results of cell testing are shown in Figure 7 and 8. A comparison of performance shows that cell #93 is more completely rechargeable than cell #94; but conversely, cell #94 gives better discharge performance than #93. These results are interpreted as follows: during discharge, cell #94 functions in the manner described for #89. Cell #93 must behave differently, because the portion of the ceramic area not covered by felt is inactive since it is covered with sulfur initially. The reduced area leads to a higher cell resistance. As polysulfide is formed and fills the open channels, the portion of ceramic covered by polysulfide becomes active. In this region, the ionic path extends through the ceramic and through the polysulfide in the open channel, and terminates on the graphite fiber surfaces on the edges of the shaped felt. The contribution of this conduction path is proportional to the height of the polysulfide in the open channels.

Although this contribution to conduction is a relatively small factor on discharge, we believe it is responsible for the improvement in chargeability of the cell. As with most cells, there are no problems charging through the one phase region because of diffusion and chemical reactions. Once $Na_2S_{5.2}$ has formed, however, the portion of ceramic covered by felt is expected to become inactive due to sulfur film formation which blocks the felt surface adjacent to the ceramic. The only remaining ionic path is through the uncovered ceramic surface. We believe that the graphite fiber surfaces at the edge of the felt remain active because these surfaces are exposed to a freely convecting liquid phase which can remove the sulfur film by convection. According to this model, one would expect the cell conductance to decrease in proportion to the remaining height of polysulfide in the open regions.

A cell designed for a more quantitative test of this concept is shown in Figure 9. The inner hole in the electrode was enlarged to provide a 1 mm gap between the ceramic surface and the electrode. The characteristics of the cell, #102, are given in Figure 10. The results can be interpreted in terms of changes in geometry associated with the varying level of $Na_2S_{5.2}$ as the state of charge of the cell is varied. If one assumes that phase separation occurs rapidly, the area of ceramic covered by the ionically conducting polysulfide varies in proportion with the amount of polysulfide in the cell. To a first approximation, one then would predict a cell conductance varying linearly with the state of charge of the cell. As can be seen in Figure 11, the agreement is quite good, both in terms of indicating the anticipated functional behavior, and also in quantitatively matching the slope expected from calculations based on cell parameters.

SUMMARY

In conclusion, we believe that these studies confirm the controlling influence of mass transfer on cell performance and demonstrate some of the effects produced by shaped electrodes. With the insight gained from these and other experiments, we are in a position to manage better the mass transport requirements pertinent to specific applications, especially those requiring high energy storage.

ACKNOWLEDGMENTS

I would like to acknowledge the contributions and helpful discussions of Drs. N. K. Gupta, F. A. Ludwig, and M. Mikkor.

This work was performed under contract NSF-C805 with the National Science Foundation, RANN division.

REFERENCES

1. F. A. Ludwig, R. P. Tischer, D. A. Aikens and K. W. Fung, "Kinetic Studies in Polysulfide Melts at a Vitreous Carbon Electrode" Extended Abstract #386, Volume 75-1, Spring Meeting of the Electrochemical Society (1975); R. P. Tischer and F. A. Ludwig, "The Sulfur Electrode in Nonaqueous Media," C. Tobias and H. Gerischer, editors, Advances in Electrochemistry and Electrochemical Engineering, Vol. 10 (in print).

2. T. G. Pearson and P. L. Robinson, J. Chem. Soc., 132, 1473 (1930); N. K. Gupta and R. P. Tischer, J. Electrochemical Soc., 119, 1033 (1972).

3. "Research on Electrodes and Electrolyte for the Ford Sodium-Sulfur Battery," Annual Report for Period June 30, 1973 to June 29, 1974, (July 1974), National Science Foundation, Contract #NSF C-805, pp 124-125.

4. J. S. Newman and others, see J. Electrochem. Soc. 109, 1183 (1962); J. Electrochem. Soc. 118, 1251, (1971); J. Electrochem. Soc. 120, 906, (1973).

5. "Research on Electrodes and Electrolyte for Ford Sodium-Sulfur Battery," Annual Report for Period June 20, 1974 to June 29, 1975 (July 1975), National Science Foundation, Contract #NSF C-805, pp 11-48 et. seq.

6. Ibid, pp 11-85 et. seq.

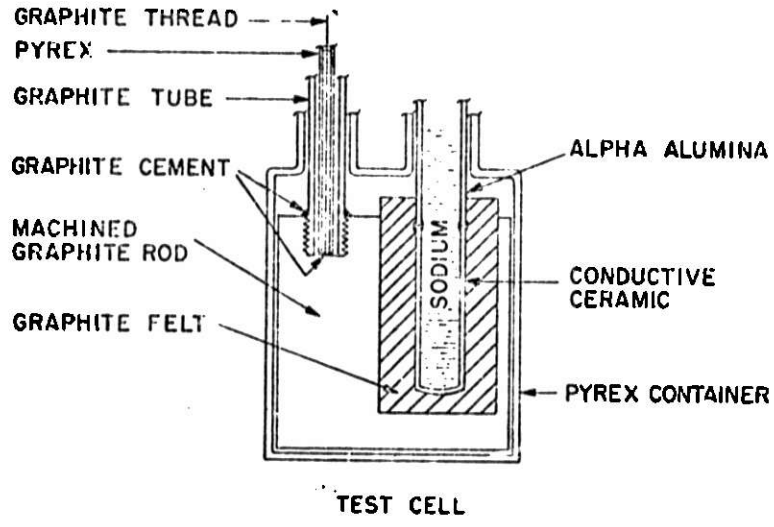

Figure 1. Schematic of test cell with electrode region filled with felt.

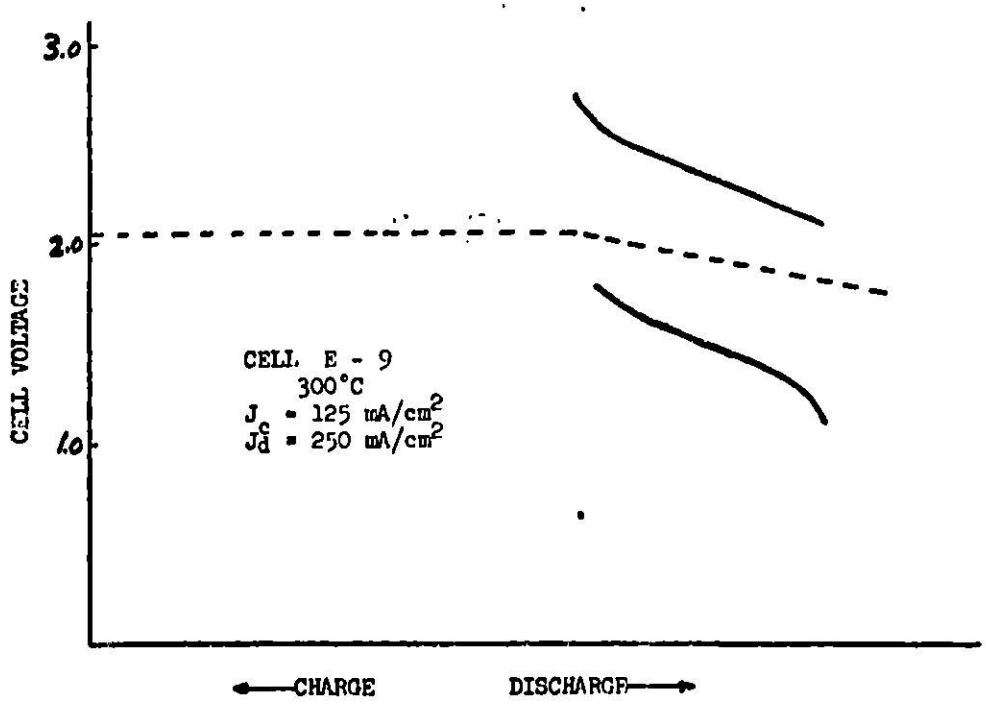

Figure 2. Cell voltage during charge and discharge shown as a function of the state of charge of the cell. The dashed curve represents the open circuit voltage. The position of cell voltage data relative to the OCV curve on the horizontal axis is approximate because of stray volume in the test cell.

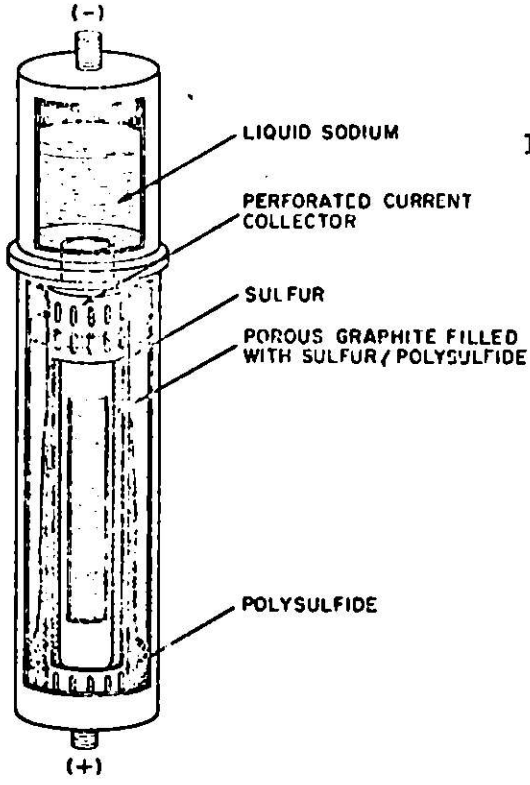

Figure 3. Schematic of a "leaky screen" cell. The graphite felt electrode is confined inside the perforated metal screen. The outer open region provides storage volume for the liquid reactants.

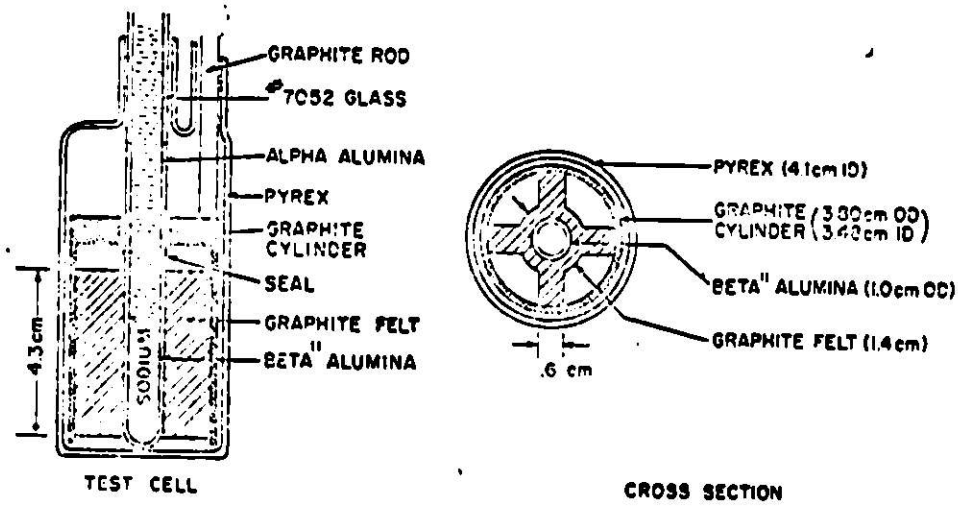

Figure 4. Schematic of a test cell employing a shaped graphite felt electrode and metal-free construction techniques for the sulfur compartment.

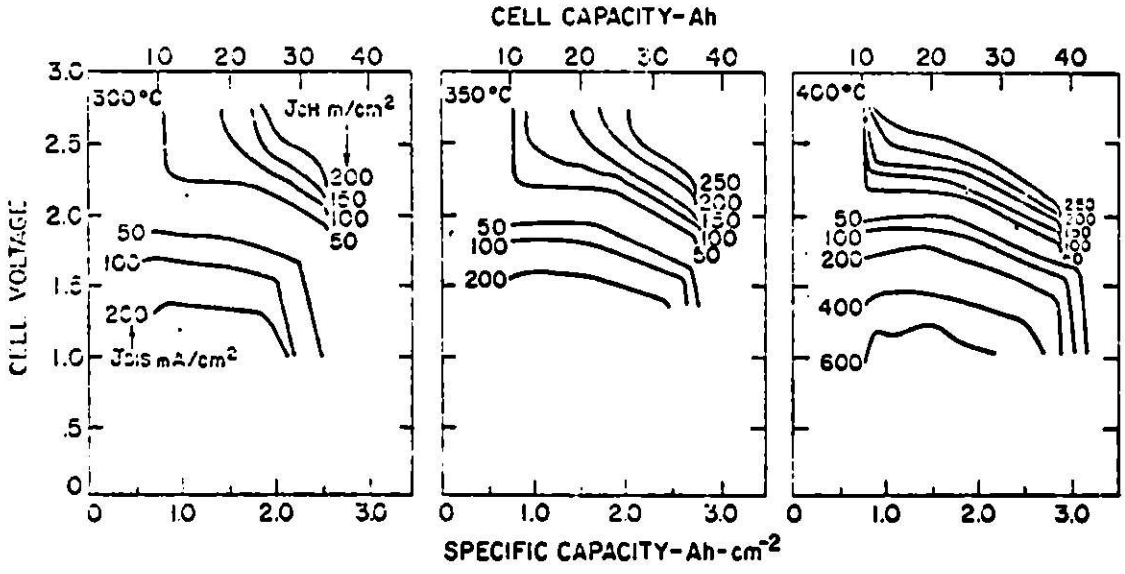

Figure 5. Charge/discharge characteristics for cell 89 with shaped electrode, at three temperatures. The current densities are referred to the surface area of the ceramic electrolyte tube covered by the felt electrode. Most of the capacity not recharged (≈ 10 Ah) at low rates is associated with the reactants stored in the stray volumes at the bottom and outer edge of the test cell.

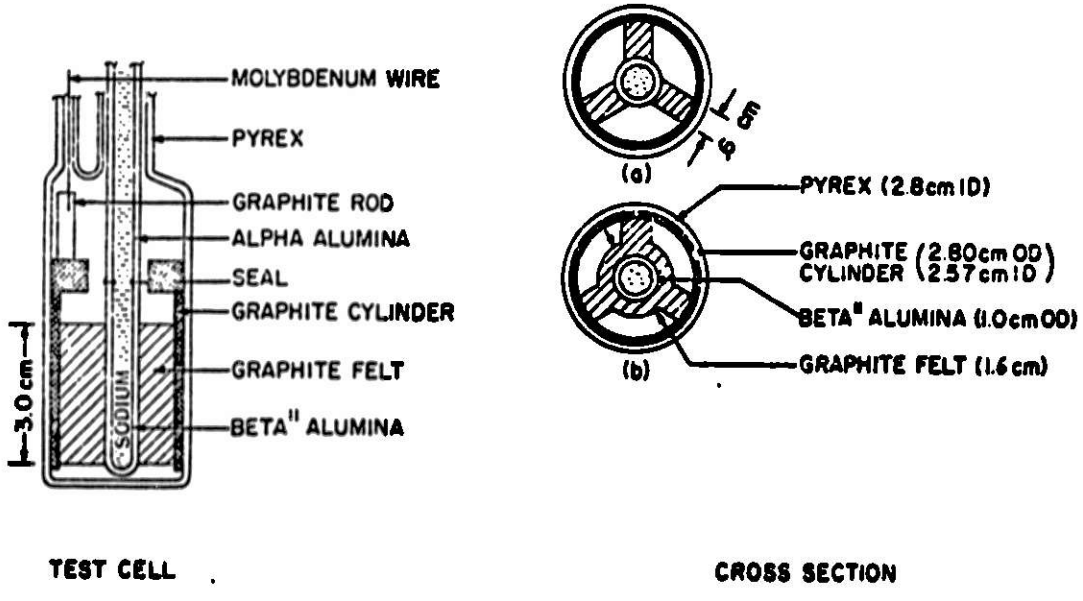

Figure 6. Schematic of metal free test cells with shaped graphite felt electrodes.

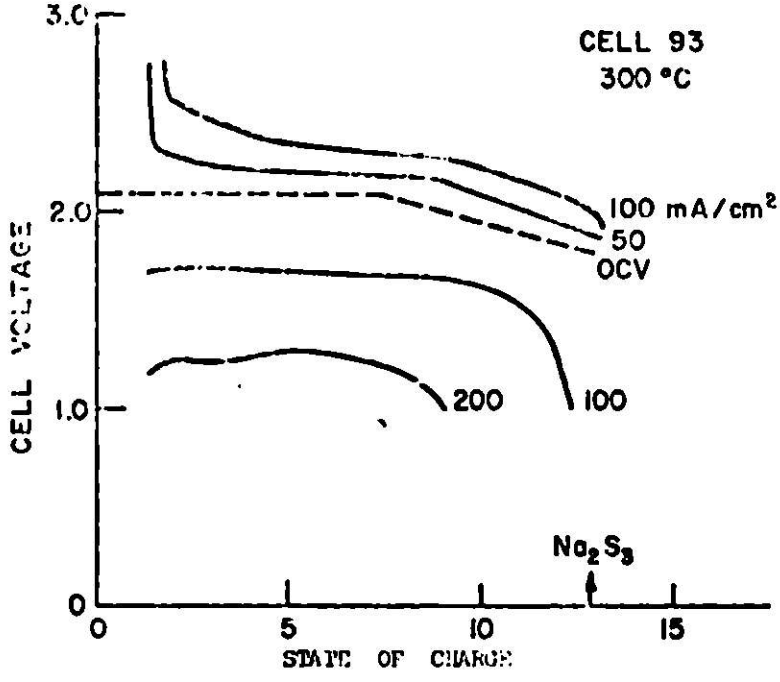

Figure 7. Charge/discharge characteristics for cell 93. Zero state of charge represents a complete recharge to sulfur.

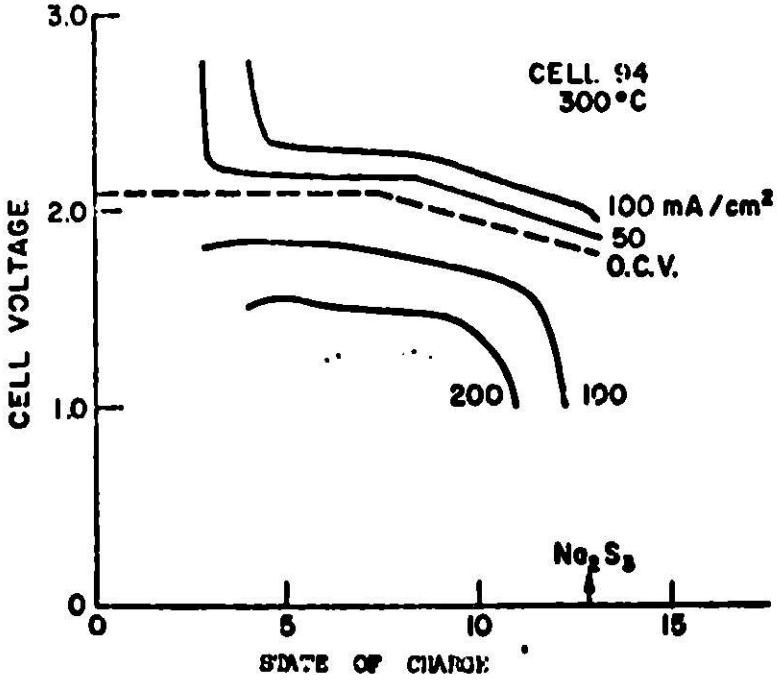

Figure 8. Charge/discharge characteristics for cell 94.

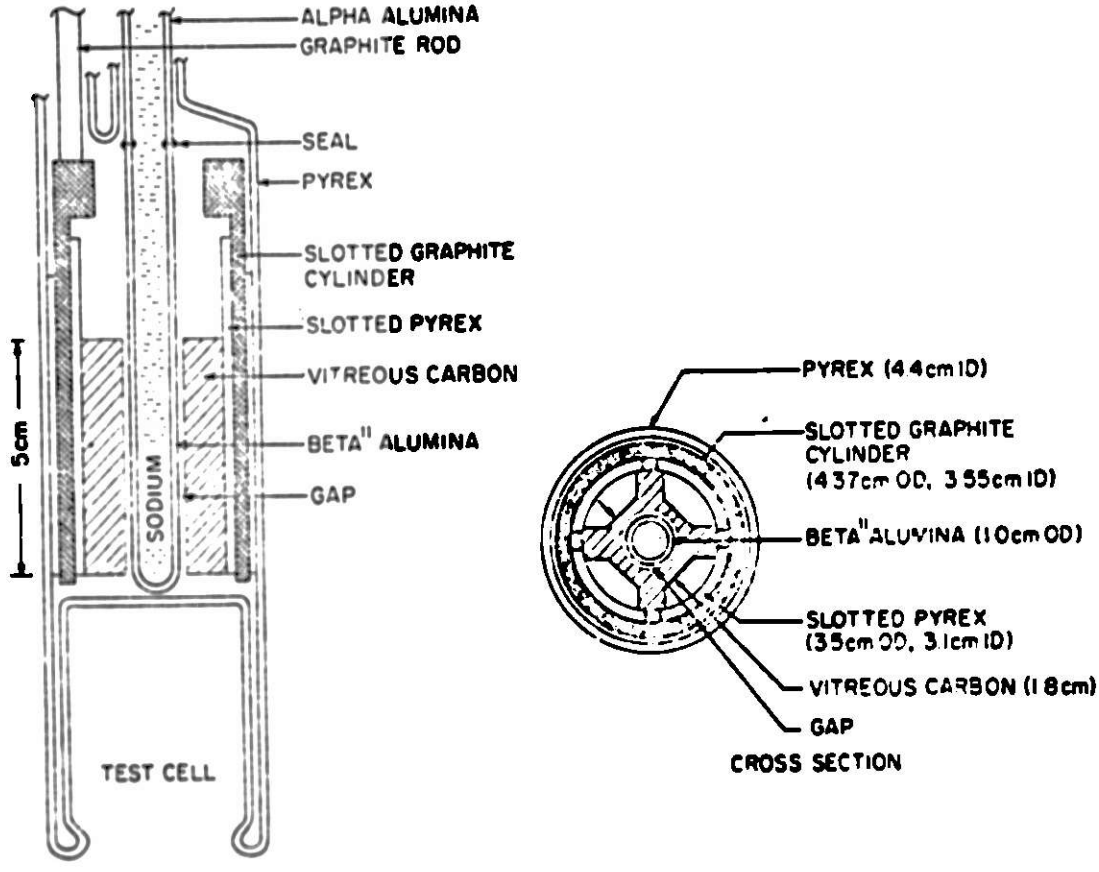

Figure 9. Schematic of cell 10% employing a shaped vitreous carbon foam electrode with a 1 mm gap between the ceramic electrolyte and the foam electrode.

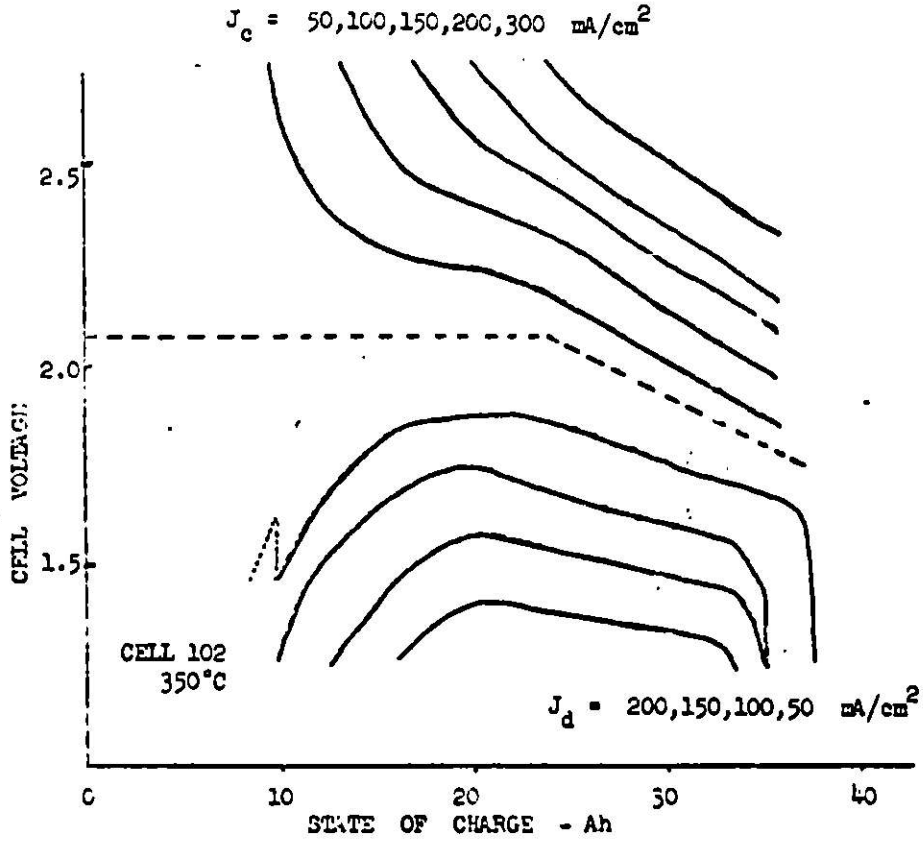

Figure 10. Charge/discharge characteristics for cell 102.

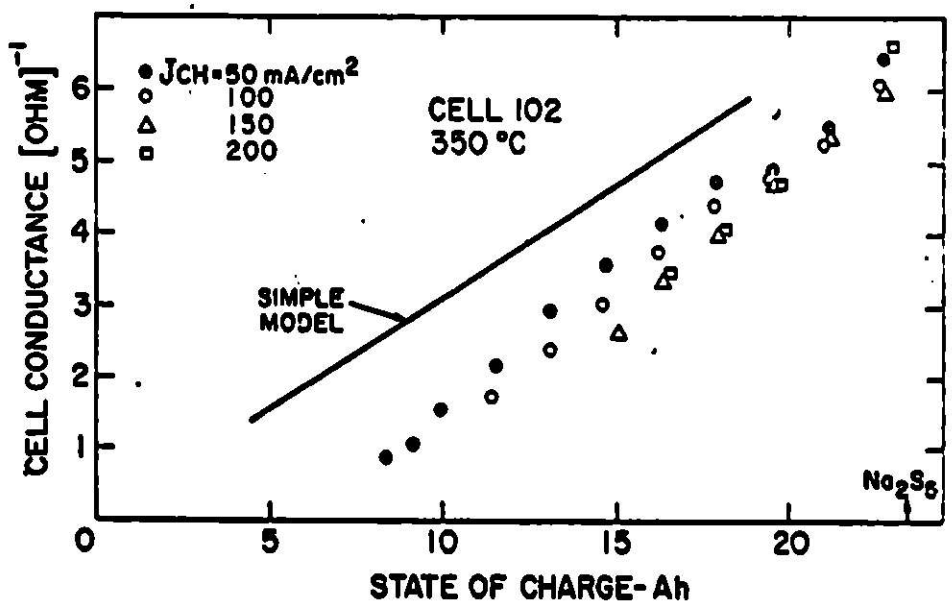

Figure 11. Cell conductance versus state of charge for cell 102. The non-zero intercept is attributed to lost capacity associated with reactants located in stray volume of the test cell.

DEVELOPMENT OF UNCHARGED Li-Al/FeS CELLS

H. Shimotake and L. G. Bartholme

Argonne National Laboratory
9700 South Cass Avenue
Argonne, Illinois 60439

ABSTRACT

Cells having negative electrodes of lithium-aluminum alloy and positive electrodes of iron sulfide (FeS) are being developed at Argonne National Laboratory for energy storage batteries to be used for utility load-leveling. This paper describes a Li-Al/FeS cell that is assembled in the uncharged state. The principal difference from previous cells is in the method of preparing the positive electrode; in this method Li_2S, iron powder, and electrolyte salt are blended and hot-pressed into a plaque (copper powder has also been included in some of the electrodes). The use of this type of electrode has overcome many previous difficulties, primarily, excessive swelling, low utilization, and gassing. The new cells have shown outstanding performance, with utilizations and energy efficiencies exceeding 85% at the 10-hr rate.

INTRODUCTION

The development of high-specific-energy secondary cells having negative electrodes of lithium-aluminum alloy and positive electrodes of iron sulfide (FeS) is under way at Argonne National Laboratory (ANL) for energy storage batteries to be used for utility load-leveling. Initial development of these cells was beset primarily by (a) excessive swelling of the positive electrodes, (b) low utilization of the positive active material in the cell, and (c) gassing from the electrodes. Postoperative examinations of FeS-type cells showed that a reaction had occurred between the FeS electrodes and potassium in the LiCl-KCl electrolyte to form a K-Li-Fe-S compound, designated J-phase.[1] This reaction caused excessive swelling of the positive electrode and high polarization, the latter of which resulted in low utilization of the positive active materials.

Accordingly, means of eliminating or minimizing this problem were sought. The addition of Cu_2S to the FeS has been found to modify the J-phase[2] and reduce the polarization of the FeS electrode, resulting in high utilization of theoretical capacity. Similar results were also obtained by raising cell temperature to 500°C from 450°C.[3] However, the excessive swelling of the electrodes still remained.[4] More recently, FeS-type cells have been operated with electrolytes containing only lithium ions, *e.g.*, LiF-LiCl-LiI or LiF-LiCl-LiBr.[5] Because of absence of potassium, J-phase did not form during the cell reaction. As a result, these cells exhibited significantly higher electrical performance and little positive electrode swelling. However, assembly of cells using these electrolytes is impractical, at present, because of high costs of the LiI and LiBr.

In this paper we describe still another solution to the problem, namely, the assembly of Li-Al/FeS cells in the uncharged state. In an uncharged cell, the positive and negative electrodes are initially prepared from a mixture of iron powder and Li_2S for the positive and a porous aluminum plaque for the negative electrode. Upon charging, the lithium in the positive electrode is electrochemically transferred to the negative electrode, forming a lithium-aluminum alloy, while in the positive electrode the sulfur from Li_2S forms FeS. Test results of engineering cells of this type showed marked improvements in terms of electrical performance, lifetimes, and costs over previous Li-Al/FeS cells.

DESIGN OF R-SERIES CELLS

The preliminary design developed for the engineering cell is shown in Fig. 1. In this design, a central positive electrode is placed between two negative electrodes; the electrodes are oriented vertically and are square (or rectangular); the cell is thus referred to as a prismatic cell. This design was selected to allow the use of steel or stainless steel housing, and to minimize the area of the cell seal. The dimensions chosen for the cell housing were 13 by 13 by 2 cm; such a housing is capable of containing active materials equivalent to a cell capacity of 120 A-hr. The LiCl-KCl eutectic

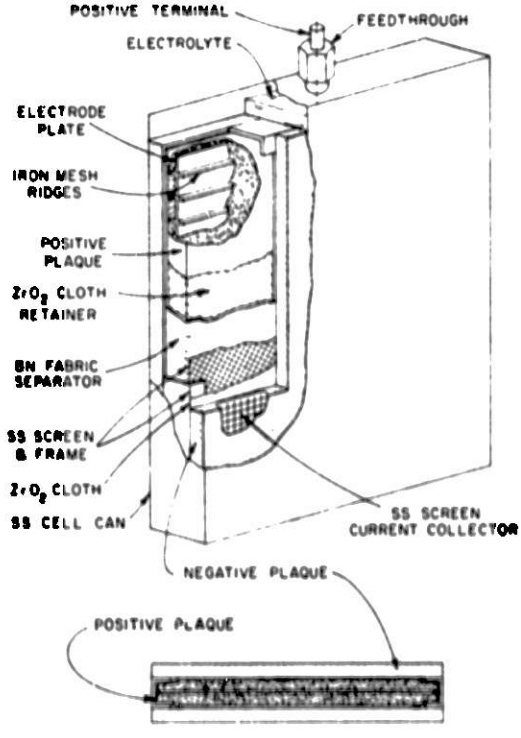

Fig. 1. Design of Prismatic Li-Al/FeS Cell

(58.5 mol % LiCl-41.5 mol % KCl, mp = 352°C) was used as the electrolyte because of its low density, low melting point and high dissociation potential (∿3.4 V). A boron nitride cloth impregnated with liquid electrolyte is used as the separator between the positive and negative electrodes, while a zirconia cloth is used as a porous barrier to retain the active material particles. A thin steel plate inserted in the center of the sulfur electrode divides the positive active material to prevent unequal utilization of the two negative electrodes.

This design of engineering cell appears to be capable of achieving a specific energy of ∿150 W-hr/kg when techniques to produce compact electrode structures are fully developed.

DEVELOPMENT OF ELECTRODES

The cells were all assembled in an uncharged state; *i.e.*, the material in the positive electrode was a mixture of iron powder, Li_2S, electrolyte, and (in some cases) copper powder as an additive; the negative electrode consisted of a porous structure of metallic aluminum. Similar electrodes were studied by Yao *et al.*,[6] and later by Martin *et al.*[7] These investigators found that low diffusional and ohmic resistance can be achieved by this type electrode. However, in this earlier work, no attempt was made to develop a compact, high-specific-energy electrode. Consequently, our work included a series of experiments in 7.5-cm-dia cells to develop such an electrode.

We found that a highly efficient and compact positive electrode can be made from a powder mixture of iron particles, Li_2S, electrolyte and, in some cases, copper particles by pressing the mixture at about 380°C on a steel substrate to form a plaque. The Li_2S is normally a fine amorphous-appearing powder that is difficult to mix uniformly. If the mixture is ground, the Li_2S smears. Martin[8] has found that the physical properties of the Li_2S can be improved significantly by sintering at 1200°C. The sintered Li_2S shrinks, thereby increasing in bulk density, and forms a hard cake, which can be ground easily without smearing and can be uniformly mixed with the iron and electrolyte powder. In tests of these electrodes, 80-90% of utilization of the active material was achieved at 2-10 hr rates. Furthermore, swelling and gassing of the electrodes were greatly reduced. In view of these results, engineering-scale cells with similar positive electrode plaques were built, first with iron powder only, and later with addition of copper powder to the mixture.

An initial consideration was that the active material on a vertical electrode plate might slump, owing to gravity. To prevent possible slumping in the engineering cells, the positive electrode plate was made with a series of ridges of steel mesh, 10 mm high and 25 mm apart, extending across the width. The pressed plaque was encased in a thin zirconia fabric, to retain any fine particles, and then in a separator of boron nitride fabric for electrical insulation. In previous cells, the boron nitride cloth was not readily wet by the molten LiCl-KCl eutectic; therefore, in the cells of this series, the boron nitride fabric was impregnated with LiCl-KCl eutectic prior to assembly by immersing it in a saturated methanol solution of LiCl-KCl eutectic and then drying in an oven. We found that such treatment made the boron nitride fabric readily wettable.

A pressed aluminum fiber plaque containing stainless steel mesh as a current collector served as the negative electrode in the 7.5-cm cell experiments. However, past experience has shown that during cell operation, the Li-Al alloy in the negative electrode gradually becomes very finely divided as a result of repeated charge and discharge operations, and the fine powder, if not contained, migrates to other parts of the cell, causing short-circuits. To prevent the migration of Li-Al particles, an additional sheet of zirconia fabric was inserted between the negative electrode and the boron nitride fabric.

ASSEMBLY OF CELLS

The required amounts of each active component can be calculated from the following equation for the cell reaction:

$$Fe + Li_2S + 2Al_x = 2LiAl_x + FeS$$

The amount of aluminum can be varied, but generally a sufficient amount was used to give a 49 at. % Li alloy, so that deposition of metallic lithium at the electrode interface was avoided. The positive electrode mixture was prepared by mixing iron, Li_2S and electrolyte, as described above. In some cells, copper powder was added, and the capacity contributed by formation of Cu_2S was taken into account. The amount of electrolyte was in general between 25 and 30 wt % of the total mixture. An amount less than 20 wt % produces a fragile plaque, whereas an amount exceeding 35 wt % is not retained in the plaque during hot-pressing. Iron powder (99.9% purity, ~200 μm dia, GAF Corporation), copper powder (99.9% pure, ~200 μm dia, Fisher Scientific), and LiCl-KCl eutectic (99.9% purity, Anderson Physics Laboratory, Champaign, Ill.) were mixed and poured over an electrode plate having a steel mesh substrate and ridges; the entire structure was then placed in a die and pressed at 380°C and 400 psig for 15 min. The resulting plaque was then encased in sheets of zirconia fabric (0.13 mm thickness, Zircar Corp.) and boron nitride fabric (2.5 mm thickness, Carborundum Corp.), which had been treated with a methanol solution of LiCl-KCl. A set of "picture-frame"-like, thin steel frames held the fabrics in position.

The aluminum plaques were made of aluminum mesh fabric (5056 aluminum, 0.15 mm wire, Otto H. York, Inc.), which had been cleaned in an ultrasonic cleaner containing trichlorofluoroethane, layered in a die, and pressed at 200°C and 1000 psig for 15 min. For current collection, a sheet of stainless steel screen was inserted between the layers of the aluminum fabric. The screen was later unfolded and spot welded to the cell casing. The aluminum plaques and the positive electrode assembly are shown in Fig. 2.

After introduction of the electrode assemblies into the cell housing, the cell lid/feedthrough assembly was clamped in place and heliarc-welded to the housing. After the feedthrough was sealed, molten salt electrolyte was introduced to the cell under vacuum at 400°C through a port provided for this purpose. A fully assembled cell is shown in Fig. 3.

The cell was heated to 450°C in a furnace tube attached to a helium-atmosphere glove box. The cell was first charged at a low current density (<10 mA/cm^2) for formation of the electrodes, followed by discharge at a

modest current density (<25 mA/cm^2). Normally, only one formation cycle is necessary for the start-up of a cell.

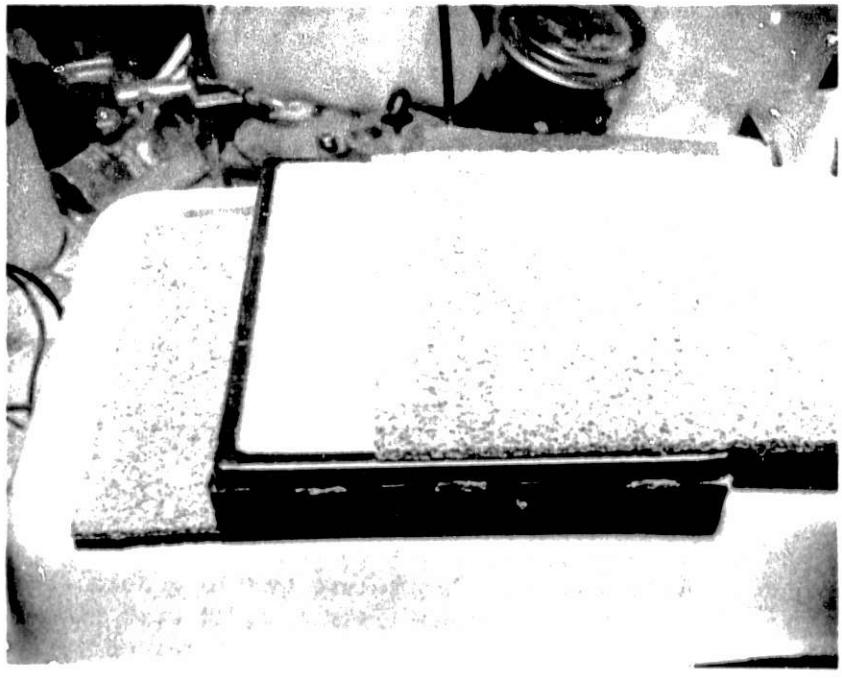

Fig. 2. Positive Electrode Assembly and Two Aluminum Plaques

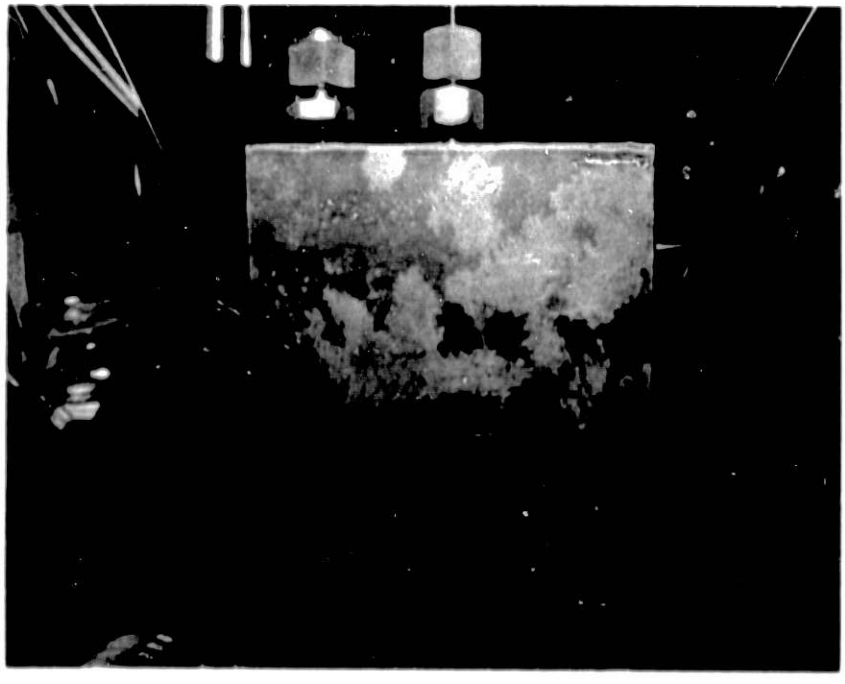

Fig. 3. A Fully Assembled Cell

RESULTS AND CONCLUSIONS

The electrical performance results for three of these cells are summarized in Table I. Figure 4 shows typical performance curves for Cell R-5,

Table I. Performance Results for Prismatic, Uncharged Li-Al/FeS Cells

Cell No.	Initial Materials[a]	Capacity, A-hr		Eff., %		Specific Energy, W-hr/kg
		Theor.	Typical	A-hr	W-hr	
R-5	Al/Fe-Li_2S	76	42	96	85	63
R-6	Al/Fe-Li_2S-Cu	73	45	96	86	67
R-7	Al/Fe-Li_2S-Cu	105	78	95	85	100

[a]The positive electrode of Cell R-6 contained 10 wt % Cu; that of Cell R-7, 20 wt % Cu.

which had a positive electrode containing iron powder but no copper, and that of Cell R-6 which had a positive electrode containing 10 wt % copper powder. Cells R-5 and R-6 showed, respectively, 55% and 62% utilizations of theoretical capacities at current densities of 35 mA/cm^2. The ohmic resistance of Cell R-6, which contained copper, was lower than that of Cell R-5; the average cell resistance of Cell R-6 was 6 mΩ, compared with 100 mΩ for Cell R-5. In view of these results, more copper powder (20 wt %) was added to the positive electrode in Cell R-7. The performance curves of this cell at current densities up to 70 mA/cm^2 are shown in Fig. 5. At a current density of 35 mA/cm^2,

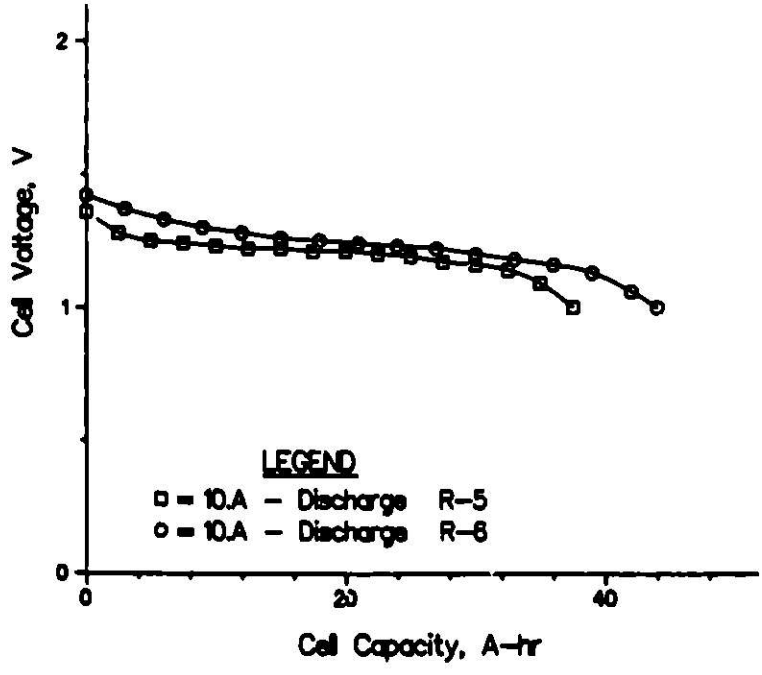

Fig. 4. Performance Curves for Cells R-5 and R-6

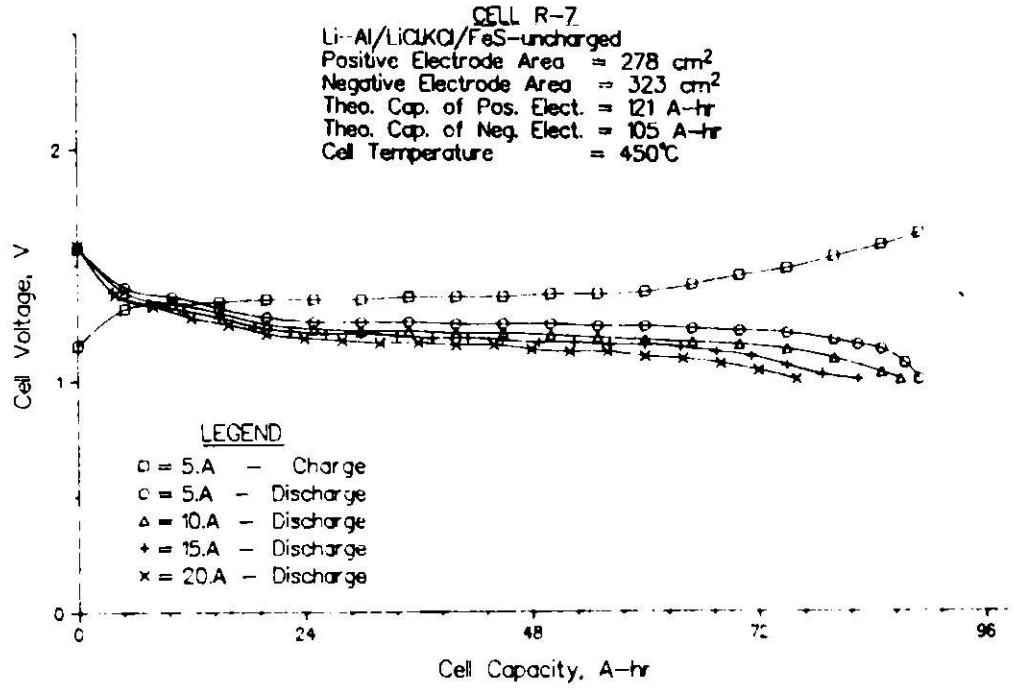

Fig. 5. Performance Curves for Cell R-7

the utilization was 85% of the theoretical capacity. The ohmic resistance of the cell was quite low, less than 4 mΩ, thereby indicating the advantage of adding copper. The coulombic efficiency was quite high, above 95%, and as a result, the energy efficiency in excess of 80% at 10-hr rate was achieved, thereby indicating that the electrical performance of this cell is satisfactory for practical application. Maximum specific energies achieved by the present cells are in the range from 70 to 100 W-hr/kg. It is believed that this figure can be further improved by making the electrodes more compact.

Figure 6 shows the capacity of Cell R-7 as a function of cycle life. This cell has accumulated over 2000 hr of operating time and 80 cycles at the time of this writing. In the figure, one can see a period of high capacities at initial cycles which gradually decline to a slightly lower but stabilized value. This is a typical pattern of cell capacity *vs.* cycle life. It is not clear at present why the cell capacities decline in the initial cycles and then reach steady value.

Swelling and gassing, which were observed in all previous Li-Al/FeS cells, did not occur in the cells of this series. One can postulate that the swelling does not occur despite the existence of J-phase in cells assembled in the discharged state, because the positive electrode materials, as initially assembled, are in their most expanded state. Disappearance of the gassing can be attributed to the use of metallic aluminum fiber plaques instead of powdered lithium-aluminum alloy or electrochemically formed lithium-aluminum alloy, either of which can be easily contaminated by oxygen, nitrogen or moisture during handling and storage.

Further improvements in performance and lifetime are expected to be achieved with this type of cell as improved component materials become available for the cell construction.

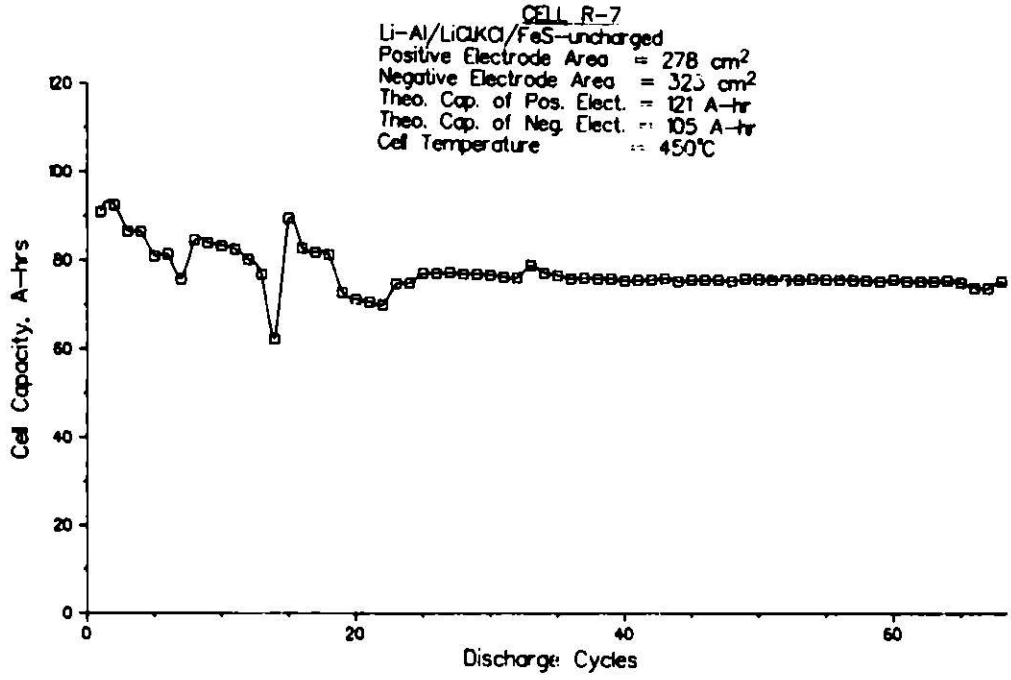

Fig. 6. Capacity *vs.* Cycle Life for Cell R-7

ACKNOWLEDGMENT

The authors gratefully acknowledge the major contributions made by Drs. A. E. Martin and D. R. Vissers in technical discussions and helpful suggestions. The encouragement of Mr. L. Burris, Jr., Dr. P. A. Nelson, and Dr. W. J. Walsh is appreciated. Thanks are also extended to Dr. S. D. Gabelnick for his help in making use of computers.

The work was conducted under the auspices of the U. S. Energy Research and Development Administration.

REFERENCES

1. F. C. Mrazek and J. E. Battles, in *High-Performance Batteries for Off-Peak Energy Storage and Electric-Vehicle Propulsion, Progress Report for the Period January-June 1974*, ANL-8109, p. 72, Argonne National Laboratory (1975).

2. Z. Tomczuk and A. E. Martin, in *High-Performance Batteries for Off-Peak Energy Storage and Electric-Vehicle Propulsion, Progress Report for the Period July-December 1974*, ANL-75-1, p. 106, Argonne National Laboratory (1975).

3. H. Shimotake and L. G. Bartholme, in *High-Performance Batteries for Off-Peak Energy Storage and Electric-Vehicle Propulsion, Progress Report for the Period July-December 1974*, ANL-75-1, p. 32, Argonne National Laboratory (1975).

4. R. C. Elliott and T. O. Cooper, "Volumetric Change of Electrodes in LiAl/FeS_x Cells," Extended Abstracts of Battery-Electronics Divisions, Electrochemical Society, Toronto, Canada, May 11-16, 1975, Vol. 75-1, pp. 85-86 (1975).

5. H. Shimotake and D. R. Vissers, Argonne National Laboratory, unpublished work (1975).

6. N. P. Yao, R. C. Elliott and J. W. Allen, "Development of a Discharged Iron Sulfide Electrode," Extended Abstracts of Battery-Electronics Division, Electrochemical Society, New York, N. Y. (October 1974).

7. A. E. Martin and Z. Tomczuk, Argonne National Laboratory, private communication (1975).

8. A. E. Martin, Argonne National Laboratory, private communication (1975).

THE SODIUM/SULFUR BATTERY: A PROGRESS REPORT*

Steven A. Weiner
Research Staff
Ford Motor Company
Dearborn, Michigan 48121

ABSTRACT

This paper presents some of the work on sodium-sulfur cells with emphasis on various aspects of cell design and testing. The baseline studies for the cell testing program were run on cells that were constructed of carbon and glass and contained no metal other than sodium. Separate cells, designed to maximize energy and power density, respectively, were studied. A preliminary discussion of materials costs is included.

INTRODUCTION

The sodium-sulfur battery consists of two liquid electrodes, sodium and sulfur, and a ceramic electrolyte membrane which allows for the transport of sodium ions.[1] The sodium electrode is well characterized and does not present material problems. Excess sodium is used in order to keep the ceramic electrolyte completely covered at all times. The use of excess sodium together with a stainless steel sodium container eliminates the need for an electrical feedthrough.

The working of the sulfur electrode is quite complex. Because elemental sulfur is an electronic insulator, graphite felt is added to provide a large area electrode. On discharge from sodium and sulfur, the sodium polysulfide formed is not soluble in sulfur. Thus, the sulfur electrode contains two liquid phases throughout some 60% of the discharge. Beyond this point, there is essentially no elemental sulfur remaining, and all of the polysulfides are miscible forming one phase. To keep this phase liquid throughout its compositional ragne (Na_2S_5 to Na_2S_3), it is necessary to operate above 270°C, with typical operating temperatures falling in the range of 300-375°C. A schematic of a cell with a cylindrical ceramic electrolyte is shown in Figure 1.

Major applications currently envisioned for the sodium-sulfur battery are vehicle propulsion and load leveling. For propulsion, the battery must meet stringent weight and volume requirements with greater emphasis on utilization of reactants than would be required for load leveling. Furthermore, the high peak to average power demand for vehicular propulsion requires a special battery design for this application. Thus our program has as one goal the development of a high power battery for vehicle application. Because of the particular nature of the sulfur electrode, the high power battery is designed to operate in the single phase region, Na_2S_3 to Na_2S_5.

In order to compare current laboratory achievement with overall program goals, the goals of the program have been translated from units of W/kg and Wh/kg to W/cm^2 and Wh/cm^2 where the unit of area is the surface area of

*Supported, in part, by the National Science Foundation.

the β''-Al_2O_3 ceramic electrolyte. The goals are given in Table I. The translation from units of weight to units of electrolyte area was necessitated by the fact that the bulk of the laboratory results were obtained using cells constructed mainly from carbon and glass to avoid the effects of corrosion products originating from metallic containers or current collectors in contact with the sulfur electrode.

Table I. High Power Cell Goals

Energy Density (Wh/cm^2)	0.2 (80 Wh/kg)
Power Density (W/cm^2)	0.7 (280 W/kg)
Utilization of Reagents (%)	25
Electrical Efficiency (%)	70
Capacity (Ah/cm^2)	0.1
Discharge Time (h)	0.3
Durability (Ah/cm^2)	250
Cycle Life	1000

RESULTS OF CELL TESTING - SODIUM/SODIUM CELLS

For purposes of ceramic evaluation, sodium-sodium test cells (Figure 2) are constructed and run at relatively high current densities of 0.75-1.25 A/cm^2 so that substantial ionic currents can be passed through the membranes in a reasonable period of time. During operation cell polarities are reversed periodically. This subjects each surface of the β''-Al_2O_3 to both a charging operation in which sodium ions are converted to sodium metal and a discharge operation in which sodium metal is converted to sodium ions. It is only after satisfactory performance in sodium-sodium cells that ceramics are tested in sodium-sulfur cells.

One of the major uses of the sodium-sodium cell test program has been to evaluate ceramic of different composition.[2] Several of the compositions tested passed over 1000 Ah/cm^2 in one direction, whereas others showed clear evidence of electrolytic degradation. The major factor in the electrolytic degradation of β''-Al_2O_3, when subjected to high current densities in a charging mode, is the Li_2O concentration. While the Na_2O content may vary within certain limits, β''-Al_2O_3 compositions containing 0.8% or less of Li_2O appear to be significantly more resistant to electrolytic degradation at high current densities than β''-Al_2O_3 compositions containing 0.9% or more of Li_2O.

Results of this study lead to recommending the composition 9.0% Na_2O - 0.8% Li_2O is recommended as a material for use in Na-S cells. Cells 1723-1 and 1723-2 each passed over 1000 amp-hrs/cm^2 undirectionally without deterioration at a current density of 1.25 amps/cm^2. The resistivity of the material (5.3 Ω-cm at 300°C) is comparable to that of the 8.7% Na_2O - 0.7% Li_2O (5.0 Ω-cm at 300°C), while its strength is greater (19,000 psi vs. 16,000 psi). A comparison of the performance of ceramic of these two compositions is given in Table II.

Table II. Summary of Data from High Current Density Na-Na Test Cells

Number	Current Density A/cm^2	Composition $\%Na_2O$	Composition $\%Li_2O$	Time On Test (Months)	Current Passed (Ah/cm^2) One Direction
1266-1	0.75	8.7	0.7	1.3	377
1266-2	0.75	8.7	0.7	6	1512
1266-3	0.75	8.7	0.7	1.5	378
1578-1	1.00	8.7	0.7	1.9	636
1269-3	1.25	8.7	0.7	1.3	525
1723-1	1.25	9.0	0.8	2.1	1155
1723-2	1.25	9.0	0.8	3.2	1575

Cells 1266-1, 1266-2, 1266-3, and 1578-1 were taken off test because of failure of the outer glass envelope. Cells 1269-3, 1723-1, and 1723-2 were taken off test because of malfunction of the cell test controller. After cell termination, most of the ceramic membranes were examined by a variety of methods including light microscopy, scanning electron microscopy (SEM), x-ray diffraction, and x-ray fluorescence. The ceramic from all test cells other than 1578-1 was intact. Some anomalies were observed however in the examination of membranes. The presence of K and Cl was found by SEM in cracked areas of tube 1578-1, but not in undamaged sections. There were several indications of seal damage but which properly could not be called seal failures in the cells built with ceramic of composition 9.0% Na_2O - 0.8% Li_2O. In these cases, the α-Al_2O_3-glass-β-Al_2O_3 seals were badly discolored or pitted, but not broken.

Now that we have found an optimum ceramic composition, the major use for sodium-sodium cell testing is to test the effects of changes in ceramic processing. In this regard, it is worth noting that ceramic tubes fabricated at the University of Utah using standard Ford processing methods have been put on test. Four such tubes of composition 8.7% Na_2O - 0.7% Li_2O have passed in excess of 850 Ah/cm^2 in one direction at a current density of 1.25 A/cm^2. These tubes are still on test and except for some asymmetry in operation appear to be intact. In the worst case, the asymmetry is of the order of 25%. At present, we have no explanation for this behavior and are awaiting the ceramic failure and results of post-test analyses before we discuss this asymmetry and its possible meaning in terms of cell life and operation.

RESULTS OF CELL TESTING - SODIUM/SULFUR CELLS

The characterization of individual sodium-sulfur cells involves two distinct testing programs -- endurance testing and performance testing.[2] The purpose of the endurance test program is to establish the durability of the cell and its components by monitoring the electrical performance at fixed operating conditions as a function of time and conditions of use. In addition to determining the time to failure, the rates of deterioration of cell performance (e.g., capacity, internal resistance) are obtained. Performance testing has as its goal the characterization of the electrical behavior of a cell at various operating conditions (e.g., temperature, charge and discharge rates) during the early stages of cell life. Specifically, these tests involve determining the capacity versus rate of charge and discharge, and the

measurement of ohmic and concentration polarizations as a function of temperature, rate, and state of charge of the cell. At the conclusion of the electrical test program, each cell is dissected and examined visually. Cell components are prepared for further examination as appropriate.

As my colleague, Dr. R. W. Minck discussed earlier in this Workshop in his paper entitled, "The Performance of Shaped Graphite Electrodes in Sodium-Sulfur Cells", a series of cells employing novel sulfur electrode shapes were constructed and tested. The electrode shapes of cells 93 and 94 are shown along with a schematic of a completely felt filled electrode in Figure 3a, b, c.

Ceramic tubes were removed from 93 and 94 and, after cleaning, were cut into segments. When feasible, rings were cut from undamaged portions of the tube for diametral strength tests, microstructures were determined and surfaces were analyzed by SEM. In selected cases electron microprobe, Auger, and x-ray fluorescence also were used.

Cell E23 was terminated while still functioning properly. The particular electrode shape used is shown in Figure 4. As is now known, its low capacity is due to the electrode shape and the absence of a metal current collector. More importantly, the ceramic was undamaged and no impurities were found on either the inner surface (that had been in contact with Na) or the outer surface (that had been in contact with sulfur). Diametral tests indicated no deterioration in strength. This sample was used as a standard and subsequent reference to contamination or impurity levels are made relative to E23 (Figure 5). This reduces the probability of misinterpreting the presence of very low level impurities resulting from normal cell construction. The appearance of tubes from 93 and 94 was quite different from that of a typical ceramic degraded in a Na-Na cell. They each displayed a single long crack, with some branching in the lower portion of the tube. The areas away from the crack appeared undamaged and diametral strength tests indicated no loss of strength. Degradation usually is manifested in Na-Na cells as multiple unconnected cracks.

The SEM techniques used for most of the surface analysis reported involves the analysis of points on a surface. To minimize the possibility of any one point being atypical because of random contamination, many points were analyzed for each sample. Some typical data are shown in Figures 5-8.

The major impurity in all of the degraded samples was K. Ca was often present with the K, but always at lower levels. Ca was never found alone. Traces of Fe, Si and Cl were also found in several cases. The K impurities were found on the outer surfaces of tubes more frequently than the inner surfaces. The K levels found on outer surfaces were often higher, but never lower than the K levels found on inner surfaces. (Compare Figures 7 and 8.) It is apparent that K is not present in the original ceramic and diffuses into the ceramic during cell operation. At this stage, it would be improper to conclude that K caused the ceramic degradation, but there are enough indications to warrant further study.

The source of potassium also is open to question. The fact that the potassium levels on the sulfur electrode side of the ceramic electrolyte were

higher than on the sodium electrode side does not compel us to assume that the potassium arises from the sulfur electrode. It may be a reflection of the fact that problems in cell operation usually show up on charge rather than on discharge.* Since all cells tested use the same quality of sodium, it is not likely that the potassium initially present in the sodium can account for these observations.

PRELIMINARY ESTIMATE OF MATERIALS COSTS

Ultimately, the utilization of the sodium-sulfur battery will depend upon its ability to compete economically with alternate means for load leveling and automotive propulsion. A cost target of $20/kWh has been chosen for the load leveling application based upon published data.[3] Construction costs of present laboratory cells provide an upper limit for battery costs. The direct cost elements can be broken down into four major categories: 1) the costs of raw materials; 2) the costs of component fabrication; 3) the costs of cell filling and assembly; and 4) the costs of external components such as leads, insulation, etc. At this time we shall concern ourselves only with the present costs of raw materials used in construction of laboratory cells.

For purposes of calculation, we have assumed a materials usage efficiency of 100% and have based all of our costs in terms of unit area of ceramic electrolyte (cm^2). In order to convert from area of electrolyte to kWh, we have used a factor of 2.3 Wh/cm^2 or 435 cm^2 ceramic electrolyte per kWh delivered. This energy density has been achieved in cells designed for load leveling.[2] Using these assumptions the major raw materials costs are shown in Table III.

Table III. Major Materials Costs for Laboratory Cells

Material	Cost ($/lb)	Amount (gm/cm^2 of β"-Alumina)	Cost ($/kWh)
Graphite felt	75	0.091	6.57
Stainless Steel	2	2.53	4.86
α- Alumina Header	10	0.35	3.18
β"-Alumina	-	0.32	50.46
Sodium	0.4	2.06	0.79
Sulfur	0.1	3.71	0.36
		Total	62.22

The cost of $3.18/kWh for α-Al_2O_3 headers can be expected to decrease at least one order of magnitude in terms of production costs. A cost reduction of a factor of four can be achieved simply by using 1" long headers rather than the 4" long headers currently used in fabrication of laboratory cells.

It is worthwhile to take a somewhat closer look at the costs associated with producing units of β"-alumina electrolyte joined to an α-Al_2O_3 insulator. In the past, we have used a cost target of $0.01/$cm^2$ of ceramic electrolyte. Using the conversion factor of 2.3 Wh/cm^2, this translates to a cost of $4.35/kWh of energy delivered.

*In β" alumina potassium ions are less mobile than sodium ions.

The raw materials costs associated with β"-alumina fabrication are shown in Table IV.

Table IV. Ceramic Materials Costs

Material (Unit)	Amount (g/cm^2)	Cost ($/unit)	Cost ($¢/cm^2$)
α-Al_2O_3 (lbs)	0.41	10.00	0.9
Na_2CO_3 (lbs)	0.07	3.60	0.06
$LiNO_3$ (lbs)	0.02	8.90	0.04
Polyurethane (boots)[1]	0.19[1]	17.50	2.6
Pt (troy ounce)[2]	0.06[2]	200.00	8.0 (39)[2]
		Total	11.6¢

[1]The conversion factor is 1.5×10^{-3} boots/cm^2.

[2]The cost of the Pt is \$0.39/cm^2 but 80% of the cost is recovered.

The cost of the polyurethane boots (molds) can be decreased by extending boot life which is now on the order of 15 pressings. The cost associated with the platinum used during sintering is shown as 20% of the cost of the formed platinum, the remaining 80% is taken as scrap value.

The results given in Table III indicate that the highest cost item is the β"-alumina ceramic electrolyte. In order to meet target costs, it is necessary to reduce the cost of β"-alumina raw materials by more than an order of magnitude. Research is continuing towards our goal of cost reduction. We are exploring the use of raw α-Al_2O_3 powders which cost less than \$1.00/lb or 0.09¢/cm^2, the elimination of platinum encapsulation, and the use of lubricants to extend the life of the polyurethane boots. Although the progress at Utah in forming ceramic electrolyte by isostatic pressing has exceeded that made using extrusion we may yet be able to use an extrusion process which would eliminate the costs associated with polyurethane boots.

SUMMARY

One key to success of the sodium-sulfur battery remains the fabrication of high strength, low resistivity, durable, and economic ceramic electrolyte. Progress in fabrication of ceramic at the University of Utah and at Ford lead us to conclude that the goals of strength, resistivity, and durability can be met in production. A comparison of goals and best laboratory results for a high power cell are given in Table V. The preliminary economic analysis indicates that we have a way to go before our cost targets can be met. Our research program in ceramic electrolytes is focussed on finding economical means of fabrication through materials substitution and process changes and we remain confident that our target cost can be met.

Table V. Comparison of Laboratory Results (Cell E17) and Program Goals for the High Power Cell

Variable	Goal	Results (Cell E17)
Power Density (W/cm^2)	0.7	0.4
Energy Density (Wh/cm^2)	0.2	0.2
Utilization of Reagents (%)	25	30
Electrical Efficiency (%)	70	62
Capacity (Ah/cm^2)	0.1	0.1
Discharge Time (h)	0.3	0.6
Durability (Ah/cm^2)	250	1060
Cycle Life	1000	6400

ACKNOWLEDGMENT

This work was supported in part by the National Science Foundation under the RANN program. I thank my colleagues at Ford, Drs. Tischer, Minck, Winterbottom, Gupta, Lingscheit, Ludwig, Mikkor and Tennenhouse, and my colleagues at the University of Utah, Drs. Gordon, G. Miller, Sosin, Cutler, Virkar, and M. Miller for allowing me to cite their work and helping me to prepare this manuscript.

REFERENCES

1. J. T. Kummer and N. Weber, "A Sodium-Sulfur Secondary Battery." SAE Transactions, Vol. 76 (1967), paper 670179.

2. S. A. Weiner et al., "Research on Electrodes and Electrolyte for the Ford Sodium-Sulfur Battery." Annual Report to the National Science Foundation under Contract No. NSF-C805, July 1975.

3. N. P. Yao and J. R. Birk, "Battery Energy Storage for Utility Load Leveling and Electric Vehicles: A Review of Advanced Secondary Batteries." Paper 759166 presented at the 10th Intersociety Energy Conversion Engineering Conference, Newark, Delaware, August 18-22, 1975.

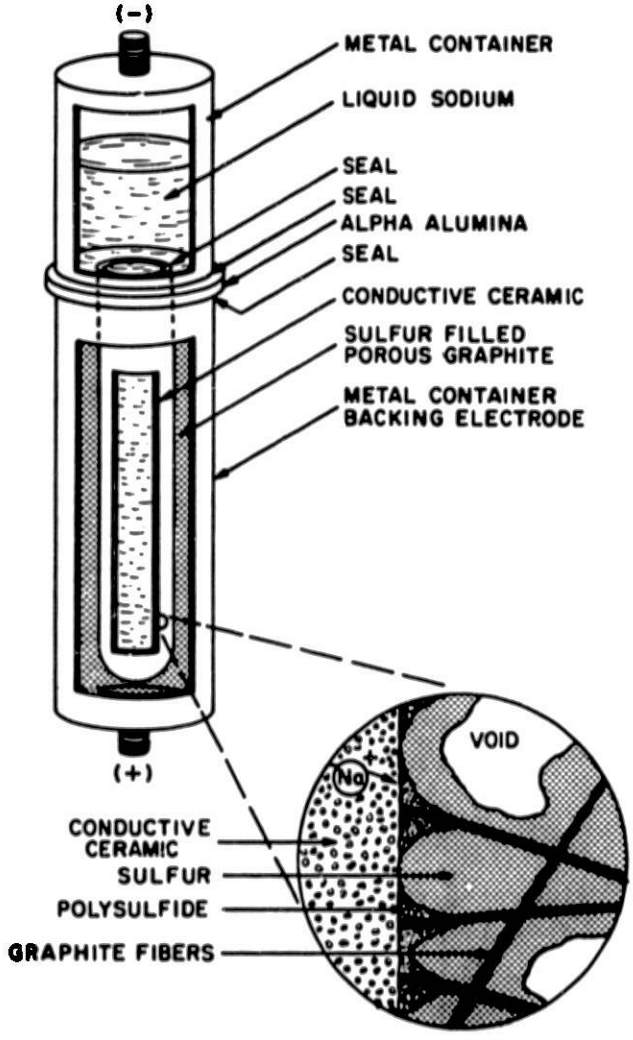

Fig. 1. Schematic of a high power sodium-sulfur cell

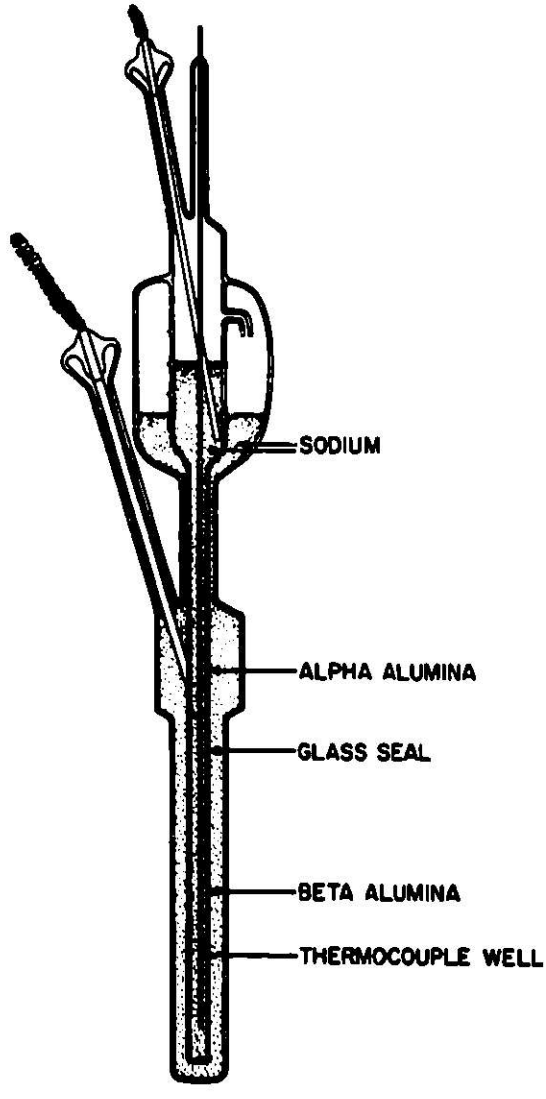

Fig. 2. Schematic of a sodium-sodium cell

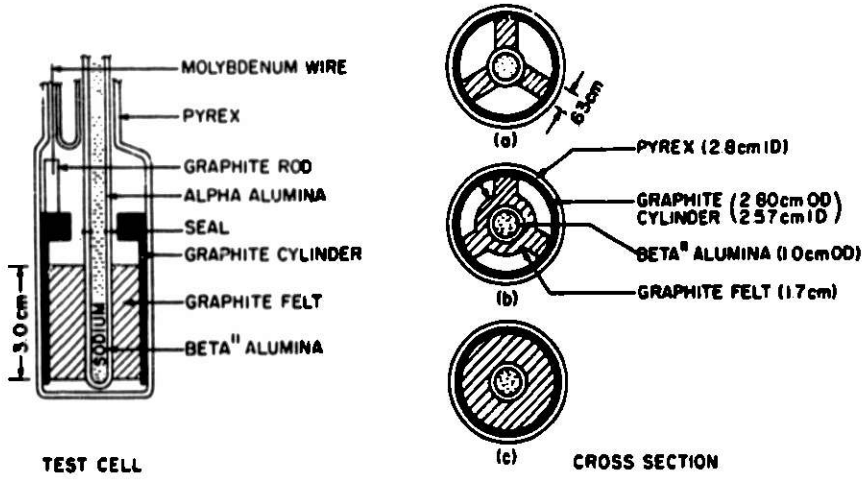

CELL DESIGN IV

Fig. 3. Schematic of sodium-sulfur cells 93(a), 94(b), and a high power cell(c)

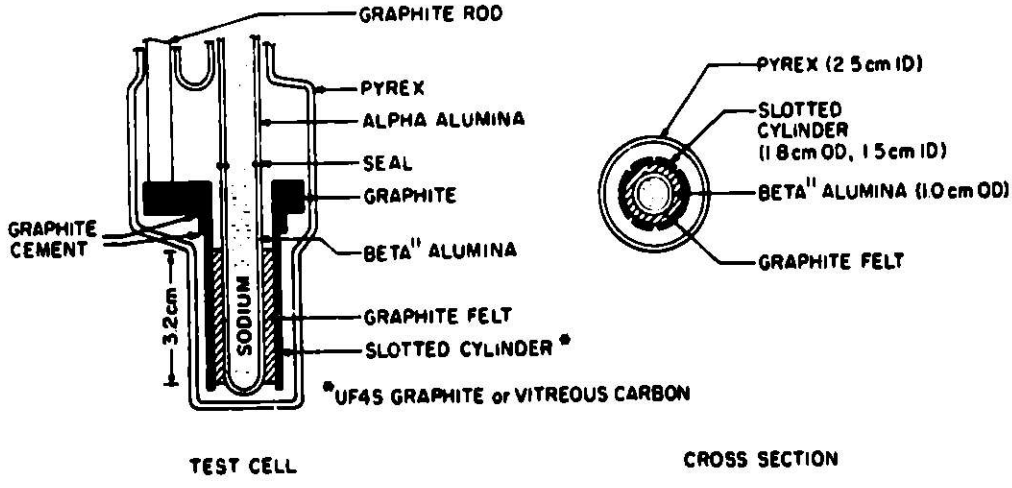

CELL DESIGN VI

Fig. 4. Schematic of sodium-sulfur cell E23

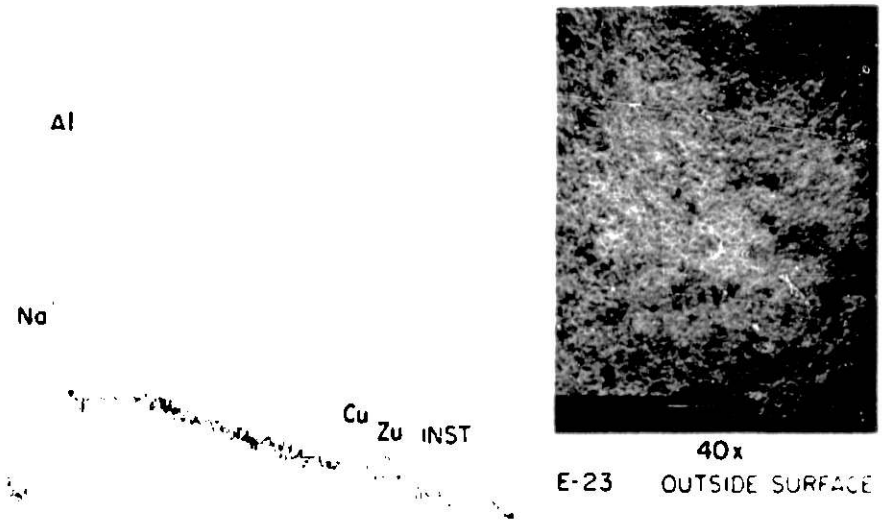

FIG. 5 Scanning electron microscope study of Tube E-23, outside surface.

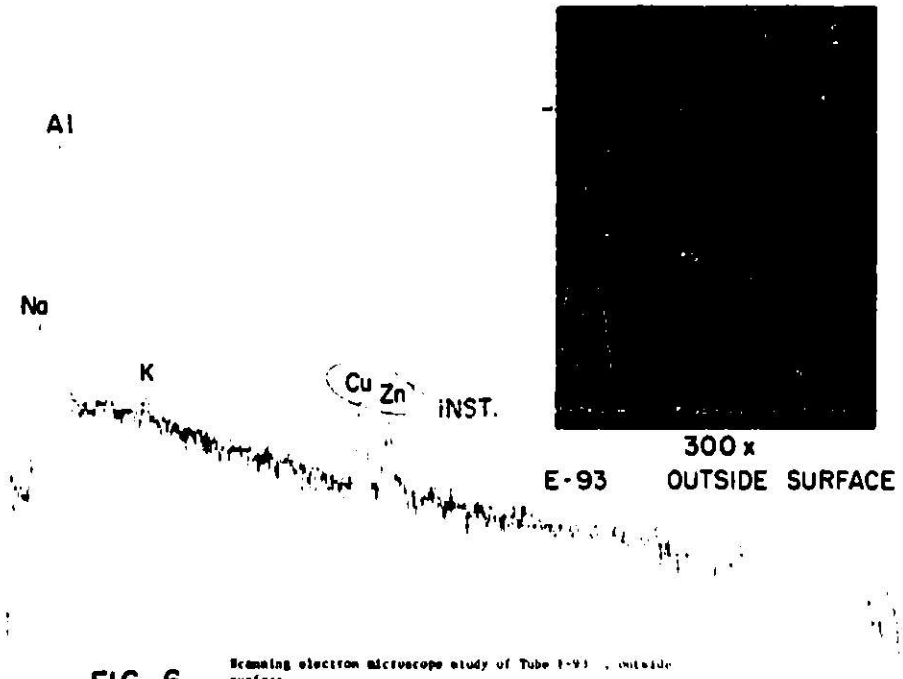

FIG. 6 Scanning electron microscope study of Tube E-93, outside surface.

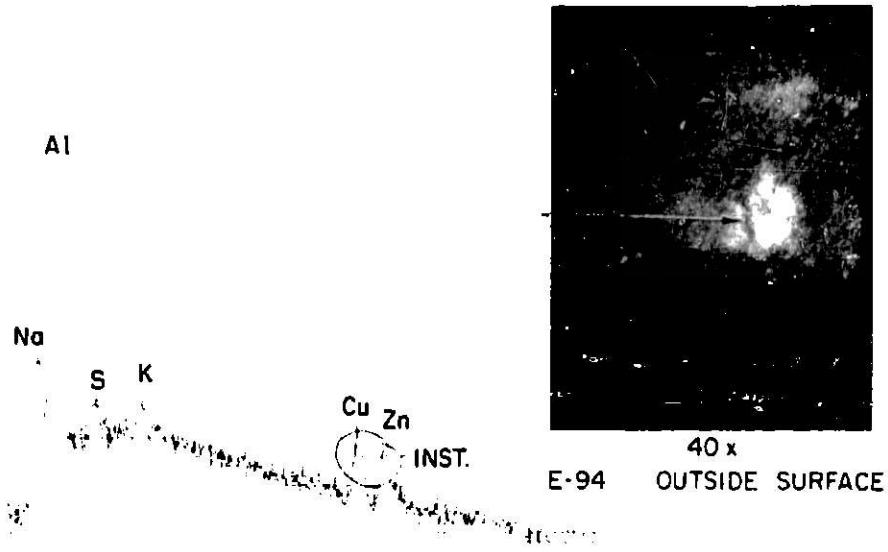

FIG. 7 Scanning electron microscope study of Tube E-94 , outside surface.

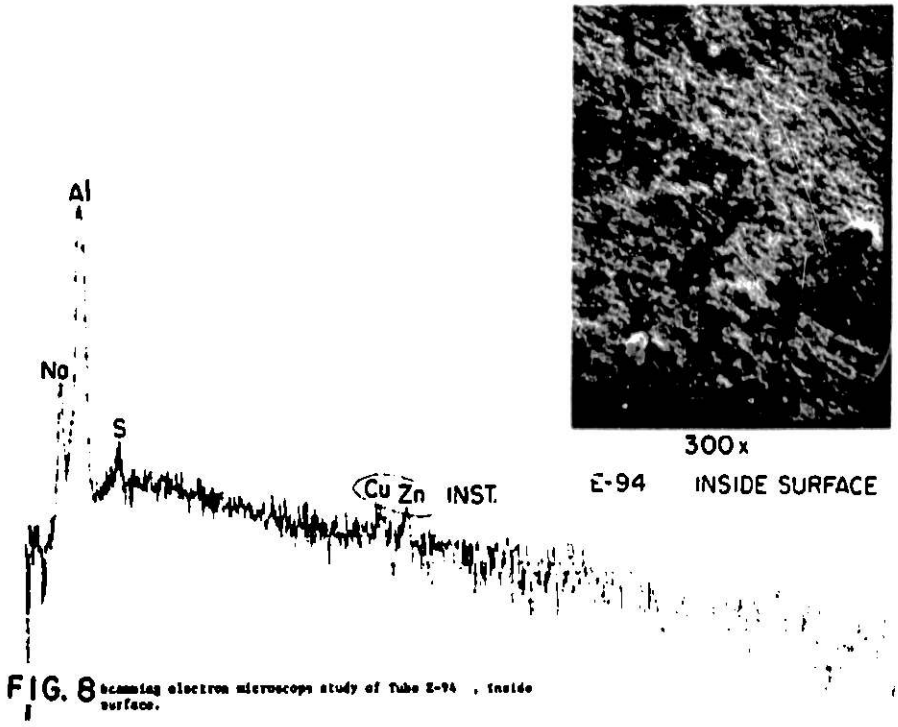

FIG. 8 Scanning electron microscope study of Tube E-94 , inside surface.

A MECHANICAL SEAL FOR THE SODIUM/SULPHUR CELL

by

A.R. Tilley
British Railways Board
Research & Development Division
Derby, U.K.

ABSTRACT

The development of a suitable sealing method is one of the technical problems that has to be solved before the high temperature sodium/sulphur battery becomes a commercial reality. This paper describes the development of a potentially low cost, lightweight seal assembly that is suitable for operation at 350°C. The results of stress analysis, seals leak tests and cell cycling studies are described.

INTRODUCTION

The sodium/sulphur battery programme at British Railways is concentrated on developing the tubular version of the cell. This cell is operated at a mean temperature of 350°C and seals are required which contain within the cell the sodium and sulphur/sodium polysulphides and prevent the sodium and sulphur from reacting chemically. In the event of ceramic electrolyte failure the direct reaction of sodium and sulphur results in high cell temperatures[1], and it is desirable to release in a controlled way any high pressures that may be built up within the cell.

The sodium/sulphur battery development in the United Kingdom is a co-ordinated joint programme between Chloride Silent Power Ltd., Harwell U.K.A.E.A. and British Railways. The British Railways seals effort is directed to developing a suitable axial compression seal system. The compression seals bear on to an alpha alumina flange which is glass sealed to the beta alumina tube as shown in Figure 1.

This paper describes the main problems encountered in the development of these seals and describes how a successful, high temperature,lightweight and potentially low cost sealing assembly has been produced.

BETA ALUMINA/ALPHA ALUMINA/GLASS SEAL

The alpha alumina collar has ground surfaces upon which the sealing gaskets are compressed. Conventional glass sealing technology is used to fabricate the beta and alpha alumina assembly. This involves careful matching of the coefficients of thermal expansion of the components. The sealing glass is required to be resistant to chemical attack from either sodium or sulphur/sodium polysulphides and during the glassing operation the glass should not react chemically with the beta alumina.

At present British Railways cells are operated with the seals uppermost and consequently chemical attack from the reactants is minimised and lives

up to one year have been obtained. When the glass seal is in contact with the reactants fairly rapid degradation of the glass seal is observed and we are presently engaged in evaluating a number of glass compositions in order to enable cells to be operated in any orientation.

COMPRESSION SEAL

Gasket Materials

Sodium seal. Flat aluminium gaskets(0.125 mm thick) have been found to be perfectly satisfactory. No sodium leaks have been observed with sealing pressures as low as 15 MNm^{-2}, even though the seals were not gas tight on assembly. It is believed that a bond is formed by chemical reaction[2] between sodium/sodium oxide and the aluminium and aluminium oxide. Aluminium seals have been operated successfully for more than 3,000 hours in charge/discharge cycling tests, and no deterioration of the gaskets has been detected. By maintaining the correct sealing stress, approximately 20-30 MNm^{-2} throughout cell operation at 350°C, a gas tight seal is obtained and reliance on the chemical sealing is not necessary.

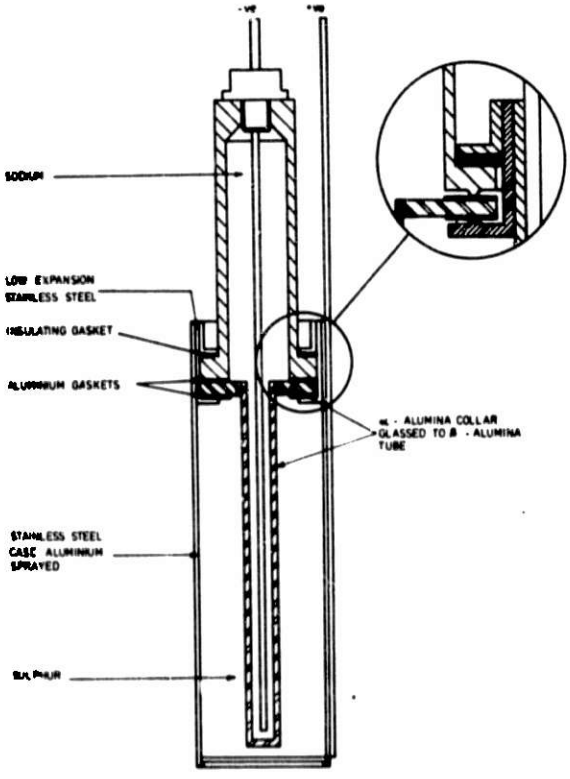

Fig.1 Sodium Sulphur Tube Cell

Flexible graphite gaskets such as "Grafoil" and "Sigraflex" have been used but special seal arrangements are needed as leakage of sodium occurs as a result of the intercalation reaction with graphite.

Sulphur seal. Flexible graphite gaskets and aluminium gaskets have been used as sulphur seals. The graphite gaskets do not perform perfectly satisfactorily. The materials are virtually non-elastic over the required sealing stress range and a constant sealing stress cannot be maintained throughout assembly and operation of the cell, which leads to leakage.

Seal tests using aluminium gaskets have shown no loss of sulphur as determined by weight loss, for over 3,500 hours. Aluminium is corroded by sodium polysulphides under polarised conditions but as the present cells are operated vertically with the seals uppermost, contact with the liquid reactants is prevented and corrosion appears to be absent. However,previous tests[3] using an immersed aluminium 'O' ring were promising and recent tests at British Railways using thin aluminium immersed seals have shown no corrosion after 69 charge/discharge cycles. This is probably due to a combination of the low surface area exposed to the melt and the attenuation

of the corrosion reaction due to build-up of the corrosion product, aluminium sulphide.

Clamping System

The initial clamping force must be such that after assembly at room temperature and operation of the cell at 350°C, the remaining clamping force is sufficient to maintain the seal. The clamping force is reduced after assembly due to relaxation of the stressed components. Flange bending and stretching of the outer clamping collar appear to be the most important effects. When the cell is heated to 350°C the load is further reduced due to differences in the coefficients of thermal expansion of the clamping components, particularly the ceramic collar (C.T.E. ca 68 x 10^{-7} K^{-1}) and the steel components (C.T.E. ca 120 x 10^{-7} K^{-1}).

Two methods of maintaining sufficient seal stress on the gaskets have been used. The first designs used a combination of metals having different coefficients of thermal expansion as shown in Figure 1. Mild steel was used for the low expansion components and initially aluminium (C.T.E. ca 230 x 10^{-7} K^{-1}) was used for the high expansion material. However, it was found that at 350°C the stresses resulted in creep of the aluminium, therefore austenitic steel was substituted. This method, however, requires stringent control of material specifications and dimensional tolerances to achieve reproducible seal stresses at 350°C and it does not overcome initial loss in clamping force after assembly.

Ideally, there should be no change in seal stress on assembly and heating and in practice this change can be reduced to a small amount by the use of disc springs. By using a disc spring of low rate compared to the stiffness of the other components of the seal assembly, the dimensional changes arising from relaxation of the clamping load and from thermal expansion do not result in a significant change in the sealing load. A typical cell design using a disc spring clamping assembly is shown in Figure 2.

Stress Analysis

A detailed stress analysis utilising finite element methods to obtain the flexibility of the components[4,5] was carried out on several cell designs in order to minimise load loss and to ensure that components were not over-stressed. Production type designs using easily formed components were also evaluated.

The calculations were as follows:-

The cell components are assembled together at room temperature as shown in Figure 3.

fi is the flexibility of the inner components 3,4,5 and 6.
fo is the flexibility of the outer components 1 and 2.

An initial clamping load P is applied and the components 1 and ` are welded as shown. The clamping load P is then removed and a reduced load R

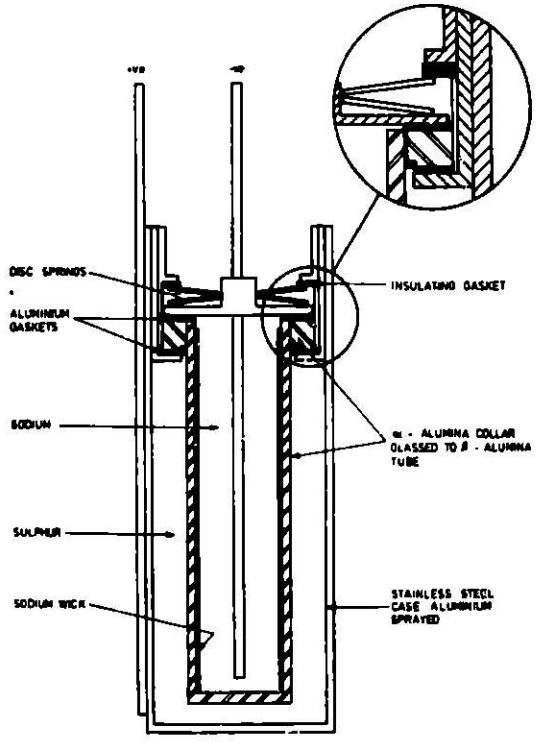

Fig.2 Sodium Sulphur Tube Cell With Disc Spring Seals Assembly

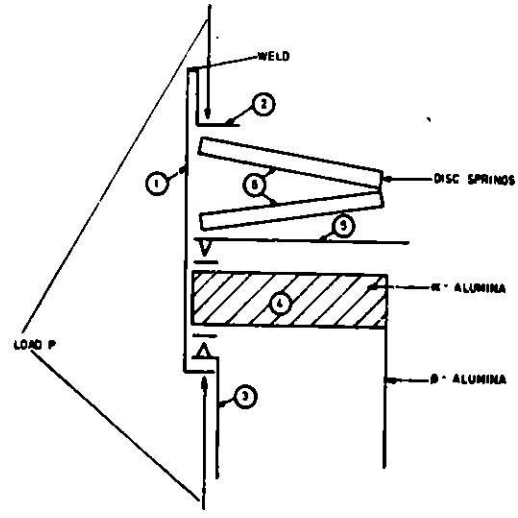

Fig.3 Arrangement Of Typical Sealing Assembly

is "locked up" in the components.

The extension of the outer components = recovery of the inner components

$$Rfo = (P - R)fi$$

$$\therefore \quad R = \frac{P}{1 + \frac{fo}{fi}}$$

On heating up to the operating temperature of 350°C the load R is further reduced due to the different thermal expansion of the components and due to a reduction in Youngs modulus of the various components. This reduced load R^{350} is given by:-

$$R^{350} = \frac{Pfi - L\alpha}{fo^{350} + fi^{350}}$$

where fo^{350} and fi^{350} are the flexibility of the outer and inner components at 350°C and $L\alpha$ is the relative dimensional change between the outer clamping collar 1 and the other components on heating to 350°C.

The various flexibilities, residual loads and maximum stresses for cell clamping arrangements are shown in Table 1.

Type of Clamping Assembly	T/10 (As Fig.3)	Modified T/10 (As Fig.3)	Production Design
Dimensions (mm)			
Outer collar diameter	50	50	44.71
Outer collar thickness	0.5	0.76	0.71
Inner collar thickness	0.5	0.5	1.01
Disc Spring			
Outer diameter	45	45	40
Inner diameter	22.4	22.4	20.4
Thickness	2.5	2.5	2.5
Height	1.0	1.0	0.95
Flexibilities ($mm/N \times 10^6$)			
Outer collar	47.3	26.3	7.1
Inner collar	10.7	10.7	6.7
2 disc springs	182.0	182.0	144.0
Load Loss (1962 N applied)	24%	17%	9%
Maximum Stresses (N/mm^2)			
Outer collar	530.0	320.0	140.0
Inner collar	276.0	276.0	165.0
Disc springs	270.0	270.0	276.0

Table 1. Stress Analysis Results

Sulphur Compartment Gasket	Approx. Stress On Gasket After Assembly (MNm^{-2})	No.Of Thermal Cycles	Seals Immersion	No.Of Electrical Cycles	Time On Test (h)	% Sulphur Weight Loss
Aluminium	30	4	No	-	3300	0.0*
Aluminium	30	1	No	-	1650	0.0*
Aluminium	30	1	No	-	1650	0.0*
Grafoil	15	-	No	-	1100	5
Grafoil	15	-	No	-	1000	6
Sigraflex	15	-	No	-	1000	6.5
Sigraflex	30	-	No	-	600	12.6
Sigraflex	15	-	Yes	-	1000	4.6
Aluminium	30	1	Yes	-	600	0.0
Aluminium	30	1	No	134	1730	0.0
Aluminium	30	-	Yes	69	720	0.0
Grafoil	12.5	2	No	229	3336	26

Table 2. Sulphur Weight Loss Results

* test still continuing

Experimental Results

Load loss measurements. Confirmation of the stress analysis results was obtained experimentally by two methods:

(i) by directly measuring the deflection of the pre-calibrated disc springs after assembly.

(ii) by strain gauging the outer clamping collar.

The T/10 (as Figure 3) assembly gave a load loss of approximately 26% and 20% by each method; this compares favourably with the stress analysis figure of 24%.

Sulphur weight loss results. It was preferred to test the seals at the operating temperature of 350°C in cells containing the reactants. This was done simply by weight loss methods. Cells were either charge/discharge cycled and weighed after test or put on long term "seals" tests where cells were partially filled with sulphur and the remaining gas space fixed to give approximately 500 KPa at 350°C which corresponds to the maximum gas pressure and maximum sulphur vapour pressure expected under normal operating conditions.

The results of these tests are given in Table 2.

As can be seen, tests are still continuing with no weight loss after several thousand hours.

Helium leak test. A production type cell design using a disc spring seals assembly was recently leak tested at 350°C using a Veeco MS17 helium leak detector. The seals were helium leak tight ($< 5 \times 10^{-10}$ litre torr sec^{-1}).

PRODUCTION AND COSTING

The commercial success of the sodium/sulphur battery depends on certain cell performance and cost targets being met. The seals assemblies in present cell designs can influence the energy density, volumetric energy density and cost quite markedly.

The early designs were made in small numbers from machined components and no real attempt to optimise for cost and weight was made. The seals assembly cannot be reduced in weight without sacrificing long term seals performance due to creep of lightened overstressed components. The weight penalty of the seals assembly can be offset, however, by increasing the length of the cells. It is anticipated that by increasing the length of the ceramic electrolyte from the present size of 160 mm to 300 mm the seals assembly will contribute less than 10% of the total cell weight. We are now in a position where large numbers of cells are required. To reduce cost a cell design was devised, the components of which could be made by semi-automatic production methods such as rotary forming and pressing. This has resulted in a considerable reduction in cost, and cells of this design show very low loss of sealing load on assembly and heat up to 350°C (< 9%). It

is estimated that the total cost of this seal assembly will account for less than 5% of the total cost.

CONCLUSIONS

The concept of using disc springs and lightweight pressed seal assemblies appears to be very satisfactory. The system has the advantages of ease of assembly, low cost and safe pressure release on cell failure. Although long term tests greater than 4,000 hours have not yet been completed, creep resulting from the high temperature operation should be avoided by careful choice of materials and reduction of stress levels.

REFERENCES

1. M.D. Hames and A.R. Tilley "Safety Of Sodium/Sulphur Cells" a paper presented at the 24th I.S.E. Meeting, Marcoussis, Paris, May 1975

2. West German Patent Application No.P.2401636.2

3. L.G. Miles and I. Wynn Jones "Performance Of Beta Alumina Ceramic Electrolyte In Sodium/Sulphur Cells" Power Sources 3, Ed. D.H. Collins Oriel Press, 1972

4. A. Scholes "NEWPAC - A Program For Linear Elastic Structure Analysis By Finite Elements" Proceedings of Finite Element Symposium at S.R.C. Atlas Laboratory, Oxfordshire, March 1974

5. R.J.M. Dodd, Private Communications

ACKNOWLEDGEMENTS

The author would like to thank the British Railways Board and the Department of the Environment for permission to publish this paper, and he is very grateful to Dr. R. Piercy and Mr. A.E. Kitchen of British Railways and Mr. M. McNamee of Chloride Silent Power Ltd. for providing some of the data.

CURRENT STATUS OF THE ATOMICS INTERNATIONAL LITHIUM – IRON SULFIDE BATTERY DEVELOPMENT*

L. Heredy, L. McCoy and S. Sudar
Rockwell International
Atomics International Division
Canoga Park, California

ABSTRACT

A program for the development of lithium-iron sulfide batteries for electric utility load-leveling is being conducted at Atomics International. These batteries use a molten KCℓ-LiCℓ electrolyte and are operated at a temperature of 400°C or higher. A lithium-silicon alloy, Li_5Si, is used as the active material in the negative electrodes. Positive electrodes contain the iron sulfides FeS, FeS_2 or their mixture. Electrode development tasks are concerned with minimizing the cost of supporting structures and optimizing electrode performance. Porous ceramic separators based upon rigid structural materials are being developed. Rigid separators used in current experimental calls are either prepared by processes under development or are purchased. Cell development is being conducted through scale-up stages involving increasing electrode area and numbers of parallel connected electrodes to reach a 2.5 kwh modular cell. A status review of this effort is presented.

INTRODUCTION

High temperature lithium-iron sulfide batteries offer considerable promise for electric utility load-leveling and electric vehicle applications because of their inherent high energy density and potentially low cost. Development programs for these batteries are being conducted at Argonne National Laboratory (ANL)[1] and at the Atomics International (AI) Division of Rockwell International.[2] General Motors is also working on this system.[3] The AI program consists of a number of tasks directed to advances in component technology and cell design and construction. The program is jointly funded by Rockwell International, the Electric Power Research Institute (EPRI) and by ANL. To date, emphasis has been placed on the load-leveling application.

The basic AI cell design is illustrated by the conceptual design of a 2.5 kwh cell shown in Figure 1. Multiple, parallel-connected electrodes are contained within a rectangular case. Porous ceramic separators provide electrical insulation between adjacent electrodes while allowing ionic conduction through the molten KCℓ-LiCℓ eutectic salt electrolyte. This salt mixture melts at 352°C, which places the operating temperature of the cell at about 400°C. Positive electrodes may use either FeS_2 or FeS as the active material. The final selection will be made on the basis of complex considerations involving both economic and performance factors. Negative electrodes will use a lithium-silicon alloy as the active component in the fully

*Jointly funded by Rockwell International, Argonne National Laboratory and the Electric Power Research Institute.

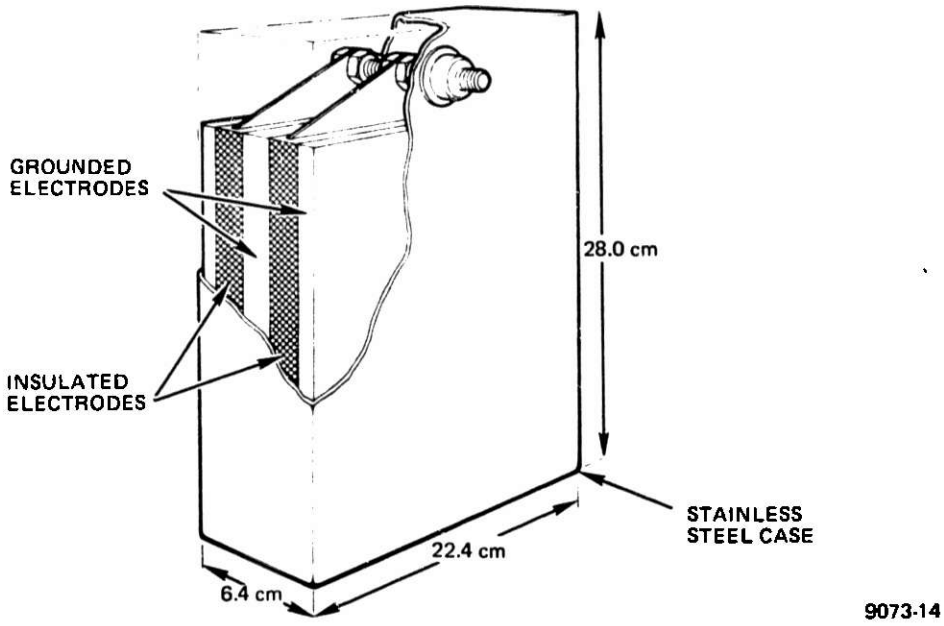

Figure 1. Conceptual Design of a 1 kwh Lithium – Iron Sulfide Cell

charged state. The cells will be hermetically sealed by welding and insulated feedthroughs will be required. A description of the current status of electrode, ceramic component, and cell development tasks is given below.

NEGATIVE ELECTRODES

Lithium electrodes may use either an alloy solid at the cell operating temperature, or liquid lithium retained in a porous metal supporting structure. The solid lithium-aluminum alloy has been used at ANL in their development program. Until last year, however, emphasis has been placed on the development of liquid lithium electrodes at AI in view of the 0.3-v advantage to the use of the liquid metal. To use this approach, means must be found to cause lithium to continually wet porous metals preferentially to the molten electrolyte saturated with Li_2S. Two additives, copper and zinc, serve this function well but, in practice, completely satisfactory electrodes of this type were not found. During charge, small quantities of dispersed lithium were formed, leading to electrode capacity loss and increased rates of self-discharge.[4]

Last year it was discovered at AI that solid alloys of lithium and silicon were electrochemically active and offered potential advantages over lithium-aluminum anodes, both in reduced voltage loss vs lithium and in greater capacity in terms of ampere-hours per gram of alloy. This development is described in detail in a separate paper. Lithium and silicon form a number of compounds with melting points around 600°C or higher. The more lithium-rich of these, Li_5Si, discharges through a series of potential plateaus ranging from 48 to 336 mv positive to liquid lithium at 400°C. The

average potential over the complete discharge is 230 mv. The theoretical capacity of Li_5Si is 2.12 amp-hr/g.

Effective utilization of these properties in practical electrodes requires the development of light weight, low cost supporting structures. A parametric study of the effect of structural variables, electrode thickness, and specific capacity loading on electrode performance with several candidate structures is being conducted.

Studies at present are confined to relatively thick electrodes suitable for low-power applications such as load-leveling. These are prepared by filling a porous steel or stainless steel structure with the molten alloy at 650 to 700°C, or by mechanically distributing the powdered solid alloy into the structure. The latter method is preferred. Superior performance is obtained with relatively large-pored supporting structures. Using a 6% dense support, structural-to-active weight ratios of ~1:1 have been reached. Specific capacities of 1.1 amp-hr/cm^3 are now being used. At a current density of 40 ma/cm^2, appropriate for load-leveling, 80% utilization of the theoretical capacity is obtained with 0.64 cm thick electrodes. This increases to 92% when thinner (0.26 cm) electrodes are used.

The voltage characteristics of Li_5Si electrodes are illustrated in Figure 2. These data were taken during the operation of a 150 w-hr cell described below. The discharge curve has been "folded back" under the charge curve for comparison purposes. The high degree of symmetry indicates excellent reversibility. These electrodes and others of similar type have now withstood hundreds of cycles over periods of thousands of hours without apparent physical deterioration.

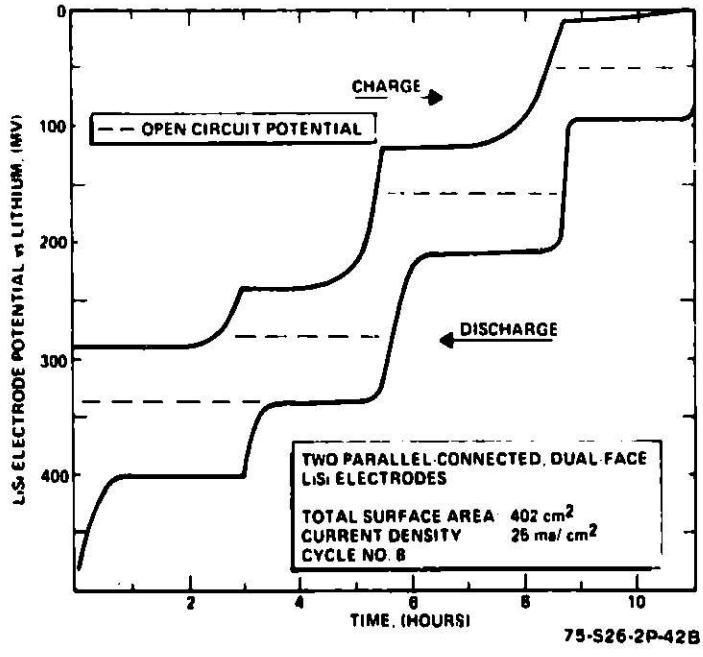

Figure 2. Potential Time Behavior of Lithium – Silicon Electrodes

The objectives of current research are to minimize the cost and weight of the supporting structure, to define the optimum loading as a function of electrode thickness, and to investigate alternate means of electrode preparation, both in the initially charged and uncharged states.

POSITIVE ELECTRODES

Two iron sulfide materials, FeS and FeS_2, are being investigated as active materials for the positive electrodes. A single voltage plateau at 1.65 v open-circuit vs lithium is obtained on discharge with FeS while FeS_2 discharges in two steps with a higher voltage of 2.05 v open-circuit for about half of the total capacity. When the average voltage is taken, FeS_2 provides an advantage of about 0.2 v over FeS. Higher energy densities and lower costs in stored energy should therefore be attainable with FeS_2 if this were the only basis for selection. However, as discussed below, materials problems are more severe with FeS_2 and FeS may be preferred on a cost basis despite the lower cell voltage. An equimolar mixture of FeS and FeS_2, $FeS_{1.5}$, has also been studied for possible advantage over the individual materials.

As in the case of the negative electrodes, a variety of supporting structures have been investigated. Graphite was used in all early work with FeS_2 and $FeS_{1.5}$ because of its outstanding resistance to chemical and electrochemical attack. Dense graphite was used as the current conductor/housing for the electrode while graphite or carbon felt was used for internal support and current collection. The powdered active material was vibrated into the felt to provide the specific capacity desired. Replacement of the dense graphite with molybdenum foil collectors has greatly reduced the weight and volume of these electrodes. Molybdenum is stable in contact with higher charge state iron sulfides and resists attack at the voltages required to charge these electrodes. Unfortunately, molybdenum is a relatively expensive metal and work is being done, both at ANL and AI, in an attempt to develop a less expensive substitute by coating steel with thin, corrosion-resistant coatings. Steel or stainless steel has been used as a current conductor/housing for an FeS electrode for almost 9000 hr. If relatively inexpensive steel can be used for this purpose, there may be an economic advantage to cells using FeS positive electrodes for load-leveling where energy density is less important than cost.

Early tests of iron sulfides were made with electrodes of about 5 cm^2 area, covered with porous Al_2O_3 plates and immersed in a molten electrode bath, together with liquid lithium or lithium-silicon electrodes. Tests were subsequently made with electrodes of 24-cm^2 area in test bed cells of the type shown in Figure 3. A number of these tests were run for extended periods of time. A summary of the results of longer term tests is given in the following table.

LONG TERM CYCLE TESTS OF IRON SULFIDE ELECTRODES

Temperature: 390 to 405°C
Electrode Area: A: ~5.0 cm^2
B: ~24.0 cm^2
Electrode Depth: 0.64 cm
Current Density: 35 to 40 ma/cm^2

Type	Active Material/ Conductive Material	Specific Capacity (amp-hr/ cm^3)	Active Utiliza- (%)*	Coulombic Efficienty (%)	Operating Life (Cycles)	Operating Life (hr)
A	FeS_2/Carbon Felt	0.6	75	96	86	2160
A	$FeS_{1.5}$/Carbon Felt	0.6	98	96	100	1970
A	FeS/Graphite Powder	0.6	100	98	456	8900
B	FeS_2/Carbon Felt	0.6	74	99	67	1080
B	$FeS_{1.5}$/Carbon Felt	0.9	60	99	172	3340
B	$FeS_{1.5}$/Graphite Felt	0.6	85	98	380	6600

*Utilization based on available sulfur

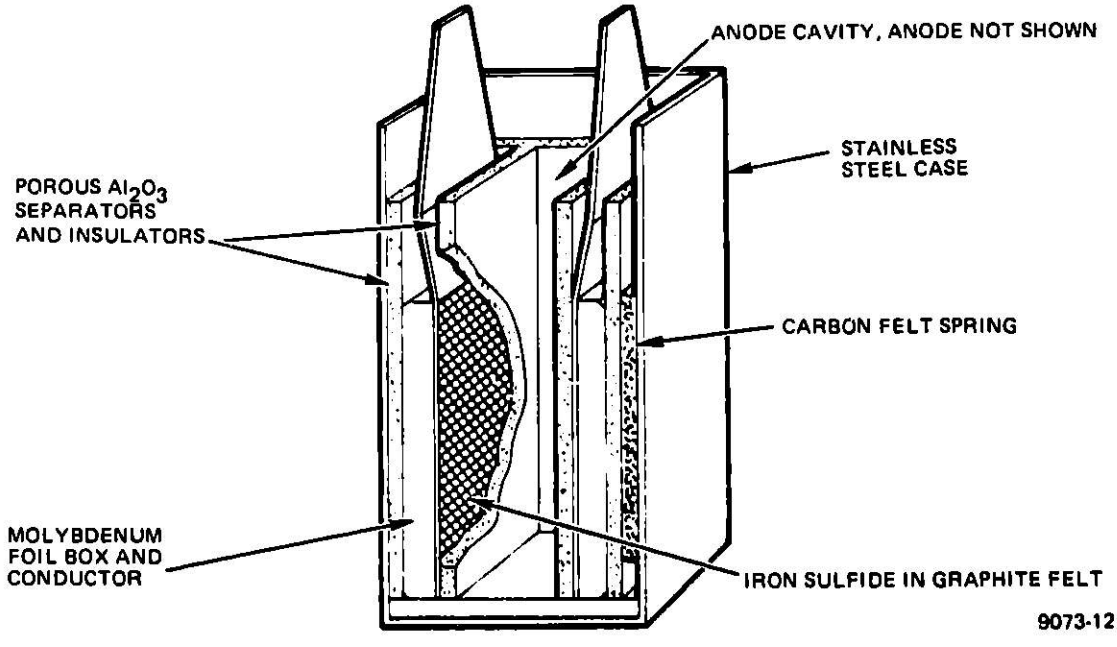

Figure 3. Test Bed Cell for 24 cm^2 Electrodes

The capacity utilization of the sulfur content of FeS_2 observed in these tests was almost uniformly around 75%. This provided the basis for tests of $FeS_{1.5}$ where the total sulfur content could be utilized experimentally. However, since $FeS_{1.5}$ yields a lower average cell voltage than FeS_2 and presents the same electrode materials problems, future tests will be made with FeS_2 alone. In a recent test, an FeS_2 electrode was operated at 500°C as well as at the more customary temperature of 400°C; the results are shown in Figure 4. A marked increase in utilization, approaching the theoretical limit, was obtained at the higher temperature.

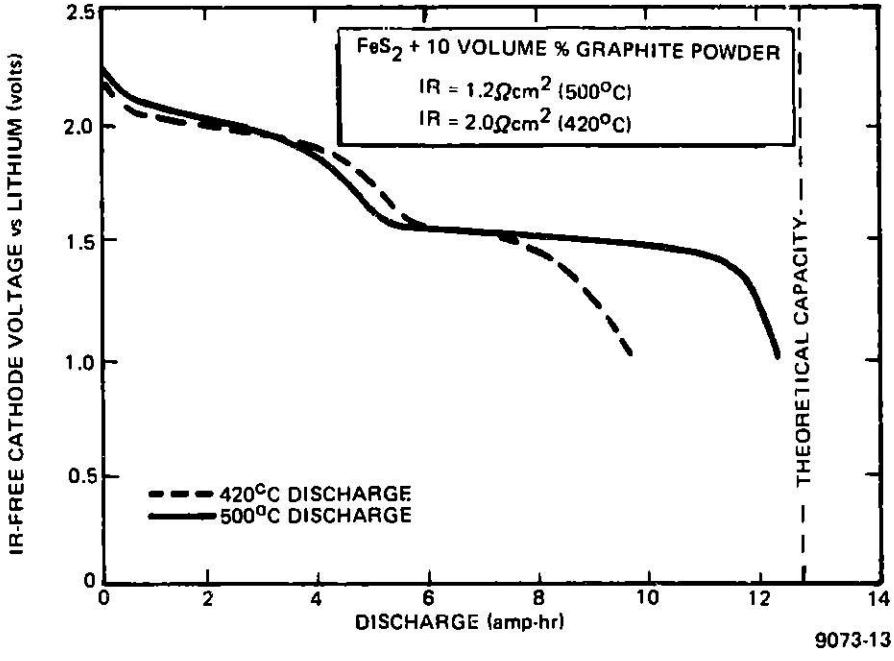

Figure 4. Discharge Capacity of FeS_2 Electrode at 420 and 500°C

In general, some difficulty has been experience in obtaining high capacity utilization with FeS in electrodes using graphite felt supports. A mixture of graphite powder with FeS has been found to increase utilization markedly as shown in the preceding table.

Emphasis in current work on positive electrodes is being placed on the use of FeS because containment in low cost steel structures appears feasible. A light weight, cellular structure has been found which resists deformation caused by swelling forces generated in the discharge of FeS. Scale-up of these electrodes to the area required for load-leveling cells will be conducted as rapidly as possible. This aspect of electrode development is described in the discussion of the cell construction task.

CERAMIC SEPARATORS

Ceramic materials for lithium-iron sulfide battery separators should be thermodynamically stable to lithium, insoluble in the electrolyte, free of harmful impurities, resist fracture by thermal shock, and be potentially low in cost. The separators may be rigid porous plates or flexible materials such as cloth, felt, or paper fabricated from ceramic fibers. Cloth made from BN fibers is now being used successfully by ANL in their lithium aluminum – iron sulfide cells. Flexible separators have mechanical advantages over rigid plates but few lithium-resistant materials are presently available in this form, and acceptably low cost remains to be demonstrated. Continued investigation of alternative materials and fabrication techniques will increase the probability of technical and economic success.

At this time, a large number of metal oxides and nitrides, prepared at AI or purchased from vendors, have been screened for their resistance to attack as determined by simultaneous exposure to liquid lithium and molten KCℓ-LiCℓ electrolyte at 420°C for 2-week periods. This test provides a more rigorous environment than might be expected by contact with solid lithium alloys where the activity of lithium is considerably lower but offers assurance that the separators will not be attacked in the event of accidental overcharge. Of the materials tested in this manner, Y_2O_2, Si_3N_4 and AℓN have been found to withstand this test without significant change in physical properties. BN cloth obtained from the Carborundum Company has shown variable resistance to attack. Poor initial results were due to insufficient removal of oxide impurities prior to test.

Techniques have been developed for preparing high purity metal oxides by chemical precipitation from aqueous solutions or by a gel process using organic acids in glycol. In the second instance, the gel is heated to decompose the organic materials. A major portion of this effort is now being placed on fabrication of porous ceramic plates of a sufficient size to permit assembly of cells with full-size electrodes ($\sim$500 cm^2 in area).

As a longer range effort, the preparation of ceramic fibers from a variety of metal oxides and nitrides will be investigated. These may be either pure ceramic materials or composite fibers utilizing a core of a different composition to provide greater strength and flexibility. Assistance in weaving these fibers into suitable separator cloth will be obtained from experts at the Rockwell Textile Machinery Division.

CELL DEVELOPMENT

The basic cell building block for utility load-leveling plants is presently based upon a unit capacity of 2.5 kwh. Electrodes 9 in. by 9 in. (522 cm^2 in area) should approximate the final size required for this application. To reach this point, it will be necessary to scale electrodes and ceramic components from the area of $\sim$25 cm^2 used in test beds to these dimensions. This will be done in a series of steps involving scale-up both in area and in the number of electrode pairs contained within a single cell casing. The former is the more difficult step. To achieve the energy density and cost goals for the load-leveling application, it will be essential that the cell configuration

be highly compact, with electrodes and separators in direct contact to minimize electrolyte weight. Cells constructed prior to this date have provided free electrolyte between the negative electrode and the ceramic separators. This design has been required by the poor resistance of Al_2O_3 separators to attack by lithium. These separators have been used because of their ready availability. Despite the low energy densities attainable in these past cell designs (~12 w-hr/lb) they have served a valuable function by demonstrating the inherent long life of iron-sulfide and lithium-silicon electrodes. As more suitable ceramic separators have become available, compact cell configurations have been designed. The performance of cells constructed in accordance with these considerations is described in the following text.

Free Electrolyte Cells

A number of these cells have been built and operated, with electrode areas ranging from 25 to 130 cm^2. The largest of these, a 150 w-hr cell constructed under ANL support, contains four electrode pairs, with positive electrodes having an area of 130 cm^2 and negative electrodes with an area of 100 cm^2. The general design of this cell is shown in Figure 5. After a brief period of operation in an inert atmosphere, this cell was closed by welding. A photograph of the internal structure of the cell is shown in Figure 6.

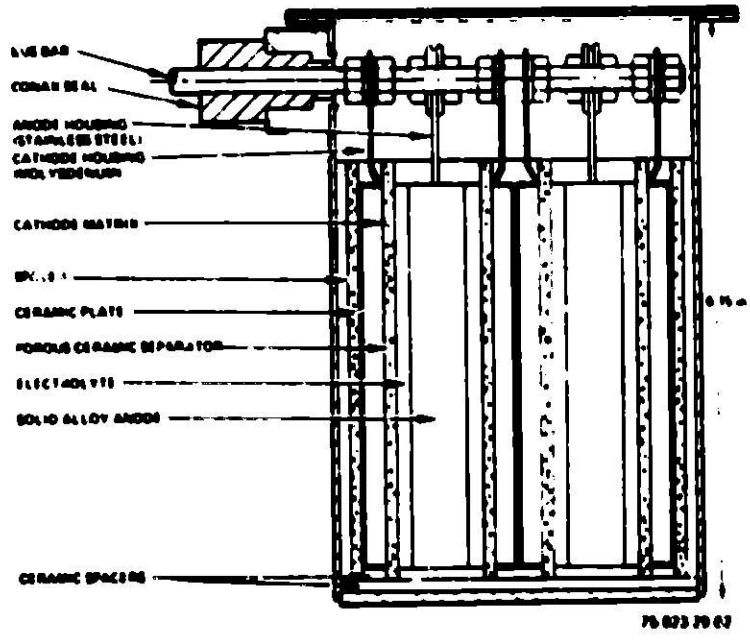

Figure 5. 150 watt-hour Cell, Side Sectional View

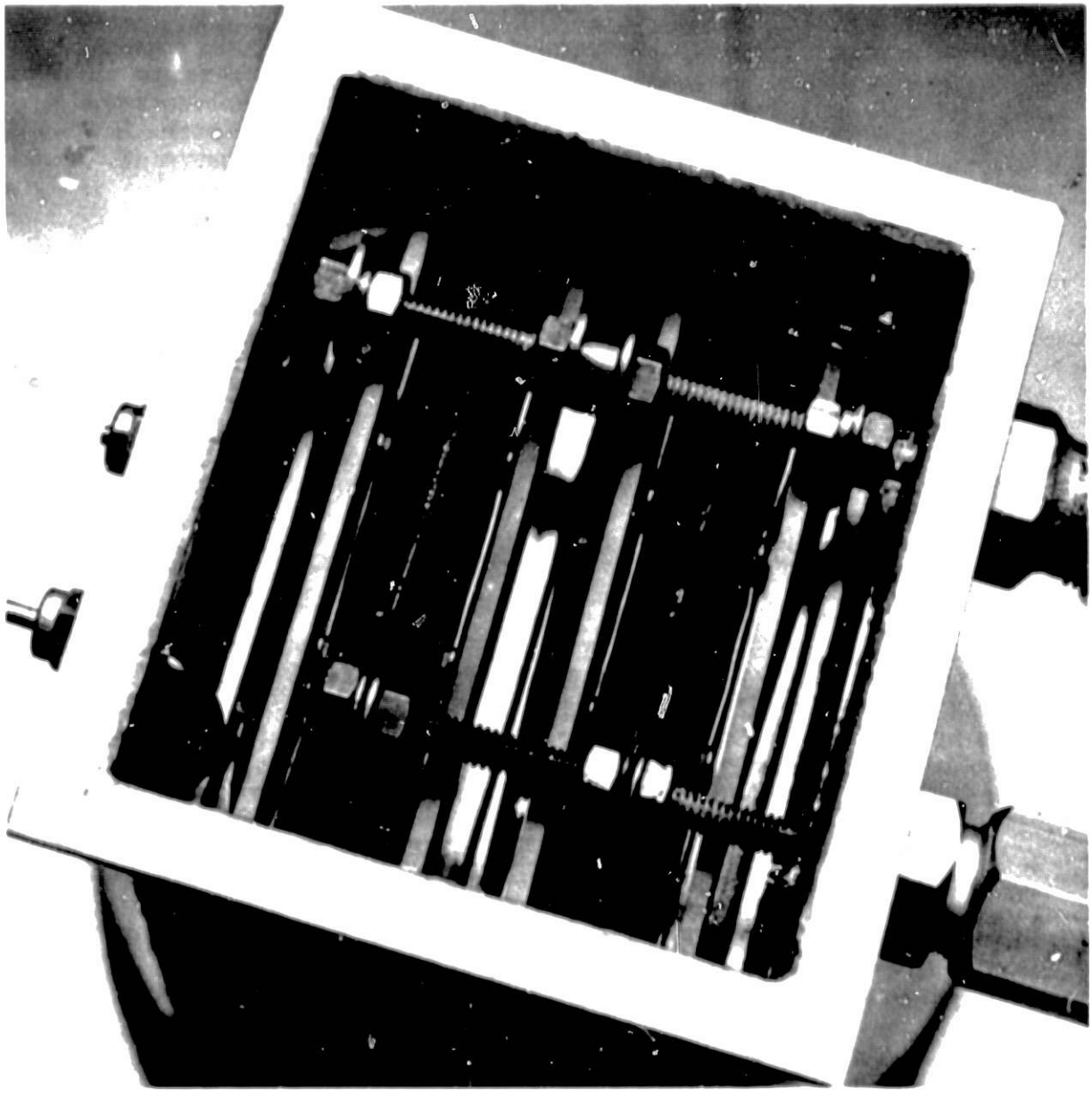

9073-8

Figure 6. Internal View of 150-w-hr Cell

The cell was characterized by operation over a range of charge and discharge rates. The results of these tests are shown in Figure 7, where the voltage behavior of the cell at various charge-discharge rates are shown together with energy efficiencies calculated for various combinations of these rates. For the mode of operation believed most pertinent to load-leveling service, a C/5 charge rate and a C/10 discharge rate, an energy efficiency of 76%, was recorded. This cell has been operated for 5540 hr and has completed 595 cycles, most of these under the 5-hr rate in both modes. The coulombic efficiency has remained high, between 98 and 100%.

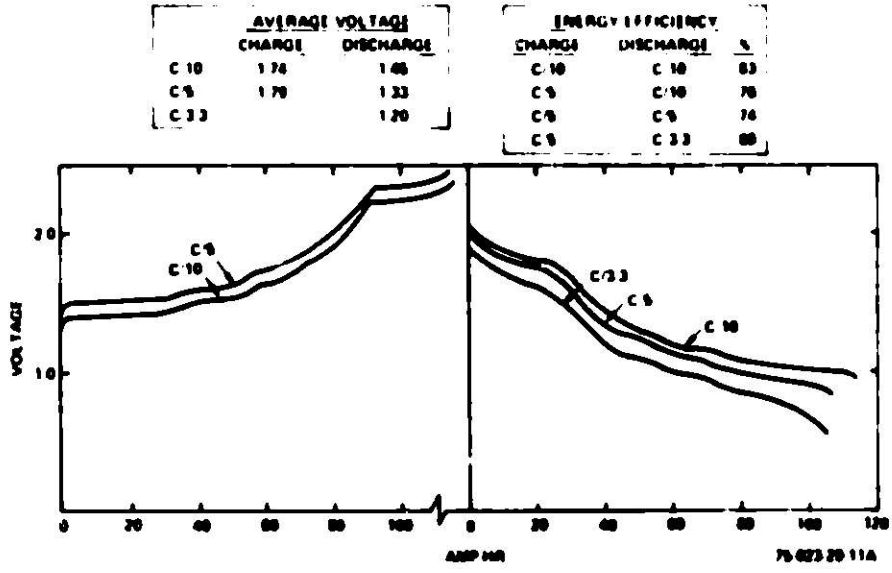

Figure 7. Performance of 150 w-hr Cell

Some small decrease in energy efficiency has occurred, as shown in Figure 8. As the cell capacity is limited by the negative electrodes, the charges shown are probably ascribable to the functioning of the lithium-silicon electrodes. The charges detected to date are, however, modest.

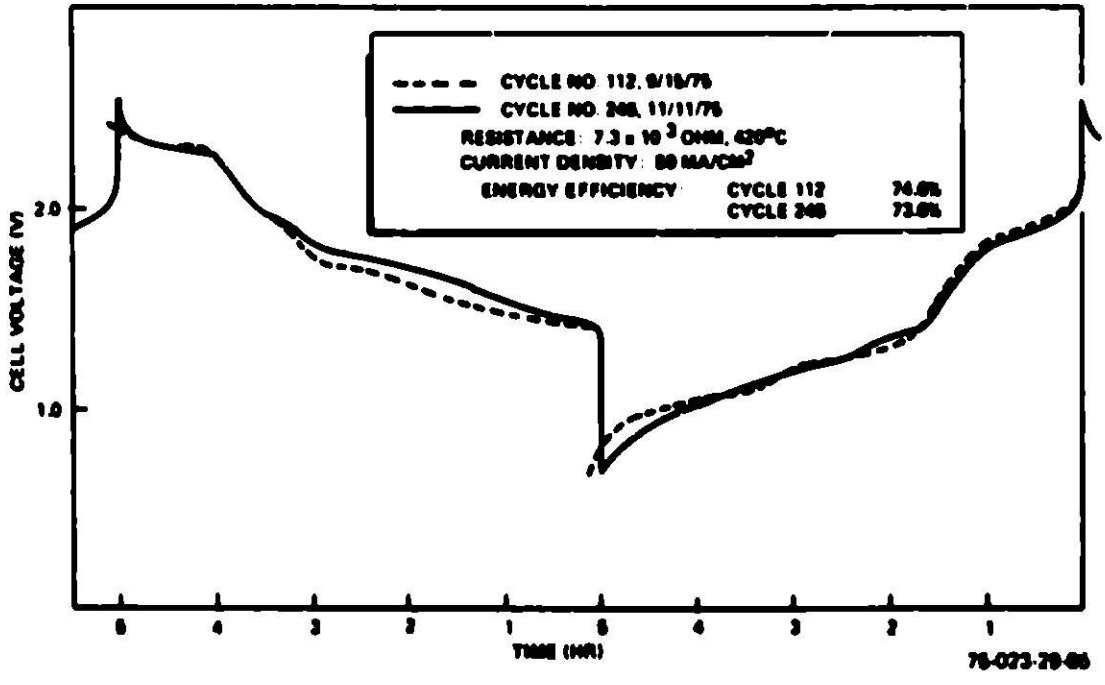

Figure 8. Performance – Time Behavior of 150 w-hr Cell at C/5 Rate

Compact Cells

Operation of compact cells with minimal electrolyte weight presents problems not associated with the type of cell described in the preceding text. A major consideration in this case is the possibility of shorting between electrodes across the narrow space occupied by the ceramic separator. This cell design requires effective containment of active materials in both electrodes and good physical integrity of the separator used in such cells. Scale-up will proceed from bicells with electrode areas of 130 cm^2 to those with electrode areas of 522 cm^2.

Smaller bicells with electrode areas of 25 cm^2 were built initially to "pilot" this effort and to establish compatibility of the ceramic separator with the positive and negative electrodes. A number of these have been built to date using FeS positive electrodes and lithium silicon negative electrodes. The first cells of this type were built using BN cloth as the separator in one instance and porous Si_3N_4 plates for this purpose in the other. In both tests, shorting was experienced when the potential of the lithium silicon electrodes approached the 50 mv plateau during charge. The shorting was transient and the cells were operated successfully thereafter at restricted states of charge. This problem now appears to have been solved by the use of composite separator materials.

Scale-up progress on construction of Li_5Si-FeS_2 cells will lag that scheduled for those containing FeS electrodes because it is possible to contain the FeS in economically practical ferrous structures. Porous Si_3N_4 shells will be used to retain the active positive material, and molybdenum current collectors will be used in FeS_2 cells. Significant lead times will be required in the design and purchase of the larger ceramic components.

The construction of compact cells of this type will provide a close approach to the design of actual load-leveling cells. An energy density in excess of 85 w-hr/kg is expected with the Li_5Si-FeS bicells. Following the design, construction, and test of these large bicells with FeS and FeS_2 electrodes, a selection of one type of these positive electrodes will be made. Larger 1.0 and 2.5 kwh cells will then be designed on the basis of that selection.

DESIGN STUDIES

As advances in component technology are made and as cell designs are refined to approach the end product, it is necessary to continually re-examine cost and energy density estimates for these batteries. This is a difficult task in a period of rapid development, but it provides an essential service by pinpointing areas where more intensive investigation is required if performance and economic goals are to be met. Recent studies based on a 1 kwh Li_5Si-Fes_2 cell using rigid silicon nitride separators and assuming specific capacities of 0.6 amp-hr/cm^3 for both negative and positive electrodes, showed that an energy density of 120 w-hr/kg is a reasonable expectation. The two factors having the greatest impact on energy density are the specific capacity loading of the electrodes and the composition and form of ceramic separator used. An increase in specific capacity beyond the 0.6 amp-hr/cm^3 used in the baseline calculation for electrodes, a value now

exceeded in both instances, would have the greatest impact. Attainment of capacities of 0.8 and 1.0 amp-hr/cm^3 for the cathode and anode, respectively, would increase the energy density to 165 w-hr/kg. Substitution of thinner flexible separators, such as BN paper, for the rigid silicon nitride plates could provide a further 15% increase in that value.

Preparation of meaningful cost estimates is a much more complex task as manufacturing and assembly costs must be determined as well as materials costs. This effort has been started but some time will be required before sufficient information is assembled to provide a basis for estimation. However, several items known to have a major impact on battery costs have been identified and steps are being taken to purchase or develop lower cost replacements. Molybdenum current leads and housings for FeS_2 positive electrodes provide one example. A task has been initiated at AI to develop less expensive substitutes. The composition and form of the ceramic separator can have a major impact on costs and this is the subject of an AI program task. In these, as well as in other areas such as feedthroughs, AI will also utilize technology developed at ANL.

SUMMARY AND PLANS

Progress has been made in developing light weight, ferrous metal supporting structures for FeS positive and lithium-silicon negative electrodes. These supporting structures are not suitable for FeS_2 electrodes, and work has been started to develop methods of applying corrosion-resistant coatings to inexpensive substrate metals to supplement similar work at ANL. Molybdenum current-conductor/housings are now being used with FeS_2. Performance characterization tests of negative and positive electrodes are being made using electrodes, 24 cm^2 in area.

Si_3N_4, Y_2O_3, and AlN have been found suitable for making porous ceramic separators resistant to attack by molten lithium and KCl-LiCl electrolyte at 420°C. These are being purchased or fabricated in the form of rigid porous plates. An in-house capability for production of such plates in sizes required for full-size cells will be established. The possibility of obtaining or producing these materials in fibrous forms for use in flexible separators will be explored.

Scale-up of FeS-Li_5Si cells will be accomplished by the construction of compact bicells with individual electrode areas of 130 and 520 cm^2. This will be followed by design, construction and test of 1 kwh multi-electrode cells. The same procedure will be followed for Li_5Si-FeS_2 cells. One of these systems will be selected for the 2.5 kwh load-leveling modular cell to be built and tested in the middle part of 1977.

REFERENCES

1. W. Schertz, A. Chilenskas, and V. Kolba, "Battery Design and Cell Testing for Electric-Vehicle Propulsion," Record of the Tenth Intersociety Energy Conversion Engineering Conference, Newark, Delaware, August 18-22, 1975, p 634

2. S. Sudar, L. McCoy, and L. Heredy, "Rechargeable Lithium/Iron Sulfide Battery," Record of the Tenth Intersociety Energy Conversion Engineering Conference, Newark, Delaware, August 18-22, 1975, p 642

3. R. Sharma, "Equilibrium Phases Between Lithium Sulfide and Iron Sulfides," Extended Abstracts, Electrochemical Society, Dallas Texas, October 5-10, 1975, p 67

4. L. McCoy, S. Lai, R. Saunders and L. Heredy, "Secondary Lithium Metal Sulfide Battery," 26th Annual Proceedings Power Sources Conference, Atlantic City, New Jersey, May 1974, p 68

HIGH TEMPERATURE RECHARGEABLE CELLS WITH DOPED CaF_2 AS A SOLID ELECTROLYTE

by

W. Baukal, W. Kuhn,
Battelle-Institut E.V., Frankfurt/Main and

E. Voss,
Forschungs- und Entwicklungszentrum der VARTA Batterie AG,
Kelkheim/Taunus, Germany

ABSTRACT

Doped calcium fluoride is applied as a solid electrolyte for high temperature secondary cells using calcium and copper fluoride as electrode materials. The cell reaction is given by the equation: $Ca + CuF_2 \rightleftharpoons CaF_2 + Cu$, the cell voltage is measured to be 3.37 V at 450° C which is in good agreement with the value of 3.39 V calculated from thermodynamic data. Results obtained on cycling experiments are reported.

INTRODUCTION

Different types of galvanic cells with solid electrolytes are increasingly finding interest in research and development work (1). A well-known example of a rechargeable cell is the $Na/\beta Al_2O_3/S$ system. It operates at 300 - 350° C and offers considerable promise for a battery of high power and high energy density. At the operational temperature both the electrode materials Na and S are in the liquid state.

Recently a new series of all-solid secondary cells has been proposed using doped CaF_2 as a solid electrolyte and Ca or Mg as negative, NiF_2, CuF_2, FeF_3 or other fluorides as positive electrode materials (2). As may be seen from table 1, cells of this type compete quite favourably in theoretical energy density with cells based on the βAl_2O_3 electrolyte.

The application of solid components only offers advantages as well as difficulties. Certainly, the problem of corrosion of grid and cell vessel material will not be as serious as in case of using corrosive liquids at high temperatures. On the other hand, however, cycling of all-solid cells may lead to void formation and other defects of the electrode/electrolyte structure which may easily be rearranged when liquids are used. But before going into further details, it will be of greater interest to investigate the fundamental properties of

the proposed CaF_2 cells. In this paper results obtained on the cell $Ca/CaF_2/CuF_2$ will be reported.

Table 1

Theoretical energy densities of high temperature secondary cells

system	reaction	temp. of op. °C	o.c.voltage V	energy density Wh/kg
$Na/\beta Al_2O_3/S$	$2Na+3S \rightleftharpoons Na_2S_3$	300	1,75	660
$Ca/CaF_2/CuF_2$	$Ca+CuF_2 \rightleftharpoons CaF_2+Cu$	450	3,41	1290
$Ca/CaF_2/NiF_2$	$Ca+NiF_2 \rightleftharpoons CaF_2+Ni$	450	2,72	1070
$Mg/CaF_2/CuF_2$	$Mg+CuF_2 \rightleftharpoons MgF_2+Cu$	450	2,82	1200

EXPERIMENTAL PART

Materials

Pellets of the composition $(CaF_2)_{0,995}(NaF)_{0,005}$ were prepared from the individual fluorides by ball-milling, pressing and sintering at 800 to 1000 °C. The pellets were about 2 mm thick and had a diameter of 11 - 12 mm. Their surface was smooth, so that they could be used as cell electrolyte without further treatment. Some pellets were ground again, and the powder was used as auxiliary electrolyte in the electrode mixtures.

These mixtures were prepared by grinding the appropriate materials together in a mortar which was placed in a glove box filled with dry nitrogen. The Ca had been filed in the same atmosphere. Table 2 presents the ratio of the materials. After grinding, the size of the Ca grains was 20 to 50 µm, the medium grain size of all other substances was less than 5 µm (microscopic inspection).

Table 2

Composition of electrode mixtures (vol. %)

	neg. electrode	pos. electrode
metal	65	45
fluoride	-	20
electrolyte (CaF_2)	35	35

Cells

For assembling an experimental cell, both sides of an electrolyte pellet were brought into contact with three construction elements in the following order: a powder layer of electrode mixture, about 200 µm thick; a so-called contacting pellet, 600 - 800 µm thick, pressed from the same electrode mixture, and a copper foil (cf fig. 1). The pellet stack was clamped together under slight spring pressure, placed into a quartz tube under streaming purified argon, and heated up to the operating temperature of 450° C. After a few hours a stable open circuit voltage and impedance could be observed.

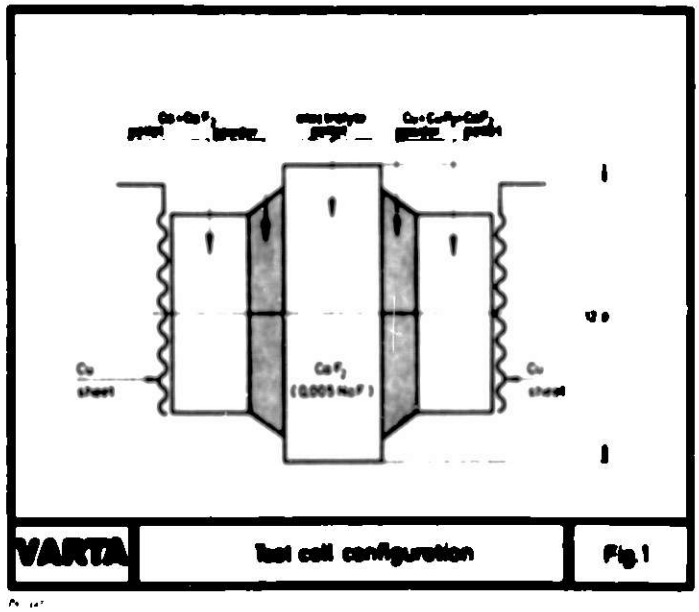

Measurements

Charge and discharge experiments were carried out under galvanostatic conditions. The open circuit voltage and the a.c. impedance at 100 kHz were measured during short intervals on open circuit. In the range of 1 to 200 kHz the ohmic part of the impedance, R_{ac}, was essentially frequency-independent and the imaginary part was negligibly small. The voltage-current densitiy characteristic was determined in the charged and discharged state of the cells. This was accomplished by quick measurements in order to maintain the actual state of charge of the cell. After the cycle experiments the cells were taken from the furnace, quickly embedded in resin, sectioned and polished under nonaqueous conditions. The cross-section was investigated by light microscopy, the SEM and microprobe analysis.

RESULTS

Electrolyte conductivity

The results of conductivity measurements on polycrystalline sintered $(CaF_2)_{0.995}(NaF)_{0.005}$ are given in fig. 2. For comparison conductivity data of monocrystals of various composition (3), (4) are also presented.

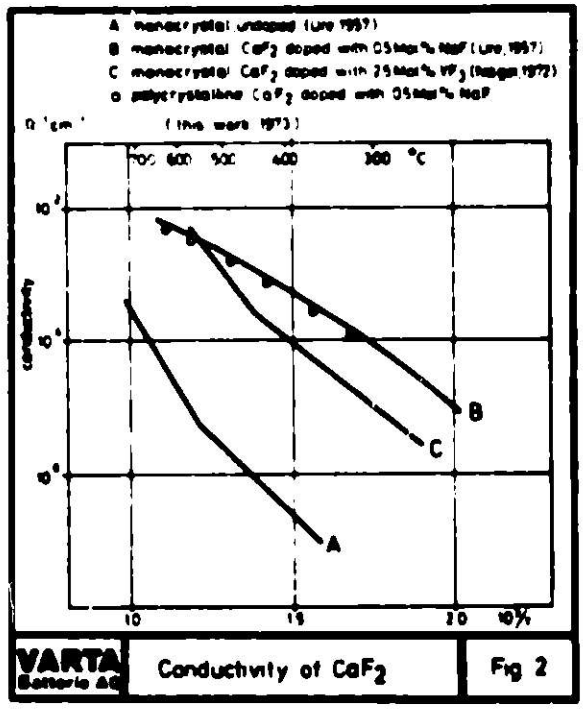

Open circuit voltage of the system $Ca/CaF_2/CuF_2$

The open circuit voltage and its constancy over a long period is an important indication for the feasibility of a cell. On heating a cell $Ca/CaF_2/CuF_2$ within a few hours up to 550° C ther maintaining a temperature of 450° C, a constant open circuit voltage of 3.37 V was observed which compares quite well with 3.39 V calculated from thermodynamic data. As will be shown later, the open circuit voltage of ca. 3.4 V was also reattained after cycling.

Current voltage relationship

Current voltage characteristics are shown in fig. 3. From the slope of the essential linear curve a, obtained on the new $Ca/CaF_2/CuF_2$ cell, an internal cell resistance of R_{ic} = 0.44 kΩ can be calculated. After 5 cycles the internal

resistance of the charged cell had increased to R_{dc} = 0.7 kΩ (curve b). An even higher increase of the cell resistance was observed in the discharged state as will be shown later. Curve c has been calculated from the electrolyte resistance, R_{el}, and the cell dimensions.

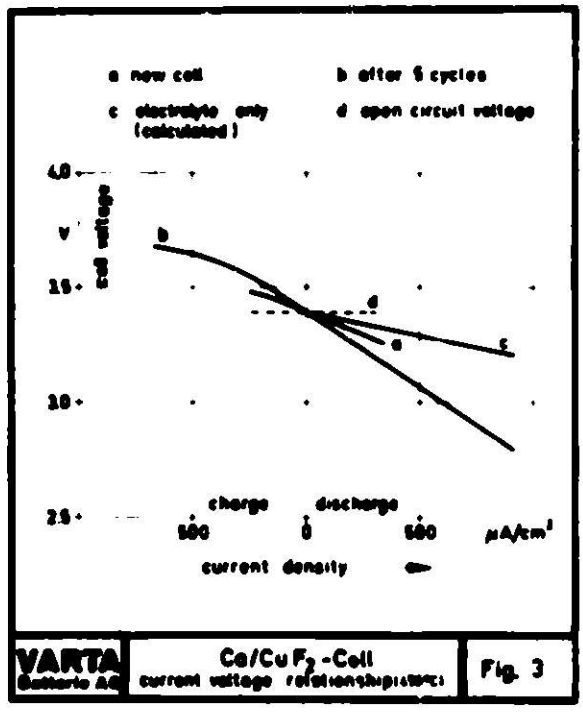

Charge and discharge behaviour

The voltage time relationship during one discharge/charge cycle at a current density of 150 $\mu A/cm^2$ is given in fig. 4. After discharge the open circuit voltage of the cell was readily reattained. On applying the charge current a high voltage peak was observed which decreased quickly to a steady state value of about 3.45 V. At the end of charge some instead iness occurred.

Cycling

During cycling at a rate of 150 $\mu A/cm^2$ the open circuit voltage, the impedance in the charged as well as in the discharged state, and the cell capacity are determined as a function of the number of cycles. The results are given in fig. 5. As can be seen up to about 15 cycles the cell behaviour is quite normal. After that point, however, a more or less abrupt change took place indicated by a decrease of the open circuit voltage and the capacity as well.

Simultaneously the impedance increased steadily, especially when measured on the discharged cell.

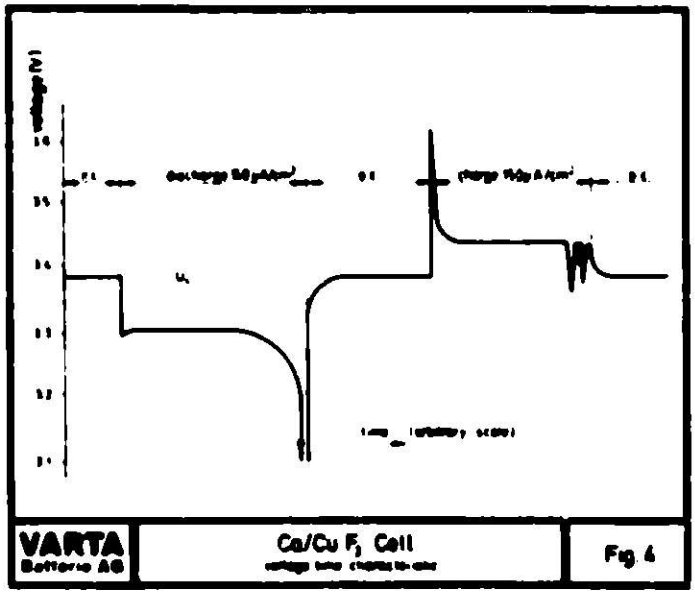

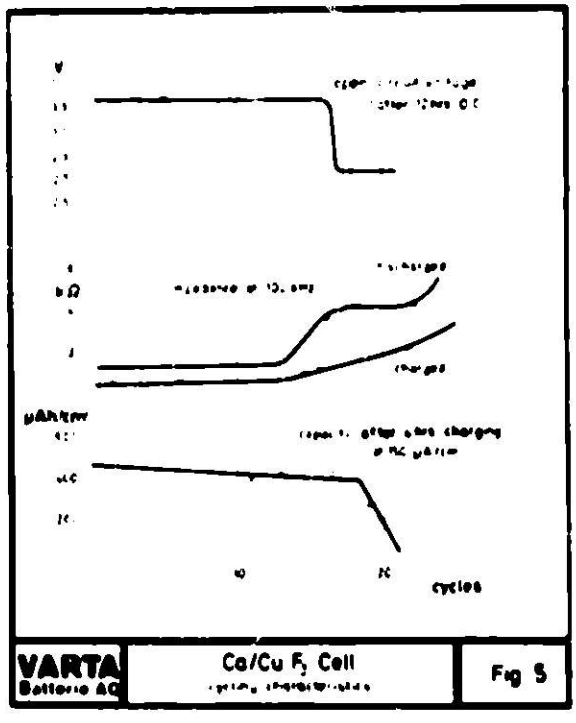

DISCUSSION

Conductivity

Fig. 2 shows that polycrystalline specimens of $(CaF_2)_{0.995}(NaF)_{0.005}$ prepared according to conventional ceramic techniques exhibit a conductivity equal to that of a single crystal of the same composition (3). Since this agreement is valid for a fairly large temperature range, it seems obvious that grain boundary conduction is negligible in these specimens. So there is no necessity to prepare monocrystals for the galvanic cells.

Open circuit voltage

As already mentioned the OCV of Ca/CuF_2 cells is in good agreement with the theoretical value of 3.39 V at 450° C. Calculations using tabulated thermodynamical data (5) produce a value of 3.41 V but a small electronic contribution to the overall conductivity (6) has to be taken into account. The ionic transference number in $(CaF_2)_{0.995}(NaF)_{0.005}$ equilibrated with metallic Ca was therefore determined. The results, reported elsewhere in full detail (7), lead to a correction of about 20 mV for a Ca-anode.

The small electronic partial conductivity does not seem to influence the performance of the experimental cells, as it should be restricted to a thin layer in the electrolyte close to the Ca-metal containing electrode. During prolonged open circuit periods of a battery, however, the electronic contribution to the conductivity could lead to self-discharge. This could be prevented by reducing the temperature during these periods. In equilibrium with Mg/MgF_2, the electronic partial conductivity in doped CaF_2 is negligible.

Self-discharge

As long as the experimental cells were in good condition, no evidence of self-discharge could be detected. The OCV was equal to its theoretical value even after a deep discharge and remained stable thereafter for an extended period of time. After one of the cells had suddenly degraded in the 15th cycle (see fig. 5) it behaved as if self-discharge was occurring. Since other cell characteristics changed at the same time, it is suggested that this self-discharge is not a primary mechanism and no intrinsic property of the system.

Cell resistance

Three resistance values, R_{el}, R_{ac} and R_{dc}, as explained earlier can be compared. R_{ac} comprises the electrolyte

resistance, contact resistances, and resistance contributions of the electrode layers and the contacting pellets. R_{dc} reflects electrode polarization effects in addition to all R_{ac}-contributions. R_{ac} and R_{dc} differed from each other and, in a characteristic way, also according to whether the cell was charged or discharged (table 3).

Table 3

Distribution of the internal resistance of a Ca/CuF_2 cell at different states of charge at 450° C (values in $k\Omega \cdot cm^2$)

	charged	discharged
electrolyte resistance, R_{el}	0.22	0.22
electrode resistance, $R_{ac} - R_{el}$	0.18	1.38
electrode polarisation, $R_{dc} - R_{ac}$	0.04	0.40
total DC resistance, R_{dc}	0.44	2.00

There also was a slight drift of both resistances towards higher values during repeated cycles. The change of R_{ac} in the course of two immediately subsequent cycles is presented in fig. 6. During discharge the R_{ac}-value of the experimental cell increased at a rather early state when only 0.2 to 0.3 mAh/cm^2 had been applied (total discharge 0.6 mAh/cm^2). On recharge, however, the impedance decreased rapidly to the original value. It should be noted that the curve was smooth; mechanical effects which one might expect as a consequence of the difference between the equivalent volumes of metal and its corresponding fluoride would result in a scattered pattern. The increase of R_{ac} upon discharge rather seems to be due to gradual changes primarily in the negative electrode: (i) a decrease in the conducting cross-section and/or (ii) a build-up of low-conductivity reaction products which interrupt the high-conductivity conduction paths. According to topochemical considerations (8) undoped CaF_2 with low conductivity is formed at the reaction sites. The F^- ions must diffuse through all layers previously formed (fig. 7). When the cell at first is subjected to a charging procedure, Ca and, for potential reasons, metallic Na is formed from the doped CaF_2. The low concentration of Na and the high temperature suggest that, at least partly, an alloy will be formed which on discharging would convert directly back to the doped high-conductivity CaF_2.

The higher values of $(R_{dc} - R_{ac})$ upon discharge (see table 3)

indicate increasing polarization effects. This shows that in addition to the topochemical considerations the charge transfer process has also to be taken into account.

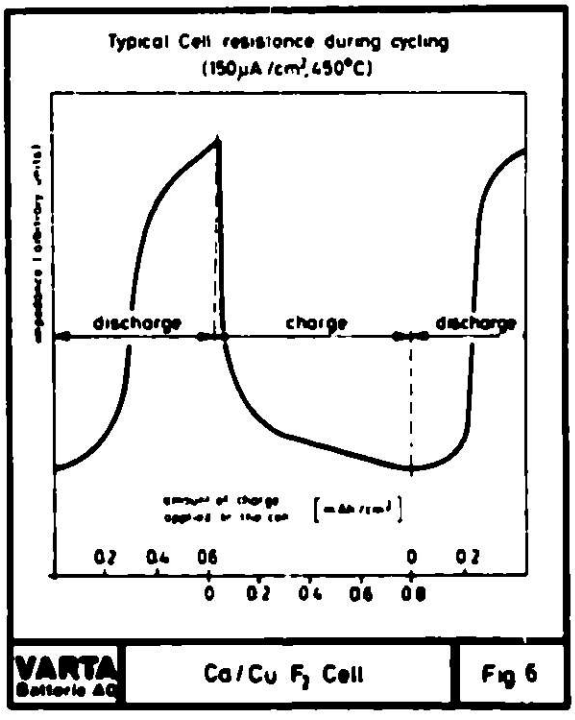

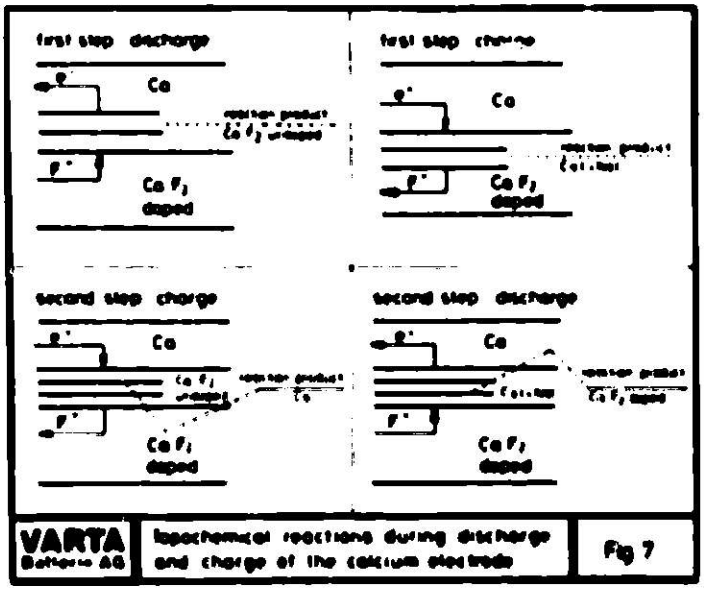

Cell capacity

A theoretical capacity in the usual sense is not well-defined because of the chosen configuration of the experimental cells (powder layers and contacting pellets of the same composition). The practical discharge capacity was given by a relatively sharp decrease in the voltage. The practical charge capacity, however, was defined arbitrarily; it was decided to terminate each charging process at the beginning of an instability of the voltage (see fig. 4).

An upper limit of the thickness of the reaction layers can be calculated assuming a model in which the electrolyte pellet is contacted by pure nonporous Ca and CuF_2. A discharge capacity of 400 $\mu Ah/cm^2$ would convert 1.9 μm Ca to 1.8 μm CaF_2 and 1.8 μm CuF_2 to 0.5 μm Cu. Microprobe examination of the electrodes revealed, however, that the reaction penetrated a few hundreds of microns deep into the contacting pellets.

The instability of the charging voltage (fig. 4) can possibly be ascribed to the relatively great difference between the equivalent volumes of Cu and CuF_2.

The sudden change of all cell characteristics in the 15th cycle (fig. 5) seems to be due to a mechanical degradation of the experimental cell. Microscopic inspection showed a relatively wide slot between the electrolyte and the positive electrode. This effect is expected to be an accidential rather than an intrinsic failure mode.

CONCLUSION

The results obtained so far demonstrate the feasibility of using doped CaF_2 as an electrolyte in all-solid secondary high-temperature cells. In a second step of development it will be necessary to increase both the power and energy density of such cells by applying a thin layer technique to the electrolyte and to the electrodes. A layer thickness of about 50 μm is envisaged. Furthermore, a certain electrode structure will be necessary to improve the cycling capability of both electrodes.

REFERENCES

(1) Rickert, H.: Einführung in die Elektrochemie fester Stoffe, Berlin-Heidelberg-New York 1973

(2) Baukal, W.: Extended Abstracts, 138th Meeting of ECS, Atlantic City, Oct. 1970

(3) Ure, R.W. jr.: J. Chem. Phys. 26 (1957) 1363

(4) Nagel, L.E., O'Keefe, M. in Fast Ion Transport in Solids/ Solid State Batteries and Devices ed. G. van Gool, p. 165, Elsevier 1973

(5) Hamer, W.J., Malmberg, M.S., Rubin, B.: J. Electrochem. Soc. 112 (1965) 750

(6) Wagner, C.: J. Electrochem. Soc. 115 (1968) 933

(7) Baukal, W.: Ber. Bunsenges. 79 (1975) 1148

(8) Baukal, W.: Electrochim. Acta 19 (1974) 687

SODIUM CHLOROALUMINATE BATTERY

J. Werth

ESB Incorporated, Technology Center
Yardley, Pennsylvania 19067

ABSTRACT

Molten salt battery technology based on low melting electrolytes containing sodium chloroaluminate will be discussed in some detail. Many sodium chloroaluminate mixtures have ionic conductivities at 200°C which compare not unfavorably with molten sodium polysulfide compositions at substantially higher temperatures. Some of the problems and advantages of batteries using sodium chloroaluminate as the major ionic conductor in the melt will be reviewed and compared with the problems and relative advantages of other molten salt concepts.

MODELING APPROACHES FOR MOLTEN-SALT LITHIUM/SULFIDE BATTERIES

T. F. Hickman* and V. M. Kolba

Argonne National Laboratory
9700 South Cass Avenue
Argonne, Illinois 60439

ABSTRACT

Methods are being sought for accurately predicting the behavior of lithium-aluminum/iron sulfide molten-salt batteries being developed at Argonne National Laboratory for electric-vehicle propulsion and off-peak energy storage on utility networks. The successful application of an analytical model would aid in design optimization studies and design iteration and testing. A literature search to determine the state of the art of electrochemical cell modeling showed that little work has been done on the modeling of cells having molten salt electrolytes. This paper presents a summary of information gained in the survey and the results obtained when several existing models were applied to data taken at the terminals of Li-Al/FeS and Li-Al/FeS_2 test cells. The present effort is expected to lead to a model which provides complete characterization of the cell and battery components and thus allow optimization of cell and battery design.

INTRODUCTION

Extensive efforts are under way at Argonne National Laboratory (ANL) and elsewhere on the development of molten-salt cells which have potential for widespread applicability to electric-vehicle propulsion and off-peak energy storage banks on electric utility networks. In support of the design phases of the effort at ANL, methods are being sought for accurately predicting, by analytical means, the behavior of cells and batteries, with a minimum of design interation and testing. An extensive literature search was undertaken to determine the state of art of modeling of electrochemical cells. The study described here had as its goal the extension of present models which appear to be applicable to cell systems with molten-salt electrolytes.

To achieve this goal the conditions to be modeled must first be defined. In the mathematical modeling of an electrical device (or "black box") it is necessary only to specify the time variation of the voltage and current functions at the device terminals, although these relationships may be affected by temperature, electromagnetic field strength, etc. This type of voltage-current characterization is well documented in the literature on linear circuit theory, for the case of circuit elements such as resistors, capacitors and inductors. For nonlinear devices such as transistors, diodes, vacuum tubes, etc., elaborate modeling techniques have been developed to facilitate their design and use. However for electrochemical storage cells, analytical

*Cooperative Student Program, University of Cincinnati, Cincinnati, Ohio.

techniques are still in the early stages of development. Significant progress along these lines has been made mainly with the lead-acid and nickel-cadmium systems.

Complete characterization of the response of a system must include both the transient and steady-state conditions. Because research on transient cell behavior is in the early stages, it will not be dealt with here. Although the frequency response of an electrical device is generally desirable, it is unnecessary for these initial modeli· studies because electrochemical cells are generally operated at quasi-steady-state conditions of constant current charge or discharge. The latter conditions have been assumed in the derivation of most models reviewed in this study.

In the two types of cell usage of interest in this study, constant power behavior is also needed and, for the case of the electric automobile application, it is desirable to model cell behavior in response to some type of driving profile (for example, the SAE J227 urban driving profile). Iterative means of predicting nonconstant cell-current behavior is a suggested method of approach.[1] This method may be described as a step wise graphical integration of the current demand at the driving profile selected.

Types of Models

The analysis of electrochemical cells has been approached by use of four major methods. These are tabular or graphical analysis and mathematical or equivalent circuit modeling. The tabular and graphical methods are similar. These consist of massive sets of test data on "typical" cells, listing the terminal relationship of the cells for each data point. The requirements of exhaustive quantities of test data, data storage, and retrieval, even if complied on a digital computer by table look-up,[2] make these methods cumbersome to apply. However, the graphical method remains the chief method of design and characterization of cells and batteries in industry today.

A more sophisticated approach is the use of mathematical equations to describe cell behavior. This method requires the initial collection of significant amounts of test data, but only enough to establish general trends. Once general trends are established for a cell of a given chemical composition, much less data are required to characterize succeeding cells.

Perhaps the ideal method of cell analysis is by an equivalent circuit model, as applied by Zimmerman and Peterson.[3] Such models, coupled with an electronic-circuit-analysis computer program such as SPICE,[4] should allow complete analysis of cell charge and discharge modes, transients, series and parallel combinations of cells, and fault analysis of a cell or battery array. This method requires extensive testing of a representative set of cells and thus would best be applied to molten-salt cells only after commercially produced cells show reproducible performance. Zimmerman and Peterson have applied this type of model to nickel-cadmium cells with considerable success. The model includes thermal affects and can include elements to represent cell changes as a function of cycle life.

Much work has been done on a more microscopic basis such as modeling of porous electrodes, examining diffusional overpotential and current

distributions in electrodes in an attempt to describe precisely the electrochemical reaction in cells and derive mathematical models for the reactions in question. The complexity of this approach renders it impractical to obtain cell-terminal-relationships under all but highly controlled conditions. Significant papers in the literature, that deal with electrochemical cell modeling and that appear to have application to our work, are listed and categorized in Table I. None of these models have been previously applied to molten-salt cells. A short description of the model output and required input data are also given in the Table. No one model is addressed to all of the desired functional relationships. The applicability of the various models to the desired relationships are reviewed in the following sections.

Cell Characterization

Before applying any of the available cell models, it is necessary to define precisely what is meant by "characterization of an electrochemical cell". A reasonably complete characterization[5] of the cell terminal relationship is found if the functional relationships of Fig. 1 can be quantitatively determined. The functional relationships desired are; cell voltage, resistance, capacity, utilization, energy efficiency and coulombic efficiency as a function of current density for charge and discharge conditions. The instantaneous power and cell voltage as a function of the state-of-charge are also desired.

For example, if a functional relationship between resistance, and ampere-hour capacity (cell size) can be found then it should be possible to quantitatively determine the functional relationship of voltage, ampere-hour capacity and current. Temperature variations affect all of these functions but until the range of temperature operation of molten-salt cells is more definitely established, no effort will be made to characterize temperature effects.

Discharge-Charge Curves

A review of the models has shown the Shepherd model[5] to be the most widely applicable. Therefore, this model was applied to data from ANL Cells R-4 and DS-11. Cell R-4 is a Li$_{Al}$/LiF-LiCl-LiBr/FeS prismatic bicell which had a theoretical capacity of 80 A-hr. Considerable data was available on this cell and its performance is considered typical of present cells of this type.

A FeS cell has been considered to be the type of cell which has a single voltage-plateau. Discharge of a FeS_2 cell proceeds to the FeS state prior to the final reduction to iron. The FeS_2 discharge has a distinct voltage plateau and the FeS discharge occurs at a lower voltage plateau. Additives to the FeS or FeS_2 produce other plateaus in addition to the two mentioned above.

The Shepherd model can be applied to FeS_2 cells, which have two voltage plateau's by modeling each voltage plateau separately. The model uses a curve-fitting technique applied to two discharge curves to arrive at an equation of the form

Table 1. Electrochemical Cell Models Found in the Literature

Author Reference	Data Needed as Input to Model[a]	Model Successfully Applied to These Cell Types	Model Output	Comments on Model
5	Two constant current density discharge curves	NiOOH/KOH/Fe; Ag_2O/KOH/Cd; NiOOH/KOH/Cd; Ag_2O/KOH/Zn; PbO_2/H_2SO_4/Pb; PbO_2/H_2SO_4/Zn; dry cell	V *vs.* f·t for all current densities; energy *vs.* it for all current densities; efficiency of utilization of active materials; theoretical watt-hour efficiency	With only an adjustment to concentration polarization term can be applied to LiAl/LiCl·KCl/FeS_x cells. Also applicable to half cells
3	Cell resistance, capacitance, and a relatively complete family of charge-discharge curves at fixed and known temperatures and currents	NiOOH/KOH/Cd	Total characterization of terminal relationships should have partial internal physical significance	Requires modification for molten salt cell and exhaustive testing of a representative cell
10	V *vs.* I curve (including short circuit) at a give state-of-charge	Mo/H_2SO_4/Fe^{3+}(SS) cell and half cells	Power output *vs.* current; maximum power output; cell resistance as a function of current; V *vs.* I including effect of concentration polarization	May apply to molten salt cells
1	"Manufacturer's data"	PbO_2/H_2SO_4/Pb; NiOOH/KOH/Cd	V *vs.* t for all currents. Allows for more than one constant current level within a discharge	Appears to be applicable to electric vehicles and may predict voltage during a driving profile
7	Charge-discharge family of curves	PbO_2/H_2SO_4/Pb	Three figures of merit; estimates of battery data at high current and energy drains	Correlates somewhat to Shepherd's model;[5] parameter calculation is considerably simpler
6,8,9	Two constant-current discharge curves	PbO_2/H_2SO_4/Pb; Ag_2O/KOH/Zn; NiOOH/KOH/Cd; Ni/KOH/Fe	V *vs.* f·t for all currents; energy *vs.* current; average voltage; rate of change of capacity with I and t	One of the easiest to apply

[a]All models use mathematical equations except Ref. 3 which is in equivalent circuit form.

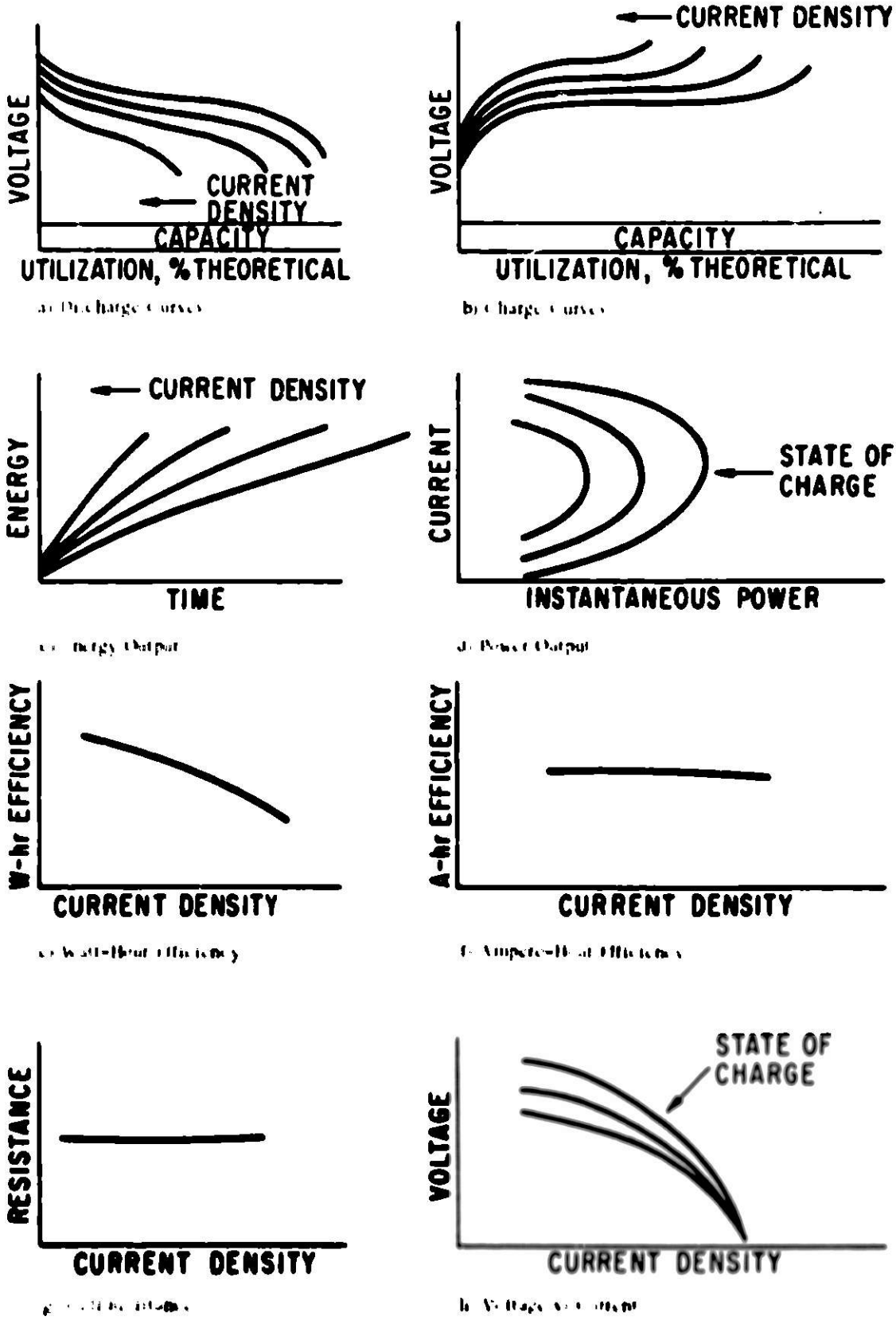

Fig. 1. Cell Characterization Curves

$$E = E_s - K\left(\frac{Q}{Q - it}\right)i - Ni + A \exp(-BQ^{-1}it) - Cit \qquad (1)$$

where

E = terminal voltage (V)

E_s = a voltage constant (V)

K = polarization coefficient (Ω/cm^2)

Q = cell capacity ($A\text{-}hr/cm^2$)

i = cell current density (A/cm^2)

t = time of charge/discharge (hr)

N = internal resistance per unit area (Ω/cm^2)

A, B and C are empirical constants, (V), (unitless) and (Ω/hr)

It has been found that, for molten-salt cells, the second order terms are better fit by a modification of Shepherd's equation. These empirical modifications were made because A, B and C were not found to be constants but varied as follows:

$$A = A_o - A_{s1}\, i \qquad (2)$$

$$B = B_o - B_{s1}\, i \qquad (3)$$

$$C = C_o \exp(C_{s1}\, it) \qquad (4)$$

where the o and s1 subscripts refer to the empirically determined slope and intercepts of the A, B and C functions. Because this complicates the original equation somewhat, it should be noted that these modifications have a significant effect only at near-zero and at large fractions of ampere-hour utilizations. With the increasing availability of programmable calculators and computers, this complication is not deemed excessive. The modified equation is as follows:

$$E = E_s - K\,[Q(Q-it)^{-1}] - Ni + \{(A_o - A_{s1}i)\exp[(B_o - B_{s1}i)\,Q^{-1}it]\} - C_o\exp(C_{s1}\,it)\,it \qquad (5)$$

It should also be noted that Eq's. 1 and 5 both have discontinuities at $i \cdot t = Q$. This should not occur until after the cutoff voltage has been achieved. However, using Shepherd's method, this is not always the case. Therefore, four points were chosen roughly in the locations on the discharge curves that Shepherd suggests, and Q was calculated. This process was repeated until the largest value of Q was found, and then the other parameters were calculated. The result was a less-than-desirable fit when the Cell R-4 achieved a capacity that was a high fraction of the theoretical. A value for Q was then estimated graphically, while the other parameters were held constant. It was also found necessary to iterate this graphically estimated Q for a better fit. In so doing, the best fit occurred when Q was replaced by $Q_o + Q_{s1}i$. The results are shown in Fig. 2. The agreement of the calculated data and experimental data is reasonable for the major portion of the discharge. However, refinements are required to more adequately represent the experimental data near the end of discharge.

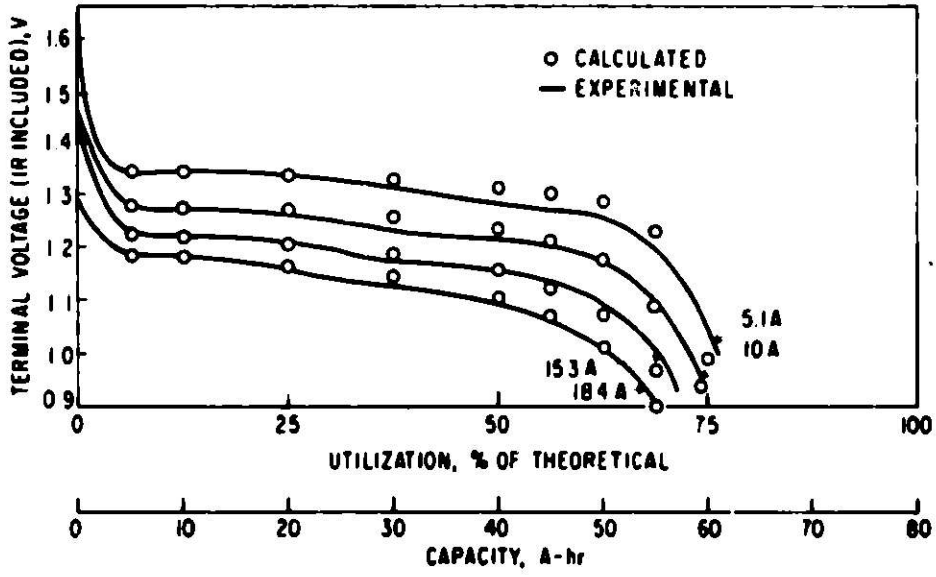

Fig. 2. Family of Constant Current Discharge Curves for Cell R-4

By integrating the product of the current and Eq. 5 over time we obtain an energy expression:

$$W_t = \int_0^t Ei\, dt = E_s it - KQi \ln (1 - it/Q)^{-1} - Ni^2 t + (A_o - A_{s1} i)\, Q/(B_o - B_{s1} i)\, [1 - \exp [-(B_o - B_{s1} i)\, it/Q)) - \frac{C}{C_{s1}} [\exp (C_{s1} it - 1)] \quad (6)$$

where W_t = energy output (W-hr). Calculated results as shown for Cell R-4 in Fig. 3 agree very well with the experimental data.

A similar curve-fitting technique can be applied to two charge curves. Merely changing the signs of all but the E_s term does not yield satisfactory results. Once the charge parameters are determined we obtain

$$E = E_s + K [Q(Q - it)]\, i + Ni - (A_o - A_{s1} i) \exp [- (B_o - B_{s1} i)\, it/Q] \quad (7)$$

and

$$W_t = E_s it + KQi \ln (1 - it/Q) + Ni^2 t - (A_o - A_{s1} i)[Q/(B_o - B_{s1} i)] [1 - \exp [- (B_o - B_{s1} i)\, it/Q]] + \frac{C}{C_{s1}} [\exp (C_{s1} it) - 1] \quad (8)$$

Energy Efficiency

An expression for watt-hour efficiency can be obtained by dividing Eq. 6 by Eq. 8. The accuracy of this method depends on the degree to which the equations fit the experimental data. Acceptable accurracy is achievable based on the fit of the data shown in Fig. 3.

Application of the model of Selis and Russell[6] failed to yield an accurate prediction for discharge watt-hours. This was largely due to the difficulty in determining the "knee-over" point in the discharge curve. If this model were modified to use a "time to cutoff" or a more accurate method of determining the "knee-over" point could be found, it could prove to be useful because it is simple to apply.

Coulombic (Capacity) Efficiency

The coulombic (A-hr) efficiency is perhaps most easily obtained by application of the Peukert[7-9] equation:

$$i^n t = C \tag{9}$$

where n and C are empirical constants

i = constant current density (A/cm^2)

t = time (hr).

For this equation to be valid the data must give a linear relationship on a plot of log t vs. log i. The experimental data for Cell R-4 yielded the linear relationship required as shown by the results plotted in Fig. 4. However, application of the Peukert equation to determine coulombic efficiency yields results showing the minimum efficiency as shown in Fig. 5.

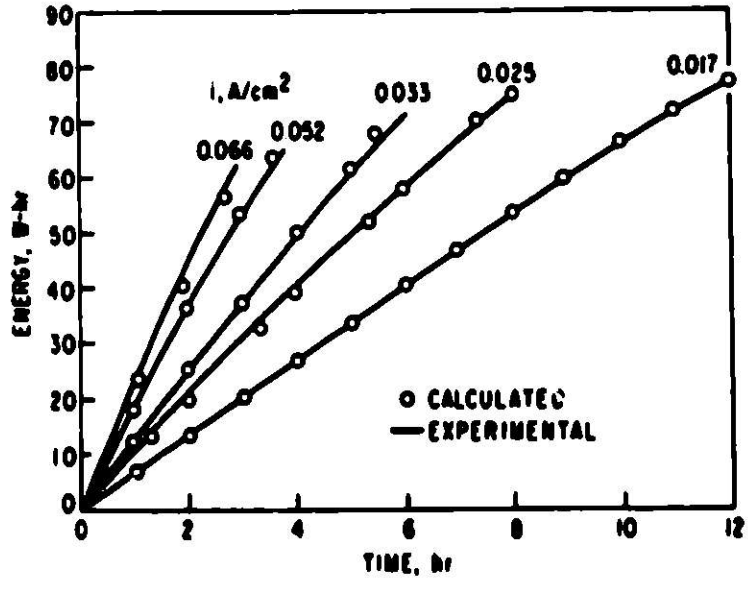

Fig. 3. Energy Output for Cell R-4

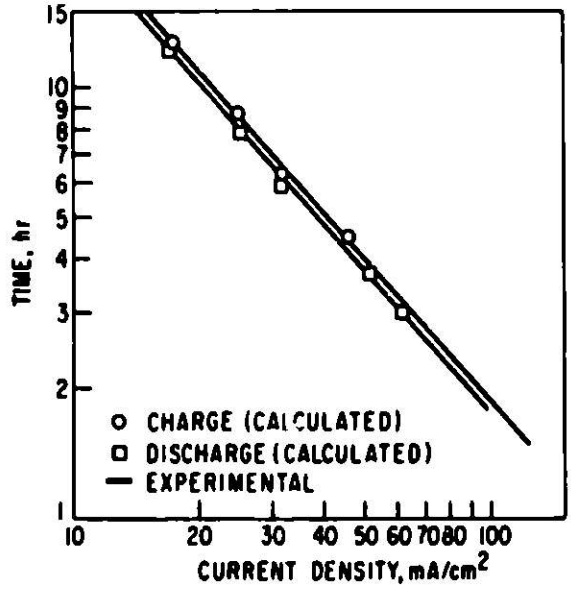

Fig. 4. Application of Peukert Equation Current *vs.* Time Curve for Cell R-4

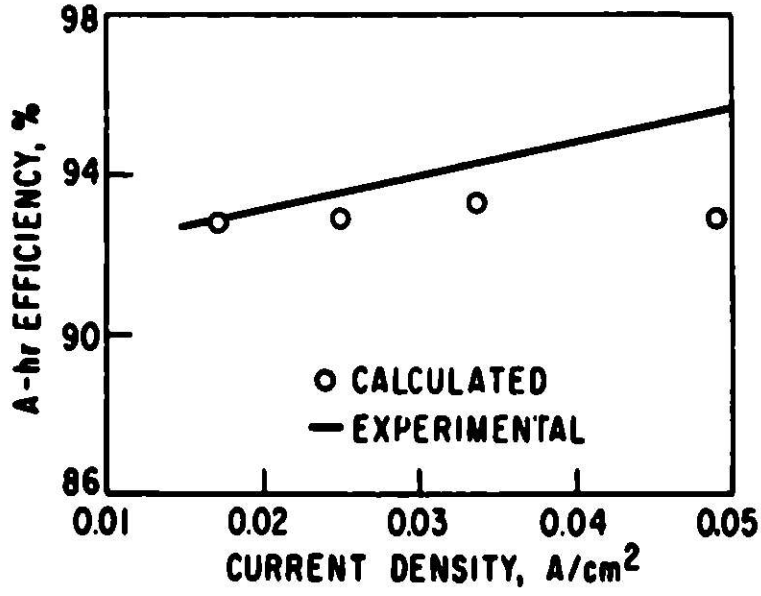

Fig. 5. Coulombic Efficiency of Cell R-4

Cell Power and Resistance

The short-duration discharges at current levels near short-circuit conditions, which are required as input to the Greene and Green[10] model, have been found[12] damaging to the cycle life of present cells. Therefore, the output of the Shepherd model was used as input data to the model of Greene and Greene at high current levels. The Shepherd model was found to yield a 15% error at high current densities ($i > 0.4$ A/cm^2). Using results from the Shepherd model and the experimental data obtained at 75% charge, the parameters for the Greene and Greene model were determined and applied to Eqs. 11 and 12 as derived by Greene and Greene to determine instantaneous power.

$$R = \frac{E_{oc}}{I'_{sc}} - \left(\frac{\gamma}{I'_{sc}}\right) \log \frac{I'_{sc}}{I_{cc}} \tag{10}$$

$$W = I_{cc} \exp\left[\left(\frac{E_{oc}-E}{\gamma}\right) \ln 10\right] \tag{11}$$

$$W_{max} = (0.16)\ \gamma\ I_{cc} \exp\left[\left(\frac{E_{oc}}{\gamma}\right) \ln 10\right] \tag{12}$$

where

R = resistance (Ω)

I'_{sc} = short-circuit current (A)

E_{oc} = open circuit voltage (V)

W = instantaneous power (W)

E = terminal voltage (V)

γ and I_{cc} are experimental constants (V) and (A)

The results obtained are shown in Fig. 6. Application of this model yields results in agreement with experimental data only in the region near peak power. At lower power levels calculational results deviate considerably from the experimental data. A more accurate means for predicting, or nondestructively gathering data, on E *vs.* I' is needed at high current densities. The Greene and Greene model applies only at currents well above I_{cc}, and requires an accurate curve of E *vs.* I' to yield good power predictions. Perhaps better agreement of the Shepherd model at higher current densities will solve this problem.

Experimentally the resistance of molten-salt cells has been found to be nearly constant with cell current and state of charge.[13] For Cell R-4, the experimentally determined cell resistance ranged from 7.0 to 10.0 mΩ while application of the Greene and Greene Eq. 10 yields a value of about 3.5 mΩ comprising both ohmic and diffusional resistance. The calculated value is not in good agreement with the measured values. However, the calculated value does agree well with anticipated cell resistance values based on theoretical design calculations.

The Lindestrom[8] model did not appear to provide new insights and similar information can be obtained from the Shepherd model. For the Kleckner[1] model, calculation of the parameters was very difficult without computer iteration.

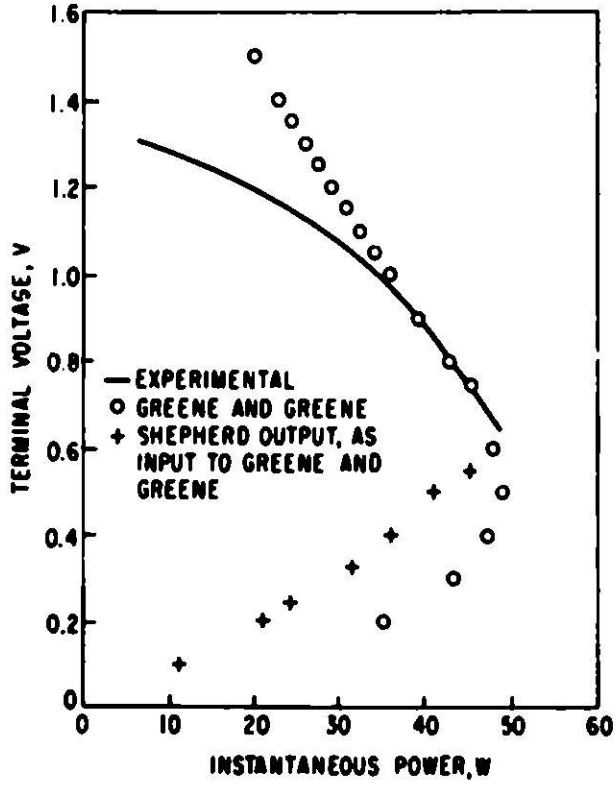

Fig. 6. Greene and Green Model for Instantaneous Power Applied to Cell R-4.

Kleckner's model may be useful, however, provided that the suggested iterative method for handling cell operation at nonconstant current conditions can be programmed. Further work in this area seems warranted.

CONCLUSIONS

A review of existing models which have been used to characterize various cells has shown that some of these are applicable to lithium-aluminum/iron sulfide molten-salt cells. Mathematical equations of several models appear to have direct application while modification of other equations provides applicable results. The Shepherd model with modifications has been applied to yield cell capacity, cell energy and energy efficiency information. Coulombic efficiency may be obtained from the Peukert equation which also provides an excellent method of determining discharge time at various current levels. The Greene and Greene method of determining cell resistance has been explored and may prove useful; however, their expression for predicting instantaneous power appears to be applicable only at the peak power region.

Work done so far indicates that a successful model and associated mathematical expressions can be developed for predicting the behavior of lithium-aluminum/iron sulfide molten-salt cells. Attainment of this goal of

complete characterization of the cells will permit the optimization of cell and battery design.

ACKNOWLEDGMENTS

The authors are grateful to L. Burris, D. S. Webster, P. A. Nelson, and A. A. Chilenskas for support and encouragement; to S. D. Gabelnick and R. H. Land, for technical support; to G. M. Kesser for editorial support; and to J. J. Johnson* and T. A. Morgan** for assistance with the calculations. This work was performed under the auspices of the Energy Research and Development Administration.

REFERENCES

1. K. R. Kleckner, "Modeling and Testing of Storage Batteries," SAE 730251 International Automotive Engineering Congress, January 8-12, 1973.

2. P. Bauer, "Computer Simulation of Satellite Electric Power Systems," IEEE Transactions of Aerospace and Electronic Systems, Vol. AES-5, November 1969, pp. 934-942.

3. H. G. Zimmerman and R. G. Peterson, "An Electrochemical Cell Equivalent Circuit for Storage Battery/Power System Calculations by Digital Computer," Intersociety Energy Conversion Engineering Conference. Vol. 1, 1970.

4. D. O. Pederson, "Simulation Program with Integrated Circuit Emphasis," University of California, Berkley.

5. C. M. Shepherd, "Design of Primary and Secondary Cells II. An Equation Describing Battery Discharge," J. Electrochem. Soc. *112*, No. 7, 657-664 (1965)

6. S. M. Selis and C. R. Russell, "Analytical Representation of the Discharge Characteristics of Commercial Secondary Batteries," Electrochemical Technology, Vol. 1, March-April 1963, pp.77-81.

7. O. Lindstrom, "A Pseudo-Resistance Method for Collating Battery Discharge Data," J. Electrochem. Soc. *117*, No. 8, 1083-1090 (1970).

8. W. Peukert, Elektrotech. Z. *18*, 287 (1897).

9. G. W. Vinal, Storage Batteries, 4th ed., John Wiley and Sons, Inc., New York, pp. 216-218 (1955).

---

*Research Associate Program - Georgia Institute of Technology.
**Cooperative Student Program - University of Cincinnati.

10. S. B. Greene and N. D. Greene, "Theoretical Analysis of Electrochemical Energy Conversion Systems," Electrochemical Technology, Vol. 1, September-October 1963, pp. 276.

11. Private communication, A. A. Chilenskas, ANL.

12. Private communication, H. Shimotake, ANL.

13. Private communication, M. Roche, ANL.

CONSIDERATIONS IN THE USE OF ELECTRICAL MEASUREMENT TECHNIQUES TO EVALUATE POTENTIAL NEW ELECTROLYTES AND MIXED CONDUCTORS

Ian D. Raistrick and Robert A. Huggins
Center for Materials Research
Stanford University
Stanford, California

ABSTRACT

Exploratory efforts are being undertaken in a number of laboratories to identify and evaluate the properties of new solid electrolytes and mixed conductors because of their potential use in such applications as high performance batteries and fuel cells. Due to large values of ionic mobility in such materials, particular care must be exercised either to avoid or to compensate for interfacial polarization effects. Methods for experimental determination of the important parameters in such cases are reviewed, with emphasis upon the interpretation of frequency-dependent a c measurements.

INTRODUCTION

There is currently a great deal of interest in solid electrolytes and mixed conductors due to their potential use in high performance battery or fuel cell systems and also because they can be employed in solid electrochemical transducers for a variety of scientific and technological purposes.

Due to the unusual range of behavior of these materials and the special requirements related to their use, particular attention must be given to the problem of appropriate measurement and evaluation methods. It is unrealistic to expect that the approaches commonly used on more conventional materials can be casually employed on solid electrolytes and related materials with success.

Various electrical measurement techniques have been used for many years to evaluate physical phenomena within both electronic and ionic conductors. These methods typically involve the determination of either electric potential differences or charge transport between the sample, or sample-electrode combination, and an external electrical measurement system. In cases in which electrodes are used, such external measurements relate to the whole sample-electrode system, and can thus be influenced by, as well as be employed to evaluate, several types of phenomena. These include long range charge transport due to the motion of charged species appreciable distances, dipolar behavior due to local motion of charged species, and various interfacial phenomena. The literature is rich with examples of the use of such methods to study semiconductors and dielectrics, as well as various electrochemical phenomena.

Electrical measurement methods are also particularly appropriate for the evaluation of mass transport in solid ionic conductors and mixed conductors (where both ionic and electronic species transport an appreciable fraction of the charge, and which may be of interest as electrode constituents). However, in cases in which ionic transport is rapid, interface polarization

effects and other related phenomena that are not normally considered when dealing with solids having low ionic mobility can be overwhelmingly important.

A number of different electrical measurement techniques can be used under both transient and steady state conditions. In many cases a time-or frequency-dependence is observed in the results. When this is found, it is common to measure various quantities, such as the apparent resistance or capacitance of the sample-electrode system, as a function of frequency, and then to relate these results to physical phenomena within the sample-electrode system.

When attempting to evaluate transport properties in more conventional ionic conductors, the general practice is to be wary whenever a frequency dependence is found. It is often ascribed to interfacial polarization effects, and one generally tries to avoid it by operating at a sufficiently high frequency that the observed system resistance is no longer frequency sensitive. This is a relatively simple matter when dealing with poorly conducting materials traditionally of interest to the solid state physics community, such as the alkali halides. However, when one is concerned with materials in which the ionic conductivity is much greater, such as those which might be considered for use as solid electrolytes, it becomes experimentally very difficult to make measurements at frequencies sufficiently high that the data are frequency-independent.

On the other hand, in another area of scientific endeavor, sometimes called "electrodics" in the electrochemical literature, attention is focused primarily upon interfacial behavior and various types of time-dependent polarization. Indeed, special attention is given to the measurement and interpretation of frequency-dependent and transient phenomena in order to elucidate, rather than avoid, interfacial behavior.

It is the purpose of this paper to discuss measurement techniques and methods of data evaluation that have been developed for a variety of purposes, and to show how they can be interrelated to provide information concerning transport processes in both ionic conductors and mixed conductors containing unusually mobile ionic species. It will be seen that the combination of concepts and techniques developed in solid state physics with those used in solid state chemistry and electrochemistry should be particularly valuable.

IMPORTANT PROPERTIES

When evaluating solid electrolytes and mixed conductors there are several important properties to be considered. These include the magnitude of the total conductivity, σ, and the fractions of the charge flux transported by ionic and electronic species, designed by the ionic transference number t_i and the electronic transference number t_e, respectively. It is obvious that $t_i + t_e = 1$, and that the ionic conductivity, σ_i, is σt_i, and the electronic conductivity σt_e. Related to these conductivities are the concentrations, mobilities, and diffusion coefficients of the respective species involved in the transport process.

It is also often important to be able to separate out the true bulk (single crystal) behavior from that due to, or influenced by, grain boundaries. Within the latter we should include the effects of porosity and second phases, as well as grain boundaries themselves.

In the case of mixed conductors, in which both ionic and electronic species are mobile, it is important to separately evaluate their respective transport parameters. This must be done with care, as interaction between them can have large effects in some cases. Particularly interesting is the large enhancement of the chemical diffusion coefficient that can sometimes occur.

In addition to these measures of the bulk transport properties, internal dipolar behavior, phenomena related to interfacial capacitance, or non-uniform imperfection distributions may also be of interest in some cases.

In general, the values of these quantities are dependent upon both the chemical environment and temperature. Therefore, it is necessary that information be obtained concerning these matters as well. In addition, the range of thermodynamic stability and the possibility of reactions with chemical species present in the environment may be especially important in connection with their use in battery or fuel cell systems employing large differences in chemical potential.

TYPES OF ELECTRODES

In general, three kinds of electrodes are available for the characterization of the electrical conduction properties of a solid electrolyte. They are: 1) Fully reversible electrodes, in which both ionic and electronic charge may cross the interface unhindered. Thus the ratio of current to potential difference across the sample gives the total conductivity σ. An example of such electrodes would be metallic silver electrodes, used to measure the total conductivity of an electrolyte, such as AgI, which conducts primarily by motion of Ag cations. Alternatively, gas/inert metal electrodes may be used, as in the cell $O_2/Pt/ZrO_2/Pt/O_2$, where the O_2 partial pressures are fixed at the same value at both electrodes. Such electrodes serve two functions, a) they maintain a constant composition across the sample, serving a thermodynamic purpose, and b) they allow all common electrochemical species to cross the interface very rapidly, i.e., also serving a kinetic purpose. It is sometimes true that although electrodes may be sufficiently reversible to fulfill function a), interfacial processes may not be sufficiently rapid with respect to all the mobile charge carriers, providing a kinetic hinderance to the electrochemical charge transfer reaction at the interface. This will result in an apparent voltage dependence of the conductivity. In the ZrO_2 cell mentioned above, for example, experimental I - V curves[1] are of the form shown in Figure 1a, and the resistance computed at each voltage is shown in Figure 1b. At low voltages an interface resistance is apparent which acts in series with the bulk resistance, giving erroneous conductivity results. At higher voltages the interface resistance becomes less than the bulk resistance, so that somewhat less error is introduced. In other words, the interfaces appear to be "non-ohmic" for kinetic reasons at low voltages in this case.

2) Electronically blocking electrodes. The electronic conductivity of the electrolyte can be suppressed by introducing a purely ionic conductor between the electrolyte and metallic electrodes. An example is the cell $Ag/AgI/Ag_2S/AgI/Ag$[2]. In this case, the ionic charge carrier can freely pass through the AgI "filters", but charge transport by electronic species is blocked. Under these conditions the measured conductivity is only the ionic portion, σ_i.

3) Ionically blocking electrodes. The ionic conductivity may be

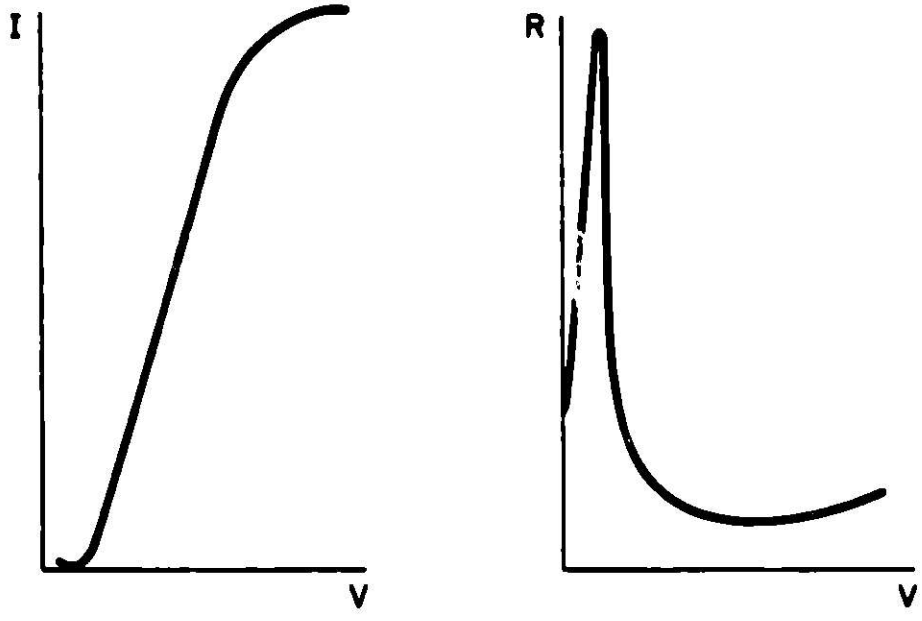

Figure 1.

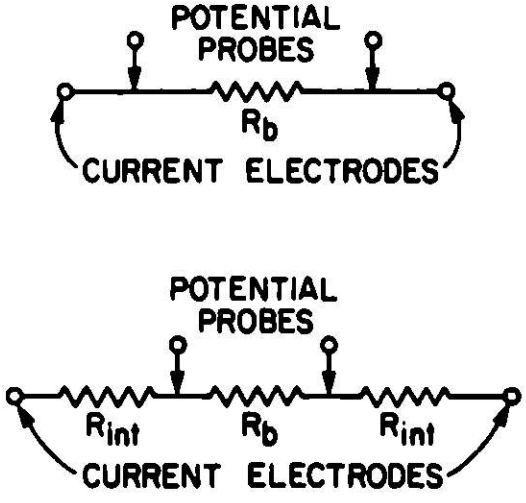

Figure 2.

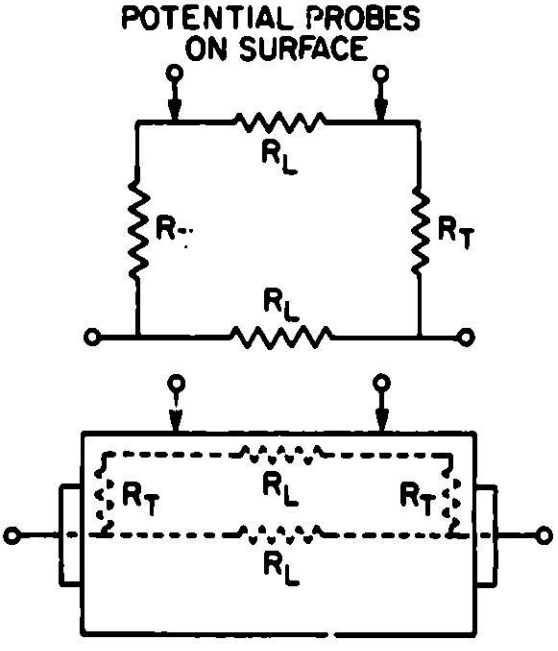

Figure 3.

suppressed,and the electronic conductivity separately measured if an electrolyte is bounded by two inert foreign metal electrodes, e.g., $Pt/Ag_2S/Pt$, if the applied potential difference is less than the decomposition potential of the electrolyte. This cell, however, has the disadvantage that the chemical potentials of the components are not fixed. Since the conductivity of minority carriers is often extremely dependent on the defect chemistry of the electrolyte, this can lead to nonreproducible results. A more satisfactory cell is therefore an asymmetric polarization cell of the type M/MX/Pt, where the chemical potentials within the electrolyte are fixed by equilibrium with the parent metal on the left and the ionic flow is blocked by the other, inert, electrode. Interpretation of the inherently non-ohmic data from such asymmetric cells was presented by Wagner[8], and will be discussed later. Alternatively the chemical potentials can be fixed by equilibria with surrounding gases, or by more complex cell arrangements[9]. One must be careful, however, for in a recent review based on the transport equations of irreversible thermodynamics,Wagner[4] showed that for materials with predominant ionic conductivity, the true ionic conductivity for uniform composition is virtually equal to the ionic conductivity value measured in the presence of suppressed electronic conductivity. On the other hand, this is not true if electronic conductivity prevails, and the electronic conductivity in the presence of suppressed ionic conductivity is in general not equal to the electronic conductivity defined by $\sigma_e = (1 - t_i)\ \sigma$.

D C MEASUREMENT OF THE TOTAL CONDUCTIVITY

Conductivity values can be obtained by a simple measurement of the relationship between the steady state charge flux and a steady applied electric potential difference between a pair of properly chosen, fully reversible electrodes, as represented by the simple equivalent circuit shown in Figure 2a. In this arrangement, sometimes called the two-point method, the total conductivity of a sample of constant cross section is given by

$$\sigma = \frac{I}{V}\left(\frac{L}{A}\right) \qquad (1)$$

where I and V are the current and voltage, and L and A are the length and cross sectional area. This technique can be employed when one can neglect the sample-electrode interfacial impedance and the impedance of the electrode system itself relative to the impedance of the sample. The absence of concentration polarization and electrochemical effects at the sample-electrode interface must also be assumed. As a result, this method is only appropriate for interesting solid electrolytes when electrodes are used that are reversible both kinetically and thermodynamically for the mobile ionic species.

A variant on this technique, the four-point method, can sometimes be used when the sample-electrode interfacial impedance cannot be neglected. The equivalent circuit representation is shown in Figure 2b. Steady state conditions are still assumed, so that the interfacial impedance must be time-independent. This technique is commonly used for measurements on semiconductors, often employing a linear arrangement of four contacts. The outer two acting as current electrodes, and the inner pair for potential measurements.

With uniform spacing between contacts, the conductivity of a homogeneous material with a flat surface is given by

$$\sigma = \frac{I}{2\pi V d} \qquad (2)$$

where d is the distance between contacts. If the spacing is not uniform, this becomes

$$\sigma = \frac{I}{2\pi V}\left[\frac{1}{d_1} + \frac{1}{d_3} - \frac{1}{d_1 + d_2} - \frac{1}{d_2 + d_3}\right] \tag{3}$$

where d_1, d_2 and d_3 are the spacing values, d_2 being the distance between the two central potential probes.

Unless special attention is given to the establishment of proper conditions at the outer two contacts, this four-point d c method may not be useful for determining the total conductivity of materials in which ionic transport is appreciable. This is due to the requisite assumption that the sample-electrode impedance can be modeled as a simple time-independent and potential-independent resistance. In order for this to be true, the interfaces must act reversibly for both ionic and electronic species.

Two further statements should be made concerning the four-point technique. Potential measurements are made at points upon the surface, and may not be representative of the bulk if the sample is not homogeneous or if special phenomena occur at the surface that are not characteristic of the interior. Likewise, the method assumes that there is good communication between the surface and the inside. In materials with anisotropic crystal structures containing layers or tunnels, as is common among solid electrolytes, this assumption may not be obeyed, particularly in the case of single crystals.

In order to see how this is the case, consider a material with resistivities ρ_L and ρ_T parallel and perpendicular to the direction of current flow. By utilization of appropriate geometric factors, these values can be converted into longitudinal and transverse resistances R_L and R_T, and the measurement system represented by the equivalent circuit shown in Figure 3. This figure neglects any interfacial impedances at the current electrodes.

This is a simple parallel circuit. For an applied voltage V, the current through the interior leg, I_{int}, is given by

$$I_{int} = \frac{V}{R_L} . \tag{4}$$

The current in the leg that includes communication between the interior and the surface through the transverse resistances, I_{ext}, is

$$I_{ext} = \frac{V}{R_L + 2R_T} . \tag{5}$$

The ratio of these currents I_{ext}/I_{int} is equal to the ratio of the potential difference measured between the potential probes on the surface and the actual potential difference across the interior portion of the sample.

$$\frac{I_{ext}}{I_{int}} = \frac{R_L}{R_L + 2R_T} . \tag{6}$$

If the sample is very anisotropic, so that $R_T >> R_L$, this simplifies to

$$\frac{I_{ext}}{I_{int}} \approx \frac{R_L}{2R_T} . \tag{7}$$

It is therefore quite evident that the actual longitudinal resistivity of a sample can be much greater than that inferred by the measurement of the potential difference between a pair of external probes in the four-point technique.

Similar difficulties may be encountered if the surface resistivity is a great deal lower than the bulk resistivity. This is an important consideration in the case of some semiconductors and dielectrics, but is often not important for solid electrolytes, due to their lower bulk resistivities.

Although these d c techniques are of limited use in evaluating either the total conductivity or the ionic conductivity of solid electrolytes or mixed conductors in which ionic transport is appreciable, they can be very useful for the determination of the electronic conductivity in mixed conductors when employed under proper conditions. Particularly important in this case is the requirement of equilibrium between the various forces tending to cause ionic transport, so that virtually all of the observed charge transport can be ascribed to the motion of electronic rather than ionic species.

D C TRANSFERENCE NUMBER MEASUREMENTS

An extremely important parameter in the assessment of a potential solid electrolyte is the electronic transference number: the fraction of the total current carried by electrons or holes. As will be seen later a c and square wave methods provide a useful estimate of this quantity as long as it is not too small. Various other methods exist for investigating minority electronic conductivities, the more important of which are discussed here.

The first of these methods is due to Tubandt[5] and is based on the fact that in the cell: $^{+}M/MX/M^{-}$ the amount of M transported from left to right is directly proportional to the quantity of electricity passed if all the current is ionic. If the amount of M transported is less than expected from Faraday's Law, then some of the current must be carried by electronic species.

The second method employs the formation cell: M/MX/X whose emf is given by the free energy of formation of MX if all the current is ionic. If some of the current is electronic, then a lower emf is measured[6]

$$t_i = (1 - t_e) = \frac{E \text{ measured}}{E \text{ calculated}} \quad . \tag{8}$$

A variation of this method employs two electrodes with different activities of M^{+}.

The third method is the most accurate and can be used to study very low levels of minority electronic conductivity: it is the Wagner [8] asymmetric polarization cell mentioned earlier: $^{-}M/MX/$ inert blocking electrode^{+} . If the above cell is biased as shown the total current at steady state is due solely to minority electronic species:

$$I_t = I_n + I_p = \frac{RTA}{LF} \{\sigma_n[1 - \exp(-u)] + \sigma_p [\exp(u)-1]\} \tag{9}$$

where $u = EF/RT$ and σ_n, σ_p are the partial conductivities due to electrons and holes.

Usually the contribution of either n or p will dominate, and the dominant species can be verified by the shape of the current voltage curve.

A useful rearrangement of the above equation[9]

$$\frac{I_t}{\exp(u)-1} = \frac{RTA}{LF} [\sigma_n \exp(-u) + \sigma_p] \tag{10}$$

allows electron and hole concentrations to be determined from a single experiment by plotting $I_c(\exp(u)-1)^{-1}$ vs. $\exp(-u)$. σ_n is calculated from the slope and σ_p from the intercept.

STEADY STATE A C MEASUREMENTS

Ideal Behavior

As was seen for the case of d c measurements it is useful to distinguish two extreme electrode types and to discuss the ideal behavior of a solid electrolyte bounded by these interfaces.

Consider first a solid electrolyte which conducts by a single ionic species interfaced to electrodes of an inert foreign metal. Transport of any charge across the interface is prevented by thermodynamic considerations if the applied a c voltage is much less than the decomposition potential of the electrolyte. Diffuse double layer or space charge theory as well as experimental results[10] on solid electrolyte-electrode systems show that each interface can be modeled as a parallel plate capacitor C_i (usually of the order of microfarads) whose rate of charging is determined by the bulk ionic resistance R_b of the electrolyte. At low frequencies therefore the appropriate equivalent circuit is that of Figure 4a. In addition it is necessary at high frequencies to consider the geometric capacitance (C_∞) which arises as a consequence of placing a material of finite dielectric constant between two metallic electrodes. C_∞ occurs in parallel to R_b and thus gives the complete circuit of Figure 4b (after lumping together the two interface capacitances). Capacitive effects related to leads between the sample and the measurement system, which are generally rather small, increase the apparent value of C_∞.

This circuit is often known as the Debye circuit and has been used (with various modifications) for many years in the interpretation of dielectric loss data for solid materials (including some solid electrolytes)[11]. In practice it makes no difference if C_∞ is placed across the entire circuit as in Figure 4b or merely across the bulk resistance[12] as it is generally of the order of picofarads and hence several orders of magnitude less than C_i.

On the other hand it is sometimes feasible to use electrodes which are both thermodynamically and kinetically reversible to the ionic carrier. Under these conditions there is no hindrance to the discharge of the ion by charge transfer and the equivalent circuit simplifies to that of Figure 4c.

In addition we may include at this stage a partial electronic conductivity. Circuit 4b becomes 4d and 4c becomes 4e, where R_e is the electronic resistance. As will be shown below it is possible, by a study of the frequency dispersion of the a c response, to determine the values of all of the components in Figure 4d, thus deriving a value for the ionic transference number. For the case of circuit 4e however, R_b and R_e are not separable and a value of the total conductivity only can be deduced.

The most common kind of a c measurement involves the use of a bridge circuit, which allows the in-phase and out-of-phase components to be balanced simultaneously. There are many kinds of bridges and the results may be expressed in terms of a variety of different parameters G_p, R_s, C_p, C_s, Q, D, etc. Most commercial bridges give readings based either on the assumption of a series representation (impedance)

$$Z^* = R_s + jX = R_s - j/\omega C_s \qquad (11)$$

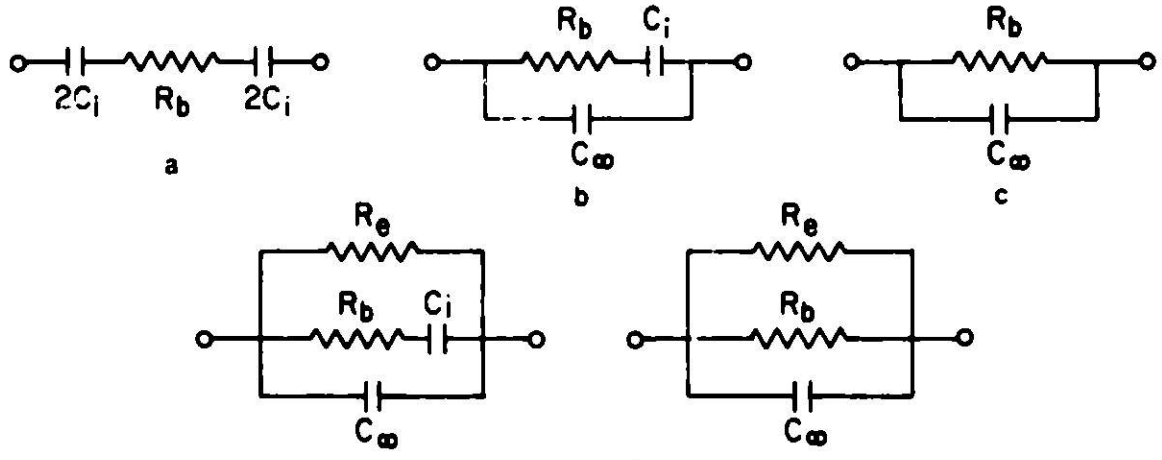

Figure 4.

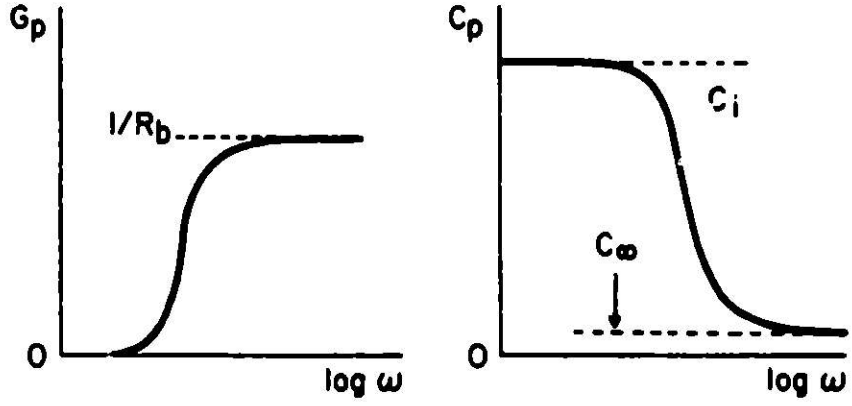

Figure 5.

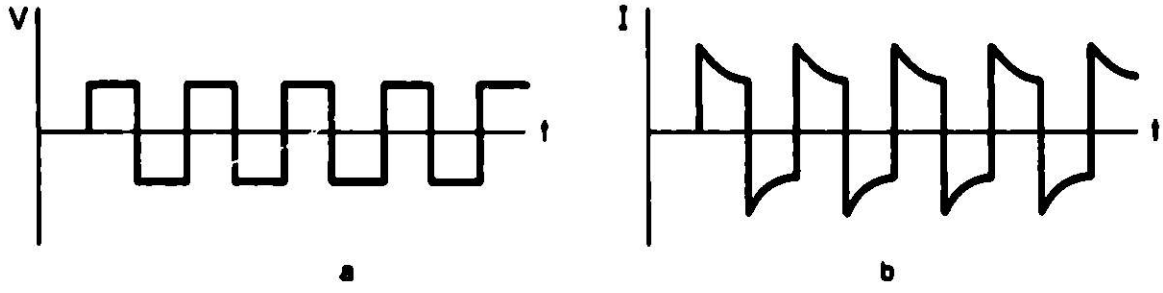

Figure 6.

or a parallel representation (admittance)

$$Y^* = 1/Z^* = G_p + jB = G_p + j\omega C_p \qquad (12)$$

In addition to frequency, however, it is only necessary to measure any two parameters and all the others may be calculated.

Circuit 4a is a series circuit and so impedance parameters are invariant as the frequency is changed. If, however, admittance parameters are measured, pronounced frequency dependence will be observed. Similarly, circuit 4c shows no frequency dispersion if admittance parameters are measured, but does if impedance parameters are determined. The Debye circuit of Figure 4b, or circuit 4d, however, show frequency dispersion no matter how the bridge is set-up. Conventionally, measurements have been extended to very high frequencies to overcome this problem. The admittance of the Debye circuit for example is given by the equation

$$Y^* = \frac{\omega^2 R_b C_i^2}{(\omega R_b C_i)^2 + 1} + j\left(\frac{\omega C_i}{(\omega R_b C_i)^2 + 1} + \omega C_\infty\right) \qquad (13)$$

as ω increases, and $(\omega R_b C_i)^2 >> 1$, $G_p \to 1/R_b$ and $C_p \to C_\infty$. Plots of G_p and C_p vs. log ω appear as in Figure 5. For a very good conductor however, it may be impossible to reach a sufficiently high frequency for G_p to be a good approximation of $1/R_b$.

Square Wave Method

One can simulate high frequency steady state a c measurements by employing a square wave generator to impose a potential difference upon the electrodes and observing the current response. Since the sudden imposition of a potential step is equivalent to the use of a very high frequency, measurement of the instantaneous current at the time of the step is equivalent to making a c measurements at a very high frequency. Indeed, the shorter the rise time of the square wave voltage, the higher the effective frequency. This is illustrated schematically in Figure 6.

If the frequency of the applied square wave is low, the level of the current at long times gives an indication of the d c (electronic) conductivity. Thus this type of measurement can give semiquantitative information about both the ionic and electronic components of charge transport.

Complex Plane Method of Data Analysis

It would obviously be useful to have a method of data analysis which allows extrapolation to correct values of R_b from measurements in a limited frequency range without recourse to the cumbersome impedance and admittance equations which demand the assumption of a particular equivalent circuit. This last point is particularly important where the electrodes may be of unknown reversibility to one or more of the conducting species, and diffusion effects become important.

A particularly convenient method of data analysis involves plotting the real and imaginary parts of the admittance, impedance, or dielectric constant against one another as a function of frequency[13,14]. Thus, in the admittance

or B-G plane, the susceptance (ωC_p) is plotted along the ordinate and conductance (G_p) along the abscissa .[p] Similarly, in the impedance (X-R) plane reactance and series resistance are plotted against one another. B-G and X-R plots for circuits 4a,b,c, and d are shown in Figure 7.

As may be seen for the case of 4d for example, all the equivalent circuit components are readily derived if measurements are made over a sufficiently extended frequency range. If measurements are made over only a limited range then one resistance and one of the capacitances might typically be found. The geometry of the figures is such that extrapolation by numerical or graphical methods is particularly straightforward. It should be noted that transference numbers are only derivable by this method if either t_i or t_e differs appreciably from unity, say by more than 1%. Very low levels of minority carrier conduction must be investigated by other methods.

Experimental Deviations from Ideal Behavior

Actually, most electrode/electrolyte systems do not conform to the ideal models discussed above. Few electrodes are so reversible that all capacitive effects at the surface can be ignored, and an electrode which may be completely blocking to a majority species may well be reversible to a minority charge carrier. Diffusion of neutral or charged species in the electrode or the electrolyte may severely complicate impedance results. Recent papers by Macdonald[15] [16] explore theoretical deviations from the simple models discussed above with some thoroughness. In addition, electrode morphology, and quality of the contact to the electrolyte are experimentally important. For example, the interface capacitance for the blocking electrode situation may be drastically reduced by having poor contacts to the sample. This results in less separation of the bulk and interface capacitance, leading to a situation similar to that shown in Figure 8a, where the correct value of conductance ($1/R_b$) is only approached slowly at high frequencies. In practice the situation is probably even more complicated in that it seems likely an additional contact R is also needed to satisfactorily model the behavior. Such effects may usually be eliminated by sputtering or evaporating the electrodes onto the electrolyte.

A very common experimental observation is that the low frequency semicircle in the B-G plots have centers lying below the real axis (Figure 8), and a corresponding deviation from verticality in the low frequency spur of the X-R plot is observed. Various explanations of this observation are possible. If, for example, the electrodes are imperfectly blocking for a conducting species, then, under certain conditions the diffusion of that species or its electrode reaction product may be rate determining. If the diffusional process obeys Fick's second law (i.e., internal fields can be neglected) then its effect can be represented at the interface by a Warburg admittance or impedance. Such a situation may exist, for example, if a neutral reaction product diffuses into the electrode material. Similarly, the situation where a minority charge carrier is free to discharge at the interface, whereas the majority carrier is blocked, leads to the same effect. This situation has been extensively discussed by Macdonald. The Warburg impedance has the complex form:

$$Z_W^* = K\omega^{-1/2} - jK\omega^{-1/2}, \qquad (14)$$

where K is a constant related to a diffusion coefficient.

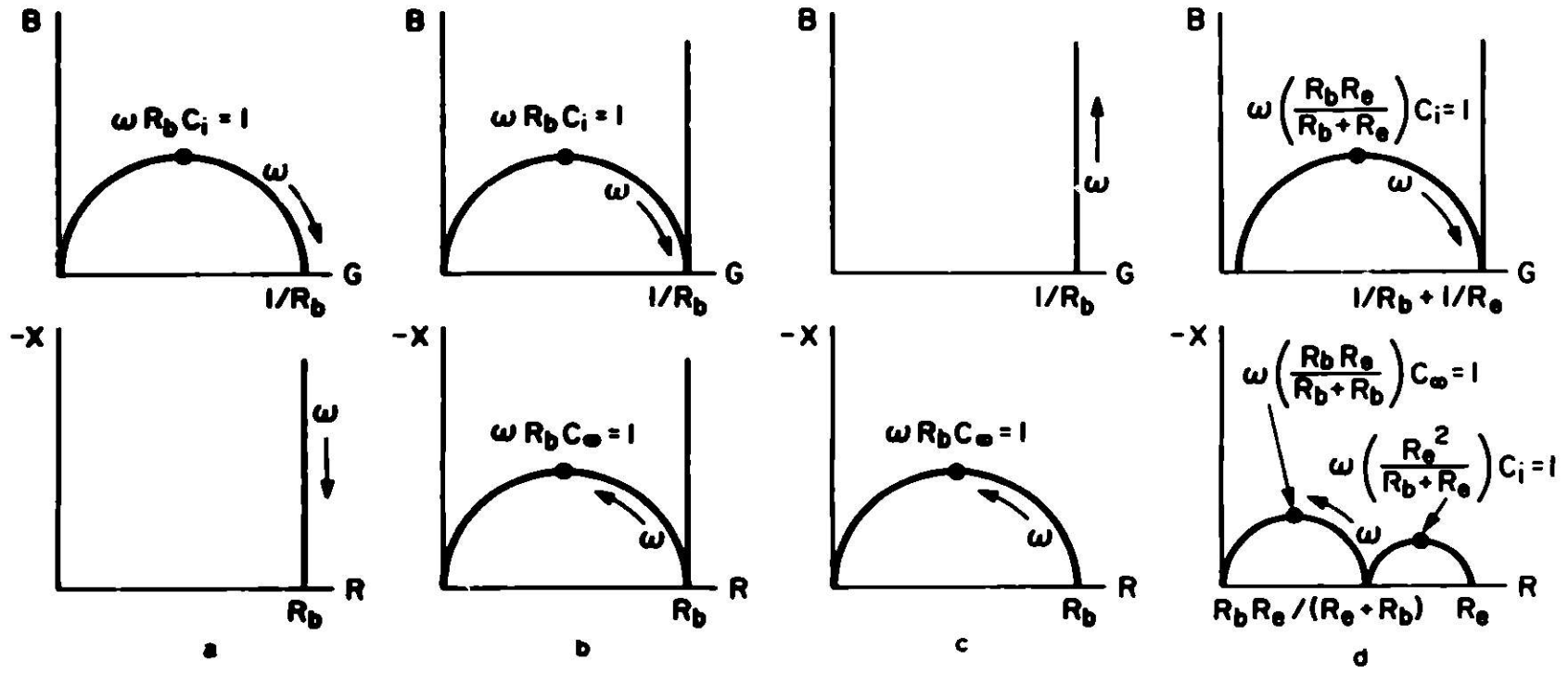

Figure 7.

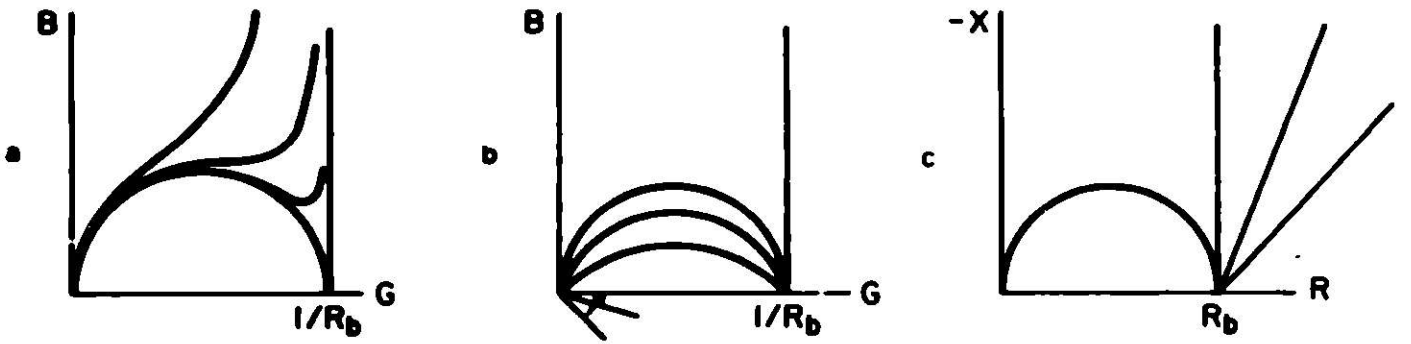

Figure 8.

If the diffusional step dominates the interface behavior then the equivalent circuit of Figure 9a is a useful approximation so long as the frequency is not too low. This gives a B-G plot of the form shown in Figure 3b. For the pure Warburg case the center of the circular arc lies on a line making an angle of 45 degrees with the real axis. Correspondingly, the X-R plot at low frequencies is a straight line inclined at 45° to the R axis.

Typically, however, the circle is not a full 45° below the G axis. It has been shown experimentally that the frequency dispersion under these circumstances can be accurately modeled using circuit 9b for a number of materials[17] where

$$Z_1^* = A_1 \omega^{-\alpha} - j B_1 \omega^{-\alpha} \tag{15}$$

and

$$R_1/A_1 = \text{cotn}\left(\frac{\alpha\pi}{2}\right). \tag{16}$$

The details of the origin of this impedance are not at present certain. Armstrong has argued[18] that such effects are primarily due to surface roughness, although diffusion effects cannot be ruled out. At the very least, equation (15) serves as a useful tool for extrapolation of data to obtain R_b if measurements have been carried out only over a limited frequency range. In particular, circuit 9b is represented by a straight line in the complex impedance plane at low frequencies, which makes the determination of R_b extremely simple (Figure 8c).

In addition to these low frequency, or interface-related effects a separate deviation from ideal Debye behavior has been observed in polycrystalline samples. The characteristic distortion of the B-G and X-R plots is shown in Figure 10. In order to model the bulk, or high frequency, response it is necessary to include, in addition to the bulk resistance and geometric capacitance, a frequency-dependent complex admittance Y_b^*

$$Y_b^* = A_b \omega^{\beta} + jB_b \omega^{\beta} \tag{17}$$

The complete admittance equation for the high frequency case is therefore

$$Y_T^* = \frac{1}{R_b} + A_b \omega^{\beta} + j\,(B_b \omega^{\beta} + \omega C_o) \tag{18}$$

obviously as ω is increased the apparent conductivity

$$C_p = \frac{1}{R_b} + A_b \omega^{\beta} \tag{19}$$

becomes indefinitely large. It has been postulated[19] that this effect is associated with energy storage and dissipation at grain boundaries in the polycrystalline samples.

Effect of Frequency Dependence on Apparent Activation Enthalpies

In the investigation of ionic conductivity of new materials an important parameter to be determined is the enthalpy of activation for conduction. Typically, a c conductivity measurements have either been made at a fixed frequency or else extrapolated to "infinite" frequency. It is quite easy to

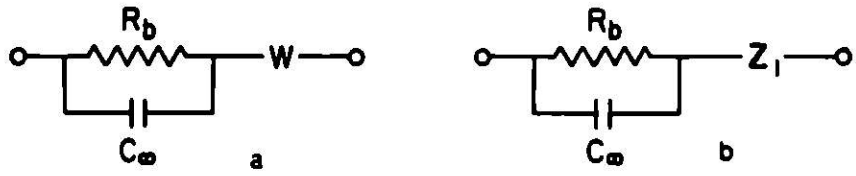

Figure 9.

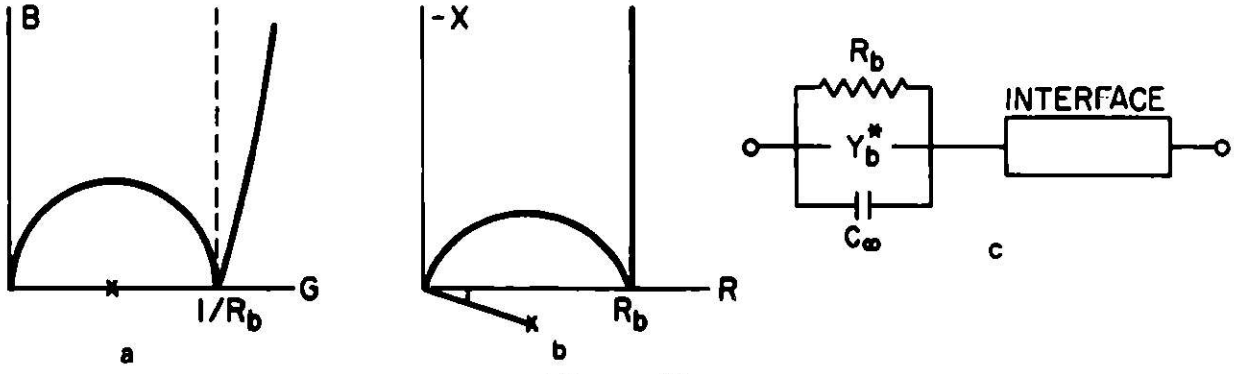

Figure 10.

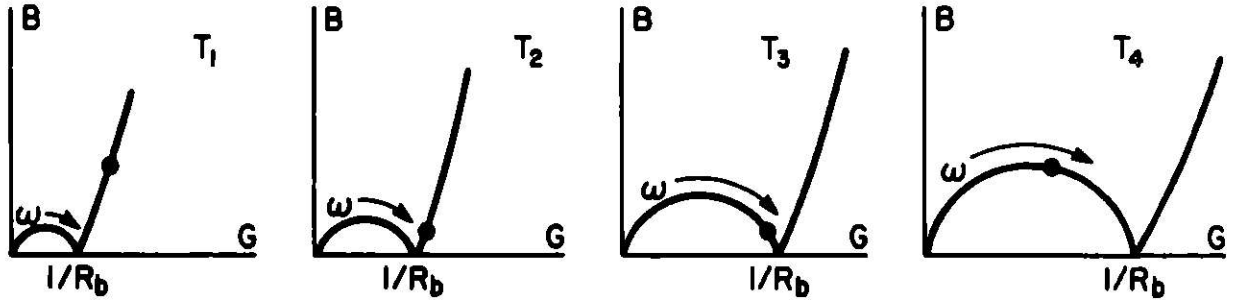

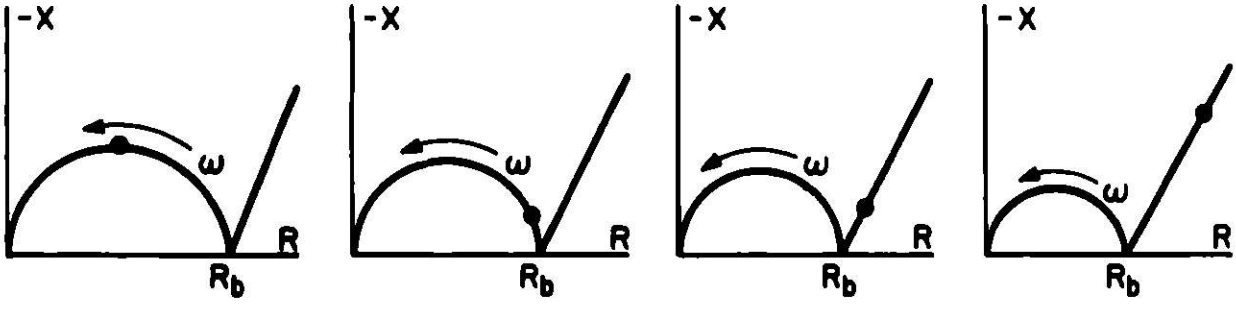

Figure 11.

derive not only wrong values of apparent conductivity, but also the wrong temperature dependence.

As shown earlier, even if the sample-electrode system behaves according to the ideal Debye circuit, the apparent value of the conductivity will vary with frequency at low frequencies if evaluated by use of the parallel approximation (G_p), and it will be frequency-dependent at high frequencies if evaluated by use of the series assumption (R_s). It can be shown that the critical frequency separating the linear from the semicircular regimes in both cases is given by

$$\omega_o = (R_b^2 C_i C_\infty)^{-1/2} \tag{20}$$

In addition to this caution about selection of the proper frequency range for the acquisition of data at any given temperature, further problems may ensue if monofrequency experiments are made over a range of temperature. Since it is expected that R_b will decrease at higher temperatures, while C_i and C_∞ should not vary so much, the value of the critical frequency ω_o will be temperature-dependent, generally increasing at higher temperatures. This means that increasing the temperature produces the same effect as decreasing the frequency of measurement, so far as the frequency-dependence of the data is concerned. Likewise, the loci of points relating to monofrequency experiments move along the complex plane figures as the temperature is changed. This effect is illustrated schematically in Figure 11, where it is readily seen that misleading results can be obtained. Looking at the B-G plots, for example, it is obvious that the apparent conductivity obtained from monofrequency experiments will tend to be higher than the correct value (where the figure intersects the real axis) at low temperatures, and lower than the correct value at high temperatures. This means, of course, that the apparent temperature dependence, expressed as the activation enthalpy, will also be incorrect. This effect is illustrated in Figure 12.

Thus it is obvious that if the frequency dependence of the response of electrolyte-electrode systems is not taken into account in the handling of a c data, misleading results can be obtained for good conductors (where R_b is relatively small), not only in the magnitude of the conductivity, but also in its temperature dependence. This is surely the origin of some of the apparently anomalous data that one finds in the literature.

ACKNOWLEDGEMENT

This work was supported by the Advanced Research Projects Agency through the Office of Naval Research under Contract N00014-67-A-0112-0075.

REFERENCES

1. T. M. Gür, Ph.D. Dissertation, Stanford (1976).
2. M. Hebb, J. Chem. Phys. 20, 185 (1952).
3. H. Rickert, Z. Physik. Chem. NF 23, 355 (1960).
4. C. Wagner, Prog. Sol. Stat. Chem. 10, 3 (1975).
5. C. Tubandt, Z. Electrochem. 26, 338 (1920).
6. C. Wagner, Adv. Electrochem. and Electrochem. Eng. 4, 1 (1966).
7. V. B. Tare and H. Schmalzried, Z. Physik. Chem. NF 43, 30 (1964).

8. C. Wagner, International Committee of Electrochemical Thermodynamics and Kinetics. Proc. 7th Meeting (1955), Butterworths, London (1956).
9. J. W. Patterson, E. C. Bogren and R. A. Rapp, J. Electrochem. Soc. 114, 752 (1967).
10. D. O. Raleigh, Electroanal. Chem. 6, 87 (1972).
11. R. H. Radzilowski, Y. F. Yao and J. T. Kummer, J. Appl. Phys. 40, 4716 (1969).
12. J. R. Macdonald, J. Electroanal. Chem. and Interfacial Electrochem. 66, 143 (1975).
13. K. S. Cole and R. H. Cole, J. Chem. Phys. 9, 341 (1941).
14. J. E. Bauerle, J. Phys. Chem. Solids 30, 2657 (1969).
15. J. R. Macdonald, Electroanal. Chem. and Interfacial Electrochem. 53, 1 (1974).
16. J. R. Macdonald, J. Chem. Phys. 61, 3977 (1974).
17. I. D. Raistrick, C. Ho, Y-W. Hu, and R. A. Huggins. To be published.
18. R. D. Armstrong, T. Dickinson and P. M. Willis, Electroanal. Chem. and Interfacial Electrochem. 53, 389 (1974).
19. I. D. Raistrick, C. Ho, and R. A. Huggins. To be published.

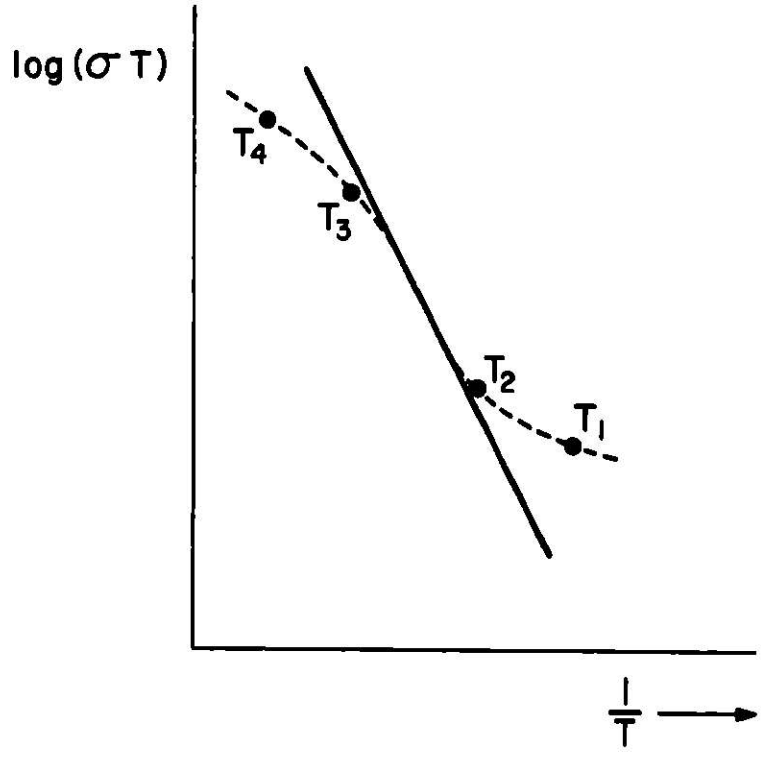

Figure 12.